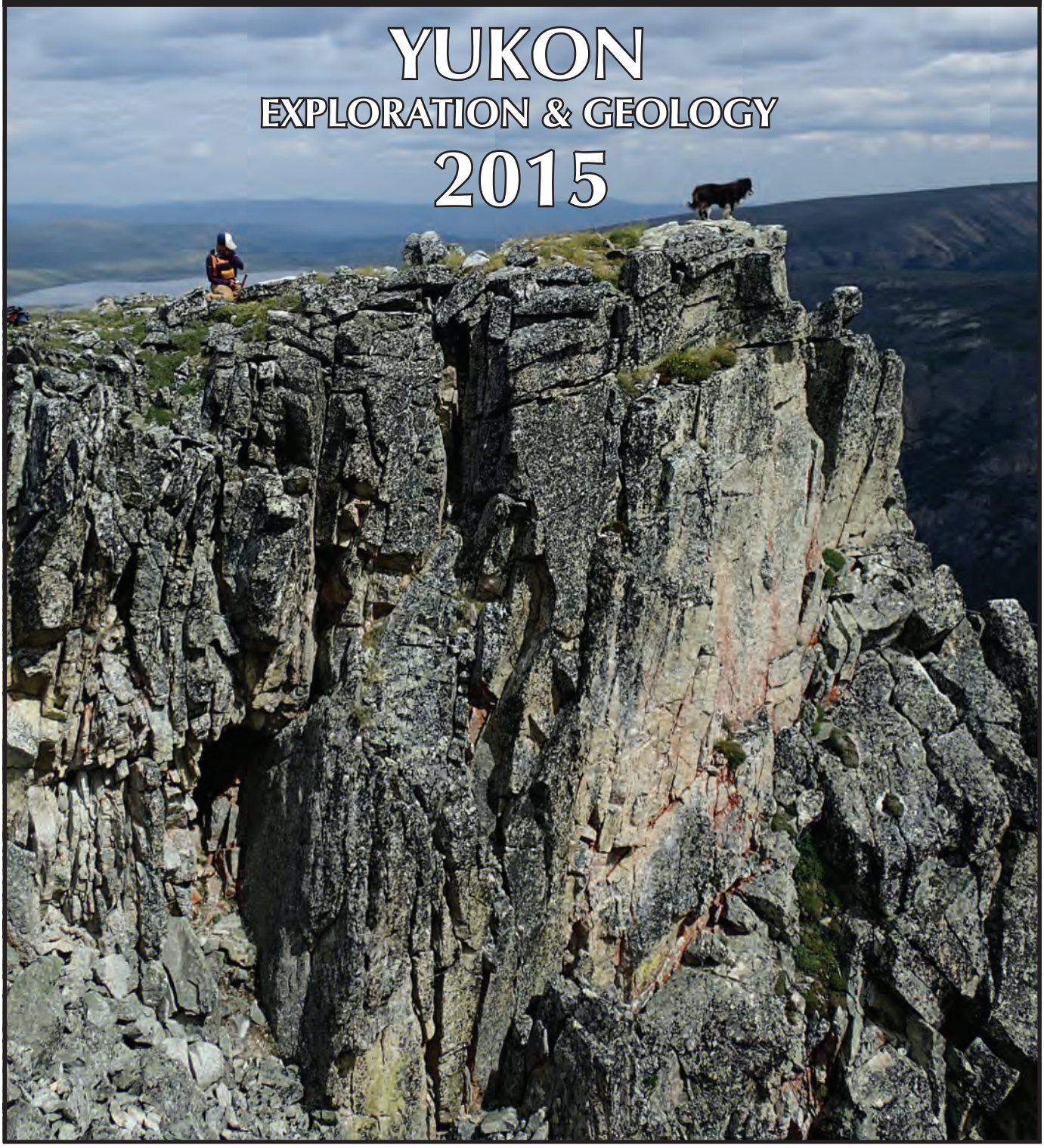
Energy, Mines and Resources • *Yukon Geological Survey*

YUKON
EXPLORATION & GEOLOGY
2015



YUKON GEOLOGICAL SURVEY

Yukon
Energy, Mines and Resources



Yukon Geological Survey staff - (left to right) Monica Nordling, Patrick Sack, Derek Torgerson, Kathy Walker, Sarah Laxton, Olwyn Bruce, Esther Bordet, Matt Hutchison, Brett Elliot, Johann Slam, Karen MacFarlane, Charlie Roots, Leigh van Drecht, Maurice Colpron, Scott Casselman, Steve Israel, Rob Deklerk, David Moynihan and Rosie Cobbett.
Missing from photo: Carolyn Relf, Lara Lewis, Jeff Bond, Kristen Kennedy, Bailey Staffen, Panya Lipovsky, Tiffani Fraser and Syd van Loon.

YUKON EXPLORATION & GEOLOGY 2015

Edited by

K.E. MacFarlane and M.G. Nordling

Yukon Geological Survey

Energy, Mines and Resources

Government of Yukon

Published under the authority of the Department of Energy, Mines and Resources, Government of Yukon ***http://www.emr.gov.yk.ca*****.**

Printed in Whitehorse, Yukon, 2016.

Publié avec l'autorisation du Ministères de l'Énergie, des Mines et des Ressources du gouvernement du Yukon, ***http://www.emr.gov.yk.ca*****.**

Imprimé à Whitehorse (Yukon) en 2016.

©Department of Energy, Mines and Resources, Government of Yukon

ISSN 1718-8326

This, and other Yukon Geological Survey publications, may be obtained from:
Yukon Geological Survey
102-300 Main Street
Box 2703 (K-102)
Whitehorse, Yukon, Canada Y1A 2C6

phone (867) 667-3201, e-mail ***geology@gov.yk.ca***

Visit the Yukon Geological Survey website at ***www.geology.gov.yk.ca*****.**

In referring to this publication, please use the following citation:
Yukon Geological Survey, 2016. Yukon Exploration and Geology 2015, K.E. MacFarlane and M.G. Nordling (eds.), 2016, 280 p.

This overview is available for download from the Yukon Geological Survey website.

Front cover photograph: Looking north at cliffs above Long Lake; composed of Early Jurassic granodiorite of the Long Lake suite. Photo by Steve Israel.

PREFACE

Yukon Exploration and Geology (YEG) and the Yukon Exploration and Geology Overview continue to be the main publications of the Yukon Geological Survey (Energy, Mines and Resources, Government of Yukon). Individual YEG papers, with colour images, are available in digital format only and can be downloaded from our website. The YEG Overview is available in a digital format; hard copies are available from a limited colour print run.

YEG 2015 contains up-to-date information on mining and mineral exploration activity, studies by industry and results of recent geological field studies. Information in this volume comes from prospectors, exploration and government geologists, mining companies and students who are willing to contribute to public geoscience for the benefit of the scientific community, general public and mineral and petroleum industries of Yukon. Their efforts are appreciated.

Joining me once again in YEG editing was Monica Nordling. A big thank you to Monica for keeping me focused and allowing editorial discussions to take place in her much warmer office. I would like to acknowledge the work of many of my Yukon Geological Survey colleagues who have submitted papers and reviewed manuscripts prior to them getting to me. Their work makes my job easier.

Sherry Tyrner of the Queen's Printer ensured that the printing process went smoothly.

We welcome any input or suggestions that you may have to improve future YEG publications. Please contact me at (867) 667-8519, or by e-mail at karen.macfarlane@gov.yk.ca.



Karen MacFarlane



TABLE OF CONTENTS

Field investigations of the Sugar gold prospect, Dawson Range, Yukon (NTS 115J/14 and 115J/15)
S.E. Bartlett, M.M. Allan, E.N. Buitenhuis, T.R. Smith and C.J.R. Hart 1

Paleozoic stratigraphy, tectonics and metallogeny of the Pelly Mountains, Quiet Lake and Finlayson Lake map areas (NTS 105F and G), central Yukon: Project outline and preliminary field results
L.P. Beranek, S.J. Piercey, R. Campbell and P. Wawrzonkowski 17

The Paradise gravel: Evidence for a pre-White Channel Gravel in the Klondike
J.D. Bond 29

Preliminary results on the Middle Triassic-Middle Jurassic stratigraphy and structure of the Teslin Mountain area, southern Yukon
E. Bordet 43

Placer-lode gold relationships in the Nansen placer district, Yukon.
R. Chapman, M. Cook, M. Grimshaw and S. Myles 63

Preliminary observations on the geology of Tay Mountain Area (parts of NTS 105K/12 and 13, 105L/09 and 16), central Yukon
R. Cobbett 79

Protopiceoxylon yukonense sp. nov. – A remarkable extinct conifer from the Mackenzie Delta area, northern Yukon
M. Dolezych and L. Reinhardt 99

Early Pleistocene glaciation and implications for placer gold deposits in Back Creek, Mount Nansen area, Yukon
P.O. Englehardt, B.C. Ward, J.D. Bond and M.J. Coleman 111

New U-Pb zircon dates from the Aishihik batholith, southern Yukon
N.L. Joyce, M. Colpron, M.M. Allan, P.J. Sack, J.L. Crowley and J.B. Chapman 131

A-type granite plutons and tin skarns in southeast Yukon: Mindy prospect and surrounding granite of 105C/9

T. Liverton 151

U-Pb zircon age and Pb isotopic constraints on the age and origin of porphyry and epithermal vein mineralization in the eastern Dawson Range, Yukon

J.K. Mortensen, C.J.R. Hart, J. Tarswell and M.M. Allan 165

Stratigraphy and structural geology of the upper Hyland River area (parts of 105H/8, 105H/9), southeast Yukon

D. Moynihan 187

Copper-gold ± silver mineralization at the Stu occurrence, central Yukon (Yukon MINFILE 115I011)

P.J. Sack, S. Casselman, D. James and B. Harris 207

Late Holocene fluctuations of the north lobe of Llewellyn Glacier, Upper Yukon River Basin

M. Samolczyk, S. Layton and J.J. Clague 223

Crustal depth of emplacement of the Early Jurassic Aishihik and Tatchun batholiths, west-central Yukon

M.J. Topham, M.M. Allan, J.K. Mortensen, C.J. R. Hart, M. Colpron and P.J. Sack 233

Digitizing and spatially analyzing historic YCGC drill data from Dominion Creek: a pilot project

S. van Loon 253

Field investigations of the Sugar gold prospect, Dawson Range, Yukon (NTS 115J/14 and 115J/15)

S.E. Bartlett
University of British Columbia

M.M. Allan[1]
Mineral Deposit Research Unit, University of British Columbia

E.N. Buitenhuis, T.R. Smith
Kaminak Gold Corporation

C.J.R. Hart
Mineral Deposit Research Unit, University of British Columbia

Bartlett, S.E., Allan, M.M., Buitenhuis, E.N., Smith, T.R. and Hart, C.J.R, 2016. Field investigations of the Sugar gold prospect, Dawson Range, Yukon (NTS 115J/14 and 115J/15). *In:* Yukon Exploration and Geology 2015, K.E. MacFarlane and M.G. Nordling (eds.), Yukon Geological Survey, p. 1-16.

ABSTRACT

The Sugar gold prospect, located 20 km southeast of the Coffee gold deposits in Yukon, is hosted in the mid-Cretaceous Dawson Range batholith, of which three mappable sub-units are recognized: a biotite hornblende quartz monzodiorite; a K-feldspar phyric hornblende biotite syenogranite; and a biotite hornblende diorite. Plutonic rocks are cut by steep, west to northwest-striking andesite dikes of uncertain age. Alteration and mineralized zones coincide with fault-fracture zones that are parallel and proximal to dikes and their margins. Alteration is characterized by an early phase of calc-sodic (albite-amphibole) and potassic (pervasive biotite and fracture-controlled K-feldspar) alteration and a later phase of silica flooding and sericite alteration. Gold mineralization is associated with disseminated sulphides in zones of silica flooding and with variably sheared veins of quartz-carbonate-arsenopyrite ± pyrite ± freibergite ± stibnite ± sphalerite. Late chalcedonic quartz-carbonate and ferroan carbonate veins mark the collapse of the hydrothermal system.

[1]*mallan@eos.ubc.ca*

INTRODUCTION

The Sugar gold prospect (Yukon MINFILE 115J 062) is a cluster of structurally-controlled gold occurrences located in the Dawson Range of west-central Yukon, approximately 20 km southeast of the 4.9 Moz Coffee Gold deposits (Yukon MINFILE 115J 110 and 111; Fig. 1). Sugar presents an opportunity to contribute to an emerging metallogenic framework for structurally-hosted gold mineralization in the Dawson Range, building on recent studies at the Coffee deposits (Wainwright *et al.*, 2011; Buitenhuis, 2014; Buitenhuis, *et al.*, 2015; MacKenzie *et al.*, 2014a,b), the Boulevard gold prospect (Yukon MINFILE 115J 052; McKenzie *et al.*, 2013) and the Moosehorn (Longline) gold deposit (Yukon MINFILE 115N 024; Joyce, 2002). The presence of significant porphyry-type mineralization at the Casino Cu-Au-Mo deposit, only 10 km to the southeast of Sugar (Fig. 1), emphasizes current uncertainties of whether gold in this area of the Dawson Range is orogenic (*i.e.*, non-magmatic fluid sources) or whether magmatism plays a role in the generation of gold-mineralizing fluids.

In 2011-2012, Kaminak Gold Corp. explored the Sugar prospect by trenching and diamond drilling 12 holes, following the identification and delineation of several gold-in-soil anomalies over an approximate 2 x 5 km area (Fig. 2). Exploration activities focused on two main zones of anomalous soil geochemistry, which will be referred to as "Sugar West" and "Sugar East" (Fig. 2).

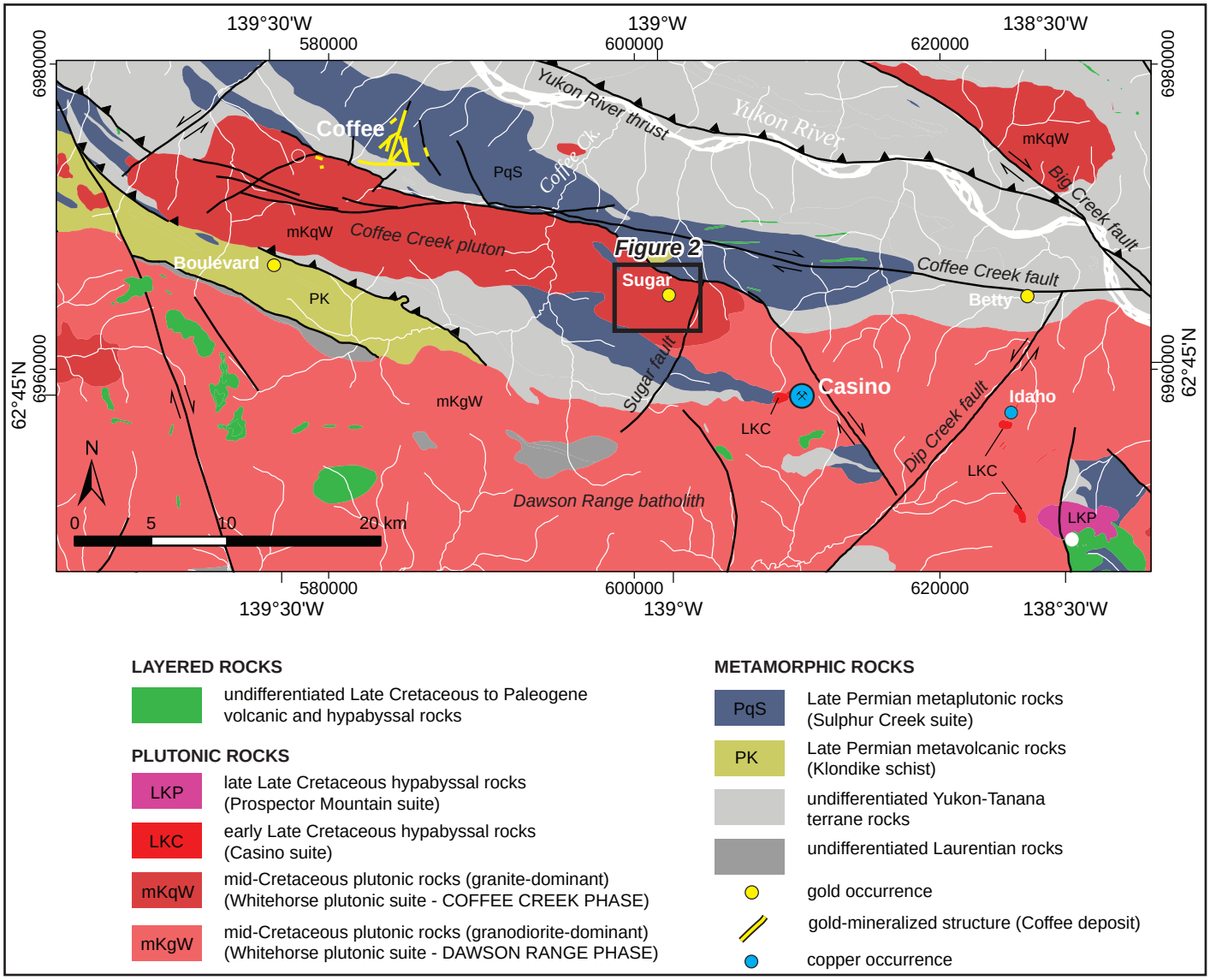


Figure 1. *Simplified regional geologic map of the western Dawson Range (Yukon Geological Survey, 2015), showing the location of the Sugar gold prospect relative to significant mineral occurrences.*

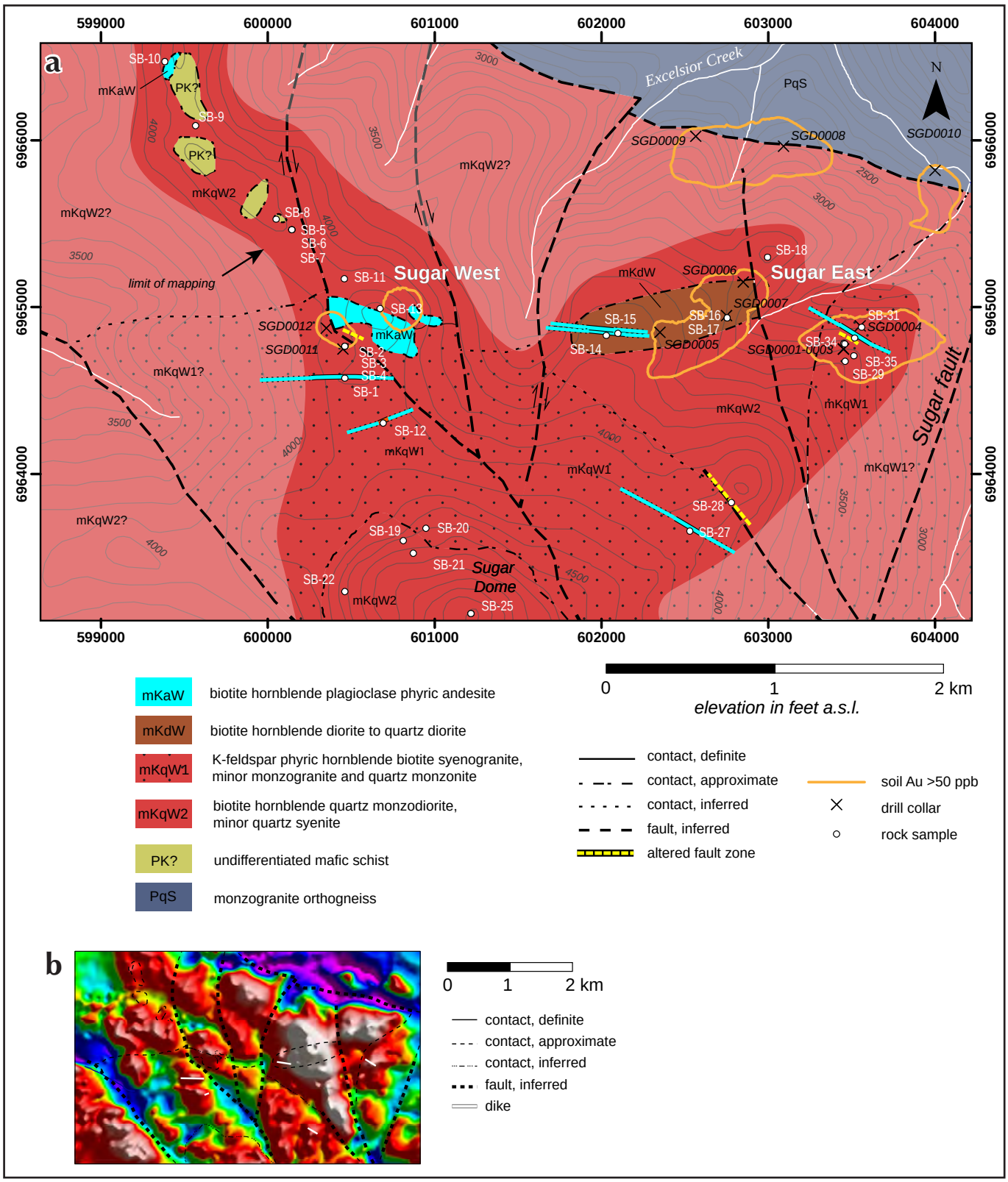


Figure 2. *(a) Geologic map of the Sugar gold prospect area based on 2015 fieldwork, with geology interpreted beyond the limit of mapping indicated by muted colours. Note that dike width is exaggerated for clarity; actual dike width is 2 to 5 m. (b) Total magnetic intensity grid of the Sugar prospect, showing position of geologic contacts and faults (same extent as Figure 2a).*

The Sugar area is on a gently north-dipping plateau at an elevation of 3500-4000 ft above sea level, and ~2 km north of the peak named "Sugar Dome" (~5200 ft; Fig. 2). The prospect drains north into Excelsior Creek, a left-limit tributary of the Yukon River. The terrain is dominated by frost-heaved felsenmeer covered by moss, lichen and low shrubs at higher elevations, and by colluvial cover and dense vegetation at lower elevations. Outcrop is limited to 4-5% of the land area, as determined by imagery analysis and field mapping. This study presents the geologic setting of the Sugar gold prospect based on 1:5000 scale geologic mapping and drill hole observations, and provides a preliminary assessment of the controls on mineralization.

REGIONAL GEOLOGIC SETTING

Gold mineralization at the Sugar prospect is hosted entirely in granitoid units of the Dawson Range batholith, a multi-phase continental arc plutonic complex of the mid-Cretaceous Whitehorse plutonic suite that intruded along the southern margin of the allochthonous Yukon-Tanana terrane in west-central Yukon (Fig. 1; Templeman-Kluit, 1974; Ryan *et al.*, 2013a,b). North of the Sugar prospect, Yukon-Tanana terrane metamorphic rocks are dominated by felsic to intermediate orthogneiss of the Late Permian Sulphur Creek plutonic suite (Figs. 1 and 2). The Sugar prospect is located ~5 km west of the mapped contact of the main Dawson Range phase of the batholith (mKgW; 112-100 Ma; Breitsprecher and Mortensen, 2004; Ryan *et al.*, 2013a,b) and the slightly younger and dominantly granitic Coffee Creek phase (mKqW; 100-99 Ma; McKenzie *et al.*, 2013; Ryan *et al.*, 2013a,b; Fig. 1).

The Sugar prospect is located ~5 km south of the west-northwest-striking, dextral strike-slip Coffee Creek fault system. The western, horse-tailing termination zone of this fault imparts a structural control on the Coffee gold deposits (Allan *et al.*, 2014a; Sanchez *et al.*, 2014). A prominent northeast-striking fault located ~2 km east of Sugar (Ryan *et al.*, 2013a), herein called the Sugar fault, parallels the normal to oblique sinistral-normal Dip Creek fault east of the Casino deposit (Fig. 1), and may have similar kinematics. North of the Sugar prospect, the Dawson Range batholith and metaplutonic rocks of the Sulphur Creek suite (PqS) are in inferred fault contact (Fig. 1; Ryan *et al.*, 2013a,b).

METHODS

Geologic map units were defined during 1:5000-scale field mapping, and have been correlated to regionally defined units (Fig. 2; Yukon Geological Survey, 2015). Thirty-five rocks samples and twenty-two drill core samples were collected for the purpose of petrographic analysis, lithogeochemistry and geochronology. Regional unit assignments will be confirmed by U-Pb geochronology. All rock names and descriptions have been based on modal mineralogy, verified by petrography and by digital image analysis of stained slabs (sodium cobaltinitrite for K-feldspar and amaranth red for plagioclase). In spite of the scarcity of outcrop, locally-derived felsenmeer provides confidence in the bedrock geology over much of the field area. The position of geologic contacts and faults in areas of cover were informed by Kaminak Gold Corp.'s total magnetic intensity and radiometric data, as well as topographic features such as slope breaks.

ROCK UNITS

The Sugar prospect is underlain primarily by the Coffee Creek phase of the Whitehorse plutonic suite (mKqW), of which two distinct, mappable subunits are identified: a K-feldspar phyric hornblende biotite syenogranite and minor monzogranite to quartz monzonite (mKqW1); and a compositionally and texturally heterogeneous unit dominated by biotite hornblende quartz monzodiorite, containing minor quartz syenite (mKqW2). The quartz monzodiorite contains locally abundant pebble to boulder-sized xenoliths of variably migmatitic, intermediate to mafic schist, which is interpreted as metavolcanic rocks of the Klondike Schist (PK) – the volcanic equivalent to metaplutonic rocks of the Sulphur Creek suite. Larger bodies of schist occur as rafts or roof pendants ~1 km northwest of Sugar West (Fig. 2). Volumetrically minor biotite hornblende diorite to quartz diorite (mKdW) forms a separate mappable body at Sugar East (Fig. 2). All units are cut by dikes of biotite hornblende plagioclase phyric diorite (mKaW), informally called "andesite" herein to differentiate it from the massive diorite unit mKdW.

More detailed rock unit descriptions are discussed below, in decreasing order of relative age. Mineralogical and textural descriptions in all cases are supported by petrographic observations of polished thin sections. Modal mineralogy and magnetic susceptibilities are included in Table 1.

BIOTITE HORNBLENDE QUARTZ FELDSPAR SCHIST (PK?)

This schist unit occurs as decimetre to metre-scale xenoliths within quartz monzodiorite of the Whitehorse plutonic suite (mKqW2). The schist also occurs as a ridge-forming series of coherent enclaves or roof pendants up to 300 m in length striking northwest from Sugar West (Fig. 2). The rock is typically fine-grained, grey-green and weathers dull brown to rusty red. Alternating sub-millimetre bands of biotite-hornblende and quartz-feldspar define a partially recrystallized metamorphic fabric. Locally discordant, undeformed granitic seams are also present, which are interpreted as a partial melt product (Fig. 3). Magnetic susceptibility of the unit is 9.0×10^{-3} SI units (Table 1).

The consistently fine-grained texture and intermediate to mafic composition of this schist unit, and its strike continuity with a large, mapped inlier of Sulphur Creek orthogneiss (Fig. 1; Ryan *et al.*, 2013b), suggests that it may be a metavolcanic equivalent, *i.e.*, Klondike Schist (PK).

BIOTITE HORNBLENDE QUARTZ MONZODIORITE TO QUARTZ SYENITE (mKqW2)

This unit forms topographic highs of outcrop and boulder talus, including Sugar Dome (Fig. 2). The unit varies from porphyritic to equigranular and from fine to coarse-grained (Fig. 4a), and contains up to 10% xenoliths of intermediate to mafic metavolcanic schist (PK?). The main lithology is a white-grey, hornblende biotite quartz monzodiorite, which is locally K-feldspar and plagioclase phyric and weathers brown-grey. The biotite commonly forms distinct euhedral, hexagonal grains, and is also interstitial with respect to phenocryst phases (Fig. 4b). The subordinate lithology is equigranular quartz syenite (Fig. 4c). Magnetic susceptibility of the unit ranges widely from 0.7 to 7.6×10^{-3} SI units (Table 1).

Table 1. *Selected samples from the Sugar gold prospect.*

Rock Unit	Sample	Northing (UTM Zone 7)	Easting (UTM Zone 7)	Modal Mineralogy	Magnetic Susceptibility ($\times 10^{-3}$ SI units)
mKaW	SB-01	600460	6964584	phenocrysts - 63% (plag - 33% hbl - 30%); matrix - 37%	19.6 ± 2.6 (n=6)
	SB-15	602097	6964853	phenocrysts - 25% (plag - 17% hbl - 5% bt - 3%); matrix - 75%	9.4 ± 2.5 (n=6)
	SB-30	603516	6964825	phenocrysts - 80% (plag - 50% hbl - 20% bt - 10%); matrix - 20%	10.7 ± 1.3 (n=6)
mKdW	SB-14	602027	6964840	qtz - 10%; plag - 60%; hbl -15%; bt - 15%	1.4 ± 0.4 (n=6)
	SB-17	602752	6964945	qtz - 2%; plag - 73%; hbl -17%; bt - 8%	7.3 ± 4.8 (n=6)
mKqW1	SGD0001_86.0m	603450	6964750	qtz - 15%; Kfs - 42%; plag - 34%; bt - 9%	5.9 ± 1.0 (n=6)
	SGD0011_38.0m	600450	6964750	qtz - 24%; Kfs - 45%; plag- 21%; hbl - 4%; bt - 6%	N/A
	SB-03	600461	6964775	qtz - 23%; Kfs - 36%; plag - 36%; bt - 5%	N/A
mKqW2	SB-06	600142	6965475	qtz - 15%; Kfs - 53%; plag - 26%; hbl - 3%; bt - 3%	0.7 ± 1.0 (n=6)
	SB-07	600142	6965475	qtz - 6%; Kfs - 20%; plag - 65%; hbl - 6%; bt - 3%	N/A
	SB-11	600457	6965180	qtz - 5%; Kfs- 23%; plag - 65%; hbl - 4%; bt - 3%	N/A
	SB-13	600672	6965001	qtz - 18%; Kfs- 47%; plag - 28%; hbl - 4%; bt - 3%	5.4 (n=1)
	SB-19	600811	6963610	qtz - 11%; Kfs- 21%; plag - 53%; hbl -10%; bt - 5%	N/A
	SB-24	601216	6963172	qtz - 10%; Kfs- 12%; plag - 45%; hbl -18%; bt - 15%	7.6 ± 4.8 (n=6)
PK?	SB-25	601291	6963038	qtz - 20%; Kfs- 15%; plag - 30%; hbl -20%; bt - 15%	9.0 (n=1)

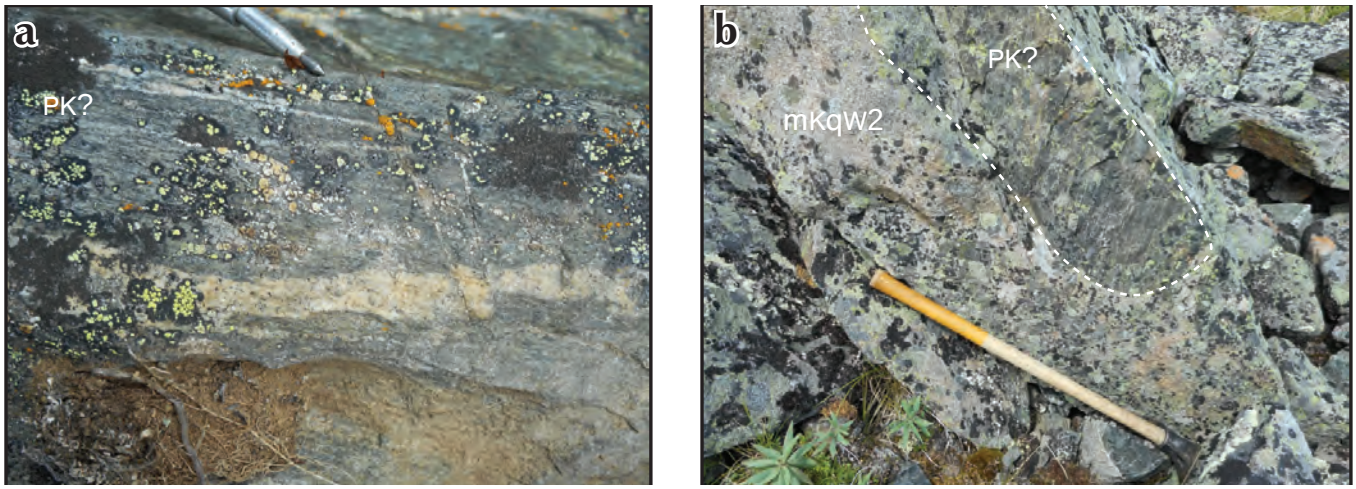


Figure 3. *Schist (unit* PK*?): (a) Xenolith of schist cut by a dikelet of granitic melt, interpreted as leucosome (pen-scribe for scale; Sample SB-9); (b) Xenolith of schist within quartz monzodiorite (*mKqW*2; Sample SB-25).*

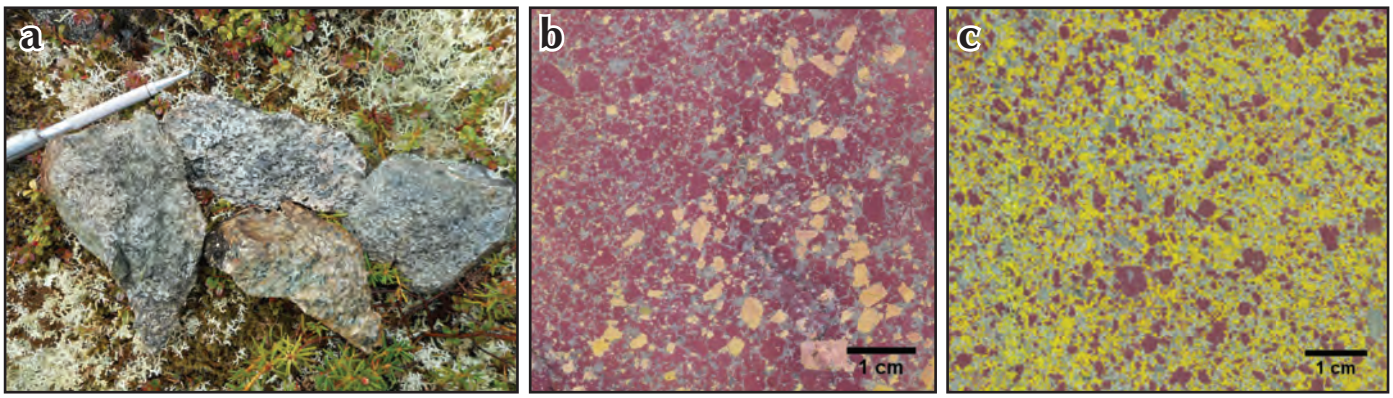


Figure 4. *Unit* mKqW*2: (a) Samples collected within a 10 m radius, indicating local heterogeneity (pen-scribe for scale; (b) Stained rock slab showing plagioclase and K-feldspar phyric quartz monzodiorite phase (Sample SB - 7) ; (c) stained slab showing quartz syenite phase (Sample SB-13).*

K-FELDSPAR PHYRIC HORNBLENDE BIOTITE SYENOGRANITE AND MINOR MONZOGRANITE TO QUARTZ MONZONITE (mKqW1)

This unit forms topographic lows and saddles and is observed mainly as float in frost-heaved felsenmeer, but also as rare outcrop near resistant andesite dikes (Fig. 5a). The unit has white-grey to chalky white weathering and contains smoky grey quartz. The unit is medium to coarse-grained and varies from equigranular to K-feldspar phyric. Plagioclase occurs interstitially to K-felspar phenocrysts and as euhedral laths in equigranular phases (Fig. 5b,c). Magnetic susceptibility of the unit is consistently ~6×10^{-3} SI units (Table 1).

BIOTITE HORNBLENDE DIORITE TO QUARTZ DIORITE (mKdW)

The diorite to quartz diorite unit intrudes granite (mKgW2) at Sugar East, and is cut by a porphyritic dike of similar composition ("andesite" below; Fig. 2). This rock unit is medium-grained and equigranular and contains subhedral plagioclase, hornblende and biotite (Fig. 6). In detail, biotite and hornblende grains are poikilitic with chadacrysts of plagioclase. Quartz content is variable, ranging from 0 to 10%. Magnetic susceptibility of the unit ranges from ~1 to 20×10^{-3} SI units (Table 1).

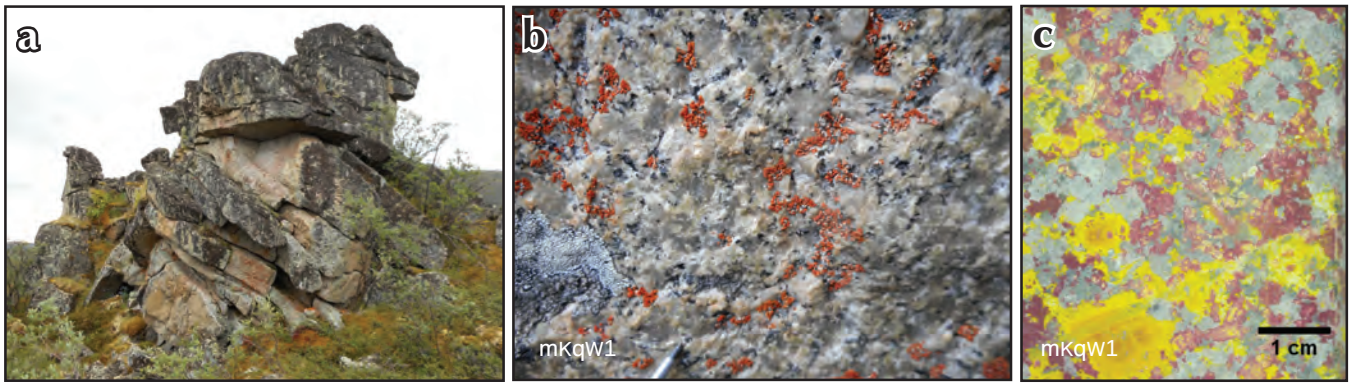


Figure 5. *Unit* mKqW*1: (a) Outcrop of granite exposed near resistant andesite dykes; (b) Representative K-feldspar phyric texture of syenogranite (pen-scribe for scale); (c) Stained slab of same granitic unit (from drill hole SGD0011).*

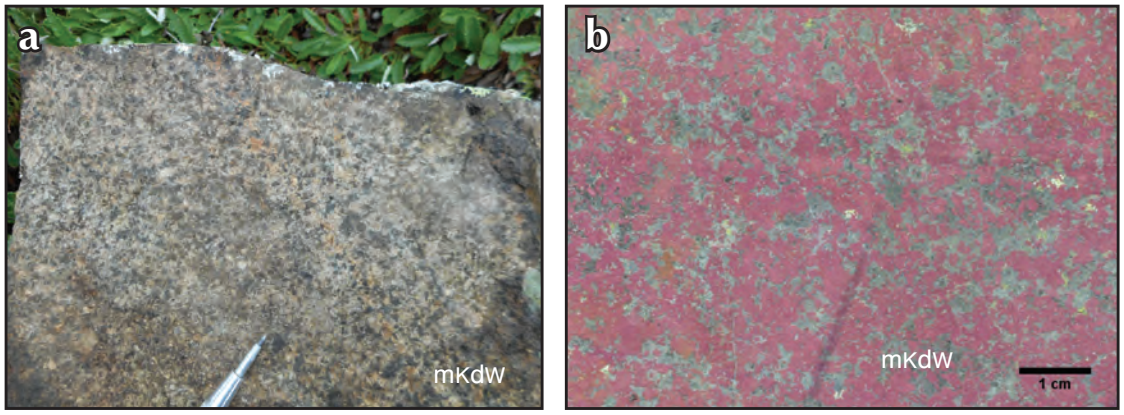


Figure 6. *Unit mKdW: (a) Biotite hornblende diorite float near drill hole (pen scratcher for scale; Sample SB-17); (b) Stained slab of biotite hornblende quartz diorite (Sample SB-14).*

BIOTITE HORNBLENDE PLAGIOCLASE PHYRIC DIORITE ("ANDESITE"; mKaW)

The unit is green-grey, weathers brown, and occurs mainly as subangular float and outcropping tors and ridges with subvertical fractures. This unit intrudes all other units as subvertical, west to northwest-striking dikes less than 10 m wide and as an irregular plug at Sugar West (Fig. 2). Intrusive contacts are subvertical and display a chilled margin of variable width (Fig. 7). Dike margins are also locally xenolithic with respect to more felsic host rocks.

Phenocryst abundance ranges from ~25% near dike margins to densely crowded (up to 90%) within dike interiors. Phenocrysts range from fine to coarse-grained with an average size of 2 to 5 mm. The groundmass is very fine-grained and comprises plagioclase, hornblende, and minor (less than 5%) quartz. This unit is magnetic (10 to 30 x 10^{-3} SI units) owing to its magnetite abundance. The unit is referred here informally as andesite, due to its porphyritic texture and to differentiate it from the equigranular phase (mKdW).



Figure 7. *Unit* mKaW*: (a) Andesite dike (*mKaW*) in contact with the more recessive syenogranite (*mKqW*1; near sample SB-1); (b) Chilled margin contact of porphyritic andesite with K-feldspar phyric syenogranite (pen-scribe for scale; near SB-12); (c) A stained slab of andesite (Sample SB-1).*

STRUCTURES

The main plutonic units (mKqW1 and mKqW2) are cut by an array of northwest to north-striking faults with apparent dextral displacement, as determined by offset geomagnetic markers in airborne magnetic data (Fig. 2b). Apparent dextral offsets on two such faults between Sugar West and Sugar East are each ~200 m. However, the timing of fault displacement relative to emplacement of the diorite and andesite units is unknown. These faults link to a southeast-striking fault that itself is a splay off the northeast-striking Sugar fault (Figs. 1 and 2).

Subvertical, hydrothermally altered fault-fracture networks occur parallel to, or coincident with, the west to northwest-striking andesite dikes and their margins (yellow dashed lines in Fig. 2a). Based on field and drillcore observations, these zones of deformation are 10s to 100s of metres wide, and are characterized by numerous individual brittle shears, fractures, veins and tectonic breccias. Three such structural corridors are recognized, and two of these are coincident with gold-in-soil anomalies (Sugar West and Sugar East, Fig. 2a). The third structural corridor is parallel to, but ~250 m north of, the andesite dike located ~1.5 km south of Sugar East. This structural corridor passes through a topographic saddle, which coincides with the intrusive contact between granite (mKqW1) to the south and quartz monzonite (mKqW2) to the north (Fig. 2a).

ALTERATION AND VEINING

Gold mineralization and both pervasive and fracture-controlled hydrothermal alteration are developed in the west to northwest-trending structural corridors described above. Pre, syn and post-mineralization veining and alteration are most intensely developed in granitoids, but also cross-cut andesite dikes. The broad spatial relationship between dikes, alteration and structural damage is evident both at Sugar West and Sugar East, as well as in a newly mapped dike and alteration zone about 1 km south of Sugar East (Fig. 2).

Because of the generally widely spaced, parallel nature of individual fractured, faulted, altered or mineralized features, some paragenetic relationships have not been observed. However, several important cross-cutting relationships establish the relative timing of magmatism, alteration and mineralization. These relationships are summarized in the paragenetic sequence shown in Figure 8, and each alteration type is described below and illustrated in Figure 9. Representative spatial relationships between dikes, veins, alteration types and mineralization are well illustrated by a graphical log of drill hole SGD0001 from Sugar East (Fig. 10).

GARNET-DIOPSIDE (EPIDOTE-CHLORITE)

Banded to massive andraditic garnet-diopside skarn-type alteration is observed overprinting xenoliths within quartz monzonite and syenogranite, and as endoskarn in immediately adjacent igneous rocks (Fig. 9a). Patchy epidote and chlorite occur as paragenetically later, overprinting alteration. The presence of calc-silicate alteration assemblages indicates a calcareous protolith, such as a calcareous member of the Snowcap assemblage (forming much of the undifferentiated Yukon-Tanana unit in Fig. 1), or potentially, a calcareous component of the Klondike schist, such as documented in the Klondike district (*e.g.*, Allan *et al.*, 2014b). The timing of this alteration relative to the timing of magmatism is unknown, but could have formed due to deuteric alteration from cooling and dehydration of the host granitoids, or by a subsequent magmatic-hydrothermal event.

EPIDOTE ± K-FELDSPAR

Epidote ± quartz ± pyrite veinlets (hairline to 2 cm wide) are observed exclusively in granitoid units, and are mantled by K-feldspar alteration haloes with a pink to brick-red hematite dusting. These veins have been cataclastically reworked with broken and randomly oriented feldspar grains cemented by epidote. Epidote-bearing veins occur both as single, widely spaced veins less than 0.5 cm wide, and as anastomosing swarms of hairline veinlets with locally pervasive K-feldspar alteration of the host granitoids (Fig. 9b). Cataclastically reworked epidote-chlorite veinlets cut andesite dike south of Sugar East; however, the timing of these veinlets relative to the epidote ± quartz ± pyrite veinlets is unknown.

AMPHIBOLE-ALBITE

Locally developed, pervasive, texturally destructive amphibole-albite alteration is observed overprinting K-feldspar phyric syenogranite proximal to a zone of garnet-diopside alteration in drill hole SGD0001 (Figs. 9c and 10). This style of alteration is manifested as albite replacement of pre-existing feldspar, and as fine-grained, dark green, randomly oriented amphibole overprinting mafic minerals. Rare vermicular amphibole-albite-pyrite veinlets with indistinct margins and albite haloes are observed in association with the pervasive albite-amphibole alteration (Fig. 9c). Alteration zones

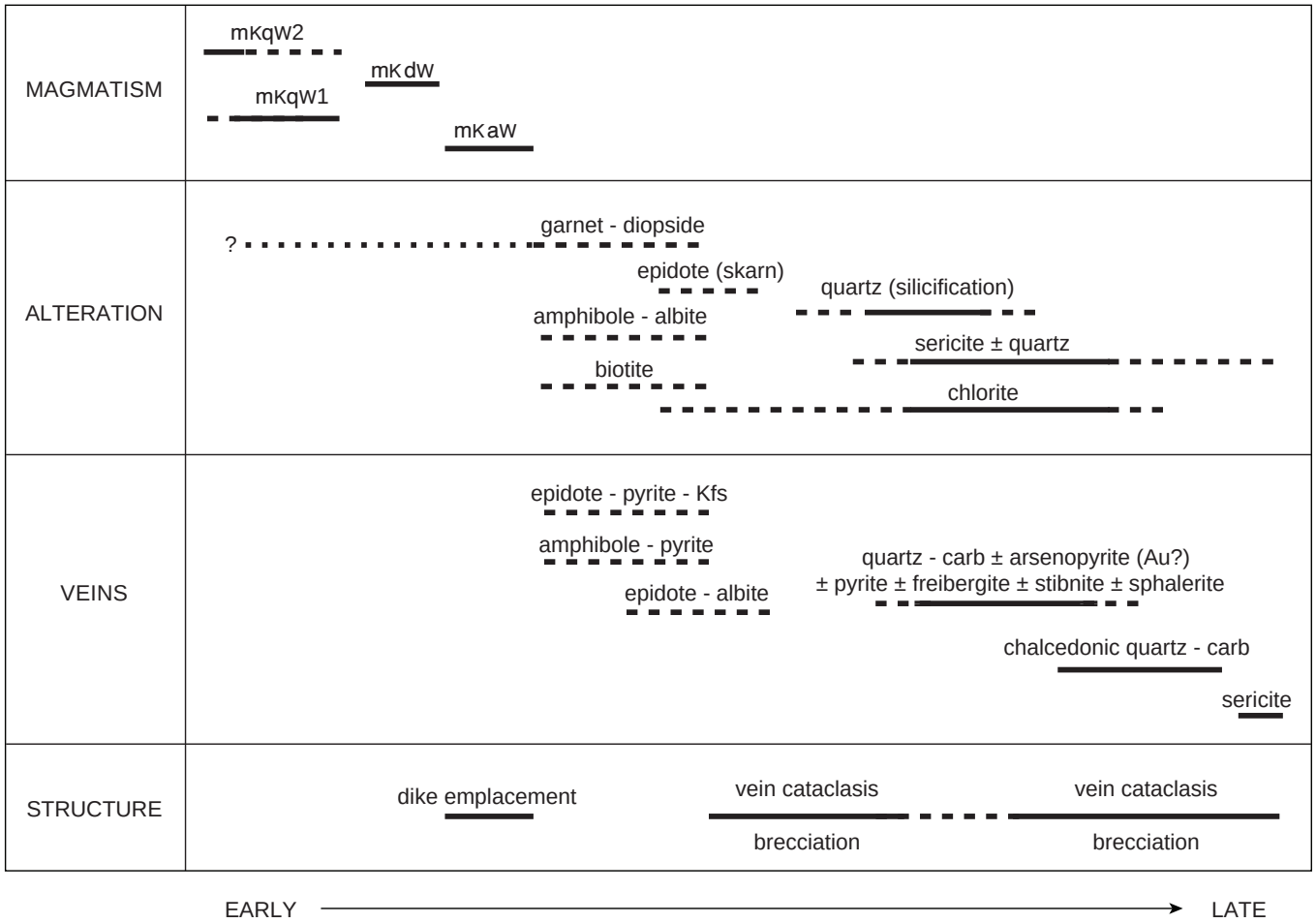


Figure 8. *Paragenetic scheme for magmatism, alteration, veining and structural activity at the Sugar prospect.*

are overprinted and obscured by silicification (Figs. 9c and 10) and by skarn-type epidote alteration (above). Therefore, the original extent of albite-amphibole alteration is unknown.

EPIDOTE-ALBITE

An epidote + albite assemblage is observed in hairline veinlets, cutting syenogranite (mKqW1) in drill hole SGD0001, along with albite-epidote alteration haloes in which albite replaces plagioclase rims (lower veinlet in Fig. 9c). Epidote in veins is subhedral and occurs in alteration haloes up to 1 cm wide.

BIOTITE

Biotite alteration is observed in porphyritic andesite in Sugar West (SGD0011) as an extremely fine-grained, pervasive and texturally destructive purple-brown overprint. This style of alteration is cut by fracture-controlled, chlorite and sericite alteration (Fig. 9d). The presence of biotite alteration in other localities has not been confirmed, and its timing relative to the epidote and albite-bearing alteration assemblages is uncertain (Fig. 8).

CHLORITE

Fracture-controlled chlorite alteration overprints hydrothermal biotite in andesite at Sugar West (Fig. 9d). Chlorite occurs as variably intense, patchy to pervasive alteration of magmatic biotite in granitic rocks distal to zones of silicification, sericitic alteration, brecciation and mineralization (Fig. 9e). However, the timing relationship of this chlorite alteration to these features is currently not well constrained.

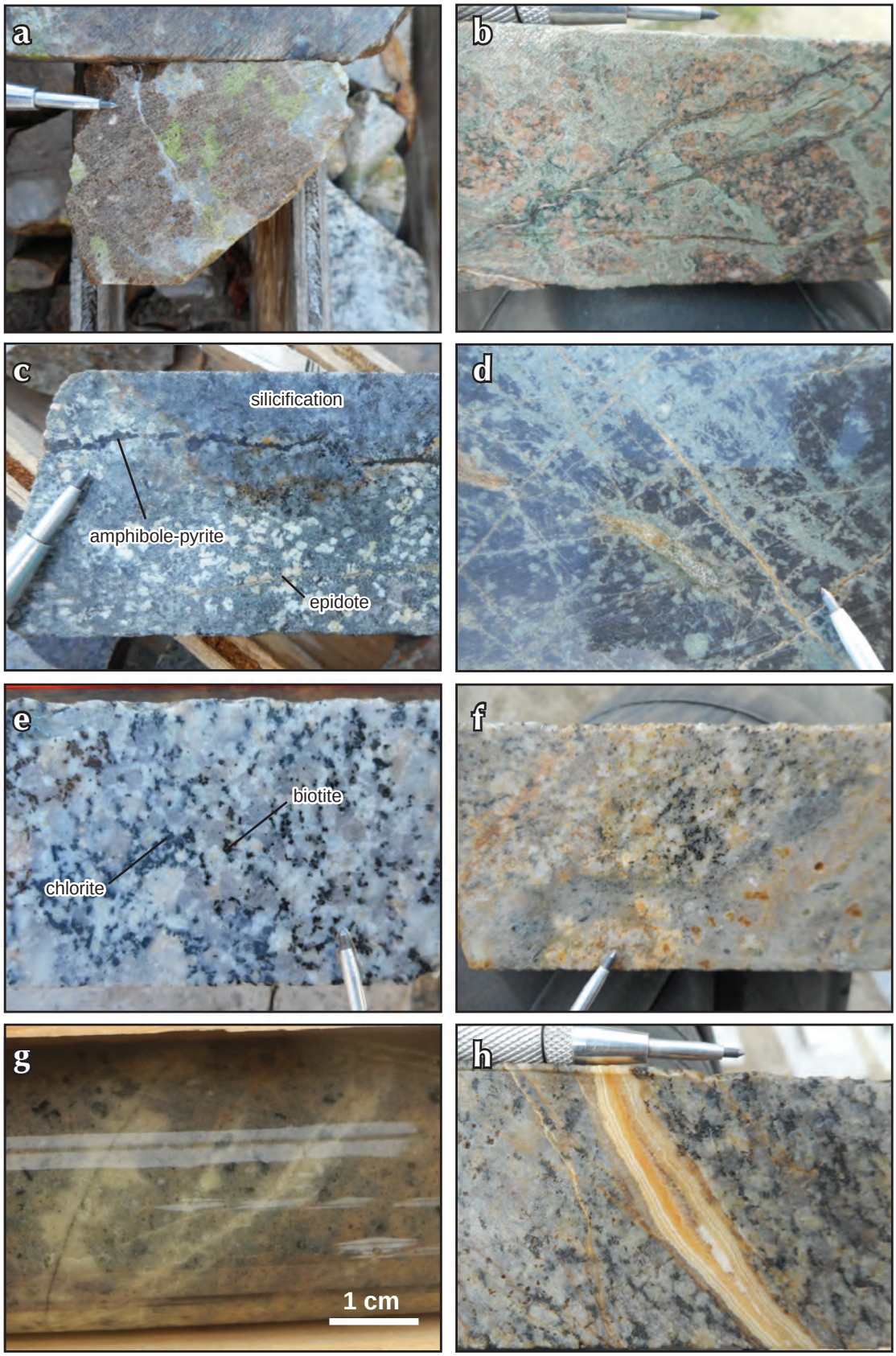


Figure 9. *Alteration styles of the Sugar prospect (pen-scribe for scale): (a) Andradite garnet-diopside-epidote skarn alteration of calcareous xenolith; (b) Wispy network of epidote veinlets with intense K-feldspar alteration cutting diorite; (c) Vermicular amphibole-pyrite veinlet with albitic halo (top) and hairline epidote vein with albite halo (bottom). Note the zone of cross-cutting silicification in the upper-right portion of the sample; (d) Pervasive biotite alteration of andesite, cut by fracture-controlled chlorite alteration (pale green) and later chalcedonic quartz-ferroan carbonate veinlets (orange); (e) chlorite alteration of magmatic biotite; (f) amoeboid front of silicification (bottom left) cutting granite (mKqW1); (g) fracture-controlled sericite alteration of previously silicified granite (note relict magmatic biotite); (h) laminated chalcedonic quartz -ferroan carbonate vein with late prismatic quartz and calcite cement.*

QUARTZ

Quartz alteration (*i.e.*, silicification) affects all rock units, including andesite dikes. It occurs as a mineralogically and texturally destructive alteration with sharp, digitate metasomatic fronts (Fig. 9f). Where silicification is intense, quartz completely replaces feldspar, but jagged, residual mafic grains are common. Silica flooding is common both in host granitoids and in andesite dikes, but is especially well developed in host rocks near dike margins (Fig. 10). Tectonic breccias not only contain clasts of silicified rock, but are overprinted by texturally destructive silicification, indicating that brecciation and silicification overlap paragenetically (Fig. 8). Zones of silicification overprint previously albite-amphibole altered rock (Figs. 9c and 10), and quartz replaces sericite-altered cores of plagioclase in both the syenogranite and quartz monzodiorite units.

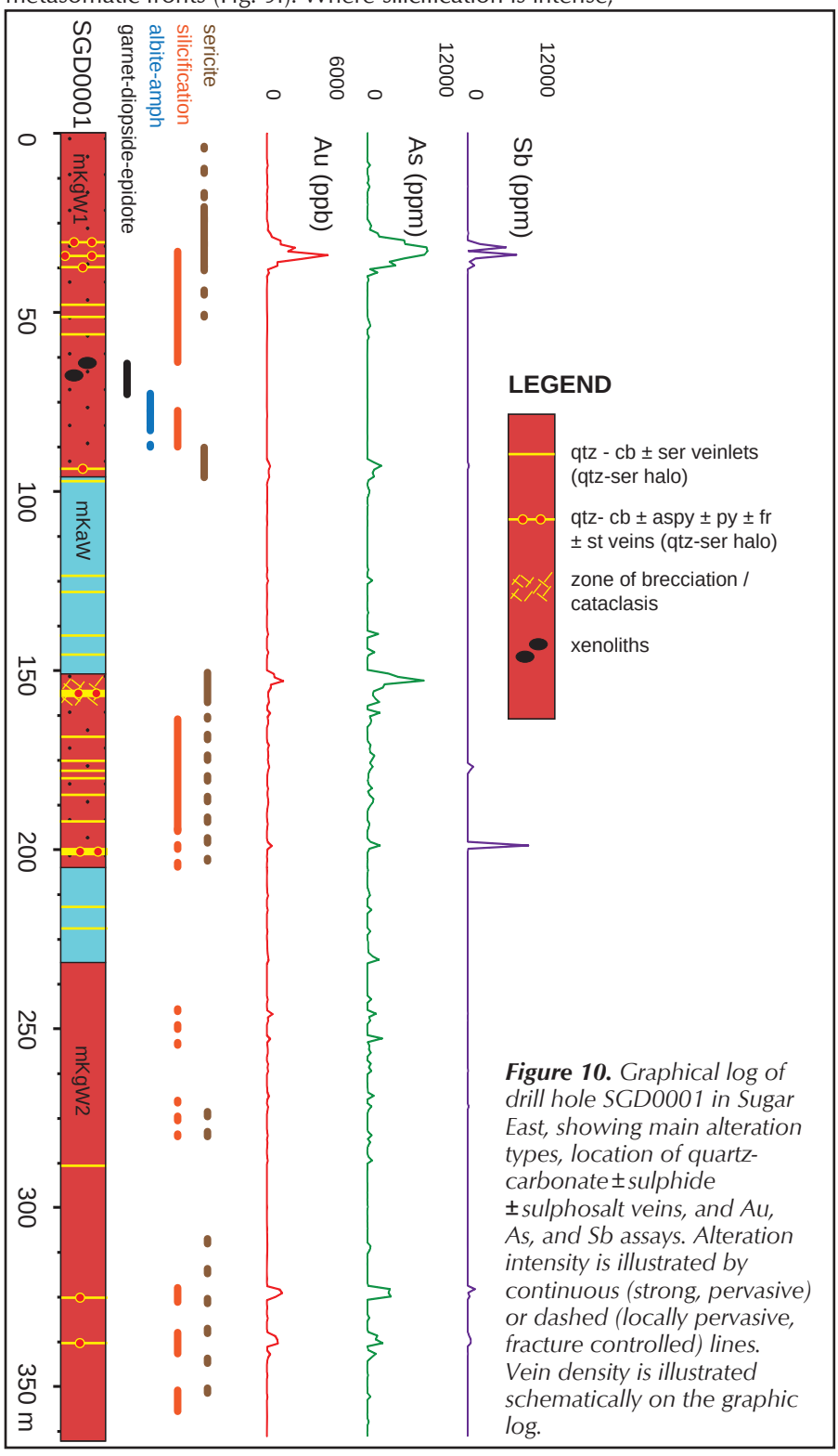


Figure 10. *Graphical log of drill hole SGD0001 in Sugar East, showing main alteration types, location of quartz-carbonate ± sulphide ± sulphosalt veins, and Au, As, and Sb assays. Alteration intensity is illustrated by continuous (strong, pervasive) or dashed (locally pervasive, fracture controlled) lines. Vein density is illustrated schematically on the graphic log.*

SERICITE

Biotite and feldspar-destructive sericitic alteration is observed as bleached haloes to both barren and mineralized quartz ± carbonate veins (see below), and clearly cross-cuts zones of silicification (Fig. 9g). Sericite also occurs in paragenetically late, hairline to 1 cm wide veinlets that cut silicified andesite and all other lithologic units. These sericite veinlets typically occur in anastomosing, variably oriented swarms.

CHALCEDONIC QUARTZ - FERROAN CARBONATE

Chalcedonic quartz-ferroan carbonate veins are observed cutting all lithologies and most alteration and vein types (Fig. 9h). Veins vary in width from hairline up to 2 cm. The hairline veins generally have ferroan carbonate concentrated along the vein margins, whereas the larger veins tend to contain sub-millimetre-scale laminations of chalcedonic quartz and ferroan carbonate, with paragenetically late, clear prismatic quartz and calcite in the vein centres (Fig. 9h). Chalcedonic quartz-ferroan carbonate veins cut zones of brecciation, but also occur as breccia clasts, suggesting that vein formation and brecciation were overlapping processes.

SECONDARY OXIDES

Sulphide-bearing zones are variably overprinted by scorodite and secondary limonite, but hypogene sulphides are preserved close to surface in all drill holes and trench exposures investigated.

ALTERATION SUMMARY

Following intrusion of the andesite dikes in the Sugar area (mKaW), hydrothermal features track a general paragenetic trend from (a) early, higher-temperature potassic (biotite) alteration of some andesite dikes, locally developed calc-sodic (albite-amphibole) alteration of host granitoids and garnet-diopside alteration of calcareous xenoliths, to (b) lower-temperature silicification, sericite alteration and variably gold-mineralized quartz-carbonate ± sulphide ± sulphosalt veins. Finally, cross-cutting chalcedonic quartz-ferroan carbonate veins and anastomosing sericite veinlets mark overprinting by the last, lowest-temperature part of the hydrothermal system.

MINERALIZATION

Gold mineralization confirmed by diamond drilling at Sugar occurs as 0.3 to 5 ppm anomalies over drill intercepts up to 10 m wide. Gold correlates strongly with arsenic in drill core assays and soil geochemistry over several orders of magnitude (Figs. 10 and 11a). Antimony is variably enriched in zones of anomalous gold, although the relationship is not strong (Figs. 10 and 11b). Zinc is also weakly anomalous in gold-mineralized zones, measuring enrichments up to several 100s of ppm compared to background levels below 100 ppm.

Gold grades correlate with occurrences of quartz-carbonate-arsenopyrite ± pyrite ± freibergite ± stibnite ± sphalerite veins and tectonic breccia cements (Fig. 12a-c). Freibergite ($(Ag,Cu)_{12}Sb_4S_{13}$) was identified as an important Sb-bearing phase as determined from Cu, Ag, Sb and S peaks in the energy-despersive X-ray spectra of three mineralized samples. The same sulphide-sulphosalt assemblage is present in the quartz-sericite alteration haloes to these veins (Fig. 12a). Mineralized features are overprinted by varying degrees of cataclastic reworking, as indicated by vein fragments in breccia zones and by shear-related microtextures.

In veins, freibergite and stibnite are interstitial with respect to quartz and carbonate, and arsenopyrite occurs as idiomorphic inclusions within freibergite and sphalerite (Fig. 12d). In disseminations proximal to veins, arsenopyrite is also idiomorphic (Fig. 12d). Gold was not observed during preliminary petrographic investigations by reflected light or scanning electron microscope.

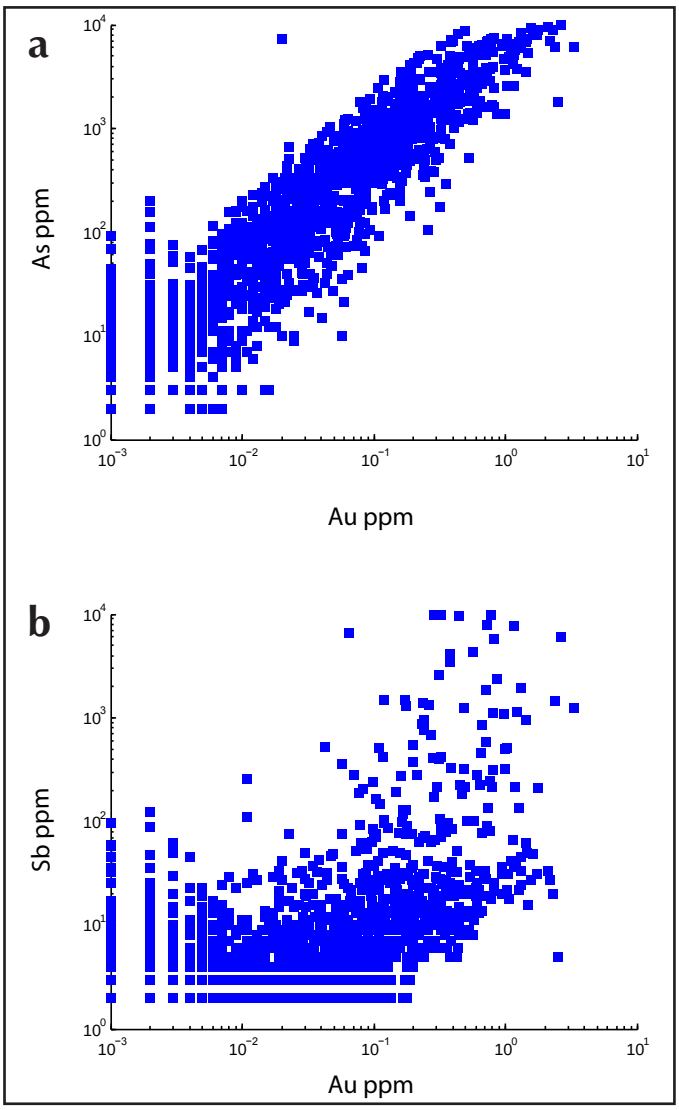


Figure 11. *Plots of (a) As vs. Au and (b) Sb vs. Au; from diamond drill hole assay data collected in 1 m intervals. The Au-As correlation is excellent over 3 orders of magnitude, whereas the Au-Sb relationship is erratic.*

Mineralization associated with cataclastic textures includes (a) 1 to 2 cm-wide veins of quartz and carbonate cementing clasts of granite, chalcedonic vein quartz and silicified rock, and (b) 1 to 3 m-wide zones of brecciation composed of granite clasts cemented by hydrothermal quartz and carbonate (Figs. 12b and 12c). Arsenopyrite within deformed veins shows grain size reduction and defines vein-parallel shear fabrics (Fig. 12e).

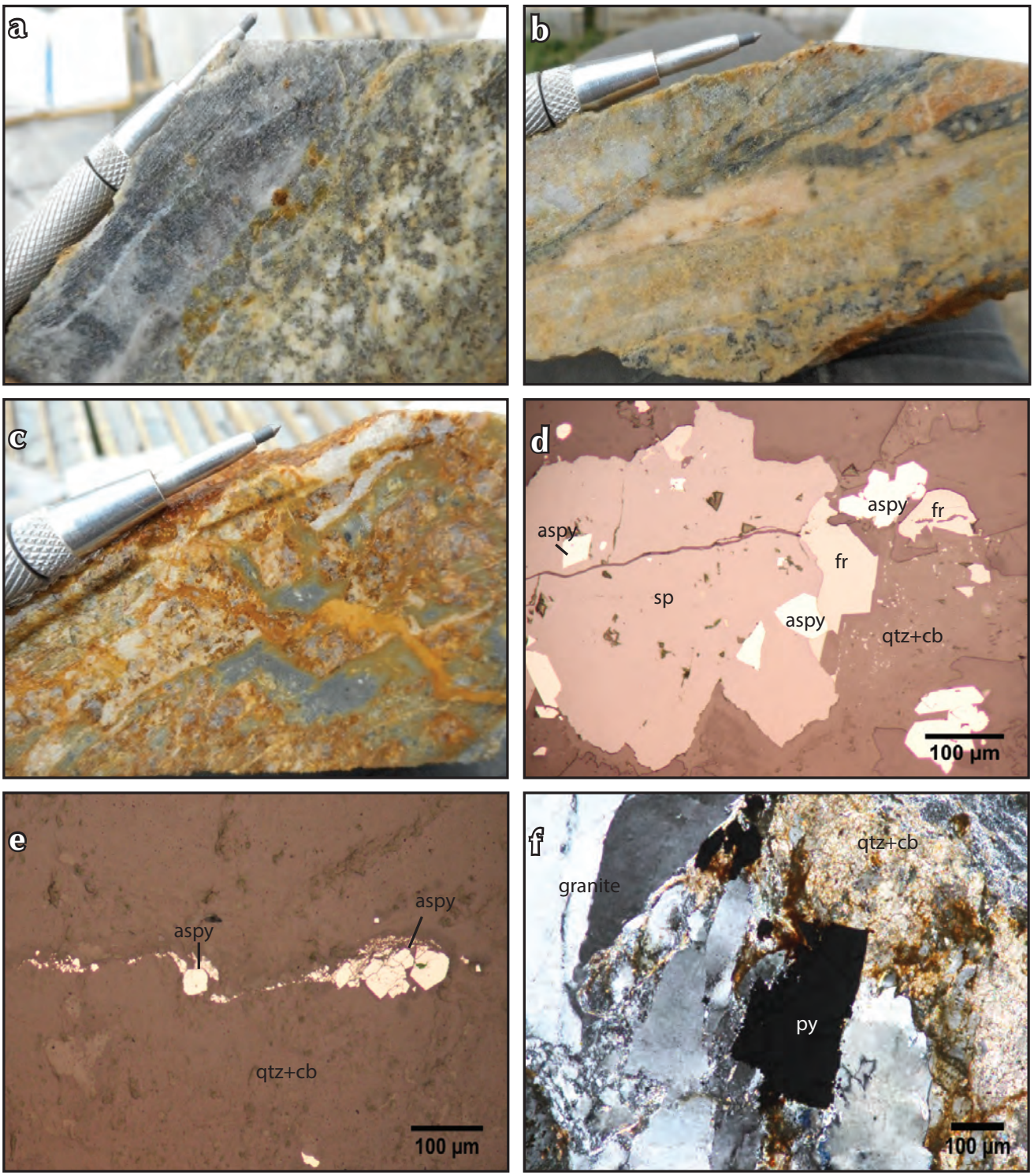


Figure 12. *Examples of mineralization styles at Sugar: (a) quartz-carbonate-arsenopyrite-freibergite-stibnite-sphalerite vein (left) with disseminated sulphides in the vein halo (right); (b) sheared quartz-carbonate-arsenopyrite-pyrite vein containing clasts of chalcedonic quartz and granite; (c) arsenopyrite-pyrite mineralized breccia with clasts of granite and chalcedonic quartz cemented by quartz and carbonate; (d) euhedral arsenopyrite (aspy) within a large anhedral sphalerite (sp) grain and blebbly, anhedral freibergite (fr) in a quartz (qtz) and carbonate (cb) matrix; (e) milled and sheared arsenopyrite grains within a deformed quartz-carbonate vein; (f) euhedral pyrite overprinting a granite clast in breccia.*

DISCUSSION

Gold mineralization at Sugar shares several features in common with mineralization at the Coffee gold deposits 20 km to the northwest. First, Sugar and Coffee share an obvious structural control, whereby mineralization is hosted in steeply dipping zones of brittle structural damage and no significant fault offsets are observed. The spatial and structural correlation of mineralization with andesitic dikes is also a common feature. Dikes are clearly pre-mineralization at Sugar due to local overprinting by silicification, quartz-carbonate veinlets, sericite alteration and mineralization. The same relative timing of dike emplacement and mineralization holds at Coffee. For both systems, dikes and hydrothermal features occupy the same structural corridors, suggesting that zones of structurally-enhanced permeability were active during both magmatic and hydrothermal episodes.

Second, both the Sugar prospect and Coffee deposits feature As and Sb anomalies coincident with Au mineralization, and the Au-As correlation is robust in both systems (Figs. 10 and 11). In hypogene sulphide ore at Coffee, most of the gold is present as solid solution in arsenian pyrite, whereas the main As-bearing phase at Sugar is arsenopyrite. This suggests that gold at Sugar is present either as solid solution in arsenopyrite, or as native gold in close paragenetic association with arsenopyrite.

Much of the mineralization at Coffee coincides paragenetically and spatially with structurally-controlled silicification (*e.g.*, Supremo zone; north-striking mineralization trends in Fig. 1). Silicification is also well-developed at Sugar, but is better characterized as proximal to mineralization, rather than having a direct genetic or spatial correlation (Fig. 10). Mineralization at Sugar is related to discrete veins (or vein breccias) of quartz-carbonate-arsenopyrite ± pyrite ± freibergite ± stibnite ± sphalerite, whereas mineralization is mainly disseminated at Coffee, and syn-mineralization veins at Coffee are rare.

Disseminated gold mineralization at Coffee is mainly associated with zones of illite-pyrite ± magnesian carbonate alteration of biotite-bearing host rocks. Carbonate is a ubiquitous gangue phase in mineralized veins and breccia zones at Sugar, but carbonate alteration of wallrocks has not been observed. Sericite (potentially illite) alteration is present at Sugar, and paragenetically overlaps with mineralization, but is mainly restricted to narrow zones of fracture-controlled alteration and is most closely associated with quartz alteration, rather than carbonate or pyrite. Whereas pyrite is abundant and closely correlated with gold mineralization at Coffee, it is a relatively minor sulphide at Sugar.

Weathering-related oxidation of pyrite along steep, mineralized structures at Coffee also played a key role in the formation of oxide facies gold mineralization. The relative lack of pyrite at the Sugar prospect has likely contributed to the poorly developed oxidation profiles. More aggressive uplift and erosion at Sugar may also play a role in the exposure of hypogene sulphides at surface.

The Sugar prospect's most significant deviation from the Coffee deposits is the presence of various high-temperature potassic and calc-sodic alteration types that pre-date mineralization. These include biotite alteration of andesite dikes, K-feldspar alteration associated with epidote veining, and albitization associated with secondary amphibole alteration of plutonic rocks. These alteration styles require high temperature and saline fluids typical of the porphyry environment. Although there is no mineralization associated with these early styles of alteration (except minor pyrite), their presence suggests the onset of a hydrothermal system shortly after, or related to, emplacement of the andesite dikes (Fig. 8).

Observations lead to the interpretation that Coffee and Sugar are broadly contemporaneous and probably genetically related hydrothermal systems on the basis of their similar structural control, Au-As-Sb association and common spatial and paragenetic relationships to andesite dikes. It is speculated that Sugar may represent a more deeply exhumed equivalent to the Coffee gold deposits, in which deeper-seated, higher-temperature alteration types and vein-controlled mineralization are exposed at the present-day erosional surface.

CONCLUSIONS

Sugar is a structurally-hosted gold system in which mineralization is tied spatially and temporally to brittle deformation along steep structures that are both proximal and parallel to mid-Cretaceous or younger andesite dikes. An early phase of calc-sodic and potassic alteration that overprints dikes and the immediate host rocks most likely signifies that a magmatic-hydrothermal system was active prior to, and potentially during, subsequent stages of silicification and gold-bearing quartz-carbonate-arsenopyrite ± pyrite ± freibergite ± stibnite ± sphalerite vein formation.

Of importance to the genetic and metallogenic interpretation of the Sugar gold prospect is the absolute timing of dike emplacement, potassic and calc-sodic alteration, and subsequent gold mineralization. Ongoing research will address the age of dikes and other magmatic phases by U-Pb dating of zircon, dating of alteration assemblages by Ar-Ar and gold deportment studies using scanning electron microscopy.

ACKNOWLEDGEMENTS

This study is the field component of a BSc Honours project by Stephen Bartlett at the Mineral Deposit Research Unit (MDRU) of the University of British Columbia, supervised by M. Allan. Helicopter-assisted fly-camp support and access to drill core was generously provided by Kaminak Gold Corp., and we are grateful in particular to Rory Kutluoglu, Geoff Newton, Adam Fage, Eric Buitenhuis and Tim Smith for technical discussions and enthusiastic logistical support. Financial support for the project was provided through the collaborative Kaminak-MDRU Yukon Coffee Gold Project, which is supported by NSERC CRD grant 474464-14. We are grateful to Farhad Bouzari for a constructive review of the manuscript.

REFERENCES

Allan, M.M., Sanchez, M.G., Mortensen, J.K. and Hart, C.J.R., 2014a. A hydrothermal record of structural overprinting and crustal exhumation in the White Gold District, Yukon. GSA Conference Abstract, Vancouver, BC, Oct 19-22, 2014.

Allan, M.M., Mortensen, J.K., and Cook, N., 2014b. Preliminary stable isotope and geochemical investigation of carbonate in the Klondike district. *In:* Yukon Exploration and Geology 2013, K.E. MacFarlane, M.G. Nordling and P.J. Sack (eds.), Yukon Geological Survey, p. 1-20.

Breitsprecher, K., and Mortensen, J.K. (compilers), 2004. Yukon Age 2004: A database of isotopic age determinations for rock units from Yukon Territory: Yukon Geological Survey (CD-ROM). Buitenhuis, E., 2014. The Latte gold zone, Kaminak's Coffee gold project, Yukon, Canada: geology, geochemistry, and metallogeny: Unpublished MSc thesis, University of Western Ontario, London, Ontario, 197 p.

Buitenhuis, E., Boyce, L. and Finnigan, C., 2015. Advances in the mineralization styles and petrogenesis of the Coffee gold deposit, Yukon. In: Yukon Exploration and Geology 2014, K.E. MacFarlane, M.G. Nordling and P.J. Sack (eds.), Yukon Geological Survey, p. 29-43.

Joyce, N.L., 2002. Geologic setting, nature, and structural evolution of intrusion-hosted Au-bearing quartz veins at the Longline occurrence, Moosehorn Range Area, west-central Yukon Territory. Unpublished MSc thesis, The University of British Columbia, Vancouver, Canada, 201 p.

MacKenzie, D., Craw, D. and Finnigan, C., 2014a. Lithologically controlled invisible gold, Yukon, Canada. Mineralium Deposita, vol. 50, p. 141-157.

MacKenzie, D., Craw, D. and Finnigan, C., 2014b. Structural controls on alteration and mineralization at the Coffee gold deposits, Yukon. In: Yukon Exploration and Geology 2013, K.E. MacFarlane, M.G. Nordling and P.J. Sack (eds.), Yukon Geological Survey, p. 119-131.

McKenzie, G.G., Allan, M.M., Mortensen, J.K., Hart, C.J.R., Sánchez, M. and Creaser, R.A., 2013. Mid-Cretaceous orogenic gold and molybdenite mineralization in the Independence Creek area, Dawson Range, parts of NTS 115J/13 and 14. *In:* Yukon Exploration and Geology 2012, K.E. MacFarlane, M.G. Nordling and P.J. Sack (eds.), Yukon Geological Survey, p. 73-97.

Ryan, J.J., Zagorevski, A., Williams, S.P., Roots, C., Ciolkiewicz, W., Hayward, N. and Chapman, J.B., 2013a. Geology, Stevenson Ridge (northeast part), Yukon. Geological Survey of Canada, Canadian Geoscience Map 116 (2nd edition, preliminary), scale 1:100 000, doi:10.4095/292407.

Ryan, J.J., Zagorevski, A., Williams, S.P., Roots, C., Ciolkiewicz, W., Hayward, N. and Chapman, J.B., 2013b. Geology, Stevenson Ridge (northwest part), Yukon. Geological Survey of Canada, Canadian Geoscience Map 117 (2nd edition, preliminary), scale 1:100 000, doi:10.4095/292408.

Sanchez, M.G., Allan, M.M., Hart, C.J.R. and Mortensen, J.K., 2014, Extracting ore deposit controlling structures from aeromagnetic, gravimetric, topographic, and regional geologic data in western Yukon and eastern Alaska. Interpretation, vol. 2, p. SJ75-SJ102.

Tempelman-Kluit, D.J., 1974, Reconnaissance geology of Aishihik Lake, Snag and part of Stewart River map-areas, west-central Yukon (115A, 115F, 115G and 115K). Geological Survey of Canada, Paper 73-41, 97 p.

Wainwright, A.J., Simmons, A.T., Finnigan, C.S., Smith, T.R. and Carpenter, R.L., 2011. Geology of new gold discoveries in the Coffee Creek area, White Gold District, west-central Yukon. In: Yukon Exploration and Geology 2010, K.E. MacFarlane, L.H. Weston and C. Relf (eds.), Yukon Geological Survey, p. 233-247.

Yukon Geological Survey, 2015. Yukon Digital Bedrock Geology, <http://www.geology.gov.yk.ca/update_yukon_bedrock_geology_map.html>, [accessed November 15, 2015].

Paleozoic stratigraphy, tectonics and metallogeny of the Pelly Mountains, Quiet Lake and Finlayson Lake map areas (NTS 105F and G), central Yukon: Project outline and preliminary field results

L.P. Beranek[1], S.J. Piercey, R. Campbell and P. Wawrzonkowski
Department of Earth Sciences, Memorial University of Newfoundland

Beranek, L.P., Piercey, S.J., Campbell, R. and Wawrzonkowski, P., 2016. Paleozoic stratigraphy, tectonics and metallogeny of the Pelly Mountains, Quiet Lake and Finlayson Lake map areas (NTS 105F and G), central Yukon: Project outline and preliminary field results. *In:* Yukon Exploration and Geology 2015, K.E. MacFarlane and M.G. Nordling (eds.), Yukon Geological Survey, p. 17-28.

ABSTRACT

Paleozoic rocks of the Pelly Mountains, central Yukon, preserve greater than 150 m.y. of sedimentation, magmatism and base-metal mineralization. To identify secular trends in regional tectonics and metallogeny, a multi-year project on the stratigraphy of the Pelly Mountains in the Quiet Lake (105F) and Finlayson Lake (105G) map areas was initiated. Field studies during summer 2015 focused on two stratigraphic intervals: (1) mafic volcanic, volcaniclastic and clastic rock successions assigned to the Cambrian-Ordovician Cloutier and Groundhog formations (Kechika group); and (2) felsic volcanic, volcaniclastic and clastic rock successions assigned to the Devonian-Mississippian Black Slate and Felsic Volcanic formations (Seagull group). Cambrian-Ordovician strata were deposited in a marine environment characterized by episodic mafic volcanism and extensional tectonism. Devonian-Mississippian strata record the transition from an extensional turbidite basin to a metalliferous volcanic rift basin, and resemble key rock assemblages of the Selwyn basin (Earn Group) and Yukon-Tanana terrane (Grass Lakes and Wolverine Lake groups).

[1]lberanek@mun.ca

INTRODUCTION

The Pelly Mountains of central Yukon (Fig. 1a) have seen a long history of bedrock mapping, stratigraphic investigations and mineral exploration (*e.g.*, Wheeler *et al.*, 1960a,b; Tempelman-Kluit *et al.*, 1976; Tempelman-Kluit, 1977, 2012; Gordey, 1981; Mortensen, 1982; Holbek and Wilson, 1997; Fonseca, 1998; Hunt, 2002). Field studies in the Quiet Lake (105F) and Finlayson Lake (105G) map areas, east of the South Canol Road and west of the Tintina fault (Fig. 1b), were in part driven by stratigraphic comparisons with rock units that host Cambrian-Ordovician and Devonian sedimentary exhalative (SEDEX) base-metal deposits in the Anvil (Faro, Grum, Vangorda and others) and Macmillan Pass (Tom, Jason) districts and Devonian-Mississippian volcanogenic massive sulphide (VMS) base-metal deposits in the Finlayson Lake district (Wolverine, Kudz Ze Kayah, GP4F and others). Despite this attention, there are many outstanding questions about the precise age, tectonic setting and base-metal potential of regionally extensive Paleozoic rock assemblages. To investigate these and other questions, a multi-year study of mineralized, prospective and barren stratigraphic units was initiated in the Saint Cyr Range (central Pelly Mountains). The short-term goals of this project are to constrain the field geology, age, petrogenesis and geochemistry of Cambrian-Ordovician and Devonian-Mississippian rocks

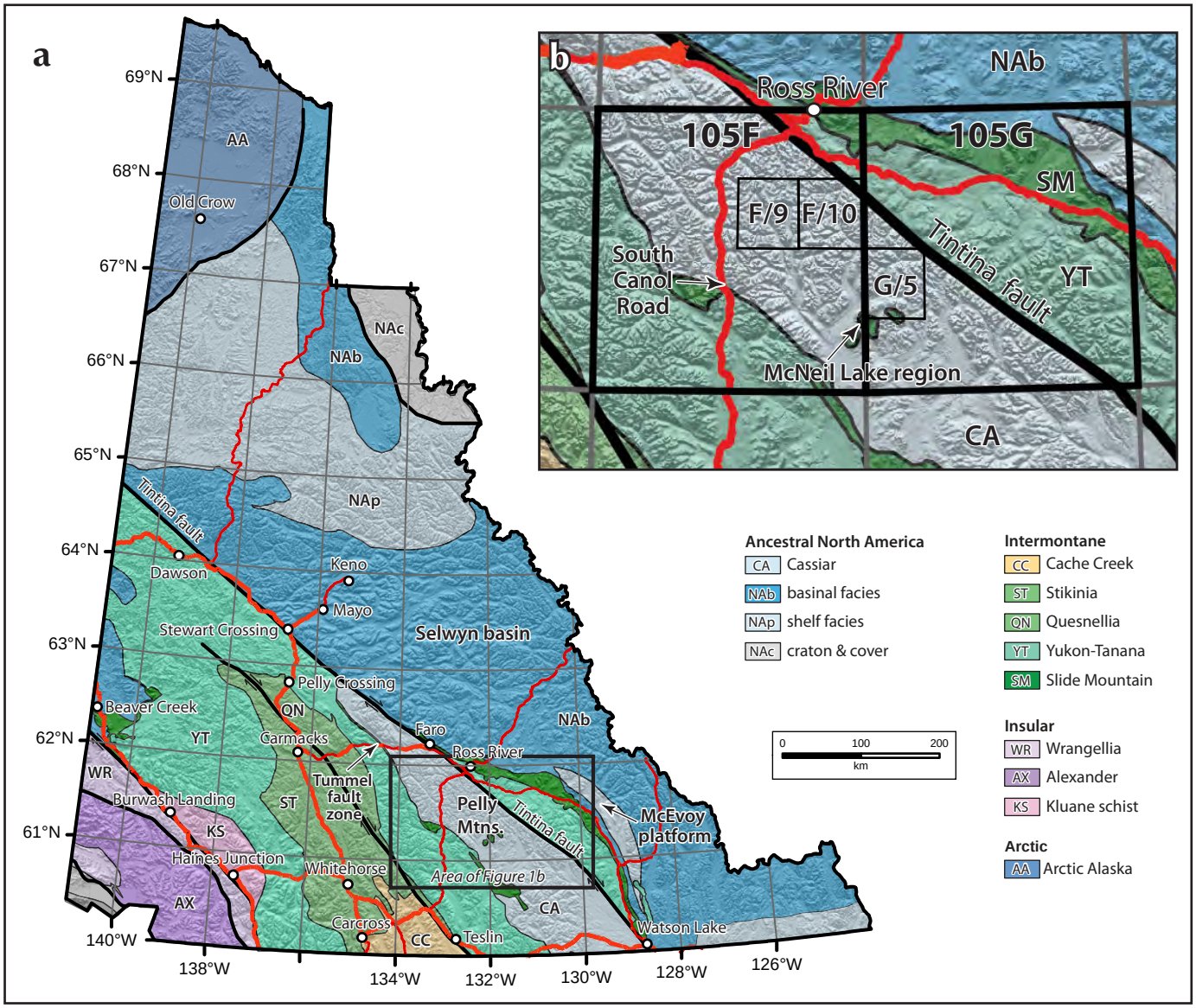


Figure 1. *(a) Yukon bedrock geology and terrane map modified from Colpron and Nelson (2011). (a) Location of the Pass Peak (105F/9), Cloutier Creek (105F/10), and Mount Placid (G/5) map areas in the Pelly Mountains between the South Canol Road and Tintina fault.*

in the Pass Peak (105F/9), Cloutier Creek (105F/10) and Mount Placid (105G/5) map areas (*see* Fig. 1b). The long-term objectives are to characterize secular trends in regional tectonics and metallogeny, especially those relevant to lithospheric architecture (*e.g.*, Cecile *et al.*, 1997; Hayward, 2015), and identify genetic relationships with coeval Paleozoic strata of the Selwyn basin, Kechika trough and Yukon-Tanana terrane.

STRATIGRAPHIC FRAMEWORK

The Pelly Mountains are mostly underlain by the Cassiar terrane (CA in Fig. 1), a parautochthonous fragment of the ancient Pacific margin that has undergone at least 430 km of dextral displacement along the Tintina fault (Gabrielse *et al.*, 2006). Lower Paleozoic strata of the Cassiar terrane comprise a distinct paleogeographic feature referred to as the Cassiar or Pelly-Cassiar platform (Gabrielse, 1967; Fritz *et al.*, 1991) or Pelly high (Cecile and Norford, 1993) that was located to the west (seaward) of inboard passive margin elements (Selwyn basin, Kechika trough, Macdonald platform; *see* discussion in Gordey, 2013). Allochthonous units of the pericratonic Yukon-Tanana and Slide Mountain terranes that evolved to the west (seaward) of the North American autochthon during the mid to late Paleozoic occur in faulted contact with the Cassiar terrane along its western edge (*i.e.*, Tummel fault zone, Glenlyon map area; Fig. 1a; Colpron *et al.*, 2006) and as overlying klippen (*i.e.*, McNeil Lake region, Finlayson Lake map area; Fig. 1b; Gordey, 1981).

Tempelman-Kluit (2012) divided the Paleozoic stratigraphy of the Cassiar terrane into five depositional sequences within the Quiet Lake and Finlayson Lake map areas, which from oldest to youngest comprise the Ketza, Kechika, Askin, Harvey and Seagull groups. Tempelman-Kluit (2012) concluded that many of these depositional sequences likely correlate with age-equivalent strata of the Cassiar terrane in northern British Columbia (Cassiar Mountains) or other passive margin elements in eastern Yukon. Figure 2 shows a schematic stratigraphic column for the study area.

KETZA GROUP

The oldest stratigraphic units in the Pelly Mountains are assigned to the Ketza group. Named for excellent exposures near the headwaters of the Ketza River, the group is at least 1000 m thick and contains a lower succession of Ediacaran(?)-Cambrian quartz sandstone, shale and limestone (Pass Peak formation), and an upper succession of Cambrian calcareous shale and archaeocyathid-bearing limestone (McConnell River formation; Fig. 3a-d). Tempelman-Kluit (2012) concluded that the Ketza group is correlative with the Atan Group (Boya and Rosella formations) of northern British Columbia.

KECHIKA GROUP

Tempelman-Kluit (2012) assigned Upper Cambrian-Ordovician strata of the Pelly Mountains to the Kechika Group based on apparent similarities with the formerly named Kechika Group (Gabrielse, 1963) in northern British Columbia. Gabrielse (1998) re-assigned such units in the Cassiar Mountains to the Kechika Formation. Herein, we refer to Upper Cambrian-Ordovician strata as the Kechika group (informal) because these units have not been formally defined according to the North American Stratigraphic Code.

The lower Kechika group comprises four laterally equivalent, interfingered sedimentary-volcanic facies (Ram, Groundhog, Cloutier and Gray Creek formations) that crop out across the Pelly Mountains (Fig. 2; Tempelman-Kluit, 2012). The Cloutier formation, named for exposures near Cloutier Creek, contains greater than 500 m of mafic lava and volcaniclastic rocks that represent the volcanic centre of the belt. To the northeast and southwest of the Cloutier Creek area, the Groundhog formation comprises greater than 800 m of shale to tuffaceous shale units that are intercalated with 1 to 8-m-thick sills of amygdaloidal basalt, pyroxene gabbro and sediment-matrix volcanic breccia (Figs. 2, 4a-d). The Ram formation occurs in the northeastern part of the facies belt and consists of up to 1000 m of platy limestone and calcareous shale. The Gray Creek formation is located in the southwestern part of the facies belt and comprises about 400 m of variably deformed and metamorphosed clastic rocks and minor mafic sills. The upper Kechika group is represented by black graphitic shale of the Magundy formation that overlies the Ram, Cloutier, and Groundhog formations in the Quiet Lake map area.

The depositional ages of Kechika group strata are constrained by Late Cambrian to Early Ordovician trilobites from the Ram formation and Ordovician graptolites from the Magundy formation (Tempelman-Kluit, 2012). Reconnaissance zircon U-Pb geochronology of a Groundhog formation pyroxene gabbro yielded a Late Cambrian age (L. Beranek and R. Friedman, 2015, unpublished data).

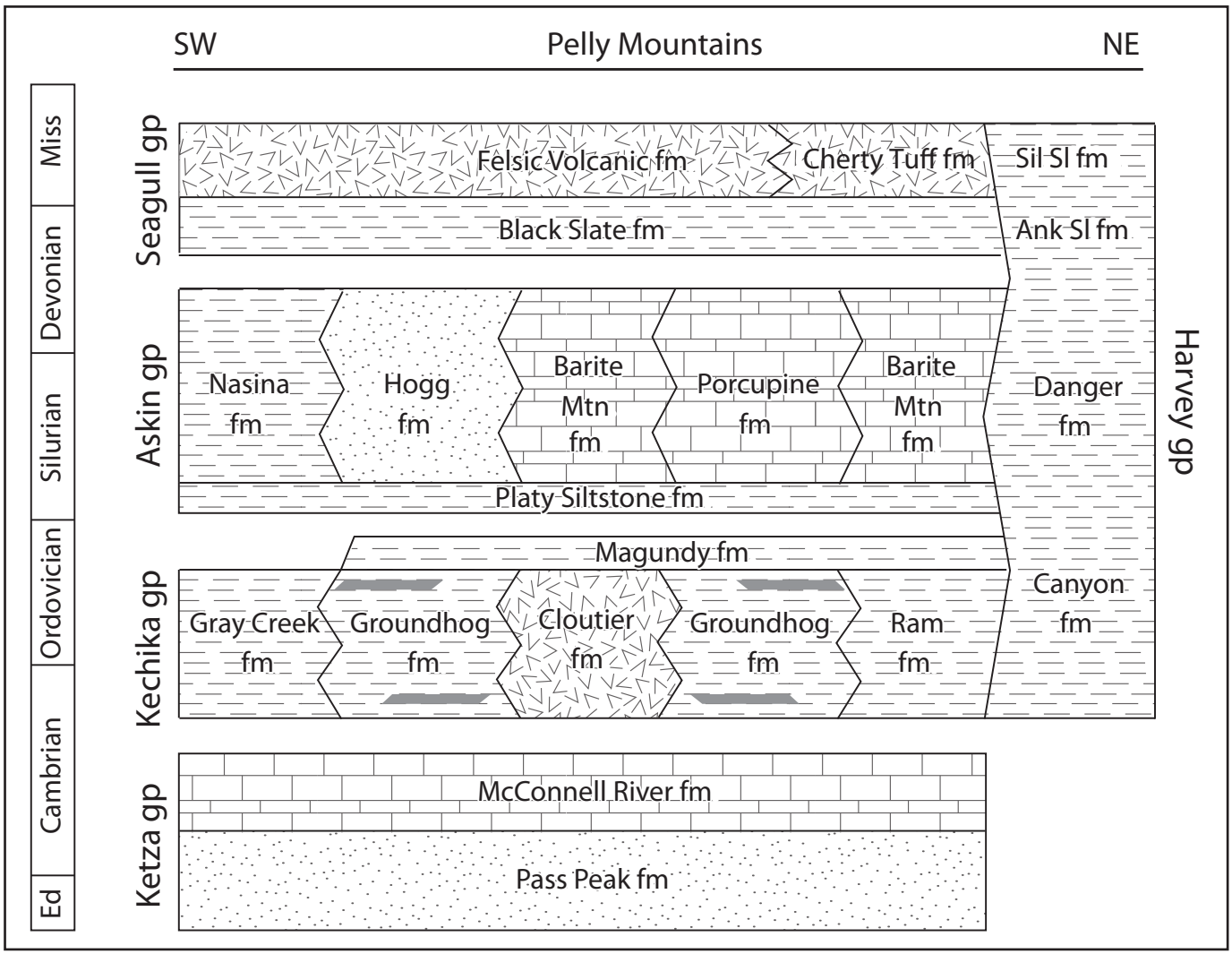


Figure 2. *Paleozoic stratigraphy of the Pelly Mountains as compiled by Tempelman-Kluit (2012). Abbreviations: Ank = Ankerite; Ed = Ediacaran; fm = formation; gp = group; Miss = Mississippian; Mtn = mountain; Sil = Siliceous; and Sl = Slate.*

ASKIN GROUP

The Silurian to Devonian Askin group (Figs. 2 and 5a,b) contains a basal succession of dolomitic siltstone and intermediate volcanic and volcaniclastic rocks (Platy Siltstone formation), a middle succession of four, laterally equivalent clastic-carbonate facies (Nasina, Hogg, Barite Mountain and Porcupine formations), and an upper succession of carbonate rocks (Grey Limestone formation; Tempelman-Kluit, 2012). The Askin group has a thickness of up to 1000 m. Tempelman-Kluit (2012) concluded that the Askin group is equivalent to rocks in the Cassiar Mountains (Sandpile and Ramhorn formations; Gabrielse, 1998), and may further correlate with Silurian-Devonian shelf strata of the McEvoy platform (Fig. 1a) to the northeast of the Tintina fault (*see* Gordey, 2013).

HARVEY GROUP

The Cambrian-Mississippian Harvey group (Fig. 2) is named for variably deformed and metamorphosed siliciclastic, carbonate and volcanic rocks that crop out between the Tintina and St. Cyr faults. Tempelman-Kluit (2012) interpreted that the lower two units (Canyon and Danger formations) correlate with the Kechika and Askin groups, respectively, whereas the upper two units (Ankeritic Slate and Siliceous Slate formations) represent basinal parts of the southwestern Selwyn basin displaced by the Tintina fault.

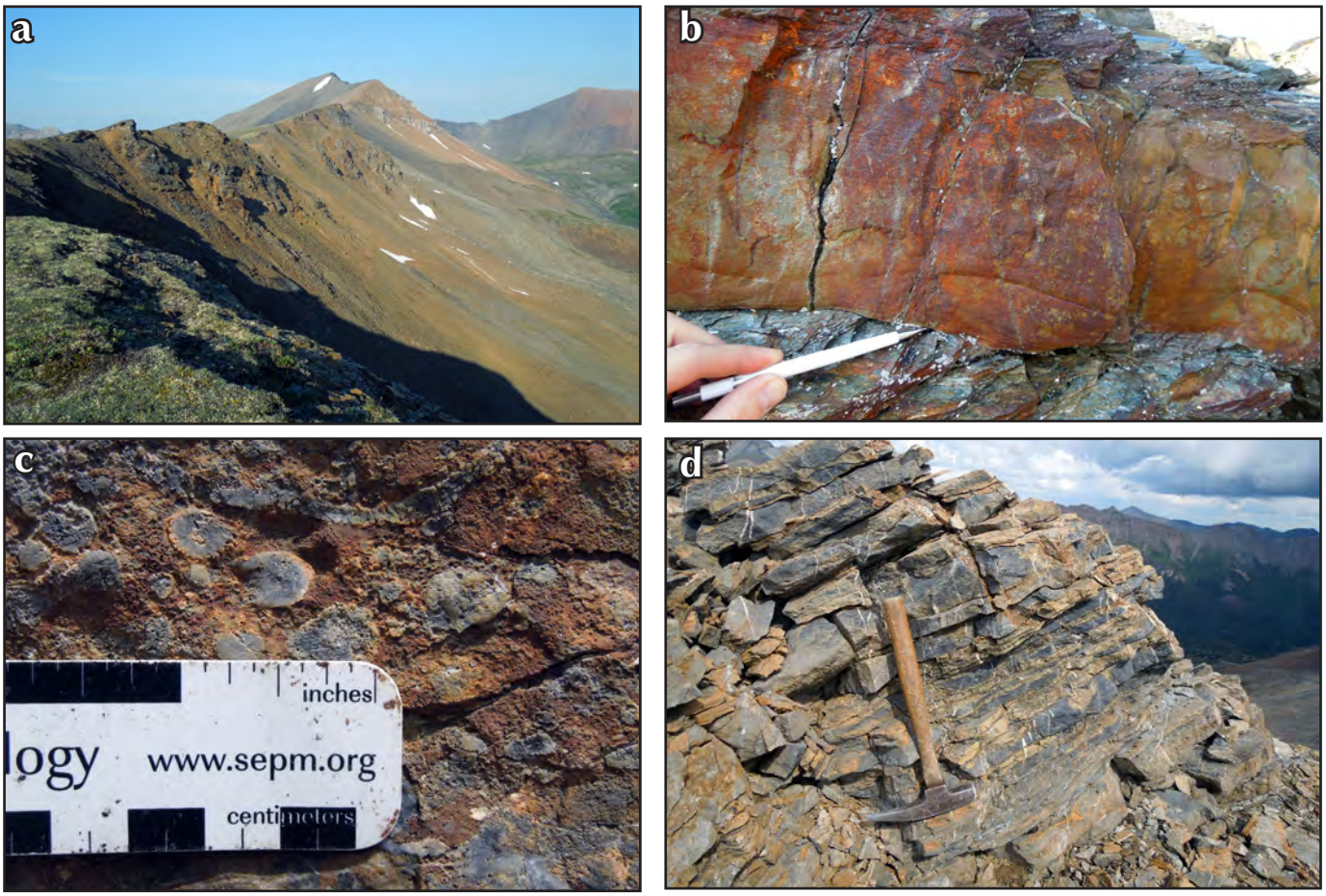


Figure 3. *Field photographs of Ediacaran(?)-Cambrian Ketza group strata, Pelly Mountains. (a) West-directed view of Pass Peak and McConnell River formation strata exposed at the Ketza River Mine, Pass Peak map area; (b) parallel laminated, medium-bedded sandstone and enclosing shale of the Pass Peak formation, Ketza River Mine area; (c) variably recrystallized archaeocyathid fossils in McConnell River formation limestone, Ketza River Mine area; and (d) thin to medium-bedded limestone and silty limestone of the McConnell River formation, Ketza River Mine area.*

SEAGULL GROUP

The Seagull group is named for Upper Devonian to Mississippian strata that are well exposed in the upper parts of Seagull Creek, central Quiet Lake map area (Tempelman-Kluit, 2012). The Black Slate formation (Fig. 2) occurs at the base of the group and contains up to 500 m of shale, lithic sandstone and chert pebble conglomerate, and minor volcanic rocks, limestone and thin-bedded barite. The overlying Felsic Volcanic formation (Figs. 2 and 6a-c) comprises about 500 m of felsic lava flows and volcaniclastic rocks that mostly occur in a 400 km^2 region between Seagull Creek and Cloutier Creek. Felsic plugs, sills and dikes assigned to the Trachyte Member are cogenetic with Felsic Volcanic formation extrusive rocks. The Cherty Tuff formation (Figs. 2 and 6d) consists of siliceous tuff that is the lateral equivalent of the Felsic Volcanic formation.

Seagull group rocks are recognized hosts of Late Devonian-Early Mississippian VMS mineralization in the Quiet Lake and Finlayson Lake map areas (*e.g.*, Mortensen, 1982; Holbek and Wilson, 1997). The timing of VMS mineralization and felsic magmatism in the Cassiar terrane is broadly coincident with that of the Selwyn basin and Yukon-Tanana terrane (Hunt, 2002). The Wolf deposit in the Mount Placid (105G/5) map area has received the most study and contains an inferred resource of over 4 million tonnes with grades of 6.2% Zn, 1.8% Pb and 84 g/t Ag (historic and not NI-43-101 compliant; Gibson *et al.*, 1999).

The depositional ages of the Seagull group are constrained by Late Devonian to Early Mississippian (Tournaisian to Visean) conodonts within Black Slate and Felsic Volcanic formation limestone (Tempelman-Kluit, 2012).

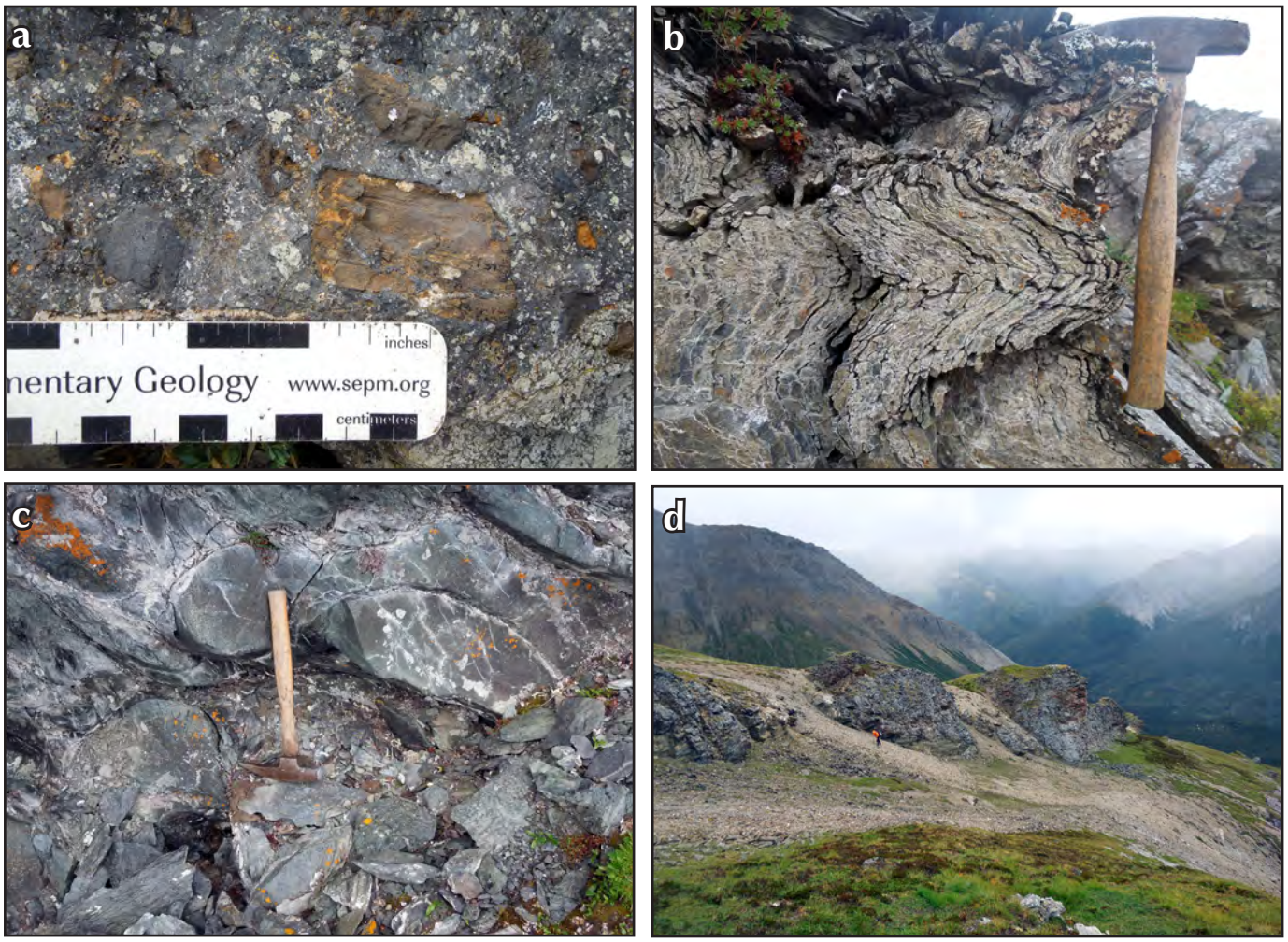


Figure 4. *Field photographs of Upper Cambrian-Ordovician Kechika group strata, Pelly Mountains. (a) Groundhog formation sediment-matrix volcanic and sedimentary lithic breccia, near Ram Creek, Pass Peak map area; (b) tightly folded Groundhog formation shale, near Groundhog Creek, Pass Peak map area; (c) pillow basalt, Mount Placid map area; and (d) east-directed view of resistant, 8 m-thick gabbro sill and enclosing shale of the Groundhog formation, near Ram Creek, Pass Peak map area.*

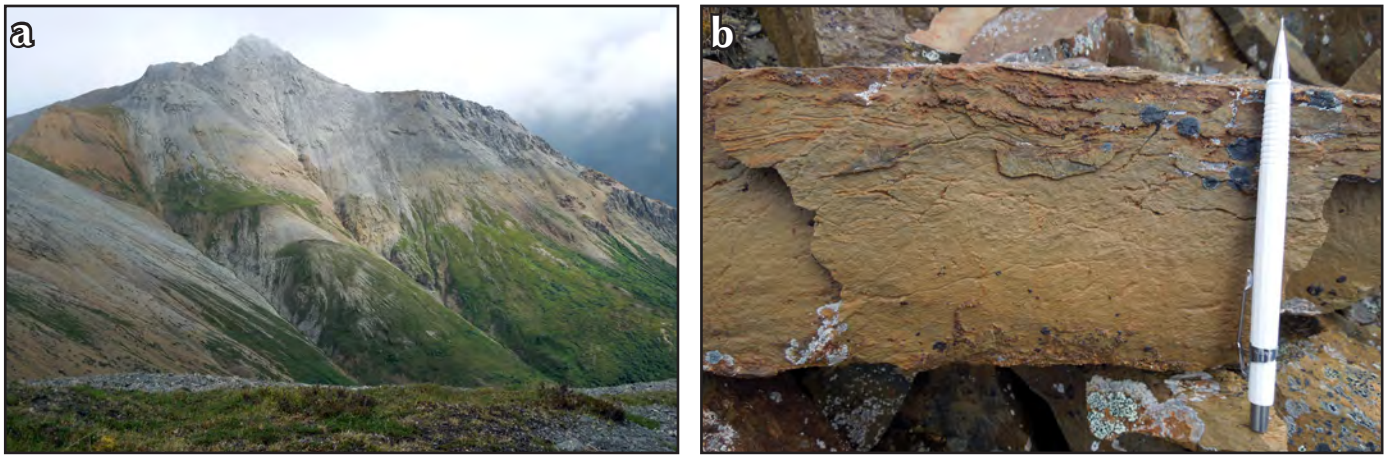


Figure 5. *Field photographs of Silurian-Devonian Askin group strata, Pelly Mountains. (a) North-directed view of Porcupine formation dolomite, near Ram Creek, Pass Peak map area; and (b) orange-weathering, intermediate ash-flow tuff or reworked derivative, Orange Volcanics Member of the Platy Siltstone formation, near Ram Creek, Pass Peak map area.*

Reconnaissance zircon U-Pb geochronology of a Felsic Volcanic formation rhyolite yielded an Early Mississippian age (L. Beranek and R. Friedman, 2015, unpublished data).

NEW FIELD STUDIES

Cambrian-Ordovician and Devonian-Mississippian stratigraphic successions were studied at several localities within the Pass Peak (105F/9), Cloutier Creek (105F/10) and Mount Placid (105G/5) map areas. Rock units were systemically sampled for whole-rock geochemistry and Nd-Hf isotope geochemistry, zircon U-Pb geochronology and thin section petrography. Folding and faulting of the rocks and significant coverage of vegetation hampered attempts for detailed stratigraphic measurement at most localities.

CAMBRIAN-ORDOVICIAN CLOUTIER FORMATION

Cloutier formation strata in the Cloutier Creek map area are best exposed along a southwest-trending ridge approximately 10 km east of the Ketza River Mine (Fig. 7a; base of section: zone 08V 654218E 6829014N NAD 83). Three principal lithofacies associations (basaltic, volcanogenic sedimentary and limestone-argillite) were identified at this locality. The basaltic facies association is related to the eruption of primary volcanic products and mostly comprises units of vesicular to amygdaloidal massive basalt (Fig. 7b), pillow basalt (Fig. 7c) and sediment-matrix basalt breccia (Fig. 7d) that are 2 to 10 m thick. The volcanogenic sedimentary facies association formed by the reworking of primary volcanic units and consists of up to 8-m-thick units of monomictic basalt breccia (Fig. 7e) and conglomerate (Fig. 7f). The limestone-argillite facies association is apparently restricted to the upper Cloutier formation and contains variably deformed argillite, limestone and granule to cobble polymictic (mafic intermediate volcanic rock, limestone) conglomerate (Fig. 7g).

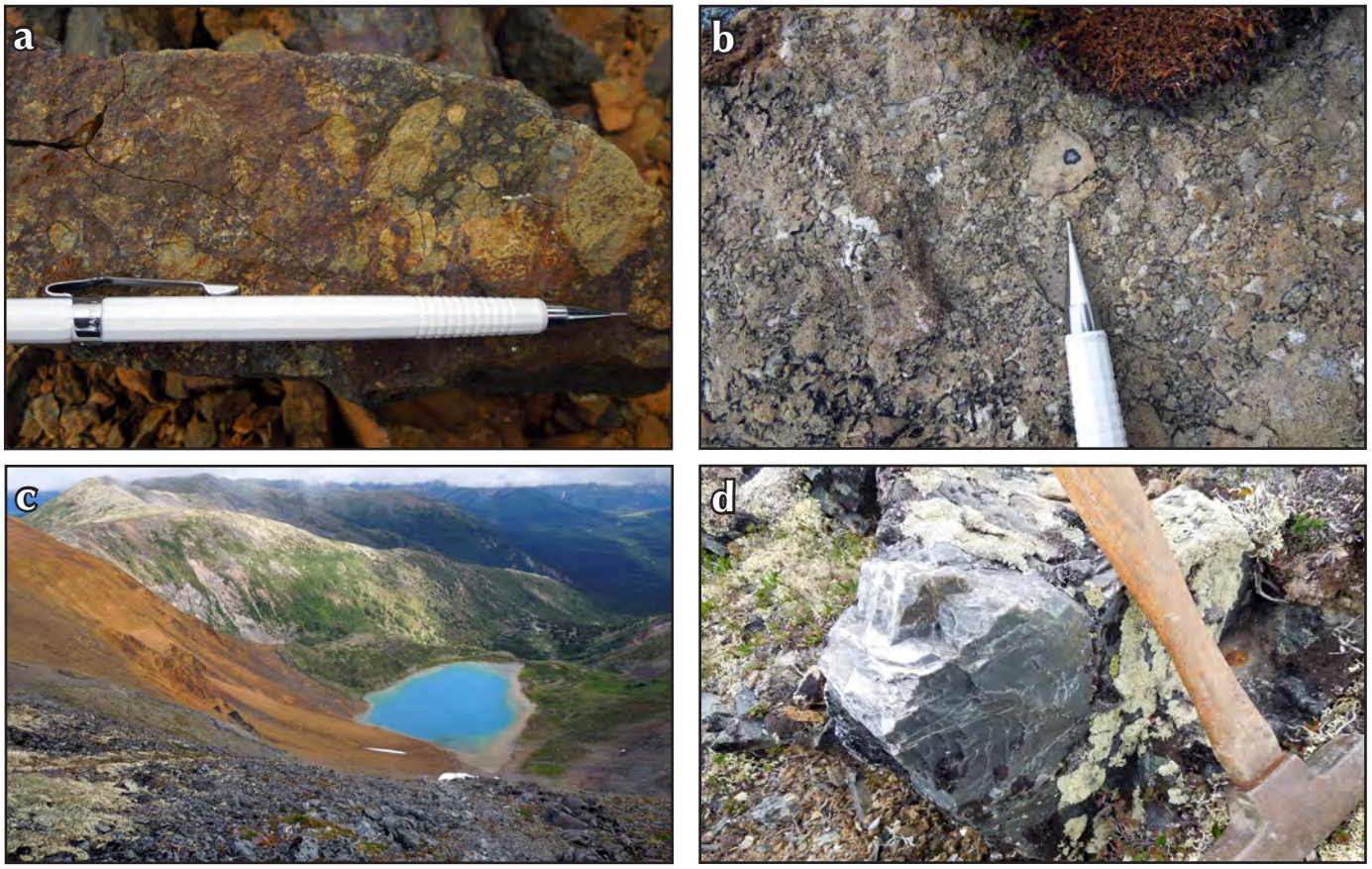


Figure 6. *Field photographs of Upper Devonian-Mississippian Seagull group strata, Pelly Mountains. (a) Felsic volcanic breccia, Wolf deposit, near Mount Vermillion, Mount Placid map area; (b) lapilli tuff, near Cloutier Creek, Cloutier Creek map area; (c) north-directed view of gossan hosted in Felsic Volcanic formation strata, near Seagull Creek, Pass Peak map area; and (d) siliceous unit of the Cherty Tuff formation, headwaters of the McConnell River, Pass Peak map area.*



Figure 7. *Field photographs of the Cloutier formation, east of the Ketza River Mine, Cloutier Creek map area. Base of section – Zone 08V 654218E 6829014N NAD 83. (a) West-directed view of Cloutier formation strata, Ketza River Mine infrastructure visible in background; (b) amygdaloidal (chlorite) basalt; (c) vesicular pillow basalt; (d) sediment-matrix basalt breccia (fluidal peperite) consisting of amoeboid- to angular-shaped, lapilli-sized fragments in volcaniclastic matrix; (e) monomictic basalt breccia (hyaloclastite) with angular, lapilli to bomb-sized fragments in volcaniclastic matrix; (f) volcanic conglomerate; (g) sheared polymictic (limestone, mafic-intermediate volcanic rock) conglomerate; and (h) thin to medium-bedded silty limestone, near Cloutier Creek, Cloutier Creek map area.*

The principal lithofacies of the Cloutier formation are consistent with a subaqueous depositional environment. Vesicular pillowed flows of the lower Cloutier formation are characteristic of subaqueous settings. Sediment-matrix basalt breccia units with lapilli-sized, amoeboid to angular-shaped clasts are likely fluidal peperites that formed from the emplacement of coherent mafic lava into/onto saturated sediment (*e.g.*, Skilling *et al.*, 2002). Monomictic basalt breccia units with lapilli to bomb-sized clasts are probably resedimented hyaloclastites that were generated from quench fragmentation of coherent flows (*e.g.*, Batiza and White, 2000). The presence of bedded limestone and limestone-bearing conglomerate units compares favourably to exposures of blue-grey carbonate and limy clastic rocks (Fig. 7h) in the upper Cloutier formation in the nearby Cloutier Creek area.

Preliminary geochemical results indicate that Cloutier formation strata yield non-arc, ocean island basalt-like (OIB) trace element and Nd-Hf isotope signatures. Age-equivalent strata of the Selwyn basin (Menzie Creek Formation, Anvil Range; Pigage, 2004) and Mackenzie platform (Marmot Formation, Misty Creek embayment; Leslie, 2009) yield analogous geochemical signatures. Our working hypothesis is that Cloutier formation mafic volcanic rocks (and mafic sills within the Groundhog formation) were generated by the partial melting of enriched lithospheric mantle during intermittent extension and rifting along the Cordilleran passive margin. Our future research will focus on the role of lithospheric architecture on Cambrian-Ordovician magmatism, including long-lived lithosphere-scale structures such as the Liard Line (Cecile *et al.*, 1997), which presumably influenced the magmatic history and metal fertility of the Pelly Mountains.

DEVONIAN-MISSISSIPPIAN BLACK SLATE AND FELSIC VOLCANIC FORMATIONS

Contact relationships between the Black Slate formation and overlying Felsic Volcanic formation are documented within an Upper Devonian-Lower Mississippian stratigraphic section that crops out near the headwaters of the McConnell River in the Pass Peak map area (base of section: zone 08V 627052E 6831980N NAD 83). The lowest stratigraphic levels of the Black Slate formation observed at this locality consist of dark grey shale with less than 2-m-thick beds of lithic sandstone and granule (shale chip) conglomerate. These strata are overlain by thin to medium-bedded, tuffaceous to siliceous (cherty) shale with 1 to 3-mm-thick laminae of white-weathering volcanic ash (Fig. 8a). The tuffaceous component in the Black Slate formation apparently increases upsection.

The basal Felsic Volcanic formation conformably overlies Black Slate formation strata and comprises 15 to 20 m of grey shale and quartz eye to lithic lapilli tuff (Fig. 8b). A 10-m-thick unit of vesicular to amygdaloidal rhyolite overlies these basal volcaniclastic and clastic units. The rhyolite unit is distinctive for its resistant weathering character and large (up to 10 mm) cavities and quartz amygdales (Fig. 8c). The upper part of the Mississippian succession at this locality mostly consists of black shale, lapilli tuff and high-level intermediate to felsic stocks (Fig. 8d,e).

Felsic Volcanic formation igneous rocks have alkaline geochemical signatures that are consistent with felsic magmatism in a rift setting (Mortensen, 1982; Hunt, 2002; Beranek, 2015, unpublished data). Although there is abundant evidence for mid-Paleozoic extension-related magmatism along the ancient Pacific margin, many questions remain about the Late Devonian-Mississippian paleogeography of the Cassiar terrane and how it relates to coeval successions in the northern Cordillera. In the Selwyn basin of central and eastern Yukon, turbidite successions (shale, lithic sandstone, chert pebble conglomerate) assigned to the Earn Group were deposited during regional extension, intermediate to felsic magmatism, and VMS and SEDEX mineralization (*e.g.*, Turner and Abbott, 1990; Gordey and Anderson, 1993; Cobbett, 2014, 2015). In the Finlayson Lake district of the Yukon-Tanana terrane, rock units of the Grass Lakes and Wolverine Lake groups record Late Devonian-Mississippian magmatism, Earn-style clastic sedimentation and VMS mineralization related to continental arc rifting (*e.g.*, Mortensen, 1992; Piercey *et al.*, 2004; Murphy *et al.*, 2006). We posit that Seagull group rocks of the Pelly Mountains likewise preserve the stratigraphic evidence for mid-Paleozoic extension along the ancient Pacific margin. Our working hypothesis calls for the Black Slate formation to comprise part of a turbidite basin that developed during regional extension and initial felsic volcanism, whereas the overlying Felsic Volcanic formation was deposited in a metalliferous volcanic rift basin that was located behind an adjacent continental arc system (Yukon-Tanana terrane).



Figure 8. *Field photographs of the Black Slate and Felsic Volcanic formations, headwaters of the McConnell River, Pass Peak map area. Base of section – Zone 08V 627052E 6831980N NAD 83. (a) Black Slate formation shale with 1-3 mm-thick laminae of white volcanic ash; (b) lapilli tuff near the base of the Felsic Volcanic formation; (c) amygdaloidal (quartz) rhyolite of the Felsic Volcanic formation; (d) intermediate to felsic rock of the Trachyte Member that is cogenetic with Felsic Volcanic formation strata; and (e) polymictic (sedimentary and volcanic lithic) breccia of the Felsic Volcanic formation.*

ACKNOWLEDGEMENTS

This project is supported by grants from the GEM (Geo-mapping for Energy and Minerals) program at Natural Resources Canada, Yukon Geological Survey and NSERC Discovery Grant program. Will Tompson of TransNorth Turbo Air provided excellent helicopter support. We are grateful to Rosie Cobbett and Maurice Colpron for help with field logistics. Comments from reviewer Rosie Cobbett improved this manuscript.

REFERENCES

Batiza, R. and White, J.D.L., 2000. Submarine lavas and hyaloclastite. *In*: Encyclopedia of Volcanics, H. Sigurdsson (ed.), Academic, San Diego, California, p. 361-381.

Cecile, M.P. and Norford, B.S., 1993. Ordovician and Silurian. *In*: Sedimentary Cover of the North American Craton in Canada, D.F. Stott and J.D. Aitken (eds.), Geological Survey of Canada, Geology of Canada no. 5, p. 125-149.

Cecile, M.P., Morrow, D.W. and Williams, G.K., 1997. Early Paleozoic (Cambrian to Early Devonian) tectonic framework, Canadian Cordillera. Bulletin of Canadian Petroleum Geology, vol. 45, p. 54-74.

Cobbett, R., 2014. Preliminary observations on the geology of the Anvil Lake area (parts of NTS 105K/11 and 12), central Yukon. *In*: Yukon Exploration and Geology 2013, K.E. MacFarlane, M.G. Nordling and P.J. Sack (eds.), Yukon Geological Survey, p. 33-51.

Cobbett, R., 2015. Geological map of the Anvil Lake area, central Yukon, parts of NTS 105K/11 and 12. Yukon Geological Survey, Open File 2015-2, scale 1:50000.

Colpron, M., Mortensen, J.K., Gehrels, G.E. and Villeneuve, M., 2006. Basement complex, Carboniferous magmatism and Paleozoic deformation in Yukon-Tanana terrane of central Yukon: Field, geochemical and geochronological constraints from Glenlyon map area. *In*: Paleozoic Evolution and Metallogeny of Pericratonic Terranes at the Ancient Pacific Margin of North America, M. Colpron, J.L. Nelson and R.I. Thompson (eds.), Canadian and Alaskan Cordillera, Geological Association of Canada Special Paper 45, p. 131-151.

Colpron, M. and Nelson, J.L., 2011. A Digital Atlas of Terranes for the Northern Cordillera. Yukon Geological Survey, <www.geology.gov.yk.ca>[accessed November 2015].

Fritz, W.H., Cecile, M.P., Norford, B.S., Morrow, D.W. and Geldsetzer, H.H.J., 1991. Cambrian to Middle Devonian assemblages. *In*: The Cordilleran Orogen: Canada, H. Gabrielse and C.J. Yorath (eds.), Geological Survey of Canada, Geology of Canada, no. 4, p. 151-218.

Fonseca, A., 1998. Structural evolution of the Ketza River gold deposit. *In*: Yukon Exploration and Geology 1997, Exploration and Geological Service Division, Yukon, Indian and Northern Affairs Canada, p. 77-81.

Gabrielse, H., 1963. McDame map area, Cassiar District, British Columbia. Geological Survey of Canada, Memoir 319, 138 p.

Gabrielse, H., 1967. Tectonic evolution of the northern Canadian Cordillera. Canadian Journal of Earth Sciences, vol. 4, p. 271-298.

Gabrielse, H., 1998. Geology of Cry Lake and Dease Lake map area, north-central British Columbia. Geological Survey of Canada, Bulletin 504, 147 p.

Gabrielse, H., Murphy, D.C. and Mortensen, J.K., 2006. Cretaceous and Cenozoic dextral orogen-parallel displacements, magmatism, and paleogeography, north-central Canadian Cordillera. *In*: Paleogeography of the North American Cordillera: evidence for and against large-scale displacements, J.W. Haggart, R.J. Enkin, and J.W.H Monger (eds.), Geological Association of Canada, Special Paper 46, p. 255-276.

Gibson, A.M., Holbek, P.M. and Wilson, R.G., 1999. The Wolf property - 1998 update: volcanogenic massive sulphides hosted by rift-related, alkaline, felsic volcanic rocks, Pelly Mountains, Yukon. *In*: Yukon Exploration and Geology 1998, C.F. Roots and D.S. Emond (eds.), Exploration and Geological Services Division, Yukon, Indian and Northern Affairs Canada, p. 237-242.

Gordey, S.P., 1981. Stratigraphy, structure, and tectonic evolution of the southern Pelly Mountains in the Indigo Lake area, Yukon Territory. Geological Survey of Canada, Bulletin 318, 44 p.

Gordey, S.P., 2013. Evolution of the Selwyn Basin region, Sheldon Lake and Tay River map areas, central Yukon. Geological Survey of Canada, Bulletin 599, 190 p.

Gordey, S.P. and Anderson, R.G., 1993. Evolution of the northern Cordilleran miogeocline, Nahanni map area (105 I), Yukon and Northwest Territories. Geological Survey of Canada, Memoir 428, 214 p.

Hayward, N., 2015. Geophysical investigation and reconstruction of lithospheric structure and its control on geology, structure, and mineralization in the Cordillera of northern Canada and eastern Alaska. Tectonics, vol. 34, doi: 10.1002/2015TC003871.

Holbek, P.M. and Wilson, R.G., 1997. The Wolf discovery: A Kuroko-style volcanogenic massive sulphide deposit hosted by rift-related, alkaline felsic volcanic rocks. *In*: Yukon Exploration and Geology 1997, Exploration and Geological Services Division, Yukon, Indian and Northern Affairs Canada, p. 115-120.

Hunt, J.A., 2002. Volcanic-associated massive sulphide (VMS) mineralization in the Yukon-Tanana Terrane and coeval strata of the North American miogeocline, in the Yukon and adjacent areas. Exploration and Geological Services Division, Yukon Region, Indian and Northern Affairs Canada, Bulletin 12, 107 p.

Leslie, C.D., 2009. Detrital zircon geochronology and rift-related magmatism: central Mackenzie Mountains, Northwest Territories. Unpublished MSc thesis, University of British Columbia, Vancouver, British Columbia, Canada, 224 p.

Mortensen, J.K., 1982. Geological setting and tectonic significance of Mississippian felsic metavolcanic rocks in the Pelly Mountains, southeastern Yukon Territory. Canadian Journal of Earth Sciences, vol. 19, p. 8-22.

Mortensen, J.K., 1992. Pre-mid-Mesozoic tectonic evolution of the Yukon-Tanana terrane, Yukon and Alaska. Tectonics, vol. 11, p. 836-853.

Murphy, D.C., Mortensen, J.K., Piercey, S.J., Orchard, M.J. and Gehrels, G.E., 2006. Mid-Paleozoic to early Mesozoic tectonostratigraphic evolution of Yukon-Tanana and Slide Mountain terranes and affiliated overlap assemblages, Finlayson Lake massive sulphide district, southeastern Yukon. *In*: Paleozoic Evolution and Metallogeny of Pericratonic Terranes at the Ancient Pacific Margin of North America, M. Colpron, J.L. Nelson and R.I. Thompson (eds.), Canadian and Alaskan Cordillera, Geological Association of Canada Special Paper 45, p. 75-105.

Piercey, S.J., Murphy, D.C., Mortensen, J.K. and Creaser, R.A., 2004. Mid-Paleozoic initiation of the northern Cordilleran marginal backarc basin: Geologic, geochemical, and neodymium isotope evidence from the oldest mafic rocks in the Yukon-Tanana terrane,

Finlayson Lake district, southeast Yukon, Canada. Geological Society of America Bulletin, vol. 116, p. 1087-1106.

Pigage, L.C., 2004. Bedrock geology compilation of the Anvil District (parts of NTS 105K/2, 3, 4, 5, 6, 7 and 11), central Yukon. Yukon Geological Survey, Bulletin 15, 103 p.

Skilling, I.P., White, J.D.L. and McPhie, J., 2002. Peperite: a review of magma-sediment mingling. Journal of Volcanology and Geothermal Research, vol. 114, p. 1-17.

Tempelman-Kluit, D.J., 1977. Geology of Quiet Lake (105F) and Finlayson Lake (105G) map areas, Yukon Territory. Geological Survey of Canada, Open File Map 486, scale 1:250000.

Tempelman-Kluit, D.J., 2012. Geology of Quiet Lake and Finlayson Lake map areas, south-central Yukon: An early interpretation of bedrock stratigraphy and structure. Geological Survey of Canada, Open File 5487, 103 p.

Tempelman-Kluit, D.J., Gordey, S.P. and Read, B., 1976. Stratigraphic and structural studies in the Pelly Mountains, Yukon Territory. Geological Survey of Canada, Paper 76-1A, p. 97-106.

Turner, R.J.W. and Abbott, G., 1990. Regional setting, structure, and zonation of the Marg volcanogenic massive sulphide deposit, Yukon. Current Research, Part E, Geological Survey of Canada, Paper 90-1E, p. 31-41.

Wheeler, J.O., Green, L.H. and Roddick, J.A., 1960a. Quiet Lake, Yukon Territory. Geological Survey of Canada, Map 7-1960.

Wheeler, J.O., Green, L.H. and Roddick, J.A., 1960b. Finlayson Lake, Yukon Territory. Geological Survey of Canada, Map 8-1960.

The Paradise gravel: Evidence for a pre-White Channel Gravel in the Klondike

J.D. Bond
Yukon Geological Survey

Bond, J.D., 2016. The Paradise gravel: Evidence for a pre-White Channel Gravel in the Klondike. *In:* Yukon Exploration and Geology 2015, K.E. MacFarlane and M.G. Nordling (eds.), Yukon Geological Survey, p. 29-42.

ABSTRACT

New stratigraphic interpretations of exposures at Dago, Preido and Paradise hills on lower Hunker Creek suggest a more complex stratigraphic framework for the development of high-level bench gravels in the Klondike than has been previously put forward. A highly-altered gravel has formerly been interpreted to be part of the lower White Channel Gravel sequence and its degree of alteration attributed to enhanced groundwater diagenesis near the bedrock contact. New mining exposures indicate this altered gravel, here informally termed 'Paradise gravel', is laterally extensive and the alteration is not restricted to the bedrock interface. Furthermore, a cross-section reconstruction shows the White Channel Gravel is stratigraphically inset into the Paradise gravel. Alteration of the Paradise gravel is possibly a function of pedogenesis, suggesting a period of landscape stability followed its deposition. This pattern of sedimentation and potential stability was repeated within the lower White Channel Gravel and recorded by a zone of clay alteration and iron oxidation.

Economically, the Paradise gravel is significant. At each locality investigated, the primary pay streak occurs in the Paradise gravel. Conversely, the White Channel Gravel is only economic where it sufficiently erodes and reworks the Paradise gravel. In nearby drainages, including upper Hunker Creek, the White Channel Gravel more completely reworks Paradise gravel to bedrock and becomes the pay unit. Preservation of the Paradise gravel documented in lower Hunker Creek may be due to its broad valley morphology. Future studies are recommended on the sedimentology of the Paradise gravel to understand gold distribution both vertically and within the pay channel(s). In addition, research into the pedogenic alteration could provide information on past climates during the Neogene.

[1]*jeff.bond@gov.yk.ca*

INTRODUCTION

Gold placers have been mined continuously from the Klondike district, Yukon since gold discovery in 1896 (Fig. 1). Reported placer gold production exceeds 10 million fine ounces and extraction continues with 90 placer mines still active in the district (Van Loon and Bond, 2014). The White Channel Gravel, a high-level Neogene[1] bench gravel, has been previously interpreted as the oldest auriferous gravel in the Klondike (Fig. 1; McConnell, 1907). The gravel owes its name to the abundance of quartz clasts, which are a residual lithology derived from weathering of the underlying Klondike Schist and its associated orogenic veins (McConnell, 1907; Tempelman-Kluit, 1982; Mortensen *et al.*, 2004; Chapman *et al.*, 2010). Reworking of the White Channel Gravel into secondary stream and terrace gravels resulted in some of the richest placer creeks in the world. Estimates from a four mile-long pay streak in Eldorado Creek, a tributary to Bonanza Creek, suggest 1.3 million fine ounces of placer gold were produced between 1896 and 1907 (McConnell, 1907). Another significant pay streak, or portions of the primary pay streak, was preserved on many of the high-level White Channel Gravel benches. Over the years these resources have been exploited by underground mining, hydraulic mining and with modern heavy equipment.

Numerous studies have described the stratigraphy and sedimentology of the White Channel Gravel; however, McConnell (1905, 1907) provided the most detailed information on contact relationships. McConnell's cross-sections for upper Bonanza Creek and the Klondike River have been cited extensively and provide a distribution framework for the primary lithostratigraphic units (Fig. 2; Tempelman-Kluit, 1982; Dufresne and Morison, 1985; Morison and Hein, 1987; Froese *et al.*, 2000; Lowey, 2002).

[1]*Tertiary is no longer recognized as a formal time period by the International Commission on Stratigraphy. The time span was subdivided between the Paleogene (66 Ma to 23.03 Ma) and Neogene (23.03 Ma to 2.58 Ma) periods, which immediately precedes the Quaternary (2.58 Ma to present).*

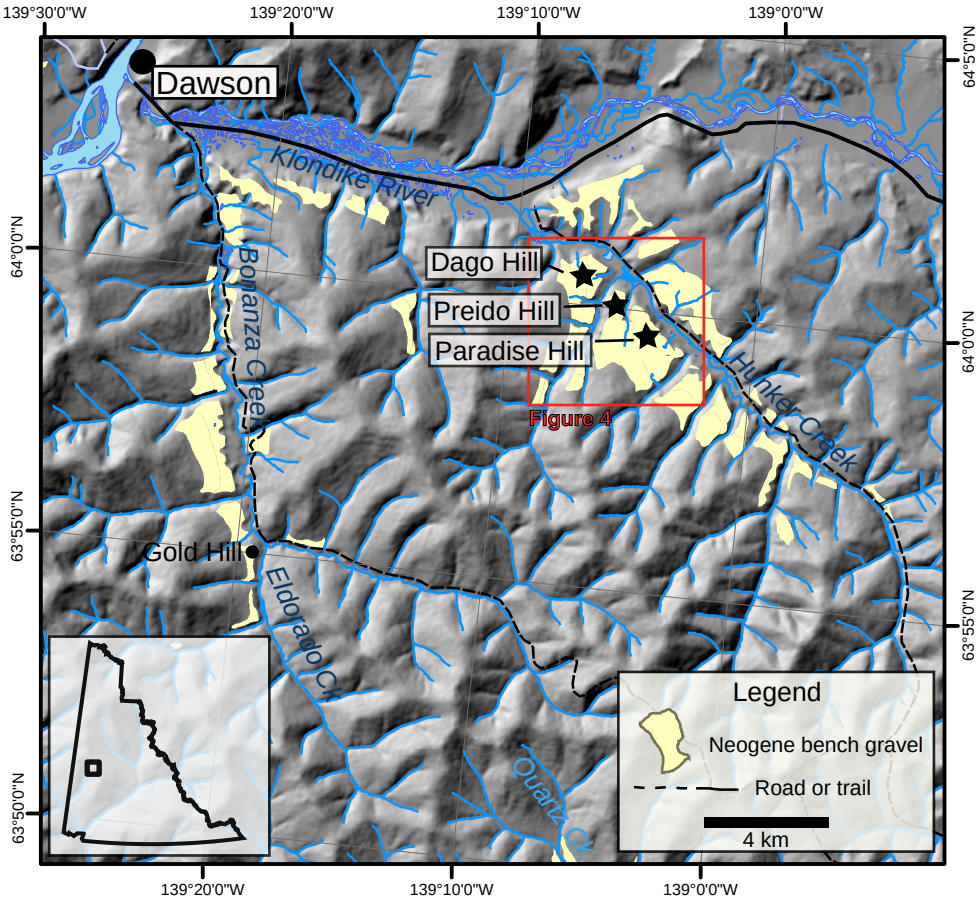


Figure 1. *Location map of the Neogene sediments in Hunker and Bonanza creeks (geology from: Froese and Jackson, 2005; McKenna and Lipovsky, 2014).*

The purpose of this paper is to present a stratigraphic re-interpretation of the White Channel Gravel based on exposures from Dago, Preido and Paradise hills on lower Hunker Creek (Fig. 1). Using the new stratigraphy, an idealized cross-section is developed that challenges the established deposit evolution, explains previously published observations and has implications for identifying new placer gold resources in the Klondike.

BACKGROUND

The high quartz content of the White Channel Gravel reflects prolonged weathering of the late Permian Klondike Schist and its gold-bearing quartz veins (Knight *et al.*, 1994; Knight *et al.*, 1999; Mortensen *et al.*, 2005). Sedimentological analyses by Morison and Hein (1987) described the White

Channel Gravel as a proximal to distal braidplain with colluvial sediment-gravity flow deposits within a confined valley. McConnell (1905, 1907) subdivided the gravel into two units: a lower 'white gravel' and an upper 'yellow gravel', and suggested the two units represented separate depositional events, consistent with a transition from preglacial to periglacial conditions as described by Froese *et al.* (2000; Fig. 2). Recent architectural analysis on sedimentary bedforms supports this interpretation by demonstrating an increase in aggradation rate (and reduction in channel size) from the lower White Channel Gravel to the upper White Channel Gravel (Lowther *et al.*, 2014). Lowther *et al.* (2014) further suggest a depositional hiatus likely occurred between the upper and lower White Channel Gravel and that it may have been caused by a tectonic event.

Alteration descriptions of the lower White Channel Gravel and underlying bedrock have been made by a number of authors. At Dago Hill, Tempelman-Kluit (1982) suggested that groundwater played a significant role in leaching the deposit and described the alteration as so intense that schist and porphyry clasts disintegrate upon thawing of permafrost. Dufresne et al. (1986) and Dufresne (1987) concluded that hydrothermal activity contributed to the alteration and subdivided the alteration into three zones: the 'Bleached Zone', the 'Iron Zone' and the 'Footwall Zone'. The alteration in all three zones is characterized by the development of secondary clay minerals with moderate to high crystallinities (Dufresne *et al.*, 1986). Furthermore, the 'Iron Zone' and 'Footwall Zone' have anomalously high concentrations of the elements Fe, Mn, As, Sb, Hg, Co, Ba and S. This hydrothermal origin for the alteration was challenged by Lowey (2002, 2006) who argued that weathering and diagenesis due to groundwater flow, coupled with time, was sufficient to explain the decomposition. Lowey (2002) also suggested the abundance of kaolinite in the 'white gravel' could be the result of deposition and weathering during a more temperate and humid climate. Lowey's arguments are consistent with McConnell's (1907) assessment that circulating surface waters had contributed to leaching.

The age of the lower White Channel Gravel is poorly constrained. McConnell (1907) estimated the gravel must date back to the Pliocene. Tempelman-Kluit (1982) thought that deposition of the White Channel Gravel was initiated in the Late Miocene or Pliocene (late Tertiary or Neogene) when differential uplift of the Klondike Plateau began. Paleomagnetic measurements indicate a change from reverse to normal polarity in the lower White Channel Gravel, attributed to the Gilbert-to-Gauss chron transition at 3.58 Ma; however, accurate placement of this change within the geomagnetic timescale is problematic (Froese *et al.*, 2000). Pollen data from the upper portions of the lower White Channel Gravel have an assemblage that is consistent with mid-Pliocene, preglacial deposits in Alaska (Ager *et al.*, 1994; Froese *et al.*, 2000; Lowther *et al.*, 2014).

The upper White Channel Gravel is a normally magnetized, unaltered gravel that exhibits periglacial weathering, including ice wedge casts and cryoturbation-related involutions (Froese *et al.*, 2000). The age of the gravel is well constrained by tephra and paleomagnetic measurements that place its age between 2.6-3.3 Ma (Froese *et al.*, 2000; Westgate *et al.*, 2003). Cordilleran Ice Sheet outwash, which overlies the upper White Channel Gravel in the Klondike River valley, dates to 2.64+0.20/-0.18 Ma, thus providing a minimum age for the cessation of White Channel Gravel deposition (Hidy *et al.*, 2013).

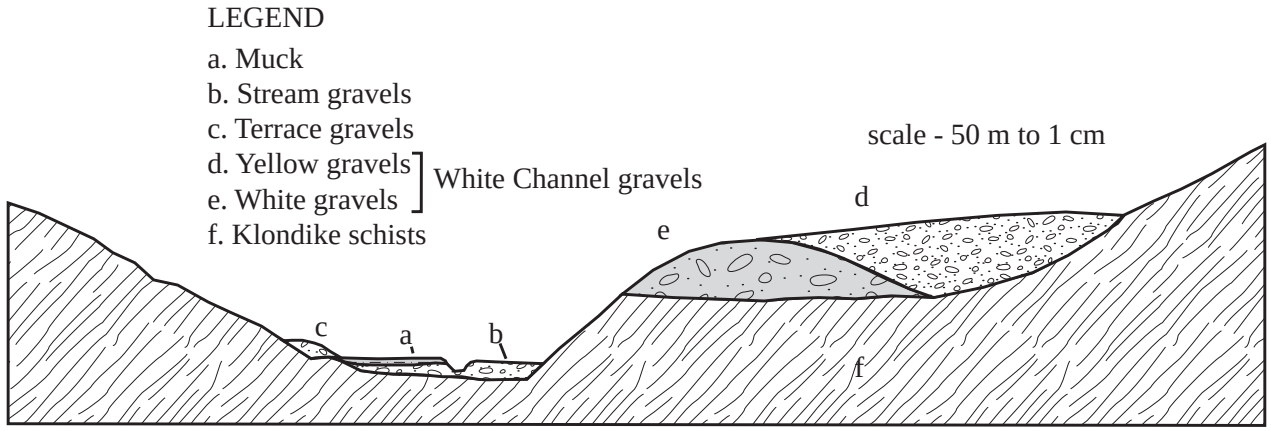


Figure 2. *Cross-section of Bonanza Creek near the mouth of Eldorado Creek. The contacts indicate that the 'yellow gravels' are cut into the lower 'white gravels' (after McConnell, 1907).*

McConnell's (1907) report on gold values in the White Channel Gravel provided a detailed account of the placer gold distribution. Throughout most of the Klondike, gold grades are considerably enriched in the lower 2 m of gravel on bedrock (Gleeson, 1970). For example, at Lovett Hill on Bonanza Creek the bottom 2 m of gravel contains the equivalent amount of gold as the overlying 44 m of gravel. In other words, 50% of the gold from a 46 m exposure is contained in the bottom 2 m. Furthermore, coarse gold is only found in this lower 2 m of gravel. An exception to this rule was documented by McConnell (1907) at Paradise Hill on Hunker Creek where the main gold zone lies 0.9-3.7 m above bedrock, at a contact with an underlying highly siliceous and coarse gravel.



Figure 3. *Aerial view to the south, looking up Hunker Creek. The Neogene benches (hills) are labelled on the west side of the valley.*

NEW STRATIGRAPHIC DESCRIPTIONS

The Neogene fluvial terraces of Paradise, Preido and Dago hills, on the southwest side of the Hunker Creek valley, were investigated for this study (Fig. 1, 3 and 4). Stratigraphic measurements, contact relationships and unit descriptions were made at each locality. The stratigraphy and sedimentology of the three sites has been described in the past and, where possible, this study relates new observations to earlier work (McConnell, 1907; Tempelman-Kluit, 1982; Dufresne *et al.*, 1986; Morison and Hein, 1987; Froese *et al.*, 2000; Lowey, 2002). Of particular relevance is the idealized stratigraphy proposed by Dufresne *et al.* (1986) that uses alteration to differentiate zones in the gravel (Fig. 5). These descriptions support a new lithostratigraphic framework that includes four units overlying a strath terrace.

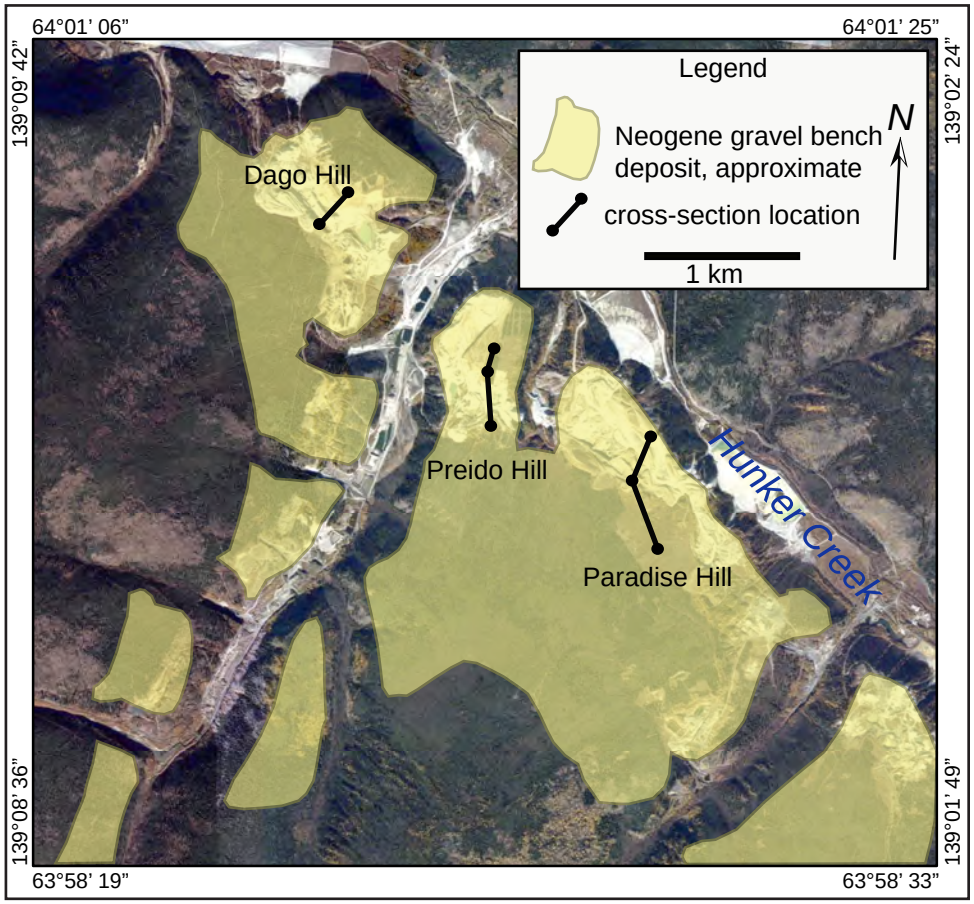


Figure 4. *Map showing the location of the cross-sections on Dago, Preido and Paradise hills. Also, the distribution of Neogene fluvial sediments are shown in yellow, which includes both Neogene pediment (thin fluvial/colluvial) and fluvial terrace (thick fluvial) deposits (geology from: Froese and Jackson, 2005; McKenna and Lipovsky, 2014).*

BEDROCK STRATH

The White Channel strath, as described by Lowey (2004), is the eroded bedrock surface that is in unconformable contact with the overlying gravel. At Paradise and Preido hills the strath lithology varies from siltstones and conglomerates of the Indian River Formation to Klondike Schist and ultramafic rocks. On Paradise Hill, a previously unmapped thin layer of Indian River Formation siltstone, pebble conglomerate and tuff overlie the Klondike Schist. At both Paradise and Preido hills the bedrock surface is intensely altered and decomposed into soft clay, and in isolated places is deformed and folded into the overlying gravel (Fig. 6). Alteration of the bedrock strath was described by Dufresne *et al.* (1986) as the 'Footwall Zone', which contained a secondary clay mineral assemblage (Fig. 5).

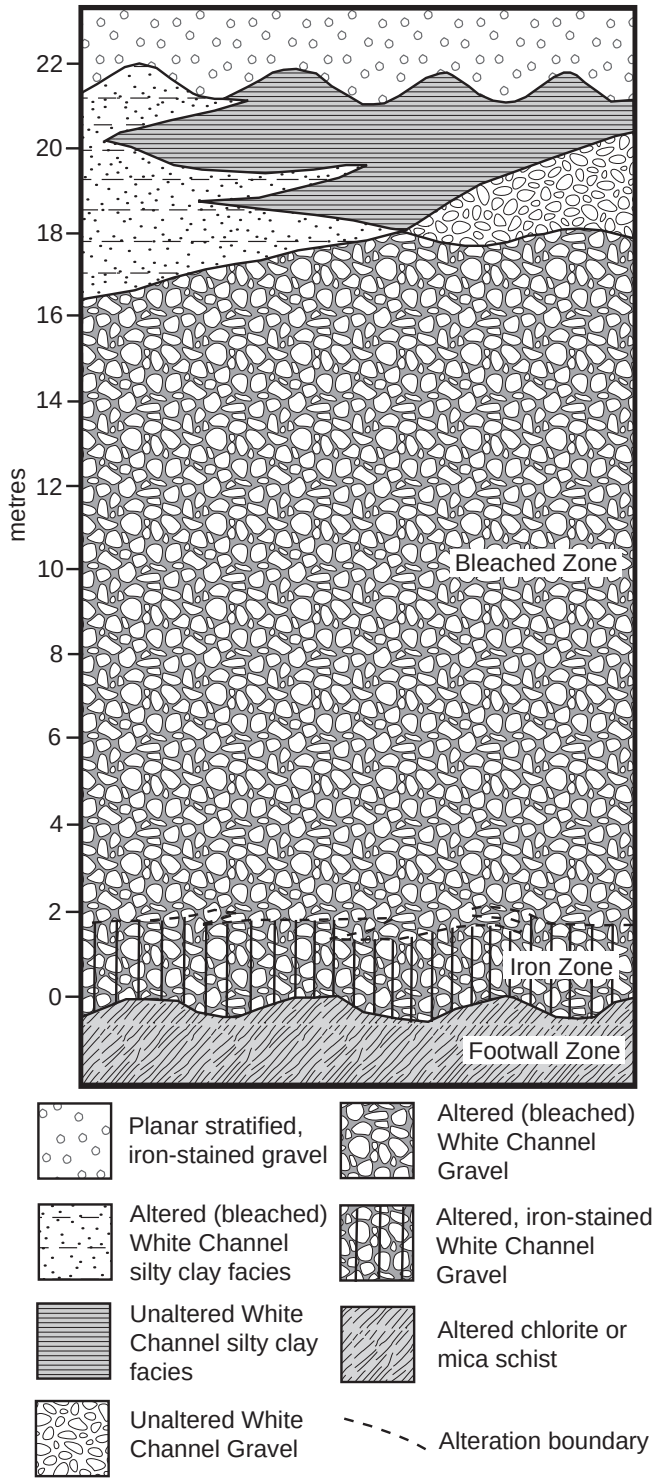


Figure 5. *Idealized section from Dago Hill showing the alteration zones within Neogene sediments (after Dufresne et al., 1986).*

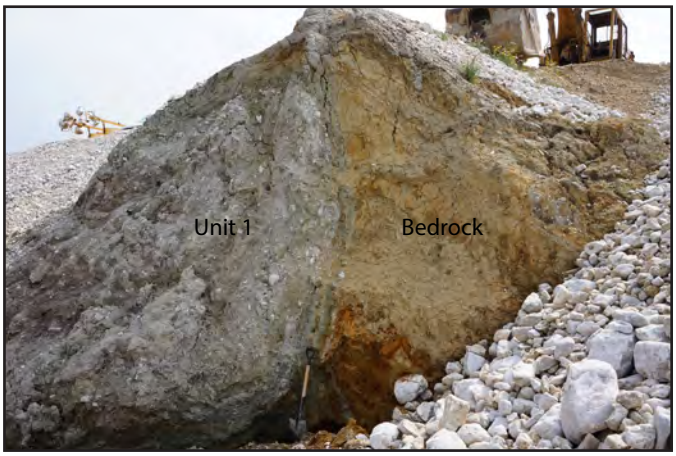


Figure 6. *Altered and deformed bedrock on Paradise Hill has produced a vertical contact between unit 1 and the Indian River Formation bedrock.*

Unit 1

The lowermost gravel unit consists of an unsorted to moderately sorted, iron-mottled to pervasively stained, intensely altered, quartz cobble-rich gravel (Figs. 7, 8 and 9). At Dago Hill, this unit is equivalent to the 'Iron Zone' as described by Dufresne *et al.* (1986; Fig. 5) and termed the 'lower White Channel Gravel' by Froese *et al.* (2000). Unpublished shafting reports from 1912-1913 on Paradise Hill refer to the lowermost gravel unit as "gumbo". Near the bedrock contact, unit 1 is clast supported, can locally resemble a diamicton due to the alteration and deformation, and contains subrounded to rounded boulders up to 100 cm in diameter (Fig. 10). Crude stratification and bedding is visible throughout and iron-staining increases upward. Dufresne *et al.* (1986) analyzed the geochemistry of the 'Iron Zone' and concluded there were anomalous concentrations of Fe, Mn, As, Sb, Hg, Co, Ba and S within the matrix. Quartz clasts represent 50-70% of the gravel with the remaining clasts

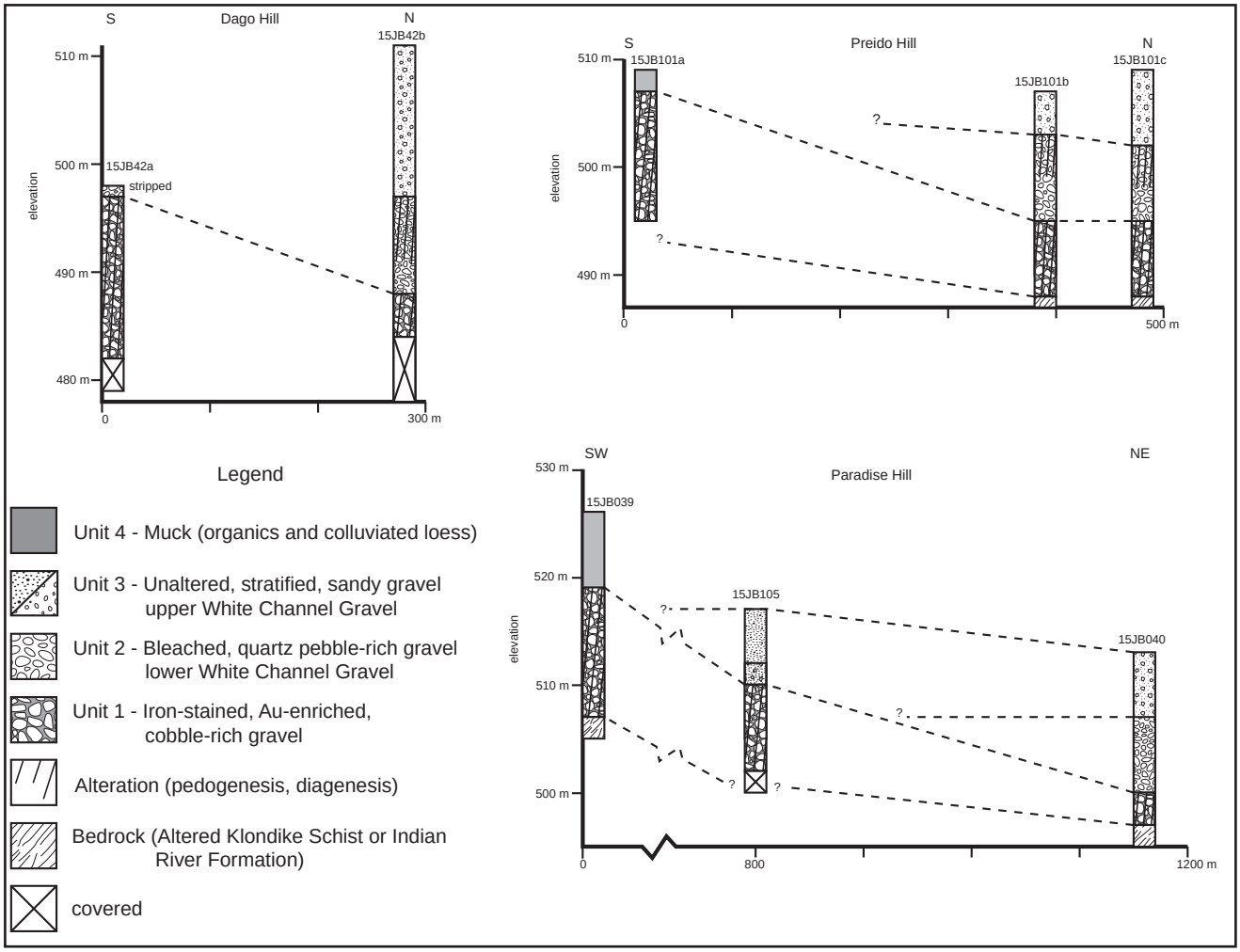


Figure 7. *Stratigraphic sections from Dago, Preido and Paradise hills. See Figure 4 for section locations.*

composed of sericite schist, mica schist, graphitic schist, rhyolite and gneiss. All of the non-quartz lithologies are soft and have been largely replaced by secondary clay minerals (Fig. 8; Tempelman-Kluit, 1982; Dufresne *et al.*, 1986). Upon thawing, the altered clasts turn to a soft incompetent clay (Tempelman-Kluit, 1982). Flattened weathered clasts are present where post-alteration deformation, perhaps from loading or mass wasting, has disturbed the gravel (Fig. 8). Unit 1 is 3.4-11.5 m thick and is consistently thickest toward the valley margin where it is overlain by muck (unit 4; Fig. 7). Unit 1 is the primary pay at Dago, Preido and Paradise hills (pers. comm., Favron Enterprises, Tamarack and Moonlight Mining, 2015).



Figure 8. *Close up photograph of unit 1 at Paradise Hill. The gravel is highly altered and clasts are visibly deformed.*



Figure 9. *View of units 1 and 4 at Paradise Hill (see Fig. 6 section 15JB039). Unit 1 is the equivalent of the 'Iron Zone' gravel described by Dufresne et al. (1986).*



Figure 10. *A small boulder exposed in unit 1 at Paradise Hill (see Fig. 6 section 15JB105). Boulders exceeding 1 m in diameter are present in unit 1. The pick is 60 cm in length.*

Unit 2

Unconformably overlying unit 1 is the bleached to iron-stained, quartz-rich gravel of unit 2 (Fig. 7 and 11). This gravel shows increased alteration towards the upper contact with unit 3, and is a stratified, moderately sorted, clast-supported, cobble-pebble gravel with less than 1% boulders. Unit 2 ranges in thickness from 2.0 to 10 m (Fig. 12). Quartz clasts comprise >70% of the unit. The composition of non-quartz clasts is similar to unit 1 although they exhibit less decomposition (Tempelman-Kluit, 1982). Unit 2 is thickest near the bench rims or proximal to the middle of the paleo-valley (Fig. 7). Unit 2 is equivalent to the 'Bleached Zone' as described by Dufresne *et al.* (1986; Fig. 5) and is part of the lower 'white gravel' subunit of the White Channel Gravel sequence described by McConnell (1907; Fig. 2). At Preido and Dago hills a pronounced weathering gradient is visible at the top of the unit (Fig. 12 and 13). The weathering gradient consists of a 5 m-thick lower zone of oxidation that is overlain by a 1.5 m-thick zone of cemented, bleached, and clay-altered gravel and capped with organic material.



Figure 11. *A close-up view of the sharp contact between unit 1 and unit 2 (lower White Channel Gravel) at Dago Hill (dashed line). Non-quartz clasts are more abundant and are more decomposed in unit 1 compared to unit 2.*

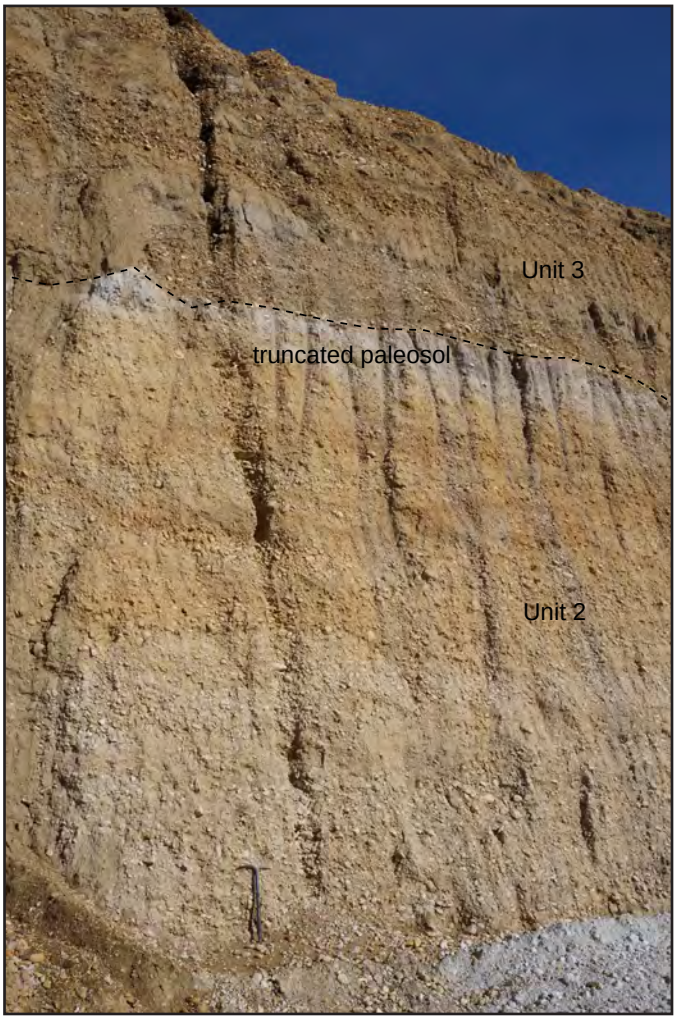


Figure 12. *View of units 2 and 3 (lower and upper White Channel Gravel) at Preido Hill. The paleosol separating the two units is truncated. Where unit 3 erodes completely through the clay-rich horizon in the paleosol, the contact between the units becomes less clear. Pick for scale.*

Unit 3

Unit 3 is 5.3 to 15 m thick and consists of unaltered, planar stratified, iron-stained, cobble-pebble gravel (Fig. 7 and 13). Unit 3 is in unconformable contact with unit 2 and the depth of erosion is variable, based on discontinuous preservation of the weathering gradient in unit 2. On Preido Hill, the contact is wavy and, in many places, erodes completely through the clay-altered zone in unit 2 (Fig. 13). Where the depth of erosion exceeds the clay-altered zone in unit 2, the contact between the two units is less obvious and unit 3 becomes diluted with clasts reworked from unit 2 (Figs. 12 and 13). Lithologically, unit 3 contains less quartz than the previous units. The distribution of unit 3 is similar to unit 2 in that it thins progressively towards the valley sides (Fig. 7). Froese et al. (2000) documented ice wedge casts in this unit and called it the upper White Channel Gravel or the 'yellow gravel' as described by McConnell (1905, 1907; Fig. 2).

Unit 4

Unit 4 is a massive to bedded silt containing organic-rich beds and wood. This material, also referred to as muck, is pervasive throughout the Klondike and often contains massive and disseminated ice (Fig. 9), vertebrate fossils and volcanic ash (Froese *et al.*, 2009). The muck increases in thickness towards the valley sides (Fig. 7).



Figure 13. *Photograph showing the contact between units 2 and 3 at Preido Hill. Unit 2 (lower White Channel Gravel) is highly altered at its upper contact, which is interpreted to be a possible Neogene paleosol. Note the erosional contact between units 2 and 3 (dashed line). Unit 3 (upper White Channel Gravel) contains more silt and sand beds compared to unit 2, which tends to be coarser.*

DISCUSSION

STRATIGRAPHY

The stratigraphy of lower Hunker Creek includes three distinct gravel sequences with consistent lithological composition and unique alteration characteristics (degree of clast decomposition). The gravel sequences are separated by erosional contacts, and units 2 and 3 are inset into unit 1 (Fig. 14).

Unit 1 is interpreted as a predecessor gravel to the White Channel Gravel and is informally referred to as 'Paradise gravel'. The Paradise gravel is defined as a distinct unit on the basis of the following observations: its position in contact with the bedrock strath (Fig. 7); contact relationships with units 2 and 3 (Figs. 7 and 14); fewer quartz clasts relative to unit 2 (Figs. 8 and 11); high gold content; high degree of clast decomposition (Fig. 8); abundance of boulders; and anomalous matrix geochemistry relative to units 2 and 3. Previous studies grouped the Paradise gravel into the lower White Channel Gravel and argued the alteration gradient was a product of hydrothermal alteration or groundwater diagenesis (Dufresne *et al.*, 1986; Lowey, 2001, 2006). However, the degree of clast decomposition in the Paradise gravel is not limited to the bedrock interface, is present where the gravel exceeds 11 m in thickness and occurs near the modern surface (Fig. 9). Importantly, the characteristically high degree of alteration does not extend into unit 2 (or unit 3) and therefore occurred prior to deposition of unit 2 (Fig. 7).

Unit 2 is interpreted to be lower White Channel Gravel (Fig. 14). This unit is inset into the Paradise gravel and its compositional character is likely a reflection of erosion and reworking of the Paradise gravel. McConnell (1907) noted that sand grains in the matrix of the White Channel

Gravel have an angular shape, suggesting limited transport. Reworking of decomposed clasts in the Paradise gravel would cause clast disintegration and a pulse of angular sand grains into the lower White Channel Gravel. Furthermore, destruction of non-quartz lithologies would have a refining effect on the lower White Channel Gravel resulting in a relative enrichment of quartz (resistant) clasts compared to the Paradise gravel (Figs. 11 and 12).

As described previously, the upper contact of the lower White Channel Gravel is marked by a variably eroded weathering gradient containing oxidation, clay alteration, cementation and organics (Fig. 13). This weathering gradient marks a hiatus in gravel sedimentation that allowed weathering and alteration to occur. Dufresne *et al.* (1986) termed this the 'Bleached Zone' and also recognized that the alteration preceded deposition of the overlying 'yellow gravel' (unit 3). Lowey (2001) argued that alteration of the 'Bleached Zone' was a product of weathering and diagenesis due to groundwater flow. Based on the weathering gradient observed at Preido Hill, consisting of organics, a leached zone and a zone of iron enrichment, it appears the alteration may be a product of pedogenesis (Fig. 13). A paleosol within the lower White Channel Gravel has not been suggested previously; however, Lowther *et al.* (2014) argue that a fluvial depositional hiatus may have occurred around this time. They identify an organic-rich lacustrine unit at the contact between the lower and upper White Channel Gravel and suggest it is related to tectonic process, such as back-tilting, causing a fluvial shut-down. Alternatively, a change in sedimentation could reflect fluvial responses to climate change.

The final phase of White Channel Gravel sedimentation is marked by unit 3, interpreted to be the upper White Channel Gravel or 'yellow gravel' (Figs. 13 and 14).

GOLD DISTRIBUTION

Detailed studies into the distribution of gold in the Paradise gravel were not completed as part of this study. General information gathered from placer miners indicates the target placer deposit at Paradise, Preido and Dago hills is the lowermost gravel at the bedrock contact (Paradise gravel). The pay channels reflect high energy conditions, marked by an abundance of subrounded to rounded quartz boulders in channels that are cut into bedrock (pers. comm., Moonlight Mining Ltd., 2015; Fig. 10). Lower grade placer concentrations occur marginally to these channels and can be economic. According to historic records, the 'heavy pay channel' in a yellow-stained gravel

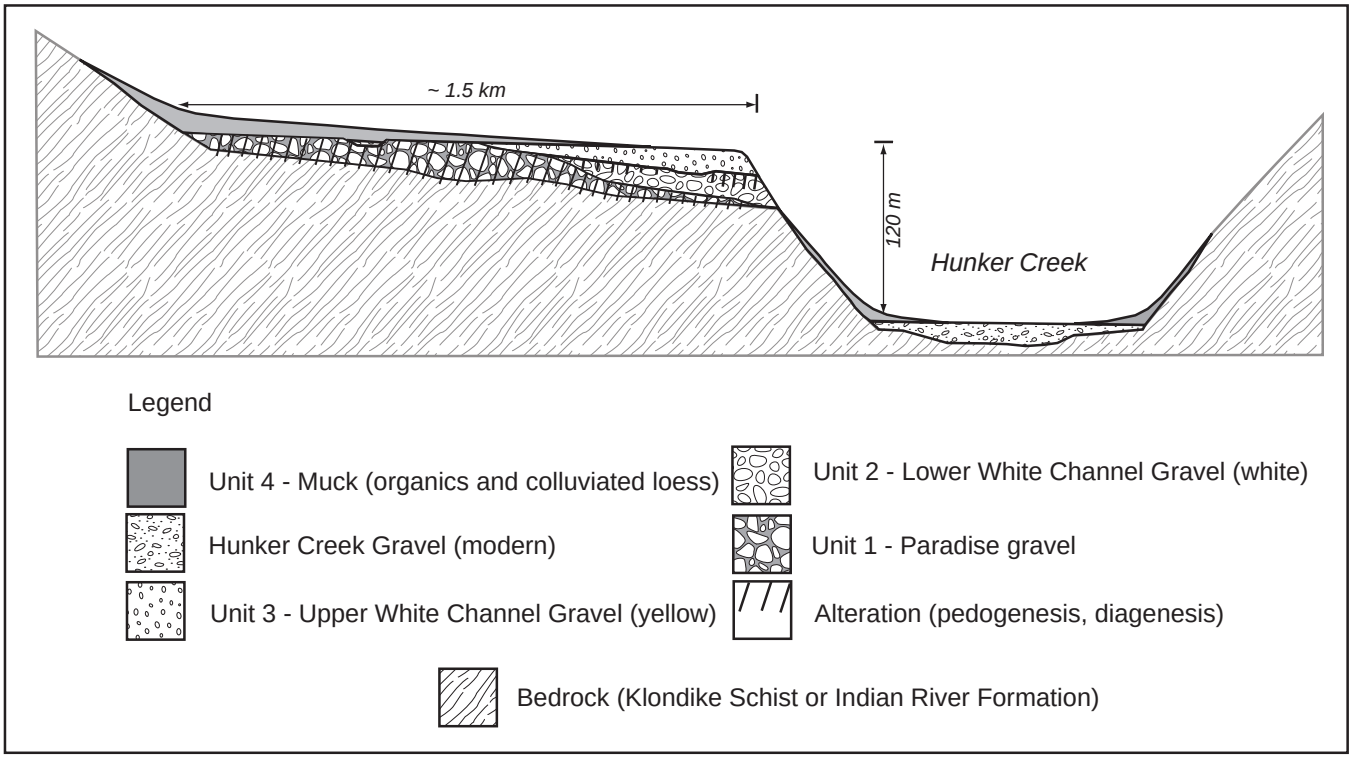


Figure 14. *An idealized cross-section (view downstream) for lower Hunker Creek depicting the Neogene stratigraphy. Note: units 2 and 3 (upper and lower White Channel Gravel) are inset into the Paradise gravel (unit 1).*

on Paradise Hill measured 50-150 m wide and 6 m thick suggesting a large channel was responsible for its deposition (Yukon Gold Company, 1913). In terms of pay thickness and modern mining, the entire 11.5 m section of Paradise gravel at Paradise Hill is processed. Locally, zones of gold enrichment occur at the upper contact with the overlying muck (Fig. 7); this is likely related to past surface weathering of the Paradise gravel and winnowing of decomposed clasts by intermittent surface runoff. At Paradise Hill, McConnell (1907) noted that there was a zone of gold enrichment on an undulating surface of siliceous gravel. This enrichment was likely emplaced when the lower White Channel Gravel incompletely eroded through the Paradise gravel and deposited a lag of placer gold. At Dago Hill, McConnell (1907) noted an important coarse gold channel on or near bedrock. This supports the economic significance of the Paradise gravel and that the White Channel Gravel is only economically enriched where it sufficiently reworks auriferous Paradise gravel.

Gold anomalies may not be the only elemental differences between the White Channel Gravel and the Paradise gravel. Dufresne *et al.* (1986) analyzed the 'Iron Zone' gravel (Paradise gravel) and concluded there were anomalous concentrations of Fe, Mn, As, Sb, Hg, Co, Ba and S within the matrix. A near-surface hydrothermal origin for the enrichment was suggested; however, these values could also reflect lithological differences associated with basin bedrock geochemistry at the time of deposition. In other words, the Paradise gravel may have been eroding bedrock containing more gold and associated pathfinder elements. However, Dufresne (1987) attempted to address this by comparing rhyolite and mica schist cobbles from different zones and concluded there were no noticeable geochemical changes. Given the decomposed nature of the Paradise gravel, his analyses may have only targeted competent clasts and ignored the decomposed lithologies. A reassessment of the clast geochemistry is recommended in order to evaluate the basin bedrock geochemistry at the time of Paradise gravel emplacement. In addition, the geochemistry of the newly mapped Indian River Formation on Paradise and Preido hills should be assessed to understand its contribution to the geochemistry of the Paradise gravel.

FLUVIAL GEOLOGY

Adding a pre-White Channel Gravel sedimentation event to the fluvial geomorphology of the Klondike has implications for placer reserves. Sedimentological studies used to reconstruct a paleoenvironment were largely focused on the upper and lower White Channel Gravel (Morison, 1985; Morison and Hein, 1987; Lowther *et al.*, 2014). The confined braided river system-model proposed for the White Channel Gravel does not necessarily apply to the Paradise gravel. Likewise, architectural element analysis completed by Lowther *et al.* (2014), while useful for characterizing the White Channel Gravel, does not address the sedimentology of the Paradise gravel. The stratigraphic reinterpretation presented here indicates that there is very little known about the river system responsible for eroding the bedrock strath and emplacing the primary placers. In particular, knowledge of channel morphology, such as width, sinuosity and number of channels has important implications for placer gold distribution.

Paradise gravel sedimentation was probably not localized at Hunker Creek. The paleovalley of lower Hunker Creek is exceptionally wide, which may have permitted stratigraphic preservation towards the valley margins. The apparent absence of Paradise gravel in Bonanza, Quartz, upper Hunker or Dominion creeks may be due to more complete reworking within these narrower valleys. Also, exposure of the lowermost gravel on the lower Bonanza Creek benches is limited in the current mining cuts. Exposures of the pay channel on the Quartz Creek bench and Gold Hill (Bonanza Creek at the mouth of Eldorado Creek) in 2015 contained relatively unaltered gravel; however, at both localities there was an abundance of subrounded quartz boulders similar to those documented in the Paradise gravel on Hunker Creek. These boulders, and a component of the placer gold, may be a residual feature of a reworked Paradise gravel.

Reworking of the Paradise gravel by the streams that deposited the White Channel Gravel, and the effect this would have on redistributing the placer gold, is poorly understood. McConnell (1907) touched on the topic of gold distribution resilience to reworking when he documented the complementary relationship between the creek and hill pay channels, despite 50-100 m of vertical incision separating the pay channels. This observation suggests that reworking may not completely destroy gold distribution patterns established during earlier emplacement events. Therefore, where the lower White Channel Gravel has completely reworked the Paradise Gravel, the gold distribution may still reflect the Paradise fluvial system. This concept of gold distribution resilience to reworking should be considered when conducting future sedimentological studies of placer deposits.

PEDOGENIC ALTERATION

Long periods of weathering and uplift were responsible for liberation of the gold-bearing veins into the Klondike fluvial environment (Morison and Hein, 1987). Our current knowledge of these weathering environments is limited, mainly because paleo-environmental information is poorly preserved. For example, no Neogene paleosols are preserved on the Klondike upland slopes due to Quaternary and Holocene periglacial weathering (Bond and Sanborn, 2006). Lowther *et al.* (2014) and Pound *et al.* (2015) provide a paleo-flora reconstruction from the middle of the White Channel Gravel sequence that suggests a much warmer climate during the Neogene. Confirmation that alteration at Paradise, Preido and Dago hills is a product of pedogenesis would present a unique opportunity to understand the interactions between Neogene climate and the fluvial, hillslope, and weathering processes that contribute to the placer emplacement and distribution.

AGE IMPLICATIONS

Paradise gravel is older than the lower White Channel Gravel, which in turn is poorly constrained to mid-Pliocene based on biostratigraphy of one pollen sample (Froese *et al.*, 2000). Accurate placement of the sample within the lower White Channel Gravel is challenging due to the cut and fill relationship between the upper and lower White Channel Gravel. A good example of this was described at Preido Hill where the lower White Channel Gravel is variably eroded by the upper White Channel Gravel. The contact between the two units is obvious where the clay-rich weathering zone is not eroded; however, if the clay altered zone is eroded then the contact between the two units is less clear (Fig. 12). For these reasons, it is possible that the pollen sample was collected within the upper White Channel Gravel and does not reflect a lower White Channel Gravel vegetation assemblage. Pound *et al.* (2015) describe a pollen assemblage from the contact between the lower and upper White Channel Gravel in upper Bonanza Creek as being similar to Late Pliocene environments from Alaska. This study adds further confirmation that the upper White Channel Gravel is Late Pliocene and is a minimum age for the lower White Channel Gravel. Additional pollen samples should be collected from the lower White Channel Gravel in sections where the contact relationships are clearly preserved. Similarly, samples for pollen analyses should be collected from the Paradise gravel. Additional studies using Terrestrial Cosmogenic Nuclides or weathering geochronology may provide an alternative technique to derive an age for the Paradise gravel.

SUMMARY

A stratigraphic reanalysis of the high-level gravel deposits on lower Hunker Creek show that a highly altered gravel is much more extensive on the bench surface than previously recognized. This gravel is responsible for eroding the bedrock strath and pre-dates the deposition of the White Channel Gravel. It is informally termed 'Paradise gravel'. Alteration of the Paradise gravel, possibly due to pedogenesis, preceded erosion and deposition of the White Channel Gravel, which facilitated the enrichment in quartz clast content in the lower White Channel Gravel. Primary gold concentrations on lower Hunker Creek bench surfaces are contained within Paradise gravel and are reworked into lower White Channel Gravel when erosion is sufficiently deep. Preservation of Paradise gravel may be due to the width of the Neogene valley at this location. Elsewhere in the Klondike, valleys are narrower, and were more likely to experience complete re-working of the primary Paradise gravel deposits.

A second alteration zone within the lower White Channel Gravel may represent a paleosol that formed prior to deposition of the upper White Channel Gravel. This period of quiescence is potentially correlative with the fluvial shut-down model proposed by Lowther *et al.* (2014). Paleosol studies are recommended as an important next step to understand whether or not surface weathering has affected these deposits. Identification of a paleosol would be significant for understanding Neogene paleo-climates in Yukon.

The paleo-river systems that deposited the Paradise gravel are poorly understood. Previous sedimentological studies have focused on the upper and lower White Channel Gravel, which typically have better exposure. Future exploration for undiscovered pay channels on the high-level benches in wide Klondike valleys will benefit from increased understanding of the Paradise gravel fluvial system. In addition, placer gold distribution within the Paradise gravel should be evaluated as thicker gravel sequences are exposed.

ACKNOWLEDGEMENTS

Advancing our geological understanding of placer deposits in Yukon depends on relationships with the placer miners. This research benefited from site access and knowledge shared by Tony and Minnie Beets (Tamarack Inc. – Paradise Hill), Kyle Bruce (Moonlight Mining Ltd. – Preido Hill), Neil Loveless and Lisa Favron (Favron Ent. – Dago Hill) and Don Ruman (Gold Hill). Appreciation is also owed to Stuart Schmidt (Schmidt Mining - Quartz Creek) for encouraging me on this Neogene stratigraphic tangent. Thank you to Alberto Reyes (University of Alberta) and Kristen Kennedy (YGS) for providing valuable technical feedback on this manuscript. Additional editorial improvements and layout were completed by Monica Nordling and Karen MacFarlane (YGS). Field tripping with Jim Mortensen (UBC) and Jim Ryan (GSC) on Paradise Hill helped identify new exposures of Indian River Formation. Finally, conversations with Sydney van Loon (YGS) on Paradise Hill helped confirm that the Paradise gravel is something different.

REFERENCES

Ager, T.A., Matthews Jr., J.V. and Yeend, W., 1994. Pliocene terrace gravels of the ancestral Yukon River near Circle, Alaska: Palynology, paleobotany, paleoenvironmental reconstruction and regional correlation. Quaternary International, vol. 22-23, p. 185-206.

Bond, J.D. and Sanborn, P.T., 2006. Morphology and geochemistry of soils formed on colluviated weathered bedrock: Case studies from unglaciated upland slopes in west-central Yukon. Yukon Geological Survey, Open File 2006-19, 70 p.

Chapman, R.J., Mortensen, J.K., Crawford, E.C. and LeBarge, W.P., 2010. Microchemical Studies of Placer and Lode Gold in the Klondike District, Yukon, Canada: 2. Constraints on the Nature and Location of Regional Lode Sources. Economic Geology, vol. 105, p. 1393-1410.

Dufresne, M.B., 1987. Origin of gold in the White Channel sediments of the Klondike region, Yukon Territory. Unpublished MSc thesis, University of Alberta, Edmonton, Alberta, 181 p.

Dufresne, M.B. and Morison, S.R., 1985. Stratigraphy and alteration of the White Channel Gravel at Dago Hill, a progress report, Klondike area, Yukon. *In:* Yukon Exploration and Geology 1983, Exploration and Geological Services Division, Yukon Region, Indian and Northern Affairs Canada, p. 55-59.

Dufresne, M.B., Morison, S.R. and Nesbitt, B.E., 1986. Evidence of hydrothermal alteration in the White Channel sediments and bedrock of the Klondike area, west-central Yukon. *In:* Yukon Geology Volume 1. Exploration and Geological Services Division, Yukon Region, Indian and Northern Affairs Canada, p. 44-49.

Froese, D.G., Barendregt, R.W., Enkin, R.J. and Baker, J., 2000. Paleomagnetic evidence for multiple Late Pliocene – Early Pleistocene glaciations in the Klondike area, Yukon Territory. Canadian Journal of Earth Science vol. 37, p. 863-877.

Froese, D.G., Zazula, G.D., Westgate, J.A., Preece, S.J., Sanborn, P.T., Reyes, A.V. and Pearce, N.J.G., 2009. The Klondike goldfields and Pleistocene environments of Beringia. GSA Today, vol. 19, p. 4-10.

Froese, D.G. and Jackson, L.E., Jr., 2005. Surficial Geology, GRAND FORKS, Yukon Territory. Geological Survey of Canada, Open File 4591, scale 1:50 000.

Gleeson, C.F., 1970. Heavy mineral studies in the Klondike area, Yukon Territory. Geological Survey of Canada, Bulletin 173, 60 p.

Hidy, A.J., Gosse, J.C., Froese, D.G., Bond, J.D. and Rood, D.H., 2013. A latest Pliocene age for the earliest and most extensive Cordilleran Ice Sheet in northwestern Canada. Quaternary Science Reviews, vol. 61, p. 77-84.

Knight, J.B., Mortensen, J.K. and Morison, S.R., 1994. Shape and composition of lode and placer gold from the Klondike district, Yukon, Canada. Exploration and Geological Services Division, Yukon Region, Indian and Northern Affairs Canada, Bulletin 3, 142 p.

Knight, J.B., Mortensen, J.K. and Morison, S.R., 1999. Lode and placer gold composition in the Klondike District, Yukon, Canada: Implications for the nature and genesis of Klondike placer and lode gold deposits. Economic Geology, vol. 94, p. 649-664.

Lowther, R.I., Peakall, J., Chapman, R.J. and Pound, M.J., 2014. A four stage evolution of the White Channel gravel: Implications for stratigraphy and palaeoclimates. *In:* Yukon Exploration and Geology 2013, K.E. MacFarlane, M.G. Nordling, and P.J. Sack (eds.), Yukon Geological Survey, p. 109-118.

Lowey, G.W., 2001. White Channel Alteration: Paradise Hill. *In:* Field Guide to Quaternary Research in Central and Western Yukon Territory, D.G. Froese, A. Duk-Rodkin and J.D. Bond (eds.), Heritage Branch, Government of the Yukon, Occasional Papers in Earth Sciences no. 2, p. 63-64.

Lowey, G.W., 2002. White Channel Gravel alteration revisited. *In:* Yukon Exploration and Geology 2001, D.S. Emond, L.H. Weston and L.L. Lewis (eds.), Exploration and Geological Services Division, Yukon Region, Indian and Northern Affairs Canada, p. 147-162.

Lowey, G.W., 2004. Placer Geology of the Stewart River (115N&O) and part of the Dawson (116B&C) map areas, west-central Yukon, Canada. Yukon Geological Survey Bulletin 14, Yukon Geological Survey, 275 p.

Lowey, G.W., 2006. The origin and evolution of the Klondike goldfields, Yukon, Canada. Ore Geology Reviews, vol. 28, p. 431-450.

McConnell, R.G., 1905. Report on the Klondike gold fields. Geological Survey of Canada, Annual Report, part B, vol. 14, p. 1-71.

McConnell, R.G., 1907. Report on gold values in the Klondike high level gravels. Geological Survey of Canada, Report no. 979, 34 p.

McKenna, K.M. and Lipovsky, P.S., 2014. Surficial geology, Dawson Region, Yukon, parts of NTS 115O/14 & 15 and 116B/1, 2, 3, & 4. Yukon Geological Survey, Open File 2014-12, 1:25000 scale.

Morison, S.R., 1985. Sedimentology of White Channel Gravels, Klondike area, west-central Yukon. Unpublished MSc thesis, University of Alberta, Edmonton, Alberta, 149 p.

Morison, S.R. and Hein, F.J., 1987. Sedimentology of the White Channel Gravels, Klondike area, Yukon Territory: fluvial deposits of a confined valley. *In:* Recent developments in fluvial sedimentology, F.G. Ethridge, R.M Flores, and M.D. Harvey (eds.). Society of Economic Paleontologists and Mineralogists, Special Publication 39, p. 205-215.

Mortensen, J.K., Chapman, R., LeBarge, W. and Jackson, L., 2005. Application of the placer and lode geochemistry to gold exploration in western Yukon. *In:* Yukon Exploration and Geology 2004, D.S. Emond, L.L. Lewis and G.D. Bradshaw (eds.), Yukon Geological Survey, p. 205-212.

Pound, M.J., Lowther, R.I., Peakall, J., Chapman, R.J. and Salzmann, U., 2015. Palynological evidence for a warmer boreal climate in the Late Pliocene of the Yukon Territory, Canada. Palynology, vol. 39, p. 91-102.

Tempelman-Kluit, D.J., 1982. White Channel Gravel of the Klondike. *In:* Yukon Exploration and Geology 1981, Exploration and Geologic Services Division, Yukon Region, Indian and Northern Affairs Canada, p. 74-79.

Van Loon, S. and Bond, J.D. (compilers), 2014. Yukon Placer Mining Industry 2010-2014. Yukon Geological Survey, p. 230.

Westgate, J.A., Sandhu, A.S., Preece, S.J. and Froese, D.G., 2003. Age of the gold-bearing White Channel Gravel, Klondike district, Yukon. *In:* Yukon Exploration and Geology 2002, D.S. Emond and L.L. Lewis (eds.), Exploration and Geological Services Division, Yukon Region, Indian and Northern Affairs Canada, p. 241-250.

White, J.M., Ager, T.A., Adam, D.P., Leopold, E.B., Liu, G., Jetté, H. and Schweger, C.E., 1999. Neogene and Quaternary quantitative palynostratigraphy and paleoclimatology from sections in Yukon and adjacent Northwest Territories and Alaska. Geological Survey of Canada, Bulletin 543, 30 p.

Yukon Gold Company, 1913. Extension of Heavy Pay Channel on Paradise Hill. Yukon Gold Company map 4222. National Archives of Canada file 011079585.

Preliminary results on the Middle Triassic-Middle Jurassic stratigraphy and structure of the Teslin Mountain area, southern Yukon

E. Bordet[1]
Yukon Geological Survey

Bordet, E., 2016. Preliminary results on the Middle Triassic-Middle Jurassic stratigraphy and structure of the Teslin Mountain area, southern Yukon. *In:* Yukon Exploration and Geology 2015, K.E. MacFarlane and M.G. Nordling (eds.), Yukon Geological Survey, p. 43-61.

ABSTRACT

Stratigraphic and structural relationships within Stikinia, and overlap assemblages of the Whitehorse trough, are investigated in the Teslin Mountain area, southern Yukon. The Middle Triassic Joe Mountain Formation is dominated by a thick sequence of aphyric basalt produced by subaqueous volcanism. The Upper Triassic Lewes River Group displays complex lateral and vertical lithological and facies changes. It illustrates synvolcanic terrane exhumation, with erosion of the volcanic upland leading to deposition of thick volcaniclastic sequences, in parallel with ongoing clastic and carbonate sedimentation in marginal basins. Unravelling the Lewes River Group stratigraphy is critical in understanding the latest stages of Stikinia arc volcanism and the onset of Whitehorse trough marine sedimentation in the Early-Middle Jurassic. Further mapping and analytical work will focus at characterizing the Joe Mountain Formation and Lewes River Group, to determine how Stikinia evolved prior to final amalgamation of the Intermontane terranes with North America.

[1]*esther.bordet@gov.yk.ca*

INTRODUCTION

The Teslin Mountain area, northeast of Whitehorse (NTS 105E/2; Fig. 1) is underlain by volcano-sedimentary rocks that are considered to be part of Stikinia, the largest of the Intermontane terranes in the Canadian Cordillera. In particular, the Middle Triassic Joe Mountain Formation (JMF; Hart, 1997) and the Upper Triassic Lewes River Group (LRG; Bostock and Lees, 1938; Lees, 1934; Tempelman-Kluit, 1984, 2009; Tozer, 1958; Wheeler, 1961) are the focus of this paper. These units are overlain by up to 3000 m of sedimentary strata of the Lower to Middle Jurassic Laberge Group, which defines the Whitehorse trough (Fig. 1; White *et al.*, 2012).

Triassic volcanic rocks are rare in the Cordillera. JMF rocks constitute a unique and geographically restricted occurrence in Yukon (Hart, 1997). The base of the JMF is not exposed, its terrane affiliation is unclear, and the transition from the JMF to LRG and their overall relationship are uncertain (Hart, 1997). Both the JMF and LRG comprise an assemblage of subaqueous basalt, volcaniclastic and sedimentary rocks. However, the basaltic portion of both units displays distinctive field, petrographic and geochemical characteristics (detailed below). In British Columbia (BC), arc volcanism within Stikinia is represented by the Upper Triassic Stuhini Group (*e.g.*, Souther, 1971) and Takla Group (*e.g.*, Monger, 1977), and the Lower to Middle Jurassic Hazelton Group (*e.g.*, Tipper and Richards, 1976). Overall, arc volcanism within the Intermontane terranes is younger in BC than in Yukon.

Bedrock mapping (1:50 000 scale) in the Teslin Mountain area was initiated during the summer of 2015 as part of a multi-year project that will investigate: (1) the relationship between the JMF and LRG, and their uncertain link with Stikinia; (2) the diachronous timing of arc volcanism in Stikinia between southern Yukon and BC; (3) the setting and nature of Triassic volcanism with respect to the development of the Whitehorse trough in Early-Middle Jurassic; and (4) the age and nature of deformation affecting strata that underlie or fill the Whitehorse trough. This study builds upon existing maps, geological datasets and previously recognized stratigraphic relationships. Early reconnaissance geological mapping (1:2 500 000 scale) was conducted by the Geological Survey of Canada around Whitehorse (NTS 105D; *e.g.*, Wheeler, 1961), and east of Lake Laberge (Fig. 1; NTS 105E; Bostock and Lees, 1938; Lees, 1934; Tempelman-Kluit, 1984, 2009; Tozer, 1958). Mapping at 1:50 000 scale (105D/2,3,6,11: Hart and Radloff, 1990; 105D/13-16: Hart and Hunt, 1994, 1995) was integrated with isotopic and biostratigraphic dates, and supports the currently used stratigraphic framework and nomenclature for Stikinia and overlap assemblages present in this region (Hart, 1997; *see* below).

This paper reports on the most recent field observations from the Teslin Mountain area, and proposes preliminary interpretations of the stratigraphic and structural relationships within the Middle to Upper Triassic volcanic sequence. A brief review of the tectonic setting and geology of southern Yukon is followed by detailed lithologies for the JMF, LRG and Laberge Group, as well as Middle and Late Cretaceous plutonic and volcanic rocks. A sedimentary sequence was identified that may constitute the base of the JMF mafic volcanic and volcaniclastic rocks at Teslin Mountain. The internal stratigraphy within the LRG is complex, and characterized by lateral and vertical facies variations. In the central part of the map area, a sedimentary sequence that underlies a mafic volcaniclastic package is inferred to represent the base of the LRG. Thick limestone beds, scattered across the map area and regionally across the Whitehorse trough may represent distinct episodes of carbonate sedimentation during the Late Triassic (*e.g.*, Lees, 1934; Tozer, 1958). Projected detailed mapping of these prominent strata will help refine stratigraphic relationships within the LRG, as well as constrain deformation of pre, syn and post-Whitehorse trough deformation.

TECTONIC SETTING

The Intermontane terranes underlie most of southern Yukon and BC southwest of the Tintina fault (Fig. 1). They represent the largest amalgamation of crustal fragments that accreted to the North American margin during the Mesozoic (Coney *et al.*, 1980). In Yukon, the outer margin of the Intermontane terranes is defined by Middle Paleozoic metasedimentary and metavolcanic rocks of the Yukon-Tanana terrane (Fig. 1; Mortensen and Jilson, 1985; Mortensen, 1992). The core and bulk of the Intermontane terranes comprise Mesozoic volcanic arc rocks of Stikinia and Quesnellia (Fig. 1; Colpron and Nelson, 2011; Wheeler *et al.*, 1991), which are juxtaposed along the Teslin fault north of Whitehorse (Fig. 1). Upper Paleozoic accretionary complex rocks of the Cache Creek terrane (*e.g.*, Monger *et al.*, 1991; Struik *et al.*, 2001) are surrounded by Stikinia and Quesnellia (Fig. 1) and extend south of Whitehorse to northern British Columbia. So far, Cache Creek rocks have not been recognized north of Whitehorse (Bickerton *et al.*, 2013), and the Teslin Mountain area is inferred to be underlain by Stikinia.

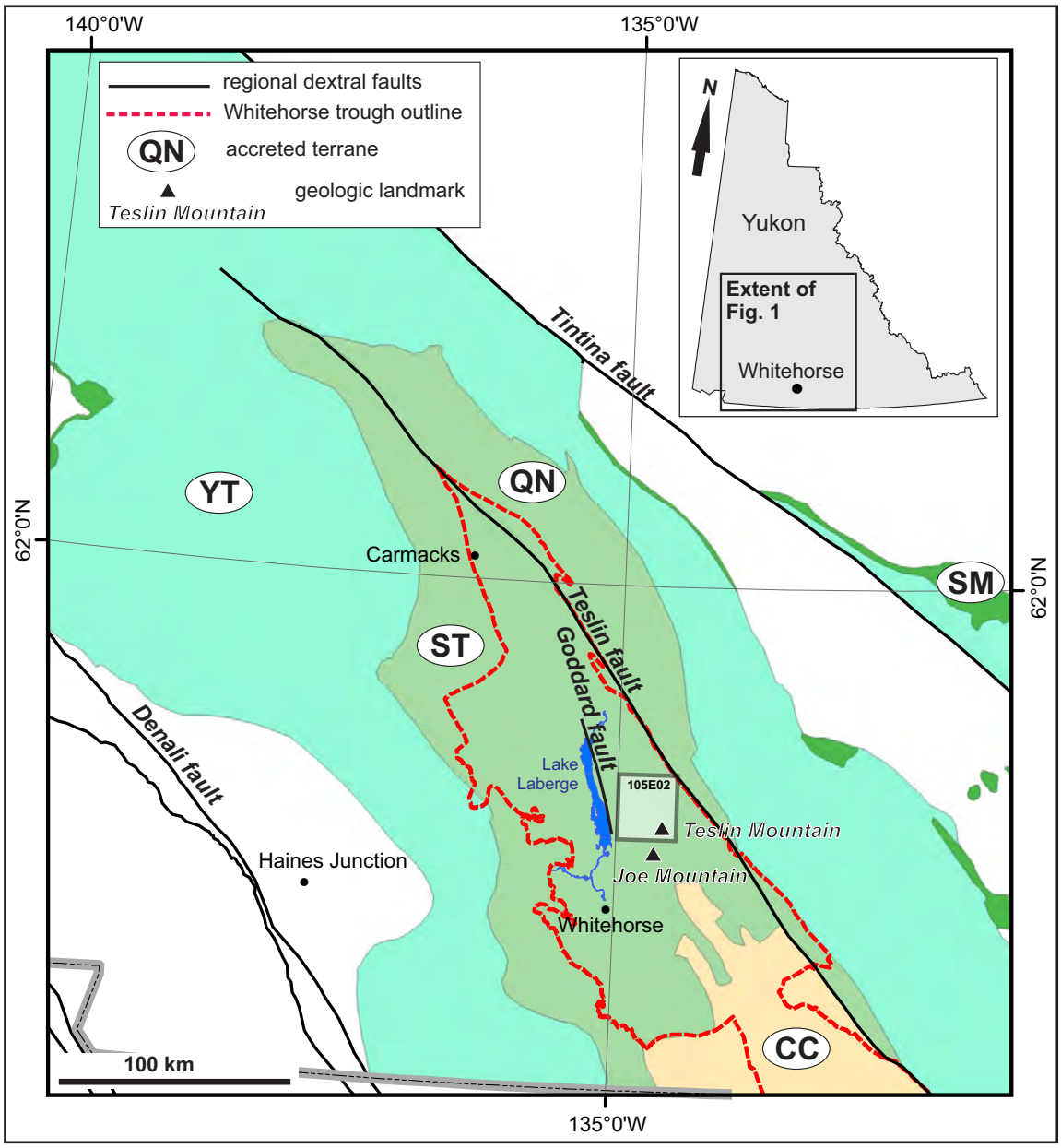


Figure 1. *Tectonic assemblage map of south-central Yukon. Intermontane terranes are ST: Stikinia, QN: Quesnellia; CC: Cache Creek, YT: Yukon-Tanana; and SM: Slide Mountain. Yukon inset map shows figure extent in square. Grey outline on figure is Teslin Mountain area (105E02). Terrane boundaries after Colpron and Nelson (2011). Whitehorse trough outline after Hutchison (pers. comm.).*

The Middle Triassic JMF and Upper Triassic LRG record arc volcanism and arc-related basin sedimentation along the North American margin in the Mesozoic (Hart, 1997). JMF sub-alkalic basalt and basaltic andesite display an iron-enriched tholeiitic signature, typical of island arc tholeiite and mid-ocean ridge basalt (Hart, 1997). The LRG mafic sequence comprises pyroxene-phyric, calc-alkaline, high-K basalt typical of island arc settings (Hart, 1997). The extensive volcaniclastic component part of the LRG (Hart, 1997; Tempelman-Kluit, 1984, 2009) suggests high rates of erosion of the arc related to exhumation and uplift of the Intermontane terranes following accretion.

Deposition of up to 3000 m of sediments of the Laberge Group (*e.g.*, Wheeler, 1961; White *et al.*, 2012) took place in the Whitehorse trough (Fig. 1) from the Early to Middle Jurassic. The Whitehorse trough extends about 650 km from Dease Lake in BC to north of Carmacks in central Yukon (Colpron *et al.*, 2015; White *et al.*, 2012).

The basin records deposition in a forearc setting, as a result of subduction of the Cache Creek ocean beneath Stikinia (Lewes River Arc) and Quesnellia in the Mesozoic (Colpron *et al.*, 2015; White *et al.*, 2012). The Whitehorse trough evolved as a northwest trending, synorogenic, intermontane piggy-back transpressional basin by Middle Jurassic (White *et al.*, 2012).

REGIONAL STRATIGRAPHY

The Teslin Mountain area is underlain by three major rock assemblages: the Middle Triassic JMF and Upper Triassic LRG are inferred to be part of Stikinia (Fig. 2), and are overlain by the Lower to Middle Jurassic Laberge Group. Other overlap assemblages include Early-Middle Cretaceous Open Creek volcanic rocks, and intrusive bodies related to the Teslin and Whitehorse plutonic suites (Fig. 2).

The JMF includes a sequence of Middle Triassic (Ladinian) pillow basalt, clastic and calcareous sedimentary rocks, microdiorite, diabase and gabbro, originally defined by Hart (1997) at Joe Mountain (type section) and Mount Byng (NTS 105D/15,16). The JMF may unconformably overlie the Upper Paleozoic Takhini assemblage (Fig. 2), a package of deformed and metamorphosed mafic volcanic rocks that constitute the base of Stikinia in southern Yukon (Hart, 1997); however this relationship is not documented. The JMF shows lithological similarities with some Cache Creek terrane rocks in southern Yukon, but the detrital link between the JMF and the Whitehorse trough supports an origin within Stikinia (Hart, 1997).

Volcanic, clastic and carbonate rocks of the Upper Triassic LRG regionally overlie the JMF, but the relationship between the two is uncertain (Fig. 2; Hart, 1997). Tozer (1958) conducted mapping northeast of Lake Laberge and built upon the first stratigraphic framework established by Lees (1934) and Bostock and Lees (1938), and introduced seven formations: four massive or bedded limestone units, interbedded with volcaniclastic and mixed volcano-sedimentary units. Wheeler (1961) mapped the Whitehorse area, south of Lake Laberge, and divided the LRG into three belts to reflect lateral changes in lithology from west to east: at the base of the sequence to the west, a coarse-grained, mixed sedimentary and volcaniclastic unit occurs, and finer, more clastic lithologies are mapped to the east; the highest stratigraphic levels seem to be dominated by limestone across the three belts. The complex stratigraphy of the LRG emphasizes important lateral facies changes across southern Yukon. The latest stratigraphic framework for the LRG introduces five lithological units grouped in two formations (Hart 1997; Tempelman-Kluit, 1984, 2009):

- The Povoas Formation, comprises aphyric to pyroxene phyric basalt and volcanic breccia, geochemically distinguished from the underlying JMF by island arc calc-alkaline geochemical characteristics (Hart, 1997).
- The Aksala Formation, comprises greywacke-shale with thick limestone lenses, and is divided into four members that variably overlie the Povoas Formation: the Casca, Hancock, Mandanna (Tempelman-Kluit, 1984) and Sheldon members (Hart, 1997). The Casca Member is lithologically heterogenous and includes a variety of calcareous siltstone, argillite, sandstone and conglomerate. The Sheldon Member comprises conglomerate, and minor sandstone and limy siltstone, and is only reported at one locality (Hart, 1997). The Hancock Member comprises thick beds of massive to bedded limestone that form a northeast trending belt east of Lake Laberge. The Mandanna Member comprises well-bedded or massive, red and green weathering greywacke and volcanic sandstone, and is mainly observed west of Lake Laberge.

The LRG is overlain by the Lower to Middle Jurassic Laberge Group (Fig. 2), but the nature of the contact is uncertain (unconformable contact: Cairnes, 1910; Lowey, 2004, 2005, 2008; Lowey *et al.*, 2009; conformable contact: Bostock and Lees, 1938; Hart, 1997; Tempelman-Kluit, 1984). The Laberge Group corresponds to deltaic and deep marine sedimentation in the Whitehorse trough from the Early to Middle Jurassic, following shallow-water, arc-related deposition of the Upper Triassic LRG strata (Colpron *et al.*, 2015; White *et al.*, 2012). Stratigraphy of the Laberge Group includes shallow marine to fluvial and coal bearing sandstone, conglomerate and shale deposits of the Tanglefoot Formation exposed north of the trough (Hart, 1997; Lowey, 2004, 2008; Tempelman-Kluit, 1984, 2009), laterally partially equivalent to deep marine turbidite and mass-flow conglomerate successions of the Richthofen Formation mapped south of the trough (*e.g.*, Lowey, 2005; Tempelman-Kluit, 1984, 2009). The Nordenskiold Formation, a distinct crystal-lithic tuff (Tempelman-Kluit, 1984, 2009), occurs at multiple stratigraphic levels in both the Richthofen and Tanglefoot formations, and represents three volcanic events between 188 and 186 Ma (Colpron and Friedman, 2008).

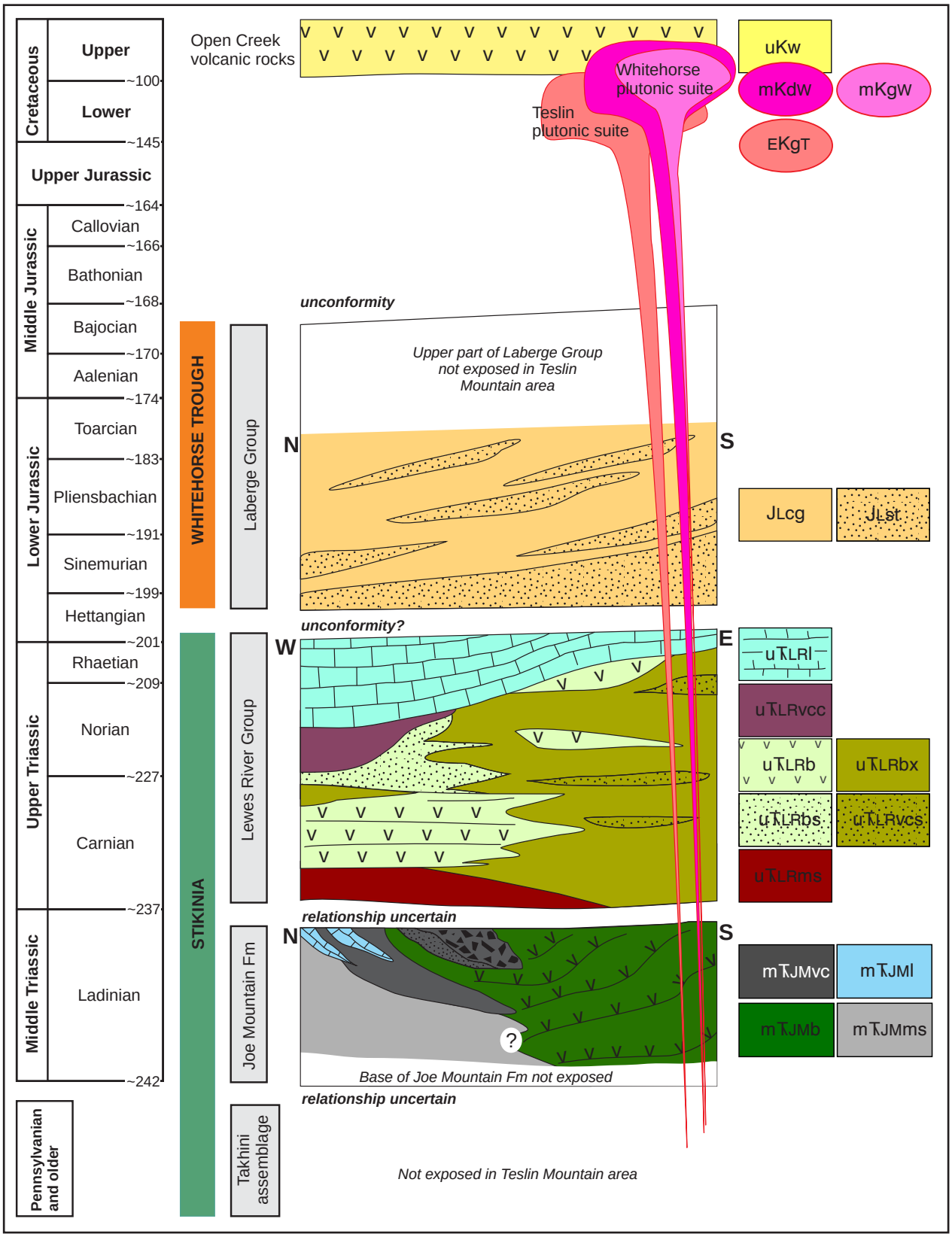


Figure 2. *Schematic stratigraphic relationships in the Teslin Mountain area based on summer 2015 mapping. See Fig. 3 for legend and description of map unit codes. Whitehorse trough extent after White et al. (2012). Stratigraphic age scale after Cohen et al. (2013; updated).*

The Middle Jurassic to Lower Cretaceous Tantalus Formation disconformably overlies the Laberge Group (*e.g.,* Tempelman-Kluit, 1984, 2009). This coal-bearing sequence of fluvial chert-pebble conglomerate and sandstone marks the end of deposition in the Whitehorse trough (White *et al.*, 2012).

STIKINIA STRATIGRAPHY

JOE MOUNTAIN FORMATION (MIDDLE TRIASSIC)

Aphyric basalt, and lesser volcanic breccia, mafic tuff and sedimentary rocks underlie high ridges and peaks near Teslin Mountain in the south and southeast of the mapped area, with a spatial extent of 6 by 16 km (Fig. 3). This sequence constitutes the geological continuity of the type section of the Middle Triassic JMF exposed at Joe Mountain about 13 km to the southeast (Hart and Hunt, 1994; Hart, 1997).

Four map units represent the JMF in the Teslin Mountain area (Figs. 2 and 3): (1) dark grey-green aphyric basalt (mTJMb); (2) a volcaniclastic sequence including chaotic volcanic conglomerate, mafic tuff and volcanic sandstone (mTJMvc); (3) a south dipping sedimentary sequence including carbonate rocks (mTJMl); (4) clastic mudstone/sandstone (mTJMms). Relationships between these map units are locally constrained, but interfingering and lateral facies variations are frequent (Fig. 2). To the north, the clastic sedimentary sequence is in erosional or structural unconformable contact with Upper Triassic volcaniclastic strata of the LRG (Fig. 3). West of Teslin Mountain, the JMF is inferred to be conformably overlain by north dipping sedimentary strata of the LRG (Fig. 3). East of the map area, JMF basalt is in contact with the Lower Jurassic Laberge Group along the Open Creek fault. Several large intrusions crosscut the JMF basalt, including an Early Cretaceous granodioritic intrusion of the Teslin Plutonic Suite in the south (EKgT), and Middle Cretaceous granodiorite to monzodiorite of the Whitehorse Suite in the east (mKgW; Fig. 3).

The thickness of the JMF is estimated at ~3000 m, including a ~1000 m thick sedimentary sequence to the north, and a cumulated thickness of 2000-2300 m for the basalt and volcaniclastic sequence. Previous thickness estimates indicate at least 3200 m for the JMF type section at Joe Mountain (Hart, 1997).

Coherent basalt (mTJMb)

Grey to rusty-brown weathering, dark grey-green, fine to medium-crystalline, amygdaloidal or vesicular aphyric basalt constitutes the dominant lithology of the JMF at Teslin Mountain. It occurs as thick-bedded (up to 1-2 m), blocky, massive to pillowed lava flows (Fig. 4a). Phenocrysts include plagioclase (up to 5%) and minor pyroxene crystals or cumulates. Coherent basalt is locally finely vesicular or amygdaloidal, and in places interbedded with autobrecciated basalt. Chlorite alteration, quartz or carbonate veinlets and disseminated pyrite (1% or less) are commonly observed. The unit is magnetite-rich, and highest magnetic values (~80 SI) are measured in clasts of hematite-magnetite iron formation similar to previously mapped occurrences at Joe Mountain (Piercey, 2005).

Petrographic observations indicate that JMF basalt have an equigranular to porphyritic texture. Interstitial space between randomly oriented plagioclase ± pyroxene crystals is occupied by a microcrystalline plagioclase-rich groundmass (Fig. 5a,b). Locally altered orthopyroxene and clinopyroxene are identified, as well as minor olivine. Chlorite is the main alteration phase (up to 30%), accompanied by lesser carbonate alteration or micro-veining.

Volcaniclastic sequence (mTJMvc)

West and north of Teslin Mountain, an ~100 m thick volcaniclastic sequence dominated by fine mafic ash tuff and chaotic volcanic conglomerate overlies the JMF basalt. Thick-bedded, polymictic, chaotic volcaniclastic conglomerate displays boulder-size clasts (30-50 cm) of quartz-plagioclase-phyric diorite, cherty glassy basaltic ash tuff, dark green finely crystalline basalt, and blocks of red-brick oxidized iron formation (Piercey, 2005). The conglomerate is interbedded with orange-brown-grey to tan weathering, pale grey-green, medium-bedded volcaniclastic sandstone, with angular dark basalt clasts (2%), quartz eyes (up to 15%) in a pale grey-green very fine matrix. North of Teslin Mountain, this unit is dominated by south-dipping, pale green weathering, dark green to grey, silicified, laminated mafic ash tuff. Disseminated pyrite is locally observed.

Petrographic observations of the quartz-phyric volcaniclastic sandstone indicate a relatively equigranular, fine-grained texture. Subangular quartz crystals are intact, the rest of the rock comprises a groundmass completely recrystallized into fine microcrystalline quartz, and extremely altered olivine or pyroxene fragments (Fig. 5c).

Possible fiammae are observed, which may correspond to compacted and elongated volcanic glass (Fig. 5c). The laminated mafic tuff displays a fine-grained texture and is dominated by isotropic ash material, with minor subangular quartz microcrysts (Fig. 5d). It is pervasively carbonate altered and displays parallel elongated fractures that may be the result of devitrification (Fig. 5d).

*Sedimentary sequence (*mTJMms and mTJMl*)*

A sedimentary sequence underlies the south dipping mafic and volcaniclastic strata of the JMF, and is bounded to the north by LRG volcaniclastic rocks (Fig. 3). Lenses of pale grey weathered thin-bedded calcareous mudstone and sandstone (mTJMl) occur within the JMF mafic ash tuff sequence (Fig. 4b). Farther north, brown-grey weathering, calcareous sandstone to pebble conglomerate contains rounded to subangular clasts of limestone, shell fragments, and fine-grained dark grey aphyric or plagioclase-phyric volcanic rock. This sequence grades northward into a south dipping mudstone/sandstone clastic sequence up to 100 m thick (mTJMms; Fig. 4c). Pale green, finely-laminated sandstone and mudstone dominate and contain less than 1% of disseminated sulphides. Coarse, matrix-supported angular conglomerate displays thick interbeds of laminated sandstone, and contains a majority of volcanic clasts and dark brown, very fine mudstone clasts in a sandstone-rich matrix. Bedded, brown grey weathering, pebble conglomerate is mapped closer to the upper contact.

Interpretation and age

Both the volcanic and clastic sequence of the JMF at Teslin Mountain suggest a shallow subaqueous environment of deposition. Basalt is generally pillowed, with subaerial, flow-banded, vesicular lava locally observed. Regular lamination within the mafic tuff sequence and the presence of pillows suggests deposition under water for at least part of the formation. The chaotic organization of the volcanic conglomerate and dominant volcanic clast composition indicate that only a minimum amount of reworking took place. The clastic sedimentary sequence and limestone lenses mapped north of Teslin Mountain suggest that a marginal shallow basin existed prior to and during JMF volcanism, at the margin of the volcanic center. A reaction rind surrounds the limestone lenses at the contact with the mafic tuff, suggesting that limestone was incorporated as the tuff was still hot. This sedimentary sequence may represent the base of the JMF north of Teslin Mountain, but a gradual lateral transition into to the mafic sequence is inferred towards the south (Fig. 2).

Conodonts extracted from limestone interbedded with JMF basalt at Joe Mountain returned a Middle Triassic (Ladinian) age (Hart, 1997). Additional conodont analysis is underway for the limestone lenses within the mafic tuff sequence near Teslin Mountain. This may provide some constraints on the age of this volcanic event and confirm the correlation with the type section of the JMF.

LEWES RIVER GROUP (UPPER TRIASSIC)

The Upper Triassic LRG is exposed in the west and centre of the Teslin Mountain map area (Fig. 3). Seven map units comprising clastic sedimentary, calcareous, volcaniclastic and mafic volcanic strata are defined based on lithology, stratigraphic associations and geographic distribution (Fig. 2).

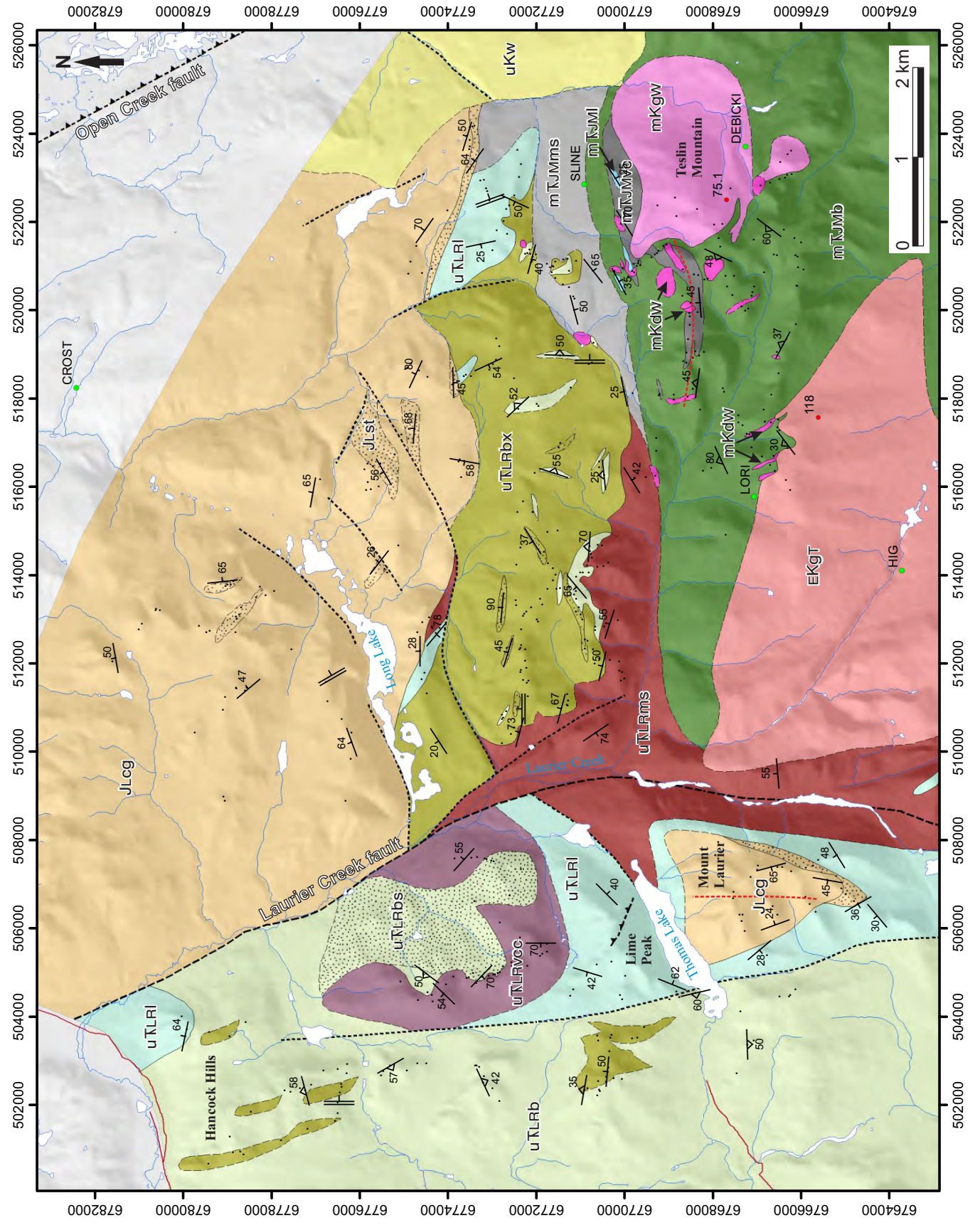
At most locations, the base of the LRG is not exposed but thickness estimations from the map and cross sections suggest that the group could be more than 2000 m. Previous thickness estimates for the LRG are between 2100 m (Tozer, 1958) to greater than 3000 m (Hart, 1997).

*Mudstone/sandstone (*uTLRms*)*

A north-dipping, ~800 m thick, well-bedded, clastic sequence of mudstone/sandstone is exposed east of Laurier Creek and south of Long Lake (Figs. 3 and 4d). It is in contact with JMF basalt to the south, possibly along a disconformity, and conformably underlies LRG volcaniclastic rocks described below. Rusty weathering of the mudstone towards the southern contact may indicate a nearby intrusive contact with the Teslin Plutonic suite (EKgT).

This unit comprises thin to medium-bedded, brown weathering, pale to dark green, fine-grained, lithic and crystal-rich laminated sandstone and mudstone and contains sparse plagioclase and mafic crystal fragments. Matrix-supported angular conglomerate interbeds contain a majority of volcanic clasts and dark brown very fine mudstone clasts in a sandstone matrix. Minor thin to medium-bedded calcareous sandstone and limestone occur in this sequence.

Similar rocks are inferred to extend along the Laurier Creek fault, east of Mount Laurier (Fig. 3), where a thick sequence of north-dipping thin to medium-bedded clastic and calcareous mudstone and sandstone was identified, however further mapping is required in this area to confirm association with this unit.


N
Open Creek fault
Laurier Creek fault
Laurier Creek
Table Lake
Thomas Lake
Lime Peak
Mount Laurier
Teslin Mountain
Hancock Hills
CROST
SLINE
DEBICKI
LORI
HIG
118
75.1
uKw
mTJMms
mTJMl
mTJMvc
mTJMb
mKgw
mKdW
uTLRl
uTLRbx
JLst
JLcg
uTLRms
EKgT
uTLRbs
uTLRVcc
uTLRb
0
1
2 km

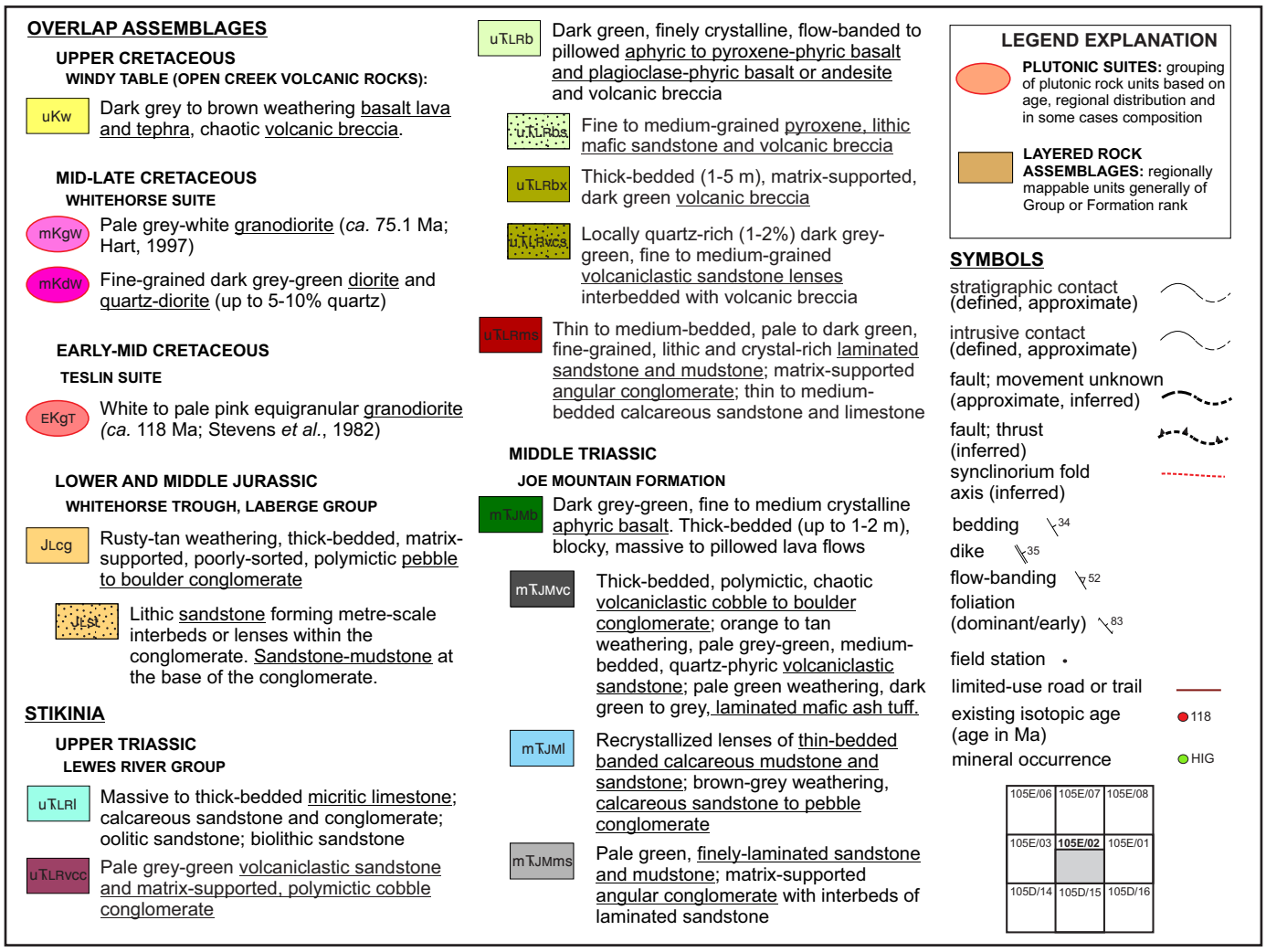


Figure 3. *Geology of the Teslin Mountain area (part of 105E/02), see map on previous page and legend above. Geology is based on 1:50 000 scale bedrock mapping conducted during the summer 2015. Intrusive contacts are after Tempelman-Kluit (1984) except where contact is indicated as "defined". Existing isotopic ages (K/Ar) after Stevens et al. (1982) and Hart (1997). Mineral occurrences from Yukon MINFILE (2015). Grid in UTM coordinates (zone 8, NAD 83).*

*Mafic volcanic sequence (*uTLRb, uTLRbs, uTLRbx, uTLRvcs*)*

A mafic volcanic sequence dominated by coherent basalt is exposed along a north-south belt in the western part of the map area, west of Lime Peak and Mount Laurier and in the Hancock Hills (Fig. 3). In the central part of the map area, this sequence is dominated by volcanic breccia, volcaniclastic sandstone and conglomerate, which show lithological similarities to the coherent lavas exposed to the west. Volcaniclastic rocks conformably overlie the clastic sedimentary sequence described above.

Coherent dark green-grey to rusty brown weathering, dark green, flow-banded to pillowed aphyric to pyroxene-phyric basalt (Fig. 4e) and plagioclase-phyric basalt or andesite dominate in the western part of the map area (uTLRb). Basalt comprises very fine (<1 mm) plagioclase crystals (1-5%), small brown pyroxene crystals (1%) and minor olivine (<1%) in a finely crystalline aphyric groundmass. Amygdules or sparse small rounded (1-2 mm) to larger irregularly shaped (1-2 cm) vesicles are visible locally. Petrographic observations display a porphyritic texture of the basalt, with plagioclase, clinopyroxene and olivine phenocrysts in a microcrystalline, equigranular,

plagioclase rich groundmass (Fig. 5e,f). Mafic crystals are locally strongly altered to chlorite. Carbonate alteration is pervasive.

Grey weathering, pale to dark grey-green, fine to medium-grained volcaniclastic sandstone and matrix-supported angular volcanic breccia (uTLRbs) occur north of Lime Peak, locally interbedded with coherent basalt lava. Sandstone contains dark grey lithic volcanic lapilli and pyroxene crystals. Mafic volcanic breccia displays a pale green rubbly matrix, supporting subrounded, pyroxene-phyric basalt blocks (Fig. 4f). Beds are up to 20 m thick. Field relationships indicate that the volcaniclastic sandstone is overlain by the coarse, chaotic volcanic breccia along a subhorizontal contact that may be a depositional unconformity. The whole section is locally crosscut by carbonate veining.

Coherent basalt is locally overlain or interbedded with tan-rusty-grey weathering, dark green, matrix-supported volcanic breccia (uTLRbx). Clasts (~ 40%) include brick-red, pyroxene, hornblende or plagioclase-phyric to aphyric, locally finely vesicular volcanic fragments. Subangular lapilli size clasts dominate, and larger clasts (20-30 cm) are subrounded. Thick-bedded (1-5 m), orange-brown-grey weathering, dark green, matrix-supported volcanic breccia also covers an area of ~12 by 4 km in the center of the map area, from the south end of Long Lake and east of Laurier Creek, northwest of Teslin Mountain (Figs. 3 and 4g). Clasts are subangular to subrounded, range from lapilli to block size, and are poorly sorted. Clast composition is volcanic, but display textural variability or various degrees of oxidation. They include red oxidized pyroxene or plagioclase-phyric basalt/andesite, vesicular to massive andesite, and lapilli size angular fragments of grey-green to red aphanitic volcanic rock. The matrix is a fine-grained, grey to green volcaniclastic sandstone, with ash to lapilli size fragments and disseminated plagioclase and pyroxene crystals. Petrographic observations of the breccia matrix indicate a relatively homogeneous clast composition. Typical clasts include plagioclase-clinopyroxene-phyric basalt with finely crystalline pyroxene-rich groundmass, and carbonate-filled vesicles (Fig. 5g).

Volcanic breccia is interbedded with lenses of volcaniclastic sandstone and coherent basalt. Brown weathering dark grey-green volcaniclastic sandstone (uTLRvcs; Fig. 4h) is fine to medium-grained with subangular volcanic clasts up to 1 cm, and is locally quartz-rich (1-2%). Petrographic observations of this lithology indicate equigranular, fine-grained crystal tuff comprising plagioclase, altered pyroxene crystals, as well as clasts of very finely crystalline plagioclase-phyric basalt and volcanic glass (Fig. 5h). Metre-scale beds of coherent, massive, flow banded or pillowed basalt (uTLRb) and angular lapilli mafic breccia are locally mapped within the volcaniclastic sequence. Basalt is tan to brown-grey weathering, dark grey-green, fine-grained, aphyric to hornblende (3-4%), pyroxene (2-3%; up to 10%) or plagioclase phyric (5-10%), with possible small crystals of olivine (1-2%).

Volcaniclastic sandstone (uTLRvcc)

Volcaniclastic sandstone (uTLRvcc) north of Lime Peak is interfingered with mafic sandstone, thick volcanic breccia and coherent pyroxene-phyric basalt of uTLRb and uTLRbs (Fig. 3). Its southern contact with uTLRl limestone is masked within an east-west oriented valley. The unit is distinguished from other volcaniclastic sandstone by its color and composition. It comprises beige-brown weathering, pale grey-green, medium-grained volcaniclastic sandstone (Fig. 4i) and matrix-supported, polymictic cobble conglomerate, with locally calcareous plagioclase-mafic-rich sandstone matrix. Subangular to subrounded clasts (up to granule size) include dark green volcanic clasts, dark grey mudstone, beige fine-grained glassy rhyolite (?), finely vesicular plagioclase-phyric volcanic rock and plagioclase-rich sandstone. The sandstone locally displays up to 5-10% apple green opaque crystals which possibly result from alteration and replacement of mafic crystals. Secondary lithologies of this unit include calcareous bioclastic sandstone and mudstone and finely laminated sandstone and mudstone interbedded with the main volcanic sandstone unit. This sequence is distinct lithologically from sedimentary rocks observed to the east across Laurier Creek. Petrographic observations illustrate pervasive carbonate alteration in this unit, which masks the original mineralogy but preserves primary igneous textures. Plagioclase crystals are locally altered to sericite.

Limestone (uTLRl)

Pale grey weathering limestone successions, between 20 and 500 m thick, are exposed along slopes and cliffs throughout the map area, at Lime Peak, west and south of Mount Laurier, south of Long Lake, and north of Teslin Mountain (Fig. 3). The main lithology comprises grey to pale yellow, finely to coarsely crystalline, massive to thick-bedded micritic limestone. Local interbeds of dark grey, fetid limestone, calcareous sandstone and conglomerate, oolitic sandstone or bioclastic wackestone



Figure 4. *Field photographs illustrating lithologies in the Teslin Mountain area. Joe Mountain Formation: (a) pillowed aphyric basalt; (b) limestone lense within laminated mafic tuff; (c) south dipping, finely bedded mudstone/volcanic sandstone sequence; Lewes River Group: (d) northeast dipping, finely laminated mudstone and sandstone; (e) pillowed pyroxene-phyric basalt; (f) matrix-supported, primary volcanic breccia; (g) partially reworked volcanic breccia possibly resulting from mass-flow depositional processes, with clasts of coherent basalt and volcaniclastic rocks shown by dashed outline; (h) volcanic sandstone; (i) beige brown weathered coarse-grained sandstone, locally grading into angular conglomerate; (j) northwest dipping limestone at Lime Peak; Laberge Gp: (k) boulder to cobble conglomerate underlain by thinly bedded mudstone and sandstone; (l) west-dipping, basal sandstone/mudstone sequence at Mount Laurier.*

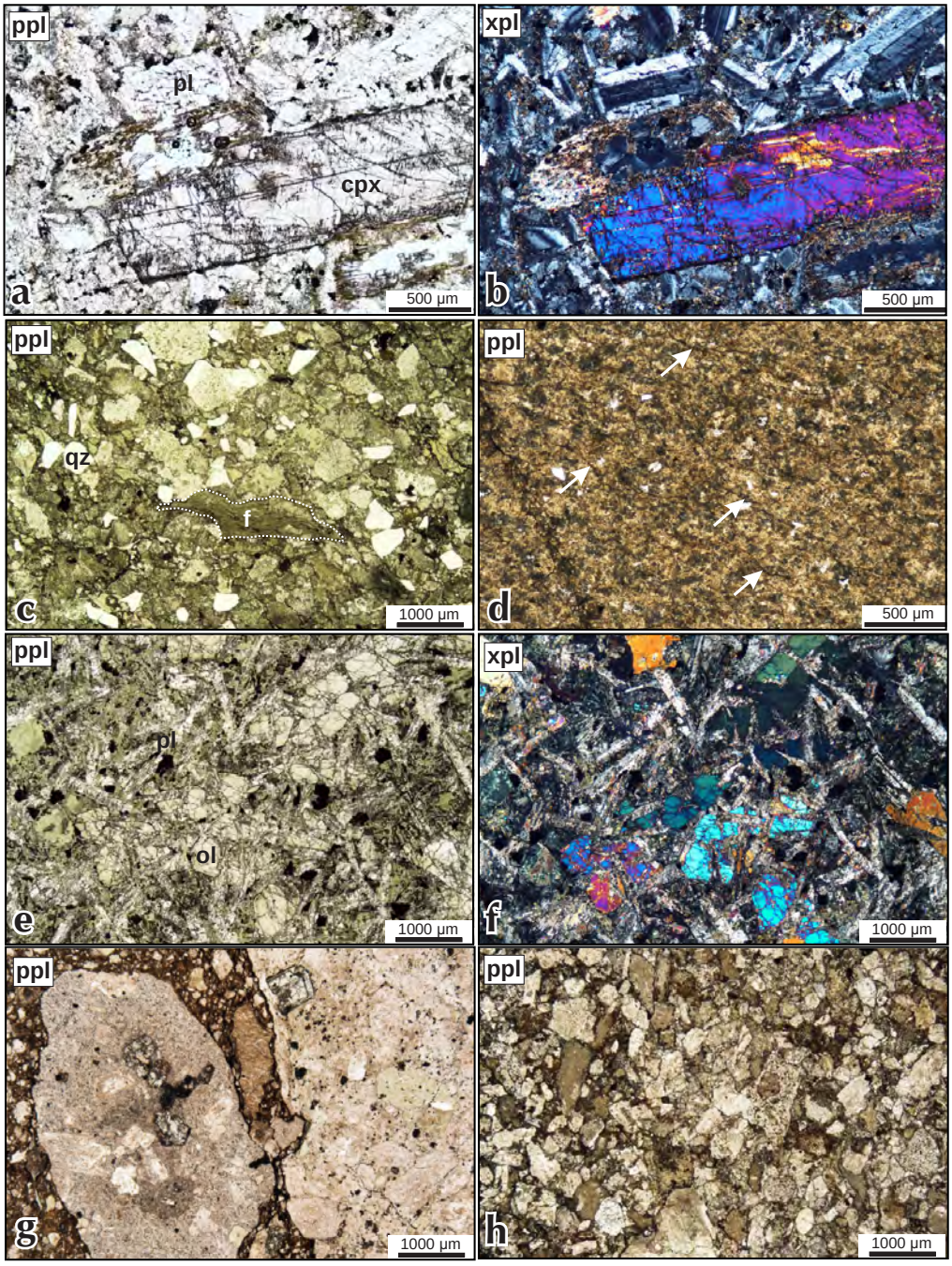


Figure 5. *Photomicrographs illustrating textures and mineralogy of selected units in the Teslin Mountain area (ppl = plain polarized light; xpl = cross polarized light). a-b and e-f are coherent rock types, c-d and g-h are volcaniclastic rock types: (a-b) Joe Mountain Formation, coherent basalt: clinopyroxene (cpx) phenocryst in an equigranular plagioclase-rich (pl) groundmass (shown in ppl and xpl); (c) Joe Mountain Formation, quartz-phyric volcaniclastic sandstone: subangular quartz grains (intact or recrystallized; qz), possible fiammae (f; dashed white outline), mafic crystal fragments and opaque volcanic glass fragments form the sandstone matrix; (d) Joe Mountain Formation, mafic ash tuff: isotropic, fine-grained ash, less than 1% very fine quartz crystals, pervasive carbonate alteration; fine dark brown fractures possibly represent compaction/devitrification features (indicated by white arrows); (e-f) Lewes River Group, coherent basalt: intergranular texture formed by plagioclase laths (pl), interstitial space is occupied by olivine crystals (ol), pervasive chlorite and carbonate alteration (shown in PPL and XPL); (g) Lewes River Group, volcanic breccia: composed of clasts of volcaniclastic rocks in a very fine grained pyroxene-rich matrix; (h) Lewes River Group, volcaniclastic sandstone: equigranular clasts and crystal fragments, grain-supported. Crystals include plagioclase and orthopyroxene, lithic fragments are very finely crystalline plagioclase phyric basalt.*

constrain bedding orientation at a few locations. The thickest and best exposed carbonate sequence is at Lime Peak, where more than 500 m of northwest to southeast dipping massive limestone is exposed (Fig. 4j). Lime Peak limestone is in possible fault contact with Lower Jurassic conglomerate at Mount Laurier.

Interpretation and age

The LRG in the Teslin Mountain area comprises mixed volcanic, clastic and carbonate units. The composition of most clastic units indicate a dominant volcanic source. Lateral lithological and textural variations, as well as thickness variations within units, reflect an active basaltic volcanic environment, with syn and post-volcanic erosion and sedimentation in an arc marginal basin.

Pillow structures in uTLRb indicate a subaqueous environment of deposition. Layering of interbedded volcanic sandstone also suggests deposition under water. The volcanic breccia (uTLRbs) is proximal, possibly a mass flow deposit as indicated by homogeneity of the clasts and the matrix, and chaotic internal structure. The volcaniclastic conglomerate that covers most of the central map area (uTLRbx) may also result from mass flow deposit processes, associated with synvolcanic (?) erosion of the coherent basalt to the west. The mixed clast composition indicates mechanical integration of other lithologies during transport and deposition, but a chaotic internal organization and very rough layering suggest that the amount of reworking was restricted.

One macrofossil analysis was conducted on a sample from a bedded, fetid limestone located northwest of Lime Peak. The sample contains small columnal crinoid ossicles (columnals), bivalved shells and poorly preserved, indeterminate solitary scleractinian corals (R. Blodgett, pers. comm., 2015). The fauna assemblage in this sample is consistent with documented relatively shallow-water, high-latitude Upper Triassic shelf fauna from northern Canada (and Alaska) and consistent with previous paleontological studies in the Whitehorse trough (*e.g.*, Reid, 1980; Yarnell *et al.*, 1999). However, there is no certainty that other limestone occurrences, particularly those north of Teslin Mountain, represent the same stratigraphic level. Conodont analyses are underway to constrain the age of different limestone occurrences across the map area.

POST-ACCRETIONARY ROCKS

WHITEHORSE TROUGH – LABERGE GROUP

Thick bedded clastic pebble to boulder conglomerate and minor sandstone of the Lower Jurassic Laberge Group occupy the northern half of the Teslin Mountain area (Fig. 3), bounded to the west by the Laurier Creek fault, to the south by Long Lake, and to the east by the Teslin River. The Laberge Group is also exposed along the rugged ridge of Mount Laurier (Fig. 3). The mapped contact with the underlying LRG is either a disconformity (Mount Laurier), or an angular unconformity (south of Long Lake). Elsewhere, the base of the Laberge Group is covered.

The upper contact of the Laberge Group is not exposed in the Teslin Mountain area, therefore the estimated thickness of 2000 m for the Laberge Group is a minimum. Previous estimates report between 1000 and 3000 m (*e.g.,* Hart, 1997; White *et al.*, 2012) across the Whitehorse trough.

*Pebble to boulder conglomerate (*JLcg*) and sandstone (*JLst*)*

An ~30 m thick sequence of brown weathering, thin-bedded sandstone to mudstone (JLst) marks the base of the Laberge Group (Fig. 4k). At Mount Laurier, this west dipping fine clastic sequence overlies LRG limestone and underlies Laberge Group conglomerate (Fig. 3). The sandstone contains fine mafic crystals (biotite, pyroxene?), minor plagioclase, in a fine, dark grey groundmass. It displays cross-stratifications on weathered surfaces and grades upward into mudstone. Finely bedded laminated mudstone is grey-brown weathered, dark grey and very fine grained. A similar relationship between the LRG and Laberge Group conglomerate is mapped north of Teslin Mountain. There, fine, brown weathering sandstone and mudstone dip north beneath thick beds of cobble conglomerate.

Grey-brown-rusty to tan weathering, thick-bedded, dominantly matrix-supported, poorly-sorted, polymictic pebble to boulder conglomerate (JLcg; Fig. 4l) is exposed along steep ridges and cliffs. It includes rounded to subrounded clasts of a variety of compositions:

- Sedimentary clasts: dark grey, very fine grained mudstone; pale grey, featureless limestone mudstone or cherty limestone;

- Intrusive clasts: dark grey-green, plagioclase ± hornblende-phyric diorite; medium-grained, biotite-plagioclase-phyric granodiorite with minor quartz; grey pyroxene-plagioclase-phyric gabbro (?); feldspar-megacrystic intrusive rock; and
- Volcanic clasts: dark grey aphyric basalt; dark green amygdaloidal basalt; hornblende-phyric mafic volcanic rock; red-oxidized finely vesicular aphyric, aphanitic volcanic rock.

Bedding thickness ranges from 10-30 cm to locally metre-scale. Matrix is a pale yellow weathering, dark grey-green calcareous sandstone rich in biotite, quartz, feldspar, and hornblende. Lithic sandstone forms metre-scale interbeds or lenses within the conglomerate.

Metre-thick, locally well sorted, crystal-rich sandstone lenses are observed within the Laberge Group conglomerate at Mount Laurier. Sandstone is grey-green weathered, grey brown, medium to coarse-grained, with lenses of very fine, grey-brown-green mudstone. The matrix contains various crystals of quartz (~20%), feldspar (~60%), lithic fragments (~5%) and mafic crystals (up to 1-2%). Mudstone is orange-brown weathered, fine-grained, bedded to brecciated (fine angular clasts, matrix supported). Local rusty weathering occurs at contact with intruding hornblende-plagioclase-phyric diorite dikes.

Interpretation and age

Exposures of the Laberge Group in the Teslin Mountain area are dominated by pebble to boulder conglomerate, over finer clastic lithologies. The best exposures of the Laberge Group are towards its southern contact with the LRG in the central part of the map area or at Mount Laurier. North of Long Lake, the area is mostly covered. The conglomerate may be interpreted as a result of mass flow processes, possibly related to submarine channels or deltas.

The age of the Laberge Group is mostly constrained by detrital zircon analyses as being Late Triassic-Early Jurassic (~220-180 Ma; Colpron *et al.*, 2015). Additional detrital zircon samples will be analyzed as part of this study in order to better characterize the ages and provenance of the Laberge Group.

IGNEOUS ROCKS

*Teslin Plutonic Suite (*EKgT*)*

A large intrusive body of ~ 4 by 10 km is exposed between Mount Laurier and Teslin Mountain in the south of the map area (Fig. 3). It intrudes mainly JMF aphyric massive basalt, but also the LRG sedimentary succession to the west. Grey to tan weathering, white to pale pink, equigranular granodiorite contains plagioclase (50%), biotite (25-30%), quartz (15%) and hornblende (up to 5%). Crystal size is generally 2 to 3 mm. A weak foliation is expressed locally. The main intrusion is accompanied by various dike phases including a tan yellow weathering, pale pink, equigranular, fine to medium-grained quartz-rich granitoid with quartz (more than 50%), plagioclase (45%), biotite (5%) and hornblende-rich veins. The main intrusion was dated at ~118 Ma (K/Ar biotite; Stevens *et al.*, 1982).

*Whitehorse Plutonic Suite (*mKW*)*

Massive, blocky, medium-grained, grey weathering, pale grey-white granodiorite (mKgW) intrudes JMF basalt over an area of ~4 by 3 km at Teslin Mountain (Fig. 3). Mineralogy includes plagioclase (40-60%), K-feldspar (up to 15%), biotite (10-15%), hornblende (10-20%) and quartz (1-3%). The intrusion locally displays magmatic layering. The main intrusive phase also includes a number of diorite and quartz-diorite bodies (mKdW) that intrude JMF basalt and occur as small stocks or dikes up to 30 m wide. These small bodies are tan to grey weathering, massive, blocky, fine-grained dark grey-green diorite (1-2% quartz) and quartz-diorite (up to 5-10% quartz) dikes. Other phenocrysts include: plagioclase (10-15%, locally up to 50%), biotite or hornblende (5-15%).

The main granodiorite body found within the map area has a K/Ar age of ~75.1 Ma (Hart, 1997), but ages reported regionally for the Whitehorse Plutonic Suite are ~112-105 Ma (Colpron, 2011). New U/Pb radiometric dating is underway as part of this project.

Late Cretaceous (?) dikes

Grey-pink to rusty weathering, pale grey-pink, quartz-phyric rhyolite metre-wide (up to 5 m) dikes are mapped across the Teslin Mountain area (Fig. 3). They variably intrude LRG basalt or volcaniclastic rocks, and Laberge Group conglomerate. The dikes are aphyric to finely plagioclase-phyric. Finely to medium-crystalline pale pink to grey groundmass contains up to 10-60% plagioclase,

5-25% K-feldspar and 1-10% quartz phenocrysts. Hornblende or biotite phenocrysts comprise up to 1-5% of the rock. Where quartz veining is abundant, the rock is orange-pale brown weathering, highly silicified and clay altered. Dikes locally display a magmatic foliation and are generally oriented NS.

Based on crosscutting relationships, and the lack of deformation of these dikes, they are probably related to a Late Cretaceous magmatic event in southern Yukon, such as Carmacks volcanism (Cairnes, 1910; Bostock, 1936; Tempelman-Kluit, 2009) or Open Creek volcanism (*see* below).

*Open Creek volcanic rocks (*uKW*)*

Dark grey to brown weathering basalt lava and tephra and chaotic volcanic breccia is exposed northeast of Teslin Mountain (Fig. 3), possibly in unconformable contact with the underlying Laberge Group and JMF. Regionally, the Open Creek volcanic rocks (informal nomenclature by Tempelman-Kluit, 2009) comprise resistant, columnar-jointed, quartz-phyric dacite flows, ash and lapilli tuff, maroon weathering basal sedimentary and epiclastic rocks, dacite flows and flow breccia, and include dikes of quartz feldspar porphyry. Their age is constrained at ~80 Ma (whole rock, K/Ar; Tempelman-Kluit, 2009). Further field mapping is required to delineate and further characterize this unit.

DISCUSSION

A summary of stratigraphic and structural observations from the Teslin Mountain area, along with preliminary interpretations and future work directions, are presented below.

STRATIGRAPHY

Field observations constrain stratigraphic relationships in the Teslin Mountain area as follows:

- The oldest rocks in the map area, exposed at Teslin Mountain, belong to the Middle Triassic Joe Mountain Formation (JMF). These are dominated by aphyric, subaqueous basalt. North of Teslin Mountain, volcaniclastic rocks and mafic tuff overlie a mixed clastic and carbonate sequence inferred to represent deposition in a shallow to medium depth marginal basin beside the volcanic center. The volcaniclastic and sedimentary units are interpreted to be coeval with basaltic subaqueous volcanism;
- The Upper Triassic Lewes River Group (LRG) overlies the Middle Triassic JMF, but the contact is mostly covered, and therefore the relationship is uncertain. North of Teslin Mountain, south dipping sedimentary strata inferred to be part of the JMF are adjacent to volcaniclastic strata of the LRG which only display rough bedding orientation. The covered contact could be structural or stratigraphic, and in the latter case it is most likely unconformable;
- JMF and LRG basalts share similar compositions and textures, but distinct macroscopic and microscopic characteristics can be identified (Figs. 4 and 5). JMF basalt is dominantly aphyric, and microscope observations indicate the presence of both clinopyroxene and orthopyroxene. LRG basalt seems to be dominantly clinopyroxene-phyric. These petrographic and field observations will be soon complemented by new lithogeochemistry, which will be compiled with existing analyses from the LRG and JMF regionally;
- Important lateral lithological and textural changes occur within the Upper Triassic LRG across the map area (Fig. 2). Coherent basalt dominate to the west, whereas chaotic and coarse volcaniclastic deposits cover most of the central part of the map. These volcaniclastic deposits likely result from erosion of the basaltic belt to the west. Bedded, clastic sedimentary rocks with a high volcanic source content, pillow basalt, and few sedimentary structures suggest a shallow, subaqueous environment of deposition for this volcanic and volcaniclastic sequence;
- Previous stratigraphic frameworks of the LRG (Hart, 1997; Tempelman-Kluit, 1984, 2009) indicate that mafic volcanic rocks (Povoas Formation) form the base of the Upper Triassic stratigraphy. However, this study indicates that a well-bedded, at least 800 m thick, clastic-carbonate sedimentary sequence conformably underlies the LRG volcanic conglomerate and breccia south of Long Lake. The LRG volcaniclastic strata have strong lithological affinities with the pyroxene-phyric basalt exposed to the west, so they are inferred to be part of the same unit. Therefore the underlying sedimentary sequence either represents a previously unrecognized upper part of the JMF stratigraphy, or it is the base of the LRG. Clastic-carbonate sedimentation took place at least before the deposition of the LRG volcaniclastic sequence, but it may have been coeval with LRG basaltic volcanism;

- Pale grey weathered, competent LRG limestone strata constitute an ideal stratigraphic and structural marker in the Whitehorse trough. Upper Triassic fauna and a carbonate shelf reef environment is confirmed by one macrofossil analysis at Lime Peak. Additional mapping of these prominent strata will help to: (1) refine stratigraphic relationships within the LRG; (2) identify distinct episodes of carbonate sedimentation during LRG arc volcanism (*e.g.*, Lees, 1934; Tozer, 1958); and (3) constrain deformation of pre, syn and post-deformation; and
- The base of the Laberge Group comprises 10-30 m of sandstone, overlain by cobble to boulder conglomerate. An angular unconformity with the underlying LRG is mapped at one location. Elsewhere, the contact may be a disconformity (*e.g.*, Mount Laurier) or conformable. Most recent studies support a regional unconformity at the base of the Laberge Group (*e.g.*, Lowey, 2004, 2005, 2008; Lowey *et al.*, 2009). Further work is required to identify the timing of deposition of the Laberge Group with respect to the rest of the Whitehorse trough, and constrain better the environment of deposition.

STRUCTURE

Previous studies in the northern Whitehorse trough suggested that northwest-trending open folds, southwest-verging thrusts and folds, and extensional structures developed under a dextral transpressive regime controlled by regional northwest and north-striking strike-slip faults (White *et al.*, 2012).

Major faults outside of the Teslin Mountain area constrain the structural pattern in this area. These include the north-northwest trending dextral strike-slip Goddard and Teslin faults (Fig.1), which deform rocks of the LRG and Laberge Group along the eastern shore of Lake Laberge and along the Teslin River respectively. Faults in the Teslin Mountain area occur in covered valleys, and are inferred from field evidence such as non-conformable stratigraphic contacts, increased strata deformation, sharp topographic breaks or intense, localized rock alteration. Folding is inferred from variations of bedding attitude, but difficult to constrain due to the lack of foliation and cleavage plans, a problem previously reported by White *et al.* (2012). Structures reported on the map (Fig. 3) are interpreted based on a combination of field evidence and preliminary interpretation of aeromagnetic patterns (Miles *et al.*, 2015):

- Flow-banding and bedding measurements indicate a sharp change of bedding polarity within the JMF near Teslin Mountain (Fig. 3) between the south (north dipping strata) and the north (south dipping strata). This suggests an east-west-trending synclinal fold axis, with outer basalt limbs wrapping around an inner core of younger volcaniclastic rocks (Fig. 3);
- Variable bedding orientation of Laberge Group strata at Mount Laurier suggest folding of the sequence along a synclinorium axis (Fig. 3). North of Long Lake, bedding is relatively consistently dipping to the north at a relatively steep angle (50-70°);
- A corridor of deformation is constrained by the Laurier Creek valley immediately east of Mount Laurier (Fig. 3). To the west, the base of Mount Laurier comprises 100 m thick north-northwest dipping beds of LRG limestone overlain by Laberge Group sandstone and conglomerate. To the east, a thick north-dipping succession of well-bedded calcareous sandstone and mudstone and volcaniclastic rocks part of the LRG is exposed. The differences in lithologies, combined with a change of bedding orientation and a sharp topographic expression, suggest the existence of a north-trending structure running through the valley, here referred to as the Laurier Creek fault. The Laurier Creek fault extends north along the Laurier Creek valley, and defines a structural contact between Laberge Group conglomerate to the east and LRG volcano-sedimentary successions exposed in the Hancock Hills to the west (Fig. 3). The Laurier Creek fault was previously interpreted as an extensional structure (Tempelman-Kluit, 1984; Colpron, 2011). Similarly, the contact between LRG basalt (west of the map area), and younger LRG limestone at Lime Peak and Mount Laurier, may be an extensional structure (Fig. 3);
- Both Thomas Lake and Long Lake are southwest-northeast trending linear features that may correspond to structural boundaries (Fig. 3). At Thomas Lake, an inferred fault delineates Late Triassic LRG limestone and Lower Jurassic conglomerate of the Laberge Group. In addition, the jagged nature of the Laberge Group contact southeast of Long Lake (Fig. 3) suggests some post-Laberge Group lateral displacements; and

- A minor thrust (?) fault was observed within LRG limestone at Lime Peak (Fig. 3), and was previously reported by Reid (1980). Movement along this fault is unconstrained.

TECTONIC SETTING

Middle Triassic JMF volcanic rocks are the oldest rocks in the Whitehorse trough, and were previously identified as a unique occurrence in the Canadian Cordillera based on their field and geochemical characteristics (Hart, 1997). JMF mafic volcanism took place within an island arc or mid-oceanic ridge environment (Hart, 1997), with one or several volcanic centers surrounded by marginal basins. Upper Triassic LRG pyroxene-phyric basalt has a distinct geochemical signature related to an island arc setting (Hart, 1997). Synvolcanic exhumation of the Intermontane terranes led to erosion of the existing volcanic belt, mass-flow deposition events and the formation of thick volcaniclastic deposits in adjacent basins. The destruction of the arc was coeval with clastic and carbonate sedimentation in marginal basins. This setting explains complex stratigraphic relationships and lateral facies changes within the LRG. If both the JMF and LRG belong to Stikinia, these assemblages result from subduction of the Cache Creek oceanic crust beneath volcanic arcs that form the Intermontane terranes. Future work will focus at clarifying the uncertain affiliation of the JMF with Stikinia (Hart, 1997), and explain their geochemical and petrographic differences with LRG basalt.

The JMF and LRG form the depositional basement to the Whitehorse trough. Unravelling the Lewes River Group stratigraphy is critical in understanding the latest stages of Stikinia arc volcanism and the onset of Whitehorse trough marine sedimentation in the Early-Middle Jurassic. It is interpreted that the southern portion of the Whitehorse trough within the map area was developed as an active forearc basin (White *et al.*, 2012). Combined structural and stratigraphic analyses of the prominent LRG limestone strata across the Whitehorse trough will help constrain the deformation history of the trough.

ACNOWLEDGEMENTS

The author thanks Steve Israel for providing constructive comments that helped improve this paper. Kyle Orr's enthusiasm and interest during the 2015 field season were greatly appreciated. Heli Dynamics Ltd. are thanked for helicopter support. Robert Blodgett conducted the macrofossil analysis.

REFERENCES

Bickerton, L., Colpron, M. and Gibson, D.W., 2013. Cache Creek terrane, Stikinia, and overlap assemblages of eastern Whitehorse (NTS 105D) and western Teslin (NTS 105C) map areas. In: Yukon Exploration and Geology 2012, K.E. MacFarlane, M.G. Nordling and P.J. Sack (eds.), Yukon Geological Survey, p. 1-17.

Bostock, H.S., 1936. Carmacks district, Yukon. Geological Survey of Canada, Ottawa, ON, Canada, Memoir 189, 67 p.

Bostock, H.S. and Lees, E.J., 1938. Laberge map-area, Yukon. Department of Mines and Resources, Geological Survey of Canada, Ottawa, ON, Canada, Memoir 217, 33 p.

Cairnes, D.D., 1910. Preliminary memoir on the Lewes and Nordenskiold rivers Coal District, Yukon Territory. Geological Survey of Canada, Memoir 5, 87 p.

Cohen, K.M., Finney, S.C., Gibbard, P.L. and Fan, J.-X., 2013; updated. The ICS International Chronostratigraphic Chart. Episodes, vol. 36, p. 199-204.

Colpron, M., 2011. Geological compilation of Whitehorse trough - Whitehorse (105D), Lake Laberge (105E), and part of Carmacks (115I), Glenlyon (105L), Aishihik Lake (115H), Quiet Lake (105F) and Teslin (105C). Yukon Geological Survey, Geoscience Map 2011-1, scale 1:250000.

Colpron, M., Crowley, J.L., Gehrels, G., Long, D.G.F., Murphy, D.C., Beranek, L. and Bickerton, L., 2015. Birth of the northern Cordilleran orogen, as recorded by detrital zircons in Jurassic synorogenic strata and regional exhumation in Yukon. Lithosphere, vol. 7, p. 541-562.

Colpron, M. and Friedman, R.M., 2008. U-Pb zircon ages for the Nordenskiold formation (Laberge Group) and Cretaceous intrusive rocks, Whitehorse trough, Yukon. *In:* Yukon Exploration and Geology 2007, D.S. Emond, L.R. Blackburn, R.P. Hill and L.H. Weston (eds.), Yukon Geological Survey, p. 139-151.

Colpron, M. and Nelson, J.L., 2011. A Digital Atlas of Terranes for the Northern Cordillera. Accessed online from Yukon Geological Survey <www.geology.gov.yk.ca> [accessed Nov. 2015].

Coney, P.J., Jones, D.L. and Monger, J.W., 1980. Cordilleran suspect terranes. Nature, vol. 288, p. 329-333.

Hart, C.J., 1997. A transect across northern Stikinia: geology of the northern Whitehorse map area, southern Yukon Territory (105D/13-16). Indian and Northern Affairs Canada, Exploration and Geological Services Division, Yukon Region, Bulletin 8, 77 p.

Hart, C.J.R. and Hunt, J.A., 1994. Geology of the Joe Mountain map area (105D/15), southern Yukon Territory. In: Yukon Exploration and Geology 1993, C.F. Roots and D.S. Emond (eds.), Exploration and Geological Services Division, Yukon Region, Indian and Northern Affairs Canada, p. 87-104.

Hart, C.J.R. and Hunt, J.A., 1995. Geology of the Mount M'Clintock map area (105D/16), southern Yukon Territory. *In:* Yukon Exploration and Geology 1994, C.F. Roots and D.S. Edmond (eds.), Exploration and Geological Services Division, Yukon Region, Indian and Northern Affairs Canada, p. 87-104.

Hart, C.J.R. and Orchard, M.J., 1996. Middle Triassic (Ladinian) volcanic strata in southern Yukon Territory, and their Cordilleran correlatives. Geological Survey of Canada, Current Research 1996-A, Cordillera and Pacific Margin, p. 11-18.

Hart, C.J.R. and Radloff, J.K., 1990. Geology of Whitehorse, Alligator Lake, Fenwick Creek, Carcross and part of Robinson map areas (105 D/11, 6, 3, 2, 7). Exploration and Geological Services Division, Department of Northern and Indian Affairs, Whitehorse, Open File 1990-4, 126 p.

Lees, E.J., 1934. Geology of the Laberge area, Yukon. Transactions, Royal Canadian Institute, vol. 20, no. 1, p. 1-48.

Lowey, G.W., 2004. Preliminary lithostratigraphy of the Laberge Group (Jurassic), south-central Yukon: Implications concerning the petroleum potential of the Whitehorse Trough. *In:* Yukon Exploration and Geology 2003, D.S. Emond and L.L. Lewis (eds.), Yukon Geological Survey, p. 129-142.

Lowey, G.W., 2005. Sedimentology, stratigraphy and source rock potential of the Richthofen formation (Jurassic), northern Whitehorse Trough, Yukon. *In:* Yukon Exploration and Geology 2004, D.S. Emond, L.L. Lewis and G. Bradshaw (eds.), Yukon Geological Survey, p. 177-191.

Lowey, G.W., 2008. Summary of the stratigraphy, sedimentology and hydrocarbon potential of the Laberge Group (Lower-Middle Jurassic), Whitehorse trough, Yukon. *In:* Yukon Exploration and Geology 2007, D.S. Emond, L.R. Blackburn, R.P. Hill and L.H. Weston (eds.), Yukon Geological Survey, p. 179-197.

Lowey, G.W., Long, D.G.F., Fowler, M.G., Sweet, A.R. and Orchard, M.J., 2009. Petroleum source rock potential of Whitehorse trough: a frontier basin in south-central Yukon. Bulletin of Canadian Petroleum Geology, vol. 57, p. 350-386.

Miles, W., Saltus, R., Hayward, N.E. and Oneschuk, D., 2015. Alaska and Yukon magnetic compilation, residual total magnetic field. Geological Survey of Canada, Open File 7862, scale 1:1 120 000.

Monger, J.W.H., 1977. The Triassic Takla Group in McConnell Creek Map-area, North-central British Columbia. Geological Survey of Canada, Paper 76-29, 45 p.

Monger, J.W.H., Wheeler, J.O., Tipper, H.W., Gabrielse, H., Harms, T., Struik, L.C., Campbell, R.B., Dodds, C.J., Gehrels, G.E. and O'Brien, J., 1991. Part B. Cordilleran terranes, Upper Devonian to Middle Jurassic assemblages (Chapter 8). *In:* Geology of the Cordilleran orogen in Canada, H. Gabrielse and C.J. Yorath (eds.), Geological Survey of Canada, Geology of Canada 4, p. 281-327, *also* Geological Society of America, The Geology of North America, vol. G-2.

Mortensen, J.K., 1992. Pre-Mid-Mesozoic tectonic evolution of the Yukon-Tanana terrane, Yukon and Alaska. Tectonics, vol. 11, p. 836-853.

Mortensen, J.K. and Jilson, G.A., 1985. Evolution of the Yukon-Tanana terrane: evidence from southeastern Yukon Territory. Geology, vol. 13, p. 806-810.

Piercey, S.J., 2005. Reconnaissance geological and geochemical studies of the Joe Mountain Formation, Joe Mountain region (NTS 105D/15), Yukon. *In:* Yukon Exploration and Geology 2004, D.S. Emond, L.L. Lewis and G.D. Bradshaw (eds.), Yukon Geological Survey, p. 213-226.

Reid, R.P., 1980. Report of field work on the Upper Triassic reef complex of Lime Peak, Laberge map area, Yukon. *In:* Geology and Exploration 1979-80, D.J. Tempelman-Kluit (ed.), Indian & Northern Affairs Canada/Department of Indian & Northern Development: Exploration & Geological Services Division, p. 110-114.

Souther, J.G., 1971. Geology and mineral deposits of Tulsequah map-area, British Columbia (104K). Geological Survey of Canada, Memoir 362, 84 p.

Stevens, R.D., Delabio, R.N. and Lachance , G.R., 1982. Age Determinations and Geological Studies, K-Ar Isotopic Ages. Geological Survey of Canada, Report 16, Paper 82-2, 56 p.

Struik, L.C., Schiarizza, P., Orchard, M.J., Cordey, F., Sano, H., MacIntyre, D.G., Lapierre, H. and Tardy, M., 2001. Imbricate architecture of the upper Paleozoic to Jurassic oceanic Cache Creek Terrane, central British Columbia. Canadian Journal of Earth Sciences, vol. 38, p. 495-514.

Tempelman-Kluit, D.J., 1984. Geology, Laberge (105E) and Carmacks (115I), Yukon Territory. Geological Survey of Canada, Open File 1101, scale 1:250000.

Tempelman-Kluit, D.J., 2009. Geology of Carmacks and Laberge map areas, central Yukon: Incomplete draft manuscript on stratigraphy, structure and its early interpretation (*ca.* 1986). Geological Survey of Canada, Open File 5982, 399 p.

Tipper, H.W. and Richards, B.C., 1976. Jurassic stratigraphy and history of North-central British Columbia. Geological Survey of Canada, Bulletin 270, 73 p.

Tozer, E., 1958. Stratigraphy of the Lewes River Group (Triassic), central Laberge area, Yukon Territory. Geological Survey of Canada, Bulletin 43.

Wheeler, J.O., 1961. Whitehorse map area, Yukon Territory. Memoir 312, 183 p.

Wheeler, J.O., Brookfield, A.J., Gabrielse, H., Monger, J.W.H., Tipper, H.W. and Woodsworth, G.J., 1991. Terrane map of the Canadian Cordillera. Geological Survey of Canada scale 1:2000000.

White, D., Colpron, M. and Buffett, G., 2012. Seismic and geological constraints on the structure and hydrocarbon potential of the northern Whitehorse trough, Yukon, Canada. Bulletin of Canadian Petroleum Geology, vol. 60, p. 239-255.

Yarnell, J.M., Stanley, G. and Hart, C.J.R., 1999. New paleontological investigations of Upper Triassic shallow-water reef carbonates (Lewes River Group) in the Whitehorse area, Yukon. *In:* Yukon Exploration and Geology 1998, C.F. Roots and D.S. Edmond (eds.), Exploration and Geological Services Division, Yukon, Indian and Northern Affairs Canada, p. 179-184.

Yukon MINFILE, 2015. Yukon MINFILE - A database of mineral occurrences. Yukon Geological Survey, <http://data.geology.gov.yk.ca> [accessed May 2015].

Placer-lode gold relationships in the Nansen placer district, Yukon

Rob Chapman[1], Matthew Cook, Matthew Grimshaw and Scott Myles
University of Leeds, UK

Chapman, R., Cook, M., Grimshaw, M. and Myles, S., 2016. Placer-lode gold relationships in the Nansen placer district, Yukon. *In:* Yukon Exploration and Geology, K.E. MacFarlane and M.G. Nordling (eds.), Yukon Geological Survey, p. 63-78.

ABSTRACT

Compositional studies have been undertaken on gold particles recovered from hypogene ore, eluvial material and placer samples in and around the Klaza property. These data have been correlated with previous descriptions of *in situ* mineralization to elucidate placer-lode relationships and systematic change in gold compositions between porphyry and epithermal environments.

Gold alloy from the porphyry environment is Ag-poor with respect to Au formed in later stage veins. Silver, and to a lesser extent Cu, have been the main discriminants for inferring the source of Au within the placers, and in general, vein mineralization is a more important source-type than porphyry mineralization.

The signature of Pb-Bi-Te previously identified in the inclusion suites of Au grains from Nucleus/ Revenue, Casino and Sonora Gulch has also been identified at Klaza, demonstrating that generic compositional signatures can underpin a robust exploration methodology. The relative sizes of porphyry and epithermal footprints of detrital Au together with their respective compositions are important considerations when targeting Cu-Au systems.

[1]*R.J.Chapman@leeds.ac.uk*

INTRODUCTION

The Dawson Range, south central Yukon is an emerging metallogenic province, and has been the focus of considerable study since 2009 (Allan *et al.* 2013). In part, this proliferation of exploration activity has been underpinned by the importance of widespread placer gold, which continues to support an important industry. The gold in the established placer regions can be broadly categorized into that derived from orogenic mineralization (*e.g.*, the Klondike, Sixtymile R., Tenmile R. and the White Gold District; Wrighton, 2013; Chapman *et al.*, 2014), and that derived from mineralization associated with early Late Cretaceous magmatism (Revenue/Nucleus, Casino, Sonora Gulch; Wrighton, 2013; Chapman *et al.*, 2014).

The Mount Nansen camp is situated at the south end of the Dawson Range (Fig.1); it comprises multiple mineral occurrences of porphyry and epithermal mineralization hosted within the 12 by 3 km 'Nansen Trend' within metasedimentary and meta-igneous rocks of the Yukon-Tanana terrane, (Hart and Langdon 1997; Fig. 1). The spatial relationships between porphyry mineralization and vein arrays, together with a parallel systematic change in mineralogy, are interpreted by Hart and Langdon (1997) as indicative of porphyry-epithermal transitions. Consequently, the mineralization in the Cyprus porphyry and gold-bearing precious metal veins of the Klaza deposit provide an excellent field area for study of mineralogical changes associated with an evolving magmatic hydrothermal system. The present study area comprises the northern part of the Nansen Trend and encompasses the Cyprus porphyry and the epithermal occurrences on the Klaza property, located between East Fork Nansen Creek and the Klaza River. The Klaza property is currently the focus of exploration by Rockhaven Resources.

In the Nansen Creek area, placer deposits are spatially located near the Klaza property, the very low grade

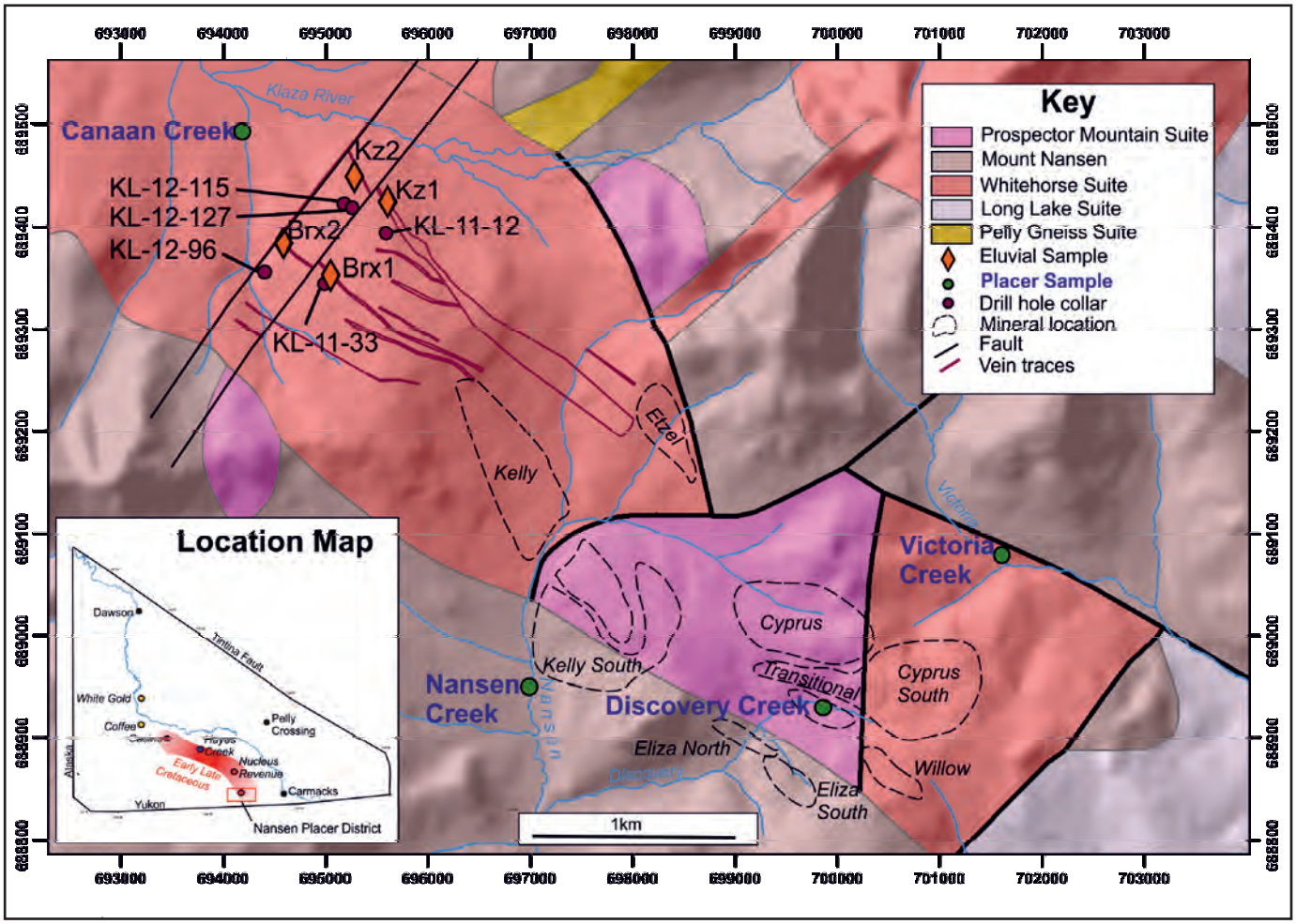


Figure 1. *Regional Geology and mineralization (after Colpron, 2006; Hart and Langdon, 1997.*

Cyprus Cu-porphyry and the Kelly occurrence. The YGS Placer Database (LeBarge, 2007) indicates that different gold fineness has been regularly reported from different creeks. Whilst bulk fineness data are only partially useful as a discriminant (due either to mixing of gold from different sources with different compositions, or derivation from a single source with a variable Au-Ag ratio), broad variation of gold composition with geographical location is suggestive of multiple sources. This study aims to establish clear compositional signatures of gold from both the hypogene and placer environments in the environs of the Klaza deposit to inform two avenues of investigation: i. evaluation of the variation in gold mineralogy within a porphyry-epithermal transition; and ii. evaluation of the relative importance of porphyry and epithermal Au as sources of local placers.

GEOLOGY AND MINERALIZATION

The regional and local geology of the study area is summarized by Hart and Langdon (1997) and depicted in Figure 1. The study area is situated in the north part of the Mount Nansen Trend; the trend is a 12 by 3 km NW-SE corridor which hosts approximately 30 mineral localities.

The locations of mineralization relevant to the present study are illustrated in Figure 1 and described in Table 1 which is organized according to the classification of Hart and Langdon, (1997)

The mineralogical descriptions of the various zones presented in Table 1 indicate a progressive decrease in Cu content away from the Cyprus porphyry both to the NW and SE, into Au-Ag-Pb-Zn dominated vein systems. The Klaza property hosts multiple sub-parallel veins of which the BRX vein and Klaza zone (Fig. 1) have been explored most extensively. The veins exhibit differences in their mineralogy with the Klaza zone containing higher levels of Pb and Ag, (Tarswell and Turner, 2014). The vein outcrops are offset by an up-thrown faulted block (throw probably around 150 m) perpendicular to strike. Tarswell and Turner (2014) propose that the Klaza veins correspond to a class of 'base metal carbonate' epithermal veins described by Corbett (2002), in which metal precipitation is induced by mixing with bicarbonate-rich groundwater. Such deposits are commonly zoned, reflecting marked differences in local temperature change, aH_2S (associated with sulphide precipitation) and degree of dilution. Samples of eluvial and hypogene material from these two zones formed part of the sample suite of the current study.

Table 1. *Descriptions of mineralized localities in the study area, adapted from Hart and Langdon (1997).*

Name	Description
Central Porphyry Zone	
Cyprus1,3	Quartz monzonite porphyry, Cu-Mo zone: py, cpy, mo, Cu 0.1-0.15%. Au anomalous but erratic
Kelly1	0.275 x 2.5km NW trending potassic alteration zone identified by soil geochemistry. Trench sample yielded 0.86 g/T Au and 0.25% Cu. cpy, Cc bn and mo
Peripheral porphyry zone	
Cyprus South1	Quartz sulphide veins and stockworks in phyllic zone. Au grade of 0.31g/T recorded in core.
Kelly South1	Au recorded in pyrite shell associated with phyllic alteration
Transitional zone	
Eliza Creek extension1	Veins and stockworks associated with porphyry stocks breccia and argillic/phyllic alteration. Au grades to 17.5g/T and Ag to 27 g/T in core
Transitional	Four veins very similar to those of the Eliza Creek extension
Epithermal veins	
Klaza Zone2	py, sp, ars, ga, sb, ss. au
BRX zone1	py, sp, ars, ga, sb, ss. au
Eliza Creek South 1	Au-Ag-Zn-Pb veins. Trench samples of Au to 3.9g/T
Eliza Creek North1	Au-Ag-Zn-Pb veins. Cu content > Eliza Creek North. Au to 10.3g/T
Etzel	Au-Ag-Pb-Zn veins
Willow1	3 Au-Ag-Pb-Zn veins containing Au to 3.5g/T

Key: py=pyrite, cpy=chalcopyrite, sp=sphalerite, ars=arsenopyrite, ga=galena, sb=stibnite. 1=(Hart and Langdon, 1997), 2=Tarswell and Turner (2014), 3=YGS Minfile 1151066.

The surficial geology of the Nansen area is described by LeBarge (1995) and comprises sediments originating in an array of pre-glacial, glacial and post glacial environments. Eight sedimentary facies are identified and each was investigated in terms of the concentration of detrital gold. Provenance of the gold in placers on Nansen and Victoria creeks and Canaan Creek was informed by clast analyses and morphological studies of the gold grains themselves. The highest concentrations of gold are observed in diamictons, interpreted to be the erosional products of pre-existing weathered ore and placers. *In situ* mineralization is observed in weathered bedrock, within the outcrop of the Cyprus porphyry such that direct liberation of gold from host to modern placer is possible at some localities. The presence of paystreaks on a false bedrock of early Pleistocene till in upper Nansen Creek till indicates that rejuvenation of the placer is ongoing (J. Bond pers. Comm.).

The Mount Nansen area has supported placer mining since the early twentieth century (LeBarge, 2007). An overview of the relative importance of various creeks is presented in Table 2, and summarizes production figures to 2005. The data show the placer resource in Nansen Creek is the most economically important. Bulk fineness data (LeBarge, 2007) indicate that most gold in the Nansen Creek system is between 800 and 850 fine, whereas gold from Victoria Creek, Canaan Creek and one of the reported Back Creek populations exhibits lower fineness values. LeBarge (2007) reports that many streams in the area were explored for their placer potential, but only a small number supported sustained activity.

PREVIOUS STUDIES OF GOLD GRAIN COMPOSITION IN THE DAWSON RANGE

Understanding the relationship between economically important placer gold deposits in Yukon and their potential lode sources has developed significantly during the last decade. Various studies have characterized gold particles derived both from lode and placers in terms of their alloy compositions and suite of mineral inclusions revealed in polished section, (*e.g.* Chapman *et al.*, 2010a,b; Chapman *et al.*, 2011; Wrighton, 2013; Chapman *et al.*, 2014). These combined data sets yield a 'microchemical signature' for a specific population of grains. Comparison of microchemical signatures of hypogene Au grains with detrital Au particles from local placer populations can establish placer-lode relationships. Wider studies are ongoing which seek to establish the characteristics of each signature which are diagnostic for different styles of gold mineralization.

A regional study of placer-lode gold relationships in the Dawson Range was undertaken between 2010 and 2012 under the auspices of the Yukon Gold Project, an academia- industry collaboration based at the Minerals Deposit Research Unit (MDRU) at UBC. Studies of placer and lode gold grains derived from the early Late Cretaceous intrusions of Revenue and Nucleus are distinct from those associated with orogenic mineralization, (Wrighton, 2013). Chapman *et al.* (2014) expanded this study to show that porphyry mineralization at Casino, Revenue/Nucleus and Sonora Gulch yield gold grains with a distinctive Bi-Pb-Te inclusion signature.

Table 2. *placer gold information (data from LeBarge 2007).*

Placer Creek	Fineness	Production (oz) to 2005	Comments
Discovery	820-850	1586	
E. Fork Nansen	No data	448	Some dendritic gold
Nansen	805-820	21,251	
Victoria	720-730	1185	
Back	760-836	3478	'Coarse' pay streak reported
Slate	800	-	Minor trib, no mining
Canaan	750	Unknown	No data in YPDB

SAMPLING

CORE SAMPLES

Core samples were selected based on the proximity of the hole collar to the localities of trench sampling (Table 3a). Selection of the intersections studied in each hole was based on the location of high Au grade. Sample preparation and analysis was undertaken at the University of Leeds.

OXIDIZED VEIN MATERIAL IN TRENCHES

The vein system at Klaza outcrops at surface and has been exposed by trenching. Decomposed vein material was collected from four localities, (*see* Table 3b and Fig. 1) and was thoroughly wetted before processing using a 'Le Trap' portable sluice. Sluice concentrates were panned to recover a 'super concentrate' containing gold grains.

COLLECTION OF PLACER SAMPLES

Samples of placer gold were collected using a combination of panning and sluicing. The details of the sample sites are provided in Table 3c and Figure 1. Characterization of Au from Nansen Creek was facilitated by study of two sample populations, the first of which is described in Table 3c. The second Nansen Creek sample comprised 56 gold grains collected by the Yukon Geological Survey close to the confluence of Nansen and East Fork Nansen creeks, although the exact locality is unknown. The inclusion assemblage of this second sample was useful to augment that observed in the sample collected slightly downstream during the current study.

Table 3. *Samples collected for this study.*

3a. Core samples used in preparation of polished blocks

Hole _ID	Close to	Sample depth m	From (m)	To (m)	Interval (m)	Collar Easting	Collar Northing	Au ppm	Ag ppm
KL-11-33	BRX 1	121.1	120.3	121.64	1.34	382080	6889865	5.51	180
KL-12-96	BRX 2	342.8	342.46	345.36	2.9	381509	6890034	10.55	92.7
KL-11-12	KZ1	221.7	221	222.6	1.6	382724	6890305	6.81	123
KL-12-115	KZ2	219.7	219.48	221.59	2.11	382340	6890627	13.75	357
KL-12-127	KZ2	169	168.11	169.11	1	382418	6890581	5.73	204

3b. Eluvial samples collected from vein outcrop

label	Trench	E	N	g/T Au	g/T Ag	intercept (m)	Volume of -2.5 cm material sluiced (L)
BRX 1	TR 13-49	382410	6889676	8.4	548	1.31	140
BRX 2	TR 13-47	381715	6890310	87	768	1.15	400
KZ 1	TR13-66	382758	6890614	25.7	449	2.27	200
KZ 2	TR 13-70	382462	6890888	16.76	1052	3.03	200

3c. Placer samples

locality	E	N	Comments	Potential sources
Discovery Ck	386521	6885312	Sample from headwaters of creek	CyS, El.N, El.S, Tr,
Victoria Ck	388391	6886630	Side pay	Unknown
Canaan Ck	381422	6891421	From active cut	BRX, Klaza zone
Nansen Ck	383700	6885781	From active cut	K, KS, Et, Cy

Abbreviations, corresponding to mineralization described in Table 1. Cy=Cyprus porphyry, CyS=Cyprus South, El.N=Eliza North, El.S=Eliza South, Tr=transitional, WC=Willow Creek, K=Kelly, KS=Kelly South.

ANALYTICAL WORK

Polished blocks were prepared from core samples and examined using both reflected light microscopy and the scanning electron microscope (SEM). Analysis of Au grains >5 µm in diameter was undertaken by electron probe microanalysis (EMP). Gold grains from eluvial and placer samples were isolated from the sluice concentrates by picking under a binocular microscope. These gold grains were mounted according to size as described by Chapman *et al.* (2000). The extreme small size of some of the gold particles necessitated the design of a new polishing technique specifically for extremely tiny (30-50 µm) particles. This involved introducing the grains into small pools of resin placed on a glass slide. The gold grains were revealed during controlled polishing of the slides in a manner similar to that employed when preparing rock thin sections to the required thickness.

Analysis of the Au grains was carried out in two stages. Firstly, qualitative analyses were undertaken using a FEI Quanta 650 FEG-ESEM. This involved inspection of each grain section and recording alloy heterogeneity and the presence of inclusions, either of minerals or intermetallic compounds. Secondly, quantitative alloy compositions were determined by EMP using a Jeol 8230 Superprobe. The minor element suite analyzed was Ag, Cu and Hg and the detection limits for each element were 0.03%, 0.02% and 0.1% respectively. All values are expressed in wt%. Polished blocks of core samples were prepared for inspection by reflected light microscopy and SEM/EMP analysis.

RESULTS

HYPOGENE ORE

The aim of this element of the project is to identify minerals coeval with the gold and that could be subsequently correlated to the suite of inclusions recorded in placer gold samples. Native gold is identified in samples from both veins, (in cores Kl-12-96 and Kl-12-115) although many of these gold grains are less than 2 µm in diameter and consequently too small to analyze by EMP. Mostly, gold is observed as small blebs in early stage pyrite, as is Bi telluride (Fig. 2a,b). Both galena and arsenopyrite post-date the pyrite, but Au is only observed in galena (Fig. 2c). Only gold in core from hole KL-12-96 (adjacent to BRX-2) is sufficiently coarse to analyse by EMP. The Ag contents of these grains are illustrated in Figure 3a, and the co- variance of Ag with Cu is illustrated in Figure 4.

SAMPLES COLLECTED FROM VEIN OUTCROPS

The alloy compositions of Au grains from BRX 1 and BRX 2 are shown in Figure 3a. Both populations are dominated by grains in the 18-25% Ag range; however there are other small contributions from other sub-populations which exhibit lower Ag contents, one of which appears similar to the Ag range of gold grains observed in the core samples. Table 4 shows that around 90% of grains from the BRX zone contain Hg to above LOD of 0.06%, although the maximum value recorded is only 1.5%. The percentage of grains containing measurable Cu is much lower at 35% and 36% in BRX 1 and BRX 2 respectively.

The low incidence of inclusions in the samples from the BRX zone grains is probably related to the tiny size of most of these gold grains. Table 4, shows the number of gold grains that contained specific minerals. Overall the inclusion assemblage reflects the mineralogy of the hypogene ore, with minerals coeval with Au observed as inclusions (*e.g.*, galena and Bi telluride; Fig. 2d,e). Arsenopyrite is not observed as an inclusion, (neither are Au grains observed within arsenopyrite in hypogene ore) but secondary As minerals are observed coating Au grains.

Covariance of minor alloying metals is investigated using the bivariate plots shown in Figure 4. Figure 4a shows the compositional fields of grains from Discovery Creek and Figure 4b superimposes these data onto that describing gold from the BRX Zone. In the Discovery Creek sample, the relationship of Ag to Cu is generally inverse, although most grains cluster in the mid-range of Ag and Cu. The distribution of alloy compositions of gold from the BRX zone shown in Figure 4b differs because the majority of points cluster in two Ag ranges, and within these Cu varies independently. A small number of grains contain relatively high Cu values but their compositional field does not correspond to that observed for grains from Discovery Creek (Fig 4a). These two differing compositional fields have been used as a template for comparison with sample populations of placer gold from the Canaan Creek (Fig. 4d), Nansen Creek (Fig. 4c) and Victoria Creek (Fig. 4e).

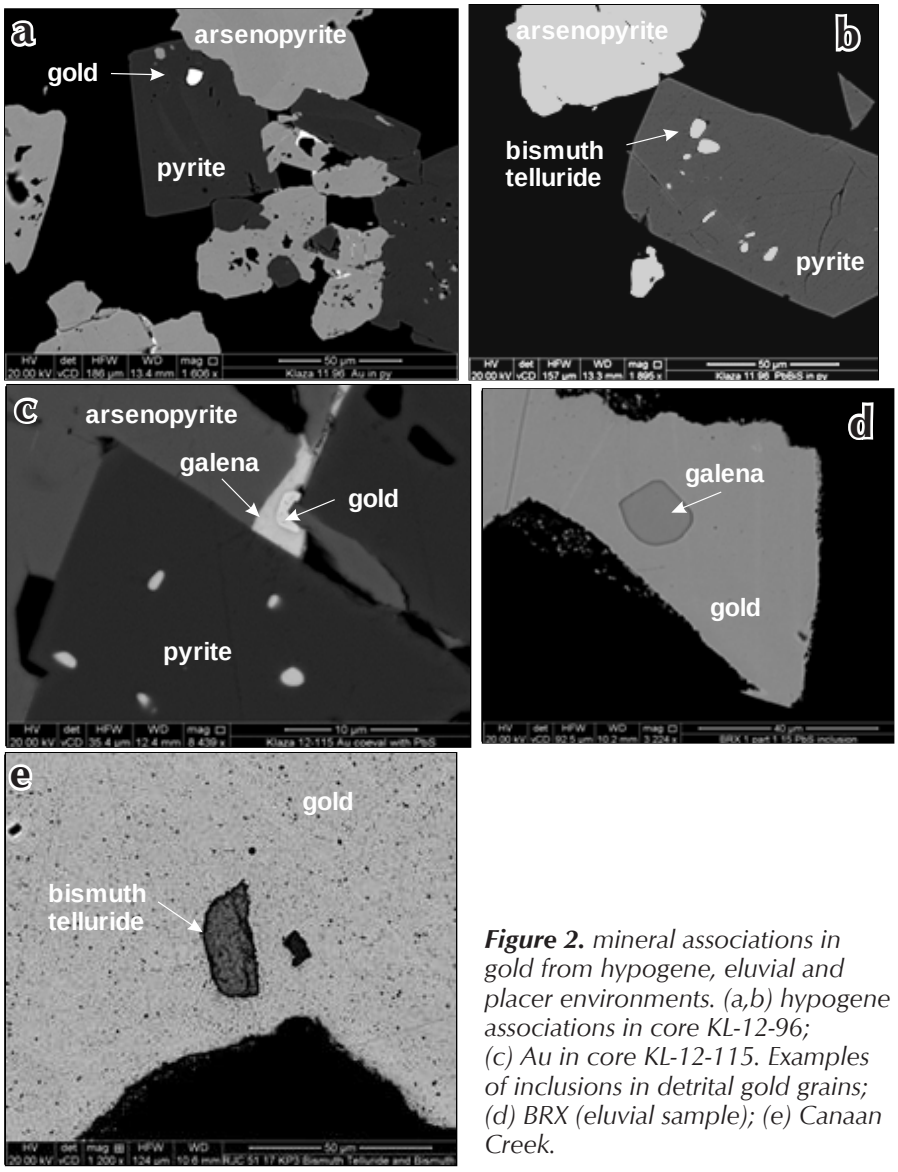


Figure 2. *mineral associations in gold from hypogene, eluvial and placer environments. (a,b) hypogene associations in core KL-12-96; (c) Au in core KL-12-115. Examples of inclusions in detrital gold grains; (d) BRX (eluvial sample); (e) Canaan Creek.*

PLACER SAMPLES

The morphology of the placer gold grains within the different sample populations are illustrated in Figure 5. Gold grains from Discovery Creek and Canaan Creek are rough, whilst the other placer samples include grains which exhibit a range of morphologies. The Ag content of the placer populations are depicted on the plots in Figure 3b. The sample from Canaan creek shows the highest overall Ag values, whilst the sample from the Discovery Creek exhibits the lowest values. These two samples have been used as 'end members' to evaluate other placer samples which exhibit features of both, but in different proportions. The placer sample from Victoria Creek resembles most closely that from the Canaan Creek, whereas that from Nansen Creek appears to conform to the Discovery Creek signature at low Ag values, but deviates thereafter.

The Ag curve describing Au from Discovery Creek also exhibits a shallow gradient for lower Ag values (Fig 3b). It also contains a substantial number of grains which contain higher levels of Ag, which could represent either an evolving system within the porphyry environment or additions from later vein mineralization as discussed above.

The covariance of Ag and Cu within the sample populations from Canaan Creek, Nansen Creek and Victoria Creek are shown in Figure 4c-e, where they are compared with the signatures of gold from both the BRX zone and Discovery Creek. The compositional field of gold from Canaan Creek overlaps with that of the gold from the BRX zones and shows the same general form, but it extends to a more Ag-rich area. Gold from Nansen Creek generally conforms to the compositional field of gold from Discovery Creek but there is also a clustering of more Ag-rich points similar to that observed in the sample from the Klaza River. Finally the small gold sample from Victoria Creek most closely resembles gold from the Canaan Creek, but a few grains show a high-Ag and high-Cu signature similar to the Discovery Creek sample.

The inclusion suites of the placer samples are shown in Table 4. Galena and Bi telluride are observed in every sample.

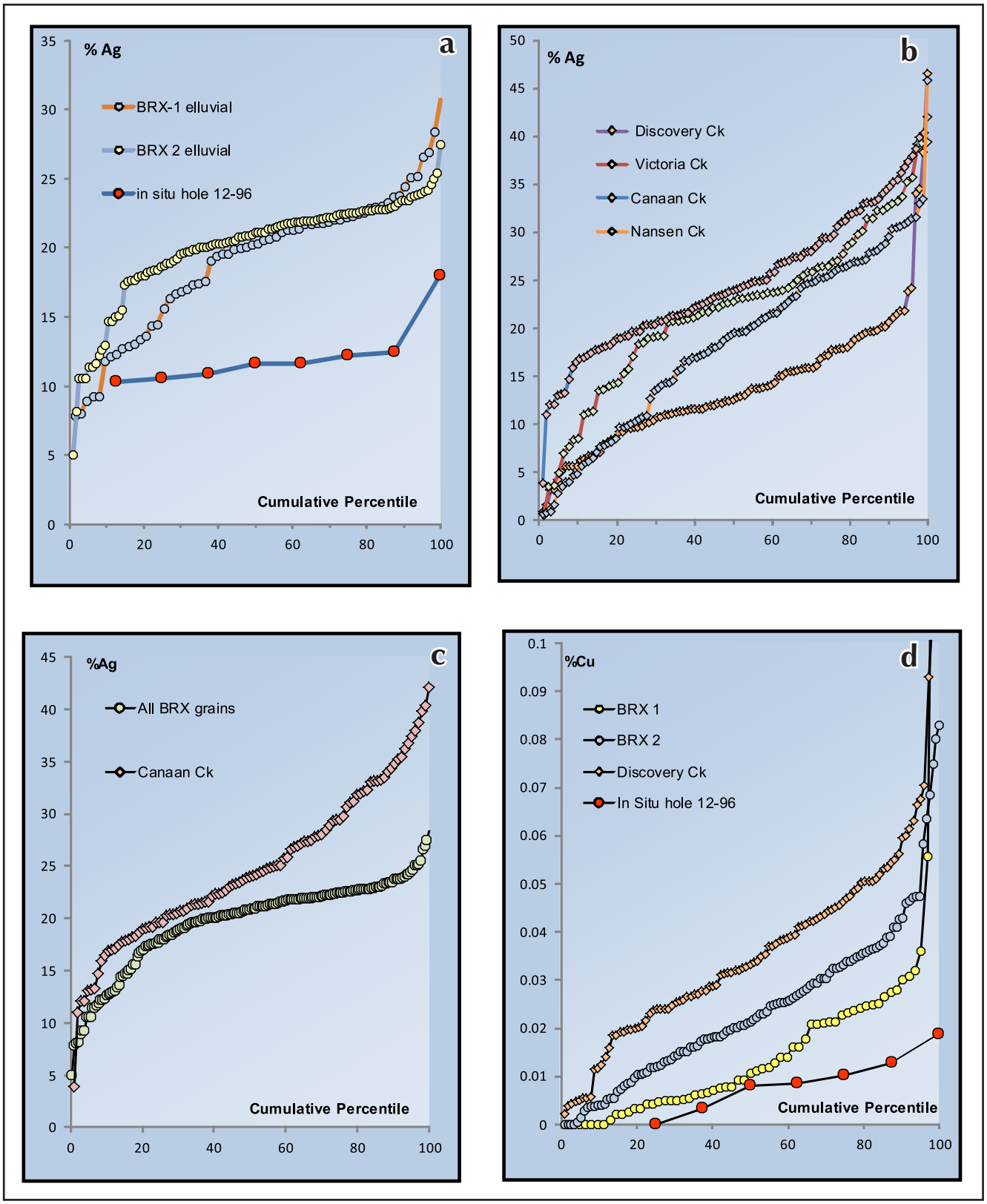


Figure 3. *Alloy compositions of gold grains from in situ eluvial and placer environments (a-c) Ag contents of alloys; (d) Cu content.*

Table 4. *Inclusion assemblages in placer and eluvial gold.*

Locality	Grains	Hg	Cu	Inclusion species											
				py	po	cpy	ga	sp	ars	Bi	ss	cv	hs	l	Sec
Discovery Ck	102	100	80				4		1	2					
Victoria Ck	78	95	54	1		1	1	1		3					
Canaan Ck	104	91	32	6		2	2			2		4			
Nansen Ck	157	100	40	12			5	2	3	3	1		1		
BRX-1	63	86	35	2		1	1				1				
BRX-2	114	90	56	1	1		1	1		2	1			1	2
Hayes Ck	122	12	32	6	2	3	8		2	3		1			

Mineral key as for Table 1, plus po=pyrrhotite, cv=cervelleite, (Ag_4TeS), hs=hessite, l=loelingite (FeAs), Sec=undetermined secondary (PbAs) bearing mineral on grain surface. 'Hg' and 'Cu'=% grains containing that metal to> LOD.

PLACER-LODE GOLD RELATIONSHIPS

RELATIONSHIP BETWEEN HYPOGENE ORE AND GOLD IN THE ELUVIAL ENVIRONMENT

The gold identified in polished blocks is much smaller in size than the eluvial grains recovered by sluicing. Consequently it is possible that there is a bias in the relationship between grain size and composition, although no such bias is observed in the data obtained from each block (where the samples are mounted according to size). Figures 3 and 4 show the relationships between the alloy compositions of hypogene and eluvial gold grains. The majority of the *in situ* grains (in core from around 340 m depth) show lower Ag content in comparison to most grains collected at surface. However, the lower Ag range exhibited by the gold in core is evident as a sub-population in the eluvial sample.

There is an overall similarity between the mineralogy of the hypogene ore and the inclusion suite observed within gold grains from the eluvial environment. Inspection of polished sections suggests that Au, Bi minerals and pyrite form the first phase of mineralization followed by arsenopyrite, galena and sphalerite. Table 4 and Figure 2 show that pyrite and Bi minerals form inclusions within the eluvial gold particles, whereas As is observed only as coatings of a Pb-As secondary mineral. Figure 2c shows that Au may also be coeval with galena, and galena inclusions in placer gold are also observed (Fig. 2d).

RELATIONSHIP BETWEEN ELUVIAL GOLD GRAINS AND PLACER GOLD GRAINS

The signatures of the BRX vein eluvial samples are used as a template to aid characterization of other placer samples in the study area. Figure 3c compares the Ag content of all grains collected from the BRX zone to the placer sample from the Canaan Creek. Gold grains containing >25% Ag form 97% of the population of grains from the Canaan Creek, but only 40% of the eluvial population of BRX vein Au. Figure 1 shows that the placer locality could also contain Au grains derived from veins situated between the BRX vein and the Klaza zone, although no information is available regarding their mineralogy. The Western Klaza zone is known to be relatively Ag-rich (Tarswell and Turner, 2014; Table 3) and Au grains from here could have travelled downslope to the placer sampling locality.

The suites of inclusion species observed within gold grains from the BRX zone and placer gold grains from Canaan Creek are largely compatible (Table 4), with the exception of cervelleite (Ag_4TeS). Four inclusions of cervelleite are observed the placer sample, but this mineral is not observed in either the BRX hypogene or the eluvial samples. All cervelleite inclusions are hosted by relatively Ag-rich Au alloy, and two of these exhibited Ag contents higher than any of the grains from the BRX vein. It is possible that the cervelleite-bearing grains are derived from the relatively Ag-rich Western Klaza zone or veins situated between the BRX and Klaza zones (Fig. 1).

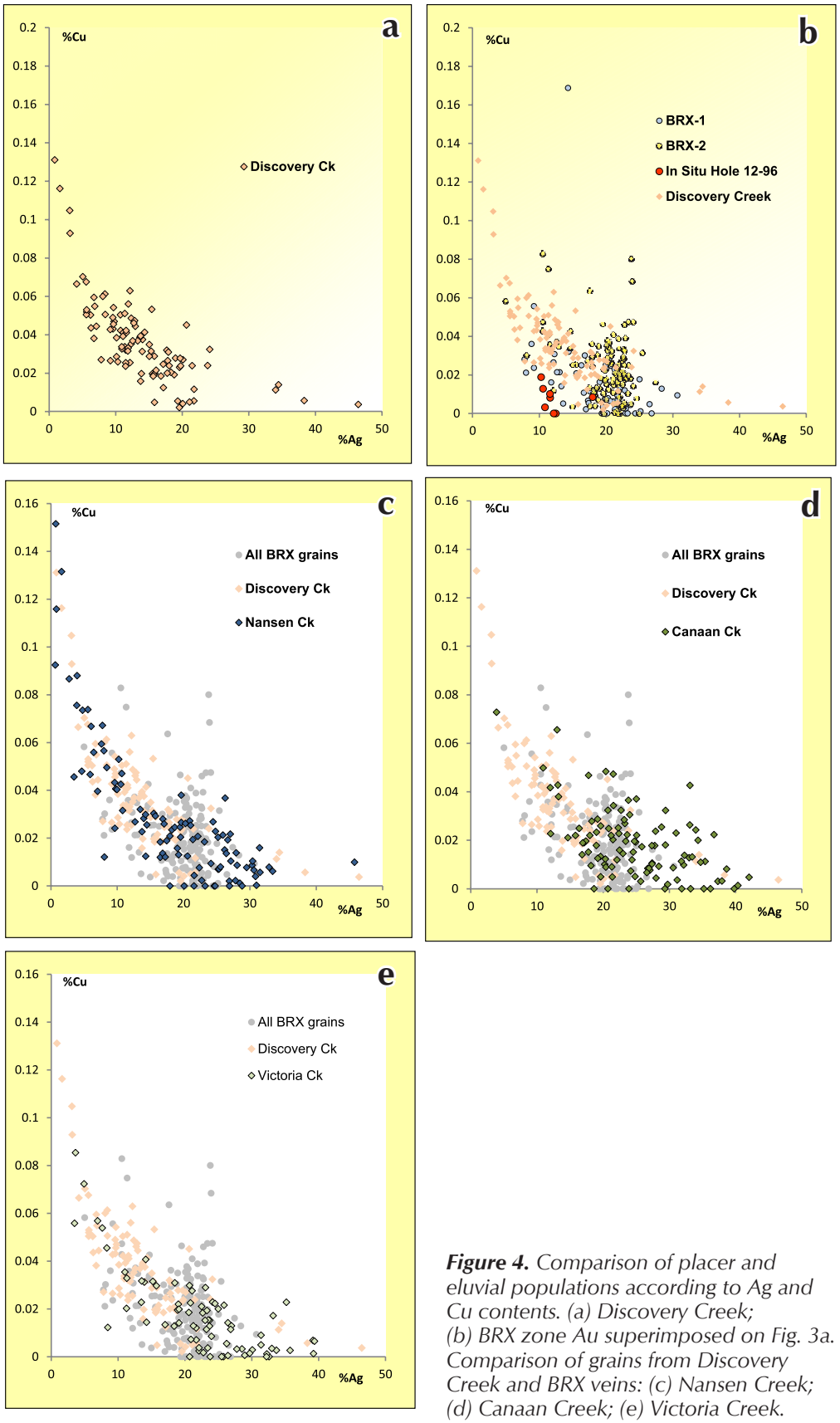


Figure 4. *Comparison of placer and eluvial populations according to Ag and Cu contents. (a) Discovery Creek; (b) BRX zone Au superimposed on Fig. 3a. Comparison of grains from Discovery Creek and BRX veins: (c) Nansen Creek; (d) Canaan Creek; (e) Victoria Creek.*

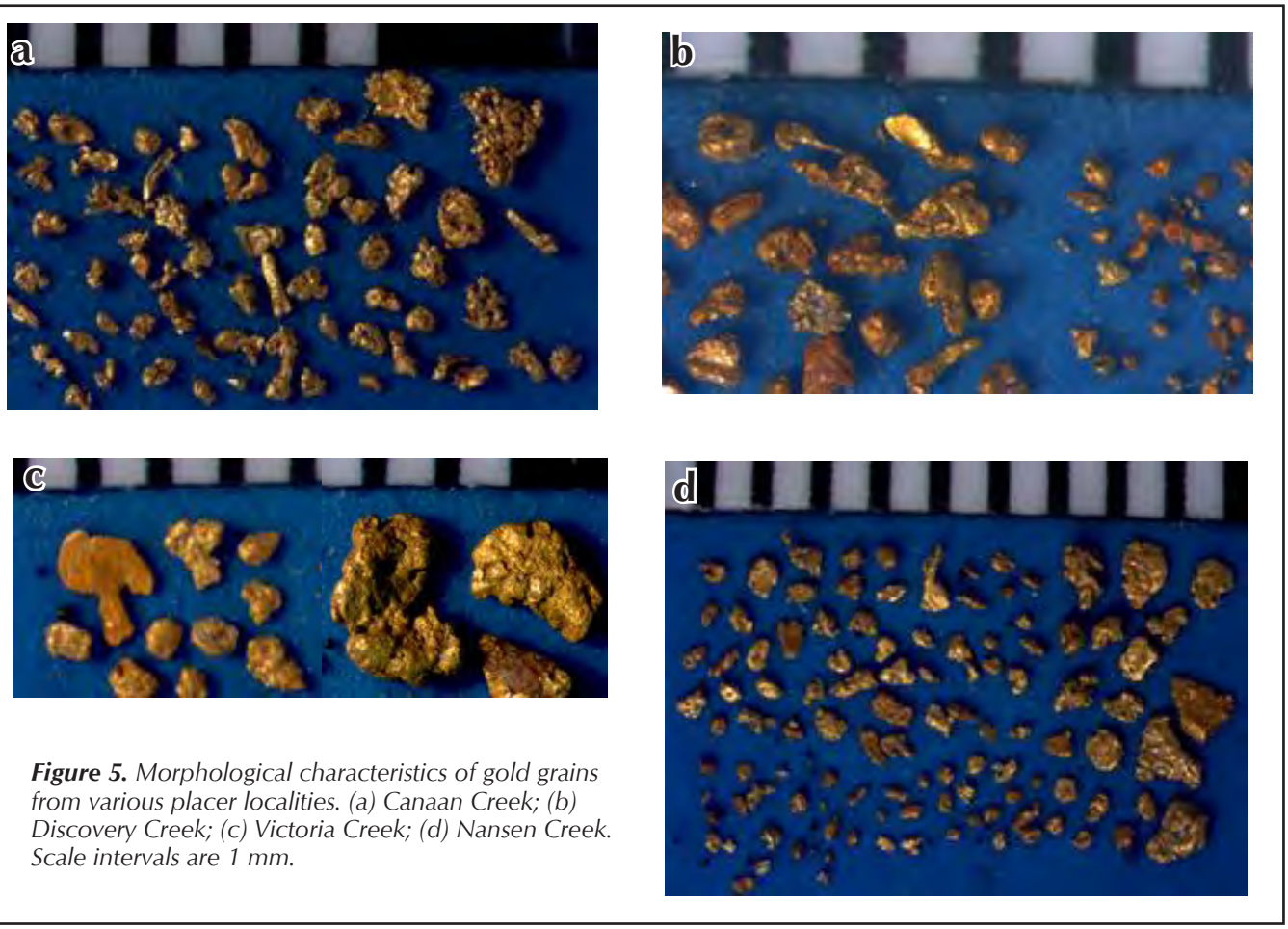


Figure 5. *Morphological characteristics of gold grains from various placer localities. (a) Canaan Creek; (b) Discovery Creek; (c) Victoria Creek; (d) Nansen Creek. Scale intervals are 1 mm.*

POTENTIAL SOURCES OF PLACERS

Consideration of the new data presented in this study has been undertaken in conjunction with bulk assay data from mining records, consideration of surficial geology (LeBarge, 1995) and the overview of regional mineralization presented in Hart and Langdon (1997) to clarify the most likely sources/source styles of mineralization for the various placers.

The Discovery Creek sample was collected from within the outcrop of the Cyprus South porphyry in the peripheral porphyry zone as defined by Hart and Langdon (1997). LeBarge (1995) reports that over 99% of the clasts in the drainage are proximal and consequently it is almost certain that all the placer Au grains were collected close to their source. Figure 5 shows that the Au grains have a rough surface texture and show little signs of fluvial transport. There are three possibilities for the source of these grains. Firstly, Au has been recorded in core samples from the phyllic alteration of the Cyprus south zone. Gold grains from this environment are probably formed from Au-bearing fluids which have stripped Au from pre-existing Cu-Au mineralization formed in the potassic zone, (Gammons and Williams-Jones, 1997). Secondly the 'Transitional' zone, in the headwaters of the Creek comprises veins and stockworks in a phyllic/argillic alteration zone (Table 1). An argillic overprint would probably not remobilize Au so the Au grains in this zone would likely resemble those in the Cyprus south mineralization. Finally there is a possibility of contribution of grains from the Eliza Creek localities although these occurrences outcrop slightly downstream of the sampling locality. From consideration of known *in situ* mineralization it could be expected that the Discovery Creek Au would consist predominantly of Au formed in an evolving porphyry environment, and indeed this sample is distinguished both by a lower Ag content (Fig. 3b) and higher Cu content (Fig. 3d).

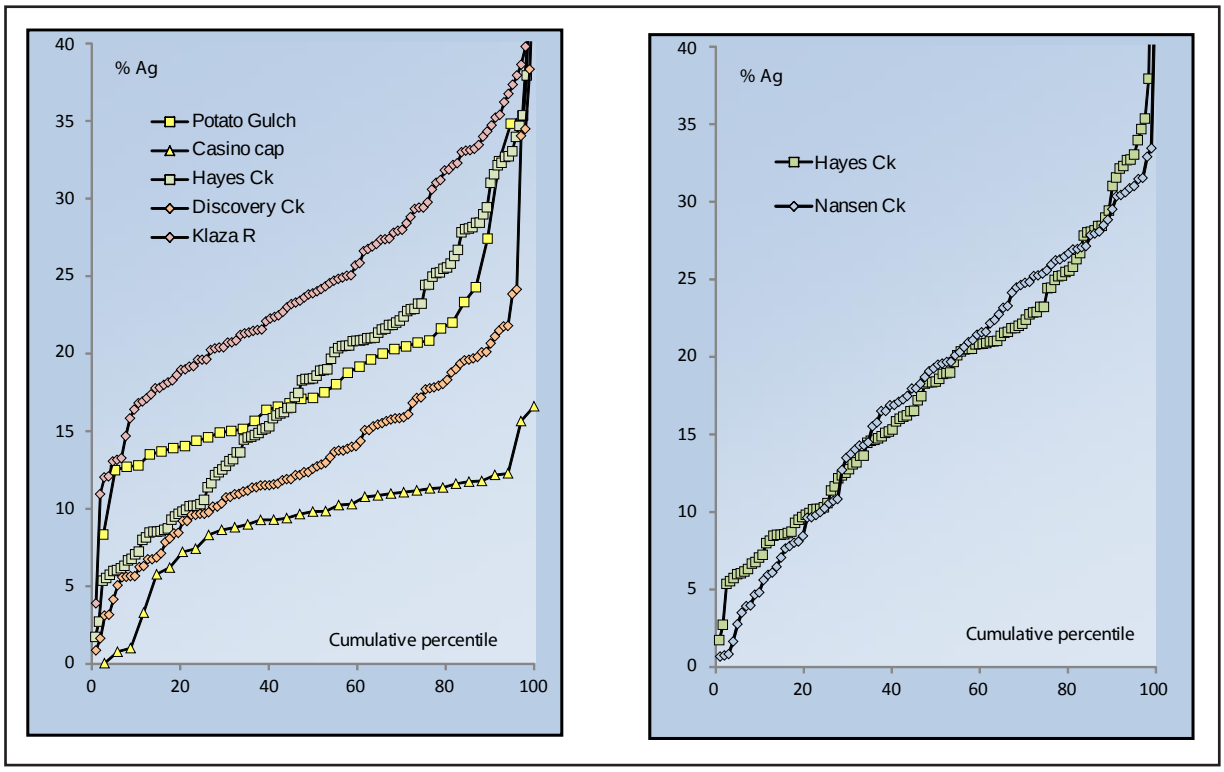


Figure 6. *Comparison of Ag contents of gold from porphyry and epithermal environments.*

Figure 3b shows that the Ag cumulative curve for Nansen Creek follows that of the gold from the Cyprus porphyry for the low-Ag component, but deviates to resemble that of the Canaan Creek sample at higher Ag values. Consideration of the Cu and Ag contents of the alloy also suggests multiple sources (Fig. 4d) as the cluster of compositions of around 30% Ag with variable Cu content is more similar to the signature of the BRX vein than the Discovery Creek gold. Figure 1 shows that Nansen Creek drains a number of potential *in situ* occurrences, principally Cyprus, Kelly and Kelly South. The Kelly and Kelly South occurrences also represent a potassic-phyllic transition, and it is entirely possible that Au from the Kelly South locality is of similar composition to that from the Cyprus south locality. There is no information available to establish whether the Au grades reported from either the Cyprus or Kelly porphyries (Table 1) relates to free Au, *i.e.*, tiny Au grains exsolved from Cu-bearing sulphides which are mostly too small to collect in placers (*e.g.*, Arif and Baker, 2004) or Au distributed within sulphide lattices.

The evidence presented in this section and the previous one, indicates that the Ag content of vein-derived Au is in general higher than that associated with porphyry mineralization. Consideration of Nansen Creek placer gold in the context of Ag content from contributing sources strongly suggests that a large proportion of the placer Au is derived from veins rather than the Kelly porphyry. Table 2 shows the large difference between the mass of placer Au recovered from Nansen and East Fork Nansen creeks. This spatial variation of Au appears incompatible with the model of the Cyprus porphyry being the major local source. It seems more probable that the bulk of Au in Nansen Creek is derived from either undiscovered or eroded veins associated with the Kelly porphyry system.

Data derived from the present study and gold fineness data (Table 2) show the Au from Victoria Creek to be relatively Ag-rich. Figure 5 shows that the grains exhibit varied morphologies, and there is a distinct population of relatively coarse, rough grains. Figure 4e shows a Ag-Cu signature very similar to that of the BRX vein sample, and it is proposed that similar, as yet undiscovered veins form the source of the Victoria Creek placer.

Although no samples of placer Au from Back Creek were available for this study, the range of fineness values reported (Table 2) suggests a contribution from both

porphyry and vein Au. van Loon and Bond (2014) report that nuggets up to 2 oz have been recovered recently, and these are most likely associated with a local vein source, rather than a porphyry environment. Figure 1 shows that the Willow Creek vein and the Cyprus South occurrences could constitute distinct sources consistent with this model.

The geomorphological development of the Nansen area described by LeBarge (1995) involves glacial erosion and transport of Au from pre-existing deep weathered material and associated fluvial sediments. LeBarge (1995) reports that Au grains are present within till, particularly at the bedrock-till contact. Consequently, it could be expected that some placer samples show an influence of relatively distal Au grains, although it is clear that that individual samples retain a strong signature of the most local source. The size of Au reservoir within present glacial sediments is unknown, consequently the placer mining records represent an unknown fraction of the total regional Au inventory. In addition, the most important placer creek (Nansen Creek) has not been mined to bedrock, but to a clay layer which is approximately 24 m thick (van Loon and Bond, 2014).

VARIATION IN GOLD SIGNATURE ASSOCIATED WITH THE PORPHYRY-EPITHERMAL TRANSITION

Whilst porphyry mineralization has a localized focus, the associated epithermal expression may be considerably more widespread, and consequently the peripheral geochemical footprint of the mineralization in the surficial environment may be influenced mostly by distal epithermal veins. From an exploration perspective, establishing the link between gold signatures in porphyries and related epithermal systems provides a mechanism to establish a vector to the most economically attractive mineralization. This study has provided the opportunity to examine the relationship between the composition of native gold formed in the porphyry environment and that of gold found in the associated epithermal expression.

EMPIRICAL CONSIDERATIONS

Hart and Langdon (1997) report four zones in the porphyry epithermal transition in the Nansen area, although this sequence is best developed to the southwest of the Nansen porphyry complex, outside the current study area. Sample suites available to the current study correspond to the peripheral porphyry zone and the epithermal zone. The most striking compositional difference is the variation in Ag content between gold derived from the placer sample from Discovery Creek (low Ag-peripheral porphyry) and the vein systems on the Klaza property (high Ag; Fig. 3b), and their placer expression at the Canaan Creek. It seems probable that the higher Cu signature of the Discovery Creek placer Au is also related to a systematic compositional trend, whereas the distribution of Hg within Au alloy appears variable.

Chapman *et al.* (2014) propose a generic relationship between porphyries and associated epithermal mineralization in which some key geochemical signatures of the porphyry system are retained (*e.g.*, a Bi and Te signature in the inclusion suite) whereas the Ag content of the Au grains increases. Studies of the Casino Creek-Canadian Creek drainage and Sonora Gulch-Hayes Creek systems provided the basis for this assertion (Fig. 6a). The similarity of the Ag content of Au grains from Hayes and Nansen creeks is striking, (Fig. 6b) and indicates that the same range of alloy compositions is evident in Au grains formed in these two different mineralizing systems. This similarity is also reflected in the inclusion assemblages (Table 4) by which Hayes Creek placer may be interpreted as derived from several sources, most of which are veins.

CONSIDERATIONS OF FLUID CHEMISTRY

Correlations between the fluid chemistry of a hydrothermal system and the resulting Au alloy compositions has been discussed in general by Morrison et al. (1991), and Gammons and Williams-Jones (1995). The alloy compositions reported above may be considered in terms of the nature of the prevailing and evolving hydrothermal systems. Gold and Ag are transported as their chloride complexes ($AuCl_2$-, $AgCl_2$-), in the environment of potassic alteration (Gammons and Williams-Jones, 1997; Williams-Jones and Heinrich, 2005). The most common manifestation of Au in this zone is as tiny exsolved blebs on grain boundaries of bornite and chalcopyrite (Kesler *et al.*, 2002), which are too small to report to the placer inventory. Subsequent remobilization of Cu and Au in propylitic and phyllic environments occurs under a different hydrothermal regime following the collapse of the original hydrothermal system (Gammons and Williams-Jones, 1997) in which Au is transported as the hydrosulphide complex. Depending on specific conditions, Au may be re-precipitated within the porphyry (together with chalcopyrite) or removed into the epithermal environment. In both cases the controls on alloy

composition are the same, *i.e.* $([Au]/[Ag])_{aq}$, temperature, pH, $aHS^-_{(aq)}$ and $aCl^-_{(aq)}$ (Gammons and Williams-Jones, 1995). Decreasing temperature results in a decrease in the Ag content of the alloy, as does decreasing $(Au/Ag)_{aq}$ resulting from the preferential precipitation of Au over Ag. It follows that small temperature variation in the porphyry setting could be expected to generate a relatively small range in Au alloy compositions, and this is observed in the grains from the hypogene environments at Casino, reported by Chapman *et al.* (2014), and in the sample from Discovery Creek reported here. Transition to the epithermal environment would be associated with more variable and generally lower temperature, and rapidly evolving $(Au/Ag)_{aq}$ following precipitation. In addition, there may be influences on fluid composition associated with fluid mixing. The net effect is to generate more Ag-rich Au alloy, and whilst locally the Au alloy signature may be constrained, it could be expected that there would be larger variation over the whole mineralizing system. This hypothesis is consistent with the observed compositional variation in the BRX and western Klaza zones as inferred by the eluvial samples and consideration of Canaan Creek placer sample. In general these observations are compatible with the 'Base-Metal-carbonate' model of Corbett (2002) but equally do not provide diagnostic evidence for that model.

Figure 4 shows two different types of relationship between the Ag and Cu contents of Au alloys. The porphyry mineralization (Discovery Creek) shows a predominant inverse relationship between Ag and Cu. The vein samples and their placer expressions yield Au in which Ag and Cu vary independently. At present, the underlying reasons for this difference in behaviour is not understood, but it has proved a useful discriminant in interpreting the origins of detrital gold in different placer populations. Similarly, the underlying reasons for the sporadic presence of Hg in some grains remain unclear.

The data presented in Table 4 show that the Bi-Pb signature is strong and pervasive. Interpretation of the significance of the abundance of other mineral inclusions is to some extent constrained by the relatively small sample sizes.

IMPLICATIONS FOR EXPLORATION

A study of the microchemical signatures of gold grains derived from the porphyry mineralization at Revenue/Nucleus, Casino and Sonora Gulch reported by Chapman *et al.* (2014) identified a common Pb-Bi-Te signature in the inclusion assemblage. This association is also observed in the present study which has further enhanced the potential for applying microchemical characterization of detrital gold grains in an exploration context. In addition, gold grains from these porphyry environments exhibit concentrations of Cu in the Au alloy consistently higher than gold grains derived from orogenic mineralization. Populations of placer grains from associated epithermal mineralization show wider variations in the concentration of Ag and perhaps substantial variation between the signatures of placer samples collected within a small area if there are multiple vein sources.

The Nansen trend is regionally atypical in the abundance of Au-bearing veins associated with the porphyry systems. Furthermore, the Cu-Au porphyry mineralization is weaker than that observed in broadly equivalent mineralized environments elsewhere. Gammons and Williams-Jones (1995) suggest that collapse of a magmatic hydrothermal system may result in overprinting of the potassic alteration zone by retrograde pyrite-rich phyllic alteration with the associated remobilization of gold in a hydrosulphide-rich fluid. Hart and Langdon (1997) report pervasive strong phyllic alteration and pyrite in a halo surrounding the potassic core of the Cyprus porphyry, and a similar feature is reported in Kelley South. Remobilization of Au provides a source for strongly developed epithermal mineralization which would inherit some of the geochemical signatures of the source mineralization, (*e.g.*, Bi, Pb and Te). It is also highly probable that the particle size of Au within late stage and epithermal veins is larger than that found in the earliest porphyry mineralization. Consequently the size and mineralogy of Au grains within placers may not correspond to the Au particles within the primary ore that are ultimately one of the targets of exploration. Understanding the genetic relationships between evolving porphyry systems and their epithermal expressions in terms of Au mineralogy is therefore key to interpretation of the characteristics of placer grains collected during reconnaissance.

CONCLUSIONS

The mineralogy of the inclusion suite revealed within polished sections of detrital gold grains from weathered outcrop in the BRX zone and the Canaan Creek placer are comparable with that of the Au-bearing stages of the hypogene ore observed in core samples, indicating that gold grains pass from the hypogene to the surface environments unmodified.

In this study, Ag content has proved a useful discriminant between porphyry and vein-derived Au. In general it has been possible to map Ag content onto end members of the porphyry-epithermal transition, and this has facilitated interpretation of the origins of placer Au in the Nansen district. The signature of gold grains collected from the BRX vein outcrop is replicated in the Canaan Creek placer, but a (very) high Ag component of the Canaan Creek placer is probably derived from other vein systems such as Western Klaza Zone. The placer Au in Nansen Creek is primarily of vein origin, although there is likely a strong contribution of Au from the Kelly rather than Cyprus porphyry. The wide range of Ag content observed in the Nansen Creek placer Au corresponds to fluctuations in fineness reported in production records and is interpreted as indicative of influx from several sources. The placer Au in Victoria Creek is predominantly vein derived although the sources remain undiscovered. Overall the study has shown that Au derived from veins is the most important contributor to placer development in the Nansen Creek area. In general the composition of Au in the various placers is consistent with the nature of the potential sources and generic relationships between porphyry and surrounding epithermal mineralization.

The values and variability of Ag and Cu contents of Au derived from porphyry and vein mineralization observed during this study may be correlated with the environment of Au precipitation. Gold veins formed during phyllic alteration from fluids which stripped Au from pre-existing mineralization in the potassic zone yielded Au of high Cu content and low Ag content and range, reflecting the relatively stable environment of mineralization. In contrast the precipitation of Au in the epithermal environment may be in response to abrupt changes in a variety of parameters and this is mirrored in the alloy signature, although the grains exhibit a similar inclusion suite as their porphyry derived counterparts.

This study augments previous work which described a generic Bi-Pb-Te signature of gold from calc-alkaline Cu-Au porphyries in Yukon, and that signature has also been identified in both porphyry and epithermal Au from the Nansen area. The importance of understanding the relationship between a porphyry system and its epithermal expression has been highlighted. The compositional ranges of populations of detrital Au particles collected during reconnaissance stream sediment sampling are more likely to be derived from relatively widespread epithermal mineralization than the relatively geographically constrained porphyry. The epithermal Au may be Cu-poor even though the primary mineralization is a Cu-Au porphyry.

The study has highlighted the need to consider stream order when interpreting Au-grain signatures. Both the Canaan Creek and the Discovery Creek placer samples were collected from first order streams, with geographically well constrained sources. The delicate nature of many Au particles reflects this proximity to source, and these samples were the most useful in developing a placer-lode model for the study area. The morphology of Au grains from Nansen Creek indicate fluvial transport, which raises the potential for multiple sources cited in various tributaries. In cases such as this it is more difficult to develop robust placer-source relationships, unless a large (typically >200) number of Au grains are available which may be considered in terms of both morphology and composition.

ACKNOWLEDGMENTS

This study was made possible by the provision of SINED funding through the Yukon Geological Survey. We are extremely grateful to Rockhaven Resources for providing us with access to the site and to excellent on-site accommodation. Finally we would like to thank Jared Tarswell and Heather Burrell of Archer Cathro; they were enthusiastically engaged with our work and went out of their way to provide maps, background information and samples of hypogene ore.

REFERENCES

Allan M.M., Mortensen J.K., Hart C.J.R., Bailey L.A., Sánchez M.G., Ciolkiewicz W.,McKenzie G.G. and Creaser R.A., 2013. Magmatic and metallogenic framework of west-central Yukon and eastern Alaska. *In:* Tectonics, Terranes, Metallogeny and Discovery in the northern circum-Pacific region, M. Colpron, T. Bissig, B. Rusk and J. Thompson (eds.), Society of Economic Geologists, Special Publication vol. 17. p. 111-168.

Arif, J. and Baker, T., 2004. Gold paragenesis and chemistry at Batu Hijau, Indoneisa: implications for gold-rich porphyry copper deposits. Mineralium Deposita vol. 39, p. 523–535.

Chapman, R.J., Leake, R.C., Moles, N.R., Earls, G., Cooper, C., Harrington, K. and Berzins, R., 2000. The application of microchemical analysis of gold grains to the understanding of complex local and regional gold mineralization: a case study in Ireland and Scotland. Economic Geology, vol. 95, p. 1753-1773.

Chapman, R.J., Mortensen, J.K., Crawford, E.C. and Lebarge, W., 2010a. Microchemical studies of placer and lode gold in the Klondike district, Yukon, Canada: 1. evidence for a small, gold-rich, orogenic hydrothermal system in the Bonanza and Eldorado Creek area. Economic Geology, vol. 105, p.1369-1392.

Chapman, R.J., Mortensen, J.K., Crawford, E.C. and LeBarge, W.P., 2010b. Microchemical studies of placer and lode gold in the Klondike District, Yukon, Canada: 2. Constraints on the nature and location of regional lode sources. Economic Geology, vol. 105, p. 1393-1410.

Chapman, R.J., Mortensen, J.K. and LeBarge, W.P., 2011. Styles of lode gold mineralization contributing to the placers of the Indian River and Black Hills Creek, Yukon Territory, Canada as deduced from microchemical characterization of placer gold grains. Mineralium Deposita, vol. 46, p. 881-903.

Chapman, R.J., Allan, M.M., Grimshaw, M.K., Mortensen, J.K., Wrighton, T.M. and Casselman, S., 2014. Pathfinder signatures in placer gold derived from Au-bearing porphyries. *In*: Yukon Exploration and Geology 2014, K.E. MacFarlane, M.G. Nordling, and P.J. Sack (eds.), Yukon Geological Survey, p. 21-31.

Colpron, M. (compiler), 2006. Tectonic assemblage map of Yukon-Tanana and related terranes in Yukon and northern British Columbia (1:1 000 000 scale). Yukon Geological Survey, Open File 2006-1.

Corbett, G., 2002. Epithermal Gold For Explorationists. Australian Institute of Geoscientists Journal - Applied geoscientific practice and research in Australia, Paper 2002-1.

Gammons, C.H. and Williams-Jones, A.E., 1995. Hydrothermal geochemistry of electrum: Thermodynamic constraints. Economic Geology, vol. 90, p. 420-432.

Gammons, C.H. and Williams-Jones, A.E., 1997. Chemical mobility of gold in the porphyry epithermal environment. Economic Geology, vol. 92, p. 45-49.

Hart, C.J.R. and Langdon, M., 1997. Geology and mineral deposits of the Mount Nansen camp, Yukon. In: Yukon Exploration and Geology 1997, Exploration and Geological Services Division, Yukon, Indian and Northern Affairs Canada, p.129-138.

Heinrich, C.A., 2005. The physical and chemical evolution of low-salinity magmatic fluids at the porphyry to epithermal transition: a thermodynamic study. Mineralium Deposita vol. 39, p. 864–889.

Kesler, S.E., Chryssoulis, S. L. and Simon, G., 2002. Gold in porphyry copper deposits: its abundance and fate. Ore Geology Reviews vol. 21, p. 103–124.

LeBarge, W.P., 1995. Sedimentology of Placer Gravels near Mt. Nansen Central Yukon territory. Exploration and Geological services Division, Indian and Northern Affairs Canada, Yukon Region, Bulletin 4, 155 p.

LeBarge, W.P. (compiler), 2007. Yukon Placer Database 2007 - geology and mining activity of placer occurrences. Yukon Geological Survey, CD-ROM.

Morrison, G.W., Rose, W.J. and Jaireth, S., 1991. Geological and geochemical controls on the silver content (fineness) of gold in gold–silver deposits. Ore Geology Reviews, vol. 6, p. 333-364.

Tarswell, J. and Turner, M., 2014. Assessment report describing excavator trenches, geophysical surveys and metallurgical tests at the Klaza property. Prepared by Archer, Cathro & Associates (1981) limited for Rockhaven Resources Ltd., Assessment Report #096667.

van Loon, S. and Bond, J.D. (compilers), 2014. Yukon Placer Mining Industry 2010-2014. Yukon Geological Survey, 230 p.

Williams-Jones, and A.E., Heinrich, C.A., 2005. Vapor Transport of Metals and the Formation of Magmatic-Hydrothermal Ore Deposits. Economic Geology, vol. 100, no. 7, p. 1287-1312.

Wrighton, T.M., 2013. Placer gold microchemical characterization and shape analysis applied as an exploration tool in western Yukon. Unpublished MSc Thesis, University of British Columbia, 140 p.

Yukon MINFILE, 2015. Yukon MINFILE - A database of mineral occurrences. Yukon Geological Survey, <http://data.geology.gov.yk.ca> [accessed September 22, 2015].

Preliminary observations on the geology of Tay Mountain Area (parts of NTS 105K/12 and 13, 105L/09 and 16), central Yukon

R. Cobbett[1]
Yukon Geological Survey

Cobbett, R., 2016. Preliminary observations on the geology of Tay Mountain Area (parts of NTS 105K/12 and 13, 105L/09 and 16), central Yukon. *In:* Yukon Exploration and Geology 2015, K.E. MacFarlane and M.G. Nordling (eds.), Yukon Geological Survey, p. 79-98.

ABSTRACT

Regional mapping north and west of Faro is aimed at improving knowledge of the geologic history of the area and at elucidating the host stratigraphy and structures of both precious and base-metal occurrences. The southern part of the Tay Mountain area is underlain by metamorphosed lower Cambrian to Silurian Selwyn basin strata. These are thrust northward over Silurian to Triassic clastic, carbonate and volcanic rocks. The entire succession is intruded by mid-Cretaceous granitic rocks of the Tay River plutonic suite. The area is deformed by folding and north-verging thrust faults and by both east-west and north-south oriented normal faults. There is evidence that north-verging thrust faults are reactivated Devonian normal faults that formed in response to regional extension and controlled the deposition of the Earn Group.

Selwyn basin strata, which are age-equivalent to the Anvil Mine host stratigraphy, crops out extensively south of the Twopete thrust fault. The end of a northwest-trending belt of silver-bearing occurrences is located at Mount Menzie. Folded chert in proximity to calcareous rocks and granitic intrusions are common features of the silver showings in the area.

[1]*rosie.cobbett@gov.yk.ca*

INTRODUCTION

In 2013 the Yukon Geological Survey initiated a multi-year, 1:50 000 scale revision mapping project focused on the western edge of the Tay River map area (NTS 105K) and the northeast corner of the Glenlyon area (NTS 105L; *see* Fig. 1). This paper describes stratigraphy and structure of the area, augmenting the preliminary report from Anvil Lake area (Cobbett, 2014) and its final map (Cobbett, 2015). The mapping described herein extends westward to Tay Mountain, including Mount Menzie and the southeast Earn Hills (Fig. 2).

The area includes the northwestern end of a trend of high-grade silver-bearing occurrences on-trend with the Keg deposit (Yukon MINFILE 105K 078; discovered in 1966, assessed through the 1970s) that parallels a NW-trending fold-thrust belt. The mineralized trend is exposed on Twopete Mountain, Mount Menzie and Earn Hills (Fig. 2).

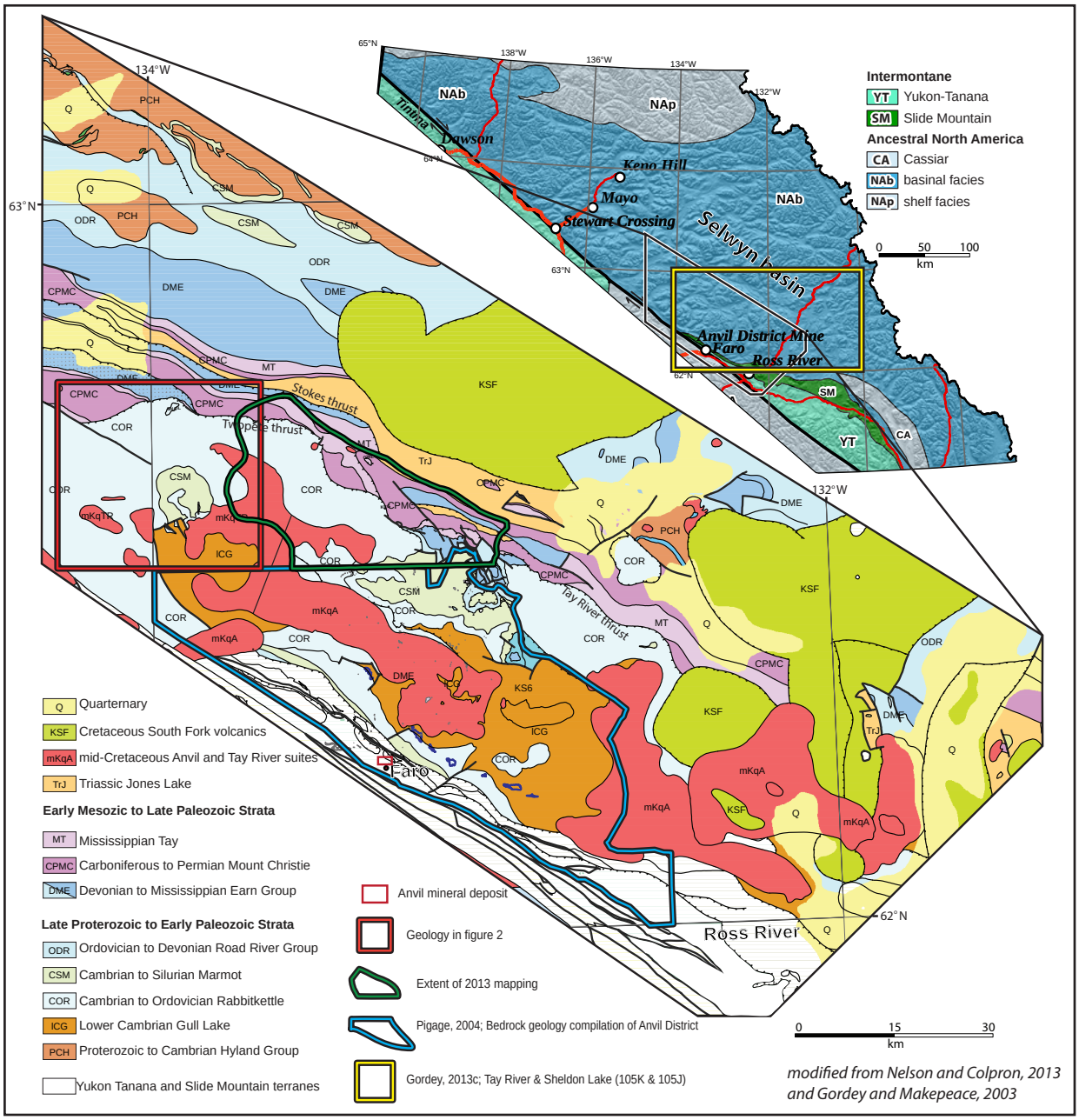


Figure 1. *Geologic terranes (from Nelson et al., 2013) shown in the top right map; mapped area lies in Selwyn basin; previous mapping by Gordey (2013c) outlined in yellow. Larger map shows geology of the Anvil district with coloured outline of previous mapping by Pigage (2004; blue) and Cobbett (2015; green).*

This project has identified previously unrecognized Lower Paleozoic strata that suggest there is potential for SEDEX-style mineralization similar to the Faro Mine within the Tay Mountain area (Figs. 1 and 2). Better understanding of Upper Paleozoic stratigraphy has allowed a re-interpretation of faults, in specific the timing and kinematic history of northeast-verging thrust faults.

GEOLOGIC FRAMEWORK

The area of interest lies in central Yukon, 50 km north of the previously mined Faro deposit (Fig. 1), within the southern part of Selwyn basin. This is a broad region underlain by mostly lower Paleozoic deep water clastic, cherty and less common thin carbonate strata (Gabrielse, 1967; Gordey and Anderson, 1993; Gordey, 2013a). Devonian through Mississippian quartz-rich sandstone, siltstone and conglomerate were deposited unconformably on the lower Paleozoic strata (Abbott *et al.*, 1986; Gordey and Anderson, 1993). Carboniferous through Jurassic clastic rocks that unconformably overlie the Devonian to Mississippian clastic rocks represent a continental shelf setting. Although of regional significance, these two major unconformities are only locally exposed in the area of interest.

The mapped area (hereafter referred to as the Tay Mountain area; Fig. 2) is within the Omenica structural province characterized by north and northeast-verging folds and thrust faults. These structures are linked to northeastward shortening that is generally accepted to have resulted from collision of continental fragments and arc assemblages with the western edge of Laurentia in Middle Jurassic (Colpron *et al.*, 2006; Mair *et al.*, 2006). Parts of these subducted terranes lie beyond the southwest corner of the area of interest and are southwest of the Tintina fault, a post-mid-Cretaceous dextral strike-slip fault (Gabrielse *et al.*, 2006; Roddick, 1967). The structurally thickened Selwyn basin strata are intruded by late Early Cretaceous granitic plutons of the Tay River suite (Gordey and Anderson, 1993; Rasmussen, 2013).

The southern half of the Tay Mountain area is made up of lower Cambrian to Silurian Selwyn basin strata, thrust over Devonian to Triassic strata in the northern half (Fig. 3). The Selwyn basin strata are metamorphosed and range from mildly foliated to completely recrystallized. The late Paleozoic strata are deformed by a northwest trending fold and thrust belt. The Anvil batholith and several small, coeval granitic plugs intrude both successions and impose a contact aureole that ranges from tens of metres to several kilometres in width.

STRATIGRAPHY

Two essentially equivalent lower Paleozoic stratigraphic successions have been used in the area of interest: one extends from regional mapping of the Selwyn basin, the other extends from mapping of the metamorphosed sequence surrounding the Anvil mine district. These units are employed in the south half of the Tay River area; from the stratigraphic oldest, Mount Mye, Vangorda, and Menzie Creek formations. This metamorphic package is unconformably overlain by a relatively unmetamorphosed Devonian through Triassic sequence including several lithologic divisions of the Earn Group, succeeded by the Mount Christie and Jones Lake formations (Fig. 3).

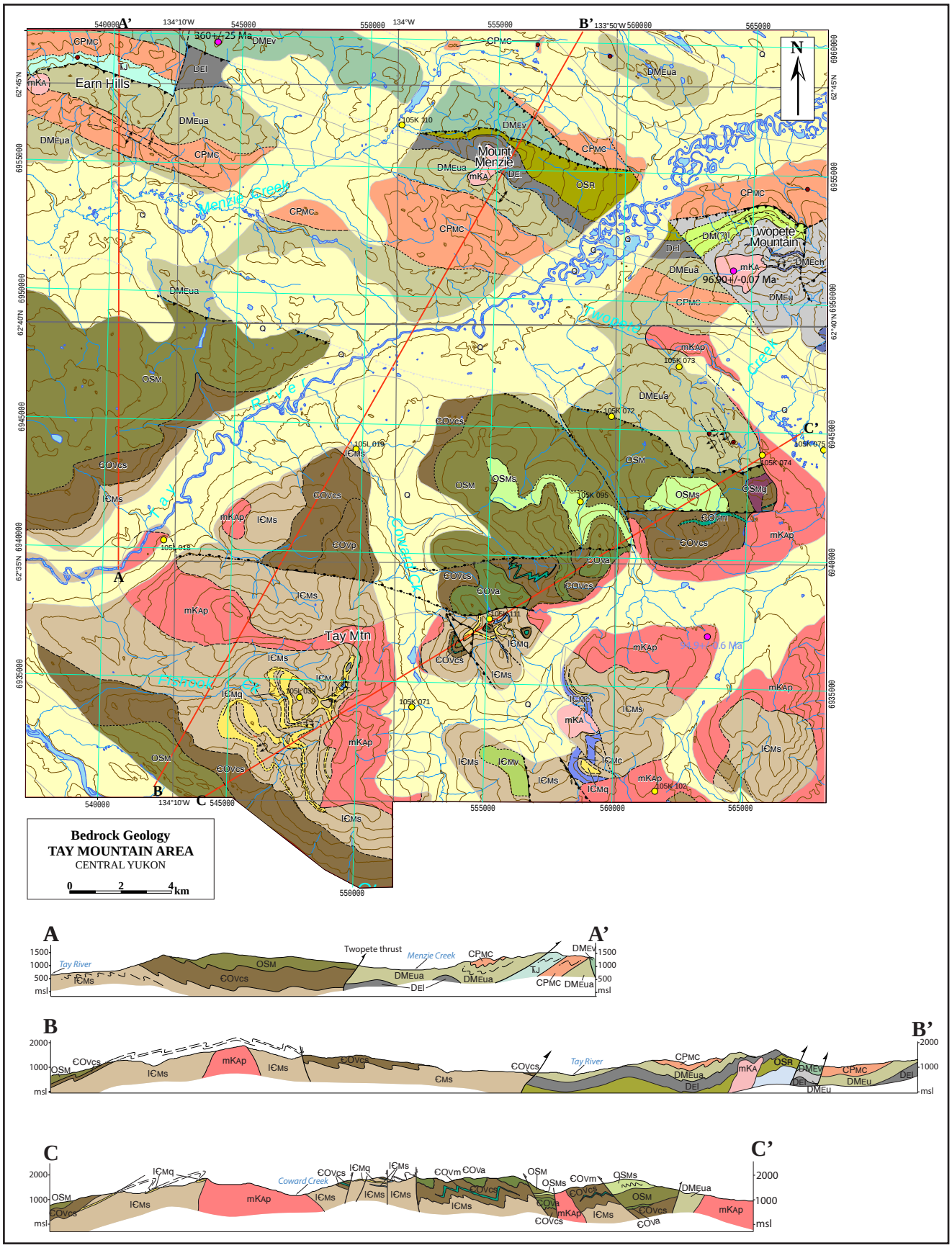
LOWER CAMBRIAN TO SILURIAN ROCKS SOUTH OF TWOPETE THRUST

Meta-clastic, carbonate and volcanic strata in the south half of the mapped area, interpreted to be lower Cambrian to Silurian, were designated as Gull Lake Formation, Rabbitkettle Formation, and overlying Menzie Creek Formation on regional maps (Gordey, 2013b,c). Currently, however, local workers have followed the leads of Jennings and Jilson (1986) and Pigage (2004), employing the informally named Mount Mye (uPCM units) and Vangorda formations (COV units), and Menzie Creek Formation (OSM units) for the equivalent strata within the Anvil District. This informal terminology is adopted here for most of the rocks in the north part of the Anvil district, and the lower-case suffixes for these units indicate predominant lithologies (not necessarily in stratigraphic order within the formation).

MOUNT MYE FORMATION

Blocky outcrops of brown weathered, well foliated mica schist comprise the dominant lithology. On Tay Mountain and along several ridges due east of Tay Mountain (Fig. 2) it is brown and grey on both weathered and fresh surfaces, fine and medium-grained, variably porphyroblastic (cordierite and andalusite) biotite-muscovite schist (Fig. 4a). The schist is interlayered with several other rock types including metavolcanic rocks, quartzite and marble.

a


Bedrock Geology
TAY MOUNTAIN AREA
CENTRAL YUKON
0 2 4 km
N
Earn Hills
Mount Menzie
Twopete Mountain
Tay Mtn
360 +/- 25 Ma
96.90 +/- 0.07 Ma
94.9 +/- 1.6 Ma
Tay River
Menzie Creek
Coward Creek
Twopete Creek
Finlayson Creek
A
A'
B
B'
C
C'
Twopete thrust
OSM
mKAp
mKA
DMEua
DMEv
DMEu
DMEch
DEl
CPMC
OSR
IEMs
IEMq
IEMv
EOVcs
EOVa
EOVm
EOVp
OSMs
OSMg
DM(2)l
105K 110
105K 073
105K 072
105K 075
105K 074
105K 095
105K 111
105K 102
105K 071
105K 039
105L 019
105K 018
msl

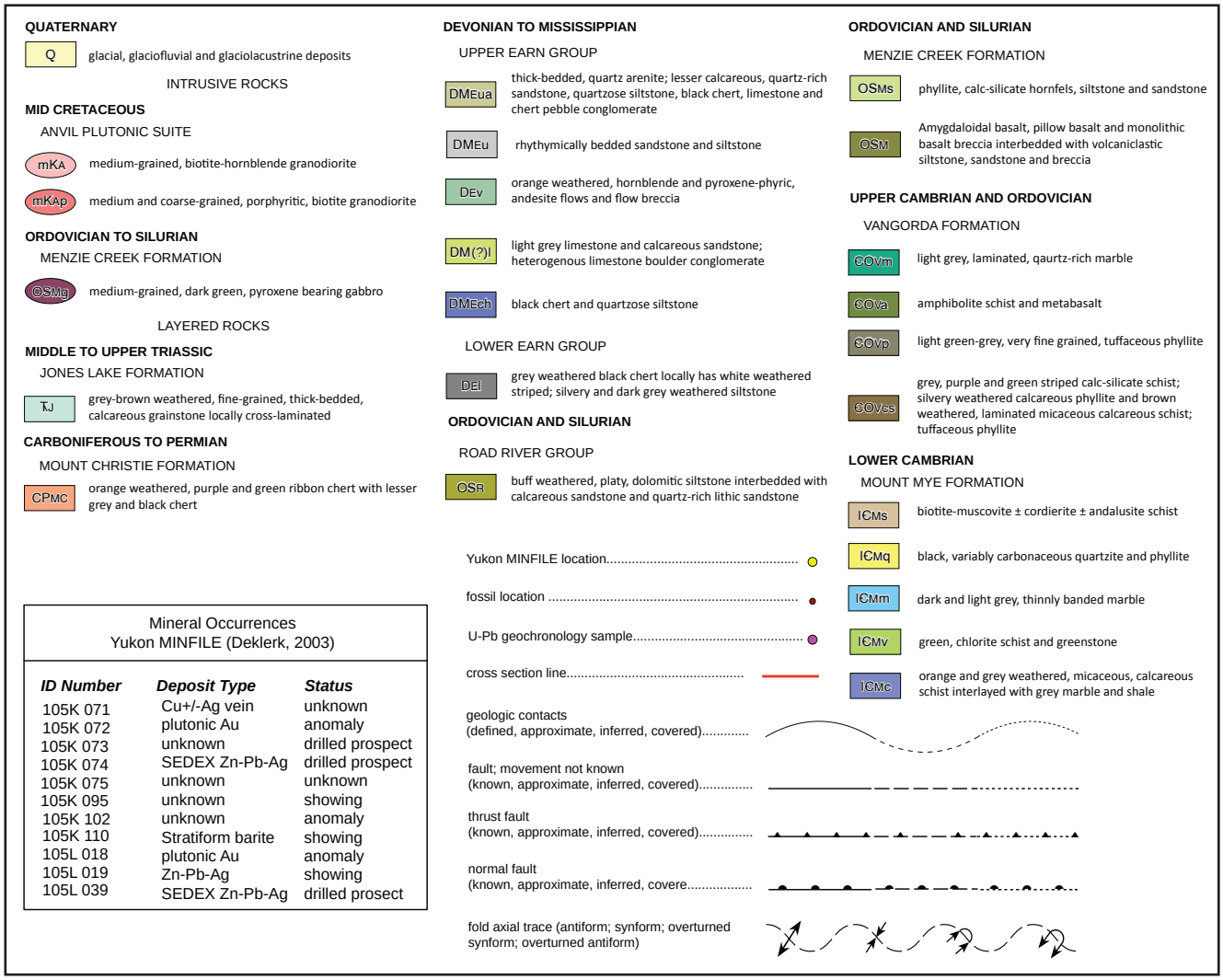


Figure 2. *(a) Bedrock geology sketch map, cross sections and (b) legend of the Tay Mountain area, based upon fieldwork in 2013 and 2015.*

The metavolcanic rocks occur in one locality a couple of kilometres southeast of the head waters of Coward Creek. Here they are green, fine-grained, well foliated chlorite phyllite and schist and dark green, fine-grained, massive greenstone with fine and medium-grained, disseminated biotite and rare pyroxene (?) crystals.

Near the top of the Mount Mye formation a dark grey to black, fine-grained, carbonaceous, micaceous quartzite provides a marker horizon within the monotonous mica-schist succession (Fig. 4b). This lithology is exposed on Tay Mountain and in several localities east of Tay Mountain and ranges in thickness from 20-60 metres.

At least two distinct calcareous horizons within the schist lie close to the quartzite. One of these horizons occurs 50 to 100 m stratigraphically below the quartzite unit east of Tay Mountain and is at least 120 m thick. This unit comprises orange and grey weathered, grey fresh, thin-bedded micaceous, calcareous schist thickly interlayered with light grey marble and minor grey shale. In other localities, including Tay Mountain, a dark and light grey striped marble crops out both above and below the quartzite and ranges in thickness from 10 to 30 m (Fig. 4c). The marble looks very similar both above and below the quartzite and could be the same depositional layer. In this case, a fold in the quartzite is necessary to make sense of the map pattern. Adjacent to dikes and sills the marble is replaced by garnet-pyroxene skarn ± semi-massive sulphide.

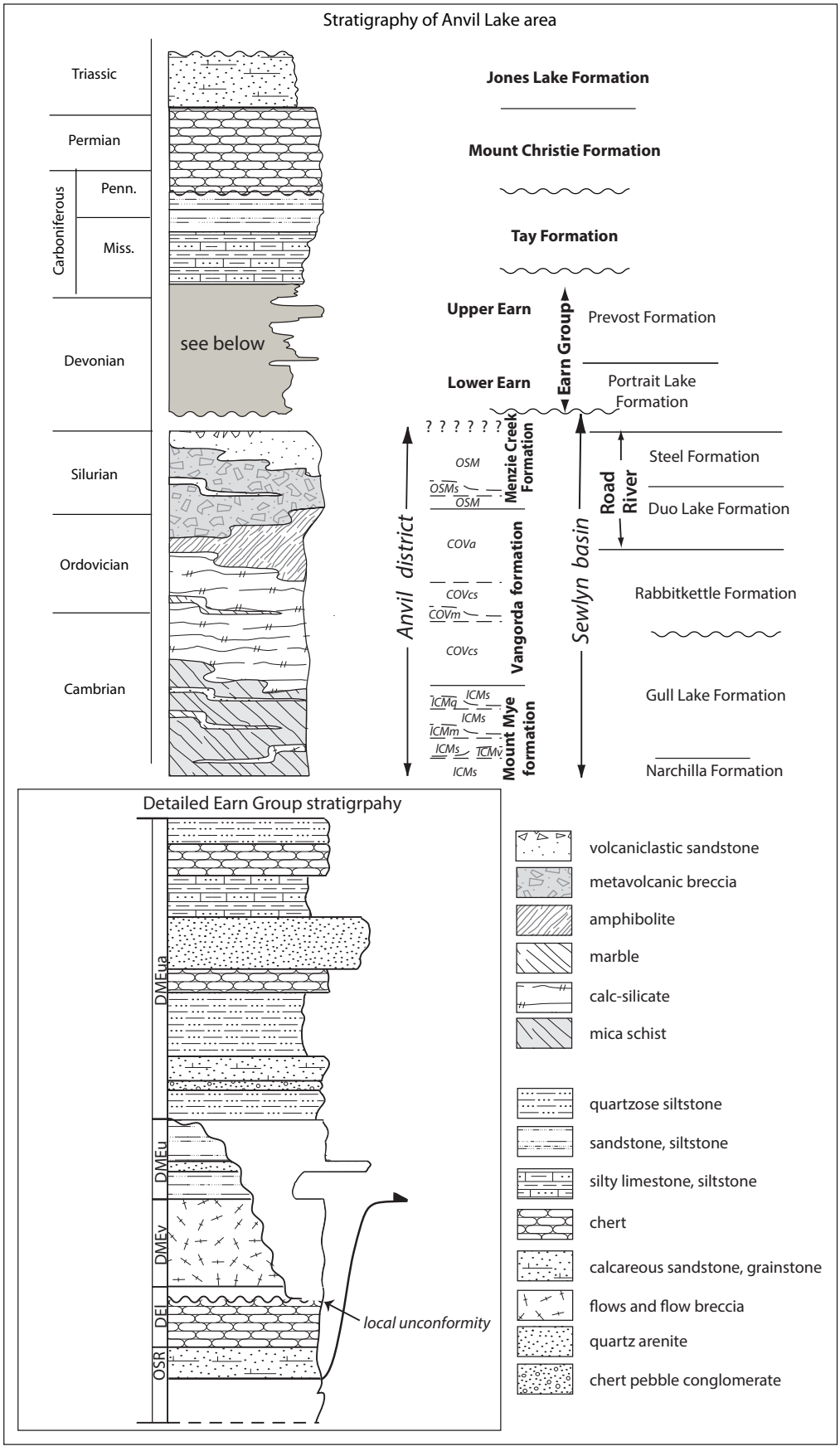


Figure 3. *Representative stratigraphy of the combined Anvil Lake and Tay Mountain areas (adapted from Cobbett, 2014). The Anvil mine district terms (left column) are used for map units in this paper; regionally equivalent Selwyn basin stratigraphy is on the right.*

The base of the Mount Mye formation is nowhere exposed. Approximately one kilometre of Mount Mye formation strata is exposed east of Tay Mountain, and assuming no structural thickening, is estimated to be a minimum thickness of this unit. The contact with the overlying Vangorda formation is unconformable based on visible truncation of strata of the Mount Mye formation, although in the Anvil Lake area a gradational boundary was interpreted (Cobbett, 2014).

This sequence of rocks has been assigned to the Mount Mye formation based on lithologic similarities to those described in the Anvil District by Pigage (2004; Fig. 3). It is interpreted to be regionally equivalent to the Gull Lake Formation and matches well with regional descriptions for the Gull Lake rocks where they have been metamorphosed (Gordey and Anderson, 1993; Gordey, 2013a).

VANGORDA FORMATION

White, chalky weathered, calcareous phyllite, mildly recessive striped calc-silicate schist and resistant, dark grey-green weathered amphibolite schist, which together make up the bulk of the Vangorda formation, crop out in an east-west orientated band across the middle of the area of interest and in the southwest corner. Rock exposures east of Coward Creek are included in the Vangorda formation but the stratigraphy differs and is best described separately.

South of Tay Mountain, the first occurrence of light grey weathered, pinkish-grey fresh, calcareous schist to calc-silicate schist marks the base of the Vangorda formation. Here, the contact between Mount Mye and Vangorda formations is unconformable because the quartzite unit near the top of the Mount Mye stratigraphy is absent beneath the calcareous schist. The Menzie Creek Formation is inferred to lie conformably above the



Figure 4. *Field photographs of lower Cambrian Mount Mye formation strata, Tay Mountain area. (a) Typical brown weathered, blocky outcrop of Mount Mye schist east of Tay Mountain. Here the schist is biotite-muscovite schist with porphyroblasts of andalusite. (559814 E, 6932356 N). (b) Well foliated, carbonaceous quartzite that is an important marker horizon in the Mount Mye formation. This outcrop is east of Tay Mountain but similar lithology is exposed on Tay Mountain. (559047 E, 6932004 N). (c) Light and dark grey banded marble east of Coward Creek. (555568 E, 6936512 N).*

Vangorda formation to the southwest but this contact was not observed in the field.

North of Tay River the base of the Vangorda formation is marked by the first occurrence of brown weathered, calcareous, mica-rich schist (Fig. 5a). The calcareous rocks that belong to the Vangorda formation are distinctly dark brown and white, finely striped schist versus calcareous rocks that belong to the Mount Mye formation that are grey and always occur interlayered with marble (Fig. 4c). Up stratigraphic section the calcareous schist grades into a calcareous phyllite and then into a calcareous siltstone (Fig. 5b) and becomes interlayered with volcanic rocks of the Menzie Creek Formation. Here the Vangorda formation is 200 m thick. North of Tay Mountain, but on the south side of Tay River, the Vangorda formation comprises brownish-grey weathered, calcareous, micaceous schist (Fig. 5a) and phyllite overlain by light greenish-grey, very fine grained, tuffaceous (?) phyllite (COVp).

East of Coward Creek the base of the Vangorda formation is marked in part by the first occurrence of purplish-brown and beige striped calc-silicate schist (Fig. 5c) and in part by a 1 to 2 m thick layer of green weathered, amphibolite schist. Sandwiched between light grey, light purple and green striped calc-silicate schist, is a grey weathered, light purple fresh, laminated to thin-bedded quartz-rich marble layer (unit COVm; Fig. 5d) 20 to 30 m thick. Locally this unit is tight to isoclinally folded creating over thickened sections that are up to 120 m thick. Conformably above the calc-silicate schist, the Vangorda amphibolite schist exhibits a distinct weathering pattern of white and green stripes which characterizes fine-grained, schistose rock of dominantly actinolite, as well as accessory feldspar and epidote (Fig. 5e). This unit locally includes a finely-foliated dark purple and dark green rock of dominantly amphibole and biotite. Locally, a porphyritic metagabbro or metabasalt is mildly foliated and contains subhedral feldspar crystals in a fine-grained, dark green and black matrix. Blocky outcrops of dark green weathered and fresh, fine-grained schistose rock that has flattened masses of chlorite (after pyroxene?) crops out in several areas right at the contact with the underlying calc-silicate schist. The Vangorda amphibolite unit (COVa) is approximately 100 m thick east of Coward Creek, however because the top of the unit is not exposed, a true thickness of this part of the Vangorda formation could not be ascertained. The Vangorda formation, including both the calc-silicate, marble and the amphibolite schist, is at least 500 m thick.

The calc-silicate schist, calcareous phyllite and calcareous schist match descriptions by Pigage (2004) for the Vangorda formation. In combination with its stratigraphic location between the Mount Mye formation and Menzie Creek Formation the lithologic similarity is the basis for the assignment. A similar unit to the amphibolite schist widely exposed south of the Anvil batholith is described by Jennings and Jilson (1986). The Vangorda formation is a variably metamorphosed equivalent to the Rabbitkettle Formation that has been mapped extensively throughout Selwyn basin (Gordey and Anderson, 1993; Cecile, 2000).

MENZIE CREEK FORMATION

Dark weathered, cliffy exposures of volcanic and volcaniclastic rocks crop out in an east-west oriented band across the middle of the mapped area. Menzie Creek Formation is geologically inferred in the southwest corner of the map but this area was not visited.

Dark green weathered and fresh, variably amygdaloidal basalt, pillow basalt and monolithic basalt breccia predominate (Fig. 6a). These rock types are commonly interbedded with chlorite schist, chert, volcaniclastic siltstone and sandstone and volcanic breccia made up of clasts of pyroxene and plagioclase-phyric basalt and andesite and fine-grained tuff in a sandy matrix (Fig. 6b). East of Coward Creek, also interbedded with the volcanic rocks, is a succession of variably metamorphosed dark grey, carbonaceous siltstone, orange-grey, thin-bedded siltstone and sandstone, grey phyllite, green-purple-beige striped calc-silicate and fine-grained, quartzose siltstone and sandstone (unit OSMs on Fig. 2; Fig. 6c).

North of Tay River the Menzie Creek volcanic rocks are in contact with the Vangorda formation (in all other locations this contact is inferred). It is interpreted as gradational because calcareous siltstone is interbedded with dioritic flows and fine-grained, banded tuffs over several hundred metres in thickness. The boundary between the two formations is drawn when the percentage of volcanic rocks is greater than siltstone. Near the confluence of Coward Creek and Tay River, the Menzie Creek Formation comprises several hundred metres of fine to coarse-grained flows or sills of intermediate to mafic composition interlayered with banded tuff and minor calcareous siltstone and phyllite. At the base of one tuff horizon thin beds of light grey, micrite are interlayered with tuffaceous material giving the rock a very distinctive weathered pattern (Fig. 6d).



Figure 5. *Field photographs of Cambrian to Ordovician Vangorda formation strata, Tay Mountain area. (a) Calcareous schist comprising micaceous bands (dark layers) between calcite seams (white layers) near the confluence of Coward Creek and Tay River. (548895 E, 6943639 N). (b) Calcareous siltstone to phyllite near the contact between the Vangorda formation and Menzie Creek formation north of Tay River. (543665 E, 6946577 N). (c) Grey, purple and beige striped calc-silicate schist east of Coward Creek. (554940 E, 6937150 N). (d) Laminated, quartz-rich marble with small porphyroblasts of andalusite (several of which are circled in red) east of Coward Creek. (557149 E, 6939325 N). (e) Amphibolite schist comprising layers of feldspar and epidote between seams of amphibole (actinolite?) east of Coward Creek. Steeply-dipping veins that cut the rock on a cm-scale are actinolite. (555173 E, 6938347 N).*



Figure 6. *Field photographs of Menzie Creek formation strata, Tay Mountain area. (a) Oblique exposure through pillow basalts east of Coward Creek. (556766 E, 6941240 N). (b) Volcaniclastic breccia: fragments of pyroxene and plagioclase-phyric basalt to andesite in a sandy, tuffaceous matrix. North of Tay River. (540884 E, 6945697 N). (c) Orange-brown to grey, thin-bedded siltstone and sandstone. (555525 E, 6942279 N). (d) Orange-green weathered, very fine grained, thin to medium-bedded tuff interbedded with grey weathered micrite north of Tay River. The tuff horizons are very thickly (10-30 m) interlayered with medium to coarse-grained andesite to basalt flows or diorite to gabbro sills. One such contact is several metres to the left of the photograph. (545643 E, 6947153 N).*

The top of the Menzie Creek Formation is not exposed within the mapped area. A minimum thickness of 500 m is estimated based on thickness of volcanic and volcaniclastic rocks exposed both north of Tay River and east of Coward Creek. The rocks have been assigned to the Menzie Creek Formation based on lithologic similarity to those described by Pigage (2004).

SILURIAN TO TRIASSIC ROCKS NORTH OF TWOPETE THRUST

ROAD RIVER GROUP

Buff weathering, platey dolomitic siltstone, greater than 400 m thick is exposed along the base of the north slope of Mount Menzie. This unit comprises thick beds of beige weathered, dolomitic siltstone with trace fossils, light green-grey weathered, fine-grained calcareous sandstone and dark grey, medium-grained quartz-rich lithic sandstone. The lower contact has been interpreted to be a thrust fault, as previously described and mapped by Gordey (2013), hindering a true thickness determination. The basis for the assignment of these rocks to the Road River Group is their similarity to descriptions of the Steel Formation (upper Road River Group) by Gordey (2013) and by the similarity of these rocks to ones observed north of Mount Mye that contain Middle Ordovician to early Silurian fossils (Gordey, 2013).

Alternatively these rocks are a variation of upper Earn Group and the lower contact with the Earn Group volcanic rocks is stratigraphic.

LOWER EARN GROUP

Recessive dark weathering chert and siltstone that are altered to beige weathered, purple hornfels near the contact with granodiorite near the peak of Mount Menzie crop out in a narrow band across Mount Menzie and locally on the eastern side of Earn Hills. The chert is dark grey and black and commonly shows white stripes on weathered surfaces (Fig. 7a). Locally, the chert is interbedded with a dark grey and silver weathered siltstone to fine-grained sandstone. On the east end of Earn Hills several outcrops and subcrops of siltstone and fine-grained sandstone have also been assigned to the lower Earn Group. At this location, brown weathered, thick-bedded, fine-grained sandstone commonly contains concretions and is interbedded with laminated and sometimes rhythmically bedded siltstone.

Although obscured by vegetation, the lower contact with the Steel Formation is interpreted to be conformable. The upper contact is an unconformity based on missing Earn Group quartz-rich clastic rocks (DMEu) and the occurrence of chert conglomerate at the base of Earn Group upper arenite (DMEua) (Fig. 3). The conglomerate has clasts of white weathered chert, presumably sourced from the underlying unit (Fig. 7b). The lower Earn Group is approximately 300 m thick near Mount Menzie, the only location where both upper and lower contacts are well constrained. The chert has been assigned to the lower Earn Group based on similar rocks mapped east of the area that contain late Early Devonian to early Middle Devonian fossils (Cobbett, 2015), however, based on the minor occurrence of chert in the Steel Formation,

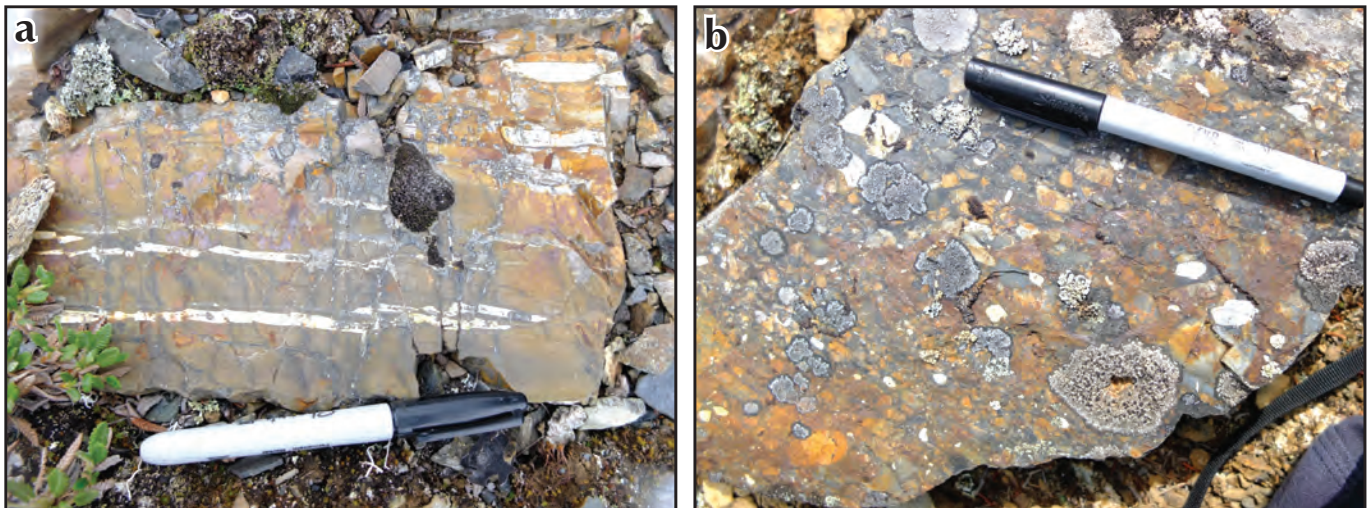


Figure 7. *Field photographs of Earn Group. (a) Lower Earn Group black chert with distinct white stripes on the weathered surface. (554980 E, 6956244 N). (b) Chert pebble conglomerate near the base of the Earn Group upper arenite (DMEua) that has clasts of white weathered, black chert. (555742 E, 6953305 N).*

assignment to this underlying unit cannot be ruled out (Gordey and Anderson, 1993; Gordey, 2013a). In the case where the Road River Group assignment is incorrect and the underlying rocks are upper Earn Group then the lower contact of this unit is a thrust fault.

VOLCANIC ROCKS WITHIN THE EARN GROUP

Rounded knobs north of Mount Menzie and Earn Hills are underlain by intermediate volcanic and volcaniclastic rocks that occur as lenses within the upper Earn Group (unit DMEv). Orange-weathering, hornblende and pyroxene-phyric, andesite flows and breccia predominate (Fig. 8a). Grey-green fresh, thin-bedded chert interbedded with green volcaniclastic siltstone crops out in one locality north of Mount Menzie. This unit is fault bounded and lacks internal structure. Its assignment to Earn Group is based on an unpublished Late Devonian U-Pb zircon age by J.K. Mortensen which is referenced in Gordey (2013a) as a personal communication. Additional volcanic layers, including felsic tuffs, are intercalated within the Upper Earn Group.

UPPER EARN GROUP

The stratigraphy documented in this section applies to the mapped area, except for Twopete Mountain, where unit DMEu was described in detail by Cobbett (2014) and is labelled as DME in that document.

Resistant, grey weathered, thick-bedded, quartz-rich sandstone (unit DMEua) crops out in both swampy and thickly treed areas between Tay River and Earn Hills. The arenite varies from a clean, medium-grained quartz arenite (Fig. 8b) to a grey chert-pebble conglomerate with a tuffaceous matrix (Fig. 8c) and also includes calcareous, medium-grained, quartz-rich sandstone. Lesser amounts (but still comprising significant portions of the upper arenite unit) of grey, medium-bedded to massive quartzose siltstone, grey and black chert, and siltstone interbedded with limestone and dark grey shale crop out on Earn Hills, Mount Menzie and south of Twopete Creek. Rare outcrops of volcanic rocks in the form of highly altered plagioclase-phyric basalt or andesite and beige weathered, felsic welded tuff (Fig. 8d) are found along Menzie Creek, south of Earn Hills. The lower contact is described above and the upper contact is not exposed but is well-constrained both on Mount Menzie and Earn Hills and is interpreted to be conformable. The thickness of this unit on Mount Menzie is approximately 350 m but may be as much as 800 m thick based on cross section interpretation (Fig. 2).

This succession has been assigned to the Earn Group upper arenite unit (DMEua) because of its lithologic similarities with this unit to the east where is has been well constrained by fossil ages and geochronology (Cobbett, 2015). It was originally interpreted to be Carboniferous to Permian in age and sit stratigraphically between the Tay Formation and the Mount Christie Formation (former unit CPa; Cobbett, 2014). New fossil and geochronological age dates show this succession to range in age from upper Devonian to lower Mississippian (unpublished data; Cobbett, 2015) and is therefore in part contemporaneous with the Tay Formation. Separating the lower Mississippian strata (Tay Formation) from the Upper Devonian strata (Upper Earn Group) is not possible within the Tay Mountain area because they always occur together in folded successions and because of repeating similar lithologic units that crop out in both levels of stratigraphy. In summary, the Earn Group upper arenite unit includes the Tay Formation northwest of Anvil Creek (Cobbett, 2015).

MOUNT CHRISTIE FORMATION

Orange weathering, purple and green banded chert cores a regional-scale syncline that trends west-northwest along the southern exposure of both Earn Hills and Mount Menzie (Fig. 2). The chert is dominantly green and maroon coloured with lesser black and grey interbeds (Fig. 9a). The maroon chert commonly has abundant siltstone interbeds. The very northwestern corner of the area of interest is shown on previous regional maps as Mount Christie Formation but has not been visited in the course of our investigation. Both the upper and lower contacts are reported as unconformable (Gordey, 2013a). A thickness could not be estimated based on the absence of upper exposures of this unit and its folded nature.

JONES LAKE FORMATION

Grey-brown weathered, thickly bedded calcareous clastic strata crop out along the northern edge of the plateau that makes up the top of Earn Hills. In most places this is a grainstone with rare cross-beds that indicate upright orientation (Fig. 9b). The grainstone has been assigned to the Jones Lake Formation based on its lithologic similarity to exposures east of the mapped area that contain Triassic fossils. Additionally a Triassic fossil locality is approximately 2 km along strike to the west (Gordey, 2013a).

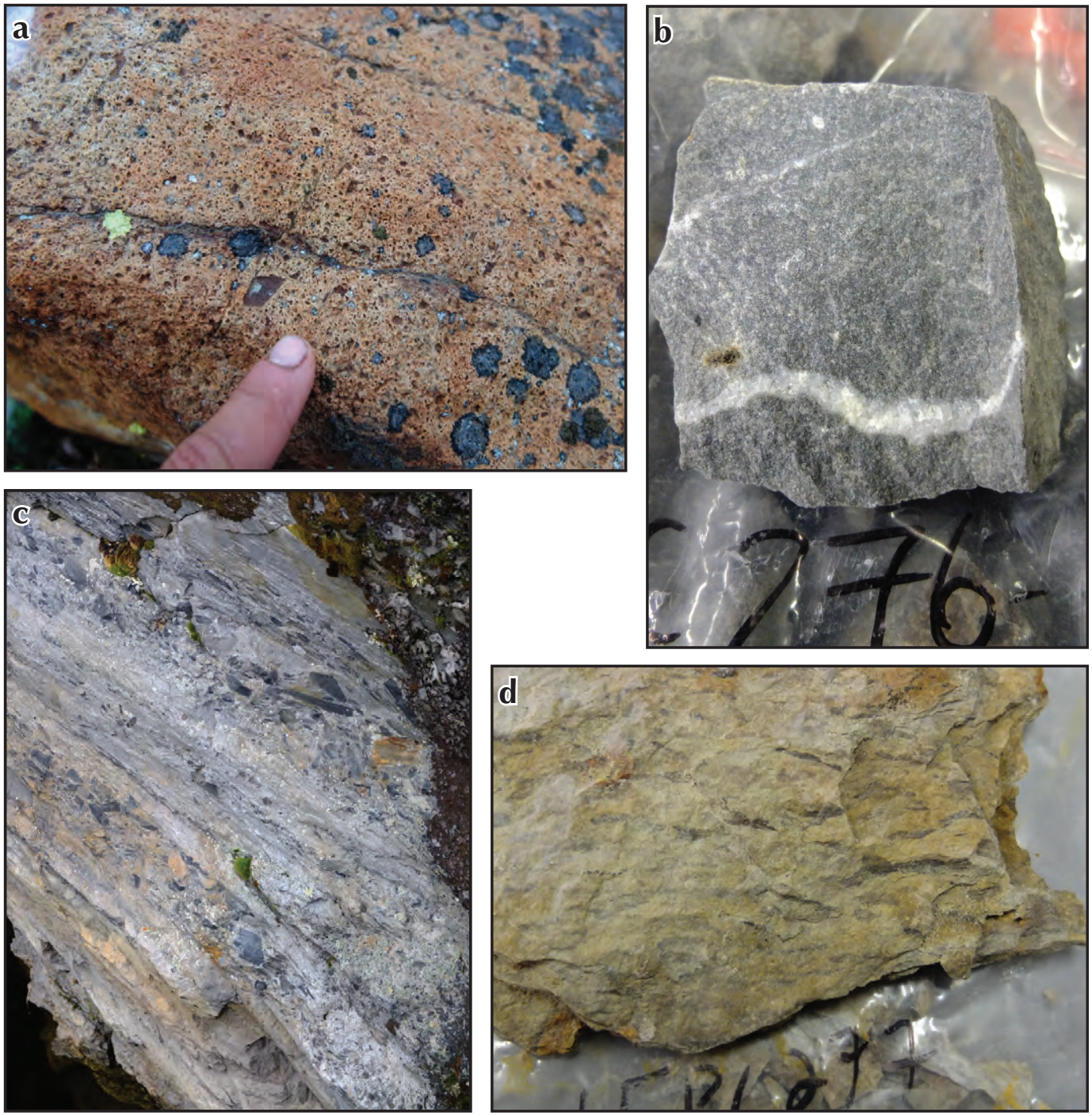


Figure 8. *Field photographs of Earn Group strata, north of Tay Mountain. (a) Orange-brown volcaniclastic rock (*DMEv*) from a rounded knob northwest of Mount Menzie and north of Earn Hills. (543990 E, 6959477 N). (b) Medium-grained, massive quartz arenite (*DMEu*, south of Earn Hills. 542269 E, 6950785 N). (c) Chert pebble conglomerate interbedded with quartz arenite (543510 E, 6953874 N). (d) Beige weathered and fresh welded tuff characterized by fiamme (flattened pumice shards) in a soft, clay-like matrix. From the heavily treed area along Menzie Creek (543628 E, 6950512 N).*

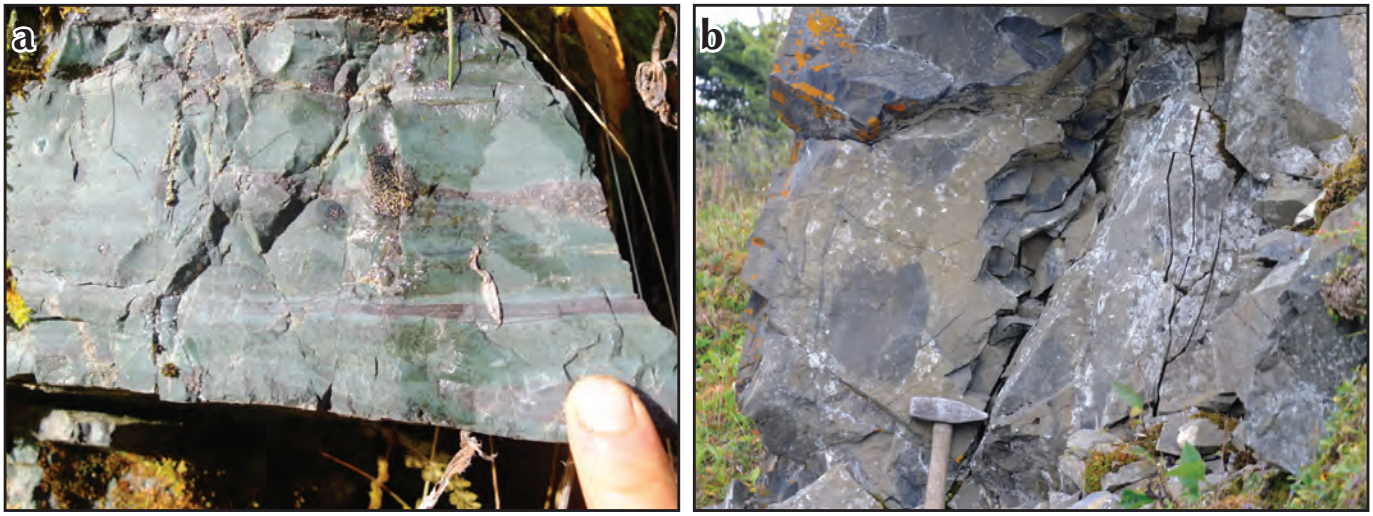


Figure 9. *Field photographs of Carboniferous to Triassic strata, Earn Hills area. (a) Typical green and maroon chert of Mount Christie Formation south side of Earn Hills. (540726 E, 6955886 N). (b) Grey-brown weathered, grey fresh, thick-bedded grainstone in nearly vertical beds that crop out along the northern edge of the plateau on Earn Hills (540776 E, 6958288 N).*

A regional unconformity between the Jones Lake Formation and Mount Christie Formation has been documented (Gordey, 2013a) but was not observed during this investigation. Instead the upper contact is a thrust fault with a hanging-wall of locally brecciated black, carbonaceous, mottled siltstone that is interpreted as the Earn Group. The lower contact is as shown on regional maps. A thickness estimate is not possible for the Jones Lake Formation in this area.

INTRUSIVE ROCKS

Pre-Cretaceous Intrusive Rocks

Several small mafic bodies are the only pre-Cretaceous intrusive rocks that were identified in the area. A green, medium-grained gabbro (unit OSMg) intrudes the contact between Vangorda calc-silicate and Menzie Creek basalt breccia south of Twopete Creek (Fig. 2). Dark green to black, medium-grained, highly magnetic, augite-phyric pyroxenite that has been partially altered to serpentinite intrude the Vangorda amphibolite schist. This 10 by 10 m exposure is located about 3 km east of Coward Creek and is too small to depict on Figure 2.

Anvil batholith

Two large bodies of light grey, medium and coarse-grained biotite granodiorite intrude the southern and central part of the area. The exposures form an irregular map pattern with some steep contacts while others appear nearly horizontal based on their relationship to topography. Most of these rocks are porphyritic with feldspar phenocrysts up to 2 cm long and exhibit no foliation, however, several traverses crossed sections of granodiorite that were non porphyritic and sometimes foliated. Contacts between these variations in the batholiths are not continuously exposed. The Anvil batholith (Pigage and Anderson, 1985) has been assigned to the Tay River plutonic suite (99-95 Ma) based on a U-Pb zircon date from the southeast corner of the mapped area (Fig. 2; Mortensen *et al.*, 2000; Pigage, 2004).

Medium-grained biotite granodiorite north of the main plutons (Fig. 2) are coeval, based on preliminary geochronology. These small bodies have a metamorphic contact aureole that range in diameter from 0.5 to 2.0 km.

The Anvil batholith is predominantly undeformed except several isolated outcrops where the batholith is weakly foliated. Marginal contacts with the schistose rocks are sharp and intrusive rocks cut both the early foliation and the dominant foliation (Fig. 10a) constraining the age of schistosity to pre 99 to 95 Ma.

STRUCTURE

Early Paleozoic strata (south part of the map area) are here considered structural domain 1, and Late Paleozoic and Early Mesozoic strata (north part of the map area) constitute structural domain 2 (Fig. 11). Domain 1, further subdivided into 3 geographic regions, is characterized by

several overprinting foliations in mica schist, calcareous schist, calc-silicate schist and marble, and a penetrative foliation in amphibolite schist and carbonaceous quartzite. The dominant foliation (late foliation, S_{n+1} on Fig. 11 and below) in the mica schist is defined by muscovite and biotite seams between microlithons of quartz that range in width from mm-scale to cm-scale. Where the microlithons are 0.5 cm and wider an early foliation (Sn) can be seen in outcrop. This early foliation is always tightly folded and sits at a high angle to the dominant foliation (Fig. 10b). It also comprises seams of mica between quartz microlithons. A late crenulation cleavage (S_{n+2}) deforms the dominant foliation in the mica schist but is only locally exhibited (Fig. 10b).

The dominant foliation in the calcareous schist of domain 1 is defined by thin laminations of quartz, calcite and mica. In the calc-silicate schist the foliation is accentuated by stripes of various colours including purple, beige, brown and light green. Typical mineral assemblages for calc-silicate rocks mapped near the Anvil mine are quartz, tremolite-actinolite, plagioclase, biotite ± diopside, calcite and epidote (Jennings and Jilson, 1986). The dominant foliation in the marble is defined by quartz laminae between thin layers of calcite. The marble, calcareous schist and the calc-silicate schist only rarely show evidence of an early foliation. Similar to the mica schist, it is exhibited as small micro-folded schistose layers between folai of the dominant foliation. The penetrative foliation in the amphibolite schist is defined by laminations of epidote and feldspar between seams of amphibole (commonly actinolite; Fig. 10c).

The volcanic and volcaniclastic rocks within this domain range from undeformed to well-foliated. Thick-bedded basalt, pillow basalt, chert and banded tuff interbedded with micrite north of the Tay River are undeformed at least at outcrop-scale (Fig. 6a,d). Volcaniclastic siltstone and sandstone and volcanic breccia of the Menzie Creek Formation are well foliated but bedding is still observable in most outcrops (Fig. 10d). Chlorite schist and meta-tuffs of the Menzie Creek Formation are commonly pervasively foliated where primary features are obliterated.

Within domain 1 several sub-domains have been identified on the basis of variations in late foliation orientations which roughly coincide with opposing flanks of the Anvil batholith (Fig. 11). The late foliations are axial planar to map-scale folds within the southwest and southeast sub-domains. In the southwest sub-domain the late foliations generally dip shallowly to moderately southwest. In both the southeast and north sub-domains the late foliation has a wider range of orientations but generally dips moderately to the east-northeast. This change in orientation is represented graphically on cross sections B-B′ and C-C′ of Figure 2 which shows a doming of this structure roughly centred on the pluton underlying Tay Mountain.

Domain 2 encompasses Late Paleozoic to Early Mesozoic rocks that are faulted against Early Paleozoic strata in the southern part of the map area (Fig. 11). Primary textures are always preserved in rocks within Domain 2. In most places, bedding is open to tightly folded in outcrop and closely folded on a regional scale. Folds are asymmetric and cylindrical, and have a steeper northeast-dipping limb that is sometimes overturned and a shallower southwest-dipping limb (Fig. 2).

The thrust fault that separates domain 1 from domain 2 is a northwestward continuation of the Twopete thrust fault; it separates Selwyn basin strata from Late Paleozoic strata. Gordey (2013c) interpreted this structure as a low angle thrust that was rooted in a detachment fault to the southwest, probably of Jurassic age. A re-interpretation of the origin of this structure as a reactivated Devonian normal fault is the reason it is drawn as a steep reverse fault in the cross sections (Fig. 2). The thrust faults that bound the volcanic rocks in the very northern part of the mapped area are also interpreted as reactivated Devonian normal faults that possibly localized volcanism during deposition of the Earn Group.

Normal faults display two trends: roughly north-south and east-west. The north-south oriented group crops out in domain 2 both on Earn Hills and Twopete Mountain and crosscut thrust faults. Estimates of offset across these normal faults range from 300 to 1000 m. The east-west oriented group crops out in the centre of the mapped area within sub-domain 1_N and accommodates north-side down movement juxtaposing younger rocks on the north side from older rocks on the south side. These faults are cut by the Anvil batholith but offset strata as young as Silurian constraining the timing of movement from post Silurian to pre mid-Cretaceous. An estimate of offset is not possible without detailed stratigraphic knowledge of the Selwyn basin strata in this area.

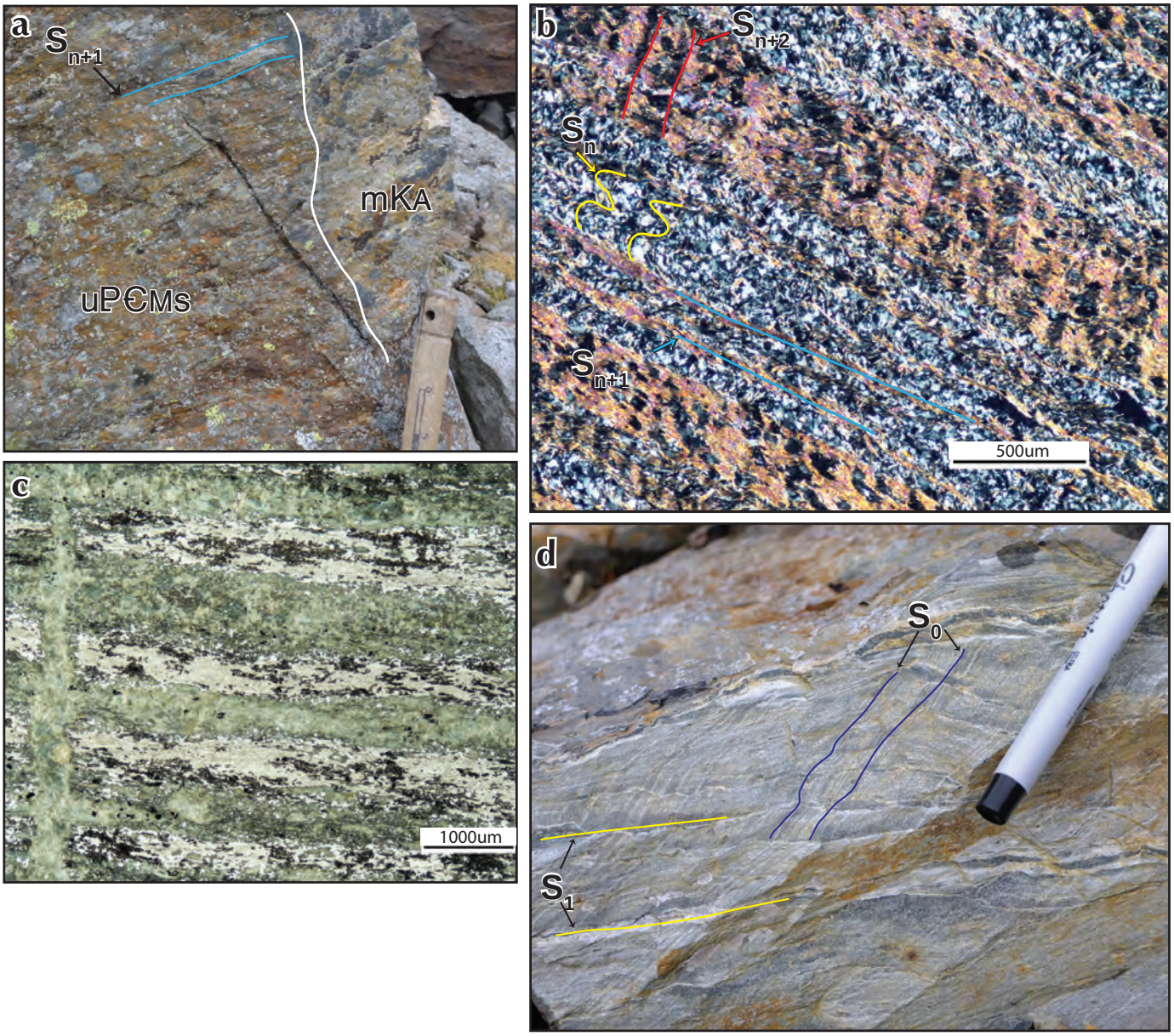


Figure 10. *Microphotographs (b, c) and field photographs (a, d) of metamorphosed Anvil district rocks. (a) Brown weathered mica schist of Mount Mye formation cut by Tay River pluton. Blue lines trace late foliation and white line traces out margin of granodiorite. Hammer handle at lower right shows a 5 cm long scale bar (558848 E, 6933152 N). (b) Biotite-muscovite-cordierite schist of Mount Mye formation that exhibits three phases of deformation. (547265 E, 6942325 N). (c) Amphibolite schist comprising layers if actinolite (green) between feldspar and epidote (lighter layers) and cut by actinolite vein. (555173 E, 6938347 N). (d) Volcaniclastic sandstone that exhibits both bedding (dark blue lines) and foliation (yellow lines). (554007 E, 6943790 N).*

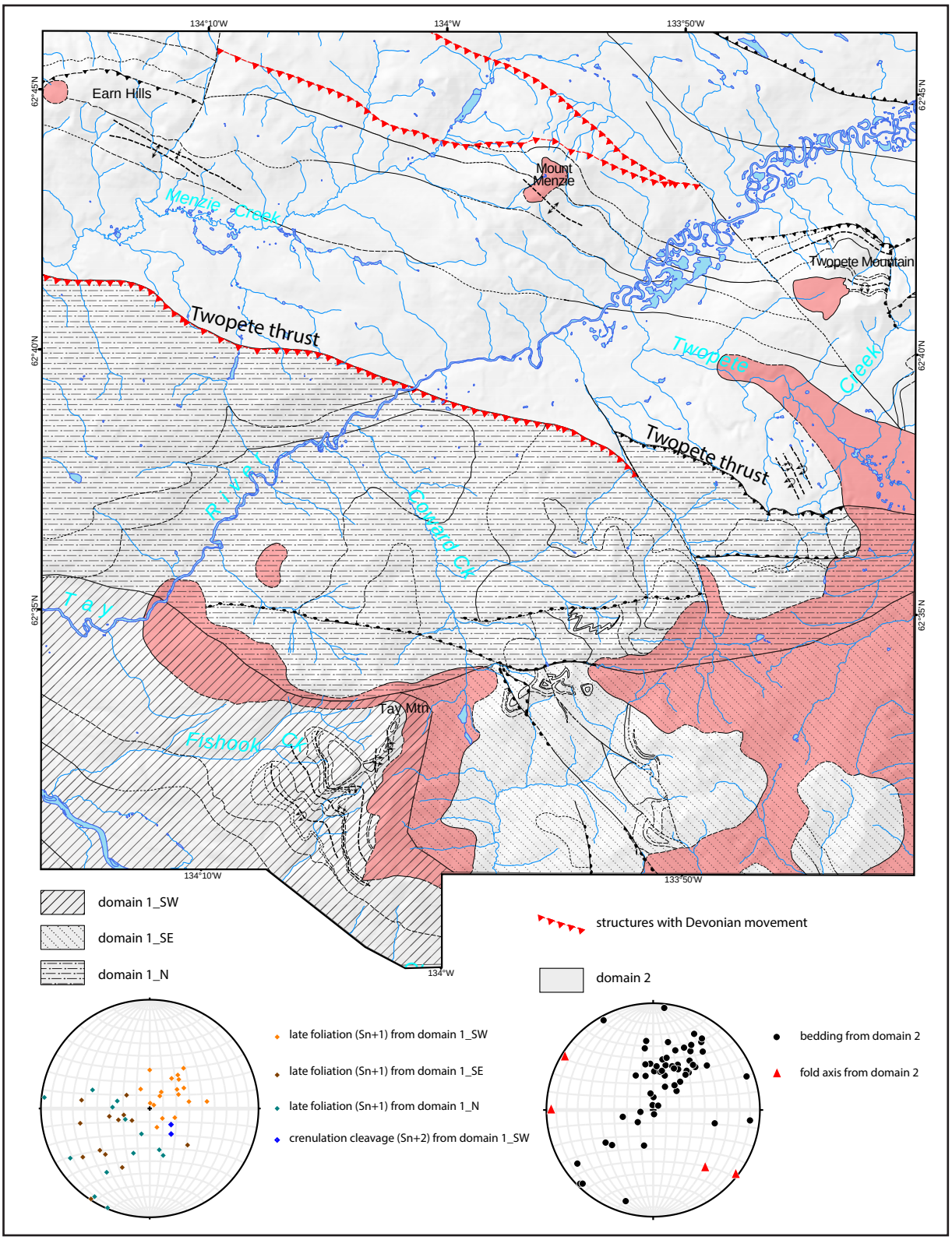


Figure 11. *Structural domains and data from the field measurements (equal area projection, lower hemisphere stereonets). Diamonds (domain 1 stereonet) are poles to foliations and crenulation cleavages. Circles (domain 2 stereonet) are poles to bedding. Triangles (domain 2 stereonet) are fold axis measurements. Map shows faults in heavy black lines and faults that are reactivated Devonian structures in heavy red lines. Fold axial traces are shown by dashed black lines and contacts are shown by fine black lines.*

DISCUSSION

The Twopete thrust fault and several other north-verging thrusts that daylight in the northern part of the mapped area are here re-interpreted as reactivated Devonian normal faults (Figs. 2 and 11). This interpretation is based upon the deduction of the deposition of upper Earn Group clastic rocks in graben and/or half-grabens that lay north of the Twopete fault during Devonian extension (Colpron and Nelson, 2009). During Jura-Cretaceous shortening the graben-bounding normal faults were reactivated as reverse faults and accommodated the thrusting of Selwyn basin rocks over Earn Group strata. Further, the normal faults may have acted as conduits for Devonian volcanism whose deposition was also controlled by graben and half-graben features.

There is an abundance of volcanism in the stratigraphy (lower Cambrian, upper Cambrian through Silurian and late Devonian) that suggest a long-lived crustal anomaly, such as a deep-seated fracture system.

MINERALIZATION

The map area lies to the northwest of the Anvil Mine district and to the west of the Keg deposit (Yukon MINFILE 105K 078). The Anvil Mine is a deformed SEDEX deposit with mineralized horizons straddling the boundary between the Mount Mye and the Vangorda formations (Jennings and Jilson, 1986; Pigage, 2004). Mineralization at the Keg deposit has been described as a Ag-Pb-Zn ± Au (polymetallic) vein system and also as a skarn or porphyry related system (Yukon MINFILE, 2015).

Other types of occurrences located within the area of interest include SEDEX Zn-Pb-Ag (Yukon MINFILE 105K 074, 105L 039), Cu-Ag vein (Yukon MINFILE 105K 071), Cu-Zn-Ag skarn (Yukon MINFILE 105K 111), sediment-hosted stratiform barite (105K 110), plutonic-related gold (Yukon MINFILE 105L 018, 105K 072) and several anomalies (Yukon MINFILE 105K 102, 105K 073) and unknown types (Yukon MINFILE 105K 073, 105K 074, 105L 019).

New mapping shows that there is more Anvil Mine host stratigraphy than was previously shown on regional maps. Mineralization examined during this mapping project within domain 1 (Selwyn basin rocks) was restricted to semi-massive sulphide lenses associated with marble horizons within the Mount Mye formation. These occur where the marble is in contact with amphibolite schist and where granodiorite dikes cut marble layers.

The Keg deposit is part of a northwest trending belt of silver-bearing mineral occurrences that has been delineated based on the prospecting of numerous soil geochemistry anomalies (www.silverrangeresources.com) in 2011 and 2012. The farthest northwest mineralized occurrence within this trend is located at Mount Menzie (Fig. 2). Generally, the silver-bearing mineral occurrences are located where chert and quartz arenite are tightly folded and in close proximity to calcareous rocks (Cobbett, 2014). Several of the occurrences also coincide with small granitic intrusions and/or steep faults. This NW-trending belt of Late Paleozoic rocks that is periodically intruded by granitic plugs and deformed by steep structures is prospective for silver and other base-metals within the Tay Mountain area and continues outside the area of interest to the northwest.

SUMMARY

The main results from mapping in the Tay Mountain area are:

1. Lower Cambrian to Silurian strata crop out extensively in the vicinity of Tay Mountain and extend the Anvil Mine host stratigraphy at least as far as this region;
2. The Tay River plutonic suite cuts the late foliation in the schistose rocks south of the Twopete thrust indicating that the metamorphism responsible for creating the schistosity in the Mount Mye and Vangorda formations is pre 99-95 Ma; and
3. Silver occurrences are spatially associated with competent late Paleozoic strata, in particular folded chert assigned to the Mount Christie Formation and within the Earn Group.

REFERENCES

Abbott, J.G., Gordey, S.P. and Tempelman-Kluit, D.J., 1986. Setting of stratiform, sediment-hosted lead-zinc deposits in Yukon and northeastern British Columbia. *In*: Mineral Deposits of Northern Cordillera, J.A. Morin (ed.), Canadian Institute of Mining and Metallurgy, Special Volume 37, p. 1-18.

Cecile, M.P., 2000. Geology of the northeastern Niddery Lake map area, east-central Yukon and adjacent Northwest Territories. Geological Survey of Canada, Bulletin 553, 120 p.

Cobbett, R.N., 2014. Preliminary observations on the geology of the Anvil Lake area (parts of NTS 105K/11 &12) central Yukon. *In*: Yukon Exploration and Geology 2013, K.E. MacFarlane, M.G. Nordling, and P.J. Sack (eds.), Yukon Geological Survey p. 33-51.

Cobbett, R.N., 2015. Geological Map of the Anvil Lake area, Central Yukon, parts of NTS 105K11 & 12. Yukon Geological Survey Open File 2015-2, scale 1:50 000.

Colpron, M., Mortensen, J.K., Gehrels, G.E. and Villeneuve, M., 2006. Basement complex, Carboniferous magmatic arcs and Paleozoic deformation in Yukon-Tanana terrane of central Yukon: Field, geochemical, geochronological constraints from Glenlyon map area. *In:* Paleozoic evolution and metallogeny of pericratonic terranes at the ancient Pacific margin of North America, M. Colpron and J. Nelson (eds.), Geological Association of Canada, Special Paper 45, p. 131-152.

Colpron, M. and Nelson, J.L., 2009. A Palaeozoic Northwest Passage: Incursion of Caledonian, Baltican and Siberian terranes into eastern Panthalassa, and the early evolution of the North American Cordillera. Geological Society, London, Special Publications, vol. 318, p. 273-307.

Gabrielse, H., 1967. Tectonic evolution of the northern Canadian Cordillera. Canadian Journal of Earth Sciences, vol. 4, p. 271-298.

Gabrielse, H., Murphy, D.C. and Mortensen, J.K. 2006. Cretaceous and Cenozoic dextral orogeny-parallel displacement, magmatism, and paleogeography, north-central Canadian Cordillera. *In:* Paleogeography of the North American Cordillera: Evidence For and Against Large-Scale Displacements, J. Haggart, R.J. Enkin and J.W.H. Monger (eds.), Geological Association of Canada, Special Paper 46, p. 255-276.

Gordey, 2013a. Evolution of the Selwyn Basin region, Sheldon Lake (105J) and Tay River (105K) map areas, central Yukon Territory. Geological Survey of Canada, Bulletin 599, 176 p., doi:10.4095/293034.

Gordey, S.P., 2013b. Geology, central Tay River, Yukon. Geological Survey of Canada, Map 2150A, scale 1:100 000, doi:10.4095/288983.

Gordey, S.P., 2013c. Geology, Selwyn Basin (105J and 105K), Yukon. Geological Survey of Canada, Open File 2149A, 2 maps at 1:250 000 scale and 1 sheet cross sections at 1:100 000 scale.

Gordey, S.P. and Anderson, R.G., 1993. Evolution of the northern Cordilleran miogeocline, Nahanni Map area (105I), Yukon and Northwest Territories. Geological Survey of Canada, Memoir 428, 214 p.

Gordey, S.P. and Makepeace, A.J. (comps.), 2003. Yukon digital geology, version 2.0. Geological Survey of Canada Open File 1749; also Yukon Geological Survey Open File 2003-9(D), 2 CD-ROMs.

Jennings, D.S. and Jilson, G.A., 1986. Geology and sulphide deposits of Anvil Range, Yukon. *In*: Mineral Deposits of Northern Cordillera, J.A. Morin (ed.), Canadian Institute of Mining and Metallurgy, Special Volume 37, p. 319-361

Mair, J.L., Hart, C.R.J. and Stephens, J.R., 2006. Deformation history of the northwestern Selwyn Basin, Yukon, Canada: implications for orogeny evolution and mid-Cretaceous magmatism. Bulletin of Geological Society of America, vol. 118, p. 304-323.

Mortensen, J.K., Hart, C.J.R., Murphy, D.C. and Heffernan, S., 2000. Temporal evolution of early and mid-Cretaceous magmatism in the Tintina Gold Belt. *In*: The Tintina Gold belt: Concepts, Exploration, and Discoveries, T.L. Tucker and M.T. Smith (eds.), British Columbia and Yukon Chamber of Mines, Special Volume 2, p. 49-58.

Nelson, J.L., and Colpron, M., 2013. The Cordillera of British Columbia, Yukon and Alaska: Tectonics and Metallogeny. Society of Economic Geology, Inc., Special Publication 17, p. 53-109.

Pigage, L.C., 2004. Bedrock geology compilation of the Anvil District (parts of NTS 105K/2,3,5,6,7 and 11), central Yukon. Yukon Geological Survey, Bulletin 15, 103 p.

Pigage, L.C. and Anderson, R.G., 1985. The Anvil plutonic suite, Faro, Yukon Territory. Canadian Journal of Earth Sciences, vol. 22, p. 1204-1216.

Rasmussen, K.L., 2013. The timing, composition, and petrogenesis of syn- to post-accretionary magmatism in the northern Cordilleran Miogeocline, eastern Yukon and southwestern Northwest Territories. Unpublished PhD theses, University of British Columbia, Vancouver, Canada, 788 p.

Roddick, J.A., 1967. Tintina Trench. Journal of Geology, vol. 75, p. 23-33.

Yukon MINFILE, 2015. Yukon MINFILE – A database of mineral occurrences. Yukon Geological Survey, <http://data.geology.gov.yk.ca> [accessed November, 2015].

Protopiceoxylon yukonense sp. nov. – A remarkable extinct conifer from the Mackenzie Delta area, northern Yukon

M. Dolezych[1]
Senckenberg Naturhistorische Sammlungen Dresden, Germany

L. Reinhardt
Federal Institute for Geosciences and Natural Resources (BGR), Hannover, Germany

Dolezych, M. and Reinhardt, L., 2016. *Protopiceoxylon yukonense* sp. nov. – A remarkable extinct conifer from the Mackenzie Delta area, northern Yukon. *In:* Yukon Exploration and Geology 2015. K.E. MacFarlane and M.G. Nordling (eds.), Yukon Geological Survey, p. 99-110.

ABSTRACT

A fossil wood remain of par-autochthonous origin was found in Paleocene sedimentary rocks of the Moose Channel Formation in the Big Fish River area in Yukon, close to the Northwest Territories border, during the CASE 15 expedition. The fossil wood was recovered from overall medium to coarse-grained units of sandstone of an inferred fluvial-deltaic origin. This contribution summarizes the current knowledge primarily on the taxonomy and paleoecology of the protopiceaceous wood specimen. The fossil wood specimen turned out to be without a relationship to extant taxa: *Protopiceoxylon yukonense* sp. nov. as a taxon of the fossil wood genus *Protopiceoxylon* Gothan 1907 belongs to the extinct family of Protopinaceae Kraeusel, 1949. The holo- and paratypes of the generotypus *Protopiceoxylon extinctum* Gothan, 1907 from the King Charles Land (Gothan, 1907) and from Green Harbour/Spitsbergen (Gothan, 1910), were available for this investigation from the Natural History Museum Berlin (NHMB). Although most of samples characteristics are comparable to be extinct genus *Protopiceoxylon*, it is differentiated by some extinct anatomical features that are intermediate between the extinct *Protopiceoxylon* and the extant *Piceoxylon* Gothan, 1905. These features manifest within the radial bordered pits, which are protopinoid in *Protopiceoxylon* and abietoid in *Piceoxylon*. Most other features demonstrate a close relationship between both fossil taxa.

[1]*Martina.Dolezych@senckenberg.de*

INTRODUCTION

Pinaceaeous and protopiceaceous fossil woods are well known from Upper Cretaceous and Cenozoic strata in the Northern Hemisphere. However, specimens from the Mackenzie Delta area, northern Yukon, have received only limited investigations and no fossil woods older than Middle Pliocene have been described to date. Hence, this taxonomic investigation is essential for research on the evolution of plants, particularly in the case of extinct woods. In addition, this research has potential for developing a paleo-ecological reconstruction, inter alia, the fossil found in Yukon represents a constituent of vegetation growing under high latitude conditions (*i.e.*, continuous daylight in arctic summer *vs.* darkness for months during arctic winters).

During the CASE 15 geological expedition, a fossil wood remain of parautochthonous origin was found in Paleocene sedimentary rocks of the Moose Channel Formation in the Big Fish River area in Yukon near the Northwest Territories border (Fig. 1).

The wood was anatomically investigated and compared with other fossil woods of the fossil genus *Protopiceoxylon* Gothan, 1907 of the extinct family Protopinaceae. Although most of samples characteristics are comparable to be extinct genus *Protopiceoxylon*, it is differentiated by some extinct anatomical features that are intermediate between the extinct *Protopiceoxylon* and the extant *Piceoxylon* Gothan, 1905. This approach allows the identification of new extinct fossil wood species. By relating the fossil wood specimen to some other *Protopiceoxylon* woods (namely from Ellesmere Island, Spitsbergen and Franz Joseph Land), it is possible to unravel additional details about the species living in the forested areas of the high latitude zone in the Cretaceous-Paleogene.

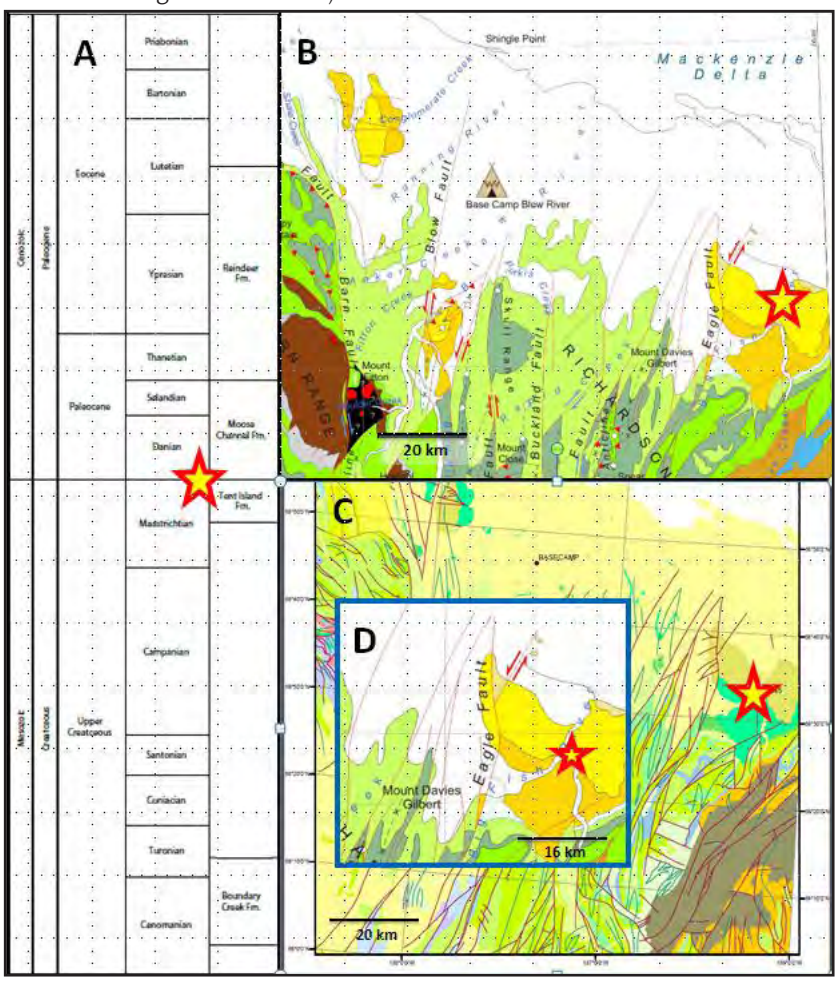


Figure 1. *Geographic and geological overview and stratigraphic reference of the sample locality. (A) Time scale with stratigraphic position of sampled specimen. (B) Geographical and geological map of a part of North Yukon and Mackenzie Delta with sample position indicated by red outlined star (sample number = Yu 045), scale 1:250 000 (Piepjohn, 2013). (C) Geological map with sample position indicated by red outlined star. (D) Detailed map of Big Fish River area (from b), sample position indicated by red outlined star.*

GEOLOGICAL SETTING

LOCALITY

Geological fieldwork on the Yukon North Slope and in the northwestern Mackenzie Delta area took place in July 2013. During a reconnaissance examination of a steep cliff outcrop in a secondary valley of the Big Fish River, Tiffani Fraser of the Yukon Geological Survey (YGS) and Lutz Reinhardt of the German Federal Institute of Geosciences and natural resources (BGR) discovered fossil wood remains on a rock pile at the base of the cliff, which had resulted from a recent rock fall. The rocks fell from a position in the steep cliff above that could be clearly identified by its fresh, unweathered colour and some remaining fossil wood (Fig. 2). The outcrop in the river valley, 68° 32′ 51.0″ N/ 136° 14′ 24.6″ W, gives access to parts of the basal sandstone member of the Lower Paleocene Moose Channel Formation.

MOOSE CHANNEL FORMATION

Deltaic sedimentation in the larger Mackenzie Delta area has persisted since the end of the Cretaceous accumulating to a total thickness of more than 10 km of Cenozoic siliciclastic rocks (Young and McNeill, 1984). The thick sedimentary succession is subdivided into nine sequences (*e.g.*, Dietrich *et al.*, 1985; Dixon *et al.*, 1992) beginning with the Fish River sequence above an unconformity with the Turonian black shales of the Boundary Creek Formation. The Fish River sequence includes the latest Cretaceous, shale dominant Tent Island Formation at its base and the overlying sandstone-dominant lower Tertiary Moose Channel Formation.

Mountjoy (1967) initially defined the Moose Channel Formation and Young (1975) subsequently modified this definition and provided a type section (Young, 1975) located near the outcrop where the fossil wood was found. The 1000 m thick Moose Channel Formation comprises a basal sandstone member overlain by the shale Ministicoog member. Originally, the Moose Channel Formation was considered to be Upper Cretaceous (Young, 1975). Subsequent detailed work on palynomorphs (*e.g.*, Sweet, 1978) and on foraminifers (McNeil, 1989) revised the formation to the Early Paleocene.

The basal sandstone member of the Moose Channel Formation is interpreted as to be of deltaic and shallow marine origin (Young, 1975). Plant remains, including woody plant fragments, coalified tree stumps, carbonaceous plant debris-, and leaf impressions, were already described in the formation's type section by Young (1975). The fossil wood examined in more detail here was recovered from a series of overall medium to coarse units of sandstone including some conglomerate layers and minor shale intercalations of inferred fluvial-deltaic origin. The several meters-long trunk or branch of a tree appears to have been transported along a channel of the Early Paleocene delta, where it was later deposited. Thus, the parautochthonous wood either originates in the direct vicinity of the former delta channel or it was transported over a longer lateral distance during a discharge event of the Early Paleocene fluvial system. This situation is assumed to be comparable to the modern depositional system of the Mackenzie River, but during generally warmer climate conditions at the end of the Cretaceous and beginning of the Paleogene.

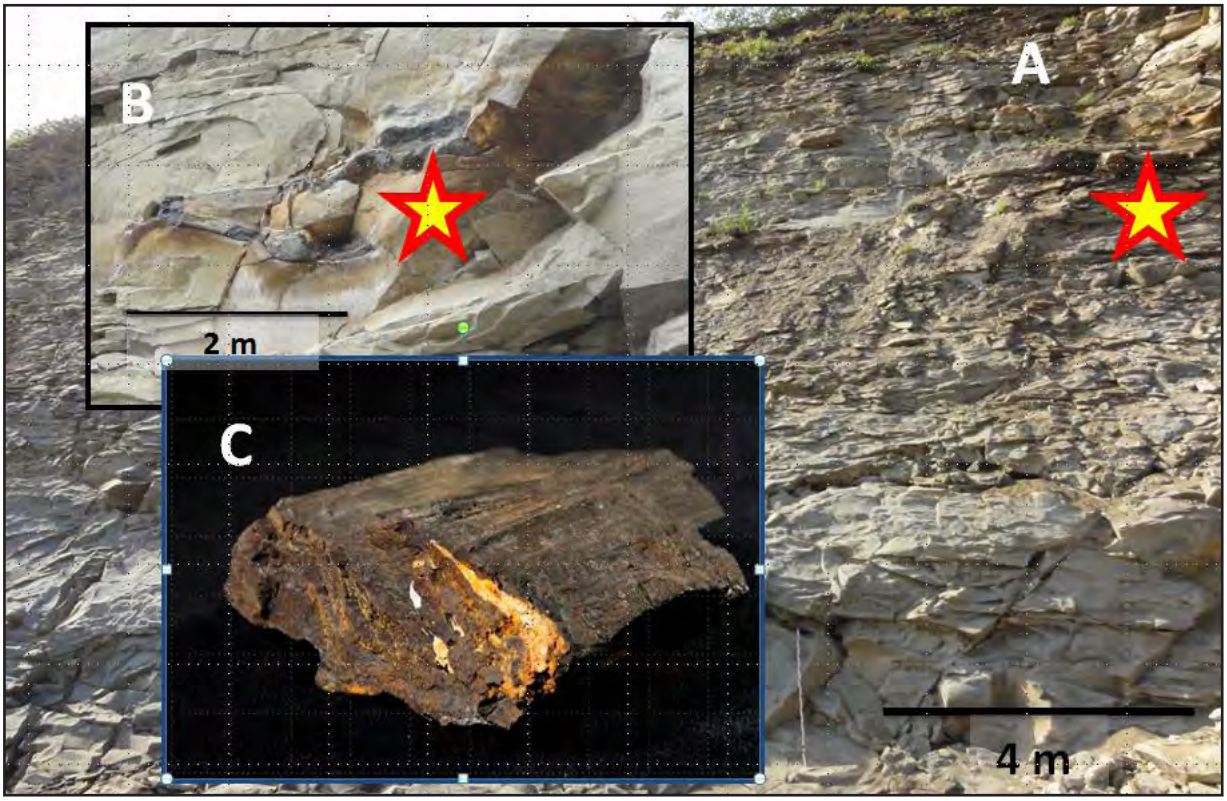


Figure 2. *(A) Outcrop in the Moose Channel Formation sample position indicated by star. (B) Zoomed detail from profil figure a, wood sample position indicated by star. (C) Petrified wood specimen No. 63049 with incrustations of Fe-silicates (in yellow), 7 cm in length.*

MATERIAL AND METHODS

The petrified parts of the wood remains were chosen for analysis. The fossil wood specimen is now housed at the Royal Ontario Museum in Toronto (collection Kevin Seymour, No. 63049; Fig. 2c). It is approximately 7 cm long and has been flattened as a result of compaction pressure, which also folded the approximately 25 growth rings of the wood. The specimen probably is most likely a thin trunk.

Additionally, the holo- and paratypes of the generotypus *Protopiceoxylon extinctum* Gothan, 1907 from King Charles Land (Gothan, 1907; Fig. 3) and from Green Harbour/Spitsbergen (Gothan, 1910; Fig. 4) were available for anatomical comparison and taxonomic classification from the Natural History Museum Berlin.

The wood fossil was extracted mechanically from the surrounding sediment and protected in a plastic bag to preserve its structure.

For xylotomical identification, the fossil wood remains were then cut into thin cross, radial-, and tangential sections, each about 20-30 µm thick. The observations were made with a Leica DM 5500 light microscope, equipped with a digital camera (DFC 480).

The wood remains were identified by comparisons with both living and fossil wood described in the literature, as well as with reference collections of living and fossil wood from the Natural History Museum Berlin, the Senckenberg Naturhistorische Sammlungen in Dresden (SNS), and from the first author's private collection. Descriptive terms correspond to current xylotomical terminology (*e.g.*, Eckhold, 1921, 1923; Kräusel, 1949; Greguss, 1955, 1967; Van der Burgh, 1973; Grosser, 1977; IAWA, 2004; Dolezych, 2005; and Philippe and Bamford, 2008).

XYLOTOMICAL INVESTIGATION

DIAGNOSIS

Protopinaceae Kraeusel, 1949

Protopiceoxylon Gothan, 1907

Protopiceoxylon yukonense sp. nov.

HOLOTYPUS: Plate I (Fig. 5d-f), Plate II (Fig. 6c-f) and Plate IV (8a-f), Royal Ontario Museum Toronto, collection Kevin Seymour, No. 63049, and Senckenberg Naturhistorische Sammlungen Dresden, collection of Martina Dolezych, Hoyerswerda, prep. 190713/4c, t, r.

LOCUS TYPICUS: Big Fish River area, northern Yukon and northwestern Mackenzie Delta area.

FORMATION: Moose Channel Formation, Paleocene.

DERIVATIO NOMINIS: After the region Yukon, Canada, where the fossil was found.

DIAGNOSIS: Coniferous wood with distinct growth rings. The transition from early to late wood is gradual. Early wood tracheids are much wider than the late wood tracheids. Pits in the radial cell walls of the early wood tracheids are protopinoid. Axial parenchyma is seldom present and diffuse. Rays are uniseriate and up to 20 cells high. Vertical resin canals occur. Horizontal resin canals occur only traumatic. Horizontal ray wall cells are about 4 to 5 µm thick and pitted. Tangential ray cell walls are often 3 to 4 µm thick and pitted. Ray tracheids are absent. Cross–field pits are mostly 2–3 (4), predominantly circular and piceoid.



Figure 3. *Slide showing generotypus Protopiceoxylon extinctum Gothan, 1907. Holotype from the King Charles Land (König Karls Land, Unterkreide). Handwriting by Walther Gothan. HNM Berlin 2001/No. 1460.*

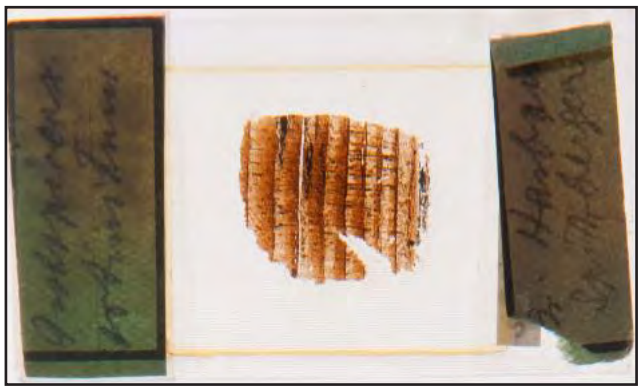


Figure 4. *Slide showing generotypus Protopiceoxylon extinctum Gothan, 1910. Paratype from Green Harbour/ Spitsbergen. Handwriting by Walther Gothan. HNM Berlin 2001/No. 1462.*

WOOD DESCRIPTION

Plate I (Fig. 5d-f); Plate II (Fig. 6c-f); Plate IV (Fig. 8a-f)

Growth rings: The growth rings vary in width. The early and the late wood are differentiated. See Figure 5d-f (Plate I).

Tracheids: The shape of the lumina is polygonal in cross section. Resin particles seldom occur. See Figure 5d-f (Plate I).

Bordered pits: The bordered pits in the radial walls of the tracheids occur in single, double and rarely in triple rows. Pits are protopinoid arranged; abietoid and araucaroid pitting occurs (Fig. 8d). Crassulae are present. The diameter of the bordered pits range from 11 to 22 µm.

Axial Parenchyma: Axial parenchyma is seldom present. The pits in the longitudinal walls are similar to those in the cross–fields and have a diameter of *ca.* 3 µm (Fig. 6c).

Rays: Rays are composed solely of parenchyma cells, are uniseriate, and are 4 to 8 cells high, up to 20 cells (Fig. 6c-f). The average height of the middle cells is 20 µm (Fig. 8a-c,e,f). The peripheral cells are somewhat higher. The horizontal cell walls are up to 6 µm thick (Fig. 8a-c,e,f). The tangential walls are up to 5 µm thick and juniperoid pitted (Fig. 8c). The cross–field pits are small and predominantly circular and piceoid (Fig. 8a-c,e). Usually 2 to 3 (4) pits with a diameter of about 6 µm are found in each cross–field (Fig. 8a-c,e). Ray tracheids are absent.

Resin canals: Vertical resin canals are surrounded by thick-walled tissue (Fig. 6f). There are approximately nine epithelium cells, which are pitted (Fig. 6e). The diameter of the vertical canals ranges between 30 and 280 µm (Fig. 6d,f).

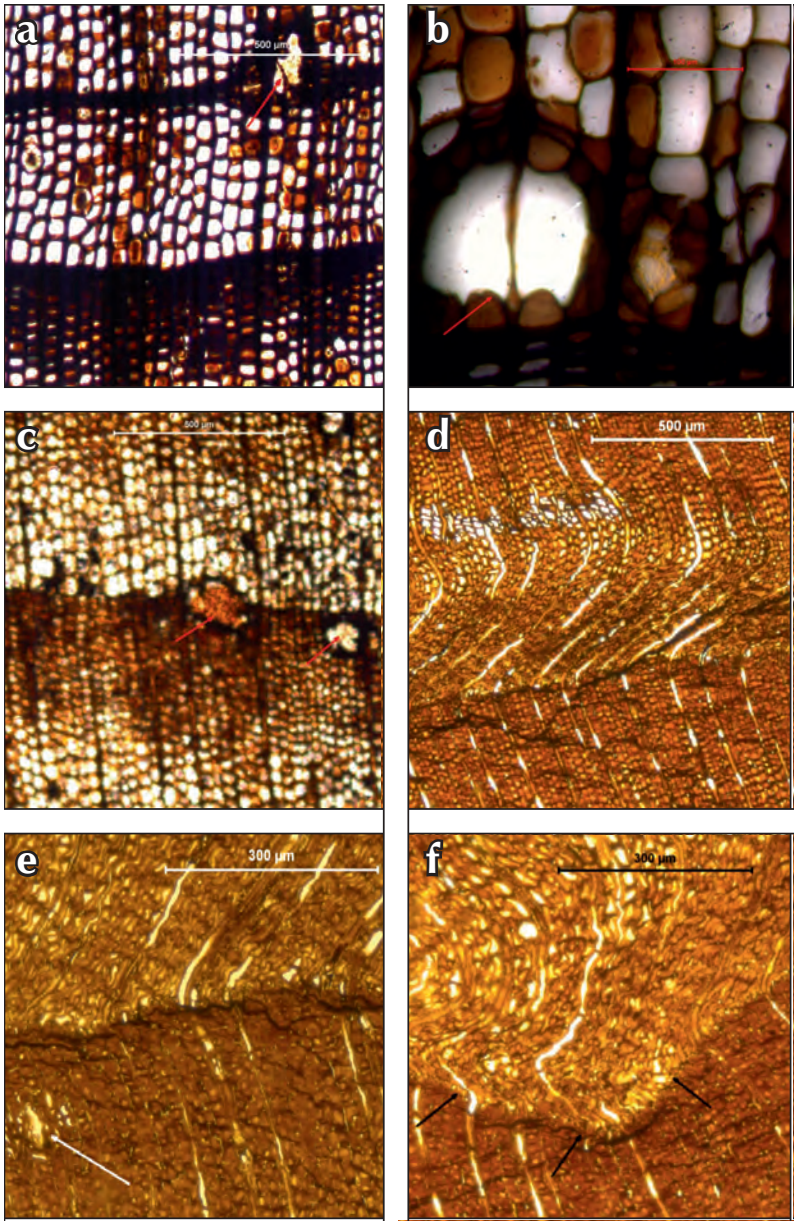


Figure 5. *Plate I: woods of Protopiceoxylon extinctum Gothan, 1907 (Berlin 2001/1460) and 1910 (Berlin 2001/1462), and Protopiceoxylon yukonense sp. nov. (a) Cross section of P. extinctum showing tracheids, distinct growth rings, resin, and a vertical resin canal (red arrow). King Charles Land, holotype by Gothan, 1907, slide no. 1460. Scale bar = 500 µm. (b) Cross section of P. extinctum showing with tracheids, a vertical resin canal, and epithelial cells (red arrow). King Charles Land, holotype by Gothan, 1907, slide no. 1460. Scale bar = 100 µm. (c) Cross section of P. extinctum showing with tracheids, distinct growth rings, resin, a gradual transition from early- to latewood, and vertical resin canals (red arrow). Green Harbour/Spitsbergen, paratype by Gothan, 1910, slide no. 1462. Scale bar = 500 µm. (d) Cross section of P. yukonense showing with tracheids, a gradual transition from the early-to the latewood, and a distinct growth ring. North Slope, prep. 190713/4c. Holotypus. Scale bar = 500 µm. (e) Cross section of P. yukonense showing with tracheids, a distinct growth ring, and a resin canal (white arrow). North Slope, prep. 190713/4c. Holotypus. Scale bar = 300 µm. (f) Cross section of P. yukonense showing with tracheids, a distinct growth ring (black arrows), and resin cannels. North Slope, prep. 190713/4c. Holotypus. Scale bar = 300 µm.*

IDENTIFICATION

A coniferous wood with a particular combination of uniseriate rays, thick and strongly pitted horizontal ray cell walls (Abietineen-pitting *sensu* Gothan, 1905), pitted tangential ray cell walls (*Juniperus*-pitting *sensu* Gothan, 1905), the occurrence of vertical resin- and traumatic horizontal resin canals, and the protopinoid pitted bordered pits corresponds to *Protopiceoxylon* (Gothan, 1907, 1910).

The generotypus of *Protopiceoxylon, P. extinctum*, was established from the Jurassic of the King Charles land (Gothan, 1907; Holotype, NHMB; Figs. 3, 5a,b, 6a,b, and 7a-c) and from the Upper Jurassic and Lower Cretaceous of Green Harbour/Spitsbergen (Gothan, 1910; Paratype, NHMB; Figs. 4, 5c, and 7c-f). *Pinites cavernosus* Cramer, 1868 *ex parte* were assigned to *P. extinctum* (Gothan, 1910). Supplementary slides, labeled as *P. extinctum*, which were used for illustration by Gothan (1907), were found by Philippe and Cantrill (2007), in the Swedish Museum of National History in Stockholm. In the holotype, Gothan (1907) did not describe the protopinoid pitting of the bordered pits, first, Gothan (1910) featured this attribute in the paratype by an extinct major anatomical feature. The protopinoid pitting is characterized by abietoid pitting with predominantly rounded pits in opposite arrangement (Fig. 7e) as well as by araucaroid pitting with predominantly angular-hexagonal pits in alternating arrangement (Fig. 7f). The term "protopinoid" goes back to Bailey (1933), who translated the "Übergangstyp" *sensu* Eckhold (1921, 1923) as "protopinaceous" type. Eckhold used this term to describe this type of bordered pitting in the tracheids walls. Furthermore, this character is also named as mixed- or transitional type (Philippe and Bamford, 2008). Vogellehner (1968) proposed a conservation of the name *Protopiceoxylon* and placed the fossil wood genus *Pinoxylon* Knowlton, 1900 and the generotypus *Pinoxylon dacotense* Knowlton, 1900 emendavit Read, 1932, from the Mesozoic of the Black Hills, into this fossil wood genus.

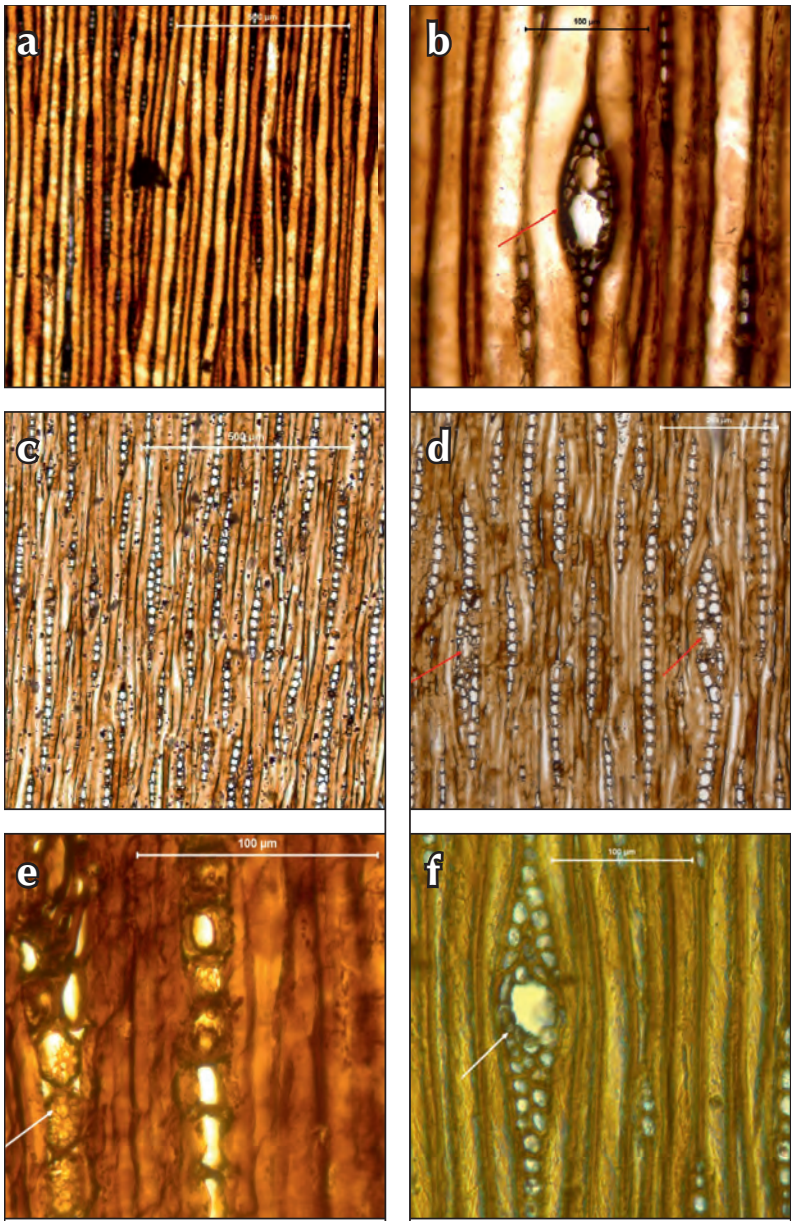


Figure 6. *Plate II: woods of Protopiceoxylon extinctum Gothan, 1907 (Berlin 2001/1460) and Protopiceoxylon yukonense sp. nov. (a) Tangential section of P. extinctum showing tracheids and rays. King Charles Land, holotype by Gothan, 1907, slide no. 1460. Scale bar = 500 µm. (b) Tangential section of P. extinctum showing tracheids, rays, and a vertical resin canal (red arrow). King Charles Land, holotype by Gothan, 1907, slide no. 1460. Scale bar = 100 µm. (c) Tangential section of P. yukonense showing tracheids, rays, and tangential pits. North Slope, prep. 190713/4t. Holotypus. Scale bar = 500 µm. (d) Tangential section of P. yukonense showing tracheids, rays, and vertical resin canals (red arrows). North Slope, prep. 190713/4t. Holotypus. Scale bar = 200 µm. (e) Tangential section of P. yukonense showing tracheids, rays, and pitted epithelial cells (white arrow). North Slope, prep. 190713/4t. Holotypus. Scale bar = 100 µm. (f) Tangential section of P. yukonense showing tracheids, rays, and a vertical resin canal (white arrow). North Slope, prep. 190713/4t. Holotypus. Scale bar = 100 µm.*

Protopiceoxylon belongs to the Mesozoic family Protopinaceae (Kräusel, 1949; Müller-Stoll and Schultze-Motel, 1990) and is known from Jurassic to Cretaceous. In addition, Grambast (1952) as well as Süss and Velitzelos (1993) classified woods of Protopinaceae into the Cenozoic. Because of the parautochthonous and allochthonous character of the Cenozoic findings of Protopinaceae, the noted origin is debatable. This family is considered extinct because there is no basis for comparisons with today's relatives. It is a transitional family between Araucariaceae and Pinaceae because it characterized by a combination of araucarian and abietineous features (Grambast, 1961; Vogellehner, 1967).

Until now the only known fossil woods from the Yukon near the Northwest Territories border are no older than Late Pliocene. Late Pliocene woods of *Picea* L. and *Larix* Mill., as well as Middle Pliocene woods of *Abies* Mill. and *Pinus* L., from the Porcupine River (Ch'ijee's Bluff) are described by Wheeler and Arnette (1994).

Protopiceoxylon spp. was found in other Arctic regions by different authors. Selmeier & Grosser (2011) identified drift wood, recovered from Early Cretaceous sediments along Reptile Creek on Ellesmere Island (Canada), as *Protopiceoxylon* sp.

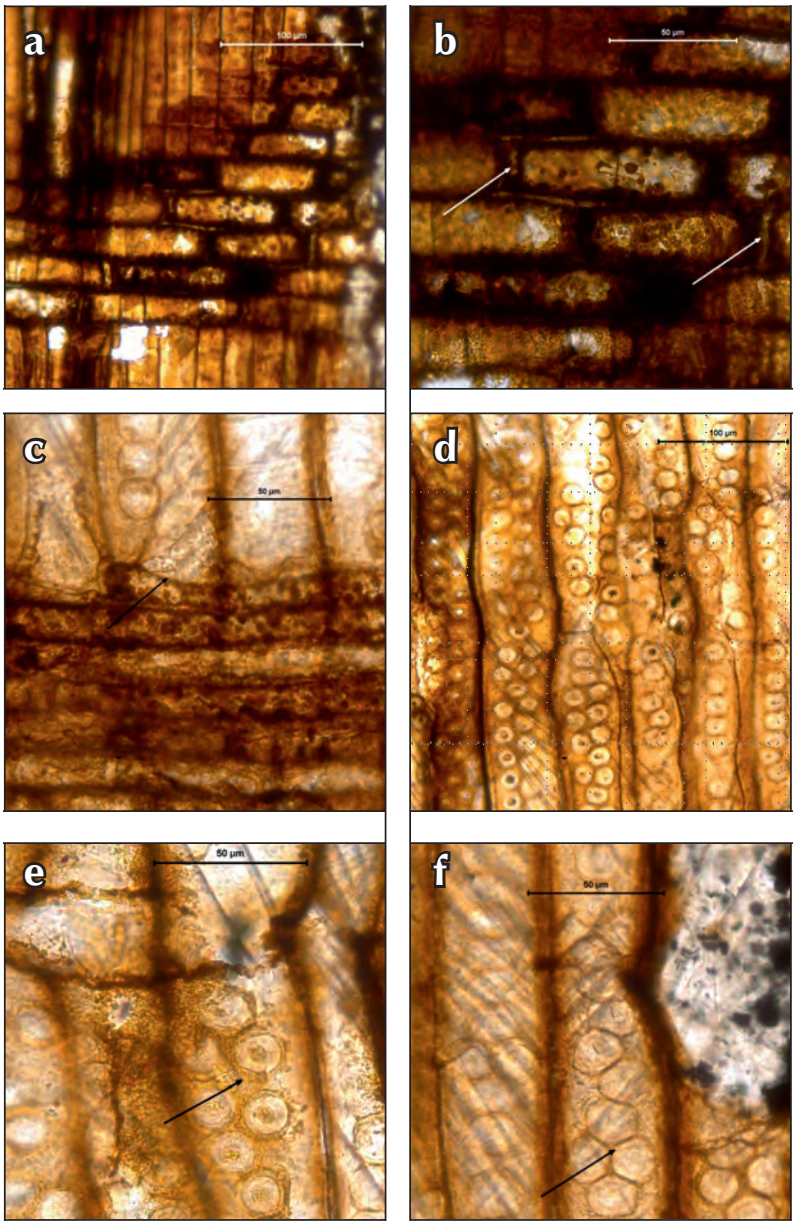


Figure 7. *Plate III: woods of Protopiceoxylon extinctum Gothan, 1907 (Berlin 2001/1460) and 1910 (Berlin 2001/1462). (a) Radial section of P. extinctum showing radial tracheids and a ray. King Charles Land, holotype by Gothan, 1907, slide no. 1460. Scale bar = 100 µm. (b) Radial section of P. extinctum showing a ray, horizontal ray cell walls, and pitted tangential ray cell walls (white arrows). King Charles Land, holotype by Gothan, 1907, slide no. 1460. Scale bar = 50 µm. (c) Radial section of P. extinctum showing radial tracheids, a ray, and a ray tracheid (black arrow). King Charles Land, holotype by Gothan, 1907, slide no. 1460. Scale bar = 50 µm. (d) Radial section of P. extinctum showing radial tracheids with protopinoid pitted bordered pits. Green Harbour/Spitsbergen, paratype by Gothan, 1910, slide no. 1462. Scale bar = 100 µm. (e) Radial section of P. extinctum showing radial tracheids with protopinoid pitted bordered pits (here a part with abietoid character, black arrow). Green Harbour/Spitsbergen, paratype by Gothan, 1910, slide no. 1462. Scale bar = 50 µm. (f) Radial section of P. extinctum showing radial tracheids with protopinoid pitted bordered pits (here a part with araucaroid character, black arrow). Green Harbour/Spitsbergen, paratype by Gothan, 1910, slide no. 1462. Scale bar = 50 µm.*

P. extinctum is known from the King Charles Land and from Spitsbergen (Gothan 1907, 1910, respectively). This fossil wood species is further characterized from the fossil wood genus *Protopiceoxylon* by the occurrence of 2 to 4 small circular cross-field pits, the lack of axial parenchyma, the lack of ray tracheids, the occurrence of tangential pits and the up to 30 cells high rays (Gothan, 1907, 1910). However, our observations of Gothan´s slides (Fig. 7c) indicate that *P. extinctum* is more characterized by the occurrence of ray tracheids than the lack of them, as previously noted. *Protopiceoxylon arcticum* Seward, 1919, a Cretaceous (Albian-Aptian) wood from the Franz Joseph Land was assigned to *P. extinctum* by Vogellehner (1968). Furthermore, Harland *et al.* (2007) identified three woods from Spitsbergen and the Canadian Arctic as *P. extinctum*. The Yukon wood differs from that fossil by the absence of ray tracheids, the fewer ray cells and the occurrence of axial parenchyma.

Protopiceoxylon johnseni Schroeter, 1880 emendavit Edwards, 1925 known from the Upper Jurassic of the King Charles Land is characterized by a small difference to *P. extinctum*. It varied only by the absence of traumatic horizontal resin canals and has somewhat fewer rays.

Another fossil wood species is known as *Protopiceoxylon wordii* Walton, 1927, from Middle Jurassic of Storfield/ Spitsbergen. On the basis of the occurrence of the traumatic origin of the vertical resin canals, this assignment is questionable.

Protopiceoxylon woods have not only been defined in from Arctic areas. Stopes (1915) described *Protopiceoxylon edwardsi* from the Early Cretaceous of England. However, this wood is not characterized by the mixed type of bordered pitting, so it probably does not belong to the *Protopiceoxylon* genus.

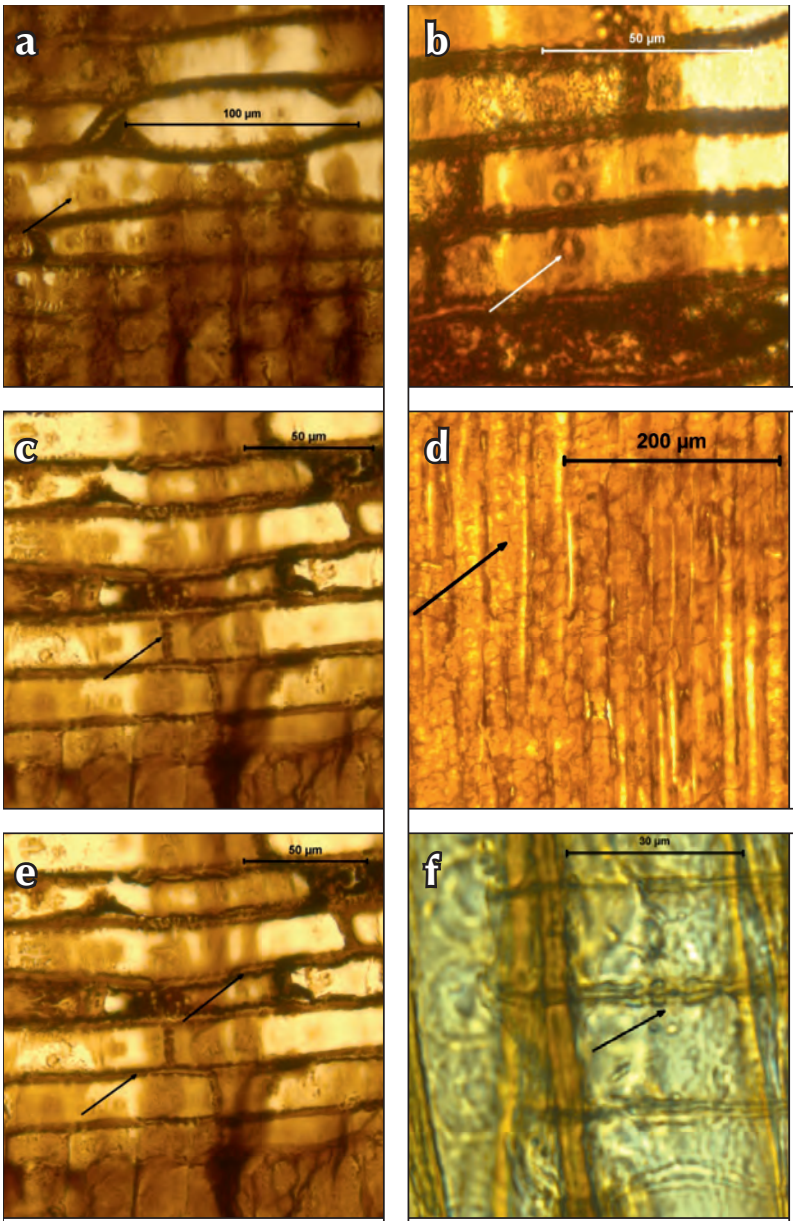


Figure 8. *Plate IV: woods of Protopiceoxylon yukonense sp. nov. (a) Radial section of P. yukonense showing a ray, pitted horizontal and tangential ray cell walls, and cross-field pits (black arrow). North Slope, prep. 190713/4r. Holotypus. Scale bar = 100 µm. (b) Radial section of P. yukonense showing a ray, pitted horizontal and tangential ray cell walls, and cross-field pits (white arrow). North Slope, prep. 190713/4r. Holotypus. Scale bar = 50 µm. (c) Radial section of P. yukonense showing a ray, pitted horizontal ray cell walls, and tangential ray cell walls (black arrow). North Slope, prep. 190713/4r. Holotypus. Scale bar = 50 µm. (d) Radial section of P. yukonense showing radial tracheids and protopinoid pitted bordered pits (black arrow). North Slope, prep. 190713/4r. Holotypus. Scale bar = 200 µm. (e) Radial section of P. yukonense showing a ray, pitted tangential ray cell walls and tangential ray cell walls (black arrow). North Slope, prep. 190713/4c. Holotypus. Scale bar = 50 µm. (f) Radial section of P. yukonense showing a ray with and pitted horizontal ray cell walls (black arrow). North Slope, prep. 190713/4r. Holotypus. Scale bar = 30 µm.*

Protopiceoxylon canadense and *Protopiceoxylon resiniferous,* established by Medlyn and Tidwell (1979), are described from the Upper Jurassic of British Columbia and Utah, respectively. However, *P. resiniferous* is not marked by the mixed type of the tracheid walls and so it is concluded that this taxon does not belong to *Protopiceoxylon*. *P. canadense* is a fossil wood species which is very similar to the Yukon fossil. It is distinguished by the higher rays and the pinoid cross-field pitting versus the circular/piceoid cross-field pitting in the Arctic wood.

A *Protopiceoxylon* wood with the combination of very high rays, up to 70 cells, the occurrence of axial parenchyma, the occurrence of tangential pits and the more abietoid- as araucaroid pitting of the radial tracheid walls is indicative of *Protopiceoxylon yabei* Shimakura,1936 emendavit Vogellehner, 1968 (Shimakura,1936; Vogellehner, 1968). This fossil is described from the Middle Jurassic of the Manschukuo/China. This taxon is distinguished from the Yukon fossil by the higher rays, the occurrence of ray tracheids, the more common occurrence of axial parenchyma and abietoid pitting of the radial tracheid walls within the protopinoid character.

Some *Protopiceoxylon* woods are also known from the Heilongjiang area in Northeast China and Russia: *P. mohense* Ding, 2000 from Lower Cretaceous sedimentary rocks and *P. amurense* Du, 1982 from Jurassic to Lower Cretaceous rocks also reported from the Late Cretaceous by Wang *et al.* (1997) and from Paleocene sedimentary rocks by Terada *et al.* (2011). Because of their lack of the protopinoid pitting of the radial tracheid walls, these woods are not considered to belong to the fossil wood genus *Protopiceoxylon*. In addition, Terada *et al.* (2011) found for *P. amurense* an affinity to the extant conifer genera *Keteleeria* Carrière, 1866 or *Nothotsuga* Hu exparte C.N. Page, 1989. Also arguable is the assignment of *Protopiceoxylon chaoyangense* Duan, 2000 and of *Protopiceoxylon yizhouense* Duan and Cui, 1995 (Duan *et al.*, 1995) to *Protopiceoxylon* based on the absence of transitional type pitting of radial tracheid walls. *P. chaoyangense* and *P. yizhouense* remains originate from Mesozoic sedimentary rocks of the Liaoning Province in Northeast China.

The Yukon fossil is characterized by a coniferous wood with distinct growth rings, the gradual transition from early to late wood, having 4 to 5 µm thick and pitted horizontal ray cell walls (Abietineen-pitting), up 3 to 4 µm thick and pitted tangential ray cell walls (*Juniperus*-pitting), the protopinoid pitting of the radial tracheid walls, the seldom occurrence of axial parenchyma, the uniseriate rays with a high of up to 20 cells, the occurrence of vertical and traumatic horizontal resin canals, the lack of ray tracheids and the mostly 2-3 (4) small and predominantly circular and piceoid cross-field pits. Because there is no identical fossil wood species known, it is required that a new fossil species of *Protopiceoxylon* be established. It is proposed that the epitheton of this new fossil wood species be named after the Yukon region where the fossil is found: ***Protopiceoxylon yukonense* sp. nov.**

This new fossil wood genus, which shares xylotomical features with both Pinaceae and Araucariaceae, is characterized by extinct anatomical features that are intermediate between *Protopiceoxylon* and *Piceoxylon*, which manifest within the radial bordered pits. These are protopinoid in the first mentioned taxon and abietoid in the other discussed taxon. Most other features, such as the general coniferous structure, the occurrence of vertical resin ducts, the thick and pitted horizontal and tangential ray cell walls and the partially piceoid cross-field pits, demonstrate a close relationship between both fossil taxa. Vogellehner (1968) considered *Protopiceoxylon*, a plant with heterobathmic character *sensu* Takhtajan, 1959, was convergent in its evolutionary line with *Piceoxylon*. In contrast, Müller-Stoll (1986) did not recognize the extinct family Protopinaceae as a necessary link in the evolutionary line, because protopinaceous and abietoid (modern) woods have their genesis in the same time period.

CONCLUSIONS

For the first time a new taxon of *Protopiceoxylon, Protopiceoxylon yukonense* sp. nov. from the Paleocene of the Moose Channel Formation in Yukon near the Northwest Territories boundary, is successfully established.

This taxon belongs to the gymnospermous family Protopinaceae. Because this family is extinct and characterized by a transitional type, the taxonomic investigation is essential for research on evolution of plants. The major anatomical feature of *Protopiceoxylon yukonense* is the protopinoid pitting which is characterized by abietoid as well as araucaroid pitted radial tracheid walls. This fossil wood species is distinct from other *Protopiceoxylon* woods by the seldom occurrence of axial parenchyma, the uniseriate rays, up to 20 cells high, the occurrence of vertical and traumatic horizontal resin canals, the lack of ray tracheids, and the mostly 2-3 (4) small and predominantly circular and piceoid cross-field pits.

Protopiceoxylon woods are distributed throughout primarily Mesozoic and Paleogene in Arctic zones of North America and Europe as well as in other regions of North America, Europe and East Asia. Relating the fossil wood specimen to some other woods of this fossil species (namely from Ellesmere Island, Spitsbergen and Franz Joseph Land), which also had been growing in high latitude zones, it is possible to provide the evidence of forested areas and to unravel additional details about the species living in the forested areas in Cretaceous and Paleogene times.

The fossil wood was recovered as a parautochthonous, petrified wood remain from the Moose Channel Formation, a formation of deltaic and shallow marine origin in the Big Fish River area. The origin of the fossil wood is either in the direct vicinity of the former delta or was transported over a longer distance during a discharge event of the Paleocene fluvial system.

ACKNOWLEDGMENTS

We are grateful for access to this area and for help during field work, especially from Tiffani Fraser (YGS), Kevin Seymour (Royal Ontario Museum, Toronto, Canada), and Karsten Piepjohn (BDR). Special thanks to Maurice Colpron (YGS) who made the project happen. Furthermore, we thank our colleagues from the National History Museum in Berlin (Germany) for making it possible to study the material in the W. Gothan collection. We owe our thanks to the reviewer for their helpful suggestions and corrections.

The 15th geological expedition of the CASE research program (CASE = Circum-Arctic Structural Events) of the German Federal Institute for Geosciences and Natural Resources in Hannover, Germany, was a joint project with the Yukon Geological Survey in Whitehorse, Canada, the Université Pierre et Marie Curie, Paris, France, and the Royal Ontario Museum, Toronto, Canada.

REFERENCES

Bailey, I.W., 1933. The cambium and its derivative tissue. VII. Problems in identifying the wood of Mesozoic Coniferae. Annals of Botany, vol. 47, p. 145-157.

Carrière, E.A., 1866. *Keteleeria fortunei* (Murr.) Carrière comb. nov. Revue Horticole, vol. 37, p. 449-451.

Cramer, C., 1868. Fossile Hölzer der arktischen Zone. *In*: Flora fossilis arctica I, 1868, O. Heer, p. 167-180.

Dietrich, J.R., Dixon, J. and McNeil, D.H., 1985. Sequence analysis and nomenclature of upper cretaceous to holocene strata in the Beaufort-Mackenzie Basin, Current research part A/Recherches en cours partie A. Geological Survey of Canada, Paper 85-1A, p. 613-628.

Ding, Q.H., 2000. *Protopiceoxylon mohense* sp. nov. from the Jiufengshan Formation in Heilongjiang Province. Chinese Bulletin of Botany, vol. 17, p. 206-209.

Dixon, J., Dietrich, J., Snowdon, L.R., Morrell, G. and McNeil, D.H., 1992. Geology and Petroleum Potential of Upper Cretaceous and Tertiary Strata, Beaufort-Mackenzie Area, Northwest Canada. AAPG Bulletin, vol. 76, p. 927-947.

Dolezych, M., 2005. Koniferenhölzer im Lausitzer Flöz und ihre ökologische Position. LLP Contributions Series No. 19, p. 1–339, Utrecht.

Du, N.Z., 1982. Two fossil woods from Heilongjiang Sheng of China. Acta Botanica Sinica, vol. 24, p. 383-387.

Duan, S.Y., 2000. Several fossil woods from Mesozoic of Western Liaoning Province, Northeast, China. Acta Botanica Sinica, vol. 42, p. 207-213.

Duan, S.Y., Cui, J.Z., Wang, X., Xiong, B.K. and Wang, Y.Q., 1995. Fossil woods from the Early Cretaceous of Western Liaoning, China. *In*: Wood anatomy research 1995, S.M. Wu (ed.). International Symposium on Tree Anatomy and Wood Formation, Tianjin, China. International Academic Publishers, Beijing, p. 166-171.

Eckhold, W., 1921. Die Hoftüpfel bei den rezenten und fossilen Koniferen. Schlesischen Friedrich-Wilhelms-Universität Breslau., p. 4.

Eckhold, W., 1923. Die Hoftüpfel bei den rezenten und fossilen Koniferen. Jahrbuch der Preußischen Landesanstalt, vol. 42, p. 472-505.

Edwards, W.M., 1925. On *Protopiceoxylon johnseni* (Schroeter), a Mesozoic coniferous wood. Annals of Botany, vol. 39, p. 1-7.

Gothan, W., 1905. Zur Anatomie lebender und fossiler Gymnospermen Hölzer. Abhandlungen der Königlichen Preußischen Geologischen Landesanstalt, Neue Folge, vol. 44, p. 1-108.

Gothan, W., 1907. Die fossilen Hölzer von König-Karls-Land. Kungliga Svenska vetenskapsakademiens handlingar, vol. 42, p. 1-44.

Gothan, W., 1910. Die fossilen Holzreste von Spitzbergen. Kungliga Svenska vetenskapsakademiens handlingar, vol. 45, p. 1-56.

Grambast, L., 1952. Sur la signification des structures généralisées chez les Coniferales et la valeur des Protopinacées en tant que groupe. C.R. Academy of Science Paris, vol. 235, p**.** 1533-1535.

Grambast, L., 1961. Évolution des structures ligneuses chez les Coniferophytes. Bulletin de la Société Botanique de France, vol. 107, p. 30-41.

Greguss, P., 1955. Xylotomische Bestimmungen der heute lebenden Gymnospermen. (Akadémiai Kiadó) Budapest. 308 p.

Greguss, P., 1967. Fossil Gymnosperm Woods in Hungary from Permian to Pliocene. (Akadémiai Kiadó) Budapest. 136 p.

Grosser, D., 1977. Die Hölzer Mitteleuropas. Ein mikrophotographischer Lehratlas. 208 p.

Harland, M., Francis, J.E., Brentnall, S.J. and Beerling, D.J., 2007. Cretaceous (Albian-Aptian) conifer wood from Northern Hemisphere high latitudes: forest composition and palaeoclimate. Review of Palaeobotany and Palynology, vol. 143, p. 167-196.

Hu, H.H. and Page, C.N., 1989. Notes from the Royal Botanic Garden. Edinburgh, vol. 45, p. 390.

International Association of Wood Anatomists (IAWA), 2004. IAWA list of microscopic features for softwood identification 2004. IAWA Journal, vol. 25, p. 1-70.

Knowlton, F.H., 1900. Description of a new genus and species of fossil wood from the Jurassic of the Black Hills. In: Status of the Mesozoic floras of the United States. I. The older Mesozoic, L.F.Ward (ed.). Annual Report U.S. Geological Survey, vol. 20, p. 420-422.

Kräusel, R., 1949. Die fossilen Koniferenhölzer (unter Ausschluss von *Araucarioxylon* Kraus). II: Kritische Untersuchungen zur Diagnostik lebender und fossiler Koniferen – Hölzer. Palaeontographica, Abteilung B, 89, p. 83-203.

McNeil, D.H., 1989. Foraminiferal Zonation and Biofacies Analysis of Cenozoic Strata in the Beaufort-Mackenzie Basin of Arctic Canada, Current Research Part G, Frontier Geoscience Program, Arctic Canada. Geological Survey of Canada, Paper 89-1G, p. 203-223.

Medlyn, D.A. and Tidwell, W.D., 1979. A review of the genus *Protopiceoxylon* with the emphasis on the North American species. Canadian Journal Botany, vol. 57, p. 1451-1463.

Mountjoy, E.W., 1967. Upper Cretaceous and Tertiary Stratigraphy, Northern Yukon Territory and Nortwestern District of Mackenzie. Geological Survey of Canada, Paper 66-16, p. 70.

Müller-Stoll, W.R., 1986. Evolutionary trends in gymnospermous wood structure during Mesozoic-Protopinaceous woods in the German Jurassic. The Palaeobotanist, vol. 35, p. 233-235.

Müller-Stoll, W.R. and Schultze-Motel, J., 1990. Gymnospermen-Hölzer des Deutschen Jura. Teil 3: Abietoid (modern) getüpfelte Hölzer. Zeitschrift der Deutschen Geologischen Gesellschaft, vol. 141, p. 61-77.

Philippe, M. and Bamford, M. K., 2008. A key to morphogenera used for Mesozoic conifer–like woods. Review of Palaeobotany and Palynology, vol.148, p. 184-207.

Philippe, M. and Bamford, M. K., 2009. Houlbert's types for fossil wood: lectotypification and taxonomic reappraisal of Abietoxylon, Ambaroxylon and Taxoxylon. Taxon, vol. 58, p. 1349–1356.

Philippe, M. and Cantrill, D.J., 2007. Nomenclatural types and taxonomy of Gothan´s Arctic fossil conifer wood. Taxon, vol. 56, p. 551-566.

Piepjohn, K., von Gosen, W., Läufer, A., McClelland, W.C. and Estrada, S., 2013. Ellesmerian and Eurekan fault tectonics at the northern margin of Ellesmere Island (Canadian High Arctic). Zeitschrift der Deutschen Gesellschaft für Geowissenschaften, vol. 164, p. 81-105

Read, C.B., 1932. *Pinoxylon dacotense* Knowlton from the Cretaceous of the Black Hills. Botanical Gazette, vol. 93, p. 173-187.

Schröter, C., 1880. Untersuchung über fossile Hölzer aus der arktischen Zone. *In*: Flora fossilis arctica VI, O. Heer. p. 1-38.

Selmeier, A. and Grosser, D., 2011. Lower Cretaceous conifer driftwood from Sverdrup Basin, Canadian Arctic Archipelago. Zitteliana A, vol. 51, p. 19-35.

Seward, A.C., 1919. Fossil plants: Ginkgoales, Coniferales, Gnetales. Cambridge University Press, 543 p.

Shimakura, M., 1936. Studies on fossil woods from Japan and adjacent lands. I. Some Jurassic woods from Japan and Manchukuo. Science Reports of the Tohoku Imperial University, vol. 18, p. 267-298.

Stopes, M.C., 1915. Catalogue of the Mesozoic plants in the British Museum (Natural History), Department of Geology. The Cretaceous flora. Part II. Lower Greensand (Aptian) plants of Britain. London, British Museum (Natural History), 360 p.

Süss, H. and Velitzelos, E., 1993. Zwei neue fossile Hölzer der Morphogattung *Pinoxylon* Knowlton emend. Read aus dem Tertiär der Insel Lesbos, Griechenland. Feddes Repertorium, vol. 120, 1-125.

Sweet, A.R., 1978. Palynology of the Lower Part, Type Section, Tent Island Formation, Yukon Territory. Current Research, Part B, Geological Survey of Canada, Paper 78-1B, p. 31-37.

Takhtajan, A., 1959. Die Evolution der Angiospermen. Gustav Fischer, Jena, 344 p.

Terada, K., Nishida, H. and Sun, G., 2011. Fossil woods from the Upper Cretaceous to Paleocene of Heilongjiang (Amur) River area of China and Russia. Global Geology, vol. 14, p. 192-208.

Van der Burgh, J., 1973. Hölzer der niederrheinischen Braunkohlenformation. 2. Hölzer der Braunkohlengruben „Maria Theresia“ zu Herzogenrath, „Zukunft West“ zu Eschweiler und „Victor“ (Zülpich–Mitte) zu Zülpich. Nebst einer systematisch–anatomischen Bearbeitung der Gattung Pinus L. Review of Palaeobotany and Palynology, vol. 15, p. 73-275.

Vogellehner, D., 1967. Zur Anatomie und Phylogenie mesozoischer Gymnospermenhölzer, 5: Prodromus zu einer Monographie der Protopinaceae. I. Die protopopinoiden Hölzer der Trias. Palaeontographica, Abteilung B, vol. 121, p. 30-51.

Vogellehner, D., 1968. Zur Anatomie und Phylogenie mesozoischer Gymnospermenhölzer, 7: Prodromus zu einer Monographie der Protopinaceae. II. Die protopopinoiden Hölzer des Jura. Palaeontographica, Abteilung B, vol. 124, p. 125-162.

Walton, J., 1927. On some fossil woods of Mesozoic and Tertiary age from the Arctic zone. Annales of Botany, vol. 41, p. 239-254.

Wang, R.F., Wang, Y.F. and Chen, Y.Z., 1997. Fossil woods from the late Cretaceous of Heilong-Jiang province, Northeast China, and their palaeoenvironmental implications. Acta Botanica Sinica, vol. 39, p. 972-978.

Wheeler, E.A. & Arnette, C.G., 1994. Identification of Neogene woods from Alaska-Yukon. Quaternary International, 22/23, p. 91-102.

Young, F.G., 1975. Upper Cretaceous Stratigraphy, Yukon Coastal Plain and Northwestern Mackenzie Delta. Geological Survey of Canada, Bulletin 249, p. 1-83.

Young, F.G. and McNeil, D.H., 1984. Cenozoic stratigraphy of the Mackenzie delta, Northwest Territories. Geological Survey of Canada, Bulletin 336, p. 1-63.

Early Pleistocene glaciation and implications for placer gold deposits in Back Creek, Mount Nansen area, Yukon

P.O. Englehardt[1], Brent C. Ward
Earth Sciences, Simon Fraser University

Jeffrey D. Bond
Yukon Geological Survey

Mark J. Coleman
Earth Sciences, Simon Fraser University

Englehardt, P.O., Ward, B.C., Bond, J.D. and Coleman, M.J., 2015. Early Pleistocene glaciation and implications for placer gold deposits in Back Creek, Mount Nansen area, Yukon. *In:* Yukon Exploration and Geology 2015, Yukon Geological Survey, p. 111-129.

ABSTRACT

Yukon has over a century of placer mining history, predominately in unglaciated regions. However, as these targets are exploited, focus turns to more complex landscapes where glaciation has buried, eroded and incorporated placer gold. This study examines how Early Pleistocene glaciation in the Mount Nansen area, central Yukon, has affected placer gold deposits. Detailed stratigraphic analysis and sample collection has focused on Back Creek, where placer mining has exposed a 22 m section with several gold bearing units. In the section, sediment from two glacial advances cap sporadically preserved pre-glacial gravel. The section is variably dissected by younger placer gold bearing fluvial gravel with enrichment related to intersection of inter-glacial or pre-glacial placer gold deposits. Analysis at Back Creek reveals the potential for deeply buried placer gold deposits in other glaciated regions of Yukon.

[1]*pengleha@sfu.ca*

INTRODUCTION

Beyond the influence of glaciation in Yukon, several lucrative placer deposits were exploited during the 1897 Gold Rush (LeBarge, 1995). As these prospects are exhausted exploration has shifted to more complex landscapes where glaciation may have obscured, eroded, and incorporated placer gold deposits (LeBarge, 1995). Several phases of Northern Cordilleran Ice Sheet (NCIS) glaciation, in Yukon, have modified the landscape (Duk-Rodkin, 1999; Duk-Rodkin *et al*., 2001; Jackson, 1993; 2000; Ward *et al*., 2007), producing the palimpsest landscape present today. The earliest phases of glaciation were the most extensive in central Yukon (Fig. 1) and likely had the largest effect on placer gold deposits. To understand the effect of early glaciation on placer gold development, the Mount Nansen Placer Mining District (NTS115/I) was investigated during the summer of 2015, to determine the stratigraphy at Back Creek, derive the geologic history, and to relate this to placer gold preservation and formation. Previous work in the Mount Nansen area is discussed and the current understanding of bedrock geology, glacial history, and placer gold development is summarized. This research is a synthesis of academic interest (early Pleistocene glacial behavior) and economic importance (placer gold development) that may be used as an analogue for future studies of placer gold in glaciated terrains.

BEDROCK GEOLOGY

Large gold deposits in Yukon formed during the repeated accretion of several terranes throughout the Mesozoic era (Colpron *et al*., 2007; Knight *et al.,* 2013; Monger *et al.,* 1972; Coney *et al.,* 1980). The Yukon Tanana terrane (YTT) formed as an island-arc back-arc basin with extensive porphyry/epithermal gold deposits, and the study area is underlain by these rocks (Colpron *et al*., 2007; Selby *et al.,* 1999). The Mount Nansen area is underlain by Proterozoic-Cenozoic bedrock, and major units are further described below (Fig. 2; Hart and Langdon, 1998; Saager and Bianconi, 1971; Tempelman-Kluit, 1984). The Proterozoic-Paleozoic metamorphic Yukon Group rocks consist of the following: chlorite schist, biotite schist, feldspathic quartzite, amphibolite, quartz-biotite gneiss and biotite-hornblende gneiss (Hart and Langdon, 1998; Mortensen *et al*., 2002; Saager and Bianconi, 1971). The metamorphic rocks host several intrusions including: the early Jurassic Long Lake Suite (hornblende-biotite granodiorite-monzogranite), mid-Cretaceous Dawson Range batholith (hornblende-biotite-quartz diorite, and granodiorite), late Cretaceous Prospector Mountain suite (quartz monzonite) and the Casino Plutonic suite (leucocratic granite, quartz monzonite and alaskite; Hart and Langdon, 1998; Johnston, 1996; Mortensen *et al*., 2002; Saager and Bianconi, 1971; Selby *et al.,* 1999; Wengzynowski *et al.,* 2015). Extensive volcanic deposits formed contemporaneously with the plutonic complexes and include the Mount Nansen Volcanic Group which comprises andesite, dacite, minor rhyolite and minor Cenozoic intrusions of quartz feldspar porphyries (Saager and Bianconi, 1971; Hart and Langdon, 1998; Mortensen *et al*., 2002). Mineralization in the Mount Nansen area is hosted within Paleozoic metamorphic rocks and Mesozoic intrusive rocks (Hart and Langdon, 1998; Mortensen *et al*., 2002). Late phase hypabyssal parts of the Mount Nansen volcanic rocks (quartz feldspars porphyries, dikes and minor pyroclastic flows) are related to significant mineralization (Hart and Langdon, 1998).

Several gold bearing porphyry-epithermal complexes are concentrated within a 3 by 12 km, northwest oriented, steeply dipping corridor called the Nansen trend (Hart and Langdon, 1998). These porphyry-epithermal complexes are the likely source for the placer gold deposits in the Mount Nansen area (Hart and Langdon, 1998; Jackson, 1993; LeBarge, 1995).

GLACIAL HISTORY

The NCIS first developed in Yukon during the late Pliocene (~2.6 Ma), and several advances produced the palimpsest surficial sedimentary record present today (Fig. 1; Barendregt *et al*., 2010; Duk-Rodkin *et al*., 2001; 2004 Hidy *et al.,* 2013). The development of the NCIS glaciation is related to complex atmospheric-oceanic interactions, Milankovitch Cycles, atmospheric composition and precipitation (Burn, 1994; Guthrie, 2001; Harris, 2005; Haug *et al*., 2005; Ward *et al*., 2008). Dawson (1889) first recognized evidence for glaciation in Yukon in 1887; however, multiple glacial advances were not recognized until Bostock (1936) worked in the Mount Nansen Area. Based on this early work there are three morphostratigraphic glacial surfaces widely recognized in Yukon: the pre-Reid, Reid/Gladstone, and McConnell (Fig. 1); each represents a discrete surface associated with a maximum extent, some of which represent two (Reid/Gladstone) or multiple (pre-Reid) NCIS advances (Bostock, 1966; Demuro *et al*., 2012; Duk-Rodkin *et al*., 1999; Hughes *et al.,* 1969; Jackson *et al.,* 1999; Jackson and Clague, 1991; Westgate *et al*., 2000; and Ward *et al*., 2007).

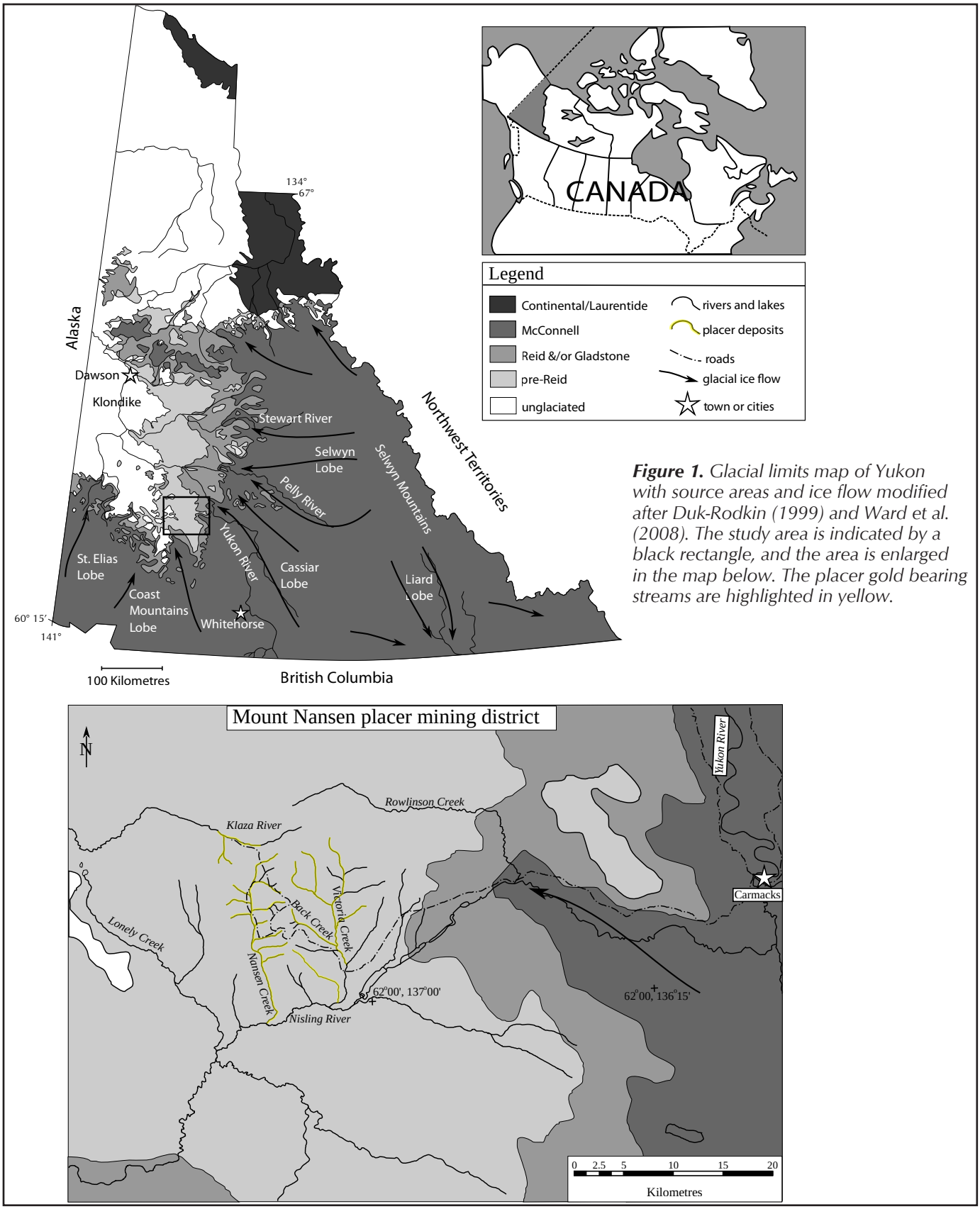


Figure 1. *Glacial limits map of Yukon with source areas and ice flow modified after Duk-Rodkin (1999) and Ward et al. (2008). The study area is indicated by a black rectangle, and the area is enlarged in the map below. The placer gold bearing streams are highlighted in yellow.*

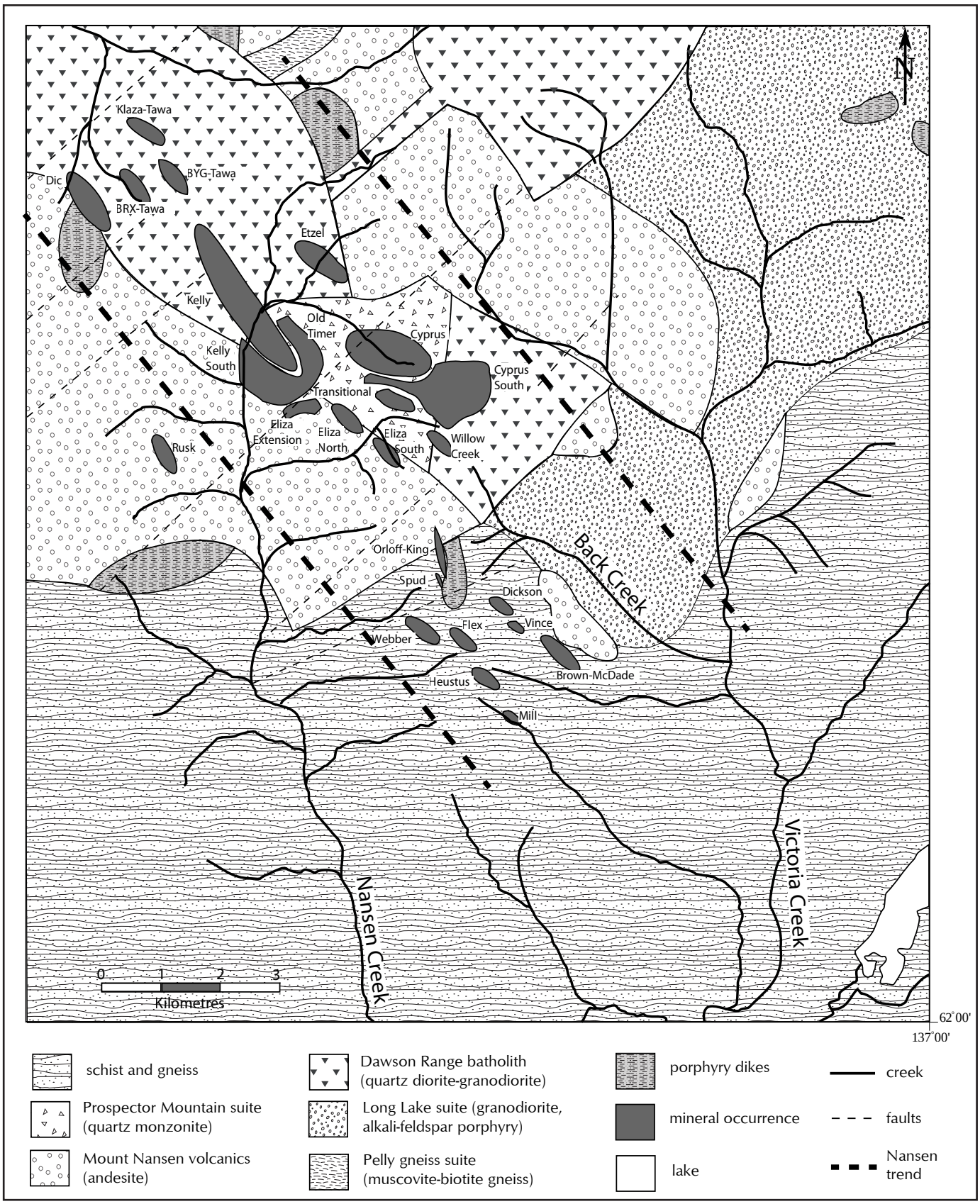


Figure 2. *Bedrock geology map of the Mount Nansen area modified after Hart and Langdon 1998.*

Glaciation in the Mount Nansen area has long been known (Cairnes, 1915), and placer mining occasionally provided insight that older glaciation had affected the area (Bostock 1966). Bostock (1966) assigned the two earliest phases of Yukon glaciation to be the Nansen (older) and the Klaza (younger) based on field observations in the 1930s. Subsequent work by Hughes *et al.* (1969), grouped the Nansen and the Klaza glacial events into the pre-Reid morphostratigraphic surface due to the challenge of separating the two advances in other areas. While several glacial periods are mapped in the Mount Nansen region only two pre-Reid glaciation events (the Nansen and Klaza) are known to have affected Back Creek (Fig. 1; Bostock, 1966; Jackson, 1993; 2000; LeBarge, 1995). The Nansen and Klaza glaciation likely advanced into the Mount Nansen area from the east and south and were part of the Cassiar and Coast Mountain ice lobes (Fig. 1; Bostock, 1966; Duk-Rodkin; 1999; Guerts and Dewes, 1993). The Nansen glaciation was extensive (affecting elevations below 1400 m), and landform evidence is restricted to meltwater channels and patchy till (Jackson, 2000; LeBarge, 1995). The antiquity of the Nansen till is reflected by the deeply weathered schist and granitic clasts contained in the till (Bostock, 1966). The timing of the Nansen glaciation is poorly constrained; however, it may be correlated to the most extensive NCIS *ca.* 2.64 Ma (Hidy *et al.*, 2013). The younger Klaza glaciation is thought to begin with local cirque glaciers developing in the Dawson Range and expanding into the valleys (Jackson, 1993; LeBarge, 1995). Further evidence of the Klaza glaciation was observed west of the study area in Lonely Creek where Bostock (1966) noted landscape modifications associated with glaciation. The Klaza glaciation may correlate to an advance in the Fort Selkirk region where basalt overlying till has been dated to greater than 1 Ma (Jackson, 2000; Jackson *et al.,* 1991; Naeser *et al.,* 1982). During subsequent mid-late Pleistocene glaciation (Reid, Gladstone and McConnell) the area was unglaciated and subjected to intense periglacial conditions (Fig. 1; Jackson, 2000; LeBarge, 1995). During the Reid and Gladstone glaciation events the Coast Mountains ice lobe dammed the Nisling River causing a glacial lake to develop. This increased the base level of the Nisling River and its tributaries Victoria and Nansen creeks (Guerts and Dewes, 1993; LeBarge, 1995). Gravel terraces associated with this episode of sedimentation are common in these tributaries to the Nisling River and are a good example of the indirect effect of more recent glaciation. This research focuses on the earliest phases of glaciation (pre-Reid) that directly affected the landscape and the associated placer gold deposits in Back Creek.

PLACER GOLD DEVELOPMENT

Placer gold deposits require mineralized bedrock and a mechanical concentration mechanism, typically colluvial and fluvial; however, it can also be glacial, eolian, or lacustrine (Els and Eriksson, 2005). In Yukon, the warmer temperatures (>4°C of current Mean Annual Temperature, MAT) and increased precipitation (>550 mm of current Mean Annual Precipitation, MAP) of the Paleogene to Neogene (66 to 2.6 Ma) produced deeply weathered bedrock mantles (>75 m) that facilitated the development of placer deposits and where lode gold became available for concentration (Ager *et al.*, 1994; Anderson and Stroshein, 1997; Dampier *et al.*, 2011; Foscolos *et al.,* 1977; Jackson, 2000; LeBarge, 1995). Beyond the reach of glaciation, placer gold deposits remained relatively undisturbed and continued accumulating throughout the Quaternary; however, in glaciated areas placer gold deposits were significantly affected by erosional and/or depositional processes (Goldfarb *et al.,* 2015; Herail *et al.,* 1989; Jackson 1993; LeBarge 1995; Levson and Blyth, 2001; Lowey, 2006).

More than 27,000 crude ounces of placer gold have been mined from several creeks in the Mount Nansen area and from various sediment types (LeBarge, 1995). A likely cause of this placer gold concentration is the abundance of mineralized bedrock in the region (Hart and Langdon, 1998; Jackson, 1993) and stable Cenozoic tectonic history that allowed residual deposits to accumulate. There are several known porphyry/epithermal deposits that may be the source of placer gold in Back Creek (Fig. 2; Hart and Langdon, 1998). Most placer mining in the Mount Nansen area extracts gold concentrated on the pervasive 'false bedrock' (till) developed on early Pleistocene pre-Reid glacial deposits (Bostock, 1966; LeBarge, 1995). These placer deposits have formed from weathering of bedrock slopes subsequent to the last regional glaciation to affect the area, and therefore, are considered relatively young. Exploitation of pre-glacial placer deposits situated on bedrock is limited due to the depth of glacial sediment cover. Recently, placer mining has exposed deeply buried deposits, which provides an important opportunity to

document stratigraphic and sedimentological information regarding multiple zones of placer gold development. This study investigates one of these deeper excavations that exposes valley bottom bedrock, pre-glacial sediment, and overlying Quaternary deposits. Information presented here may provide an analogue for future placer gold exploration in neighboring drainages, such as Nansen and Victoria creeks, and in other in glaciated areas.

METHODS

During the 2015 field season several locations in the Mount Nansen Area were visited; however, this study focuses on the stratigraphy of Back Creek due to its exceptional exposure of potential pre-glacial gravel and pre-Reid glacial sediment (Figs. 3 and 4). To understand the stratigraphy at Back Creek, sediment descriptions, clast orientation measurements, and paleomagnetic samples were collected. Several units (2, 3, 4, 6 and 11) were also sampled for placer gold to characterize gold provenance.

Sedimentary analysis was completed in the field where estimates of clast character (size, shape, orientation and surface features), and matrix character (size, abundance, compaction and structures) aided in assigning separate units (Table 1 and Fig. 5). Samples from several of these units were collected for further analysis. The presence of unique features including: 'decomposed clasts', cryoturbation, iron/manganese staining and organics were noted. The term 'decomposed clasts' refers to clasts that are pervasively weathered and may be easily broken by hand; Bostock (1966) used similar terminology (rotten clasts) when describing clasts from the Mount Nansen area.

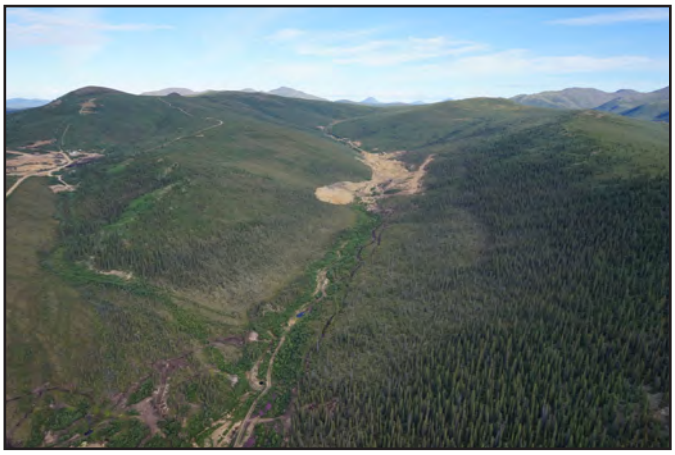


Figure 3. *A view of Back Creek looking northwest; current placer mining is in the centre of the valley.*



Figure 4. *A view of the deep (>22 m) placer mining exposure at Back Creek. The lowest unit visible is the deeply weathered bedrock (Unit 1). In the center of the section are two till units (Units 3 and 5) separated by interglacial sediments (Unit 4). Above this is cover sediment that includes various amounts of colluviated material (Unit 9), organics (Unit 8), tephra (Unit 9), and anthropogenic sediment (Unit 12).*

Table 1. *Unit interpretations and descriptions with respective landscape evolution phases.*

Unit	Interpretation	Description	Landscape Evolution Phase
12	Anthropogenic Sediment	All of the material that has been disturbed by mining. Characteristics, contacts and lateral extent all vary based on style of formation.	Cover Development (G)
11	Modern Gravel	Moderately stratified, poorly-consolidated, clast-supported gravel with ~70% clasts and a silty sand matrix. Clasts are subrounded to rounded and clast lithology is variable but local. Lower contact is sharp and erosive, and the unit forms the base of the modern creek.	
10	White River Tephra	Pale grey-white, finely laminated, fine-medium sand sized glass shards.	
9	Colluvium	Brown, poorly stratified to massive, organic-rich, matrix-supported, diamicton with ~30% clasts, variable lithologies. Lower contact is sharp and erosive, and the unit is laterally extensive.	
8	Colluviated Organics	Organic-rich, matrix-supported, poorly-consolidated, colluviated organics, with clay to fine sand, and abundant macrofossils. Lower contact is sharp and erosive, and this unit is laterally extensive.	
7	Fluvial Sand	Tan, sub-horizontally bedded silty-sand, with minor organics. Lower contact is erosive and unit is not laterally extensive.	
6	Fluvial Gravel (pay)	Variably Fe/Mn stained, stratified, poorly-consolidated, clast-supported gravel with ~80% boulder, cobble pebble clasts. Clasts are subrounded, imbricated with variable lithologies. Lower contact is erosive and unit is laterally extensive.	Pay Gravel Development (F)
5	Klaza Till	Dark grey, massive, over-consolidated, matrix-supported, diamicton with ~20% clasts, and a clayey silt matrix. Clasts were commonly decomposed, striated and or exotic.	Klaza Glaciation (E)
4	Paleosol/ inter-glacial gravel	Sediment present includes: i) an over-consolidated, matrix-supported diamicton with a clayey silt matrix ii) yellowish red disorganized pebbly gravel with Fe/Mn staining; iii) an organic bearing normal and reversely magnetized silt/clay (Fig. 8b,c).	Inter-Glaciation (D)
3	Nansen Till	Yellowish brown, massive, over-consolidated, matrix-supported, diamicton with ~20% clasts and a clay silt matrix (Fig. 7). Clasts are commonly decomposed, striated and/or exotic. Clast fabrics indicate a shift in ice flow direction from parallel to valley to orthogonal to valley which separates the two Nansen glacial phases (Landscape Evolution Phase B and C). Lower contact is sharp erosive and unit is laterally extensive.	Maximum Nansen Glaciation (C) Early Nansen Glaciation (B)
2	Pre-Glacial Gravel	Yellowish brown, weakly stratified, matrix/clast supported, poorly-consolidated gravel, with a ~50% clasts and a variably iron stained silty sand matrix (Fig. 6). The clasts are commonly decomposed and have variable but local lithologies. Within this unit a fine-grained magnetically reversed silty clay is also present (Fig. 8a). Lower contact is gradational and lateral extent is unknown.	Cenozoic Weathering (A)
1	Long Lake Suite	Buff coloured, variably weathered (highly fractured - completely decomposed), granitoid with some sulphide mineralization.	

Clast orientations were measured to reconstruct paleo-flow directions (Fig. 5). In diamictons only clasts with a greater than 2:1 length (A): width (B) were measured and utilized for trend analysis. Trend and plunge measurements were plotted using a Stereonet Program (version 9.3.3 by Dr. Allmendinger; website www.geo.cornell.edu/geology/faculty/RWA/programs.html). This technique is used to determine the direction of ice flow and the style of deposition (*cf*., Hicock *et al*., 1996). The A:B plane orientation was also measured in stratified gravel, to determine the approximate flow direction during deposition.

Paleomagnetic dating is very useful for late Pliocene-early Pleistocene glaciation (Duk-Rodkin *et al*., 1996), and several paleomagnetic samples collected from fine-grained units were analyzed by Dr. N. Roberts at the University of Lethbridge. The Earth's magnetic field can align magnetic minerals in sediment and rocks, recording polarity changes (Walker, 2005). Recognition of polarity changes can be used to assign ages to the sediment analyzed (Walker, 2005). Analysis first determined the bulk magnetic susceptibility, with a Sapphire Instruments Model SI-2B magnetic susceptibility and anisotropy meter. The natural remnant magnetism (NRM) was determined using an AGICO JR-6A spinner magnetometer and samples were incrementally demagnetized to determine their detrital remnant magnetism (DRM) acquired during deposition. Too few paleomagnetic samples were collected for a detailed determination of sediment age; however, analysis reveals the original polarity present during deposition which may indicate approximate ages.

Organic samples were collected for paleoenvironmental reconstructions and radiocarbon dating. Samples were sent to Alice Telka at Paleotec services for analysis. Organic material thought to be within the range of radiocarbon ages were dated while other samples were analyzed for macrofossil identification in an attempt to understand the environment at the time of deposition. Results from this analysis will be presented in a later publication.

Chemical characterization of gold grains is being completed from strategic placer-bearing facies in Back Creek. Sediment was sieved and panned to separate the heavy minerals and gold grains. The gold grains will be submitted for later laboratory analysis. At this time only the presence of placer gold grains in a unit are noted (Fig. 5).

RESULTS

Large exposures (>22 m) at Back Creek (Fig. 4) reveal a complex Quaternary history. During the 2015 field season twelve sections were analyzed at Back Creek, and these data were synthesized into an idealized stratigraphic column (Fig. 5) containing 12 units. The following is a brief synopsis of the stratigraphy and sedimentology present at Back Creek (Table 1 and Fig. 5).

The lowermost unit in the section is a variably weathered (minor jointing to highly decomposed) granite with sporadic sulphide mineralization (Unit 1). Based on previous mapping, Unit 1 is interpreted to be part of the Long Lake suite (Fig. 2) and is a potential source for gold mineralization in the drainage (Fig. 5 and Table 1).

Unit 2 is a matrix/clast-supported, poorly-consolidated gravel (Fig. 6). Unit 2 is less than 1 m thick with a gradational lower contact with Unit 1. This unit is locally exposed and lateral extent is unknown. The matrix is silty sand with variable iron staining and the colour is yellowish brown (10YR 5/6). There are ~50% clasts that are dominantly rounded to subrounded. The clasts are commonly decomposed and have variable, but local lithologies. The unit is crudely stratified in some exposures and a fine-grained clayey silt layer ~15 cm thick was sampled for paleomagnetic dating. Unit 2 contains placer gold, but due to the limited volume exposed it was not the main target for placer development.

Unit 3 is an over-consolidated, matrix-supported diamicton (Fig. 7). The lower contact is sharp and erosive with Units 1 or 2. Unit 3 is 5 to 10 m thick and laterally extensive across the valley bottom of Back Creek. The unit is thickest towards the valley margins and thinnest towards the valley center. The matrix is clayey-silt with minor sand, and yellowish brown (10YR 5/4) at the base and brown (7.5YR 5/4) at the top (7.5YR 5/4; brown). It contains 20-25% subrounded clasts that range from pebbles to boulders and many are striated or decomposed. Diverse clast lithologies are present in this diamict, including some not found within the Back Creek basin (sedimentary). Clast orientation changes upsection from parallel to orthogonal to the valley (Fig. 5). Based on the consolidation, extent, striated clasts, erosional lower contact, diverse clasts lithologies and fabric orientation, Unit 3 is interpreted as a regionally extensive glacial diamict. Since this represents the oldest known glaciation in the Mount Nansen area it is assigned to the Nansen glaciation.

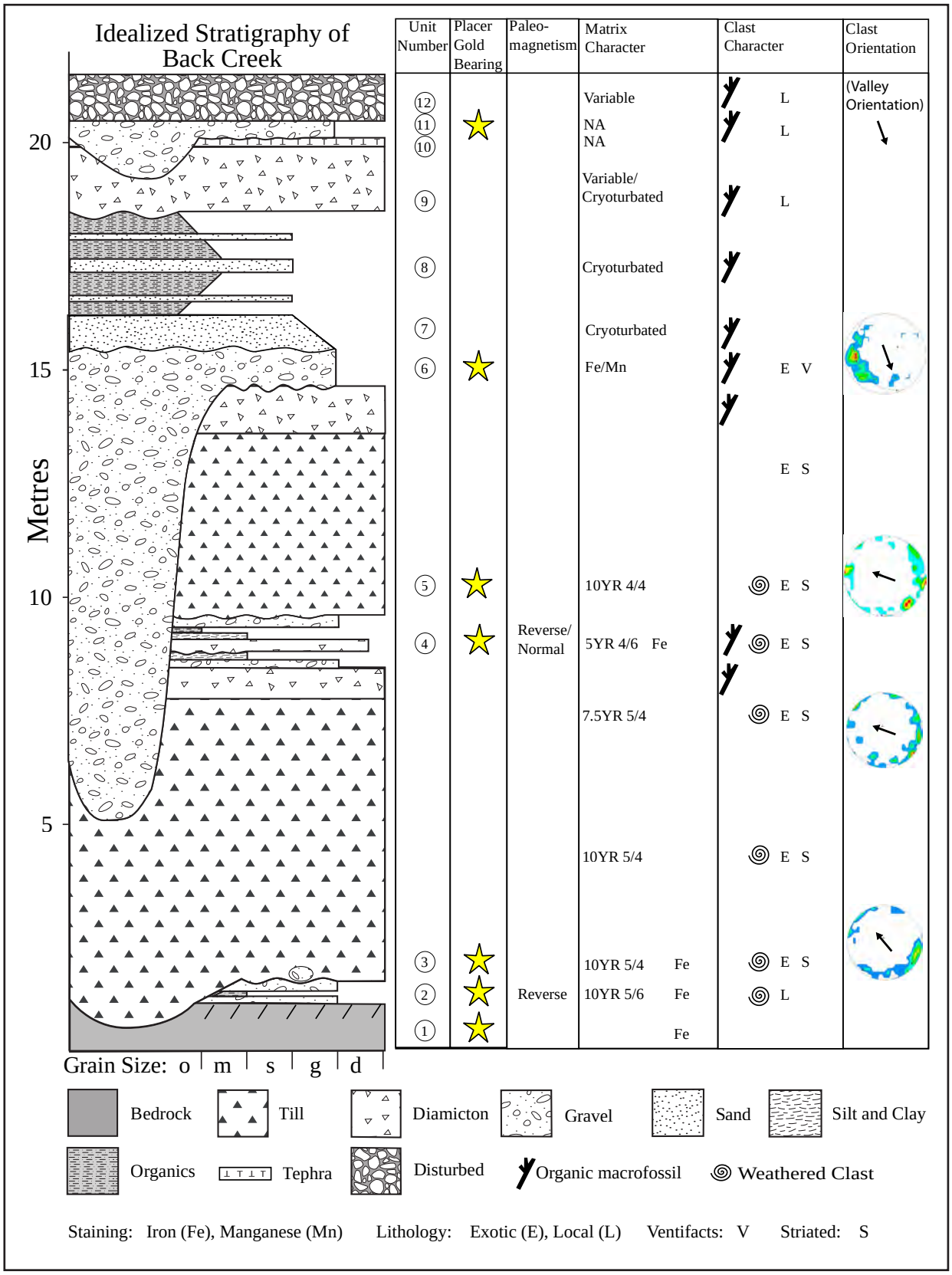


Figure 5. *Idealized stratigraphy of Back Creek. Each unit is numbered (1-12) and is further described in the results.*

Unit 4 is less than 2 m thick, laterally extensive and has a sharp, erosional lower contact. The materials and stratigraphic relationships of the sediment in Unit 4 are variable and include diamict, gravel, silt/clay and organic material (Fig. 8b,c). One sediment type is an over-consolidated, matrix-supported diamict with an erosional lower contact. The diamict has a clayey silt matrix, with 20-30% pebble-boulder sized, and subrounded to subangular clasts (Fig. 8c). Two clast-supported gravel beds are variably present in Unit 4 (Fig. 8b,c). The gravel has a silty sand matrix that is variably iron and manganese-stained. Clasts are greater than 55% pebble-cobble sized and subrounded to subangular. Furthermore, some of the clasts in the gravel are decomposed. Bedded silt/clay sediment is variably present in Unit 4 (Fig. 8b,c). Two sets of paleomagnetic samples were collected from this Unit 4 and normal (N) and reversely (R) magnetized sediment is present. Due to the small number of paleomagnetic samples collected and stratigraphic complexity it is unknown whether sediment records an N-R or an R-N-R sequence. There is an organic rich layer interstratified with silty clay. This layer was sampled for macrofossil analysis. Based on the presence of several sediment types, weathering representing potential paleosol processes and organics, Unit 4 is interpreted as inter-glacial sediment.



***Figure 6**. Pre-glacial gravel (Unit 2) exposed in lower Back Creek. Gravel is pervasively weathered and iron-stained. Clasts are variable in lithology but local in source.*

Unit 5 is an over-consolidated, matrix supported diamict. The lower contact is sharp and erosional. It is 3 to 6 m thick, and laterally extensive. The matrix is a clayey-silt with minor sand. It contains 15-20% subrounded clasts that range from pebbles to boulders, and have diverse lithologies. Striated and decomposed clasts are abundant, and several exotic lithologies are present. The clast fabric measured in this unit indicates ice flow orthogonal to the valley (Fig. 5). Based on the exotic lithologies, extent and striated clasts, Unit 5 is interpreted as a regionally extensive till. Since this represents the second oldest known glaciation in the Mount Nansen area, and it is beyond the Reid limit, it is assigned to the Klaza Glaciation.

Unit 6 is a poorly-consolidated, clast-supported gravel. The bottom contact is sharp and erosive, and this unit incises the pre-existing stratigraphy to Nansen till (Unit 3). Unit 6 is approximately 20 m wide and is presumed to



***Figure 7.** Nansen Till (Unit 3), containing striated and weathered clasts. Clasts can be quite large and several exotic clast lithologies are present indicative of regional glaciation.*



Figure 8. *Paleomagnetic sample locations. (a) Paleomagnetic samples of the pre-glacial gravel (Unit 2). Pervasive iron staining is visible in this photo. (b) Paleomagnetic samples of the interglacial sediment (Unit 4) right below an organic rich horizon. (c) Several inter-glacial sediments (Unit 4) and paleomagnetic sample locations are shown.*

extend down valley for some distance. The matrix is predominately sand with minor silt, and it is variably iron and manganese stained. It contains 60 to 70% subrounded to subangular clasts that range in size from boulder to pebble. Fabric measurements in Unit 6 indicate paleo-flow direction is approximately parallel to the modern creek valley (Fig. 5). This unit is the target of current placer mining and the gold character will be analyzed and presented in a later publication.

Unit 7 is a poorly-consolidated, with sub-horizontal bedded silty sand with minor organics. It is ~1 m thick and has a sharp erosive contact. This unit is not laterally extensive. Based on the sub-horizontal bedding, organics and sharp erosive lower contact Unit 7 is interpreted to be fluvial sand.

Unit 8 is matrix-supported, poorly-consolidated clay to fine sand colluviated organics. This unit is 2 to 3 m thick and laterally extensive. The unit has interstratified sand and it contains well-preserved macrofossils. Unit 8 contains several cryoturbation features (cryoturbated sediment and ice wedges) and the unit is predominately frozen. Based on the presence of organics and the interstratification of silt/clay, and sand Unit 8 is interpreted as a valley bottom floodplain deposit.

Unit 9 is a variably thick (1-4 m), matrix/clast-supported, moderately-consolidated diamicton. Unit 9 has an erosive lower contact and is laterally extensive. This unit contains organics and it has crude stratification. Based on these features it is interpreted to be a colluvium.

Unit 10 is a variably thick (5-50 cm), pale grey, silty sand, composed of tephra. This unit has a sharp non-erosive lower contact and it is laterally extensive. Based on the sediment location and previous work in the Mount Nansen area (LeBarge, 1995), Unit 10 is interpreted as the White River Tephra (WRT).

Unit 11 is a clast-supported, poorly-consolidated gravel. The gravel has a sharp erosive lower contact, and it is variably thick (0.5-2 m). The unit has a silty sand matrix with ~70% clasts. Clasts are cobble to pebble sized, and subrounded. The unit forms the base of the modern stream and this unit contains a minor amount of placer gold; however, it is not the current target of exploration. Based on these features, Unit 11 is interpreted as the modern/recent fluvial gravel.

Unit 12 includes all material that has been disturbed during mining. This includes a variety of sediment types such as diamictons or bedded silt and sand, depending on how the material was affected. Furthermore the thickness and lateral variability of this unit is highly variable.

LANDSCAPE EVOLUTION

By synthesizing the stratigraphy of Back Creek a seven phase landscape evolution model was created (Table 1 and Fig. 10). The following interpretations relate to the model, and explain the concentration mechanisms, preservation potential, and timing of placer gold development in relation to the landscape evolution of Back Creek.

CENOZOIC WEATHERING

The first phase of development was dominated by deep weathering and fluvial concentration of placer gold (Fig. 10a). The bedrock exposed at Back Creek is highly oxidized suggesting pervasive weathering occurred over a significant time period. The pre-glacial development of placer gold is theoretically the period of greatest gold accumulation in Back Creek due to long periods of weathering and tectonic stability. The presence of highly weathered bedrock (>2 m thick) suggests that it was sub-aerially exposed for a significant amount of time. Weathering is so intense that many of the feldspar grains have become pervasively stained and decomposed in the bedrock. Pre-glacial gold concentration developed as mineralized bedrock present at the surface, weathered, and incorporated in fluvial deposits of paleo-Back Creek.

The mineralized bedrock that supplied gold in Back Creek may be from several mineral occurrences (*eg.,* Willow Creek, Orloff-King and Dickson; *see* Fig. 2), and further analysis is required to determine its origin. Weathered bedrock is commonly in contact with, and incorporated into the Nansen till (Unit 3). Unit 2 (pre-glacial gravel) is only exposed in the deepest part of the valley and has a very limited lateral extent, likely related to variable paleo-bedrock topography. The valley bottom may have once had more extensive pre-glacial fluvial deposits; however, erosion during the first glaciation effectively removed most of these deposits.

NANSEN GLACIATION

The second phase of landscape evolution is during the Nansen glaciation (Fig. 10b,c). Reversely magnetized sediment sampled from overlying Unit 4 indicate the Nansen till is >780 ka, and normally magnetized sediment is interpreted to have formed during the Jaramillo (0.90-1.06 Ma) or Olduvai (1.78-2.00 Ma) subchron (Fig. 9). There are two phases during the Nansen glaciation, the advance phase (Fig 10b) and the maximum phase (Fig. 10c); these phases are based on changes in till characteristics and ice flow reconstruction from till fabric data. During the advance phase, ice flowed up-valley and likely produced a glacial lake (Fig. 10b). The ice was significantly erosive to incorporate highly weathered bedrock and pre-glacial gravel. The incorporation of oxidized bedrock produced a visible colour change from the base (10YR 5/4; yellowish brown) to the top (7.5YR 5/4; brown) of the Nansen till. As glaciation continued, ice thickened and flow became orthogonal to the valley unconstrained by underlying topography (Fig. 10c). During Nansen glacial maximum it is likely that large parts of the region were covered in ice. Both advance and maximum phases were likely significantly erosive depending on the topographic position. The glacial advance was parallel with the valley and therefore eroded the valley bottom, whereas at glacial maximum, ridge tops were likely eroded and the valley bottom remained protected.

INTER-GLACIATION

The next phase of landscape evolution occurred during a non-glacial or inter-glacial period (Fig. 10d). Unit 4 contains organic material, and a zone of weathering resembles a paleosol. These attributes suggest a period of stability following the Nansen glaciation. Two sets of paleomagnetic samples were collected from this unit

and normal and reversely magnetized sediment are present. The reversely magnetized sediment suggests a minimum age of deposition >780 ka, forming when the Earth's magnetic field last had a reversed polarity. Due to the number of samples collected and the complex stratigraphic relationships between samples, the exact age of the sediment remains unresolved (Fig. 9). It is likely however, that the paleomagnetic results record the Jaramillo or Olduvai subchron (Fig 9), due to suggested age (>1 Ma) of the overlying sediment from the Klaza glaciation (Jackson, 2000). The gravel from the inter-glacial unit has pervasive staining and several weathered clasts that represent fluvial activity over a significant period of time. This inter-glacial gravel may be another target for placer exploration, although its volume is limited particularly near the valley sides where it is exposed. It is possible this gravel sub-unit is larger towards the valley center; however, it was only seen in the left limit.

KLAZA GLACIATION

The Klaza glaciation (Fig. 10e) produced till with similar sedimentological characteristics to the Nansen till; however, clast orientations have a larger range in value that may be related to post-glacial disturbance or to the primary depositional environment. This unit is laterally extensive on the side of the valley, but placer excavation in the center of the valley effectively removed most of this unit. The preserved paleosol (Unit 4) below the Klaza till suggests that ice was largely non-erosive, which is encouraging for preserving inter-glacial placer gold deposits. The Klaza till is likely the 'false bedrock' that is pervasive throughout the Mount Nansen area and is known to have placer gold concentrated on it or in it.

PAY GRAVEL DEVELOPMENT

The next phase of landscape evolution (Fig. 10f) is the formation of post-glacial fluvial gravel. Fluvial incision following the Klaza glaciation eroded into the Nansen till, and potentially into the pre-glacial gravel. Currently, this gravel is the main placer gold target at Back Creek. Placer gold has four potential sources in the area i) bedrock; ii) till enriched with placer gold; iii) inter-glacial fluvial gravel; or iv) pre-glacial gravel. Additional studies into gold character may highlight the amount of reworked gold that is contributing to the placer deposit.

COVER DEVELOPMENT

The final phase of landscape evolution is the formation of cover (Fig. 10g). Hillslope colluviation, periglacial weathering and eolian processes were all dominant after glaciation. These processes produced thick cover (>5 m)

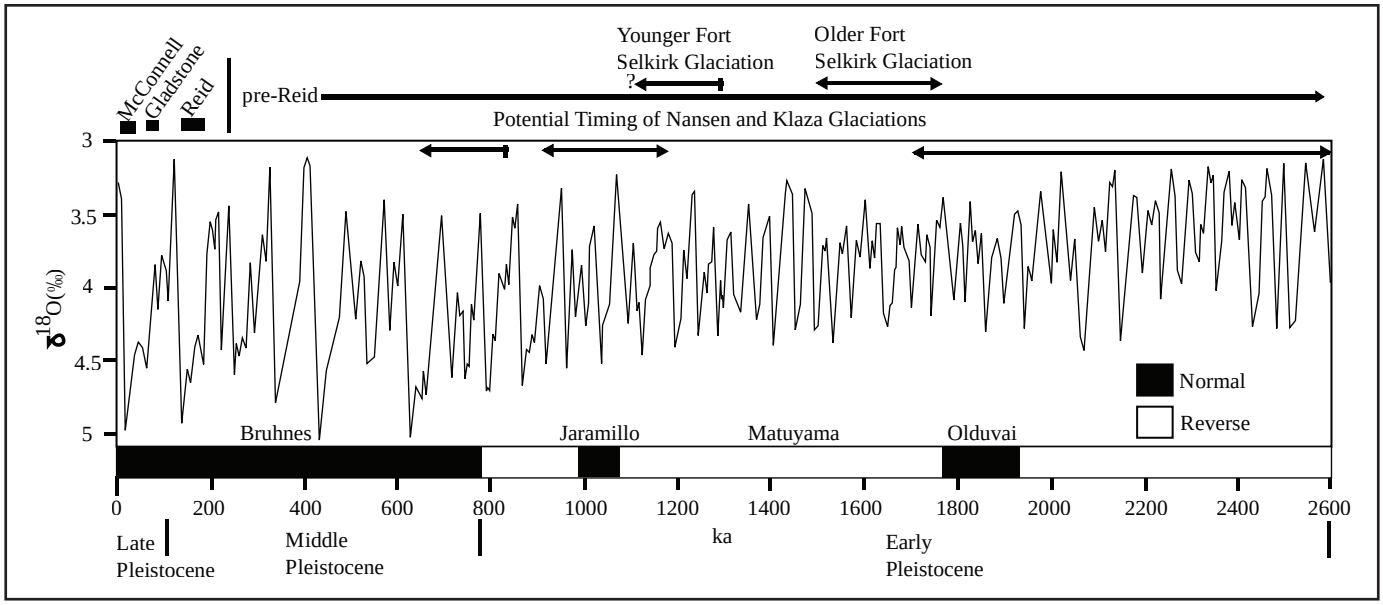


Figure 9. *Paleomagnetic timescale and the oxygen isotope ($\delta^{18}O$) curve modified from Lisieki and Raymo, 2005. The ($\delta^{18}O$) curve fluctuations indicate climate changes, where troughs denote glacial stages and the peaks are non-glacial. The timing of local glaciation is summarized for reference (after Nelson et al., 2009; Bond and Lipovsky, 2010), and the potential timing of the glaciation of Nansen and Klaza are highlighted*

with a variety of characteristics. The cover sediment is generally depositional in nature and therefore has not removed the underlying units. The presence of marker horizons such as the White River tephra (Unit 10) deposited ~1200 years ago (*cf.*, Clague *et al.,* 1995), indicate sediment has remained undisturbed since deposition. Most cover sediment contains little placer gold (Unit 11) and is not a placer mining target.

PLACER POTENTIAL

Two distinct tills are present at Back Creek and based on their extent, striated clasts, diverse clasts lithologies, and an intercalated paleosol, they are interpreted to represent Nansen and Klaza glaciation. This assignment is consistent with earlier glacial stratigraphy work in the region (Bostock, 1966; LeBarge, 1995). Nansen and Klaza glaciation has significantly impacted placer gold deposits in Back Creek. To understand the evolution of placer gold deposits at Back Creek, concentration mechanisms, preservation potential and a timing of placer gold deposits were synthesized into a model (Fig. 10) which highlighted three main placer gold targets (pre-glacial, inter-glacial, and post-glacial fluvial sediment). The influences of the Nansen and Klaza glaciation on these deposits are examined below.

PRE-GLACIAL DEPOSITS

Pre-glacial placer deposits should contain the highest gold concentrations because these deposits formed over a sustained period during the Paleogene and Neogene when climate was warmer, resulting in significant weathering of mineralized bedrock and fluvial concentration of gold (Ager *et al*., 1994; Anderson and Stroshein, 1997; Dampier *et al*., 2011; Foscolos *et al.,* 1977; Jackson, 2000; LeBarge, 1995). Channel avulsion may have resulted in laterally extensive pre-glacial placer deposits across Back Creek valley. Significant erosion likely occurred during the Nansen glaciation because Nansen till is in direct contact with bedrock near the valley side and incorporates weathered bedrock. Therefore, extensive removal of pre-glacial placer deposits likely occurred during this glaciation. Variable bedrock topography would decrease the efficiency of glacial erosion and this may preserve placer gold deposits. In Back Creek, gold-bearing pre-glacial placer deposits are most likely preserved in valleys oriented at a high angle to ice flow and where local bedrock topographic features like paleo-canyons or bedrock highs provide protection from glacial erosion. For exploration, preserved pre-glacial placer gold deposits could be anticipated by identifying areas of undulatory bedrock (canyons or ledges) using geophysics. Highlighting these areas might increase the chance of successfully drilling into a pre-glacial gravel. The discontinuous nature of these pre-glacial placer deposits in valleys aligned with regional ice flow makes them a challenging exploration target.

INTER-GLACIAL DEPOSITS

Inter-glacial gold deposits are another target for placer gold exploration. In these deposits gold must be sourced from either mineralized bedrock or from the Nansen till. LeBarge (1995), found that till may contain large quantities of gold grains, so the Nansen till could be a significant source of placer gold. In addition the Nansen till provides a false-bedrock for placer gold deposits to accumulate on. The Klaza glaciation did not result in significant erosion of these inter-glacial placer gold deposits. The deposits may be extensive and represent a favorable exploration target due to their shallow depth relative to pre-glacial deposits. Drilling and geophysical surveys could be employed to identify these inter-glacial targets within the Mount Nansen area.

POST-GLACIAL DEPOSITS

Post-glacial placer gold deposits have historically been the primary exploration targets in the Mount Nansen area, and they are most continuous deposits present in Back Creek. Gold in the post-glacial deposits may be sourced from (i) bedrock; (ii) till enriched with placer gold; (iii) inter-glacial fluvial gravel; or (iv) pre-glacial gravel. The gold abundance in post-glacial deposits may reflect various sources. Significant increase in gold abundance likely reflects intersection of underlying placer gold deposits, and should warrant detailed study to determine if intersected deposit is an extensive target. Sand, organics, colluvium, tephra, gravel, and anthropogenic deposits cover the post-glacial placer gold deposits. The thickness of this overlying material dictates the economic viability of mining post-glacial placer deposits.

DISCUSSION

This research shows that the early Pleistocene Nansen and Klaza glaciation had a significant impact on placer gold concentration in Back Creek. Three placer gold targets exist in the Back Creek area including the pre, inter and post-glacial deposits. Although historical exploration

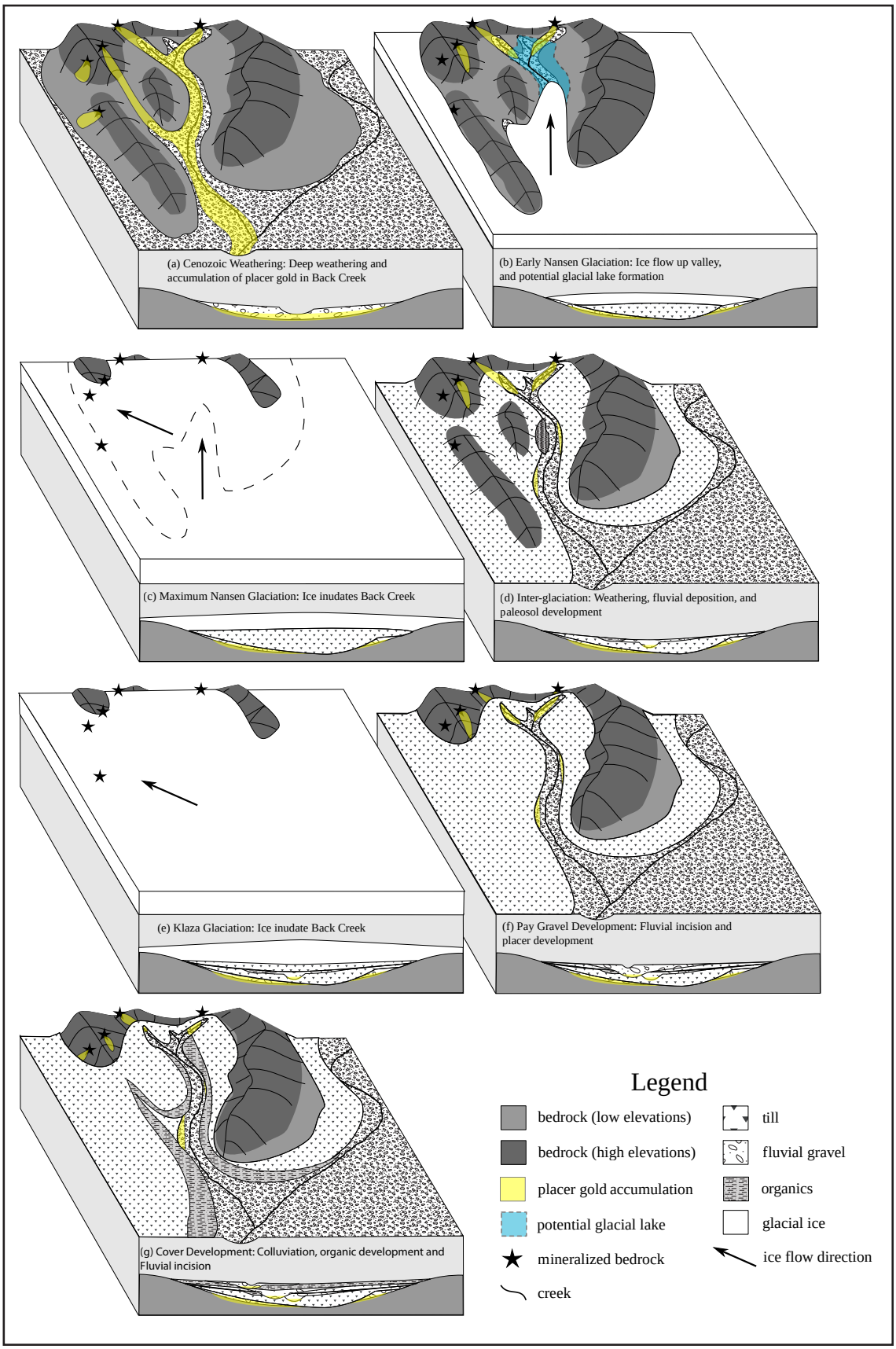


Figure 10.
The landscape evolution of Back Creek is described in these 7 block diagrams. This model illustrates both the spatial and stratigraphic distribution of placer gold from pre-glacial to modern time.

has focused on the post-glacial deposits, it is likely that lucrative pre-glacial and inter-glacial deposits exist at depth where glacial erosion was minimal. The landscape evolution model presented here is for Back Creek (Fig. 10); however, could be applied to other placer gold exploration targets in the Mount Nansen district and in early Pleistocene glaciated fringe of Yukon (Fig. 1).

CONCLUSION

Early Pleistocene glaciation had a significant effect on placer gold deposits in Back Creek. Two phases of glaciation are present and were separated by a period of weathering and pedogenesis. These two glacial events likely represent the Nansen and Klaza and are interpreted to have occurred before the Jaramillo or Olduvai subchron based on paleomagnetic results. The Nansen glaciation destroyed much of the earliest placer gold deposits leaving little evidence of pre-glacial gravels, only where bedrock topography permitted preservation. The Nansen glaciation was pervasive in the landscape and till fabrics recorded ice thickening and changing directions. Between periods of glaciation, a long period of pedogenesis occurred and inter-glacial placer gold deposits formed. The Klaza glaciation did not result in significant erosion of these inter-glacial placer gold deposits, and they may represent an important target for placer exploration. Post-glacial fluvial gravels are the main target for placer gold mining in Back Creek and variable gold abundance is likely related to incision of previous concentrations of placer gold. The thickness of sediment covering the post, inter or pre-glacial placer gold deposits has a significant impact on the economics of the deposit and should be considered during exploration. In conclusion, analysis at Back Creek reveals the potential for deeply buried placer gold deposits in other glaciated regions of Yukon.

ACKNOWLEDGEMENTS

First, I would like to thank the Canadian Northern Economic Development Agency for graciously providing the funding for this project. I would like to thank Ross Agnosti for access to the section and insightful information. I appreciate the Yukon Geological Survey for providing funding, training and guidance. I would also like to thank the Geological Survey of Canada, specifically Jim Ryan, for logistical support and guidance. I would also like to thank Nick Roberts for processing the paleomagnetic samples, and providing insight into Early Pleistocene glaciation. Furthermore, this research would not be possible without the countless hours of help from Mark Coleman and Kyle Orr. Further thanks go to Alice Telka for analysis of the macrofossil analysis and radio carbon dating. Finally, I want to thank my esteemed colleges Anna Haiblen and Gioachino Roberti who helped review my work and provided feedback on several ideas.

REFERENCES

Ager, T.A., Matthews, J.V. and Yeend, W., 1999. Pliocene terrace gravels of the ancestral Yukon River near Circle, Alaska: Palynology, paleobotany, paleoenvironmental reconstruction and regional correlation. Quaternary International, vol. 22/23, p. 185-206.

Anderson, F. and Stroshein, R., 1997. Geology of the gold-silver vein system, Mount Nansen area, Yukon. *In*: Yukon Exploration and Geology 1997, C.F. Roots and D.S. Emond (eds.), Exploration and Geological Services Division, Yukon Region, Indian and Northern Affairs Canada, p. 129-143.

Barendregt, R.W., Enkin, R.J., Duk-Rodkin, A. and Baker, J., 2010. Paleomagnetic evidence for multiple late Cenozoic glaciations in the Tintina Trench, west-central Yukon, Canada. Canadian Journal of Earth Science, vol. 47, p. 987-1002.

Bond, J.D., Lipovsky, P.S., and Gaza, P., 2007. Surficial geology investigations in Wellesley basin and Nisling Range, southwestern Yukon. In: Yukon Exploration and Geology 2007, D.S. Emond, L.L. Lewis and G.D. Bradshaw (eds.), Yukon Geological Survey, p. 125-138.

Bostock, H.S., 1936. Carmacks District, Yukon. Geological Survey of Canada, Memoir 189.

Bostock, H.S., 1966. Notes on glaciation in central Yukon Territory. Geological Survey of Canada, Paper 65-36, p. 18.

Burn, C.R., 1994. Permafrost, tectonics, and past and future regional climate change, Yukon and adjacent Northwest Territories. Canadian Journal of Earth Science, vol. 33, p. 182-191.

Cairnes, D.D., 1915. Summary Report 1914, Part A. Geological Survey of Canada, Memoir 284, p. 25-30.

Clague, J.J., Evans, S.G., Rampton, V.N. and Woodsworth, G.J., 1995. Improved age estimates for the White River and Bridge River tephras, western Canada. Canadian Journal of Earth Science, vol. 32, p. 1172-1179.

Colpron, M., Nelson, J.L. and Murphy, D.C., 2007. Northern Cordilleran terranes and their interactions through time. GSA Today, vol. 17, p. 4-10.

Coney, P.J., Jones, D.L. and Monger, J.W.H., 1980. Cordilleran suspect terranes. Nature, vol. 288, p. 329-333.

Dawson, G.M., 1889. Report on an exploration in the Yukon District, N.W.T. and adjacent northern portion of British Columbia, 1887. Geological Survey of Canada, Annual Report, 1887-88.

Dampier, L., Sanborn, P., Smith, S., Bond, J. and Clague, J.J., 2011. Genesis of upland soils, Lewes Plateau, central Yukon. Part 2: Soils formed in weathered granitic bedrock. Canadian Journal of Soil Science, vol. 91, p. 579-594.

Demuro, M., Froese, D.G., Arnold, L.J. and Roberts, R.G., 2012. Single-grain OSL dating of glaciofluvial quartz constrains Reid glaciation in NW Canada to MIS 6. Quaternary Research, vol. 77, p. 305-316.

Duk-Rodkin, A., 1999. Glacial limits map of Yukon Territory. Geological Survey of Canada, Open File 3694, Indian and Northern Affairs Canada Geoscience Map 1999-2, scale 1:1 000 000.

Duk-Rodkin, A., Barendregt, R.W., Froese, D.G., Weber, F., Enkin, R., Smith, I.R., Zazula, G.D., Waters, P. and Klassen, R., 2004. Timing and extent of Plio-Pleistocene glaciations in north-western Canada and east-central Alaska. Quaternary Glaciations-Extent and Chronology, Part II, p. 313-342.

Duk-Rodkin, A., Barendregt, R.W., Tarnocai, C., and Phillips, F.M., 1996. Late Tertiary to late Quaternary record in the Mackenzie Mountains, Northwest Territories, Canada: stratigraphy, paleosols, paleomagnetism, and chlorine-36. Canadian Journal of Earth Science, vol. 33, p. 875-895.

Duk-Rodkin, A., Barendregt, R.W., White, J.M. and Singhroy, V.H., 2001. Geologic evolution of the Yukon River: implications for placer gold. Quaternary International, vol. 82, p. 5-31.

Els, G. and Eriksson, P., 2005. Placer formation and placer minerals. Ore Geology Review, vol. 28, p. 373-375.

Foscolos, A.E., Rutter, N.W. and Hughes, O.L., 1977. The use of pedological studies in interpreting the Quaternary history of central Yukon Territory, Geological Survey of Canada, Bulletin 271.

Geurts, M. and Dewez, V., 1993. Le lac glaciaire Nisling et le Pleistocene dans le basin superieur de la Nisling River, au Yukon. Geographie physique et Quaternaire, vol. 47, no. 1, p. 81-92.

Guthrie, R.D., 2001. Origin and causes of the mammoth steppe: a story of cloud cover, wolly mammal tooth pits, buckles and inside-out Beringia. Quaternary Science Reviews, vol. 20, p. 549-574.

Goldfarb, Y.I., Petrov, A.N., Preis, V.K. and Skurida, D.A., 2015. Geological prerequisites for differentiated approach to prospecting and exploration of alluvial gold placers: an example from the northeast of Russia. Russian Journal of Pacific Geology, vol. 9, p. 166-177.

Harris, S.A., 2005. Thermal history of the Arctic Ocean environs adjacent to North America during the last 3.5 Ma and a possible mechanism for the cause of the cold events (major glaciations and permafrost events). Progress in Physical Geography, vol. 29, p. 218-237.

Hart, C.J.R. and Langdon, M., 1998. Geology and mineral deposits of the Mount Nansen camp, Yukon. *In:* Yukon Geology and Exploration 1997, Exploration and Geological Services Division, Yukon Region, Indian and Northern Affairs Canada, p. 129-138.

Haug, G.H., Ganopolski, A., Sigman, D.M., Rosell-Mele, A., Swann, G.E.A., Tiedemann, R., Jaccard, S.L., Bollmann, J., Maslin, M.A., Leng, M.J. and Eglinton, G., 2005. North Pacific seasonality and the glaciation of North America 2.7 million years ago. Nature, vol. 433, p. 821-825.

Herail, G., Fornari, M., Viscarra, G., Laubacher, G., Argollo, J. and Miranda, V., 1989. Geodynamic and Gold Distribution in the Tipuani-Mapiri Basin (Bolivia). International Symposium on Intermontane Basins: Geology and Resources, p. 342-352.

Hidy, A.J., Gosse, J.C., Froese, D.G., Bond, J.D. and Rood, D.H., 2013. A latest Pliocene age for the earliest and most extensive Cordilleran Ice Sheet in northwestern Canada. Quaternary Science Reviews, vol. 61, p. 77-84.

Hicock, S.R., Goff, J.R., Lian, O.B. and Little, E.C., 1996. On the Interpretation of Subglacial Till Fabric. Journal of Sedimentary Research, vol. 66, p. 928-934.

Hughes, O.L., Campbell, R.B., Muller, J.E. and Wheeler, J.O., 1969. Glacial limits and flow patterns, Yukon Territory, South of 65 Degrees North Latitude. Geological Survey of Canada, Paper 68-34, p. 1-9.

Jackson, L.E. Jr., 1993. Origin and stratigraphy of Pleistocene gravels in Dawson Range and suggestions for future exploration of gold placers, southwestern Carmacks map area, Yukon Territory. Current Research, part A; Geological Survey of Canada, paper 93-1A, p. 1-10.

Jackson, L.E. Jr., 2000. Quaternary geology of the Carmacks map area, Yukon Territory. Geological Survey of Canada, Bulletin 539, p. 1-74.

Jackson, L.E. Jr. and Clague, J.J., 1991. The Cordilleran Ice Sheet: one hundred and fifty years of exploration and discovery. Geographie physique et Quaternaire, vol. 45, p. 269-280.

Jackson, L.E. Jr., Tarnocai, C. and Mott, R, J., 1999. A middle Pleistocene paleosols sequence from Dawson Range, Central Yukon Territory. Geographie physique et Quaternaire, vol. 53, p. 313-322.

Johnston, S.T., Mortenson, J.K. and Erdmer, P., 1996. Igneous and metaigneous age constraints for the Aishihik metamorphic suite, southwest Yukon. Canadian Journal of Earth Sciences, vol. 33, p. 1543-1555.

Knight, J.B., Morison, S.R. and Mortensen, J.K., 1999. The relationship between placer gold particle shape, rimming, and distance of fluvial transport as exemplified by gold from the Klondike district, Yukon Territory, Canada. Economic Geology, vol. 94, p. 635-648.

Knight E., Schneider, D.A. and Ryan, J., 2013. Thermochronology of the Yukon-Tanana Terrane, west-central Yukon: Evidence for Jurassic extension and exhumation in the northern Canadian Cordillera. The Journal of Geology, vol. 121, p. 371-400.

LeBarge, W.P., 1995. Sedimentology of Placer Gravels near Mt. Nansen, Central Yukon Territory, Bulletin 4, Exploration and Geological Services Division, Indian and Northern Affairs Canada, Yukon Region, p. 155.

Levson, V.M. and Blyth, H., 2001. Formation and preservation of a Tertiary to Pleistocene fluvial gold placer in northwest British Columbia. Quaternary International, vol. 82, p. 33-50.

Lisiecki, L.E. and Raymo, M.E., 2005. A Pliocene-Pleistocene stack of 57 globally distributed benthic $\delta 18O$ records. Paleoceanography, vol. 20, PA 1003.

Loen, J.S., 1994. Origin of placer gold nuggets and history of formation of glacial gold placers, Gold Creek, Granite County, Montana. Economic Geology, vol. 89, p. 91-104.

Lowey, G.W., 2006. The origin and evolution of the Klondike goldfields, Yukon, Canada. Ore Geology Reviews, vol. 28, p. 431-450.

Monger, J.W.H., Souther, J.G. and Gabrielse, H., 1972. Evolution of the Canadian Cordillera: a plate-tectonic model. American Journal of Science, vol. 272, p. 577–602.

Mortensen, J.K., Appel, V.L. and Hart, C.J.R., 2002. Geological and U-Pb age constraints on base and precious metal vein systems in the Mount Nansen area, eastern Dawson Range, Yukon. *In:* Yukon Exploration and Geology 2002, D.S. Emond and L.L. Lewis (eds.), Exploration and Geological Services Division, Yukon Region, Indian and Northern Affairs Canada, p. 165-174.

Naeser, N.D., Westgate, J.A., Hughes, O.L. and Pewe, T.L., 1982. Fisson-track ages of late Cenozoic distal tephra beds in the Yukon Territory and Alaska. Canadian Journal of Earth Sciences, vol. 19, p. 2167-2178.

Nelson, F.E., Barendregt, R.W. and Villeneuve, M., 2009. Stratigraphy of the Fort Selkirk Volcanogenic Complex in central Yukon and its paleoclimatic significance: Ar/Ar and paleomagnetic data. Canadian Journal of Earth Science, vol. 46, p. 381-401.

Saager, R. and Bianconi, F., 1971. The Mount Nansen gold-silver deposit, Yukon Territory, Canada. Mineralium Deposita, vol. 6, p. 209-224.

Selby, D., Creaser, R.A. and Nesbitt, B.E., 1999. Major and trace element compositions and Sr-Nd-Pb systematics of crystalline rocks from the Dawson Range, Yukon, Canada. Canadian Journal of Earth Science, vol. 36, p. 1463-1481.

Tempelman-Kluit, D.J., 1984. Geology of the Laberge (105E) and Carmacks (115I) map areas. Geological Survey of Canada, Open File 1101, maps with legends, 1:250 000 scale.

Ward, B.C., Bond, J.D., Froese, D. and Jensen, B., 2008. Old Crow tephra (140±10 ka) constrains penultimate Reid glaciation in central Yukon Territory. Quaternary Science Reviews, vol. 27, p. 1909-1915.

Walker, M., 2005. Quaternary Dating Methods. John Wiley and Sons Ltd. London. p. 1-286.

Ward, B.C., Bond, J.D., Froese, D., Jensen, B., (2008). Old Crow tephra (140±10 ka) constrains penultimate Reid glaciation in central Yukon Territory. Quaternary Science Reviews 27, 1909-1915.

Ward, B.C., Bond, J.D. and Gosse, J.C., 2007. Evidence for a 55-50 ka (early Wisconsin) glaciation of the Cordilleran Ice Sheet, Yukon Territory, Canada. Quaternary Research, vol. 68, p. 141-150.

Wengzynowski, W.A., Giroux, G.H., and Martin, C.J., 2015. Geology mineralization, geochemical surveys, geophysical surveys, diamond and percussion drilling, metallurgical testing and mineral resources on the Klaza property Yukon, Canada. NI43-101 technical report. <http://www.rockhavenresources.com/projects/klaza-project> [accessed November 20, 2015].

Westgate, J.A., Preece, S.J., Froese, D.G., Walter, R.C., Sandhu, A.S. and Schweger, 2000. Dating early and middle (Reid) Pleistocene glaciations in central Yukon by tephrochronology. Quaternary Research, vol. 56, p. 335-348.

New U-Pb zircon dates from the Aishihik batholith, southern Yukon

N.L. Joyce
Geological Survey of Canada, Ottawa, ON

M. Colpron[1]
Yukon Geological Survey

M.M. Allan
Mineral Deposit Research Unit, University of British Columbia

P.J. Sack
Yukon Geological Survey

J.L. Crowley
Isotope Geology Laboratory, Boise State University, Boise, ID

J.B. Chapman
Geological Survey of Canada, Vancouver, BC

Joyce, N.L., Colpron, M., Allan, M.M., Sack, P.J., Crowley, J.L and Chapman, J.B., 2016. New U-Pb zircon dates from the Aishihik batholith, southern Yukon. *In:* Yukon Exploration and Geology 2015, K.E. MacFarlane and M.G. Nordling (eds.), Yukon Geological Survey, p. 131-149, plus digital appendices.

ABSTRACT

New U-Pb zircon dates (SHRIMP and LA-ICPMS) from granitoid rocks of the Aishihik batholith indicate a range of *ca.* 190-180 Ma for the Long Lake plutonic suite, as previously indicated by less precise, multi-grain TIMS dates. None of the phases in the Aishihik batholith are as old as the Minto suite to the north, therefore limiting the potential for Minto-style Cu-Au-Ag mineralization in the batholith. However, local occurrences of apparently shallow-level intrusions suggest that parts of the Aishihik batholith may present suitable targets for more typical porphyry Cu-Au mineralization. LA-ICPMS U-Pb zircon dating of two orthogneiss samples from the western margin of the Aishihik batholith yielded Early Mississippian protolith ages akin to the Simpson Range plutonic suite (Yukon-Tanana terrane), and Jurassic overgrowths consistent with partial melting related to intrusion of the Aishihik batholith.

[1]*maurice.colpron@gov.yk.ca*

INTRODUCTION

The Aishihik batholith is one of a series of large, composite Late Triassic to Early Jurassic granitoid batholiths that intrude the Intermontane terranes in southern Yukon (Fig. 1). These plutons form the northern extension of a pair of plutonic belts related to arc magmatism of Stikinia and Quesnellia in British Columbia, where they are associated with a number of significant Cu-Au(Mo) porphyry deposits (Logan and Mihalynuk, 2014). The BC porphyry deposits are typically large tonnage, low grade and formed at shallow crustal levels. In Yukon, high-grade (but low tonnage) Cu-Au-Ag mineralization is locally hosted in latest Triassic-Early Jurassic plutons (*e.g.*, Minto, Carmacks Copper), but the style of mineralization is not typical of porphyry deposits. All indications are that the Yukon deposits either formed, or were deformed, at mid-crustal levels during emplacement of the latest Triassic-earliest Jurassic plutons (*e.g.*, Tafti, 2005; Hood, 2012). These plutons and associated mineralization were emplaced prior to, or during accretion of the Intermontane terranes to western North America and the onset of Cordilleran orogenesis (*e.g.*, Nelson *et al.*, 2013; Logan and Mihalynuk, 2014; Colpron *et al.*, 2015). To date, Minto-style mineralization has only been confirmed in a relatively restricted area northwest of Carmacks, commonly referred to as the Carmacks Copper belt, despite the fact that plutons inferred to be coeval with the Granite Mountain and Minto plutons (which host the Carmacks Copper and Minto deposits, respectively) are much more extensive in southern Yukon.

Despite the economic importance of the Late Triassic-Early Jurassic plutons, they have so far received little attention in Yukon and as a result they generally remain poorly characterized. Previous studies focused primarily on areas known to host mineralization (*e.g.*, Tafti, 2005; Hood, 2012). Regionally, the Late Triassic-Early Jurassic plutons were locally characterized as part of regional mapping programs (*e.g.*, Gordey and Stevens, 1994; Johnston *et al.*, 1996; Colpron *et al.*, 2002; Gordey and Ryan, 2005). These programs produced some U-Pb dates and geochemical data for the plutons, but no attempts were made at understanding their petrogenesis, locally or regionally.

In 2014, the Yukon Geological Survey embarked on a regional study of Late Triassic to Jurassic magmatism in Yukon in order to fill this knowledge gap. This program aims at developing a standardized, modern and high-quality geochronological, geochemical and isotopic dataset for Late Triassic to Jurassic plutons in Yukon in order to elucidate the regional petrogenesis of these magmatic belts. Specific objectives are to identify other plutons with potential to host Minto-style Cu-Au-Ag mineralization, and to evaluate the potential for Early Jurassic plutons in Yukon to host porphyry Cu-Au mineralization.

In this contribution, we report new U-Pb zircon dates from eight samples collected during regional reconnaissance of the Aishihik batholith. These results add to previously published Thermal Ionization Mass Spectrometry (TIMS) dates (Johnston *et al.*, 1996; Hart, 1997; Table 1; Fig. 2) which were obtained by analyzing multi-grain zircon fractions, and generally yielded discordant dates attributed to either inheritance or lead-loss. Most of the new analyses presented in this paper were obtained by *in-situ* spot analyses of zircon using either Sensitive High Resolution Ion Microprobe (SHRIMP) or Laser Ablation-Inductively Coupled Plasma Mass Spectrometry (LA-ICPMS), coupled with Scanning Electron Microscope (SEM) based imaging, thereby permitting better spatial resolution of the different age components.

LATE TRIASSIC - JURASSIC PLUTONIC SUITES IN YUKON

Late Triassic to Jurassic plutons in Yukon are grouped into four distinct plutonic suites: 1) the Late Triassic Stikine suite; 2) the latest Triassic to Early Jurassic Minto suite (formerly Klotassin and/or Aishihik suite; *see* discussion below); 3) the Early Jurassic Long Lake suite; and 4) the Middle Jurassic Bennett-Bryde suite (following subdivisions of Woodsworth *et al.*, 1991; Gordey and Makepeace, 2001; Colpron *et al.*, 2016). Only the Minto and Long Lake suites will be discussed in this paper, as both were previously considered to comprise the Aishihik batholith (Tempelman-Kluit, 1974; Woodsworth *et al.*, 1991; Johnston and Erdmer, 1995; Johnston *et al.*, 1996).

The Late Triassic-Early Jurassic suite of mainly granodiorite plutons, including the Minto, Granite Mountain, Tatchun, Lokken and part of the Aishihik batholith (Fig. 1), was originally thought to extend to the western Dawson Range and include the Klotassin batholith (Tempelman-Kluit, 1974, 1984, 2009; Tempelman-Kluit and Wanless, 1975). The suite was named the Klotassin suite and presumed to be of Late Triassic age (Tempelman-Kluit and Wanless, 1975; Woodsworth *et al.*, 1991). However, subsequent K-Ar and U-Pb dating of the Klotassin suite in the Dawson Range indicated a mid-Cretaceous age for the former

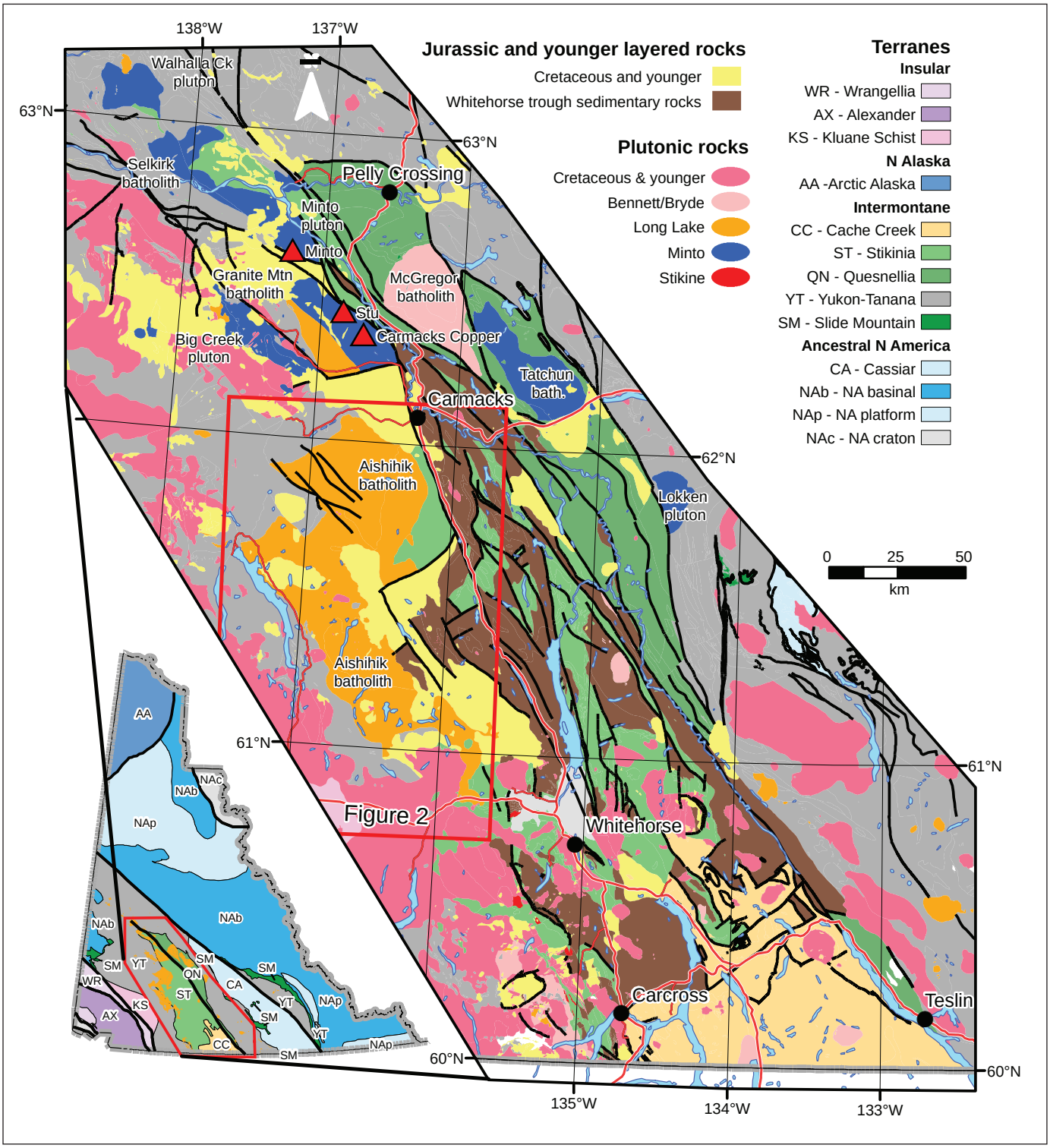


Figure 1. *Terrane map (Colpron and Nelson, 2011) and regional geology of southern Yukon (www.geology.gov.yk.ca/update_yukon_bedrock_geology_map.html). Main map coloured by terrane with Whitehorse trough and younger cover sequences shown in brown and yellow, respectively. Late Triassic to Jurassic plutonic rocks are subdivided into 4 suites as described in text. Inset Yukon terrane map to lower left shows the area of the main map; note that all Late Triassic to Jurassic plutonic rocks are shown in orange in the inset map.*

Klotassin batholith (*ca.* 100 Ma; now known as the Dawson Range batholith; Godwin, 1975; Breitsprecher and Mortensen, 2004). This led Johnston and Erdmer (1995) to abandon the name Klotassin suite and rename presumed Early Jurassic granodiorite as the Aishihik suite (*ca.* 186 Ma; Johnston *et al.*, 1996). Granodiorite of the Aishihik batholith is intruded by 'younger', more felsic quartz monzonite and granite of the Long Lake suite (pink quartz monzonite of Tempelman-Kluit, 1974; Woodsworth *et al.*, 1991; Johnston and Erdmer, 1995) that also yielded a *ca.* 186 Ma date (Johnston *et al.*, 1996).

Further studies of the Minto, Granite Mountain, Big Creek and Tatchun plutons indicated U-Pb zircon ages ranging from *ca.* 204-196 Ma (Tafti, 2005; Hood, 2012; Colpron, 2011; Breitsprecher and Mortensen, 2004), restoring a Late Triassic to Early Jurassic age range for the Aishihik suite. The suite has important economic significance because it hosts Cu-Au-Ag mineralization at the Minto and Carmacks Copper (formerly Williams Creek) deposits (Fig. 1; Tafti, 2005; Hood, 2012). We present below new U-Pb data suggesting that none of the granodiorite phases in the Aishihik batholith are as old as the Minto, Granite Mountain and Tatchun plutons (which became archetypical examples of the Aishihik suite). Hence, assignment of these older plutons to the Aishihik suite no longer seems appropriate. Instead, we propose assignment of the Late Triassic-Early Jurassic granodiorite plutons to the newly defined Minto plutonic suite (*e.g.*, Colpron *et al.*, 2016).

Table 1. *Summary of dates from Aishihik batholith.*

Sample	Date		Error (2 σ)	MSWD	Lithology	Mineral dated	Comment	Latitude	Longitude	Reference
CDB10-102	182	±	2	1.2	porphyritic granite	zircon	SHRIMP - weighted mean of 9 analyses	61.22232	-136.28342	this study
CDB10-103	181	±	2	1.4	quartz monzonite	zircon	SHRIMP - weighted mean of 7 analyses	61.36263	-136.59095	this study
CDB10-105	188	±	2	1.3	hbl-bt granodiorite	zircon	SHRIMP - weighted mean of 9 analyses	61.64177	-136.7876	this study
CDB10-106	183	±	2	1.4	porphyritic granodiorite	zircon	SHRIMP - weighted mean of 15 analyses	61.89086	-136.77289	this study
CDB10-107	187	±	2	1.4	hbl-bt tonalite	zircon	SHRIMP - weighted mean of 12 analyses	61.79203	-136.28931	this study
10-SI-223	344	±	6		granodiorite orthogneiss	zircon	LA-ICPMS - weighted mean of 15 oldest zircons	61.44778	-137.06437	this study
	193	±	5			zircon	LA-ICPMS - weighted mean of 2 youngest zircons			this study
MA14-AB9	186	±	2	1.5	quartz porphyry	zircon	LA-ICPMS - weighted mean of 19 analyses	61.88169	-136.93544	this study
MA14-AB6	345	±	4	1.5	granodiorite orthogneiss	zircon	LA-ICPMS - weighted mean of 17 cores	61.91717	-137.21234	this study
	187	±	5	0.5		zircon	LA-ICPMS - weighted mean of 2 rims			this study
Previously published dates										
92CH-75-8	183	±	2		quartz monzonite	zircon	TIMS - 3 pt regression, lower intercept	60.93667	-135.80829	Hart (1997)
STJ86-82	185.6	±	2.4	0.5	quartz monzonite	zircon	TIMS - 5 pt regression, lower intercept	61.33336	-136.6781	Johnston et al. (1996)
STJ87-108	186.0	±	2.8		granodiorite	zircon	TIMS - mean age of two concordant fractions	61.55728	-137.3277	Johnston et al. (1996)
QM87-92	187.7	±	0.6		quartz monzonite	titanite	TIMS - mean age of two concordant fractions	61.69866	-136.27249	Johnston et al. (1996)
STJ-OG	352.3	±	2.4	0.2	granitic orthogneiss	zircon	TIMS - 3 pt regression, upper intercept	61.48042	-137.17689	Johnston et al. (1996)
	184.4	±	0.5			titanite	TIMS - most precise of 2 concordant analyses			Johnston et al. (1996)

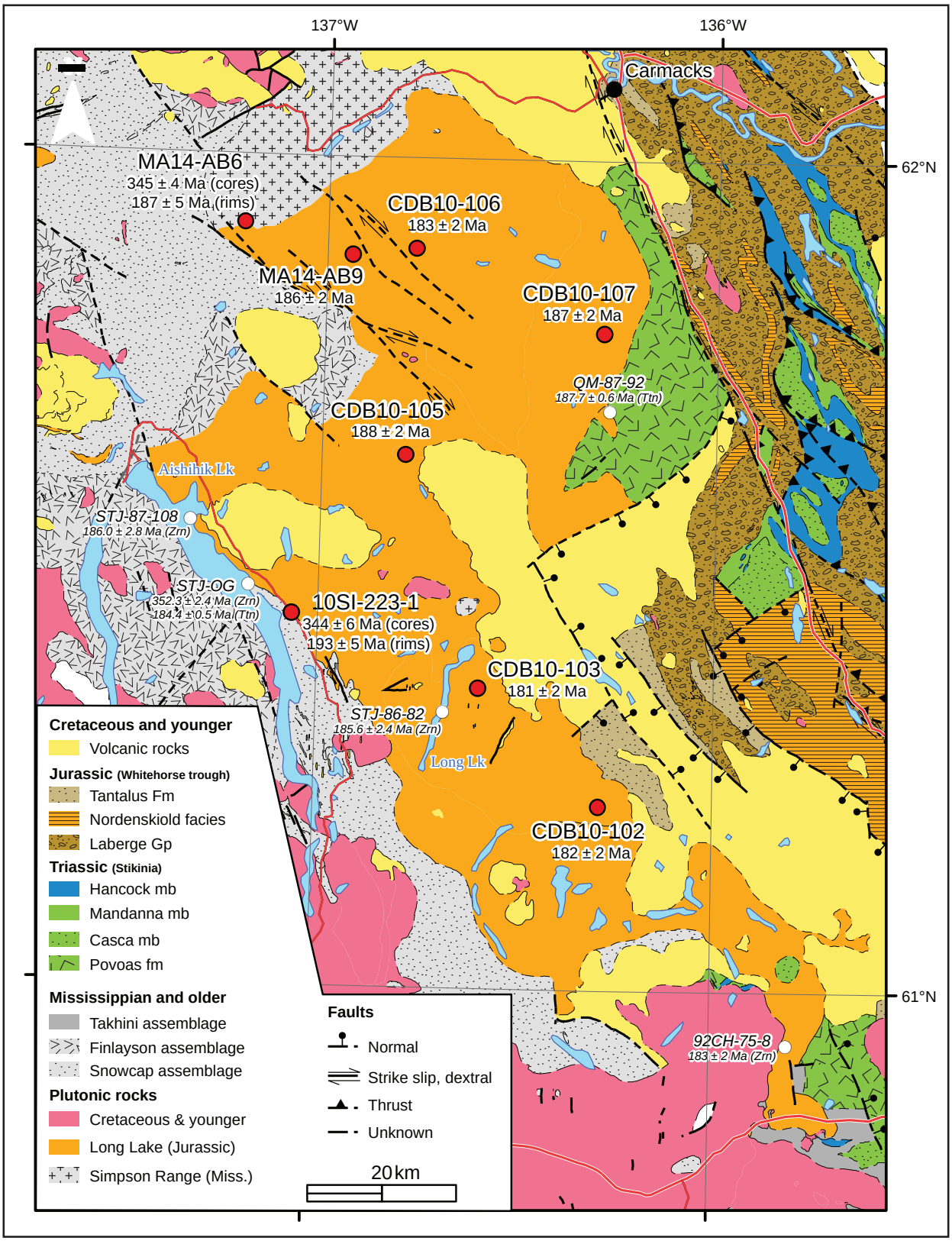


Figure 2. *Geological map of the area surrounding the Aishihik batholith (geology from www.geology.gov.yk.ca/update_yukon_bedrock_geology_map.html). Geology is coloured by terrane affinity with patterns showing regional units. Red circles are geochronology samples reported in this paper; small white circles show location of previous geochronology samples (see Table 1 for details).*

AISHIHIK BATHOLITH

The Aishihik batholith is the largest of the Late Triassic-Early Jurassic composite plutons in Yukon (Fig. 1). It extends from near Whitehorse to the vicinity of Carmacks, and intrudes strata of Stikinia and Yukon-Tanana terranes west of the Whitehorse trough (Figs. 1 and 2). The batholith comprises granitoid lithologies that range in compositions from quartz diorite, tonalite and granodiorite, to quartz monzonite and granite, with the various compositions mutually intermixed and with gradational contacts (Tempelman-Kluit, 1974; Johnston and Erdmer, 1995; Johnston *et al.*, 1996). Originally the name Aishihik batholith was primarily applied to rocks of granodioritic composition, and the two regions dominated by quartz monzonite and granitic compositions, near Long Lake and at the north end of the batholith near Carmacks, were referred to as the Long Lake and Carmacks batholiths, respectively (Tempelman-Kluit, 1974; Woodsworth *et al.*, 1991; Johnston and Erdmer, 1995). More recently, the entire area underlain by Jurassic granitoid rocks has been called the Aishihik batholith (Gordey and Makepeace, 2001; Colpron *et al.*, 2016), and this is the usage followed in this paper (Fig. 1).

Granodiorite and tonalite are the dominant intermediate compositions within the Aishihik batholith. They are generally medium to coarse-grained, equigranular to K-feldspar porphyritic, and typically contain hornblende and biotite, with hornblende commonly more abundant than biotite (Figs. 3a-c). Johnston and Erdmer (1995) reported occurrence of magmatic epidote from granodiorite of the Aishihik batholith; an observation that could not be replicated in our suite of samples. The presence of magmatic epidote is a key argument to suggest emplacement of the granodiorite-tonalite in the Aishihik batholith at >25 km depth (Johnston and Erdmer, 1995; Johnston *et al.*, 1996).

Quartz monzonite and granite of the Aishihik batholith are typically coarse-grained and K-feldspar porphyritic, and also commonly contain biotite and hornblende (Figs. 3d-e). The local abundance of large, pink K-feldspar phenocrysts led Tempelman-Kluit (1974) to assign the name of 'pink quartz monzonite' to these rocks (Fig. 3e). Occurrences of granite are commonly associated with late aplite and pegmatite dikes, local miarolitic cavities, and locally finer grained quartz porphyry (Figs. 3f). These more felsic, and apparently shallowly-emplaced rocks appear to be more common in (but not exclusive to) the northern part of the batholith (Fig. 2). The various compositions that make up the Aishihik batholith are variably intermixed with gradational internal contacts, though field relationships generally suggest that granodiorite-tonalite phases are older, and quartz monzonite-granite phases are relatively younger (Tempelman-Kluit, 1974; Johnston and Erdmer, 1995; Johnston *et al.*, 1996).

Johnston and Erdmer (1995, p. 67) described the rocks of the Aishihik batholith as "characteristically foliated". Although we observed weak to moderate foliation (both magmatic and solid state) in many locations throughout the batholith, for the most part granitoid rocks in the Aishihik batholith are undeformed (Figs. 3a-f). Johnston and Erdmer (1995, p. 75) further suggested that foliation intensity increased toward the western margin of the Aishihik batholith and was locally gneissic in character (their S_t fabric). Our observations, and the geochronological data we present below, indicate that the granodiorite gneiss at the western margin of the Aishihik batholith (Fig. 3g-h) is part of the Mississippian Simpson Range plutonic suite of the Yukon-Tanana terrane (*e.g.*, Mortensen, 1992; Colpron *et al.*, 2006). A series of late upright folds are superposed on the gneissic foliation and also fold the western intrusive contact of the batholith near Aishihik Lake (Israel and Borch, 2015).

Previous U-Pb geochronology of the Aishihik batholith is limited to multi-grain, generally discordant TIMS dates from five samples (Fig. 2). Johnston *et al.* (1996) reported a $^{207}Pb/^{206}Pb$ date of 186.0 ± 2.8 Ma for two concordant zircon fractions in a foliated granodiorite from the western part of the Aishihik batholith. A sample of quartz monzonite from Long Lake yielded a lower intercept U-Pb zircon date of 185.6 ± 2.4 Ma (Johnston *et al.*, 1996). Another sample of quartz monzonite yielded a $^{206}Pb/^{238}U$ titanite date of 187.7 ± 0.6 Ma (Johnston *et al.*, 1996). A quartz monzonite from the southern tail of the Aishihik batholith yielded a lower intercept U-Pb zircon date of 183 ± 2 Ma (Hart, 1997). Finally, a granitic orthogneiss from the western margin of the Aishihik batholith yielded an upper intercept U-Pb zircon date of 352.3 ± 2.4 Ma, considered the age of the protolith, and a titanite cooling date of 184.4 ± 0.5 Ma (Johnston *et al.*, 1996).

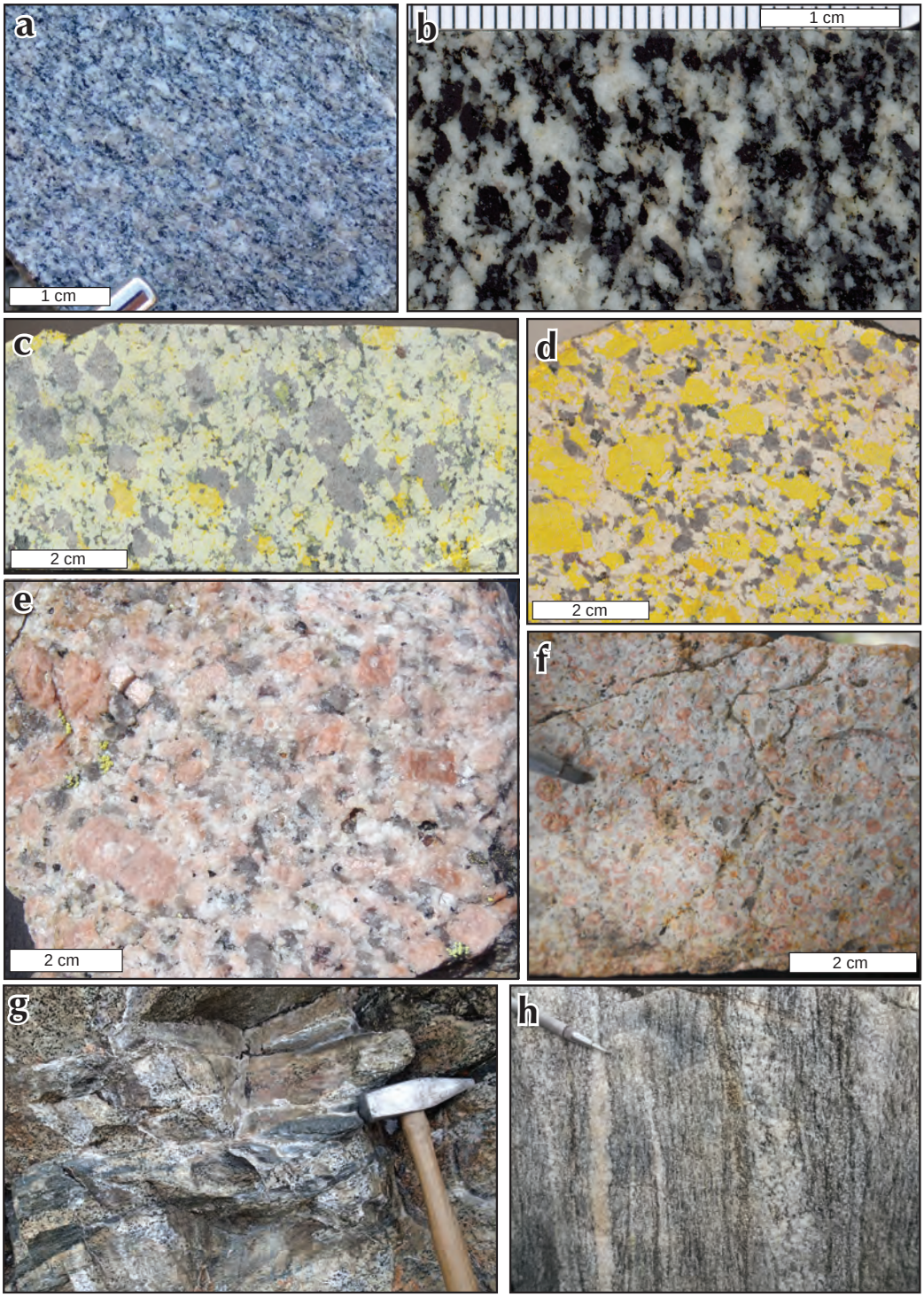


Figure 3. *Representative lithologies in the Aishihik batholith. (a) K-feldspar porphyritic granodiorite from central part of the batholith; (b) hornblende-biotite granodiorite at sample locality CDB-10-105; (c) stained slab of coarse-grained tonalite from the same locality as sample CDB-10-107. K-feldspar is stained yellow; (d) stained slab of K-feldspar porphyritic granite collected near sample CDB-10-103; (e) hand sample of K-feldspar porphyritic granite from station CDB-10-103. Note the large quartz phenocrysts characteristic of granite to quartz monzonite phases of the Aishihik batholith. (f) Weathered surface of quartz monzonite porphyry at location MA14-AB9. (g) Foliated, medium-grained, hornblende-biotite granodiorite with mafic schlieren at locality 10-SI-223; (h) sample of biotite granodiorite orthogneiss (MA14-AB6) from the northwestern margin of the Aishihik batholith.*

GEOCHRONOLOGY

In this contribution, we report new U-Pb zircon dates from eight samples collected during regional reconnaissance of the Aishihik batholith. Five samples were collected by J. Chapman and M. Colpron during a reconnaissance visit in August 2010. They were analyzed by N. Joyce using the Sensitive High Resolution Ion Microprobe (SHRIMP) at the Geological Survey of Canada laboratory in Ottawa (CDB-10-102, 103, 105, 106, 107; Table 1; analytical methods are given in Appendix 1 and data are presented in Appendix 2 and on Fig. 4). Sample 10-SI-223 was collected by S. Israel, M. Colpron and D. Murphy during a field visit of the Aishihik Lake area in September 2010 (Table 1). The sample was dated by J. Crowley using both Chemical Abrasion-Thermal Ionization Mass Spectrometry (CA-TIMS) and Laser Ablation-Inductively Coupled Plasma Mass Spectrometry (LA-ICPMS) at the Isotope Geology Laboratory at Boise State University (analytical methods detailed in Appendix 1; data are presented in Appendix 3 and 4, and on Fig. 5). Finally, samples MA14-AB6 and MA14-AB9 were collected by M. Allan during the early stages of our 2014 field studies. They were analyzed by LA-ICPMS at the Pacific Centre for Isotopic and Geochemical Research, University of British Columbia by M. Allan (analytical methods detailed in Appendix 1; data are presented in Appendix 5 and on Fig. 6). In general, these results confirm the ranges of dates previously obtained from multi-grain zircon fractions analyzed by TIMS (Table 1), but single-grain CA-TIMS analyses and the spatial resolution of laser and SHRIMP provide more accurate and precise results, circumventing problems of discordance in older TIMS ages caused by inheritance, post-crystallization Pb loss and mixing of age domains (Johnston *et al.*, 1996; Hart, 1997). Two of the samples (10-SI-223 and MA14-AB6) were collected from strongly foliated orthogneiss along the western margin of the Aishihik batholith (Fig. 2).

CDB-10-102 (Z11234) – PORPHYRITIC GRANITE

CDB-10-102 is a mafic-poor, K-feldspar porphyritic, coarse-grained, unfoliated, pink granite collected from the southern part of the Aishihik batholith (Fig. 2). The granite is characterized by large quartz phenocrysts (similar to Fig. 3e), and contains ~20% quartz, 30-35% plagioclase, 35-50% K-feldspar, and <10% hornblende. The granite is locally highly altered with fine Fe-oxide veinlets and extensive sericite and clay alteration of plagioclase relics.

Zircon grains recovered from this sample are 100-220 µm euhedral stubby prisms; results are shown in Figure 4a. In transmitted light the crystals are clear and colourless or pale yellow, and rarely contain inclusions. In both backscatter (BSE) and cathodo-luminescence (CL) scanning-electron microscope (SEM) images, the majority of the grains mounted for SHRIMP analysis show distinct oscillatory zoning. Cores were observed in about 15% of the grains. U content ranged between 181 and 456 ppm and Th/U values were moderate to high (0.37-0.85). Nine spots on individual grains returned a weighted mean $^{206}Pb/^{238}U$ date of 182 ± 2 Ma (mean square of weighted deviates [MSWD] = 1.2).

CDB-10-103 (Z11235) – QUARTZ MONZONITE

CDB-10-103 is a coarse-grained, unfoliated, biotite quartz monzonite collected from the top of Red Granite Mountain, near Long Lake (Fig. 2). It also has the 3-5 mm smokey quartz crystals characteristic of the more felsic compositions in the Aishihik batholith (Figs. 3d-e). Quartz makes up 19-30% of the rock, with 40-50% plagioclase, 15-31% K-feldspar, and up to 15% biotite. The plagioclase is commonly Fe-stained imparting a pink to red colouration to the weathered rock.

Zircon grains recovered from this sample are ~80-225 µm euhedral stubby prisms; results are shown in Figure 4b. In transmitted light the crystals are clear and colourless or pale yellow, and contain minor clear bubble-shaped inclusions. Cores, which have varying CL responses, are commonly sieve-textured in BSE, and are found in over 25% of the mounted grains. In both BSE and CL SEM images, the majority of the grains show distinct oscillatory zoning. Of the 16 analyses in Appendix 2, four are clearly from inherited zircons (Calibration 2; 197, 204, 361, and 1866 Ma). Dates of the 10 concordant analyses from Calibration 3 vary between 177 and 187 Ma, the weighted average of which is 182 Ma. The MSWD, however, is elevated at 3.3, suggesting more than one population is present. The weighted mean $^{206}Pb/^{238}U$ date of the 7 youngest analyses is 181 ± 2 Ma (MSWD = 1.4), which is interpreted as the crystallization age of the quartz monzonite. U content of this population of zircons ranged between 166 and 723 ppm, and Th/U values were moderate (0.16-0.37). Three analyses at ~187 Ma (grains 23, 46, and 47) are interpreted to be inherited from a slightly older intrusive phase. Grain 20 clearly has a *ca.* 197 Ma core mantled by a *ca.* 177 Ma rim (Fig. 4b).

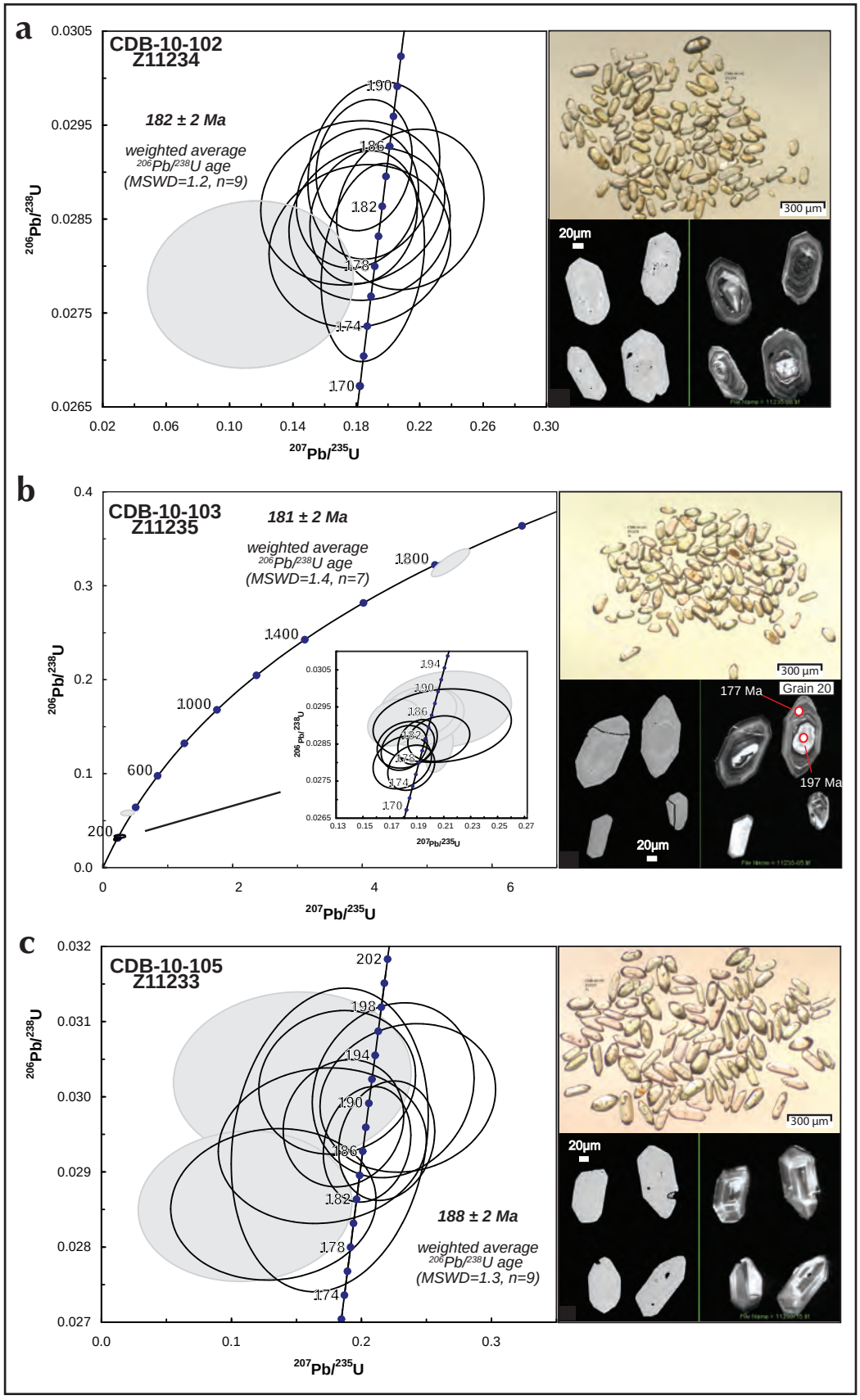


Figure 4. *U-Pb concordia plots for five samples analyzed by SHRIMP methods at the Geological Survey of Canada geochronology laboratory in Ottawa. Each diagram consists of: a Concordia plot on the left, a photograph of zircon grains recovered in the upper right, and paired SEM backscatter (L) and CL images (R) in the lower right. Photograph of recovered grains shows the range in morphology, colour and size of zircons analyzed, and representative BSE and CL images show internal structure of the grains. For each Concordia plot, error ellipses are at the 2σ confidence level, unfilled ellipses are analyses used in calculating the mean weighted average age for each sample; light grey ellipses are analyses rejected from age calculations for reasons discussed in text.*

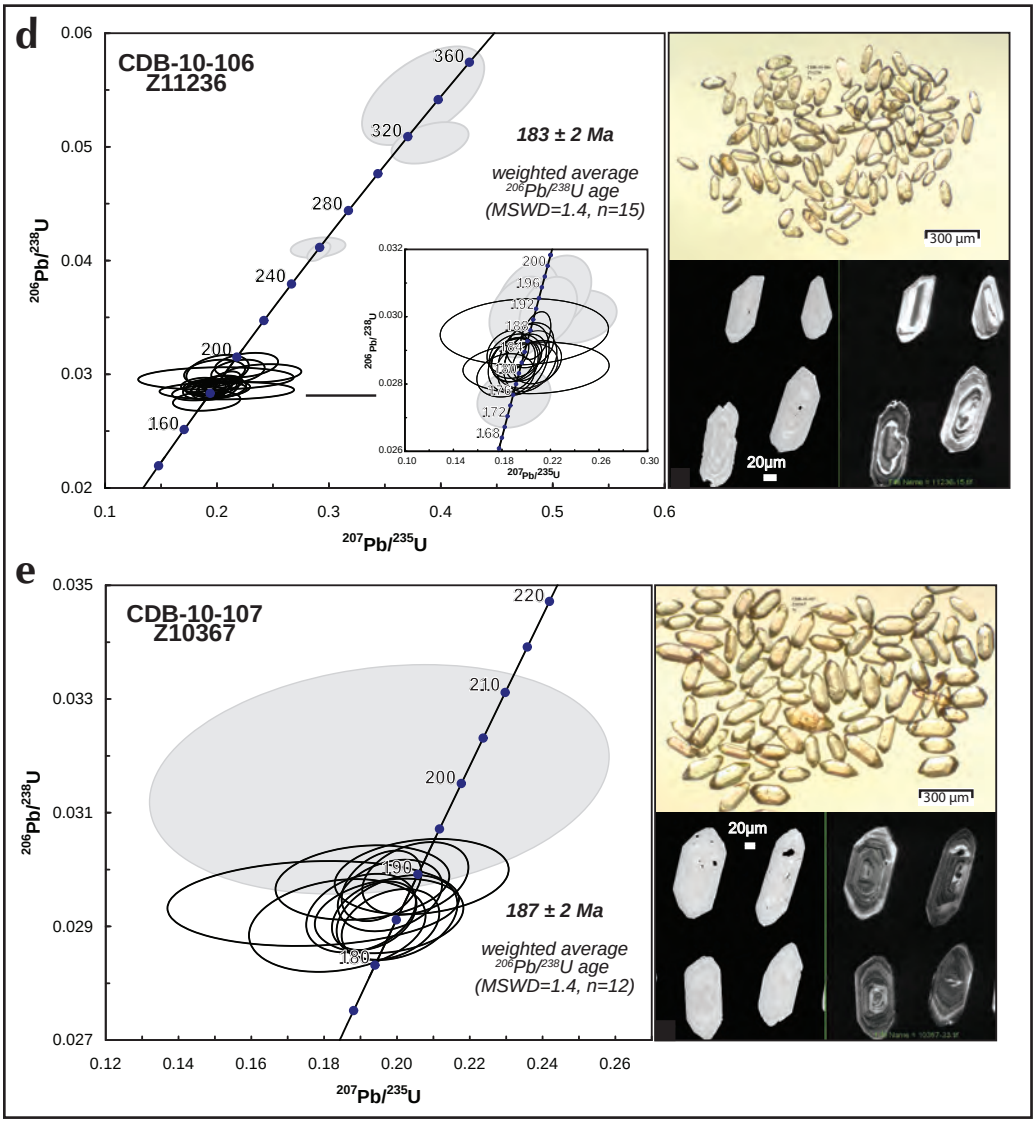


Figure 4 continued. *U-Pb concordia plots for five samples analyzed by SHRIMP methods at the Geological Survey of Canada geochronology laboratory in Ottawa. Each diagram consists of: a Concordia plot on the left, a photograph of zircon grains recovered in the upper right, and paired SEM backscatter (L) and CL images (R) in the lower right. Photograph of recovered grains shows the range in morphology, colour and size of zircons analyzed, and representative BSE and CL images show internal structure of the grains. For each Concordia plot, error ellipses are at the 2σ confidence level, unfilled ellipses are analyses used in calculating the mean weighted average age for each sample; light grey ellipses are analyses rejected from age calculations for reasons discussed in text.*

CDB-10-105 (Z11233) - WEAKLY FOLIATED HORNBLENDE-BIOTITE GRANODIORITE

CDB-10-105 is a mafic-rich, weakly foliated, medium-grained, equigranular hornblende-biotite granodiorite from the central part of the Aishihik batholith (Figs. 2 and 3b). It contains 15-25% fine-grained quartz, 35-50% plagioclase, 5-25% K-feldspar, up to 35% hornblende and 10% biotite. The weak magmatic foliation is shown by crude alignment of mafic minerals. Mafic minerals are locally altered to chlorite and epidote, with biotite more commonly altered.

Zircon grains recovered from this sample are 150-250 µm in size, stubby to elongate euhedral prisms; results are shown in Figure 4c. In transmitted light the crystals are clear and colourless or pale yellow, and commonly contain clear bubble or rod-shaped inclusions. Backscatter SEM images of the grains mounted for SHRIMP analysis reveal few internal textures of the grains, with the exception of inclusions and fractures. In CL, the majority of grains exhibit c-axis-parallel, broadly banded or striped zoning patterns, mantled by variably developed oscillatory-zoned growth (up to ~20 µm thick). Faint sector zoning is visible in grains polished normal to the c-axis. U content ranged between 130 and 245 ppm and Th/U values were moderate (0.36-0.68; Appendix 2). Cores were seen in only two of the grains. Nine spots on individual grains returned a weighted mean $^{206}Pb/^{238}U$ date of 188±2 Ma (MSWD=1.3). A 196 Ma date obtained for grain 85 is considered to reflect an inherited component (Appendix 2).

CDB-10-106 (Z11236) – PORPHYRITIC GRANODIORITE

CDB-10-106 is a coarse-grained, variably K-feldspar porphyritic, quartz-phyric hornblende (±biotite) granodiorite from Buffalo Mountain in the northern part of the Aishihik batholith (formerly the Carmacks batholith of Tempelman-Kluit, 1974; Johnston and Erdmer, 1995). Smokey quartz phenocrysts are up to 4 mm, in a 0.5-2 mm groundmass, as commonly noted in other quartz-rich rocks to the south, near Long Lake (*e.g.*, CDB-10-102 and 103; Figs. 2 and 3d). Quartz makes up 25-35% of the rock, with 40-50% plagioclase, 7-20% K-feldspar, and up to 10-15% hornblende (±biotite). The granodiorite is fresh and unfoliated.

Zircon grains recovered from this sample are ~90-225 µm stubby to elongate euhedral prisms; results are shown Figure 4d. In transmitted light the crystals are clear and colourless or pale yellow, and contain minor bubble-shaped clear inclusions. In both BSE and CL SEM images, the majority of the grains mounted for SHRIMP analysis show distinct oscillatory zoning. Cores were observed in about 20% of the grains. U content for the igneous grains ranged between 114 and 701 ppm and Th/U values were moderate (0.26-0.51; Appendix 2). Fifteen spots on individual grains returned a weighted mean $^{206}Pb/^{238}U$ date of 183±2 Ma (MSWD=1.4). Because the core regions of the grains in this sample were the largest and easiest to analyze, more analyses were carried out on this sample compared to the other four to characterize the inheritance profile of the Aishihik batholith. Eight inherited cores were analyzed, yielding dates of *ca.* 190, 260, 316 and 343 Ma (Appendix 2).

CDB-10-107 (Z10367) - HORNBLENDE-BIOTITE TONALITE

CDB-10-107 is a medium-grained, equigranular, hornblende-biotite tonalite to granodiorite collected from the northeastern portion of the Aishihik batholith (Figs. 2 and 3c). The rock contains up to 25% mafic minerals (hornblende and biotite), 35-55% plagioclase, 5-15% K-feldspar, and 25-40% quartz, but lacks the distinctive smokey-grey quartz phenocrysts characteristic of more felsic compositions to the west and south (*e.g.,* CDB-10-102, 103 and 106). A weak (magmatic) alignment of mafic minerals is locally apparent. Secondary epidote and titanite are locally important accessory phases.

Zircon grains recovered from this sample are ~100-300 µm stubby to slightly elongate euhedral prisms; results are shown in Figure 4e. In transmitted light the crystals are clear and colourless, and contain clear minor bubble and rod-shaped inclusions. In both BSE and CL SEM images, the majority of the grains mounted for SHRIMP analysis show distinct oscillatory zoning. Cores were observed in about 15% of the grains. U content for the igneous grains ranged between 234 and 826 ppm and Th/U values were moderate (0.34-0.64; Appendix 2). Twelve spots on individual grains returned a weighted mean $^{206}Pb/^{238}U$ date of 187±2 Ma (MSWD=1.4).

10-SI-223 - GRANODIORITE GNEISS

Sample 10-SI-223 is a strongly foliated, hornblende-biotite granodiorite to quartz diorite gneiss from the western margin of the Aishihik batholith, near the eastern shore of Aishihik Lake (Fig. 2). The rock is medium-grained with hornblende and biotite-rich schlieren (Fig. 3g)

Zircon is CL dark with weak to moderate sector and oscillatory zoning (Fig. 5 and Appendix 6). One third of the grains exhibit CL bright cores that were avoided during selection of grains for dating using the CA-TIMS method. Most grains have rims a few microns wide that grew after a period of zircon dissolution. CA-TIMS analyses (Fig. 5a and Appendix 3) form a discordant array nearly parallel to concordia that indicates the zircon is a mixture of two ages, 357±5 and 208±26 Ma (Fig. 5a).

The *in-situ* LA-ICPMS method was then performed to better resolve the age components (Appendix 4 and Fig. 5b). LA-ICPMS analyses show a similar spread of dates as seen in CA-TIMS analyses. The 15 oldest dates are equivalent, with a weighted mean date of 344±6 Ma (Fig. 5b). These zircons have uniformly high total REE contents of 3000-6000 ppm (Fig. 5d), Th/U of 1.1 to 1.6, and Ti-in-zircon temperatures of ~800°C (Appendix 4; Watson *et al.*, 2006). The next 5 oldest dates are between 329±5 and 314±6 Ma. These analyses have similar chemical characteristics as the older zircon, and thus likely are part of the same population, with the younger dates being due to slight mixing in the analysis with Jurassic rims. Two analyses of rims yielded a weighted mean of 193±5 Ma (Fig. 5c and Appendix 4). The Jurassic rims have similar CL brightness as the majority of the Mississippian igneous zircon, making it difficult to distinguish the components using CL images alone (Appendix 6). The rims have low total REE contents of ~460 ppm (Fig. 5d), especially light and middle REE contents, and Th/U of 0.03 to 0.25.

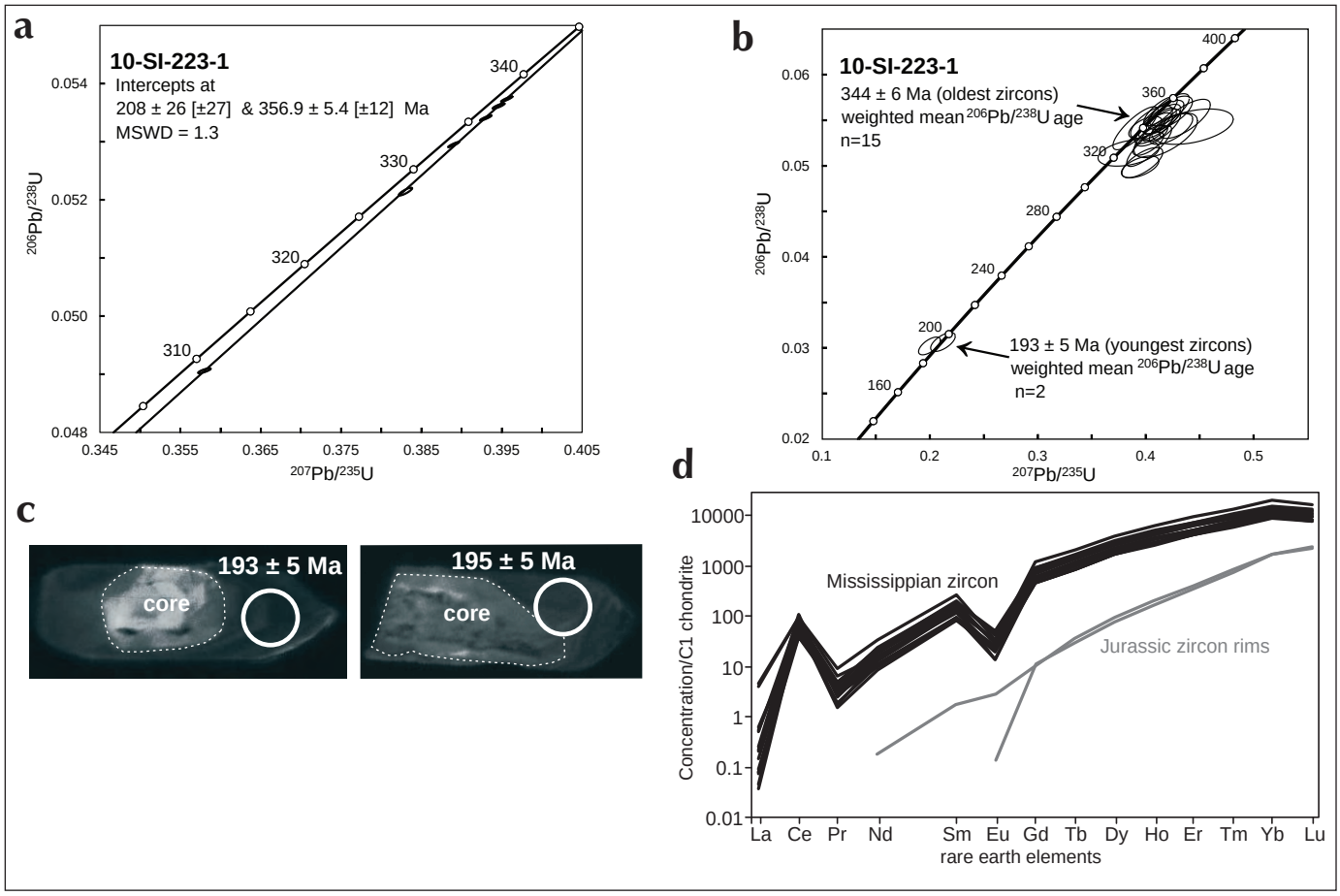


Figure 5. *U-Pb concordia plots for sample 10-SI-223, analyzed at the Isotope Geology Laboratory at Boise State University. (a) concordia plot for CA-TIMS analyses; (b) concordia plot for LA-ICPMS analyses; (c) CL images showing spot yielding Jurassic analyses from zircon rims. Errors are at 2σ. Errors on intercepts defined by CA-TIMS analyses are given without and with U decay constant uncertainties.*

MA14-AB9 – QUARTZ MONZONITE PORPHYRY

MA14-AB9 is a buff-weathering, quartz monzonite porphyry, which contains 35% 2–4 mm K-feldspar phenocrysts and 5% 1–4 mm euhedral to rounded and embayed quartz phenocrysts in a pervasively sericitized quartzofeldspathic groundmass (Fig. 3f). The porphyry forms a recessive topographic saddle between prominent tors of massive, white weathering, coarse-grained, weakly foliated, K-feldspar porphyritic biotite-hornblende granodiorite of the Aishihik batholith west of Buffalo Mountain (Fig. 2).

The 20 zircon grains analyzed by LA-ICPMS were colourless, doubly-terminating prisms with lengths between 100 and 150 μm and with aspect ratios ranging from 2:1 to 4:1. Nineteen of the 20 grains yielded concordant or nearly concordant dates (Fig. 6a and Appendix 5), which, with the exception of one statistically rejected analysis, yielded a weighted average $^{206}Pb/^{238}U$ date of 186 ± 2 Ma (MSWD = 1.5; probability of fit = 0.074).

MA14-AB6 – BIOTITE GRANODIORITE ORTHOGNEISS

MA14-AB6 is a grey, medium-grained biotite granodiorite orthogneiss with a strongly-developed, planar gneissocity, which was collected along the northwest margin of the Aishihik batholith (Figs. 2 and 3h). This flaggy-weathering, outcrop-forming rock has a moderately south-dipping foliation at this locality, and is locally folded about south-plunging axes. Compositional layering ranges from mm-scale biotite-only seams to coarse, granitic layers up to 1-cm thick.

The 19 zircon grains analyzed by LA-ICPMS from the orthogneiss were stubby prisms with lengths between 100 and 150 µm and an average aspect ratio of 1:2. Fifteen of these grains had a colourless and slightly cloudy core with low average CL intensity, rimmed by higher-clarity zircon with higher average CL intensity (Fig. 6b iii-vi). The remaining four zircons imaged contained only the core growth stage. Laser ablation rasters were planned to sample only the core or overgrowth zircon stage with a 25 µm spot. However, where overlap of the two mutually contaminating growth zones was unavoidable, only the portion of the time-series signal that represented a single growth stage was integrated. Seventeen of the 19 analyses represent zircon cores (Fig. 6b iv-vi), whereas in two grains, later stages of zircon overgrowths were sufficiently broad to sample and analyze (Fig. 6b iii-iv).

The 17 analyses of zircon cores fell on or very near to concordia (Fig. 6B iv and Appendix 5), and their weighted average $^{206}Pb/^{238}U$ date is 345 ± 4 Ma (MSWD = 1.5; probability of fit = 0.10). The two analyses of zircon overgrowths were concordant (Fig. 6b i and Appendix 5), and their weighted average $^{206}Pb/^{238}U$ date is 187 ± 5 Ma (MSWD = 0.45; probability of fit = 0.50).

DISCUSSION

The new U-Pb zircon dates reported here generally confirm the age range previously determined by TIMS analyses of multi-grain zircon fractions from samples of the Aishihik batholith (Johnston *et al.*, 1996; Hart, 1997). The SHRIMP dates range from ~190 to ~179 Ma (approximate range including errors; Table 1), with the more mafic rocks (CDB-10-105, 107) yielding older dates (~190-185 Ma), and felsic rocks (CDB-10-102, 103, 106) giving distinctly younger dates of ~184-179 Ma (Fig. 7). This apparently confirms the general field observations suggesting that tonalite-granodiorite phases are older and quartz monzonite-granite phases are relatively younger; although in detail the various phases in the Aishihik batholith appear to be closely related with gradational contacts (Tempelman-Kluit, 1974; Johnston and Erdmer, 1995; Johnston *et al.*, 1996; *this study*). The LA-ICPMS date of 186 ± 2 Ma from a quartz porphyry in the northern part of the Aishihik batholith (MA14-AB9; Fig. 2 and Table 1) is intermediate between the two populations revealed by SHRIMP dates, and may indicate more frequent intrusive episodes leading to batholith construction (Fig. 7). More precise CA-TIMS analyses are required to resolve whether the batholith was constructed from intrusion of two discrete phases or more frequent magma injections.

Johnston and Erdmer (1995) considered the granodiorite-tonalite compositions to be part of the Aishihik plutonic suite (which also included the Granite Mountain, Minto and Tatchun plutons), and the more felsic compositions as belonging to the Long Lake suite (following Tempelman-Kluit, 1974, 1984; Woodsworth *et al.*, 1991). However, the available geochronological dataset (Fig. 7 and Table 1) and the close inter-relations of the various phases in the Aishihik batholith do not warrant division of the batholith into two distinct plutonic suites. We favour assigning granitoid rocks of the Aishihik batholith to the Long Lake suite, ranging from *ca.* 190-180 Ma (Colpron *et al.*, 2016), to avoid potential confusion with recent use of the term Aishihik plutonic suite for older plutons (*see* below).

It is notable that none of the dates obtained from the Aishihik batholith are as old as the *ca.* 204-196 Ma granodiorite of the Granite Mountain, Minto and Tatchun batholiths (Fig. 1; *e.g.*, Tafti, 2005; Hood, 2012; Colpron, 2011; Breistprecher and Mortensen, 2004). These older plutons were previously assigned to the Aishihik suite (*e.g.*, Gordey and Makepeace, 2001) based on their predominantly granodioritic compositions (Johnston and Erdmer, 1995). Because these plutons are distinctly older than any phases dated in the Aishihik batholith, it is recommended that the latest Triassic-Early Jurassic granodiorite plutons that occur mainly north of Carmacks, and host Cu-Au-Ag mineralization at Minto and Carmacks Copper, be assigned to the Minto plutonic suite (*e.g.*, Colpron *et al.*, 2016; Fig. 1). The absence of Minto-age granodiorite in the Aishihik batholith may also suggest lower probability of hosting Minto-style Cu-Au-Ag mineralization in these younger phases.

The range of U-Pb zircon dates from the Aishihik batholith overlaps in part with the range of dated pyroclastic deposits (*ca.* 189-186 Ma; Fig. 7) in the Whitehorse trough, to the east (Nordenskiöld facies, Fig. 2; Colpron and Friedman, 2008). A petrogenetic association between these deposits and the batholith was previously suggested by Hart (1997) and Fillmore (2006). Late Triassic to Early Jurassic plutons of the Minto and Long Lake suites (and their eroded volcanic cover) were also the most significant contributors of detritus in sedimentary rocks of the Whitehorse trough as indicated by abundant plutonic clasts and detrital zircons (Colpron *et al.*, 2015).

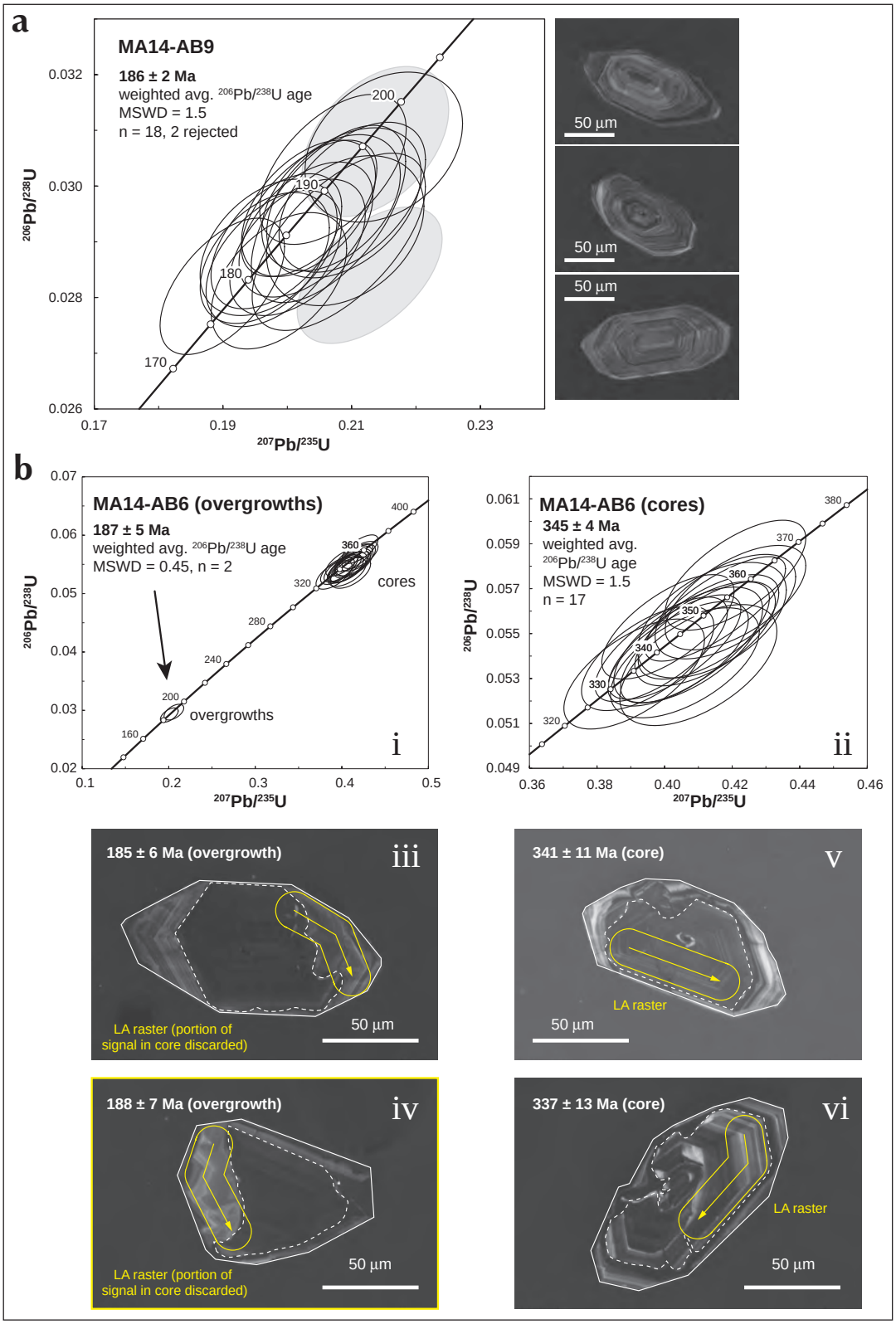


Figure 6. *U-Pb concordia plots for two samples analyzed by LA-ICPMS methods at the Pacific Centre for Isotopic and Geochemical Research at the University of British Columbia. (a) Conventional U-Pb concordia plot for sample MA14-AB9. Error ellipses correspond to 2σ uncertainties in $^{206}Pb/^{238}U$ and $^{207}Pb/^{235}U$ ratios. The two rejected analyses have light grey fill. SEM-CL images of three representative, internally zoned zircon grains are shown to the right. (b) Conventional U-Pb concordia plots for zircon from sample MA14-AB6 (i); greater detail of the dominant Early Mississippian population are shown in (ii). Error ellipses correspond to 2σ uncertainties in $^{206}Pb/^{238}U$ and $^{207}Pb/^{235}U$ ratios. (iii-iv) SEM-CL images of zircon with Early Jurassic overgrowths; (v-vi) SEM-CL images of zircon with embayed, weakly luminescent, Early Mississippian cores and luminescent overgrowths.*

Previous zircon TIMS analyses from the Aishihik batholith typically yielded discordant dates that resulted in large part as a result of mixing of inherited components and/or post-crystallization Pb loss (Johnston *et al.*, 1996; Hart, 1997). Our new results allow better resolution of inherited versus magmatic components by using a combination of SEM imaging and *in-situ* dating techniques. Inherited cores were identified in 15-25% of zircons imaged with CL SEM (Figs. 4-6). Larger cores were analyzed with the SHRIMP for a few samples (CDB-10-103, 105, 106; Appendix 2). Xenocrystic cores typically reflect interaction with local Paleozoic 'host' rocks (*ca.* 360, 343, 316 and 260 Ma; Yukon-Tanana and/or Stikinia) and older early Mesozoic intrusions (*ca.* 204-196 Ma; Minto suite). A single core was dated at *ca.* 1866 Ma reflecting interaction with either Paleoproterozoic 'basement' or incorporation of a detrital zircon component from metasedimentary rocks of the Yukon-Tanana terrane (Snowcap assemblage; Piercey and Colpron, 2009).

The porphyritic texture in sample MA14-AB9 could be interpreted to indicate it was emplaced at shallower (subvolcanic?) crustal depths, or under H_2O-saturated conditions. Shallow emplacement and/or high volatile content in the magma are also suggested by common occurrences of pegmatite, miarolitic cavities and aplite dikes in the northern part of the batholith. Shallow (<5 km) emplacement of the *ca.* 186 Ma quartz porphyry is unexpected compared to apparently deeper crystallization pressures (3.4-4.2 kbar; ~10-12 km) indicated by Al-in-hornblende analyses of nearby granitic rocks dated at *ca.* 187-183 Ma (CDB-10-106, 107; Fig. 2; Topham *et al.*, 2016). Either this reflects differential exhumation of various parts of the batholith, or the quartz porphyry could be younger than the *ca.* 186 Ma date indicated in Figure 6a. Closer examination of the data in Appendix 5 show a spread of ages between ~196 and ~180 Ma that could represent multiple populations of young zircons (*see* also Fig. 6a). Further analyses using the CA-TIMS method would help improve resolution of these different events. More significantly, the presence of apparently shallower intrusive rocks may indicate potential for porphyry-type Cu-Au mineralization in parts of the Aishihik batholith, especially given that both the Mount Milligan and Lorraine porphyry Cu deposits in northern BC are associated with Early Jurassic intrusions broadly coeval with the Long Lake plutonic suite (Nelson and Bellefontaine, 1996; Jago *et al.*, 2014; Devine *et al.*, 2014; Bath *et al.*, 2014). However, the BC deposits are hosted in alkalic rocks; the Aishihik batholith is generally calc-alkalic to transitional; lithogeochemistry of the Aishihik batholith will be discussed in a future publication.

Two of the samples analyzed in this study are from orthogneiss along the western margin of the Aishihik batholith (10-SI-223 and MA14-AB6; Fig. 2). A previous attempt at dating the orthogneissic rocks along the shore of Aishihik Lake (STJ-OG; Table 1 and Fig. 2) yielded a discordant scatter of zircon analyses suggesting mixing between a predominantly mid-Paleozoic (*ca.* 352 Ma) population of zircons representing the protolith age, and a younger, Mesozoic event of Pb loss or remelting (Johnston *et al.*, 1996). A titanite age of *ca.* 184 Ma provided further constraints on the possible Mesozoic event (Johnston *et al.*, 1996).

CA-TIMS analyses of zircon from orthogneiss at 10-SI-223 yielded a discordant array nearly parallel with concordia, also indicating mixing of mid-Paleozoic and early Mesozoic age components, similar to the sample dated by Johnston *et al.* (1996; Fig. 5a and Appendix 3). LA-ICPMS analysis shows two distinct age clusters, with most zircon being Mississippian (344±6 Ma) and rare rims being Early Jurassic (193±5 Ma; Fig. 5b-c and Appendix 4). LA-ICPMS analysis of another orthogneiss to the north (MA14-AB6; Fig. 2) yielded similar results, with a dominant cluster of older Mississippian zircon (345±4 Ma), and rare Early Jurassic (187±5 Ma) zircon rims (Fig. 6b and Appendix 5). CL images show resorbed Mississippian cores mantled by well-zoned overgrowths (Fig. 6b iii-vi), a pattern that is most consistent with a period of zircon dissolution in a zircon-undersaturated melt, followed by re-precipitation in the presence of a zircon-saturated melt in the Jurassic. Chemical compositions suggest that the Jurassic zircon formed during partial melting of the orthogneiss, rather than crystallizing from a granitoid magma. In both samples, the Jurassic zircon has lower Th/U (0.03-0.25) than typical magmatic zircon (Tables 4 and 5). In sample 10-SI-223, the Jurassic zircon has much lower light and middle REE contents (Fig. 5d) than zircon in typical granitoid magmas. In summary, the zircon textural, age, and chemical data are most consistent with the orthogneiss being an Early Mississippian granitoid of the Simpson Range plutonic suite, which experienced partial melting and ductile strain during emplacement of the Aishihik batholith in the Early Jurassic.

CONCLUSIONS

Five new SHRIMP and one LA-ICPMS U-Pb zircon dates from various granitoid phases in the Aishihik batholith confirm a range of *ca.* 190-180 Ma (Fig. 7); the various phases are all assigned to the Long Lake plutonic suite. Older (*ca.* 204-196 Ma) granodiorite of the Minto suite, host to Cu-Au-Ag mineralization north of Carmacks, appear absent from the Aishihik batholith, but are locally reflected in inherited zircon cores. The Aishihik batholith is therefore an unlikely target for Minto-style mineralization, but local occurrence of apparently shallow-level intrusions in the northern part of the batholith could represent a crustal level permissible for more typical porphyry mineralization. LA-ICPMS U-Pb zircon dating of two orthogneiss samples from the western margin of the Aishihik batholith indicate an Early Mississippian protolith age similar to that of the Simpson Range plutonic suite of Yukon-Tanana terrane. Jurassic overgrowths on several zircon grains indicate an episode of partial melting of the orthogneiss likely related to intrusion of the Aishihik batholith.

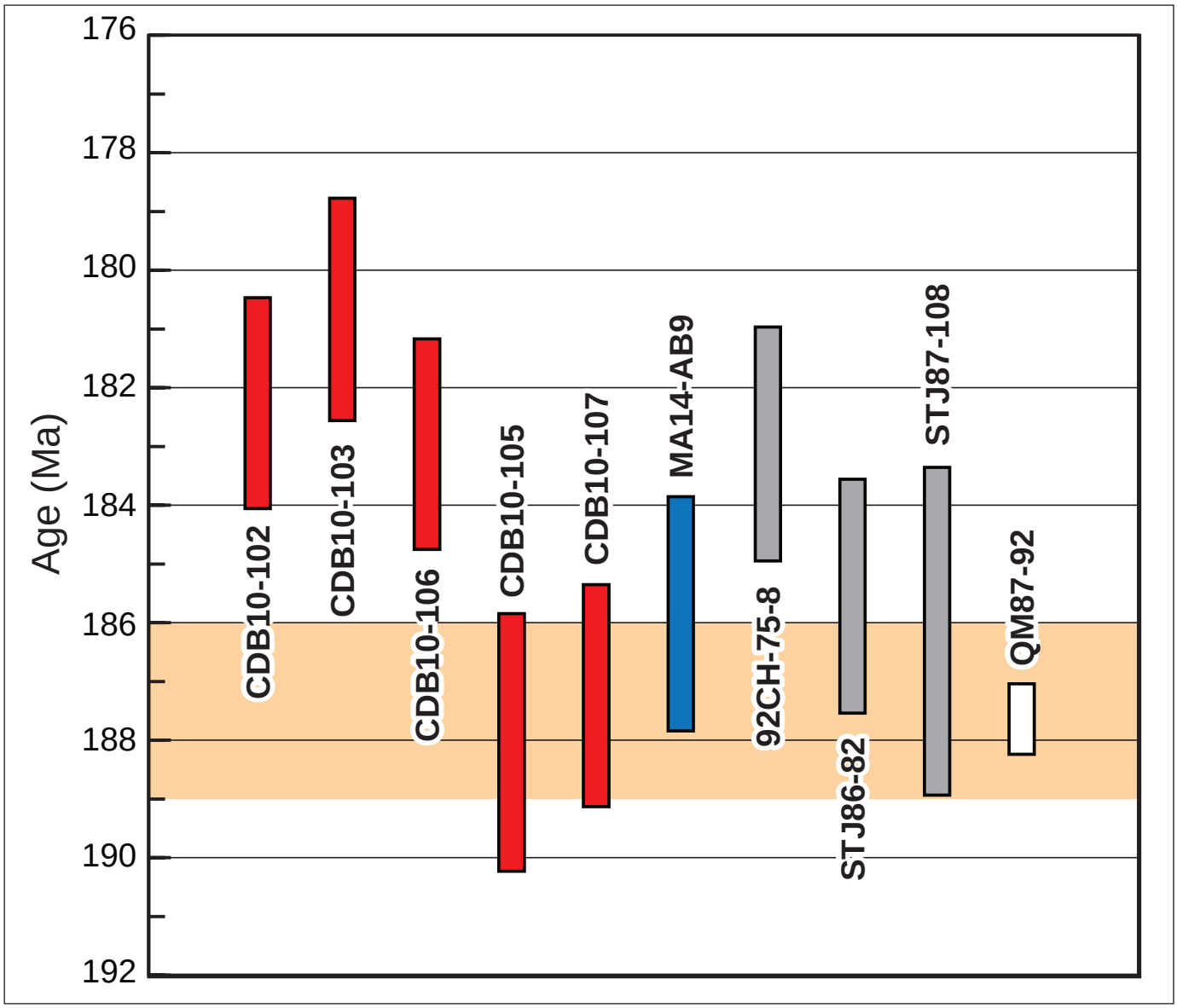


Figure 7. *Summary of U-Pb dates for granitoid samples of the Aishihik batholith (Table 1). Results from orthogneiss samples are omitted. All dates are shown with 2σ errors. Red – SHRIMP zircon date (this study); Blue – LA-ICPMS zircon date (this study); Grey – TIMS multi-grain zircon fractions (Johnston et al., 1996; Hart, 1997); White – TIMS titanite age (Johnston et al., 1996). Orange interval in background indicates the range of dates from pyroclastic rocks in the Whitehorse trough (e.g., Nordenskiöld facies of the Laberge Group; Colpron and Friedman, 2008).*

ACKNOWLEDGMENTS

This study was funded by the Geomapping for Energy and Minerals program of Natural Resources Canada and the Yukon Geological Survey. It is a contribution to the Yukon-Alaska Metallogeny project of the Mineral Deposit Research Unit at the University of British Columbia. Linda Cataldo and Pat Hunt (GSC Ottawa) are thanked for grain mounting and SEM imaging, respectively, for the CDB-10 samples. We thank Tom Pestaj, Bill Davis and Nicole Rayner for their expert guidance and assistance at the GSC SHRIMP facility. Steve Israel collected sample 10-SI-223 and provided the data for this paper. A review by Alex Zagorevski improved the manuscript. This is ESS Contribution number/Numéro de contribution du SST: 20150368.

REFERENCES

Bath, A.B., Cooke, D.R., Friedman, R.M., Faure, K., Kamenetsky, V.S., Tosdal, R.M. and Berry, R.F., 2014. Mineralization, U-Pb geochronology, and stable isotope geochemistry of the lower main zone of the Lorraine deposit, north-central British Columbia: a replacement-style alkalic porphyry. Economic Geology, vol. 109, p. 979-1004,

Breitsprecher, K. and Mortensen, J.K., 2004. Yukonage 2004: A database of isotopic age determinations for rock units from Yukon Territory, Canada. Yukon Geological Survey, Whitehorse, Yukon, www.geology.gov.yk.ca.

Colpron, M., 2011. Geological compilation of Whitehorse trough - Whitehorse (105D), Lake Laberge (105E), and part of Carmacks (115I), Glenlyon (105L), Aishihik Lake (115H), Quiet Lake (105F) and Teslin (105C). Yukon Geological Survey, Geoscience Map 2011-1, scale 1:250 000.

Colpron, M. and Friedman, R. M., 2008. U-Pb zircon ages for the Nordenskiold formation (Laberge Group) and Cretaceous intrusive rocks, Whitehorse trough, Yukon. *In:* Yukon Exploration and Geology 2007, D.S. Emond, L.R. Blackburn, R.P. Hill and L.H. Weston (eds.), Yukon Geological Survey, p. 139-151.

Colpron, M. and Nelson, J.L., 2011. A digital atlas of terranes for the northern Cordillera. Yukon Geological Survey, accessed November, 2015; *also, BC Geological Survey, GeoFile 2011-11.*

Colpron, M., Nelson, J. L. and Murphy, D. C., 2006. A tectonostratigraphic framework for the pericratonic terranes of the northern Canadian Cordillera. *In:* Paleozoic evolution and metallogeny of pericratonic terranes at the ancient margin of North America, Canadian and Alaskan Cordillera, M. Colpron and J.L. Nelson (eds.), Special Paper 45, Geological Association of Canada, p. 1-23.

Colpron, M., Crowley, J.L., Gehrels, G.E., Long, D.G.F., Murphy, D.C., Beranek, L.P. and Bickerton, L., 2015. Birth of the northern Cordilleran orogen, as recorded by detrital zircons in Jurassic synorogenic strata and regional exhumation in Yukon. Lithosphere, vol. 7, p. 541-562.

Colpron, M., Israel, S., Murphy, D.C., Pigage, L.C. and Moynihan, D., 2016. Yukon Bedrock Geology Map 2016. Yukon Geological Survey, Open File 2016-1, scale 1:1 000 000.

Colpron, M., Murphy, D.C., Nelson, J.L., Roots, C.F., Gladwin, K., Gordey, S.P., Abbott, G. and Lipovsky, P.S., 2002. Preliminary geological map of Glenlyon (105L/1-7,11-14) and northeast Carmacks (115I/9,16) areas, Yukon Territory (1:125 000 scale). Exploration and Geological Services Division, Yukon Region, Indian and Northern Affairs Canada, Open File 2002-9, scale; *also Geological Survey of Canada, Open File 1457*.

Devine, F.A.M., Chamberlain, C.M., Davies, A.G.S., Friedman, R.M. and Baxter, P., 2014. Geology and district-scale setting of tilted alkalic porphyry Cu-Au mineralization at the Lorraine deposit, British Columbia. Economic Geology, vol. 109, p. 939-977.

Fillmore, J.A., 2006. Character and origin of the Lower Jurassic (Pleinsbachian) Nordenskiold dacite, Whitehorse trough, Yukon Territory, Canada. Unpublished Honours BSc thesis. Laurentian University, 28 p.

Godwin, C.I., 1975. Alternative interpretations for the Casino complex and Klotassin batholith in the Yukon crystalline terrane. Canadian Journal of Earth Sciences, vol. 12, p. 1910-1916.

Gordey, S.P. and Makepeace, A.J., 2001. Bedrock geology, Yukon Territory. Geological Survey of Canada, Open File 3754, scale 1:1 000 000; *also Yukon Geological Survey, Open File 2001*

Gordey, S.P. and Ryan, J.J., 2005. Geology, Stewart River area (115N, 115O and part of 115J), Yukon Territory. Geological Survey of Canada, Open File 4970, scale 1:250 000.

Gordey, S.P. and Stevens, R.A., 1994. Geology, Teslin, Yukon Territory. Geological Survey of Canada, Open File 2886, scale 1:250 000.

Hart, C.J.R., 1997. A transect across northern Stikinia: Geology of the northern Whitehorse map area, southern Yukon Territory (105D/13-16). Exploration and Geological Services Division, Yukon, Indian and Northern Affairs Canada, Bulletin 8, 112 p.

Hood, S.B., 2012. Mid-crustal Cu-Au mineralization during episodic pluton emplacement, hydrothermal fluid flow, and ductile deformation at the Minto deposit, YT, Canada. Unpublished MSc thesis, University of British Columbia, 220 p.

Israel, S. and Borch, A., 2015. Preliminary geological map of the Long Lake area, parts of NTS 115H/2 and 115H/7. Yukon Geological Survey, Open File 2015-32, 1:50 000 scale.

Jago, C.P., Tosdal, R.M., Cooke, D.R. and Harris, A.C., 2014. Vertical and lateral variation of mineralogy and chemistry in the Early Jurassic Mt. Milligan alkalic porphyry Au-Cu deposit, British Columbia, Canada. Economic Geology, vol. 109, p. 1005-1033,

Johnston, S.T. and Erdmer, P., 1995. Magmatic flow and emplacement foliations in the Early Jurassic Aishihik Batholith, southwest Yukon: Implications for northern Stikinia. *In:* Jurassic Magmatism and Tectonics of the North American Cordillera, D.M. Miller and C. Busby (eds.), Geological Society of America, Special Paper 299, p. 65-82.

Johnston, S.T., Mortensen, J.K. and Erdmer, P., 1996. Igneous and meta-igneous age constraints for the Aishihik metamorphic suite, southwest Yukon. Canadian Journal of Earth Sciences, vol. 33, p. 1543-1555.

Logan, J.M. and Mihalynuk, M.G., 2014. Tectonic controls on Early Mesozoic paired alkaline porphyry deposit belts (Cu-Au±Ag-Pt-Pd_Mo) within the Canadian Cordillera. Economic Geology, vol. 109, p. 827-858.

Mortensen, J.K., 1992. Pre-Mid-Mesozoic tectonic evolution of the Yukon-Tanana terrane, Yukon and Alaska. Tectonics, vol. 11, p. 836-853.

Nelson, J.L. and Bellefontaine, K.A., 1996. The geology and mineral deposits of north-central Quesnellia: Tezzeron Lake to Discovery Creek, central British Columbia. BC Ministry of Energy, Mines and Petroleum Resources, Bulletin 99, 112 p.

Nelson, J.L., Colpron, M. and Israel, S., 2013. The Cordillera of British Columbia, Yukon, and Alaska: Tectonics and metallogeny. *In:* Tectonics, Metallogeny and Discovery: The North American Cordillera and Similar Accretionary Settings, M. Colpron, T. Bissig, B.G. Rusk and J.F.H. Thompson (eds.), Society of Economic Geologists, Inc., Special Publication 17, p. 53-103.

Piercey, S.J. and Colpron, M., 2009. Composition and provenance of the Snowcap assemblage, basement to the Yukon-Tanana terrane, northern Cordillera: Implications for Cordilleran crustal growth. Geosphere, vol. 5, p. 439-464, doi: 10.1130/GES00505.1.

Tafti, R., 2005. Nature and origin of the Early Jurassic copper (-gold) deposits at Minto and Williams Creek, Carmacks copper belt, western Yukon: examples of deformed porphyry deposits. Unpublished MSc thesis, University of British Columbia, 213 p.

Tempelman-Kluit, D.J., 1974. Reconnaissance geology of Aishihik Lake, Snag and part of Stewart River map-areas, west-central Yukon. Geological Survey of Canada, Paper 73-41, 97 p.

Tempelman-Kluit, D.J., 1984. Geology, Laberge (105E) and Carmacks (105I), Yukon Territory. Geological Survey of Canada, Open File 1101, scale 1:250 000.

Tempelman-Kluit, D.J., 2009. Geology of Carmacks and Laberge map areas, central Yukon: Incomplete draft manuscript on stratigraphy, structure and its early interpretation (*ca.* 1986). Geological Survey of Canada, Open File 5982, 399 p.

Tempelman-Kluit, D.J. and Wanless, R.K., 1975. Porassium-Argon age determinations of metamorphic and plutonic rocks in the Yukon crystalline terrane. Canadian Journal of Earth Sciences, vol. 12, p. 1895-1909.

Topham, M.J., Allan, M.M., Mortensen, J.K., Hart, C.J.R., Colpron, M. and Sack, P.J., 2016. Crustal depth of emplacement of the Early Jurassic Aishihik and Tatchun batholiths, west-central Yukon. *In:* Yukon Exploration and Geology 2015, K.E. MacFarlane and M.G. Nordling (eds.), Yukon Geological Survey, p. 233-251.

Watson, E.B., Wark, D.A. and Thomas, J.B. 2006. Crystallization themometers for zircon and rutile. Contributions to Mineralogy and Petrology, vol. 151, p. 413-433.

Woodsworth, G.J., Anderson, R.G. and Armstrong, R.L., 1991. Plutonic Regimes, Chapter 15. *In:* Geology of the Cordilleran Orogen in Canada, H. Gabrielse and C.J. Yorath (eds.), Geological Survey of Canada, Geology of Canada, no. 4, p. 491-531; *also Geological Society of America, The Geology of North America, vol. G-2*.

APPENDICES

The six appendices for this paper are only available digitally. They are included in a .zip file with this document and available from http://data.geology.gov.yk.ca/.

Appendix 1. Analytical methods

Appendix 2. Data table of all SHRIMP analyses for samples CDB-10-102, 103, 105, 106, 107, analyzed at the Geological Survey of Canada. Bold ^{207}Pb-corrected apparent ages are those used in final weighted mean age calculation, data in italics are rejected from age calculations as discussed in text.

Appendix 3. Data table for CA-TIMS analyses for sample 10-SI-223, analyzed at Boise State University.

Appendix 4. Data table for LA-ICPMS analyses for sample 10-SI-223, analyzed at Boise State University.

Appendix 5. Data table for LA-ICPMS analyses for samples MA14-AB6 and 9, analyzed at the University of British Columbia. Bold ^{206}Pb/^{238}U isotopic ages are those used in final weighted mean age calculation, data in italics are rejected from age calculations as discussed in text.

Appendix 6. CL images of zircon from 10-SI-223. Locations of LA-ICPMS spots are shown with dates in Ma. Spot size is 25 microns. Two analyses of Jurassic rims are shown in yellow. Fraction labels for grains dated by CA-TIMS are shown in red.

A-type granite plutons and tin skarns in southeast Yukon: Mindy prospect and surrounding granites of 105C/9

Tim Liverton
Watson Lake, Yukon

Liverton, T., 2016. A-type granite plutons and tin skarns in southeast Yukon: Mindy prospect and surrounding granite of 105C/9. *In:* Yukon Exploration and Geology 2015, K.E. MacFarlane and M.G. Nordling (eds.), Yukon Geological Survey, p. 151-164.

ABSTRACT

In the southeast Yukon, immediately southwest of the mid-Cretaceous Cassiar suite plutons,is a northwest-trending suite of anorogenic one-mica granites called the Seagull suite. This suite is comprised of the Seagull and Hake batholiths, Ork and Thirtymile stocks and an un-named intrusion to the northwest. These B and F enriched granites are associated with various forms of tin mineralization, including skarns. The Mindy prospect in the Thirtymile Range contains a variety of metasomatic silicate and borate and fluoride minerals. Tin (Sn) mineralization is found as cassiterite and borate mineral phases. Mapping has shown that faulting active during metamorphism-metsomatism controlled the distribution of the skarn mineralization. Both mineral chemistry and structural control of mineralization have a significant effect on the economic potential of the Mindy prospect.

[1]*timliv@northwestel.net*

INTRODUCTION

A northwest-trending line of mid-Cretaceous granite plutons in southeast Yukon (Seagull and Hake batholiths, Ork stock, Thirtymile stock and one un-named stock) have been recognized as being distinct from the larger Cassiar suite of intrusions that are immediately to the east of the Seagull suite trend. They are one-mica monzo to alkali feldspar granites which have similar to A-type plutons in chemistry, texture (occasional rapakivi texture) and fluorine-boron-tin (F-B-Sn) mineralization. Tin-rich skarns, greisens and tin±niobium (Nb)±tantalum (Ta) sheeted vein stockworks are associated with the Seagull batholith but the Thirtymile and Ork stocks have peripheral tin or tungsten (W) skarns.

The Mindy prospect (Fig. 1), tested with shallow diamond drilling by Newmont Mining Corp. in 1981, is a greisen-altered skarn characterized by primary, high temperature calc-silicate assemblages that have been formed in, and peripheral to, extensional faults above a buried stock and have been replaced by iron-rich greisenized B-F-Sn skarn mineral assemblages.

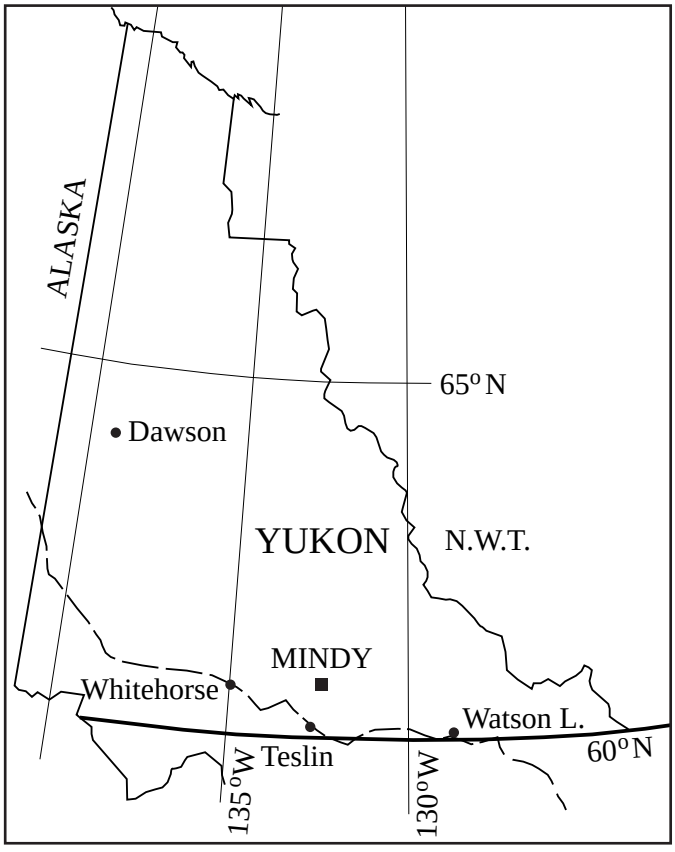


Figure 1. *Location of the Mindy prospect.*

Skarn mineralization may have a variety of tin minerals: cassiterite, vonsenite [$3(Fe,Mg)O{\cdot}2Fe_2O_3{\cdot}SnO_2{\cdot}3B_2O_3$], hulsite [$(Fe^{2+},Mg)_2{\cdot}(Fe^{3+},Sn)BO_5$], nordenskiöldine [$CaSn(BO_3)_2$] and malayaite [$CaSn(SiO_5)$] associated with fluoborite [$Mg_3(F,OH)_3BO_3$]. The borates and silicates are metallurgically refractory and only the cassiterite is of economic interest; as a result, a total Sn analysis may give a misleading result for evaluation of a prospect. The proportion of oxide tin (as cassiterite) to tin borates and fluorides in the Mindy prospect is estimated to be somewhat greater than 50%.

This paper discusses some of the 1992 work plus a re-evaluation of Sn mineralogy through examination of original thin sections and 23 new thin and polished sections cut from drill core stored in the H.S. Bostock Core Library.

GRANITES

The Thirtymile Range contains mid-Cretaceous (101 Ma; Liverton, 1992; Liverton *et al.*, 2001) stocks of monzogranite to alkali feldspar granite according to the Streckeisen classification (LeMaitre, 2004). Two lithofacies of biotite-only granite make up the bulk of the outcropping Thirtymile stock to the northwest of the Mindy prospect (Fig. 2). A volumetrically minor hornblende-bearing porphyry forms a disaggregated syn-plutonic dike within the Thirtymile stock and is the only amphibole-bearing lithofacies seen in the pluton and the Seagull suite. A lithium-mica topaz leucogranite crops out at the southeast corner of the Thirtymile stock and forms ladder dikes in the biotite-bearing 'even-grained' lithofacies. The leucogranite also forms 1-5 m dikes and three sills that contain spectacular concentrations of topaz. The leucogranite may be classified as an alkali feldspar granite *sensu stricto* since the plagioclase is at least 95% albite. A similar lithofacies forms the just-exposed Ork stock and adjacent dikes that are 2.5 km southeast of the Mindy prospect. The Thirtymile and Ork leucogranites consist of a quartz-albite-orthoclase-zinnwaldite-topaz-fluorite mineral assemblage contianing accessory fergusonite.

The Thirtymile and Ork stocks, together with the Seagull and Hake batholiths, were considered as a sub-suite of the Cassiar intrusions by Liverton (1992), called the Seagull-Thirtymile suite and identified as having A-type affinity (Liverton and Alderton, 1994; Liverton and Botelho, 2001; Liverton *et al.*, 2005). Subsequent work on the Cretaceous granites of the Northern Cordillera added a further pluton to the NW as being part of this suite, renamed

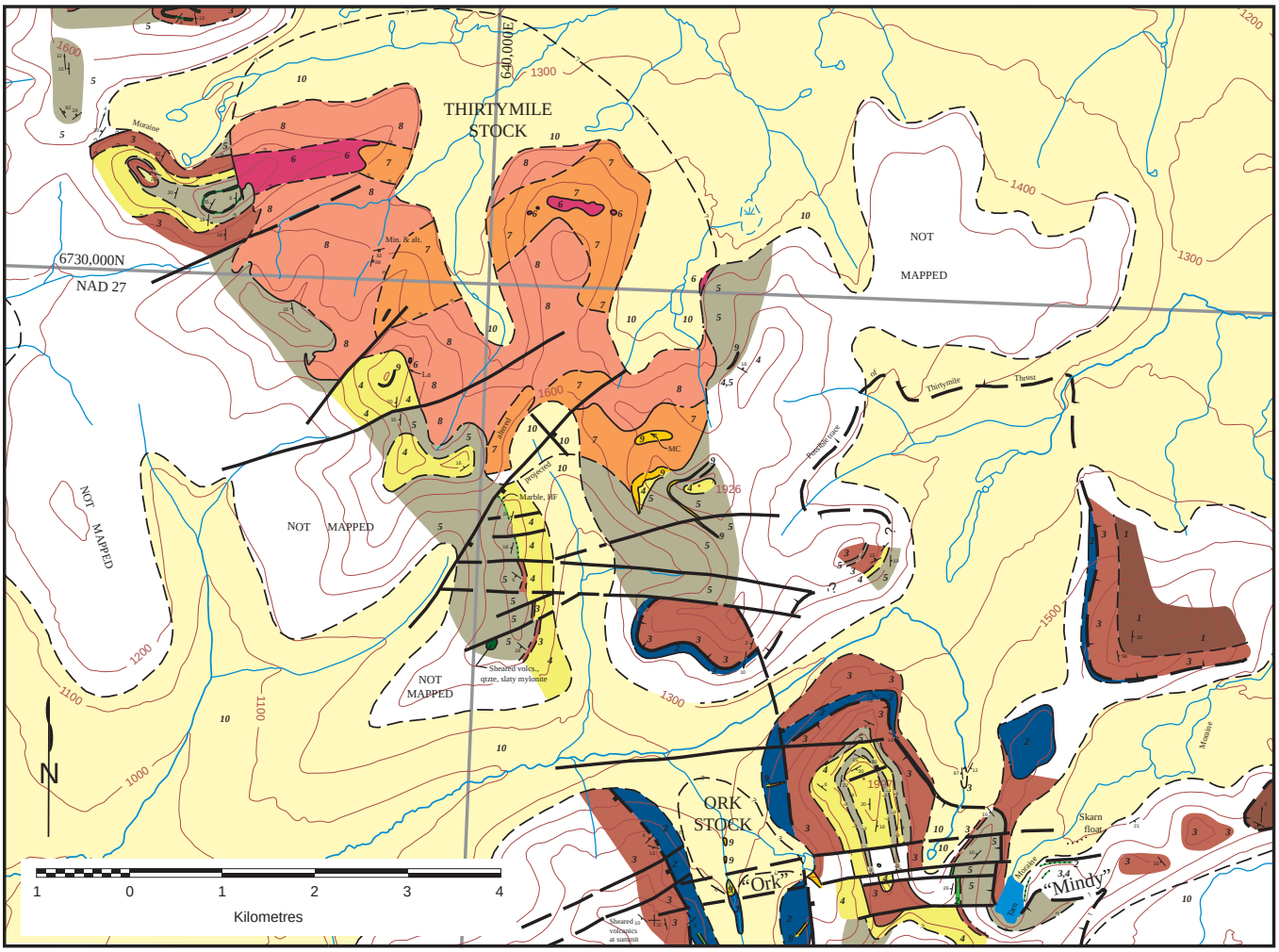


Figure 2. *Geology of the Thirtymile Range. Mapping 1987-1988, by T. Liverton.*

them as simply the Seagull suite, which is recognized as distinct from the Cassiar intrusions, and confirmed their anorogenic nature (Rasmussen, 2013). They are metaluminous to weakly peraluminous and conform to type A_1 of Eby (1992), *i.e.*, they are anorogenic (Fig. 3; Liverton and Botelho, 2001).

The Thirtymile and Ork leucogranites are the most chemically evolved (*i.e.*, fractionated) granites in the Northern Cordillera (Rasmussen, 2013), having Rb/Sr contents exceeding 3000. They might be considered the plutonic analogue to the topaz rhyolites, such as found from Colorado to New Mexico (Christianson *et al.*, 1986). They form the apical portion of batholiths which were emplaced at shallow depth (no more than 2 km), as indicated by common miarolitic cavities and pod pegmatites. These magmas were highly enriched in alkalis, Rb, Li, with B and anions (F^-, Cl^-). This B and halogen enrichment would have allowed the granitic magma to remain as a melt to <650°C, producing a compositional trend different to the 'normal' quartz enrichment process (Fig. 4a). Halogen-enriched granites fractionate to albite-enriched compositions, and due to protracted melt/aqueous fluid and fluid/vapour fractionation, as well as their reduced nature, are able to concentrate high field strength elements (HFSE) into the hydrothermal phase: notably Sn, Nb, Ta (Lehman 1990). Shallow depth of emplacement of the pluton, and being located in the apical part of a batholith, is essential for the development of the F-B mineralization. An 'inheritance' of those metals (*i.e.*, that the source rocks were anomalous in HFSE) might be possible (Lehmann, 1990) but fractionation processes in low-temperature reduced melts are most important for mineralization. In the Seagull suite, halogen enrichment is reflected in the unusual mineralogy at the Mindy and Ork prospects, these are greisenized skarn in the classification of Kwak (1987).

Analyses of Fe-Li micas ranging from siderophyllite to zinnwaldite from the Seagull suite granites indicate a sequence of Li-enrichment in the micas displaying progressive fractionation from the least evolved lithofacies, the Thirtymile porphyry, through the Hake granite, Seagull granite, and the Thirtymile biotite granite, to the zinnwaldite of the leucogranite (leucogranite and biotite-bearing lithofacies of the Thirtymile plutons are shown in Figure 4b,c). Biotite compositions indicate that these granites were distinctly reduced (Fig. 4c): biotite $\{Fe^{2+}/(Fe^{2+}+Fe^{3+})\} = 0.811\text{-}0.965$, magma $fO_2 \leq$ NNO buffer (Liverton and Botelho, 2001). The progression to extremely Li-rich micas (trioctahedral 1M zinnwaldite) may be a particular trait of the anorogenic granite.

The Li-mica leucogranite of the Mindy stock exhibits three forms of hydrothermal mineralization at its southern contact: rare cm-scale beryl pegmatite, cm-scale lepidolite-topaz greisen veins and, presumably the last event, mm-scale joints that carry hematite. It is remarkable that a granite carrying very little total iron is capable of exsolving Fe-rich hydrothermal fluid, but this is evident in the retrograde/greisen stage skarn mineralization at the Mindy prospect.

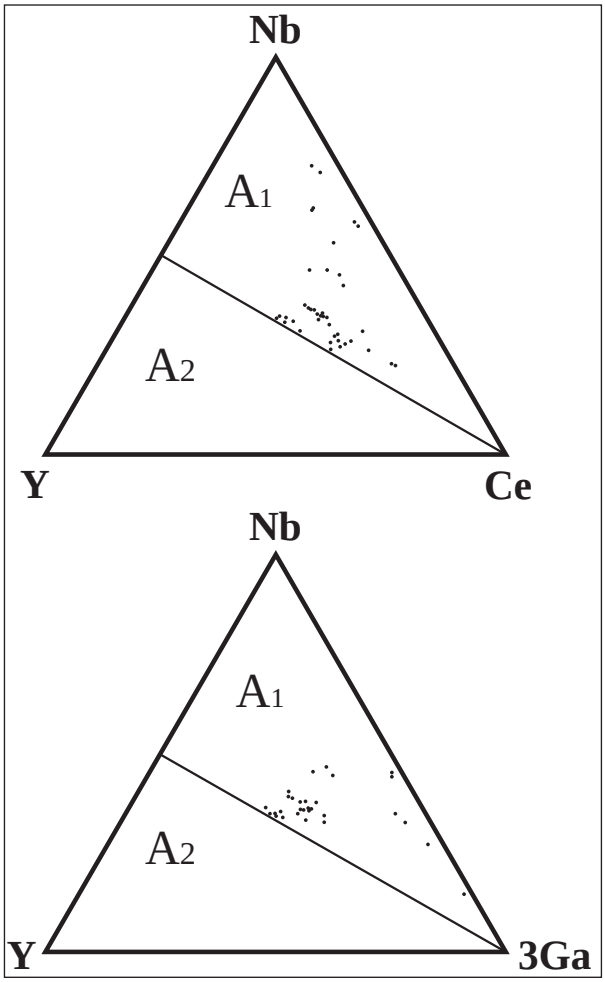


Figure 3. *Eby discriminant plots for anorogenic granites showing compositions of the Thirtymile and Ork stocks (Eby, 1992).*

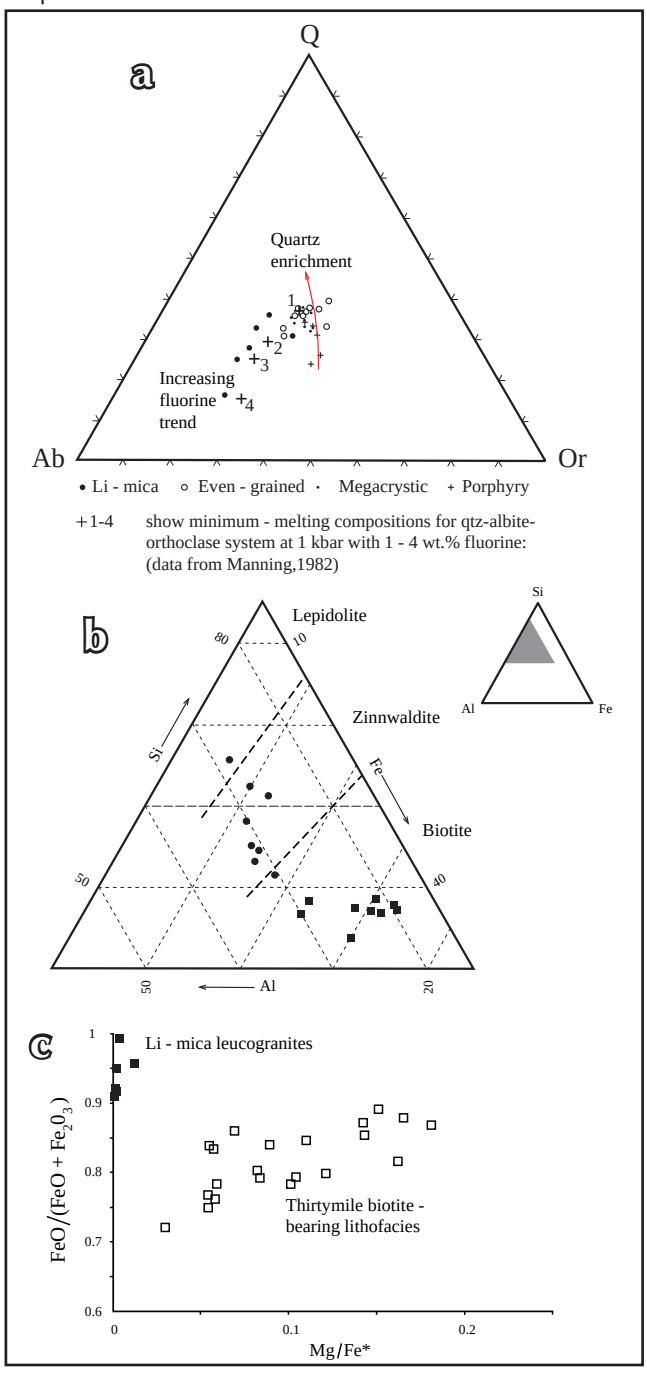


Figure 4. *(a) Proportions of quartz-albite-orthoclase for the various lithofacies of the Thirtymile and Ork stocks compared to experimental data for a fluorine-bearing system. (b) Chemical data for Thirtymile and Ork micas. Cation proportions of Al-Si-Fe for Fe-Li micas from Thirtymile granites. (c) Chemical data for Thirtymile and Ork micas. Ferrous iron proportion to Mg/Fe ratio of micas ($FeO/(FeO + Fe_2O_3)$ vs. Mg/Fe* plot).*

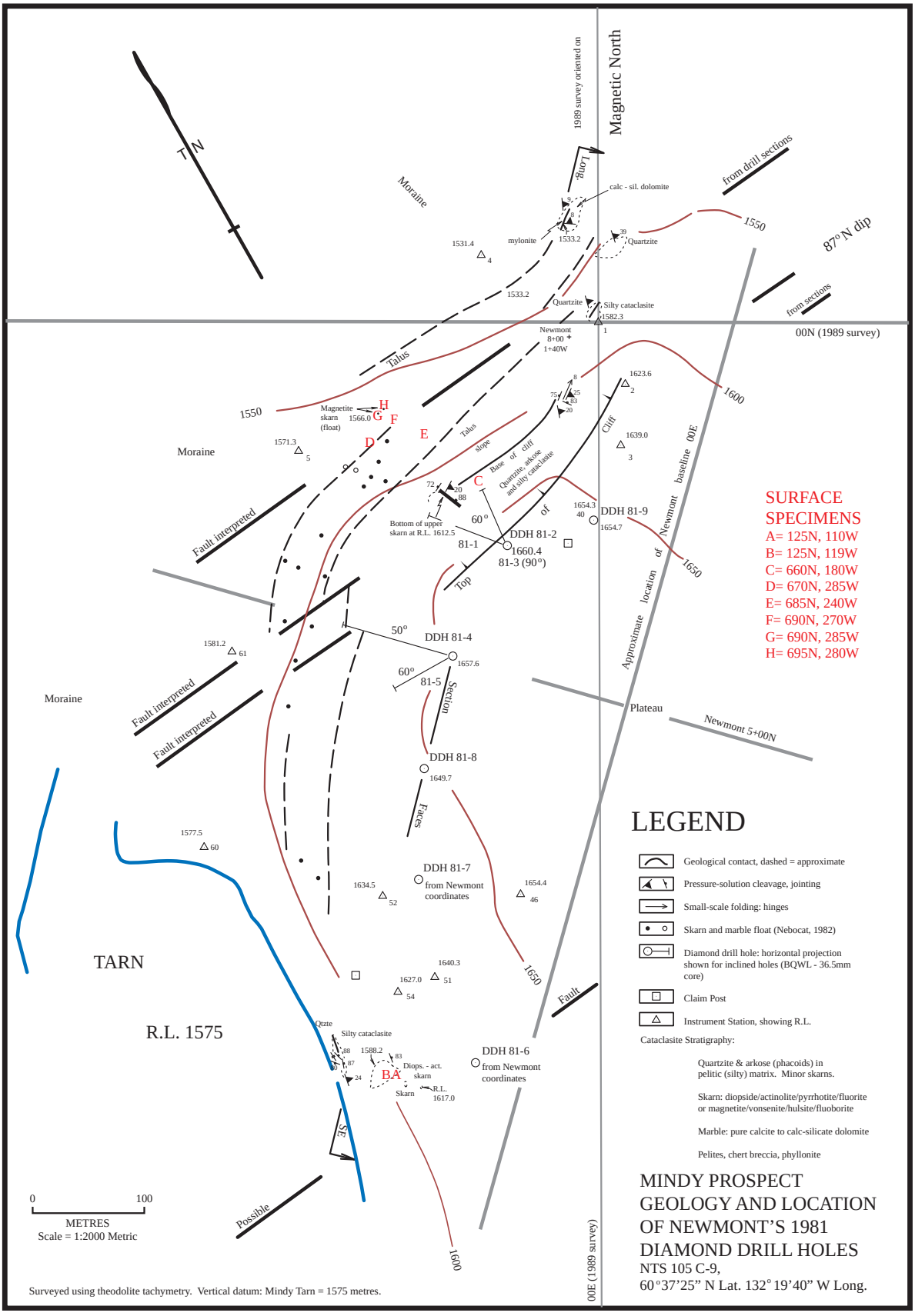


Figure 5. *Detailed map of the Mindy prospect showing trend of the lower skarn horizon and location of diamond drill holes.*

MINDY PROSPECT

The Mindy prospect (Fig. 5) consists of sparse exposure and frequent float of two marble-skarn horizons within siliciclastic rocks that are similar to Proterozoic to lower Paleozoic continental assemblages, probably the rifted continental basement for the Yukon-Tanana terrane. Imbrication of the siliciclastic sequence is likely, and a phacoidal fabric predominates throughout the Range. Mapping (Liverton, 1992) indicated the presence of at least three east-striking extensional faults that transect the property and which have been interpreted to be the principal 'plumbing' for the introduction of hydrothermal fluids into the carbonates. These faults have little obvious displacement and likely were associated with granite intrusion. This is best shown to the west of Mindy where a scheelite-bearing diopside skarn is developed alongside one such fault (Figs. 2 and 5), which projects through the mineralized portion of the Mindy prospect. An interpretation of diamond drill sections (Liverton, 1990) indicates that the lower carbonate-skarn unit, the only potentially economic horizon, is boudinaged (Fig. 6). Away from the extensional faults it consists of pure calcite marble. On the Mindy property the carbonates locally dip from 9° to 25° to the east. Two skarn horizons crop out at the Mindy prospect.

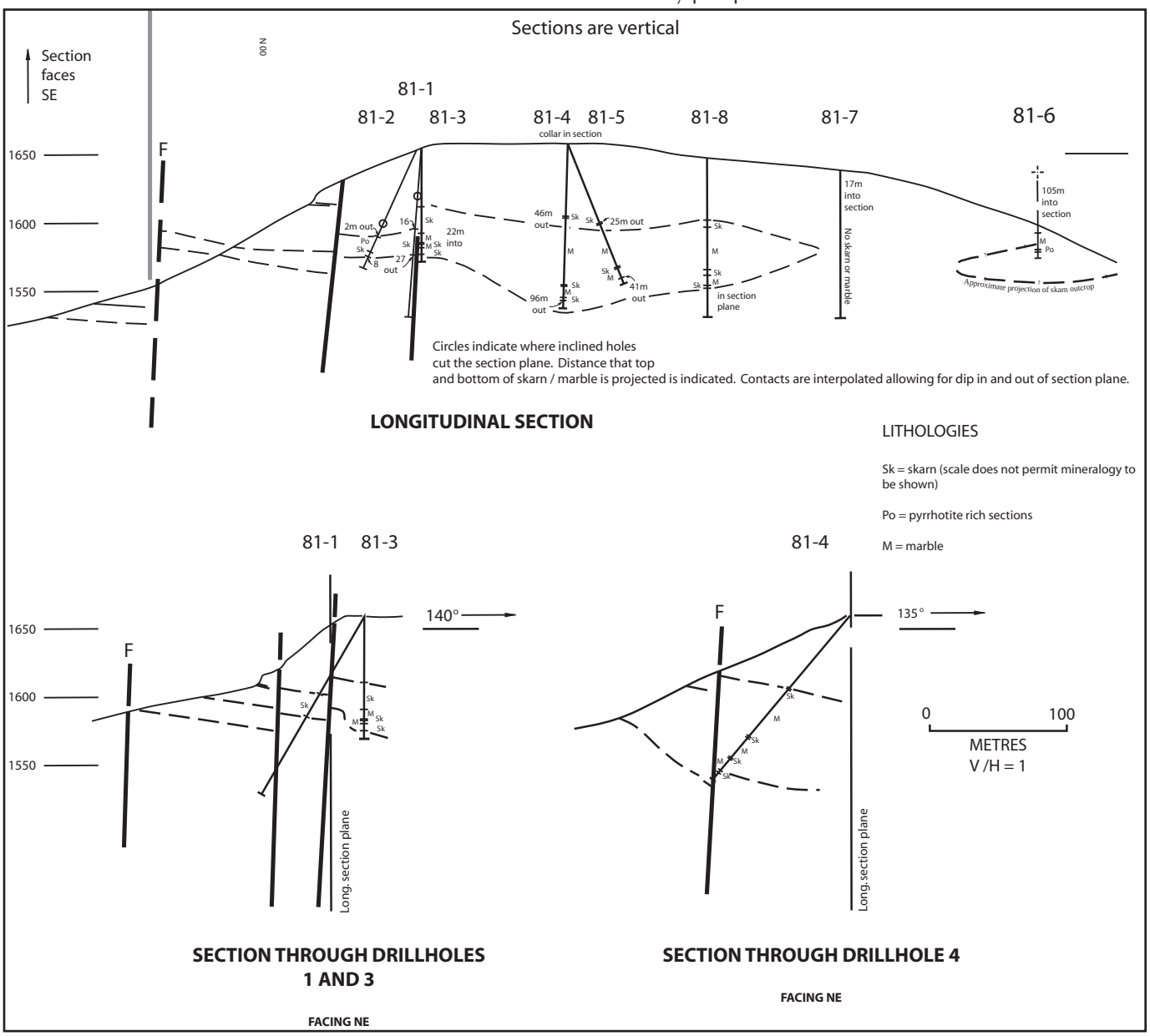


Figure 6. *Longitudinal and cross sections through drillholes 81-1 to 8, of the 1981 Newmont diamond drilling at Mindy prospect.*

The upper skarn consists of vesuvianite-grossular-calcite skarn with acicular vesuvianite crystals up to 40 mm long. No tin mineralization has been noted from this horizon. The margins of the coarse skarn grade into aphanitic 'calc-silicate hornfels' (diopside-hedenbergite) in contact with siliciclastic metsediments, that corresponds to the bimetasomatic skarn type of Kwak (1987). The garnet of this horizon (approximately 21% andradite) is significantly more aluminous than that of the lower skarn, presumably reflecting separate protoliths of different chemistry.

The skarn of the lower horizon developed in the major marble unit adjacent to the extensional faults. Textural evidence indicates that the original protolith controlled much of the skarn mineralogy, and that migration of many chemical components during contact metamorphism and metasomatism was limited. The fine-grained hornfels S-C fabric that developed during imbrication is preserved in calc-silicate mineralogy.

The process of skarn formation has had an obvious structural control. Development of successive retrograde and greisenized skarn assemblages has each accompanied fracturing of earlier skarn. Cataclasis of pyroxene, that has a range of compositions from salite to ferrosalite, indicates continued early brecciation. Disequilibrium in composition over the scale of a thin section is common in the central mineralized part of the skarns (Fig. 7).

The most striking texture of later greisenized skarn is the intricately banded 'wrigglite' (*c.f.*, Kwak and Askins, 1981; Kwak, 1987). Wrigglite texture displays contorted layers of magnetite and sulphides with phengite or talc, lesser amounts of fluorite, fluoborite and corroded relicts of chondrodite and vesuvianite. The wrigglite zones are discordant to host-rock bedding, hence representing fracture systems and the wrigglite layers themselves may be cut by several generations of microfractures, <1 mm to 3 mm wide that carry phengite, talc and scarcer ferrophengite or serpentine.

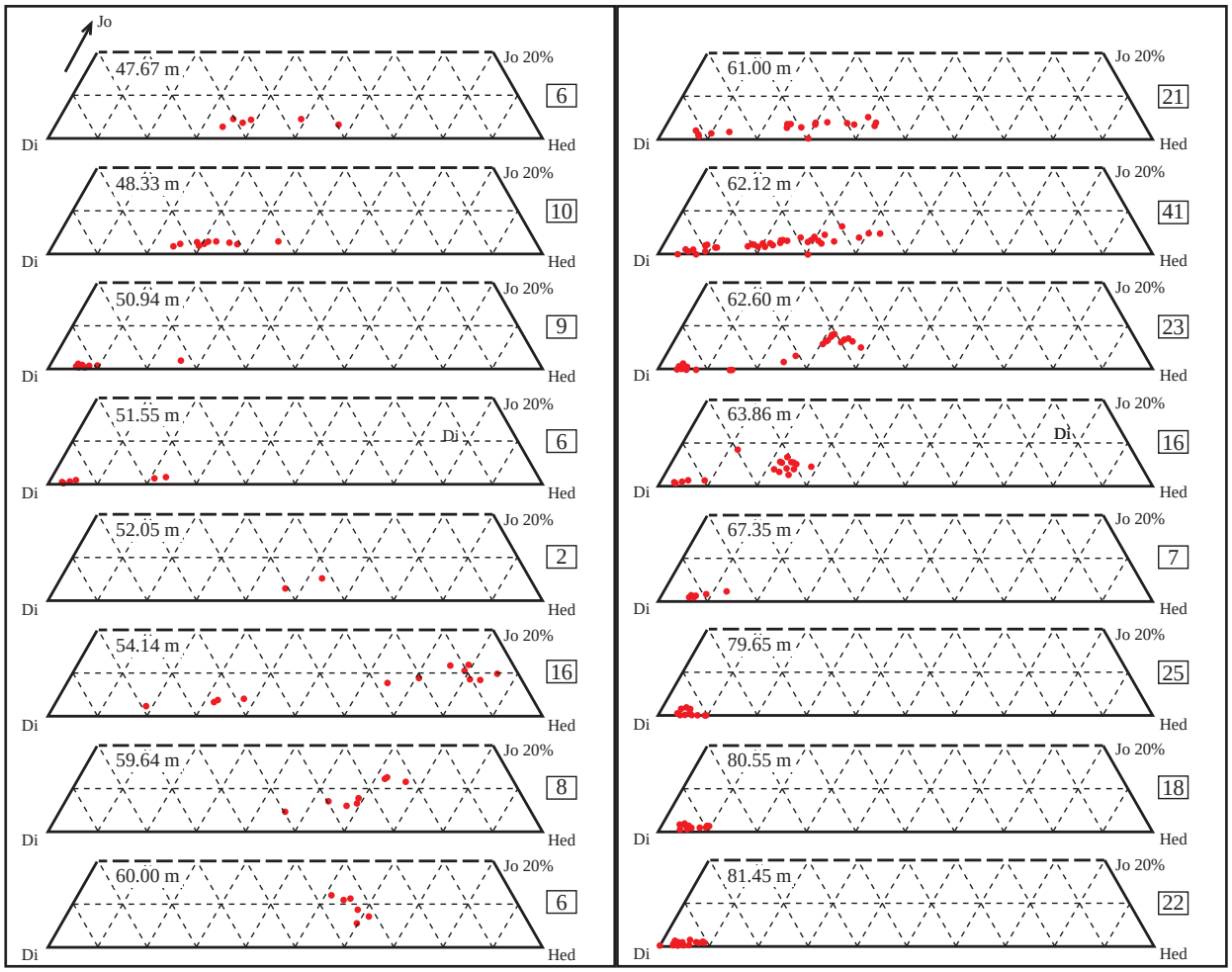


Figure 7. *Proportions of diopside-johannsenite-hedenbergite in skarn pyroxenes from drill hole 81-3, from electron microprobe analyses. Each diagram shows the range of compositions across one thin section. Numbers of analyses are shown in boxes to the right.*

Figure 8 gives a graphical log of DDH 2 to illustrate skarn distribution through the marble horizon and Figures 9-13 illustrate mineralogy, structure and texture of the skarn units.

The various stages of skarn mineralization are as follows:

- *Primary skarn:* garnet-vesuvianite, diopside ± larnite, wollastonite in calcite marble. Increasing Fe content from pyroxene to hedenbergite. Vein skarns of garnet ± arsenopyrite in pure marble. First fluorine mineralization as chondrodite.
- *Early Fe-F-Sn mineralization:* replacement of marble by magnetite-fluorite-cassiterite.
- *Retrograde alteration:* tremolite to actinolite along fractures altering garnet and pyroxene.
- *Greisen alteration and mineralization:* fluoborite alteration of pyroxene skarns, later (?) alteration to massive magnetite-vonsenite-hulsite-fluoborite (often containing relict chondrodite); pyroxene skarn replaced by fluoborite-vonsenite; voluminous wrigglite skarn.
- *Late retrograde alteration:* serpentine growth along fractures and grain boundaries.

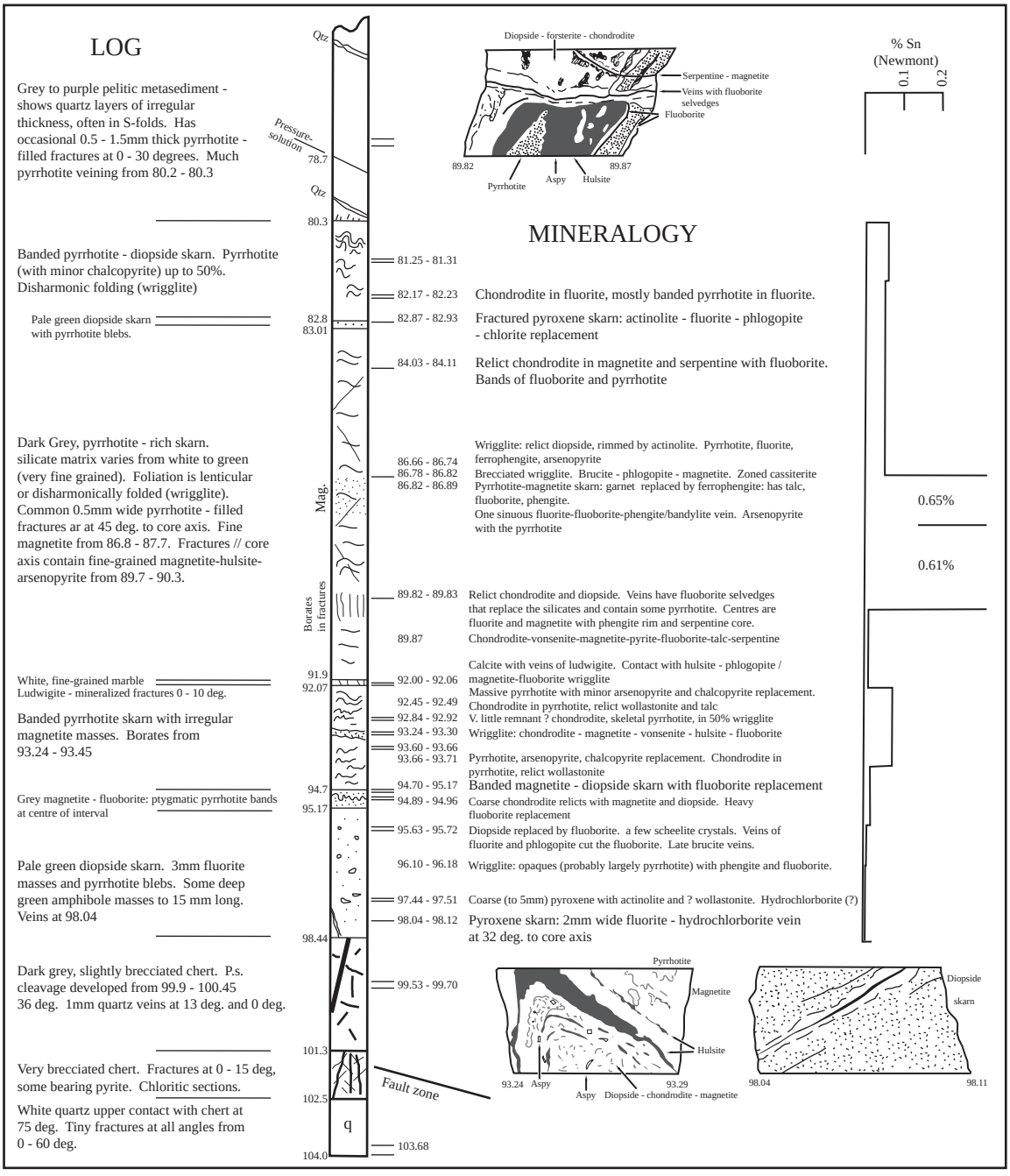


Figure 8. *Log of skarn horizon from Mindy DDH 81-2: dip -60°; Az 006°; Collar R.L. 1660.4 m.*

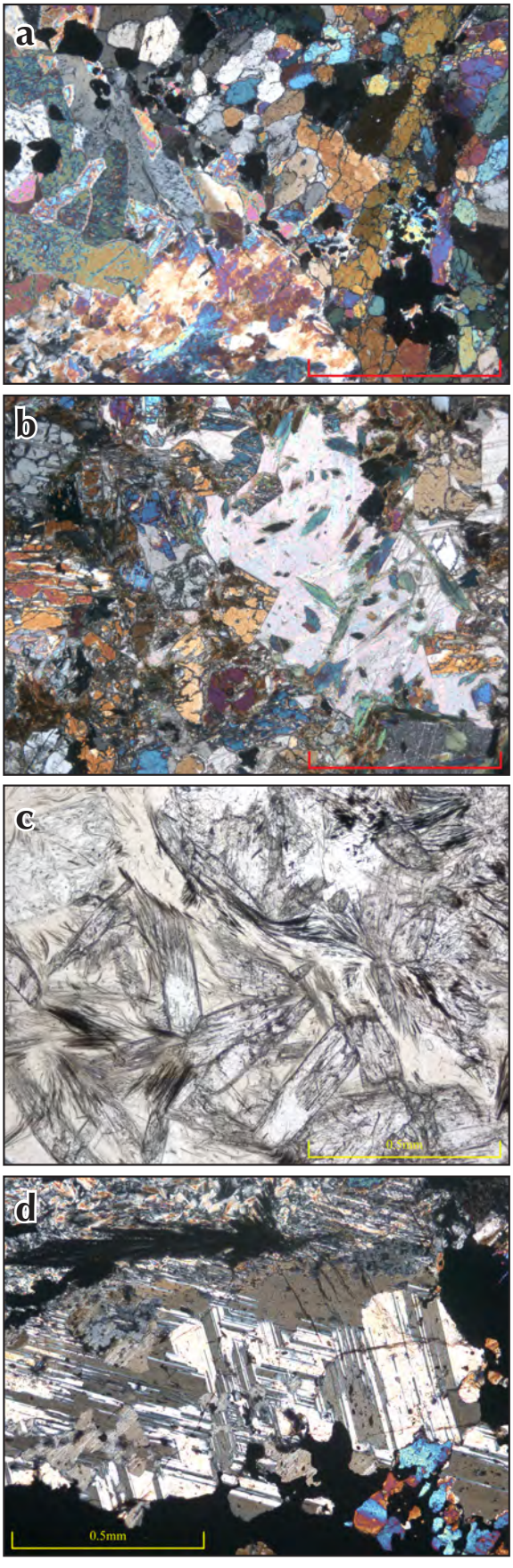




Figure 10. *Drillhole 81-4, 149.72 m. Plane polarized transmitted light on: 'stitched' mosaic of 60 photomicrographs. Sheared and retrograde altered skarn. Garnet in the bottom-right corner and centre, showing some zoning. Diopside is in the bottom-left corner and upper part of the image. Actinolite alteration has followed horizontal fractures which carry fluorite and some serpentine. Three en-echelon tension gashes in the top-left corner are filled with serpentine and quartz. These show evidence of at least six crack-seal events. Scale bar 1 mm.*

Figure 9. *(a) Surface sample (670N, 285W): diopside skarn replaced by fluoborite (SW half of the image). Transmitted light, crossed polarizers, 1 mm scale bar. (b) Surface sample (125N, 110W): diopside skarn with remnant carbonate containing actinolite and crystals of (?) larnite. Serpentine alteration has followed cleavages and gain boundaries in the pyroxene. Transmitted light, crossed polarizers, scale bar 1 mm. (c) Surface sample (670N, 285W): detail of the fluoborite field in (9a). Acicular inclusions are vonsenite and the irregular SE-NW vein is serpentine. Plane polarized transmitted light, 0.5 mm scale bar. (d) DDH 81-2 sample (92.45 m): chondrodite in sulphide. Transmitted light, crossed polarizers, scale bar 0.5 mm.*

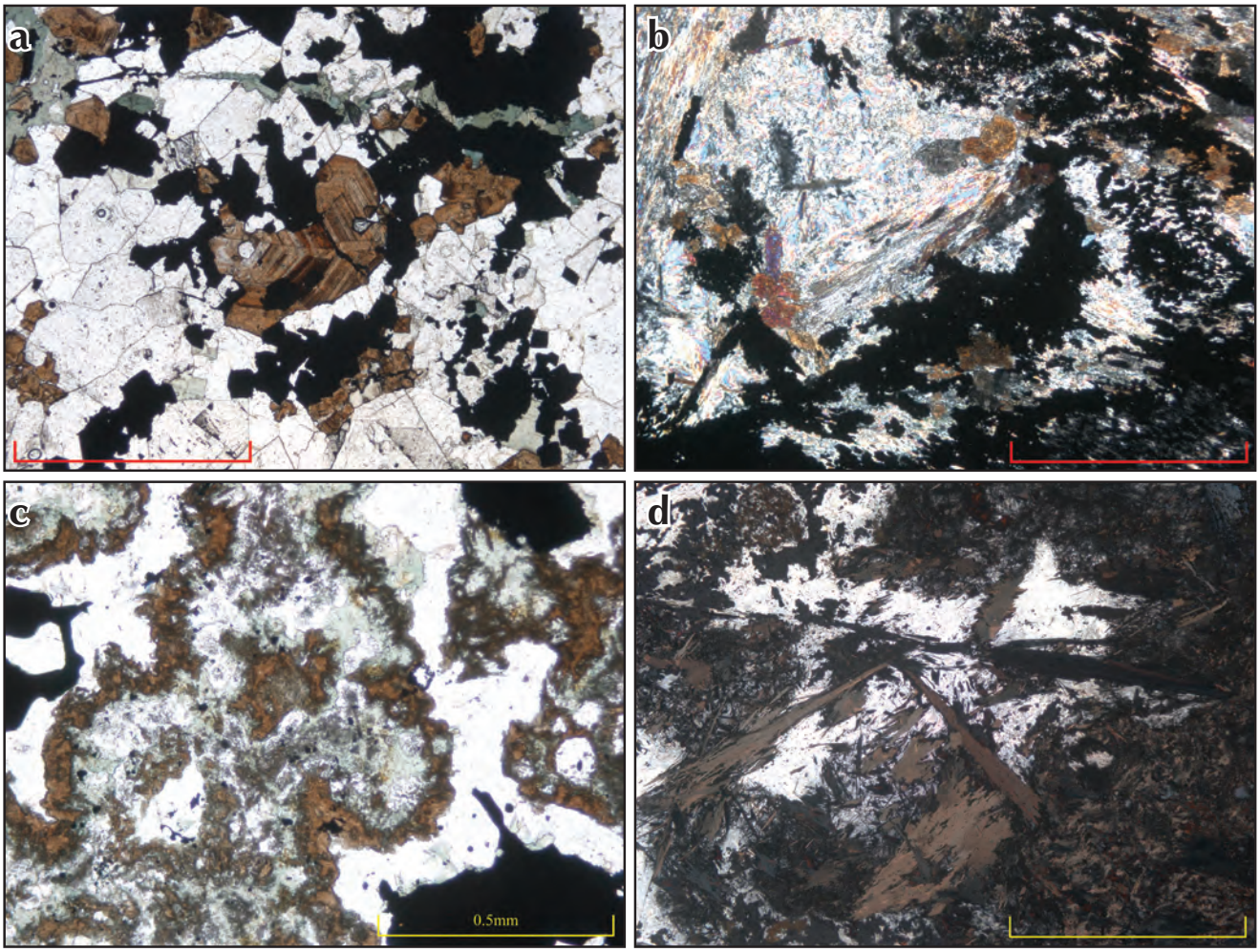


Figure 11. *(a) DDH 81-5B (109.06 m): cassiterite in fluorite with magnetite. The section has cut the cassiterite through a geniculate twin. Plane polarized transmitted light, 1 mm scale bar. (b) DDH 81-8 (49.0 m): wrigglite with cassiterite. Pyrite forms the wrigglite texture and the cassiterite is in a matrix of talc and possibly some phengite. Transmitted light, crossed polarizers, scale bar 1 mm. (c) DDH 81-5B (106.75 m): wrigglite texture shown by cassiterite (brown). Fluoborite and fluorite fill the atoll-like structure. The opaques are sulphides. Plane polarized transmitted light, 1 mm scale bar. (d) DDH 81-8 (48.92 m). Borates: vonsenite (acicular) and hulsite (curved). Incident (reflected) light with polarizers at 85°. Scale bar 1 mm.*

SKARN CHEMISTRY

Compositions of pyroxenes, amphiboles, garnets and vesuvianite were determined using energy dispersive X-ray analysis with a Jeol electron microprobe on polished thin sections and block specimens taken from diamond drill core. The most complete section of pyroxene analyses through the lower (main) skarn was obtained from drill core of DDH 81-3. Two populations of pyroxene are evident: a tight group of 0-12% hedenbergite (interpreted as the 'primary' pyroxene) and a group defined by a wide variation of compositions from the same stratigraphic intervals, interpreted as being formed by successively iron-rich metasomatic fluid events (Fig. 7). The garnet of the main skarn horizon is andradite-grossular, composed of <4% spessartine and <6% almandine components (the method of Droop (1987) was used to estimate Fe^{3+}). The main skarn varies from 58-99% andradite, with the exception of the garnet found with vesuvianite of DDH 81-3, 81.45 m (andradite ≈ 18%).

Chemical evolution of the skarn metsomatism is interpreted to have begun as a high temperature alteration of the carbonate host rock by mostly silica introduction to produce the larnite high temperature (800°C) calcic skarn. Subsequent garnet-vesuvianite skarns, followed by diopside-rich primary skarns, and then successive Fe-enrichment of the hydrothermal fluid resulted in a

range of pyroxene, from salite to hedenbergite; retrograde alteration produced amphibole assemblages. Late introduction of HF produced the fluorite/chondrodite which was followed by the greisenized magnetite-phengite-talc wrigglite skarns that contain the bulk of the tin. Cassiterite was probably first to crystallize in the F-rich massive magnetite stage, and the crystallization of borate-fluoride minerals accompanied the later greisen alteration. The latest retrograde stage is represented by serpentine formation and occasional bandylite [CuB(OH)4Cl] (Fig. 12d). Prominent bleached zones as selvages to fractures in the siliciclastic unit above the lower skarn, which have been attributed elsewhere to $CaCl_2$ 'exhaust solutions' from metasomatism, indicate that abundant chloride was present with the boron to form this unusual mineral, bandylite.

TIN MINERALIZATION

Although no quantitative analysis for tin was performed on the silicate phases, the spectra from electron microprobe energy-dispersive analyses were frequently examined qualitatively for tin peaks. None were found, and tin levels in the garnet, pyroxene, amphiboles and vesuvianite are expected to be significantly less than 0.5%. Tin mineralization does not obviously occur until the early greisenized skarn stage, appearing first as cassiterite in magnetite-phlogopite altered marble, and later as fluoride-borate minerals accompanying magnetite-fluorite-fluoborite in the wrigglite skarn. The visible tin mineralization, as cassiterite, vonsenite or hulsite phases (Fig. 12), accompanies a massive introduction of iron as magnetite and often lesser amounts of pyrrhotite and

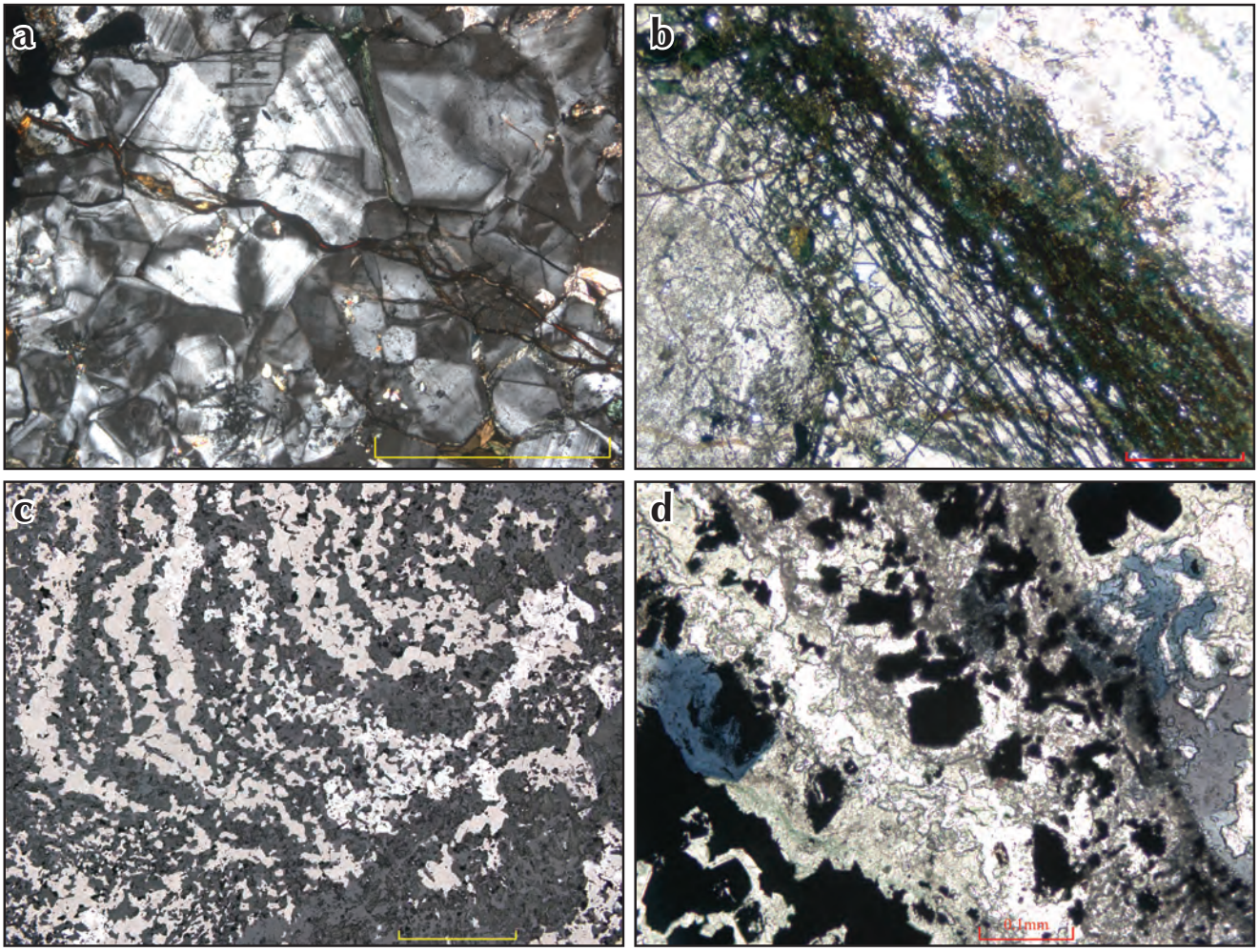


Figure 12. *(a) DDH 81-4 (150.0 m): birefringent, sector-twinned andradite. Transmitted light, crossed polarizers, scale bar 1 mm. (b) DDH 81-5B (105.08 m): microfaulting in skarn. Garnet at the bottom-left, vesuvianite at the top-right and actinolite retrograde alteration along the shear zone. Transmitted light, crossed polarizers, scale bar 1 mm. (c) DDH 81-2 (86.66 m): wrigglite comprised of magnetite and pyrrhotite (pale yellow) in fluorite and fluoborite. Incident (reflected) light with crossed polarizers. Scale bar 1 mm. (d) DDH 81-4 (148.4 m): bandylite (blue, hexagonal) in fluorite and serpentine. Plane polarized transmitted light, 0.1 mm scale bar.*

pyrite into the skarn. In one specimen, pyrite alone has been observed to form wrigglite texture with the fluorides and phengite (Fig. 12c). Nordenskiöldine was indicated by SEM scan from the sample collected at 685N, 290W (Fig. 5). A summary of skarn mineralogies (tin minerals in bold) can be found in Tables 1 and 2.

DISCUSSION

The approximately 100 Ma Seagull suite has peripheral Sn±Ta±Nb mineralization that is particular to southeast Yukon, and is consistent with the anorogenic nature of the intrusions. At the Mindy prospect, B-F rich magma with a low solidus temperature and shallow depth of emplacement allowed protracted melt-aqueous fluid interaction and development of a tin-enriched hydrothermal fluid. This fluorine and boron-rich nature of the A-type granite magma is reflected in greisenized skarn mineralization at the Mindy prospect. Tin mineralization as cassiterite was introduced into the granite aureole with the first massive amounts of iron and fluorine. Subsequent greisenization produced exotic minerals such as vonsenite, hulsite and rare nordenskiöldine. At the Mindy prospect, the mineralization has a structural control: skarns are found within and adjacent to extensional faults that presumably formed the 'plumbing' for hydrothermal fluids released by a shallowly emplaced Li-mica leucogranite stock.

Only cassiterite is viable as a tin ore, and at the Mindy prospect only slightly more than half the tin minerals present are cassiterite which reduces any potential grade. The structural control by faulting active during mineralization has also reduced tonnage potential of the prospect by limiting the areal extent of the skarns. It is possible that the greater tin target at Mindy was never tested by drilling during the 1981 Newmont program: greisens would have been developed in the apical part of the underlying granite, and these might be the larger tin target which is likely to be dominated by cassiterite and possibly contain wolframite.

The Seagull batholith (105B/3) has nine tin skarns recorded in the Yukon MINFILE database. Of these, the JC and Val prospects have recorded the presence of borate or silicate tin minerals. Similar skarn prospects are likely to contain borates, but if only total tin is determined during assay, they would have an exaggerated estimate made of economic potential. An accompanying assay of oxide tin is needed to distinguish economically viable minerals (cassiterite) from total tin. Recognition of the structural control on the skarns (which was not emphasized during the 1981 work at Mindy) is also vital.

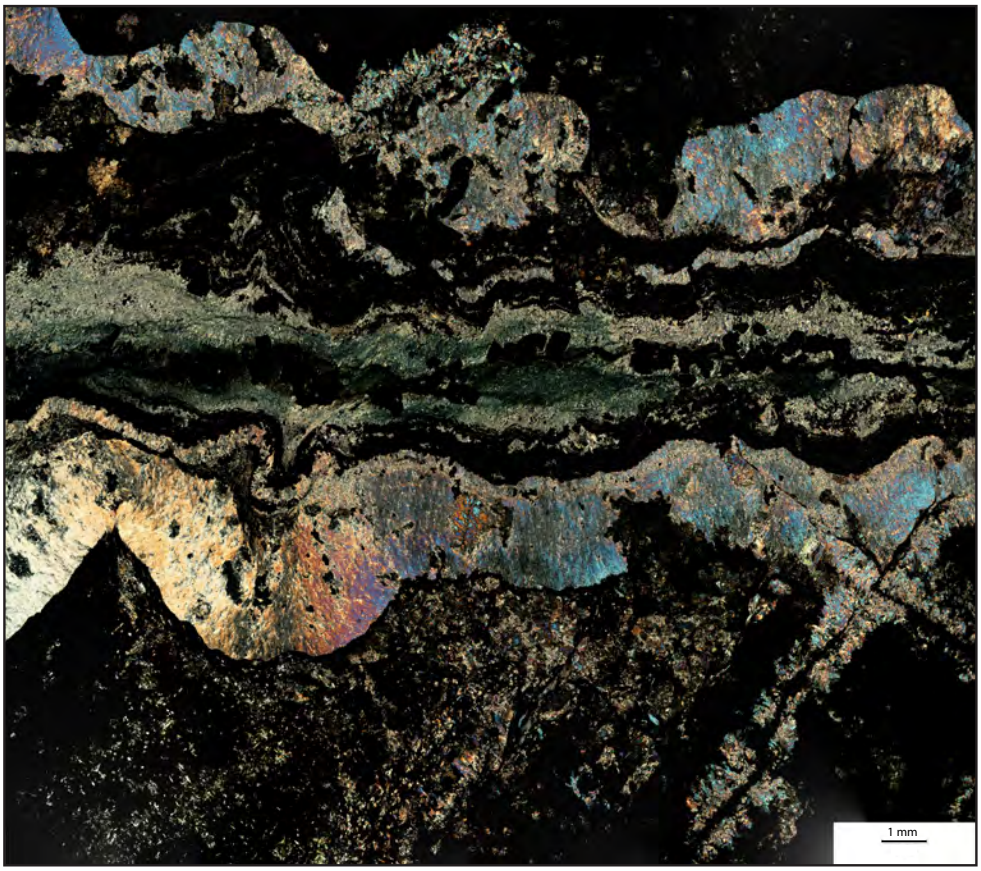


Figure 13. *Transmitted light with crossed polarizers: 'stitched' mosaic of approximately 45 photomicrographs, Massive magnetite-vonsenite mineralization, containing some chondrodite relicts, that has been cut by various generations of veins. The somewhat ptygmatic horizontal vein has fluoborite along its outer margins and euhedral magnetite in serpentine in the centre. A broad intermediate margin of talc contains corroded chondrodite. Magnetite, talc and fluoborite form the diagonal veins. Scale bar 1 mm.*

Table 1. *Mineralogy of the skarn samples from 1981 Newmont diamond drilling.*

Drill hole	Interval/Depth (m)	Mineralogy
81-1	65.2-65.3	Rock is a quartzite, contains diopside, actinolite
81-1	67.0-67.08	diopside, carbonate, serpentine
81-1	69.55-69.62	diopside, actinolite, serpentine
81-1	73.4-73.49	**cassiterite,** magnetite, talc
81-1	75.42-75.49	wollastonite, fluoborite, **vonsenite**
81-1	76.52-76.56 *pts*	diopside, **hulsite,** pyrrhotite. magnetite
81-1	76.60-76.67	diopside, carbonate, scapolite, magnetite, **cassiterite,** sulphide, phengite.
81-1	77.88-77.92 *pts*	magnetite, wollastonite, fluoborite, **cassiterite.**
81-1	88.0-88.90	vesuvianite, diopside, serpentine
81-1	83.9-84.02	vesuvianite, diopside
81-1	88.4-88.61	Rock is a quartzite, contains biotite, cordierite
81-2	89.87 *lts*	chondrodite, **vonsenite,** magnetite, pyrite, fluoborite, talc, serpentine
81-2	86.66-86.74 *pts*	diopside, actinolite, pyrrhotite, fluorite, ferrophengite, pyrite, chalcopyrite
81-2	86.82-86.89 *lts*	pyrrhotite, ferrophengite, talc, fluoborite, bandylite, arsenopyrite
81-2	89.87 *lts*	chondrodite, **vonsenite,** magnetite, pyrite, fluoborite, talc, serpentine
81-2	92.45-92.49 *pts*	pyrrhotite, arsenopyrite, chalcopyrite, chondrodite, wollastonite, diopside, talc
81-2	93.66-93.71 *pts*	fluoborite, fluorite, pyrrhotite, arsenopyrite
81-2	96.10-96.18	pyrrhotite, phengite, fluoborite, serpentine.
81-4	70.17-70.25 *pts*	diopside, magnetite, pyrrhotite, arsenopyrite, garnet
81-4	142.50	magnetite, sphalerite, talc, fluoborite, bandylite, phengite
81-4	148.30 *pts*	magnetite, pyrrhotite, fluoborite, fluorite, arsenopyrite
81-4	148.40-148.5 *pts*	ferrophengite, magnetite, pyrrhotite, arsenopyrite, chalcopyrite, bandylite, serpentine
81-4	149.72-149.82 *lpts*	garnet, salite, ferroactinolite, pyrrhotite, fluorite
81-4	150.00 *pts*	garnet, hedenbergite, actinolite, pyrrhotite
81-4	151.15-151.23 *pts*	diopside, pyrrhotite
81-5B	66.72 *pts*	garnet, salite, actinolite, pyrite
81-5B	103.47-103.51	andradite, diopside
81-5B	104.85-104.92 *pts*	actinolite, fluorite, **cassiterite,** ferrophengite
81-5B	105.08	garnet, vesuvianite, actinolite
81-5B	106.75 *pts*	magnetite, pyrrhotite, chalcopyrite, ferrophengite, **cassiterite**
81-5B	108.87 *pts*	magnetite, pyrrhotite, arsenopyrite, fluorite, talc, **cassiterite**
81-5B	109.06-109.11	**cassiterite,** phengite, quartz, pyrrhotite
81-5B	111.25-111.34 *pts*	fluorite, phengite, fluoborite, quartz, amphibole, pyrrhotite, **cassiterite**
81-8	48.92-49.0 *lpts*	magnetite, **hulsite, vonsenite**
81-8	49.00 *pts*	pyrrhotite, **vonsenite, hulsite,** fluoborite, serpentine
81-8	66.8 *pts*	garnet, diopside

Note: *pts* indicates a polished thin section of 25 x 50 mm, *lts* a 50 x 75 mm covered thin section, *lpts* a large polished thin section on a 50 x 75 mm slide. Tin minerals are shown in bold.

Grid location*	Mineralogy
125N 110W – 1.5 m	diopside, larnite, actinolite, fluorite
125N 110W – 4 m	diopside, serpentine, fluorite, actinolite, carbonate
125N 119W – 1.5 m	diopside, larnite, calcite, actinolite
660N 180W	rock is a quartzite with phacoidal garnet and diopside
660N 180W (2nd slide)	diopside, vesuvianite, garnet.
670N 285W	diopside, magnetite, garnet, vesuvianite, epidote, **borates**
685N 240W	Rock is a quartzite with a little plagioclase, carbonate layers
690N 270W	chlorite, carbonate in siliciclastics, diopside, epidote
690N 285W	garnet, vesuvianite, carbonate, pyroxene, sphene, epidote
695N 280W	**vonsenite**

*****Coordinates refer to the original Newmont grid (Fig.5). Distances (*e.g.*, 1.5 m) give depth from top of a near vertical face. Tin minerals in bold.

Table 2. *Mineralogy of the skarn hand samples.*

REFERENCES

Christiansen, E.H., Sheridan, M.F. and Burt, D.M. 1986. The geology and geochemistry of Cenozoic topaz rhyolites from the Western United States. Geological Society of America Special Paper 205, p. 82.

Droop, G.T.R. 1987. A general equation for estimating Fe^{3+} concentrations in ferromagnesian silicates and oxides from microprobe analyses, using stoichiometric criteria. Mineralogical Magazine, vol. 51, p. 431-435.

Eby, G.N., 1992. Chemical subdivision of the A-type granitoids: Petrogenetic and tectonic implications. Geology, vol. 20, p. 641-644.

Kwak, T.A.P., 1987. W-Sn skarn deposits and related meteamorphic skarns and granitoids. Developments in Economic Geology, Elsevier, vol. 24, p. 451.

Kwak, T.A.P. and Askins, P.W., 1981. Geology and genesis of the F-Sn-W (-Be-Zn) skarn (wrigglite) at Moina Tasmania. Economic Geology, vol. 76, p. 439-467.

Lehmann, B., 1990. Metallogeny of tin. Lecture Notes in Earth Sciences 32, Springer-Verlag, Berlin, p. 211.

LeMaitre, R.W. (ed.), Strekeisen, A., Zanettin, B., Le Bas, M.J., Bonin, B., Bateman, P., Bellieni, G., Dudek, A., Efremova, S., Keller, J., Lameyre, J., Sabine, P.A., Schmid, R., Sørensen, H. and Woolley, A.R., 2004. A classification of igneous rocks and glossary of terms, 2nd edition. Cambridge University Press, p. 236.

Liverton, T. 1990. Tin-bearing skarns of the Thirtymile Range, NTS Sheet 105 C/9: a progress report. *In:* Yukon Geology Volume 3, T.J. Bremner (ed.), Exploration and Geological Services Division, Indian and Northern Affairs Canada, p. 52-70.

Liverton, T. 1992. Tectonics and metallogeny of the Thirtymile Range, Yukon Territory, Canada. PhD thesis, Royal Holloway, University of London.

Liverton, T. and Alderton, D.H.M., 1994. Plutonic rocks of the Thirtymile Range, Dorsey Terrane: ultrafractionated tin granites in the Yukon. Canadian Journal of Earth Sciences, vol. 31, p. 1557-1568

Liverton, T. and Botelho, N.F., 2001. Fractionated alkaline rare-metal granites: two examples. Journal of Asian Earth Sciences, vol. 19, p. 399-412.

Liverton, T., Mortensen, J.K. and Roots, C.F., 2005. Character and metallogeny of Permian, Jurassic and Cretaceous plutons in the southern Yukon-Tanana Terrane. *In:* Yukon Exploration and Geology 2004. D.S. Emond, L.L. Lewis and G.D. Bradshaw L.H. (eds.). Yukon Geological Survey, p. 147-165.

Liverton, T., Mortensen, J.K. and Roots, C.F., 2005. Character and metallogeny of Permian, Jurassic and Cretaceous plutons in the southern Yukon-Tanana Terrane. *In:* Yukon Exploration and Geology 2004, D.S. Emond, L.L. Lewis and G.D. Bradshaw (eds.), Yukon Geological Survey, p. 147-165.

Manning, D.A.C., 1982. An experimental study of the effects of fluorine on the crystallisation of granitic melts. *In:* Metallization associated with acid magmatism, A.M. Evans (ed.), p. 191-203.

Rasmussen, K., 2013. Mid-Cretaceous magmatism and mineralization in the southwestern Northwest Territories and southern Yukon: a geochronological, geochemical, and isotopic approach towards a model for the Cretaceous tectonic, magmatic, and metallogenic evolution of the northern Cordillera. PhD thesis, University of British Columbia.

U-Pb zircon age and Pb isotopic constraints on the age and origin of porphyry and epithermal vein mineralization in the eastern Dawson Range, Yukon

J.K. Mortensen, C.J.R. Hart
Mineral Deposit Research Unit, University of British Columbia

J. Tarswell
Rockhaven Resources Ltd.

M.M. Allan
Mineral Deposit Research Unit, University of British Columbia

Mortensen, J.K., Hart, C.J.R., Tarswell, J. and Allan, M.M., 2016. U-Pb zircon age and Pb isotopic constraints on the age and origin of porphyry and epithermal vein mineralization in the eastern Dawson Range, Yukon. *In:* Yukon Exploration Geology 2015, K.E. MacFarlane and M.G. Nordling (eds.), Yukon Geological Survey, p. 165-185, including appendices.

ABSTRACT

Six dikes that are closely associated with the Klaza epithermal vein system in the Mt. Nansen district yield early Late Cretaceous U-Pb zircon ages (78.2-76.3 Ma); this age is similar to that obtained from the porphyry stock that hosts the Cyprus Cu-Mo-Au porphyry occurrence immediately to the southeast. These results support the interpretation that epithermal veins in the Mt. Nansen district are likely genetically related to subvolcanic magmatism. Granodiorite of the Dawson Range batholith that underlies most of the Klaza property gives a U-Pb zircon age of 107.9±0.3 Ma. These dates overlap with previously reported mid-Cretaceous U-Pb zircon ages for felsic dikes associated with the Brown-McDade and related vein and breccia deposits in the Mt. Nansen mine. The new results, together with regional dating and Pb isotopic data from western Yukon, emphasize the metallogenic importance of the "early Late Cretaceous" magmatic-hydrothermal event in this region.

[1]*jmortensen@eos.ubc.ca*

INTRODUCTION

The eastern Dawson Range in west-central Yukon hosts a wide variety of porphyry, epithermal and related styles of mineralization, including those in the Sonora Gulch area as well as the Freegold and Mt. Nansen camps (Fig. 1). Much of the mineralization in this region is known to be "early Late" Cretaceous in age and associated with the Casino plutonic suite (~78-72 Ma; Sonora Gulch, Nucleus, Revenue, Casino); however, at least some intrusion-related deposits, such as Antoniuk (Fig. 1), have yielded unambiguous mid-Cretaceous formation ages (Allan *et al.*, 2013). In addition, some occurrences, such as the Bonanza vein swarm in the Prospector Mountain area (Fig. 1) are spatially and temporally associated with the "late Late" Cretaceous (71-67 Ma) Prospector Mountain suite magmatism and deposition of Carmacks Group volcanic rocks (Allan *et al.*, 2013).

The timing of formation of epithermal vein systems in the Mt. Nansen camp, including the main "Brown-McDade cluster" (Brown-McDade, Huestis, Weber, Flex and Dickson veins; Fig. 2), as well as the extensive area of veining in the Klaza deposit area to the north ("Klaza cluster"; Fig. 2), has been problematic. Mortensen *et al.* (2003) report U-Pb zircon ages ranging from 107.9 ± 0.9 Ma to 109.0 ± 0.7 Ma for northwest-trending quartz-feldspar porphyry dikes that are closely associated with the veins in the main Brown-McDade cluster, and, in the absence of any other direct constraints on the timing of mineralization, concluded that the veins formed at approximately the same time. Hart and Langdon (1998) had previously argued that epithermal veins in the Mt. Nansen camp (including both those in the main camp and the Klaza system) could represent parts of a "porphyry-to-epithermal transition" that was centered on the Cyprus porphyry and contained Cu-Mo-Au porphyry-style mineralization (Fig. 2). However, a Re-Os age of 71.1 ± 0.3 Ma reported by Selby and Creaser (2001) for molybdenite from the Cyprus porphyry deposit was incompatible with such a model if the Mt. Nansen veins were indeed middle Cretaceous in age.

A U-Pb dating study of intrusive rock units that either host or are spatially closely associated with mineralization in the Mt. Nansen area was undertaken. This study also evaluates existing and new measured Pb isotopic compositions of igneous feldspar minerals from many of the intrusions as well as sulphides (mainly galena) from the various deposits and occurrences. The aim of the work is to better constrain the timing of mineralization throughout the eastern Dawson Range, and to test models such as the "porphyry-to-epithermal transition" that was proposed for the Mt. Nansen area. New results resolve some of the questions concerning the age(s) of mineralization in much of the area, although some areas of uncertainty still exist.

GEOLOGY OF THE EASTERN DAWSON RANGE

The eastern Dawson Range is mainly underlain by intermediate to felsic intrusive rocks of the Early Cretaceous Dawson Range batholith (Whitehorse plutonic suite; Fig. 1). Eruptive equivalents of the Whitehorse suite are locally preserved as the Mt. Nansen Group volcanic rocks in the vicinity of Mt. Nansen (Figs. 1 and 2). The batholith was intruded into metamorphic rocks of the Yukon-Tanana terrane, as well as large bodies of Late Triassic and Early Jurassic plutonic rock of the Minto plutonic suite that underlie much of the easternmost end of the Dawson Range (Fig. 1). Small bodies of hypabyssal felsic porphyry of early Late Cretaceous age are widespread in the region; some of these host, or are spatially closely associated with, some of the main mineral deposits and occurrences in the area (*e.g.*, Casino, Nucleus, Revenue). The slightly younger late Late Cretaceous Carmacks Group mafic volcanic rocks cover extensive areas in the eastern Dawson Range (Fig. 1). Paleocene and Eocene felsic intrusive and extrusive rocks are increasingly abundant along the southwestern flank of the Dawson Range.

MINERALIZATION IN THE MT. NANSEN DISTRICT

The Mt. Nansen district (Fig. 2) includes two main concentrations of mineralized veins: the "Brown-McDade cluster", centered approximately 11 km southeast of the top of Mt. Nansen and includes the Brown-McDade vein system that was mined by BYG Resources in 1995-98; and the "Klaza cluster", centered approximately 3 km east-northeast of Mt. Nansen and based on recent exploration work by Rockhaven Resources, contains an inferred resource of 948 koz of gold and 21.8 Moz of silver (Wegnzynowski *et al.*, 2015; Fig. 2).

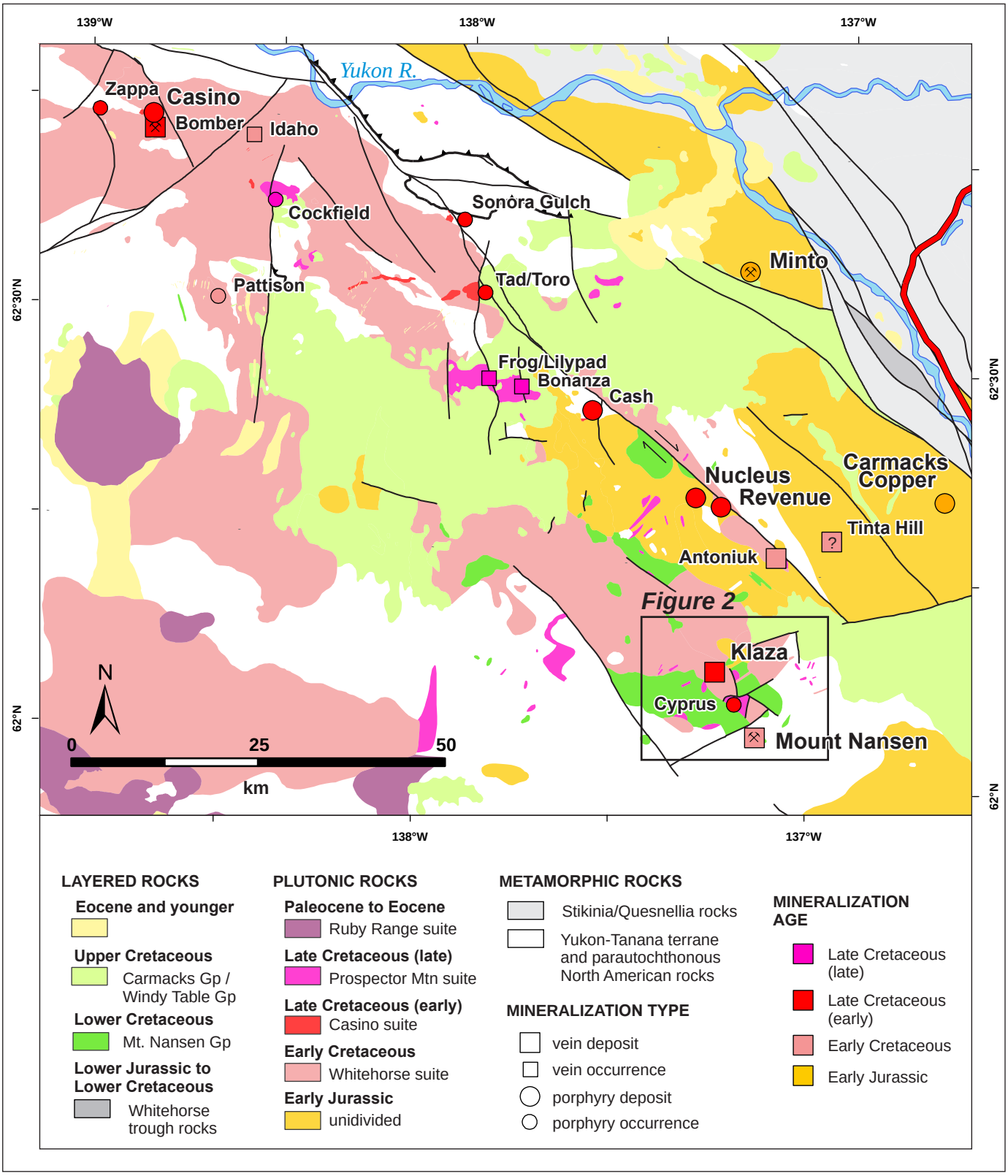


Figure 1. *Regional geology of the central and eastern Dawson Range, showing locations of some of the main mineral deposits and occurrences referred to in the text. Box shows the location of Figure 2.*

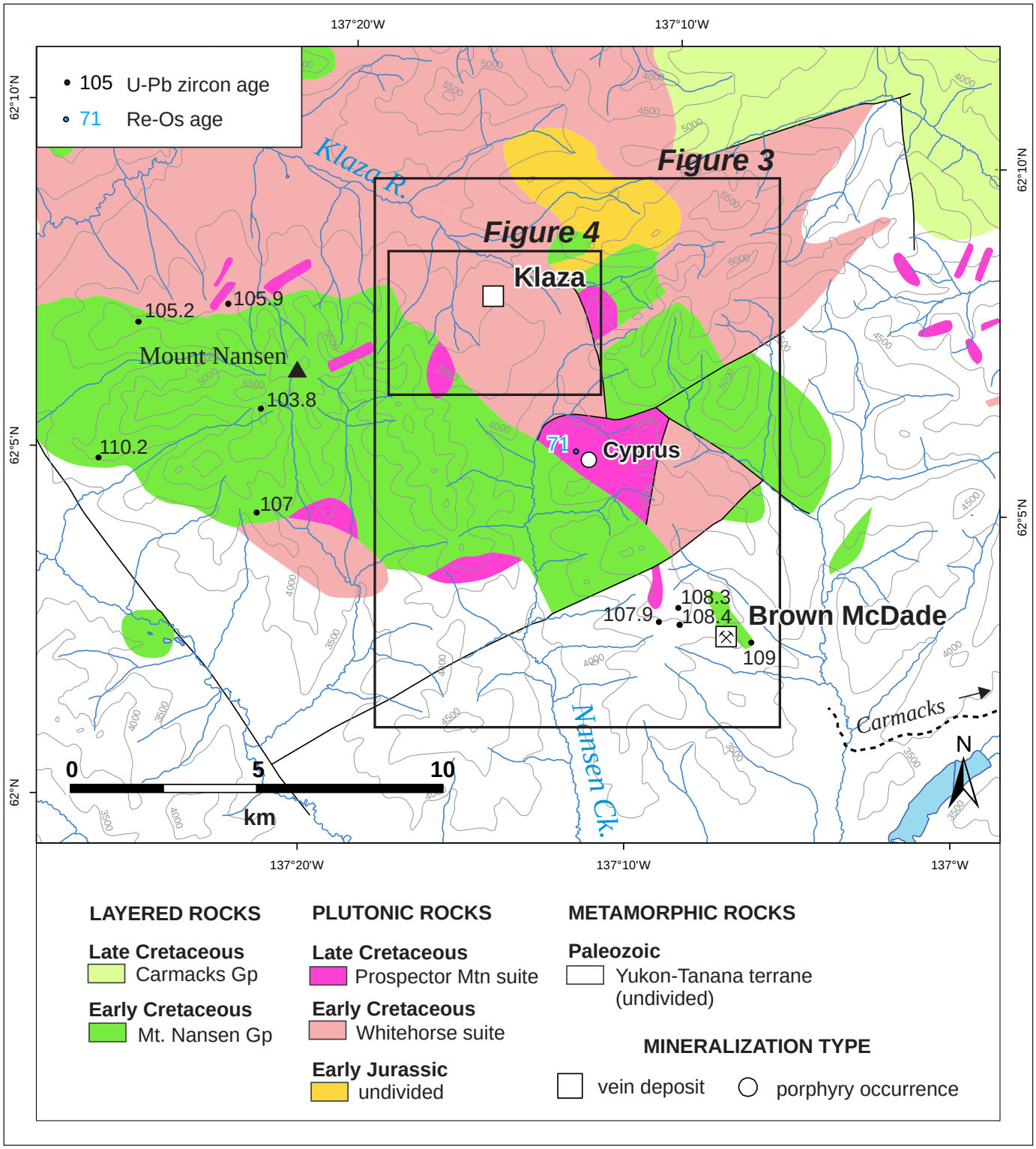


Figure 2. *Geology of the Mt. Nansen District, showing locations of the Klaza and Brown-McDade vein clusters and the Cyprus porphyry. Ages shown in the Brown-McDade cluster are ID-TIMS U-Pb zircon ages from Mortensen et al. (2003); ages for the Mt. Nansen Group are from Mortensen et al. (unpublished); Re-Os age from the Cyprus porphyry is from Selby and Creaser (2001).*

The Brown-McDade cluster consists of veins and deposits south of the Dickson fault, comprising the Webber, Flex, Heustis, Dickson, Vince and Brown-McDade occurrences (Fig. 3; Hart and Langdon, 1998; Anderson and Stroshein, 1998; Stroshein, 1999). These are historically amongst the most economic in the district and cumulatively host a resource of about 1 Mt with grades ranging from 5 to 14 g/t Au and 50 to 300 g/t Ag.

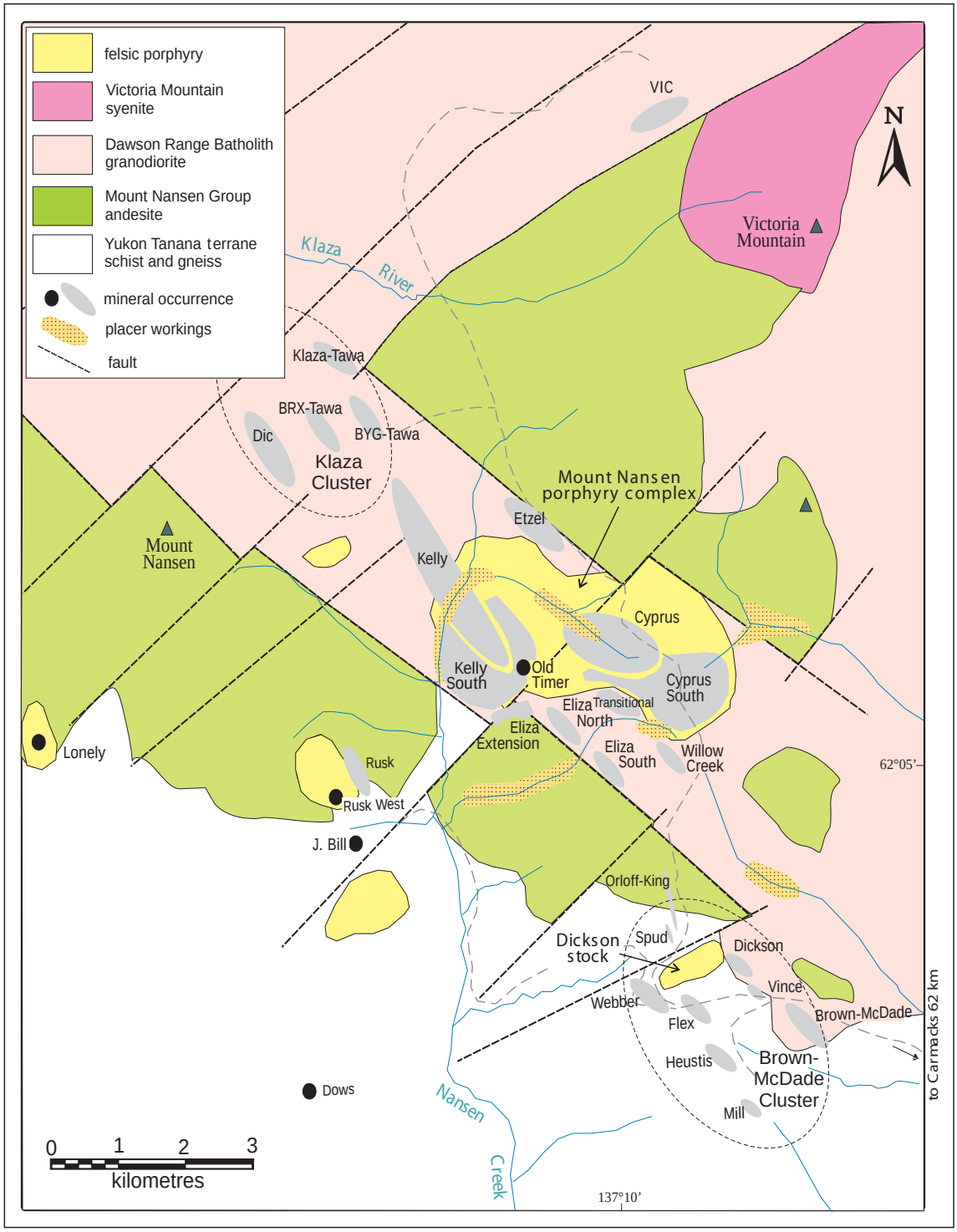


Figure 3. *Geology the Mt. Nansen District including the Brown-McDade cluster in the southeast, the Cyprus porphyry and related occurrences in the central area, and the Klaza cluster in the northwest (modified from Hart and Langdon, 1998).*

Most occurrences are hosted in Yukon-Tanana terrane schist and gneiss, but the Brown-McDade deposit, which is the largest, is mostly hosted in granodiorite. Each occurrence typically includes a 'swarm' of several veins, but may be dominated by a larger, single vein. Most veins are at least partly hosted by, northwest-trending quartz-feldspar porphyry dikes and small quartz-porphyry plugs. Most veins strike northwesterly between 320 and 340° and dip moderate to steeply (65 to 80°) to the southwest. Many of these veins have strike lengths of 500 m or greater, but their extents are variably displaced along north-northeast-striking sinistral strike slip faults. They are typically 0.2 to 0.8 m wide, but locally up to 2.5 m thick. The thicker parts result from intersections with 020°-striking fractures.

The veins are typically crudely banded, but are locally, variably brecciated. The Brown-McDade deposit occurs mostly as a breccia pipe (Stroshein, 1999). All veins are generally similar in mineralogy consisting of 'cherty' fine-grained grey and white quartz, with varying abundances of sulphide minerals dominated by pyrite and arsenopyrite, with essential galena and sphalerite typically to 10%, and lesser stibnite, tetrahedrite and various sulphosalt minerals such as boulangerite and jamesonite.

The Klaza area (Fig. 4) is mainly underlain by massive and unfoliated, medium to coarse-grained, equigranular hornblende-biotite granodiorite and quartz monzonite of the Dawson Range batholith, which is part of the regionally developed Whitehorse plutonic suite. A stock of quartz monzonite to granite, termed the Cyprus porphyry, intrudes the Dawson Range batholith on the southeastern corner of the Klaza property (Figs. 2 and 3). The Dawson Range batholith is cut by a set of northwest-trending, steeply to moderately southwest-dipping fault zones, along which dikes of vari-coloured (grey, green, tan, red and purple) feldspar and quartz-feldspar porphyry have been emplaced (Fig. 4). Individual porphyry dikes commonly pinch and swell along strike, and are up to 30 m wide. They consist of an aphanitic groundmass with up to 15% K-feldspar phenocrysts (1 to 2 mm) and minor biotite and rare quartz phenocrysts. Contacts with the granodiorite range from sharp and undulating to brecciated with locally abundant gouge development. A second, much less common set of northwest-trending dikes is also locally present, particularly in the southeastern part of the Klaza property, near the Cyprus porphyry stock. These dikes are typically fine grained to aphanitic, and appear to be intermediate to mafic in composition. They contain a significant amount of magnetite, and are locally strongly magnetic. These mafic dikes are up to 100 m in width, and are larger and more abundant near the Cyprus porphyry.

The main mineralized zones at Klaza range from 1 to 100 m wide and are usually associated with feldspar porphyry dikes. Mineralization occurs as veins, sheeted veinlets and tabular breccia bodies. The feldspar porphyry dikes generally occupy the same northwest-trending structural zones as the mineralized veins and they are commonly strongly fractured. They are locally cut by the main mineralized veins as well as by late stage white carbonate veinlets. Mineralization at Klaza mainly consists of gold and silver bearing, sulphide-rich veins that comprise pyrite, arsenopyrite, galena, sphalerite, various sulphosalts and electrum in a gangue of quartz, rhodocrosite and barite. The mafic dikes are also locally mineralized, hosting small amounts of disseminated pyrite and pyrite stringers, together with minor chalcopyrite and rare molybdenite. The strongest copper mineralization on the property is always associated with argillic altered versions of the mafic dikes.

The feldspar porphyry dikes at the Klaza property have been interpreted to emanate from the Cyprus porphyry stock to the southeast. Two distinct centres of Cu-Mo ± Au porphyry-style mineralization have been identified within the Cyprus porphyry stock, the Cyprus zone and the Kelly zone (Fig. 3). These zones appear to contain modest grades and be of limited extent (Wengzynowki *et al.*, 2015).

The northwest-trending feldspar porphyry dikes and the mineralized structures at Klaza have been displaced by two northeast trending faults (Fig. 4). The exact timing of these faults is uncertain; however, they appear to be coeval with, or post-date, the mineralized zones on the property.

U-PB ZIRCON GEOCHRONOLOGY

METHODOLOGY

Zircons were separated from 2-4 kg samples using conventional crushing, grinding, wet shaking table, heavy liquids and magnetic separation methods. U-Pb dating of zircons was done using laser ablation (LA-) ICP-MS methods at the Pacific Centre for Isotopic and Geochemical Research (PCIGR) at the University of British Columbia. Analytical techniques employed are as described by Allan *et al.* (2013). Twenty individual

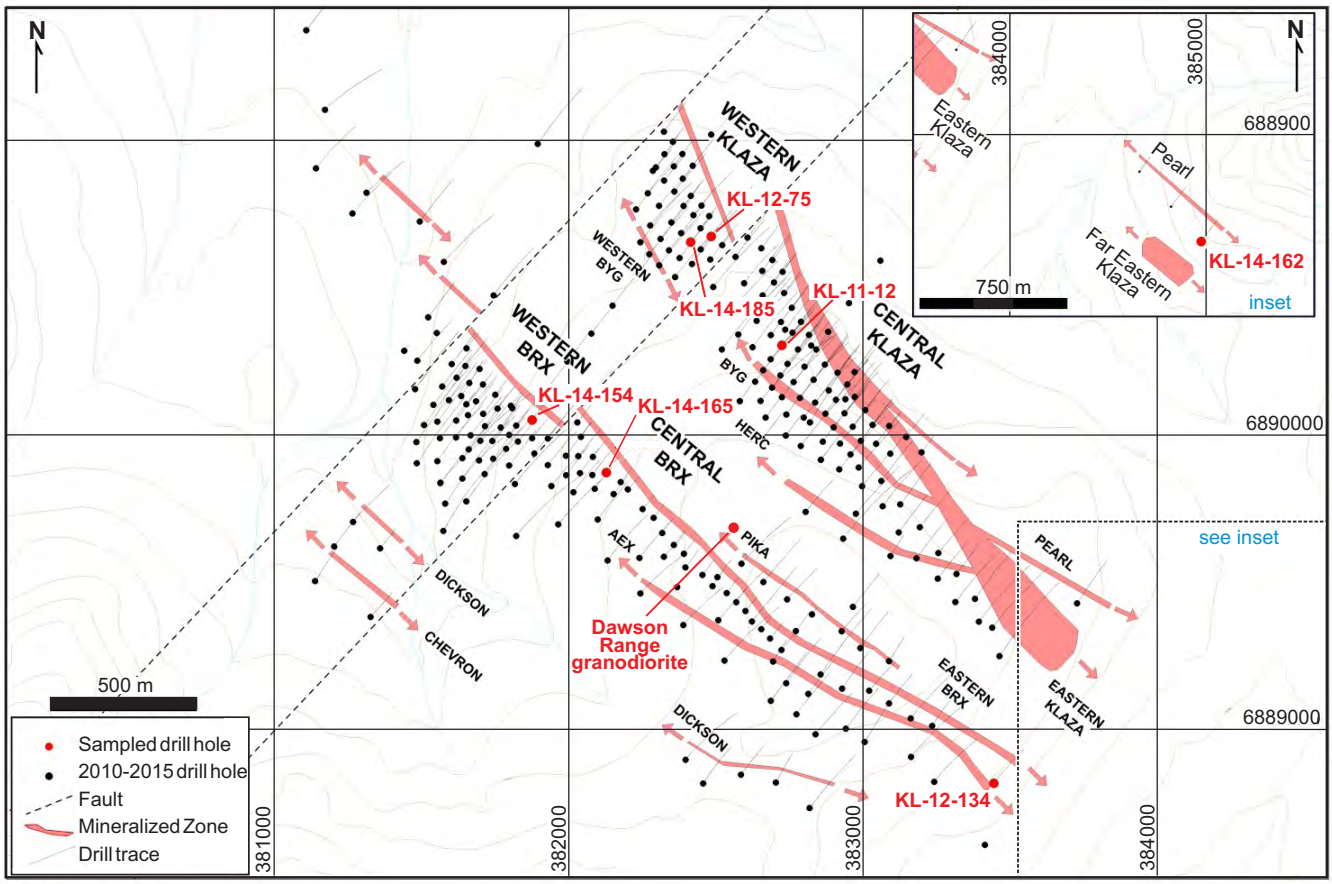


Figure 4. *Map of the Klaza property showing the distribution of the various zones as well as drill holes and the specific locations of samples that were analyzed in this study (modified from Wengzynowki et al., 2015). UTM coordinates are in NAD83 datum.*

zircon grains were analyzed from each sample. Complete analytical data are provided in Appendix 1 and the results are plotted as compilations of the calculated $^{206}Pb/^{238}U$ ages for individual sample analyses in Figures 3 and 4. Errors quoted for final assigned ages are given at the 2σ level.

RESULTS

All zircons analyzed from the Klaza U-Pb samples yielded concordant analyses. Sample locations are shown on Figure 3, and interpretations of the results for each of the samples are presented briefly below.

Granodiorite of the Dawson Range batholith

Twenty zircon analyses from a sample of massive medium-grained granodiorite from the Pika Zone (Fig. 4) yield a weighted $^{206}Pb/^{238}U$ age of 107.9±0.3 Ma (MSWD=0.74; POF=0.78; Fig. 5a).

Feldspar porphyry dikes in the Western Klaza Zone

Twenty zircon grains from a sample of feldspar porphyry from DDH KL-12-75 (189-191 m; Fig. 4) yield a weighted $^{206}Pb/^{238}U$ age of 76.9±0.3 Ma (MSWD=1.00; POF=0.45; Fig. 5b). Eighteen zircon grains from a second feldspar porphyry dike from the Western Klaza Zone in DDH KL-14-185 (0-11.5 m; Fig. 4) yield a weighted $^{206}Pb/^{238}U$ age of 76.8±0.4 Ma (MSWD=1.4; POF=0.14; Fig. 5c). A single grain from this sample gives a much older age ($^{207}Pb/^{206}Pb$ age of 1600.6±40.6 Ma) and represents an older xenocryst likely entrained from underlying metamorphic basement rocks. One of the analyses gave a significantly younger $^{206}Pb/^{238}U$ age, likely related to post-crystallization Pb-loss, and is not included in the calculated weighted average age.

Feldspar porphyry dike from the Western BRX Zone

Eighteen zircon grains from a porphyry dike sample in DDH KL-14-154 (52.1-52.5 m; Fig. 4) yield a weighted $^{206}Pb/^{238}U$ age of 77.1 ± 0.4 Ma (MSWD = 0.78; POF = 0.72; Fig. 5d). Two grains give $^{206}Pb/^{238}U$ ages of 102.6 and 105.0 Ma, and are interpreted to have been xenocrystic zircons entrained from the underlying Dawson Range batholith.

Feldspar porphyry dike from the Central BRX Zone

Sixteen zircon grains from a porphyry dike in DDH KL-14-165 (85.7-87.5 m; Fig 4) give a weighted $^{206}Pb/^{238}U$ age of 76.5 ± 0.4 Ma (MSWD = 0.68; POF = 0.80; Fig. 5e). Four grains give $^{206}Pb/^{238}U$ ages of 105.0-105.7 Ma and a single grain gives an age of 369.7 Ma; these are interpreted to have been xenocrysts from the Dawson Range batholith and the metamorphic basement rocks, respectively.

Feldspar porphyry dike from the Central Klaza Zone

Seventeen zircon grains from a porphyry dike in DDH KL-11-12 (181-187 m; Fig. 4) give a weighted $^{206}Pb/^{238}U$ age of 71.6 ± 0.3 Ma (MSWD = 0.55; POF = 0.92; Fig. 5f). Two grains give slightly younger $^{206}Pb/^{238}U$ ages and are not included in the calculated weighted average age. A single grain gave a $^{206}Pb/^{238}U$ age of 77.1 ± 1.7 Ma. The calculated age for this sample is significantly younger than that of most of the other Klaza dikes that were dated, and it appears to represent a distinctly younger intrusion. The presence of the single 77.1 Ma zircon indicates that the magma did interact to some extent with the "early Late" Cretaceous rocks.

Mafic dike in the Eastern BRX Zone

Sixteen zircon grains from a mafic dike in DDH KL-12-134 (218-221.5 m) give a weighted $^{206}Pb/^{238}U$ age of 78.2 ± 1.0 Ma (MSWD = 0.34; POF = 1.00; Fig. 6a). Four grains give $^{206}Pb/^{238}U$ ages of 107.4-109.8 Ma, and are interpreted to have been xenocrysts entrained from the Dawson Range batholith.

Feldspar porphyry dike from the Far Eastern Klaza/ Pearl Zone

Fifteen zircon grains from a feldspar porphyry dike in DDH KL-14-162 (86.2-86.5 m; Fig. 4) give a weighted $^{206}Pb/^{238}U$ age of 76.3 ± 0.3 Ma (MSWD = 0.49; POF = 0.94; Fig. 6b). Two grains give slightly older $^{206}Pb/^{238}U$ ages and are excluded from the weighted average age calculation. Two other grains gave $^{206}Pb/^{238}U$ ages of 101.4 and 102.6 Ma, and a single grain gave an age of 446.9 Ma; these are interpreted to have been xenocrysts from the Dawson Range batholith and the underlying metamorphic bedrock, respectively.

Cyprus porphyry

Seventeen zircon grains from sample 97-CH-33-3 in the Cyprus porphyry stock give a weighted $^{206}Pb/^{238}U$ age of 76.0 ± 0.4 Ma (MSWD = 0.75; POF = 0.74; Fig. 6c). Three grains give slightly younger $^{206}Pb/^{238}U$ ages, likely reflecting the effects of post-crystallization Pb-loss and were excluded from the weighted average age calculation.

SUMMARY OF KLAZA DATING RESULTS

Results from the dating study of the Klaza samples confirm an Early Cretaceous age of 107.9 ± 0.6 Ma for granodiorite of the Dawson Range batholith in the Mt. Nansen area. All but one of the northwest-trending dikes associated with Klaza mineralization give ages ranging from 78.2 to 76.0 Ma, indicating that these intrusions are part of the ~78-72 Ma Casino plutonic suite. An intermediate composition dike that contains disseminated chalcopyrite and minor molybdenite (sample KL-12-134; Eastern BRX zone), and was initially speculated to be part of the younger Prospector Mountain suite, actually yielded the oldest age at 78.2 ± 1.0 Ma. A sample of the felsic porphyry that hosts the Cyprus Cu-Mo-Au porphyry occurrence returned a crystallization age of 76.0 ± 0.4 Ma, confirming that this body is coeval and likely co-magmatic with the felsic dikes in the Klaza area. One of the quartz-feldspar dike samples from Klaza (KL-11-12; Central Klaza zone) gave a significantly younger age of 71.6 ± 0.3 Ma, suggesting that this body either represents a late stage Casino suite intrusion or (less likely) an early intrusion of the Prospector Mountain suite.

RE-EXAMINATION OF DATING RESULTS FROM THE BROWN-MCDADE CLUSTER

The porphyry dikes at Klaza are very similar to those previously dated in the Brown-McDade cluster, in terms of composition, structural setting in northwest-trending faults, and association with sulphide-rich epithermal veins. However, Mortensen *et al.* (2003) report multi-grain TIMS zircon ages for five porphyry dikes and small stocks from the Brown-McDade cluster ranging from 109.0 to 107.9 Ma, suggesting that these intrusions are temporally related to the Dawson Range batholith. The TIMS data for

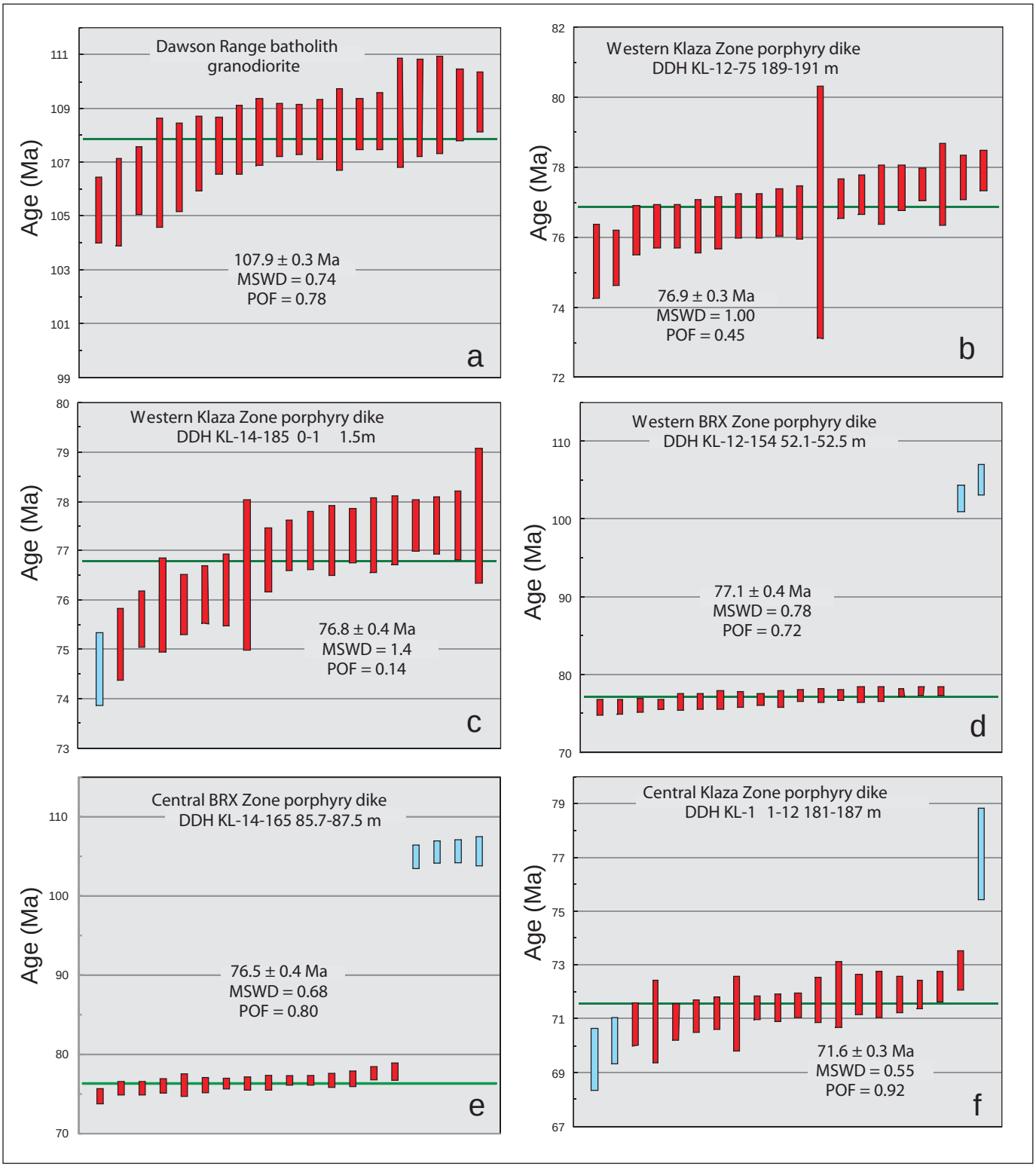


Figure 5. *Plots of $^{206}Pb/^{238}U$ ages for zircons from Klaza igneous samples, with calculated weighted average ages. Error bars are shown at the 2σ level. Analyses shown by blue boxes were not used in calculation of the weighted average ages.*

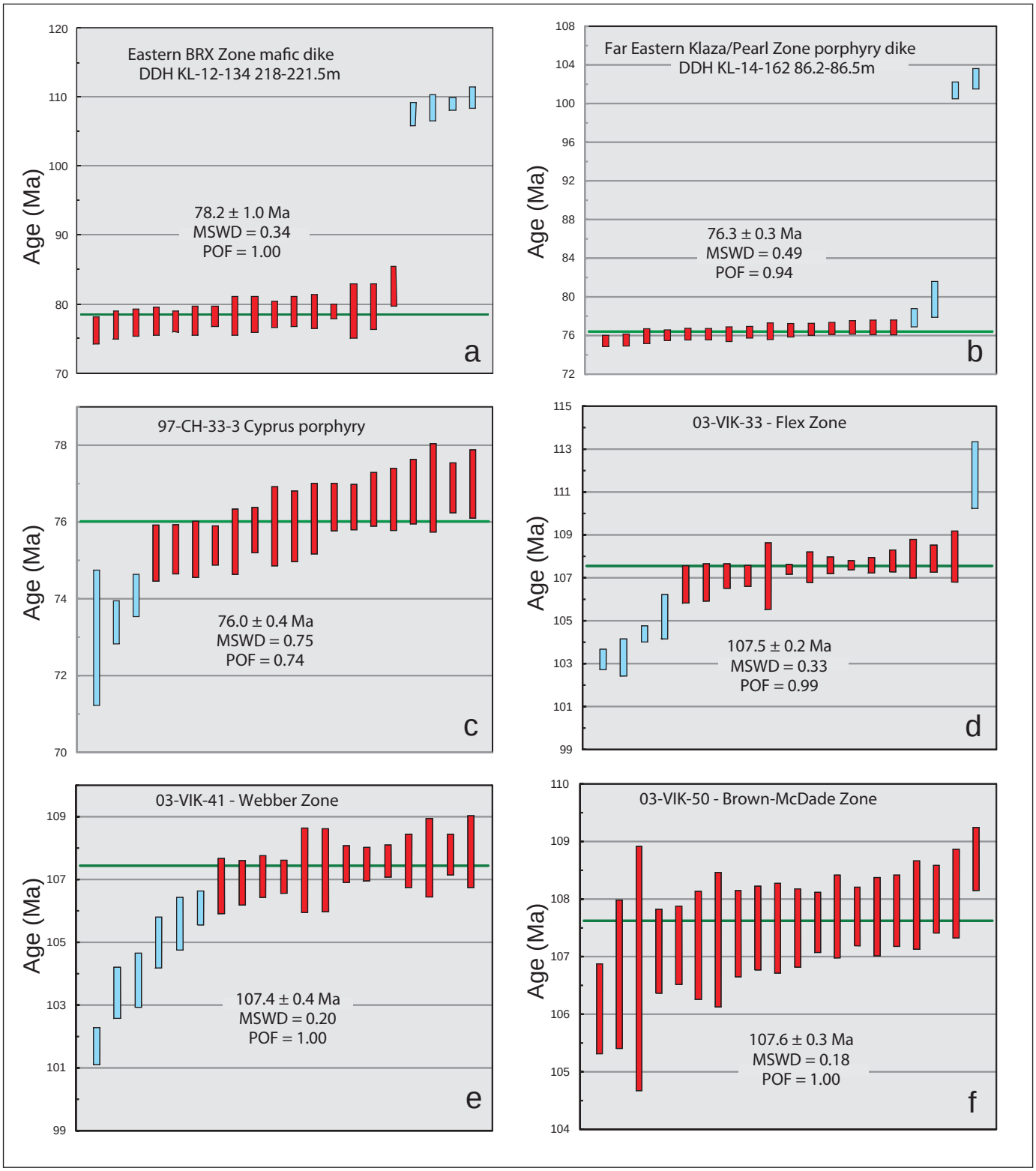


Figure 6. *Plots of $^{206}Pb/^{238}U$ ages for zircons from Klaza igneous samples, as well as the Cyprus porphyry and re-analysis of three porphyry samples from the Brown-McDade cluster. Error bars are shown at the 2σ level. Analyses shown by blue boxes were not used in calculation of the weighted average ages.*

some of the samples show considerable scatter and there is evidence for a substantial amount of older inherited zircon present in some cases. Although considered unlikely, it is conceivable that the Early Cretaceous zircons dated in 2003 might have been of xenocrytic origin, and entrained from underlying bodies of 108 Ma Dawson Range batholith; the Brown-McDade cluster dikes and plugs are mostly emplaced into Yukon-Tanana terrane metamorphic rocks at the present level of exposure. In order to evaluate this possibility, twenty zircon grains from each of three samples from the 2003 study, selected as representative of the entire range of grain size and morphology present in the concentrate, were analyzed using LA-ICP-MS methods (Appendix 1; Fig. 6d-f). The new results confirm the original age assignments: Flex zone porphyry, 108.4±0.7 Ma TIMS and 107.4±0.2 Ma LA; Weber zone porphyry, 107.9±0.9 Ma TIMS and 107.4±0.4 LA; Brown-McDade porphyry: 109.0±0.7 Ma TIMS; 107.6±0.3 Ma LA. Therefore, the reanalysis of zircons from these samples strongly argues for an Early Cretaceous crystallization age for the intrusions in the Brown-McDade cluster. The most reasonable conclusion, therefore, is that two similar, but completely unrelated sets of felsic dikes and small stocks were emplaced into northwest-trending faults in the Mt. Nansen area.

Pb ISOTOPES

METHODOLOGY

In general the Pb isotopic compositions of sulphides precipitated from magmatic-hydrothermal fluids in intrusion-related vein systems are very similar to the Pb isotopic compositions of igneous feldspar within the genetically related intrusions (Tosdal *et al.*, 1999). Lead isotopes therefore provide a powerful tool for determining the source(s) from which Pb (and by analogy, other metals) in a deposit is derived, and in the case of intrusion-related mineralization, for identifying which intrusion (or intrusive suite) is genetically associated with the mineralization. In some cases, Pb compositions can also yield some indication of the age of formation of epigenetic mineralization, although this must be utilized with caution. Lead isotopic compositions of several samples of galena from veins from both the Brown-McDade and the Klaza cluster were determined at the PCIGR, using TIMS methods as described by Mortensen and Gabites (2002). Analytical data are given in Appendix 2. An extensive Pb isotopic database for both igneous feldspar minerals from intrusive rocks and galena and other sulphides from various mineral deposits and occurrences from throughout west-central Yukon, including data from various published and unpublished sources, is also discussed.

RESULTS

New galena Pb isotopic analyses from Klaza (n=3) and Brown-McDade (n=3) from this study are plotted on a $^{207}Pb/^{204}Pb$ *vs.* $^{206}Pb/^{204}Pb$ diagram in Figure 7. Also shown for comparison on this plot are fields of Pb isotopic compositions from additional Klaza and Brown-McDade vein samples, as well as sulphides from a number of other epigenetic, polymetallic vein occurrences (Fig. 1) in the Dawson Range and elsewhere in western Yukon, including the Prospector Mountain area (Frog and Lilypad occurrences), the Tinta Hill deposit in the Freegold Mountain area, the Longline Au deposit in the Moosehorn Range (Yukon MINFILE 115N 024), the Bomber vein at Casino, and numerous other Late Cretaceous vein occurrences in the region (data from Godwin *et al.*, 1988; Glasmacher, 1990; Smuk, 1999; Selby *et al.*, 2001; Joyce, 2002; Selby *et al.*, 2001; Bineli-Betsi *et al.*, 2013; Mortensen, unpublished data). Also shown on the plot are fields for igneous K-feldspars from Early Cretaceous intrusions in the Moosehorn Range (from Joyce, 2002) and Late Cretaceous intrusions in the Casino area (from Selby *et al.*, 1999), as well as other Early and Late Cretaceous intrusions from throughout west-central and western Yukon (Mortensen, unpublished data).

The Pb isotopic study tries to resolve the question of whether veins in the Brown-McDade cluster formed at the same time as those in the Klaza cluster (*i.e.*, early Late Cretaceous), and coincidentally happen to be spatially associated with a lithologically similar but ~35 my older set of porphyry dikes, or represent a completely unrelated mineralizing event. The study also evaluates the relative importance of mid-Cretaceous *vs.* early Late and late Late Cretaceous mineralizing events in western Yukon.

The field for Early Cretaceous igneous feldspar from the Moosehorn Range (dotted green line in Fig. 7) is completely separate from that for sulphides in gold-bearing veins from the Longline occurrence that is hosted by those intrusions (solid green line). This observation led Joyce (2002) to conclude that the metals in the Longline veins were not derived from the host intrusions, or indeed from any other intrusions in western Yukon or eastern Alaska, but were actually orogenic rather than intrusion-related.

The field for igneous feldspar from other Early Cretaceous intrusions in western Yukon (dotted red line in Fig. 7)

overlaps with the Moosehorn Range feldspar data but shows somewhat more scatter. Feldspar from early Late Cretaceous Casino suite intrusions and from other early and late Late Cretaceous intrusions in western Yukon (blue dotted lines on Fig. 7; including the Cyprus porphyry in the Mt. Nansen district, shown as the blue triangle) show considerable scatter; although there is substantial overlap with the fields for the Early Cretaceous feldspar, most of the Late Cretaceous feldspar show higher $^{206}Pb/^{204}Pb$ ratios and slightly lower $^{207}Pb/^{204}Pb$ ratios (Fig. 7). The field for galena from the Bomber veins, which are considered to be related to the early Late Cretaceous Casino porphyry deposit, overlap with both the more radiogenic (higher Pb/Pb compositions) part of the Early Cretaceous feldspar Pb field and the less radiogenic (lower Pb/Pb compositions) part of the Late Cretaceous feldspar field. However, galena from other early and late Late Cretaceous intrusion-related veins in western Yukon (solid blue line on Fig. 7), show a good overlap with Late Cretaceous feldspar but are completely separate from the Early Cretaceous feldspar field. Taken together, the data suggest: 1) Early and Late Cretaceous igneous feldspar minerals yield partly overlapping compositional fields, but most Late Cretaceous samples have higher $^{206}Pb/^{204}Pb$ and slightly lower $^{207}Pb/^{204}Pb$ ratios than the bulk of the Early Cretaceous samples; and 2) epigenetic vein occurrences that are known to be of Late Cretaceous age more closely match the compositional fields for the Late Cretaceous igneous feldspar than the Early Cretaceous samples, which is consistent with the bulk of the metals in these occurrences having been derived predominantly from the Late Cretaceous intrusions.

Sulphide Pb isotopic compositions from four separate areas (Klaza, Brown-McDade, Prospector Mountain, Tinta Hill), however, are more puzzling. Field relationships discussed above provide unequivocal evidence that the Klaza veins (pink field in Fig. 7) are spatially and temporally related with late Late Cretaceous porphyry intrusions, whereas very similar veins in the Brown-McDade cluster (blue field in Fig. 7) are most reasonably interpreted to be Early Cretaceous in age. Both of these compositional fields overlap with the least radiogenic part of the compositional ranges for the Early and Late Cretaceous igneous rocks. Veins in the Prospector Mountain area, whose galena Pb isotopic compositions overlap almost perfectly with the Brown-McDade galena field (Fig. 7), are interpreted to cut Late Cretaceous Carmacks Group volcanic rocks, and must therefore be Late Cretaceous in age. The Tinta Hill Au-Ag-Cu-Pb-Zn deposit in the Mt. Freegold area is a polymetallic, epithermal vein that closely resembles the Klaza and Brown-McDade veins in most respects (Bennett and Bineli Betsi, 2010). The age of the Tinta Hill veins is uncertain; Bineli Betsi and Bennett (2010) stated that the vein is crosscut by a porphyry dike that yielded a 108 Ma U-Pb zircon (TIMS) age; however, there is somewhat less certainty regarding this crosscutting relationship in subsequent publications (Bineli Betsi, 2012; Bineli Betsi *et al.*, 2013). These four vein systems were each emplaced into very different host rocks that would be expected to have quite distinct Pb isotopic characteristics. The Brown-McDade cluster of veins are mainly hosted by Yukon-Tanana terrane metasedimentary rocks; whereas the Klaza veins are hosted by the Early Cretaceous Dawson Range batholith, the Prospector Mountain veins by Late Cretaceous Carmacks Group volcanic rocks, and the Tinta vein by the Early Jurassic Granite Mountain batholith. The fact that sulphides from these four vein systems show rather similar Pb isotopic compositions suggests that the Pb in each was likely derived mainly from the associated intrusions rather than the host rocks, and in general the Pb isotopic compositions of the sulphides is more consistent with the metals having been derived from Early, rather than Late, Cretaceous magma.

The implications of the Pb isotopic study are therefore uncertain at this time. It is very difficult to directly date epithermal veins such as those in the eastern Dawson Range, and vein ages typically must be inferred from contact relations with dated igneous rock units. More detailed geological investigations will be required to resolve the age relations between the various intrusive suites and vein systems in the area.

IMPLICATIONS FOR THE METALLOGENY OF WEST-CENTRAL YUKON

At least three distinct ages of porphyry-style mineralization are known to exist in western Yukon: Early Cretaceous (*e.g.*, Pattison, Idaho); early Late Cretaceous (*e.g.*, Casino, Cash, Cyprus, Nucleus, Revenue, Sonora Gulch, Tad/Toro and Bluff/Taurus in eastern Alaska); and late Late Cretaceous (*e.g.*, Mt. Cockfield, Sixtymile; Allan *et al.*, 2013). Similarly there are gold-bearing vein and breccia systems of the same three ages: Early Cretaceous (*e.g.*, Antoniuk, possibly Brown-McDade, possibly Tinta Hill); early Late Cretaceous (*e.g.*, Klaza); and late Late Cretaceous (*e.g.*, Prospector Mountain, Connaught (Yukon

MINFILE 115N 040)). The largest and most prospective porphyry systems, however, appear to be related to the early Late Cretaceous Casino suite, and the most significant epithermal vein systems identified thus far appear to be the Klaza deposit and some zones in the Sonora Gulch area, also of early Late Cretaceous age. Our new age constraints strongly support the "porphyry-to-epithermal transition" model that was proposed by Hart and Langdon (1998), at least for veins of the Klaza cluster and the Cyprus and Kelly porphyry deposits. The age of the epithermal veins in the Brown-McDade cluster, however, is still not resolved, and it remains unclear whether the Brown-McDade veins have any relationship to any of the Late Cretaceous magma in the Mt. Nansen area.

Lead isotopic studies of many of the mineral deposits and occurrences in western Yukon, together with analyses of igneous feldspars from potentially related intrusive rocks, indicate that there is a substantial amount of scatter within each of the plutonic suites in the region. It appears that lead isotopes do not provide a simple tool for identifying which intrusive rocks are genetically related to specific mineralization in this region. It is unclear whether this is because of the isotopic heterogeneity of the igneous rocks themselves, or the fact that some amount of mixing has occurred between metal-bearing magmatic fluids and metals derived from compositionally variable host rocks.

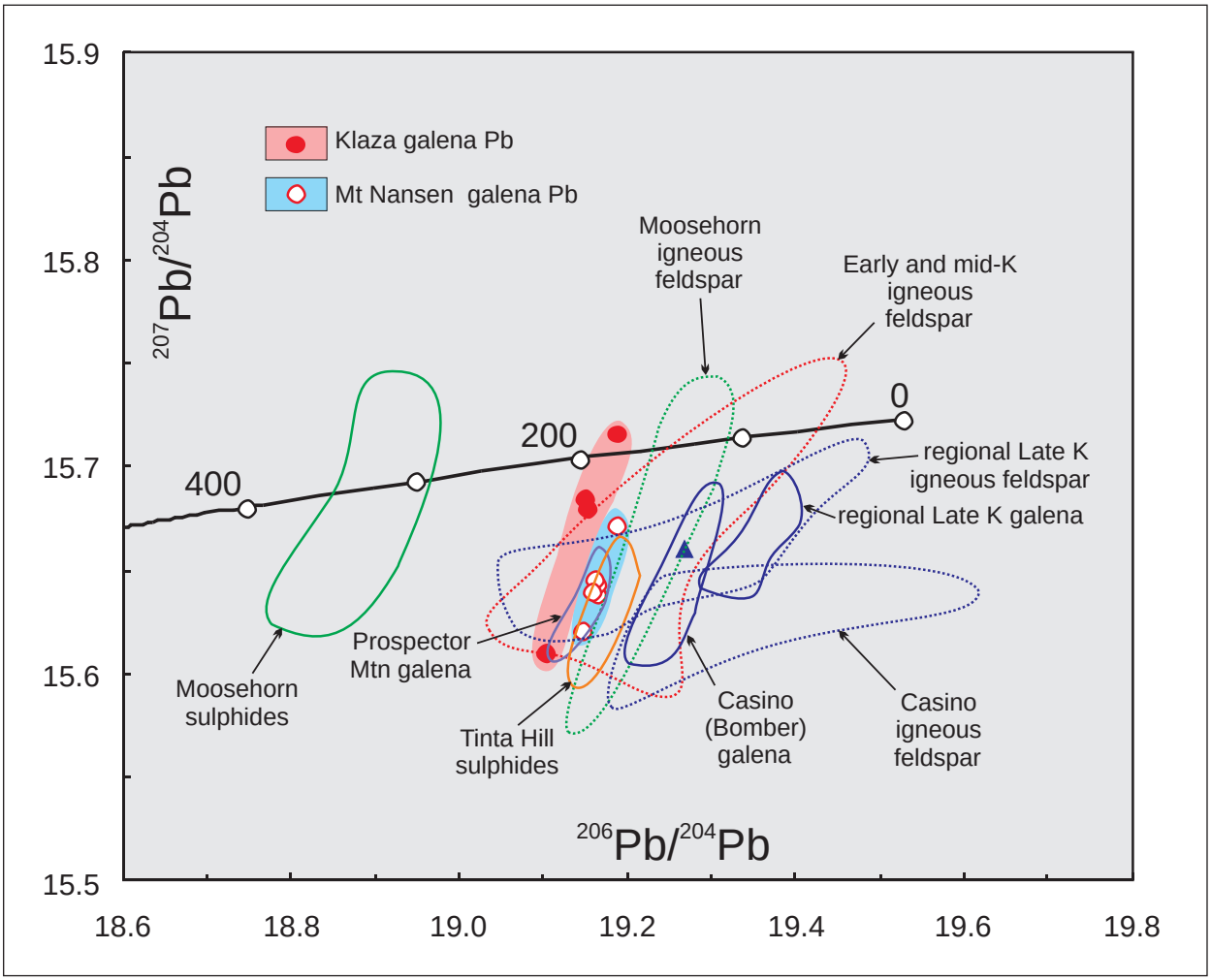


Figure 7. *Compilation plot showing Pb isotopic compositional fields for igneous feldspars from Early to Late Cretaceous intrusions from west-central Yukon, together with sulphide (mainly galena) compositions from a variety of intrusion-related orogenic gold deposits and occurrences. Fields for sulphide Pb analyses from the Mt. Nansen veins and from the Klaza deposit are shown as colored fields. The Cyprus porphyry feldspar Pb is shown by the blue triangle. Sources of data are discussed in the text.*

ACKNOWLEDGMENTS

We thank Rockhaven Resources for providing access to the Klaza drill core for sampling purposes and for permission to publish the results of the Klaza dating. We also thank Steve Israel for a critical review of an early draft of the manuscript.

REFERENCES

Allan, M.M., Mortensen, J.K., Hart, C.J.R., Bailey, L.A., Sánchez, M.G., Ciolkiewicz, W., McKenzie, G.G. and Creaser, R.A., 2013. Magmatic and metallogenic framework of west-central Yukon and eastern Alaska. *In:* Tectonics, Terranes, Metallogeny and Discovery in the Northern Circum-Pacific Region, M. Colpron, T. Bissig, B. Rusk, and J. Thompson, J. (eds.), Society of Economic Geologists, Special Publication 17, p. 111-168.

Andersen, F. and Stroshein, R., 1998. Geology of the Flex gold-silver vein system, Mount Nansen area, Yukon. *In:* Yukon Exploration and Geology 1997, Exploration and Geological Services Division, Yukon, Indian and Northern Affairs Canada, p.139-143.

Bineli Betsi, T., 2012. Petrogenesis of Au-Bi-As-Cu, Cu-Mo±W, and base metal-Au-Ag mineral occurrences, in the Mount Freegold region (Dawson Range), Yukon, Canada. Unpublished PhD thesis, University of New Brunswick, Fredericton, Canada, 515 p.

Bineli Betsi, T. and Bennett, V., 2010. New U-Pb age constraints at Freegold Mountain: Evidence for multiple phases of polymetallic mid- to Late Cretaceous mineralization. *In*: Yukon Exploration and Geology 2009, K.E. MacFarlane, L.H. Weston and L.R. Blackburn (eds.), Yukon Geological Survey, p. 57-84.

Bineli Betsi, T., Lentz, D., Chiaradia, M., Kyser, K. and Creaser, R.A., 2013. Genesis of the Au–Bi–Cu–As, Cu–Mo±W, and base-metal Au-Ag mineralization at the Mountain Freegold (Yukon, Canada): constraints from Ar-Ar and Re-Os geochronology and Pb and stable isotope compositions. Mineralium Deposita, vol. 48, p. 991-1017.

Glasmacher, U., 1990. Petrogenetic and metallogenetic evolution of selected areas in the Yukon-Tanana Terrane and the ´Stikine Terrane´, Yukon Territory, Canada, during the Upper Cretaceous and Lower Tertiary (in German). Unpublished PhD thesis, Rhenish Westphalian Technical University, Aachen, Germany, 351 p.

Godwin, C.I. and Sinclair, A.J., 1982. Average lead isotope growth curves for shale hosted zinc-lead deposits, Canadian Cordillera. Economic Geology, vol. 77, p. 675-690.

Godwin, C.I., Gabites, J.E. and Andrew, A., 1988. Leadtable – a galena lead isotope database for the Canadian Cordillera, with a guide to its use by explorationists. BC Mineral Resources Division, Geological Survey Branch, Paper 1988-4, 188 p.

Hart, C.J.R. and Langdon, M., 1998. Geology and mineral deposits of the Mount Nansen camp, Yukon. *In:* Yukon Geology and Exploration 1997, Exploration and Geological Services Division, Yukon Region, Indian and Northern Affairs Canada, p. 129-138.

Joyce, N.L., 2002. Geologic setting, nature and structural evolution of intrusion-hosted Au-bearing quartz veins at the Longline occurrence, Moosehorn Range area, west-central Yukon Territory. Unpublished MSc thesis, University of British Columbia, 199 p.

Mortensen, J.K. and Gabites, J.E., 2002. Lead isotopic constraints on the metallogeny of southern Wolf Lake, southeastern Teslin and northern Jennings River map areas, Yukon and British Columbia: Preliminary results. *In*: Yukon Exploration and Geology 2001, D.S. Emond, L.H. Weston and L.L. Lewis (eds.), Exploration and Geological Services Division, Yukon Region, Indian and Northern Affairs Canada, p. 179-188

Mortensen, J.K., Appel, V.L. and Hart, C.J.R., 2003. Geological and U-Pb age constraints on base and precious metal vein systems in the Mount Nansen area, eastern Dawson Range, Yukon. *In:* Yukon Exploration and Geology 2002, D.S. Emond and L.L. Lewis (eds.), Exploration and Geological Services Division, Yukon Region, Indian and Northern Affairs Canada, p. 165-174.

Selby, D. and Creaser, R.A., 2001. Late and mid-Cretaceous mineralization in the northern Canadian Cordillera: constraints from Re-Os molybdenite dates. Economic Geology, vol. 96, p. 1451-1467.

Selby, D., Creaser, R.A. and Nesbitt, B.E., 1999. Major and trace element compositions and Sr-Nd-Pb systematics of crystalline rocks from the Dawson Range, Yukon, Canada. Canadian Journal of Earth Sciences, vol. 36, p. 1463-1481.

Selby, D., Nesbitt, B.E., Creaser, R.A., Reynolds, P.H. and Nuehlenbachs, K., 2001. Evidence for a nonmagmatic component in potassic hydrothermal fluids of porphyry Cu-Au-Mo systems, Yukon, Canada. Geochimica et Cosmochimica Acta, vol. 65, p. 571-587.

Smuk, K.A., 1999. Metallogeny of epithermal gold and base metal veins of the southern Dawson Range, Yukon. Unpublished MSc thesis, McGill University, 155 p.

Stroshein, R., 1999. A summary report on the geology of the Brown-McDade gold-silver deposit, Mount Nansen mine area, Yukon. *In:* Yukon Exploration and Geology 1998, C.F. Roots and D.S. Emond (eds.), Exploration and Geological Services Division, Yukon, Indian and Northern Affairs Canada, p. 231-236.

Tosdal, R.M., Wooden, J.L. and Bouse, R.M., 1999. Pb isotopes, ore deposits, and metallogenic terranes. Society of Economic Geology, Reviews in Economic Geology, vol. 12, p. 1-28.

Wengzynowki, W.A., Giroux, G.H. and Martin, C.J., 2015. NI 43-101 Technical Report describing geology, mineralization, geochemical surveys, geophysical surveys, diamond and percussion drilling, metallurgical testing and mineral resources on the Klaza Property. Rockhaven Resources, NI 43-101 Technical Report, 173 p., <http://www.rockhavenresources.com/assets/projects/2015-06-19_Klaza_NI-43-101.pdf> [accessed November 26, 2015].

APPENDIX 1. *U-Pb analytical data by laser ablation (LA)-ICP-MS methods.*

Fraction	Isotopic Ratios							Isotopic Ages						Background corrected mean counts per second at specified mass							
	$^{207}Pb/^{235}U$	% 1σ	$^{206}Pb/^{238}U$	% 1σ	rho	$^{207}Pb/^{206}Pb$	% 1σ	$^{207}Pb/^{235}U$	1σ	$^{206}Pb/^{238}U$	1σ	$^{207}Pb/^{206}Pb$	1σ	202	204	206	207	208	232	235	238
Dawson Range batholith granodiorite - Pika Zone																					
1	0.11355	0.00624	0.01703	0.00032	0.34	0.04933	0.00256	163.7	117.2	109.2	5.69	108.8	2.02	1	15	4014	194	378	21508	692	72551
2	0.11273	0.00341	0.01708	0.00018	0.35	0.04837	0.00138	117.5	65.74	108.5	3.11	109.2	1.11	24	32	3436	163	524	32456	585	61901
3	0.11333	0.00504	0.0165	0.00025	0.34	0.04987	0.0021	188.8	94.96	109	4.6	105.5	1.61	50	0	6206	304	605	31463	1084	115710
4	0.11395	0.00431	0.01678	0.00022	0.35	0.04926	0.00176	160.4	81.28	109.6	3.93	107.3	1.38	0	8	7453	361	630	36829	1279	136678
5	0.1122	0.0033	0.01684	0.00017	0.34	0.04839	0.00134	118.4	63.98	108	3.01	107.6	1.05	36	9	4504	214	456	24503	771	82318
6	0.11538	0.00401	0.01646	0.00019	0.33	0.04969	0.00163	180.7	74.67	110.9	3.65	105.2	1.22	0	0	5200	254	671	37560	889	97243
7	0.11335	0.00304	0.01693	0.00015	0.33	0.04901	0.00124	148.2	58.03	109	2.77	108.2	0.98	0	0	5375	259	743	42442	922	97722
8	0.10818	0.00282	0.01693	0.00015	0.34	0.04706	0.00116	51.7	57.93	104.3	2.59	108.2	0.94	27	2	12980	601	1285	76215	2241	235989
9	0.1135	0.00625	0.01706	0.00028	0.3	0.0491	0.00258	152.8	118.81	109.2	5.7	109.1	1.8	0	1	1309	63	175	8412	224	23616
10	0.11789	0.0034	0.01698	0.00017	0.35	0.05042	0.00137	214.3	61.62	113.2	3.09	108.5	1.06	16	3	4327	214	483	23909	734	78429
11	0.11212	0.0039	0.01691	0.0002	0.34	0.04837	0.00159	117.5	75.51	107.9	3.56	108.1	1.25	55	0	3592	171	429	24405	615	65367
12	0.11682	0.00349	0.01692	0.00017	0.34	0.05148	0.00144	262.3	63.16	112.2	3.17	108.2	1.1	0	21	3481	176	437	24168	609	63311
13	0.10328	0.00474	0.01671	0.00026	0.34	0.04829	0.00211	113.3	99.98	99.8	4.36	106.8	1.65	0	0	4156	197	595	33906	771	76564
14	0.10225	0.00436	0.01693	0.00024	0.33	0.04474	0.00181	0.1	26.11	98.9	4.02	108.2	1.52	26	7	4808	211	781	43916	835	87436
15	0.11135	0.00301	0.01696	0.00015	0.33	0.04807	0.00123	102.5	59.18	107.2	2.75	108.4	0.96	68	7	4579	216	491	25890	784	83092
16	0.11023	0.00562	0.01706	0.00028	0.32	0.04823	0.00234	110.4	110.52	106.2	5.14	109	1.78	0	24	2028	96	173	9235	352	36607
17	0.11931	0.00658	0.01667	0.00032	0.35	0.05012	0.0026	200.6	115.98	114.4	5.97	106.6	2.01	0	0	6677	329	409	14809	1113	123250
18	0.10491	0.00371	0.01686	0.0002	0.34	0.04726	0.00158	61.8	78.25	101.3	3.41	107.8	1.28	0	17	5088	236	660	38469	910	92867
19	0.10711	0.00416	0.01707	0.00021	0.32	0.04467	0.00164	0.1	13.97	103.3	3.82	109.1	1.32	0	0	3610	158	431	27237	597	65101
20	0.05001	0.00549	0.01662	0.0002	0.11	0.022	0.0024	0.1	0	49.5	5.31	106.3	1.26	0	0	3772	81	601	32671	658	69853
Western Klaza Zone porphyry dyke - DDH KL-12-75 189-191m																					
1	0.07326	0.00194	0.01197	0.00011	0.35	0.04433	0.00113	0.1	0	71.8	1.83	76.7	0.67	0	10	9147	399	485	36628	2197	235218
2	0.07988	0.00195	0.01196	0.0001	0.34	0.04959	0.00117	175.9	53.97	78	1.83	76.6	0.64	7	0	5256	256	290	20110	1295	135282
3	0.0782	0.00189	0.01191	0.0001	0.35	0.04733	0.0011	65.2	55.14	76.5	1.78	76.3	0.62	0	0	5489	255	310	24373	1318	141857
4	0.07836	0.00221	0.01192	0.00012	0.36	0.04742	0.0013	69.6	64.35	76.6	2.08	76.4	0.74	27	22	8117	379	357	29685	1950	209572
5	0.0708	0.00299	0.01175	0.00017	0.34	0.04369	0.0018	0.1	0	69.5	2.83	75.3	1.06	32	16	6166	265	363	29922	1510	161600
6	0.07708	0.00209	0.01189	0.00011	0.34	0.04727	0.00124	62.4	61.84	75.4	1.97	76.2	0.7	26	7	6747	314	268	18457	1642	174712
7	0.07658	0.0014	0.01209	0.00007	0.32	0.04638	0.00081	17.3	40.8	74.9	1.32	77.5	0.47	18	12	10463	478	410	34578	2515	266434
8	0.07786	0.0017	0.01204	0.00009	0.34	0.04766	0.001	81.8	49.9	76.1	1.6	77.2	0.57	0	15	6838	321	322	23773	1661	174846
9	0.07456	0.0022	0.01198	0.00012	0.34	0.04383	0.00125	0.1	0	73	2.08	76.7	0.75	18	10	6340	273	296	23159	1479	162987
10	0.082	0.00258	0.01205	0.00013	0.34	0.04928	0.0015	161	69.69	80	2.42	77.2	0.84	9	6	5790	281	333	24996	1381	147866
11	0.07627	0.0021	0.01195	0.0001	0.3	0.04541	0.00121	0.1	29.72	74.6	1.98	76.6	0.63	19	3	5472	245	340	25093	1293	140995
12	0.07299	0.01077	0.01198	0.00057	0.32	0.04686	0.00682	41.7	315.76	71.5	10.19	76.7	3.6	0	20	580	26	80	6594	147	14916
13	0.08298	0.00366	0.01209	0.00018	0.34	0.04825	0.00206	111.4	97.75	80.9	3.43	77.5	1.16	0	0	2593	123	62	5205	598	66035
14	0.07909	0.00191	0.0119	0.0001	0.35	0.04831	0.00112	114.7	54.01	77.3	1.8	76.3	0.63	0	8	5443	259	258	21769	1320	140839
15	0.07854	0.00241	0.01177	0.00012	0.33	0.04744	0.00141	70.6	69.64	76.8	2.26	75.4	0.78	5	1	5609	262	265	20678	1344	146734
16	0.07708	0.00234	0.01191	0.00012	0.33	0.04674	0.00137	35.6	69.02	75.4	2.21	76.3	0.76	5	1	4816	222	191	14864	1159	124492
17	0.07665	0.00167	0.01215	0.00009	0.34	0.04598	0.00095	0.1	45.6	75	1.57	77.9	0.57	25	3	6977	316	302	23875	1661	176803
18	0.0739	0.00178	0.01213	0.0001	0.34	0.04496	0.00104	0.1	0	72.4	1.68	77.7	0.62	0	17	6020	267	293	20051	1453	152876
19	0.07548	0.0019	0.01208	0.0001	0.33	0.04594	0.00111	0.1	51.19	73.9	1.79	77.4	0.65	0	12	5154	233	383	27285	1245	131415
tt	0.07909	0.00169	0.01203	0.00009	0.35	0.04767	0.00097	82	48.46	77.3	1.59	77.1	0.56	0	0	7301	343	314	23695	1746	186893
Western Klaza Zone porphyry dyke - DDH KL-14-185 189-191m																					
1	0.07721	0.0022	0.01165	0.00012	0.361498244	0.0489	0.00135	142.9	63.64	75.5	2.07	74.6	0.74	4	1	8362	398	613	49708	2090	217369
2	0.07886	0.00193	0.01198	0.0001	0.341069312	0.0477	0.00113	83.6	55.92	77.1	1.81	76.8	0.64	0	0	9871	459	559	42674	2357	249407
3	0.0804	0.00289	0.01184	0.00015	0.352450201	0.04953	0.00173	172.9	79.7	78.5	2.72	75.9	0.95	0	13	3126	151	571	47198	760	79977

Fraction	Isotopic Ratios							Isotopic Ages						Background corrected mean counts per second at specified mass							
	$^{207}Pb/^{235}U$	% 1σ	$^{206}Pb/^{238}U$	% 1σ	rho	$^{207}Pb/^{206}Pb$	% 1σ	$^{207}Pb/^{235}U$	1σ	$^{206}Pb/^{238}U$	1σ	$^{207}Pb/^{206}Pb$	1σ	202	204	206	207	208	232	235	238
4	0.07703	0.0017	0.01204	0.00009	0.338709205	0.04757	0.00101	77.1	50.65	75.4	1.61	77.2	0.58	14	0	6750	313	283	24680	1646	169744
5	0.08021	0.00408	0.01212	0.00021	0.340631673	0.04918	0.00244	156.3	112.36	78.3	3.84	77.7	1.36	39	7	1249	59	186	14525	302	31219
6	0.08055	0.00223	0.01189	0.00011	0.334173119	0.04931	0.00132	162.6	61.39	78.7	2.09	76.2	0.72	0	10	5212	250	208	16508	1260	132781
7	0.07726	0.00154	0.01209	0.00008	0.331969106	0.04702	0.0009	49.8	44.2	75.6	1.45	77.5	0.52	8	5	8588	393	350	27676	2064	215233
8	0.08345	0.00177	0.01209	0.00009	0.350969424	0.05051	0.00103	218.5	46.5	81.4	1.66	77.5	0.57	7	1	7115	350	301	22047	1700	178400
9	0.07668	0.00153	0.01203	0.00008	0.333284436	0.04676	0.0009	36.8	44.6	75	1.44	77.1	0.52	0	0	8677	395	394	28650	2090	218657
10	0.0729	0.00203	0.01205	0.00011	0.32782127	0.04424	0.0012	0.1	0	71.4	1.92	77.2	0.71	13	1	6910	298	234	18684	1656	173922
11	0.07594	0.00163	0.01207	0.00009	0.347390732	0.04568	0.00094	0.1	29.92	74.3	1.54	77.3	0.55	16	0	10163	452	662	52701	2415	255440
12	0.07951	0.00222	0.01172	0.00011	0.33615057	0.0485	0.00131	123.7	62.48	77.7	2.09	75.1	0.72	7	3	6853	324	707	49634	1651	177445
13	0.08379	0.00485	0.01194	0.00024	0.347262084	0.04941	0.00278	167.4	126.55	81.7	4.54	76.5	1.52	0	0	2799	134	79	5193	652	71104
14	2.5523	0.13393	0.19079	0.0025	0.249711333	0.09875	0.00218	1600.6	40.58	1287.1	38.28	1125.7	13.53	0	12	9579	922	2135	9061	146	15236
15	0.0809	0.0018	0.01187	0.00009	0.340775063	0.04947	0.00106	169.9	49.22	79	1.69	76.1	0.58	0	8	6820	328	310	23322	1647	174347
16	0.08017	0.00215	0.0121	0.00011	0.338985201	0.04833	0.00125	115.5	59.94	78.3	2.02	77.5	0.7	30	0	5068	238	232	15379	1207	127180
17	0.07627	0.00171	0.0118	0.00009	0.340187333	0.04659	0.00101	28.1	50.32	74.6	1.61	75.6	0.57	46	0	7794	354	537	40609	1881	200631
18	0.07654	0.0022	0.01206	0.00012	0.3461782	0.04507	0.00125	0.1	14.02	74.9	2.07	77.3	0.75	0	0	4391	192	239	20370	1021	110565
19	0.08083	0.00215	0.01208	0.00011	0.342341753	0.04892	0.00126	143.9	59.31	78.9	2.02	77.4	0.69	2	8	4718	225	478	37962	1128	118664
20	0.0783	0.00182	0.01185	0.0001	0.363054667	0.04909	0.0011	152.1	51.67	76.5	1.71	75.9	0.61	5	24	8008	383	509	36882	1984	205312
Western BRX Zone porphyry dyke - DDH KL-12-154 52.1-52.5m																					
1	0.07857	0.00308	0.01194	0.00016	0.34	0.04797	0.00183	96.5	88.86	76.8	2.9	76.5	1.02	23	0	3149	149	192	15596	763	81217
2	0.12332	0.00648	0.01643	0.0003	0.35	0.05707	0.00285	493.5	107.18	118.1	5.85	105	1.89	37	0	1241	69	110	5766	228	23282
3	0.10066	0.00516	0.01604	0.00028	0.34	0.04701	0.00229	49.2	112.8	97.4	4.76	102.6	1.76	22	0	4055	188	260	14533	751	77855
4	0.08324	0.00309	0.01209	0.00015	0.33	0.04793	0.00172	94.6	83.76	81.2	2.9	77.5	0.99	45	0	5123	242	378	27894	1171	130489
5	0.08827	0.00424	0.01198	0.0002	0.35	0.05256	0.00245	309.7	102.69	85.9	3.95	76.8	1.24	13	0	1334	69	129	11351	315	34303
6	0.07564	0.00318	0.01199	0.00016	0.32	0.04462	0.00182	0.1	20.42	74	3	76.9	1.02	0	0	2102	92	330	24144	492	53970
7	0.07502	0.00218	0.01207	0.00012	0.34	0.04653	0.00131	25	65.09	73.5	2.06	77.3	0.75	17	11	4022	184	548	41025	990	102669
8	0.08131	0.00165	0.01212	0.00008	0.33	0.04803	0.00092	100.5	44.61	79.4	1.55	77.7	0.53	0	12	8726	413	371	27849	2045	221743
9	0.08134	0.00209	0.01189	0.0001	0.33	0.04863	0.0012	129.9	56.89	79.4	1.96	76.2	0.66	15	0	5058	242	506	37076	1200	131005
10	0.08249	0.00289	0.01184	0.00014	0.34	0.04933	0.00166	163.8	77	80.5	2.71	75.9	0.92	56	0	4163	202	533	42260	988	108256
11	0.07457	0.00284	0.01199	0.00016	0.35	0.04548	0.00168	0.1	56.52	73	2.68	76.8	0.99	35	3	3911	175	570	45074	946	100459
12	0.08073	0.00267	0.01206	0.00014	0.35	0.04707	0.0015	52.5	74.57	78.8	2.51	77.3	0.87	2	0	2915	135	349	28126	674	74440
13	0.0762	0.00309	0.01182	0.00016	0.33	0.04648	0.00183	22.6	91.94	74.6	2.92	75.8	1.03	5	11	4247	195	447	35211	1028	110631
14	0.07933	0.00307	0.01196	0.00016	0.35	0.04814	0.0018	106.2	86.2	77.5	2.89	76.6	1.02	0	0	4290	204	124	10926	1033	110482
15	0.0717	0.00225	0.01199	0.00012	0.32	0.04417	0.00134	0.1	0	70.3	2.13	76.8	0.78	42	2	3632	158	499	42268	888	93326
16	0.07925	0.00292	0.01209	0.00015	0.34	0.04803	0.00171	100.9	82.15	77.4	2.75	77.5	0.97	54	0	3064	145	249	20693	737	78067
17	0.07647	0.00262	0.01187	0.00013	0.32	0.04828	0.0016	113.2	76.55	74.8	2.47	76.1	0.86	13	0	2868	136	312	23742	718	74399
18	0.07375	0.00213	0.01207	0.00011	0.32	0.04515	0.00125	0.1	18.28	72.3	2.01	77.4	0.73	4	5	4228	188	230	19216	1027	107871
19	0.07802	0.00175	0.01216	0.00009	0.33	0.04633	0.00098	14.7	49.77	76.3	1.65	77.9	0.59	13	3	7029	321	364	30861	1656	178127
20	0.07852	0.00166	0.01215	0.00009	0.35	0.04747	0.00094	72.5	47.14	76.7	1.56	77.9	0.56	14	4	7944	372	521	40287	1906	201352
Central BRX Zone porphyry dyke - DDH KL-14-165 85.7-87.5m																					
1	0.4214	0.02236	0.05902	0.00094	0.300159007	0.05357	0.00215	352.8	88.13	357.1	15.97	369.7	5.73	0	0	4977	259	464	7052	250	25637
2	0.07612	0.00177	0.01198	0.00009	0.323080841	0.04639	0.00104	17.9	52.3	74.5	1.67	76.8	0.6	20	6	7759	350	588	44796	1869	196970
3	0.08222	0.00191	0.01198	0.0001	0.359324878	0.04959	0.00111	176	51.21	80.2	1.79	76.8	0.61	27	0	5991	289	556	42236	1428	152096
4	0.07761	0.00247	0.01213	0.00013	0.336746648	0.04787	0.00148	91.7	72.61	75.9	2.33	77.7	0.83	0	0	3283	153	450	33599	800	82357
5	0.07443	0.00265	0.01183	0.00013	0.308646071	0.0453	0.00157	0.1	42.22	72.9	2.5	75.8	0.85	7	1	2898	128	169	15214	697	74560
6	0.08214	0.00448	0.01189	0.00022	0.339248168	0.04969	0.00264	180.3	119.42	80.2	4.21	76.2	1.42	10	11	1770	85	119	8716	423	45320
7	0.08011	0.00336	0.01215	0.00017	0.333595434	0.04669	0.0019	33.3	94.74	78.3	3.16	77.9	1.09	31	0	3059	139	102	9127	705	76636
8	0.103	0.00434	0.01652	0.00023	0.33041921	0.04609	0.00184	2.5	92.31	99.5	3.99	105.7	1.45	35	15	2680	120	399	20584	474	49377
9	0.07675	0.0029	0.01166	0.00015	0.340465488	0.04738	0.00174	67.9	85.72	75.1	2.73	74.8	0.96	32	0	2691	124	188	13815	657	70253

Fraction	Isotopic Ratios							Isotopic Ages						Background corrected mean counts per second at specified mass							
	$^{207}Pb/^{235}U$	% 1σ	$^{206}Pb/^{238}U$	% 1σ	rho	$^{207}Pb/^{206}Pb$	% 1σ	$^{207}Pb/^{235}U$	1σ	$^{206}Pb/^{238}U$	1σ	$^{207}Pb/^{206}Pb$	1σ	202	204	206	207	208	232	235	238
10	0.0763	0.00204	0.01192	0.00011	0.345152323	0.04743	0.00122	70.1	60.85	74.7	1.92	76.4	0.68	21	0	4743	219	231	17288	1165	121141
11	0.07701	0.00265	0.01187	0.00014	0.34275087	0.04914	0.00164	154.5	76.43	75.3	2.5	76.1	0.91	0	0	3779	181	202	17852	953	97018
12	0.07456	0.00244	0.01183	0.00013	0.335795352	0.04725	0.0015	61.3	74.49	73	2.3	75.8	0.85	12	9	3181	146	376	29971	797	81920
13	0.07798	0.00247	0.01192	0.00013	0.344312964	0.04789	0.00147	92.9	72.21	76.2	2.33	76.4	0.83	6	0	3070	143	286	20322	745	78502
14	0.07638	0.00287	0.01189	0.00015	0.335743151	0.04759	0.00174	78.2	85.39	74.7	2.71	76.2	0.96	39	1	3602	167	282	22474	887	92353
15	0.10795	0.0055	0.01654	0.00029	0.344129933	0.05074	0.00245	229.1	107.96	104.1	5.04	105.7	1.84	39	12	2382	117	277	16336	442	43923
16	0.10907	0.00459	0.01642	0.00023	0.332849042	0.04976	0.00198	184	90.28	105.1	4.2	105	1.48	0	0	2615	126	304	16974	472	48563
17	0.11018	0.00446	0.01652	0.00022	0.328988371	0.04905	0.00188	150.4	87.4	106.1	4.08	105.6	1.4	7	13	2596	124	321	18549	457	47945
18	0.06905	0.00269	0.01201	0.00015	0.320597148	0.04333	0.00165	0.1	0	67.8	2.56	77	0.98	8	2	5098	215	853	65617	1265	129486
19	0.07623	0.00275	0.01193	0.00015	0.34853311	0.04807	0.00168	102.7	80.72	74.6	2.59	76.5	0.93	0	6	3122	146	345	26623	778	79838
20	0.08083	0.00276	0.01199	0.00014	0.34195767	0.04837	0.00159	117.3	75.89	78.9	2.59	76.8	0.89	0	4	3892	183	220	15896	921	99036
Central Klaza Zone porphyry dyke - DDH KL-11-12 181-187m																					
1	0.07448	0.00364	0.01084	0.00018	0.339767244	0.04901	0.00234	148.3	108.21	72.9	3.44	69.5	1.16	5	20	2757	131	225	19019	718	77966
2	0.07481	0.0024	0.01105	0.00012	0.338506787	0.04945	0.00153	169.4	70.65	73.3	2.27	70.8	0.79	18	8	7257	349	600	53997	1900	201387
3	0.073	0.00244	0.01118	0.00013	0.347884102	0.04887	0.00158	141.8	74.04	71.5	2.31	71.7	0.83	2	11	8464	403	641	56851	2244	232176
4	0.0792	0.00515	0.01204	0.00027	0.344869851	0.04701	0.00297	49.5	144.68	77.4	4.85	77.1	1.69	0	6	2273	104	539	37604	534	57918
5	0.06699	0.0038	0.01122	0.00019	0.298529412	0.04307	0.0024	0.1	0	65.8	3.62	71.9	1.21	34	0	2368	99	341	34958	603	64751
6	0.07674	0.00495	0.01106	0.00024	0.336412954	0.04963	0.00313	177.8	140.63	75.1	4.67	70.9	1.52	29	5	1227	59	249	22588	314	34054
7	0.07187	0.00216	0.01121	0.00011	0.326498332	0.04655	0.00134	26	66.76	70.5	2.05	71.9	0.73	0	0	9272	420	752	58934	2379	253765
8	0.07572	0.00262	0.01121	0.00014	0.360937277	0.04947	0.00166	170.4	76.31	74.1	2.48	71.9	0.86	32	12	4320	208	289	22619	1118	118276
9	0.07565	0.00187	0.0111	0.00009	0.328009828	0.04915	0.00115	154.9	53.99	74	1.77	71.2	0.6	8	0	7332	351	1037	88488	1887	202730
10	0.07119	0.00202	0.01106	0.0001	0.318648954	0.04669	0.00127	33.4	62.68	69.8	1.91	70.9	0.67	0	0	5329	242	410	34305	1385	147894
11	0.0744	0.00413	0.01111	0.00022	0.356723324	0.05107	0.00278	243.8	120.58	72.9	3.91	71.2	1.38	0	2	2417	120	199	15090	657	66888
12	0.07431	0.00265	0.01095	0.00013	0.332912897	0.04698	0.00161	47.7	80.35	72.8	2.51	70.2	0.85	0	0	9223	422	920	80042	2310	258871
13	0.0736	0.00141	0.01114	0.00007	0.327998268	0.04705	0.00083	51.5	40.78	72.1	1.34	71.4	0.45	3	17	12350	566	1332	113347	3129	340633
14	0.07094	0.00151	0.01114	0.00008	0.337379766	0.04591	0.00091	0.1	39.81	69.6	1.43	71.4	0.5	11	5	9350	418	751	70332	2398	257988
15	0.07458	0.00142	0.01116	0.00007	0.329433591	0.04805	0.00084	101.7	40.73	73	1.34	71.5	0.46	0	18	12284	574	1185	97514	3137	338457
16	0.07397	0.0022	0.01135	0.00011	0.325859031	0.04655	0.00132	25.9	65.81	72.5	2.08	72.8	0.71	0	16	6118	277	1038	85866	1526	165778
17	0.07529	0.00177	0.01127	0.00009	0.339689892	0.0496	0.00109	176.5	50.52	73.7	1.67	72.2	0.57	9	0	7123	344	563	48264	1860	194460
18	0.07442	0.00207	0.01122	0.00011	0.352467557	0.04901	0.0013	148.1	60.98	72.9	1.96	71.9	0.68	3	7	7404	353	501	46832	1933	203052
19	0.07411	0.00165	0.01121	0.00008	0.320536318	0.04865	0.00101	130.9	48	72.6	1.56	71.9	0.54	10	0	7872	373	941	76164	2048	216055
ttt	0.07248	0.00184	0.01109	0.00009	0.319676951	0.04785	0.00114	90.7	56.67	71.1	1.74	71.1	0.61	0	6	7918	368	728	60397	2072	219614
Eastern BRX Zone porphyry dyke - DDH KL-12-134 218-221.5m																					
1	0.07253	0.00674	0.01231	0.00034	0.3	0.04388	0.00401	0.1	92.74	71.1	6.38	78.9	2.15	0	0	744	32	132	10868	178	18607
2	0.08244	0.00745	0.01201	0.00032	0.29	0.04826	0.00428	111.9	196.98	80.4	6.99	77	2.02	22	0	716	33	126	9651	166	18353
3	0.11223	0.00478	0.01718	0.00024	0.33	0.04928	0.00199	161.4	91.69	108	4.36	109.8	1.55	0	26	2445	118	347	19648	426	43790
4	0.0689	0.00647	0.0121	0.00033	0.29	0.04549	0.00424	0.1	182.37	67.7	6.15	77.5	2.08	21	0	530	23	57	5774	139	13490
5	0.08195	0.00849	0.01225	0.0004	0.32	0.0503	0.00512	208.7	219.94	80	7.97	78.5	2.56	35	13	648	32	93	8795	157	16277
6	0.07507	0.00415	0.0122	0.00023	0.34	0.0457	0.00247	0.1	107.82	73.5	3.92	78.2	1.44	24	17	1405	63	236	16881	339	35437
7	0.08152	0.00661	0.01211	0.00032	0.33	0.05007	0.00399	198.5	174.99	79.6	6.21	77.6	2.07	16	0	806	39	94	8161	196	20473
8	0.11126	0.00587	0.01695	0.00029	0.32	0.04729	0.00237	63.3	115.64	107.1	5.36	108.3	1.85	0	4	1678	77	253	14575	283	30463
9	0.10709	0.00515	0.0168	0.00026	0.32	0.04667	0.00214	32.3	106.29	103.3	4.72	107.4	1.62	10	14	2180	99	262	15335	377	39906
10	0.06928	0.00672	0.01232	0.00038	0.32	0.04149	0.00394	0.1	0	68	6.38	78.9	2.39	19	1	1136	46	139	11505	270	28387
11	0.07806	0.00325	0.01231	0.00017	0.33	0.04595	0.00186	0.1	88.68	76.3	3.06	78.9	1.09	0	9	2373	107	131	9687	554	59314
12	0.07277	0.00798	0.01289	0.00045	0.32	0.04469	0.00481	0.1	171.16	71.3	7.55	82.6	2.88	21	15	753	33	141	10173	183	17971
13	0.07544	0.00993	0.01242	0.00051	0.31	0.04592	0.00594	0.1	278.95	73.8	9.38	79.6	3.24	0	3	737	33	161	10879	178	18258
14	0.08267	0.00654	0.01225	0.0003	0.31	0.04839	0.00375	118.4	173	80.7	6.13	78.5	1.89	45	0	792	37	121	10968	184	19914
15	0.10015	0.01412	0.01234	0.00061	0.35	0.05407	0.00737	373.8	280.9	96.9	13.03	79	3.91	0	0	657	34	105	8427	141	16402

Fraction	Isotopic Ratios							Isotopic Ages						Background corrected mean counts per second at specified mass							
	$^{207}Pb/^{235}U$	% 1σ	$^{206}Pb/^{238}U$	% 1σ	rho	$^{207}Pb/^{206}Pb$	% 1σ	$^{207}Pb/^{235}U$	1σ	$^{206}Pb/^{238}U$	1σ	$^{207}Pb/^{206}Pb$	1σ	202	204	206	207	208	232	235	238
16	0.07928	0.00508	0.0121	0.00024	0.31	0.04704	0.00296	50.9	143.99	77.5	4.78	77.5	1.52	41	9	932	43	134	9851	219	23715
17	0.11182	0.00284	0.01704	0.00015	0.35	0.04773	0.00114	85	56.58	107.6	2.59	108.9	0.92	41	0	6592	309	1728	97796	1117	119019
18	0.09223	0.00926	0.01222	0.00044	0.36	0.05166	0.00503	270.6	208.22	89.6	8.61	78.3	2.8	73	0	664	33	93	5998	147	16728
19	0.08685	0.006	0.01189	0.00031	0.38	0.05622	0.00383	460.3	144.96	84.6	5.61	76.2	1.99	55	7	613	33	96	7680	157	15883
20	0.08647	0.00788	0.01207	0.00032	0.29	0.04942	0.00441	167.8	196.17	84.2	7.37	77.3	2.03	29	6	620	30	84	5436	140	15815
Far Eastern Klaza/Pearl Zone porphyry dyke - DDH KL-14-162 86.2-86.5m																					
1	0.07827	0.00191	0.01189	0.0001	0.344651452	0.04709	0.0011	53.3	55.29	76.5	1.8	76.2	0.61	46	0	6051	277	259	20298	1440	155386
2	0.07727	0.00261	0.01194	0.00014	0.347131571	0.04738	0.00155	67.8	76.58	75.6	2.46	76.5	0.86	4	0	4427	204	445	35175	1074	113202
3	0.08229	0.00186	0.01192	0.00009	0.334041459	0.05048	0.00108	217.1	49	80.3	1.74	76.4	0.6	28	0	6395	314	376	28739	1552	163878
4	0.07904	0.00183	0.0119	0.00009	0.326656564	0.04809	0.00106	103.7	51.41	77.2	1.72	76.2	0.59	3	0	6711	314	417	30824	1616	172337
5	0.08151	0.00192	0.0118	0.0001	0.359772246	0.0502	0.00113	204.4	51.36	79.6	1.8	75.6	0.62	29	6	5823	284	376	28965	1419	150761
6	0.11074	0.00335	0.01604	0.00017	0.350351733	0.04903	0.00139	149.3	64.98	106.6	3.06	102.6	1.05	0	14	11681	558	542	30614	2047	222507
7	0.1019	0.00263	0.01585	0.00014	0.342229312	0.04707	0.00114	52.5	56.96	98.5	2.42	101.4	0.87	0	6	11506	527	479	29190	2104	221925
8	0.07809	0.00284	0.01216	0.00015	0.339183539	0.04443	0.00156	0.1	0	76.3	2.68	77.9	0.94	34	0	5510	238	298	24746	1241	138511
9	0.07699	0.00226	0.01188	0.00012	0.344104764	0.04724	0.00134	60.7	66.54	75.3	2.13	76.2	0.76	0	0	7854	361	446	33974	1907	202081
10	0.08125	0.00237	0.01186	0.00012	0.346873866	0.05065	0.00142	224.8	63.52	79.3	2.22	76	0.77	10	8	3672	181	162	11947	906	94665
11	0.08182	0.0022	0.012	0.00011	0.340916667	0.04929	0.00127	161.7	58.98	79.9	2.06	76.9	0.7	0	7	4653	223	176	16420	1109	118630
12	0.07927	0.00177	0.01178	0.00009	0.342162815	0.04875	0.00103	135.9	49.06	77.5	1.67	75.5	0.58	15	12	7001	332	529	42440	1704	181784
13	0.08199	0.00177	0.01188	0.00009	0.350924499	0.04967	0.00101	179.4	46.76	80	1.66	76.1	0.55	0	15	7759	375	614	50901	1861	199932
14	0.07562	0.00185	0.01196	0.0001	0.341769864	0.0467	0.00109	33.8	54.27	74	1.75	76.7	0.62	12	0	6169	280	275	20459	1508	157848
15	0.07864	0.00188	0.01198	0.0001	0.349163499	0.04814	0.0011	106.2	52.99	76.9	1.77	76.8	0.62	7	11	6204	291	379	28025	1504	158536
16	0.07673	0.00542	0.01246	0.00029	0.329492753	0.04572	0.00315	0.1	141.25	75.1	5.11	79.8	1.85	0	5	2354	104	170	14159	555	57850
17	0.07093	0.00236	0.012	0.00012	0.300550847	0.04396	0.00142	0.1	0	69.6	2.24	76.9	0.76	3	5	5406	231	273	22454	1326	137967
18	0.07774	0.00234	0.012	0.00012	0.332222222	0.04807	0.00139	102.9	66.91	76	2.2	76.9	0.77	11	9	4768	223	279	20907	1167	121672
19	0.87863	0.02022	0.07178	0.00053	0.32084649	0.09108	0.00139	1448.2	28.84	640.2	10.93	446.9	3.17	17	20	26815	2379	1477	12699	1100	114451
20	0.08145	0.00216	0.01196	0.00011	0.346815775	0.04941	0.00125	167.3	58.02	79.5	2.03	76.6	0.7	21	18	6977	335	284	20493	1676	178794
Cyprus porphyry - 97-CH-33-3																					
1	0.07823	0.00319	0.01200	0.00018	0.37	0.04851	0.00204	76.5	3.0	76.9	1.2	124.3	96.3	0	31	4058	199	206	25117	2866	369794
2	0.07570	0.00202	0.01173	0.00011	0.35	0.04732	0.00130	74.1	1.9	75.2	0.7	65.0	64.6	0	12	7167	344	338	40058	5103	667546
3	0.07585	0.00193	0.01195	0.00011	0.36	0.04580	0.00120	74.2	1.8	76.6	0.7	0.1	48.5	39	0	7408	344	404	47264	5094	677031
4	0.07751	0.00180	0.01175	0.00010	0.37	0.04765	0.00113	75.8	1.7	75.3	0.6	81.0	56.4	85	0	8408	406	568	63811	5887	781633
5	0.07898	0.00227	0.01195	0.00013	0.38	0.04740	0.00140	77.2	2.1	76.6	0.8	69.0	69.4	14	0	8927	429	429	51214	6103	815232
6	0.07714	0.00251	0.01188	0.00014	0.36	0.04752	0.00159	75.4	2.4	76.1	0.9	74.9	78.5	85	0	6582	317	481	54016	4619	604393
7	0.07893	0.00207	0.01175	0.00011	0.36	0.04860	0.00131	77.1	2.0	75.3	0.7	128.5	62.3	0	0	7530	371	881	107359	5281	698728
8	0.07811	0.00139	0.01177	0.00008	0.38	0.04815	0.00087	76.4	1.3	75.4	0.5	106.5	42.3	0	0	10572	517	731	89253	7423	979639
9	0.07701	0.00153	0.01155	0.00009	0.39	0.04836	0.00098	75.3	1.4	74.1	0.6	116.8	47.2	0	1	10923	537	658	82360	7814	1030032
10	0.07753	0.00610	0.01139	0.00028	0.31	0.04750	0.00383	75.8	5.8	73.0	1.8	73.9	181.9	0	0	827	39	117	16137	577	79103
11	0.07882	0.00172	0.01193	0.00010	0.38	0.04750	0.00106	77.0	1.6	76.4	0.6	73.8	52.9	15	6	8534	412	591	70917	5859	779124
12	0.07273	0.00292	0.01184	0.00016	0.34	0.04439	0.00182	71.3	2.8	75.9	1.0	0.1	8.5	0	11	3281	148	1781	211812	2281	301746
13	0.07789	0.00177	0.01200	0.00010	0.37	0.04794	0.00111	76.2	1.7	76.9	0.7	95.1	55.2	58	24	7898	385	485	60332	5537	715886
14	0.07904	0.00163	0.01183	0.00009	0.37	0.04854	0.00102	77.2	1.5	75.8	0.6	125.5	48.8	22	0	8236	406	424	53690	5762	756780
15	0.07945	0.00160	0.01145	0.00009	0.39	0.04968	0.00102	77.6	1.5	73.4	0.6	180.0	47.3	21	13	10015	506	758	90551	7134	950501
16	0.07935	0.00166	0.01192	0.00009	0.36	0.04778	0.00102	77.5	1.6	76.4	0.6	87.4	50.9	38	15	9466	460	567	67342	6494	862678
17	0.08048	0.00245	0.01202	0.00014	0.38	0.04931	0.00155	78.6	2.3	77.0	0.9	162.4	71.8	2	17	10521	528	496	67269	7344	950693
18	0.07165	0.00234	0.01198	0.00013	0.33	0.04314	0.00144	70.3	2.2	76.8	0.8	0.1	0.0	1	0	4580	201	272	32364	3142	415040
19	0.07959	0.00240	0.01178	0.00013	0.37	0.04898	0.00152	77.8	2.3	75.5	0.9	147.0	71.1	35	15	7221	360	405	43613	5064	665072
20	0.07719	0.00254	0.01185	0.00014	0.36	0.04751	0.00161	75.5	2.4	75.9	0.9	74.0	79.4	0	15	8200	396	579	76078	5750	750960

Fraction	Isotopic Ratios							Isotopic Ages						Background corrected mean counts per second at specified mass							
	$^{207}Pb/^{235}U$	% 1σ	$^{206}Pb/^{238}U$	% 1σ	rho	$^{207}Pb/^{206}Pb$	% 1σ	$^{207}Pb/^{235}U$	1σ	$^{206}Pb/^{238}U$	1σ	$^{207}Pb/^{206}Pb$	1σ	202	204	206	207	208	232	235	238
Mt. Nansen - Weber Zone porphyry dyke - 97-VIK-41																					
1	0.11622	0.00205	0.01686	0.0001	0.34	0.04938	0.00086	166.1	40.26	111.6	1.87	107.8	0.65	100	24	12054	604	5903	271666	3360	472169
2	0.10882	0.00201	0.01675	0.00011	0.36	0.04718	0.00086	57.9	43.49	104.9	1.84	107.1	0.67	0	0	12377	593	1682	88518	3520	488017
3	0.37652	0.00348	0.05209	0.00017	0.35	0.05173	0.00042	273.7	18.41	324.5	2.57	327.4	1.05	49	28	107919	5675	18825	282402	9725	1367797
4	0.10947	0.00257	0.01652	0.00013	0.34	0.04683	0.00109	40.4	53.84	105.5	2.36	105.6	0.84	49	48	12368	588	2916	126309	3470	494365
5	0.11301	0.00247	0.01617	0.00013	0.37	0.0502	0.00109	204.2	49.52	108.7	2.26	103.4	0.81	54	33	17940	915	3187	155430	5225	732383
6	0.1091	0.00341	0.01688	0.00018	0.34	0.04748	0.00147	72.7	72.62	105.1	3.12	107.9	1.14	11	18	9949	480	1859	75784	2839	388812
7	0.1117	0.00371	0.01685	0.0002	0.36	0.04762	0.00156	79.5	76.83	107.5	3.38	107.7	1.25	19	0	14532	704	2557	130584	4061	568758
8	0.1101	0.00259	0.01623	0.00013	0.34	0.04775	0.00111	86.2	55.28	106.1	2.37	103.8	0.86	0	41	15475	752	30213	1370423	4400	628805
9	0.1117	0.00177	0.01681	0.00009	0.34	0.04829	0.00076	113.7	36.57	107.5	1.62	107.5	0.59	14	35	12343	607	8736	393269	3498	484000
10	0.10929	0.00155	0.01681	0.00008	0.34	0.04696	0.00066	46.7	32.64	105.3	1.42	107.5	0.53	95	0	21874	1046	16503	749173	6161	857643
11	0.11399	0.00153	0.01675	0.00008	0.36	0.04982	0.00066	186.6	30.45	109.6	1.39	107.1	0.53	1	11	30706	1560	36053	1691828	8796	1207075
12	0.10762	0.00157	0.01659	0.00009	0.37	0.04711	0.00068	54.4	33.38	103.8	1.44	106.1	0.55	37	0	33669	1618	39525	2042991	9659	1335921
13	0.10744	0.00233	0.01641	0.00013	0.37	0.04815	0.00103	106.8	49.87	103.6	2.13	105	0.81	55	0	26875	1320	16315	842788	7893	1077725
14	0.11181	0.00151	0.01683	0.00008	0.35	0.04725	0.00063	61.6	30.83	107.6	1.38	107.6	0.51	18	9	22550	1087	3211	142410	6245	881542
15	0.11593	0.00216	0.01673	0.00011	0.35	0.04997	0.00092	193.4	42.14	111.4	1.96	106.9	0.71	0	0	16180	825	14023	598261	4569	636482
16	0.39148	0.00203	0.05341	0.00011	0.40	0.05245	0.00025	305.2	10.65	335.4	1.48	335.4	0.69	0	12	354473	18990	11302	162561	31120	4366004
17	0.11003	0.00406	0.01678	0.00021	0.34	0.04646	0.00169	21.5	85.29	106	3.71	107.3	1.35	0	6	10115	480	6752	290829	2798	396492
18	0.10786	0.00186	0.01589	0.00009	0.33	0.04757	0.00081	77.1	40.71	104	1.7	101.7	0.59	42	13	12246	595	2856	130622	3538	506584
19	0.11267	0.00265	0.0167	0.00014	0.36	0.04852	0.00113	124.8	53.9	108.4	2.42	106.8	0.88	29	0	13591	674	3025	143236	3834	534812
20	0.10673	0.00381	0.01679	0.00021	0.35	0.04628	0.00163	12.1	81.71	103	3.49	107.3	1.32	0	0	12271	580	9596	414715	3485	480350
21	0.10925	0.00253	0.01682	0.00013	0.33	0.04661	0.00107	29	53.27	105.3	2.32	107.6	0.85	38	6	13523	644	6781	314510	3778	528108
Mt. Nansen - Brown-McDade Zone porphyry dyke - 97-VIK-50																					
1	0.1541	0.00195	0.017	0.00009	0.42	0.06621	0.00083	812.9	25.96	145.5	1.72	108.7	0.55	80	1	20267	1340	6383	234736	5733	797876
2	0.1204	0.00257	0.0166	0.00012	0.34	0.05156	0.00109	265.7	47.88	115.4	2.33	106.1	0.78	89	34	10529	542	8336	355830	2968	424498
3	0.11153	0.00191	0.01686	0.0001	0.35	0.04799	0.00081	97.4	40.87	107.4	1.74	107.8	0.62	170	0	14668	703	2465	108137	4154	582055
4	0.11731	0.00408	0.01668	0.0002	0.34	0.04989	0.00171	189.8	78.04	112.6	3.7	106.7	1.29	47	7	12135	605	2160	99934	3397	486530
5	0.11672	0.00366	0.01678	0.00018	0.34	0.04981	0.00155	186.1	70.74	112.1	3.33	107.3	1.17	12	0	11396	567	2831	125265	3201	454282
6	0.11181	0.0024	0.01687	0.00012	0.33	0.04843	0.00103	120.5	49.44	107.6	2.19	107.9	0.77	62	22	10951	530	2834	129312	3122	433859
7	0.12392	0.00215	0.01677	0.00011	0.38	0.05386	0.00093	365.2	38.47	118.6	1.94	107.2	0.68	0	0	21807	1176	12607	561864	6238	868993
8	0.113	0.00236	0.01691	0.00012	0.34	0.04831	0.001	114.3	48.04	108.7	2.15	108.1	0.77	30	14	12928	625	3307	139039	3637	510714
9	0.11333	0.00233	0.01684	0.00011	0.32	0.04876	0.00099	136.2	47.24	109	2.12	107.7	0.72	66	31	9535	465	1874	81384	2699	378233
10	0.08741	0.00798	0.01671	0.00033	0.22	0.03812	0.00347	0.1	0	85.1	7.45	106.8	2.12	52	0	2214	84	686	33952	635	88497
11	0.11359	0.00224	0.0168	0.00012	0.36	0.04833	0.00094	115.6	45.39	109.2	2.04	107.4	0.75	52	0	26295	1274	18559	842315	7360	1044630
12	0.11154	0.0022	0.01676	0.00012	0.36	0.04925	0.00096	159.8	45.14	107.4	2.01	107.1	0.73	0	15	16401	810	7649	328817	4763	653059
13	0.12065	0.00234	0.01681	0.00012	0.37	0.05149	0.00099	262.9	43.61	115.7	2.12	107.5	0.73	0	0	10623	548	2288	99116	2982	421409
14	0.11116	0.0016	0.01684	0.00008	0.33	0.04766	0.00068	81.4	34.37	107	1.46	107.6	0.52	23	14	16174	773	4043	174440	4560	640548
15	0.11204	0.00183	0.0169	0.00009	0.33	0.04743	0.00077	70.3	38.6	107.8	1.67	108	0.59	21	5	12471	594	2761	124309	3472	492136
16	0.11209	0.00152	0.01684	0.00008	0.35	0.04778	0.00064	87.6	32.43	107.9	1.38	107.7	0.51	0	0	27343	1312	20987	968835	7664	1081990
17	0.1071	0.00236	0.01682	0.00012	0.32	0.04675	0.00102	36.2	50.88	103.3	2.17	107.5	0.78	12	0	10097	474	7130	297126	2897	399998
18	0.11516	0.00215	0.01684	0.00011	0.35	0.04868	0.0009	132.6	42.87	110.7	1.96	107.7	0.68	123	0	11597	567	2010	81549	3223	458584
19	0.11107	0.00289	0.01677	0.00015	0.34	0.04711	0.00121	54.4	60.77	106.9	2.64	107.2	0.94	121	22	11220	531	1640	73941	3128	445418
20	0.11466	0.002	0.01681	0.00011	0.38	0.05039	0.00087	212.9	39.57	110.2	1.82	107.5	0.68	0	0	28797	1459	26846	1200323	8319	1140298

Appendix 2. *Pb isotopic analyses of igneous feldspar from the Cyprus porphyry and galenas from the Klaza and Brown-McDade clusters. Errors are given at the 1σ level.*

Sample	$^{206}Pb/^{204}Pb$	error	$^{207}Pb/^{204}Pb$	error	$^{208}Pb/^{204}Pb$	error	$^{207}Pb/^{206}Pb$	error	$^{208}Pb/^{206}Pb$	error
Cyprus porphyry feldspar (97CH33-3)	19.267	0.09	15.6602	0.04	39.0727	0.1	0.8128	0.085	2.028	0.028
Brown-McDade - Dickson Zone galena	18.829	0.012	15.634	0.011	38.552	0.013	0.8303	0.005	2.0475	0.003
Brown-McDade - Flex Zone galena	19.156	0.006	15.64	0.005	38.816	0.009	0.8165	0.003	2.0263	0.007
Brown-McDade - Heustis Zone galena	19.186	0.002	15.672	0.002	38.92	0.002	0.8168	0.001	2.0285	0.001
Klaza - Pika vein galena	19.1485	0.01	15.685	0.01	38.9112	0.01	0.8191	0.008	2.0321	0.007
Klaza - KL11-12-196 galena	19.1859	0.01	15.7165	0.01	39.026	0.02	0.8192	0.006	2.0341	0.011
Klaza - KL14-165 galena	19.1518	0.01	15.68	0.01	38.9108	0.01	0.8187	0.005	2.0317	0.006

Stratigraphy and structural geology of the upper Hyland River area (parts of 105H/8, 105H/9), southeast Yukon

D. Moynihan
Yukon Geological Survey

Moynihan, D., 2016. Stratigraphy and structural geology of the upper Hyland River area (parts of 105H/8, 105H/9), southeast Yukon. *In:* Yukon Exploration and Geology 2015, K.E. MacFarlane and M.G. Nordling (eds.), Yukon Geological Survey, p. 187-206.

ABSTRACT

The upper Hyland River area of southeast Yukon is mostly underlain by rocks of the Neoproterozoic-Cambrian Hyland Group. The Yusezyu Formation, which forms the lower part of the Hyland Group, was previously undivided; however, good exposure in the upper Hyland River area facilitates the identification of marker horizons, including marble/limestone layers and thick units of quartz granule-pebble conglomerate. A new 1:50 000-scale map of part of the area includes ten stratigraphic subdivisions in rocks previously assigned to the Yusezyu Formation. From northeast to southwest, the structure of the area is characterized by: (1) a southwest-vergent fold and thrust belt; (2) a central region with upright, northwest-trending folds; and (3) a highly deformed region characterized by tight-isoclinal folding, in which folds and stretching lineations are at a high angle to the trend of the orogen. This deformation was accompanied by amphibolite facies, low-pressure metamorphism. A steeply-dipping fault with long strike-length is coincident with the upper Hyland River valley.

[1]*david.moynihan@gov.yk.ca*

INTRODUCTION

Large parts of eastern Yukon are underlain by rocks of the Hyland Group, a thick sequence of Neoproterozoic-Cambrian clastic and lesser carbonate rocks that form part of the Windermere Supergroup (Fig. 1). The Windermere Supergroup records sedimentation during extension that eventually led to the breakup of the Supercontinent Rodinia and the formation of the ancient Laurentian margin (Ross, 1991). The Hyland Group is the upper part of the Windermere sequence in Yukon and British Columbia. It is exposed in the core of the Selwyn fold-thrust belt, east of the Tintina fault and south of the Yukon stable block (Fig. 1).

The Hyland Group is overlain by rocks that record sedimentation in the Selwyn basin, an embayment in the Laurentian margin that was fringed by carbonate platforms from late Early Cambrian until the Middle Devonian. Rocks deposited in Selwyn basin were subsequently uplifted and eroded during rifting that accompanied deposition of the Devonian-Mississippian Earn Group. During the Mesozoic, the formation of the Cordillera led to development of the Selwyn fold-thrust belt and the emplacement of numerous mid-Cretaceous granitic intrusions (Gordey and Anderson, 1993; Rasmussen, 2013).

Gordey and Anderson (1993) defined the Hyland Group in the Little Nahanni River area (105I; Fig. 1) and recognized two major units – a lower unit with abundant coarse clastic rocks (Yusezyu Formation), overlain by fine clastic rocks of the Narchilla Formation. A thin limestone member at the top of the Yusezyu Formation was recognized (Gordey and Anderson, 1993) and a thicker limestone sequence in the same stratigraphic position was later defined as the Algae Formation in the Niddery Lake area (105O) to the north (Cecile, 2000).

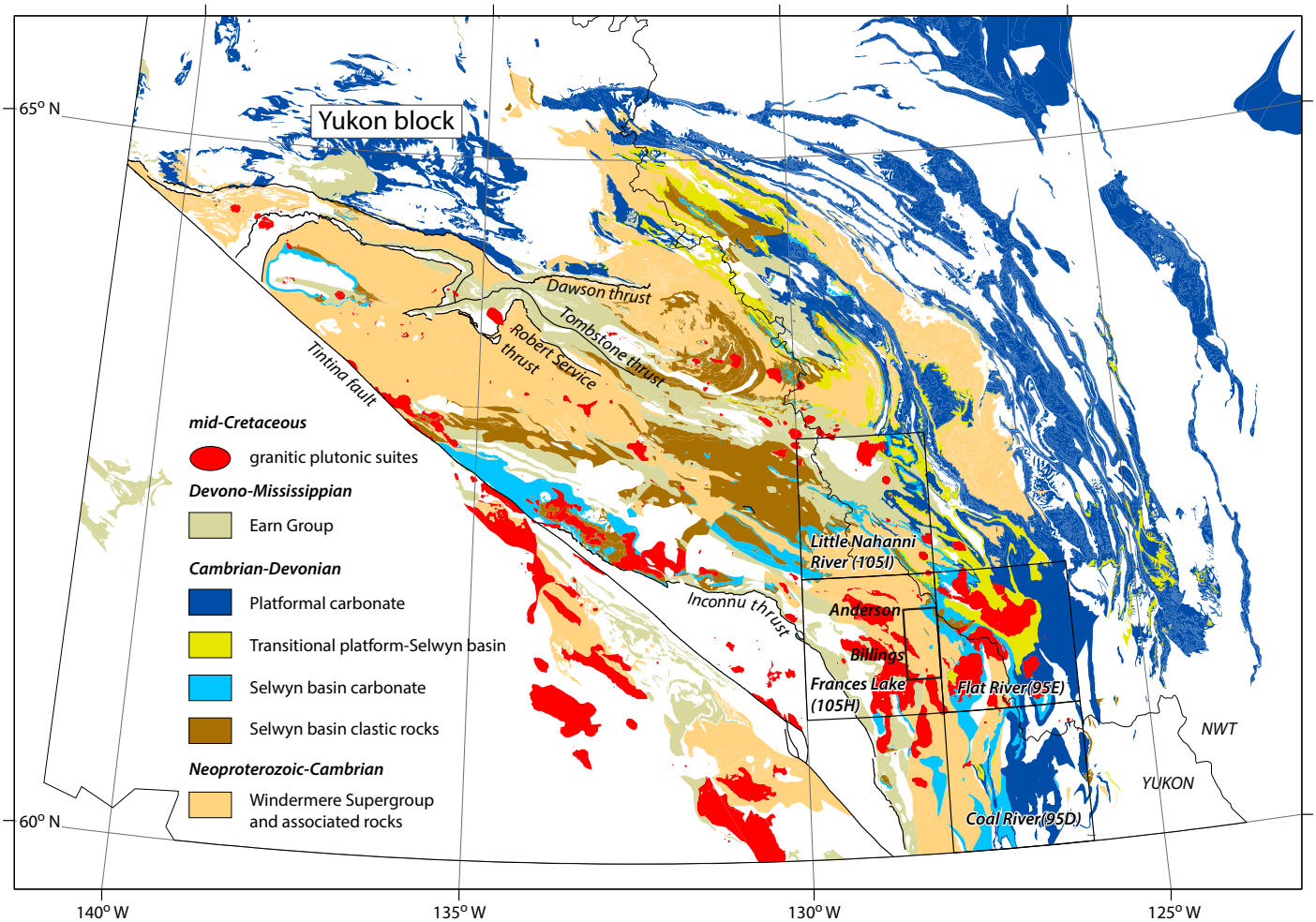


Figure 1. *Simplified geology of the Selwyn fold and thrust belt. Only major faults discussed in the text are shown for clarity. The small black box within the Frances Lake area shows the combined outline of 105H/8 and 105H/9. The plutons/batholiths shown are those of the mid-Cretaceous Cassiar, Hyland, Anvil, Tombstone, Tungsten, Tay River and Mayo plutonic suites. The largest intrusions in the Frances Lake area are the Billings and Anderson batholiths of the Hyland suite (labelled).*

The Yusezyu Formation comprises an ostensibly monotonous sequence of brown shale, sandstone, grit and subordinate calcareous rocks. Gordey and Anderson (1993) estimated a stratigraphic thickness of at least 3 km in the Little Nahanni River type area, but the base was not observed. The lack of stratigraphic subdivisions of the Yusezyu Formation presents an impediment to understanding the structure of the interior part of the Selwyn fold-thrust belt. Large structures (*e.g.*, the Dawson, Robert Service and Tombstone thrust faults; Fig. 1) have been recognized where the Hyland Group is juxtaposed with younger (Palaeozoic-Mesozoic) units, but the absence of known marker units in the Yusezyu Formation prevents recognition of faults and characterization of the structural geometry elsewhere.

This report contains preliminary results on the structure and stratigraphy of the Hyland Group and overlying units in the upper Hyland River area of southeast Yukon (Frances Lake map area, 105H). The report is based on mapping (Fig. 2) that was carried out from two-person fly camps during the summer of 2015 and the latter part of the summer of 2014. It accompanies a 1:50 000 scale open file map covering parts of NTS sheets 105H/8 and 105H/9 (Moynihan, 2016b; summarized in Fig. 2). Previously, bedrock geology of the Frances Lake area (105H) had only been mapped at a scale of 1:250 000 (Roots *et al.*, 1966).

A broad area around the Billings and Anderson batholiths (Fig. 1) is affected by syn to post-kinematic, low-pressure amphibolite-facies metamorphism (Moynihan, 2013) and this includes the western part of the mapped area (Fig. 2). Metamorphic grade increases structurally downward towards the batholiths, though their intrusion post-dates the syn-kinematic metamorphism. In order of increasing grade, metapelitic rocks belong to the Crd+Bt, And+Crd+Bt, And+Bt, And+St+Bt, Sil+St+Bt and Sil+Kfs+melt (muscovite-free) zones. Outside of this area, the regional metamorphic grade is low (chlorite zone). This report focuses on stratigraphy and structure of the area, and a full account of metamorphism will be given elsewhere.

STRATIGRAPHY

The oldest rocks in the map are currently included in the Yusezyu Formation, which extends across the map boundary from Little Nahanni River type area into Frances Lake. As a large structural culmination underlies eastern Frances Lake map sheet (centred on the Billings and Anderson batholiths), the area is likely to include deeper parts of the stratigraphy than is exposed in Little Nahanni River (105I).

Mountainous terrain in the mapped area allowed recognition of ten stratigraphic units below the Yusezyu Formation-Narchilla Formation boundary. The most prominent stratigraphic marker is a thick marble, informally referred to here as the 'Hyland marble' that appears to be widely distributed in 105H. A thick marble marker horizon was not mapped by Gordey and Anderson (1993), and it is likely that it is occurs at a lower stratigraphic level than was observed in 105I. Rather than referring to the entire sub-Narchilla stratigraphy as Yuseyu Formation, here the term is only applied to rocks between the Hyland marble and the Narchilla Formation. This allows distinction between rocks described by Gordey and Anderson (1993), which are characterized by the presence of abundant coarse grit layers and older rocks, which are not. Rocks stratigraphically below the 'Hyland marble' are assigned to the sub-Yusezyu Fm portion of the Windermere Supergroup. Future work will determine the extent to which the provisional stratigraphic subdivisions identified in this area can be traced regionally.

UNDIVIDED WINDERMERE SUPERGROUP (UNDERLYING THE HYLAND MARBLE)

Heterolithic schist in the western part of the area has been affected by amphibolite-facies metamorphism and intense penetrative deformation. This area is dominated by compositionally layered, rusty brown weathering, quartzofeldspathic and micaceous schist (uPs; Fig. 3a). Schist is mostly psammitic and semipelitic, containing thin folia/layers of pelitic schist and some white quartzite layers; marble and calc-silicate schist is also common. White to pale grey weathering, pale to medium grey, coarsely crystalline marble forms layers ranging from <1 m to several tens of metres thick. Thick, continuous bands of marble were mapped separately as unit uPm (Fig. 3b).

Metapelitic layers are thin in the heterolithic schist unit (uPs), but the area contains at least two intervals predominantly composed of orange-brown to rusty-brown weathering metapelitic and semipelitic schist (uPmp; Fig. 3c) The thickest of these bands (in western 105H/8) contains a distinctive unit, approximately 20 m thick, of laminated rock (meta-chert?) comprising alternating quartz-rich and argillitic layers (uPbq; Fig. 3d). This was referred to as banded argillite by MacLeod (1982).

HYLAND MARBLE (uPHm)

The thickest marble layer that was encountered can be traced across the mapped area and beyond, forming a distinctive stratigraphic marker. This marble approximately coincides with the upper limit of the low-pressure, amphibolite facies metamorphism that affects low structural levels (*i.e.*, most of the rocks west of the Hyland River).

The Hyland marble (Fig. 3e) is composed of pale grey to white weathering, coarsely crystalline, grey banded marble and calc-silicate. In some places, the unit is represented by a discrete band of marble/calc-silicate, tens of metres thick, under and overlain by rusty brown weathering schist units. Elsewhere, the unit is characterized by a mixed zone containing intercalated marble/calc-silicate and schist up to 200 m thick. This intercalation and variation in thickness is attributed to tight to isoclinal infolding of marble/calc-silicate with surrounding clastic metasediments. The Hyland marble is notably discontinuous where it is exposed in steep slopes overlooking the east side of the Hyland River in 105H/8. The lenticular nature of the unit here may result from boudinage of this layer.

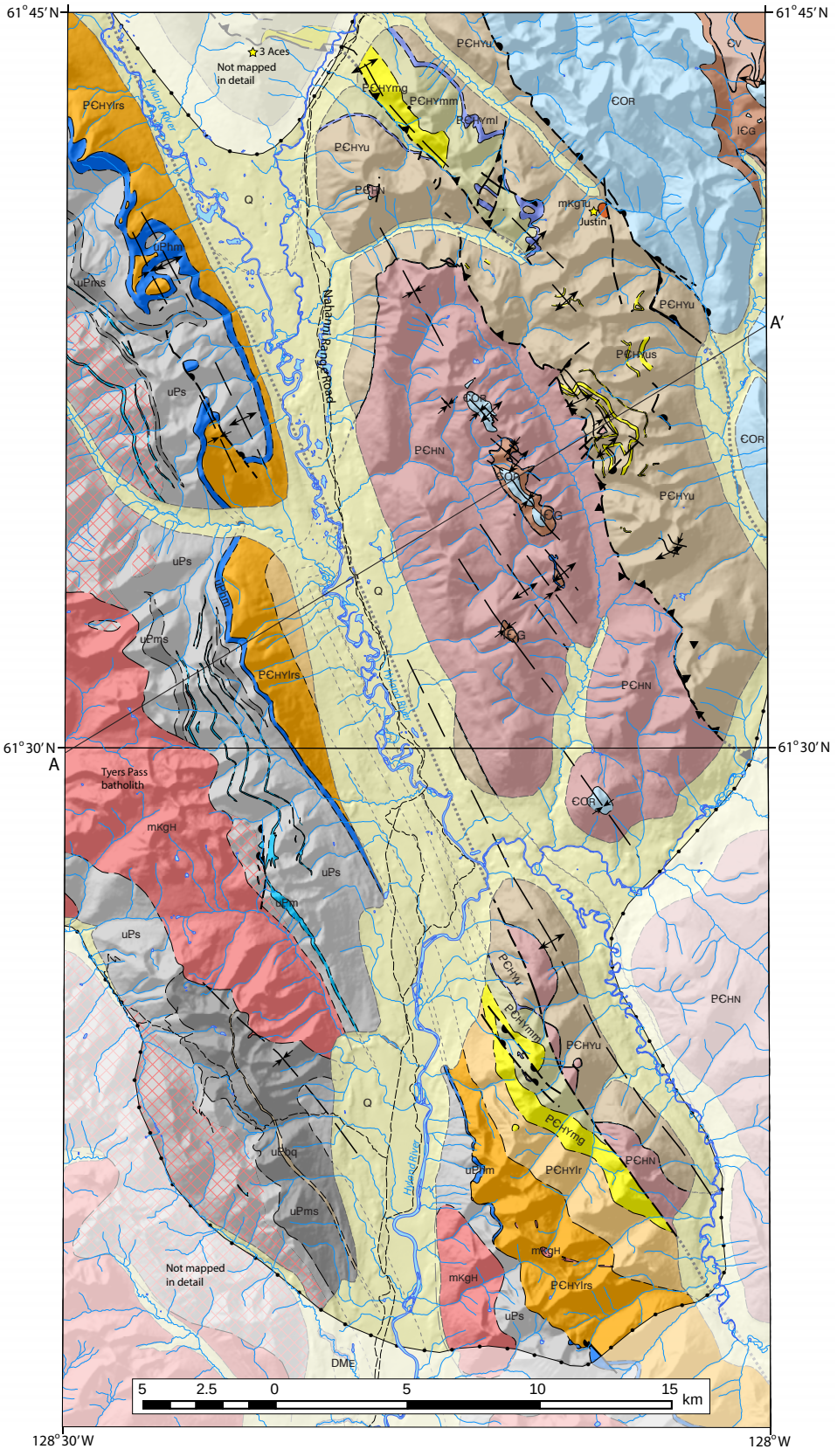


Figure 2. *Geological map and legend. The outline of the study area (105H/8 and 105H/9) is marked by a black box in Figure 1.*

PLUTONIC ROCKS

MID-CRETACEOUS

mKgTu — **TUNGSTEN SUITE:** *biotite granodiorite*

mKgH — **HYLAND SUITE:** *biotite +/- hornblende biotite granodiorite, quartz monzonite and quartz diorite*

SEDIMENTARY AND METASEDIMENTARY ROCKS

QUATERNARY

Q — **QUATERNARY**: *unconsolidated glacial, glaciofluvial and glaciolacustrine deposits; fluviatile silt, sand, and gravel, and local volcanic ash, in part with cover of soil and organic deposits*

UPPER DEVONIAN TO LOWER MISSISSIPPIAN

DME — **EARN GROUP:** *brown-weathering, brown and black shale, black and grey chert, quartzite, greywacke, chert-pebble conglomerate*

UPPER CAMBRIAN TO LOWER ORDOVICIAN

ЄOR — **RABBITKETTLE FORMATION:** *Thinly bedded and laminated cream, grey and buff-coloured argillacous limestone; thinly-bedded grey limestone.*

CAMBRIAN SERIES 2-3

lЄG — **GULL LAKE FORMATION, upper member:** *Rusty weathering, chocolate-brown weathering, dark brown to black shale; grey weathering, laminated, bioturbated mudstone-siltstone; thin-medium beds of limestone near base.*

lЄGb — **GULL LAKE FORMATION, basal member:** *Boulder conglomerate comprising grey limestone clasts in a siliciclastic, variably calcareous matrix; limestone; medium-thick bedded quartz arenite; minor greenschist*

NEOPROTEROZOIC-CAMBRIAN WINDERMERE SUPERGROUP

TERRENEUVIAN-CAMBRIAN SERIES 2

PЄHN — **NARCHILLA FORMATION:** *green, maroon and grey, well-cleaved, rhythmically-bedded mudstone and siltstone and phyllite; upper part of formation is heavily bioturbated; white-weathering thin to medium-bedded, planar and*

ЄV — **VAMPIRE FORMATION:** *grey phyllite/mudstone-siltstone; medium- to thick-bedded sandstone; minor calcareous phyllite*

EDIACARAN

HYLAND GROUP

PЄHYul — **YUSEZYU FORMATION, UPPER, limestone:** *grey and buff, thin-bedded, planar and cross-laminated limestone; thin-bedded limestone and green shale; thin to medium-bedded grey limestone pebble conglomerate and breccia; bright yellow-orange to orange-brown dolostone; correlative with Algae and Risky formations elsewhere in Yukon and NWT.*

PЄHYus — **YUSEZYU FORMATION, UPPER, sandstone/conglomerate:** *pinkish-brown, white-grey weathering, limonitic, coarse sandstone, granule and pebble conglomerate; subordinate phyllite*

PЄHYu — **YUSEZYU FORMATION, UPPER (undivided):** *grey and pale green phyllite, sandstone, granule and pebble conglomerate; calcareous phyllite, siltstone and sandstone; silty and sandy limestone*

PЄHYml — **YUSEZYU FORMATION, MIDDLE, fetid limestone:** *thin, locally medium-bedded, medium to dark grey, generally fetid limestone; includes calcilutite, calcarenite and calcirudite; brownish-grey silty/sandy limestone*

PЄHYmm — **YUSEZYU FORMATION, MIDDLE, mixed unit:** *grey, maroon and green phyllite, sandstone, granule and pebble conglomerate (grit); grey limestone, silty/sandy limestone*

PЄHYmg — **YUSEZYU FORMATION, MIDDLE, 'grit':** *white or pale grey weathering, poorly sorted coarse sandstone, granule and pebble conglomerate; mostly quartz grains, with 10-15% milky-white feldspar grains in argillaceous/micaceous matrix.*

PЄHYlr — **YUSEZYU FORMATION, LOWER, recessive unit:** *grey, brown-weathering phyllite with subordinate thick to massive beds of coarse sandstone and granule-pebble conglomerate*

PЄHYlrs — **YUSEZYU FORMATION, LOWER, resistant unit:** *medium to thick bedded sandstone and granule conglomerate; brown-weathering grey phyllite; thin-bedded siltstone-fine sandstone; minor thin-bedded grey limestone*

SYMBOLS

geologic contacts (defined, approximate, inferred, covered).....

fault; movement not known (defined, approximate, inferred, covered).....

thrust fault (defined, approximate, inferred, covered).....

normal fault (defined, approximate, inferred, covered).....

anticline (upright, overturned).....

syncline (upright, overturned).....

Au mineralization.....

cross-hatching indicates regions that comprise a mix of country rock and unit mKgH. In these regions, dikes, sills and other small bodies of mKgH form 25-75% of the rock.

uPHm — **"HYLAND MARBLE":** *pale grey to white weathering marble; calc-silicate schist; thin folia of metapelitic schist; locally abundant (structural?) intercalations of micaceous schist*

uPs — **HETEROLITHIC SCHIST:** *semi-pelitic schist, psammitic schist, metapelitic schist; marble; calc-silicate; quartzite*

uPm — **MARBLE:** *pale grey to white weathering, medium to dark grey marble*

uPbq — **"BANDED QUARTZITE":** *Laminated to thinly-bedded silica-rich rock with thin, dark, micaceous folia.*

uPms — **METAPELITIC SCHIST:** *rusty orange-brown weathering, medium to coarse-grained metapelitic and semi-pelitic schist; pasmmitic schist*

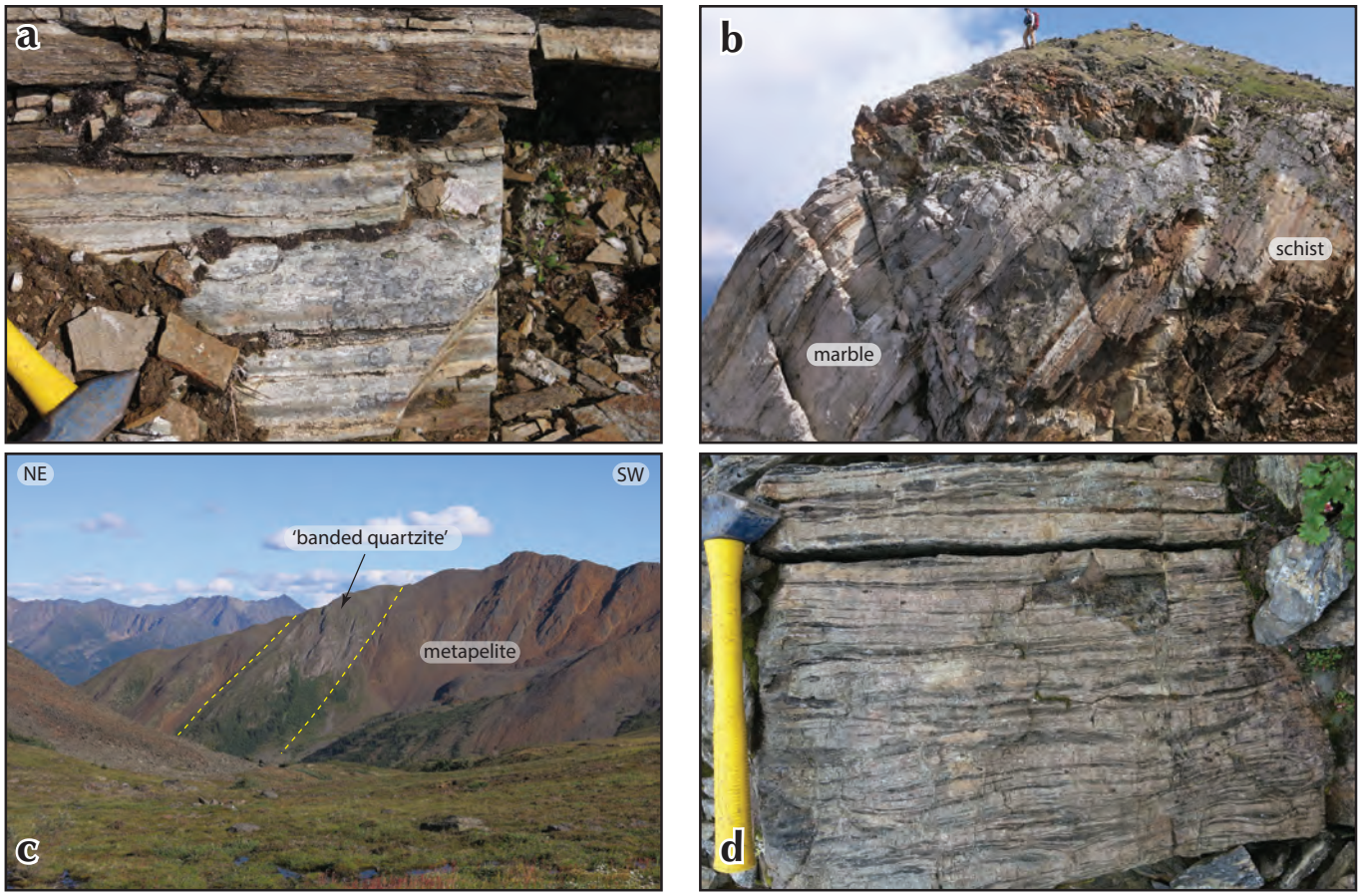


Figure 3. *(a) Interlayered quartz-rich and mica-rich schist of unit* uPs*. Hammer for scale. (b) Grey marble (~5 m thick) interlayered with rusty brown micaceous schist, unit* uPs*. Person for scale. (c) Rusty brown weathering metapelite (*uPms*), with grey-coloured band of 'banded quartzite' (*uPbq*) surrounded by rusty, orange-brown weathering metapelite. Relief on the photographed ridge is approximately 350 m. (d) 'Banded quartzite' (*uPbq*) unit forms a distinctive marker tens of metres thick in the west-central part of 105H/8. It comprises interlayered lamellae of grey, fine-grained quartzite and dark green-grey to black argillite. Numerous pinch and swell (boudinage) structures are visible. Hammer for scale.*

YUSEZYU FORMATION

LOWER YUSEZYU FORMATION

The lowest part of the Yusezyu Formation is a resistant unit (PЄHYlr) that is dominated by medium to thickly bedded, medium to coarse-grained, brown to cream weathering sandstone (Fig. 3f). In most of the unit, phyllite is subordinate and forms thin layers between sandstone beds. However, the sandstone: phyllite ratio is variable, and there are some thick intervals (tens of metres) composed exclusively of laminated phyllite. Phyllite in the lowest part of the unit is metamorphosed to cordierite-biotite spotted hornfels. The uppermost part of this unit also includes some thin (2-3 m) silty limestone layers. This unit forms resistant topography and the sandstone beds impart a ribbed appearance to hillsides underlain by these rocks (Fig. 3g).

The resistant unit is overlain by a recessive interval (PЄHYlrs) that forms brown shaly slopes. Phyllite is the dominant rock type, but there is also fine to medium-grained sandstone, and widely spaced intervals of thick to very thickly-bedded granule-pebble conglomerate ('grit') that forms pinnacles on ridge-tops.

MIDDLE YUSEZYU FORMATION

The lowest part of the middle Yusezyu Formation (PЄHYmg) comprises a thick sequence of pale grey to white weathering, medium to very thickly bedded coarse sandstone and granule-pebble conglomerate ('grit'). The conglomerate (Fig. 3h) is moderately sorted and is dominated by quartz grains, with 10-15% milky-weathering feldspar grains. Unlike elsewhere in the formation, grit is the dominant rock type and phyllitic interbeds are thin and volumetrically minor. Calcareous sandstone is locally also a constituent of this unit. The thick grit interval is overlain by a mixed sequence (PЄHYmm) including varicoloured phyllite (maroon, green, grey and blue-grey), thickly-bedded sandstone and granule conglomerate, medium-bedded sandstone, calcareous phyllite and thinly-bedded grey limestone. The top of this mixed unit is a thick sandstone-conglomerate interval, which is overlain by a distinctive fetid limestone marker horizon (PЄHYml; Fig. 3i). This limestone, which is approximately 30 m thick, is thin to medium bedded with internal planar laminations and less common cross-laminations. The weathered surfaces are mostly pale to medium grey and locally pale creamy brown. Freshly broken surfaces are dark grey and crystalline. Most of the rock is recrystallized grainstone, but some thin-medium limestone conglomerate layers are present. In some cases, the conglomerate layers contain distinctive bright orange or red shaley clasts. A notable feature of the limestone is the sulphurous smell emitted by much of the unit when it is walked over or hammered. This limestone may be equivalent to a "black, fine crystalline, thin(?)-bedded limestone" noted by Gordey and Anderson (1993, p. 41) in the Yusezyu Formation type section.

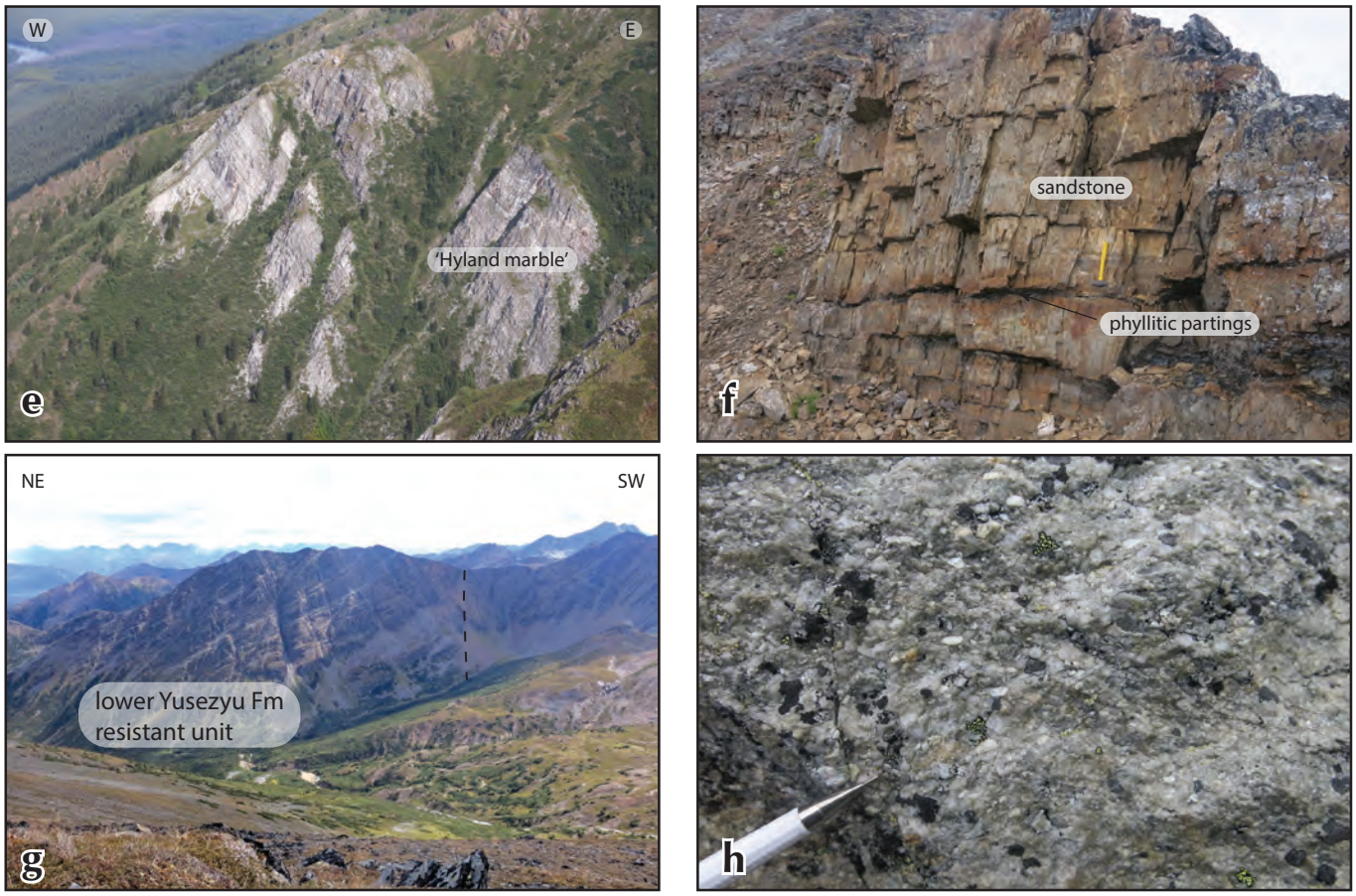


Figure 3 (continued). *(e) Pale grey weathering, marble band ('Hyland marble',* uPHm*) forms cliffs on the East side of the Hyland River in central 105H/8. It is approximately 75 m thick here. (f) Thickly bedded sandstone layers with thin phyllitic partings in the lower Yusezyu Fm, resistant unit that lies directly above the 'Hyland marble'. Hammer for scale. (g) Sandstones of the Lower Yusezyu Fm, resistant unit lends a ribbed appearance to this ridge in the eastern part of 105H/8. The elevation difference between the top of the ridge and the creek in the middle ground is approximately 550 metres. Dashed line marks the trace of a fault. (h) Granule-pebble conglomerate ('grit') of unit* PЄHYmg*. The clasts are mostly grey quartz, with prominent milky-white feldspar grains. Pencil for scale.*

UPPER YUSEZYU FORMATION

The upper part of the Yusezyu formation (PЄHYu) comprises a heterogeneous mix of variably calcareous, mostly fine-grained clastic rocks. The dominant rock type is well-cleaved, brown-weathering, medium grey, pale grey and pale green phyllite. Phyllite is thinly-bedded and laminated with graded bedding and ripple cross-lamination in silty layers; locally, the phyllite is calcareous (Fig. 3j). Other rocks types include thin to very thickly bedded sandstone and conglomerate, and thin to medium-bedded calcareous sandstone and silty-sandy limestone. Though most of this unit is relatively fine-grained, it also includes a number of resistant, thick to very thickly bedded intervals of coarse sandstone and pebble-granule conglomerate (PЄHYs). These intervals are generally 5-20 m thick and form excellent structural markers. Coarse sandstone and conglomerate layers are commonly graded and have erosive bases, some of which contain abundant rip-up clasts (Fig. 3k). The base of this unit is marked by one such layer of quartz (+subordinate feldspar) granule-pebble conglomerate.

A distinctive aspect of the upper part of the Yusezyu Formation is the presence of one or more layers (approximately 15-20 m thick) of olistostrome. This rock comprises clasts of massive orange weathering dolostone, up to 1 m diameter, in a green matrix (Fig. 3l). The matrix is a wacke composed of green shale with abundant poorly sorted, variably sized subangular to subrounded quartz grains.

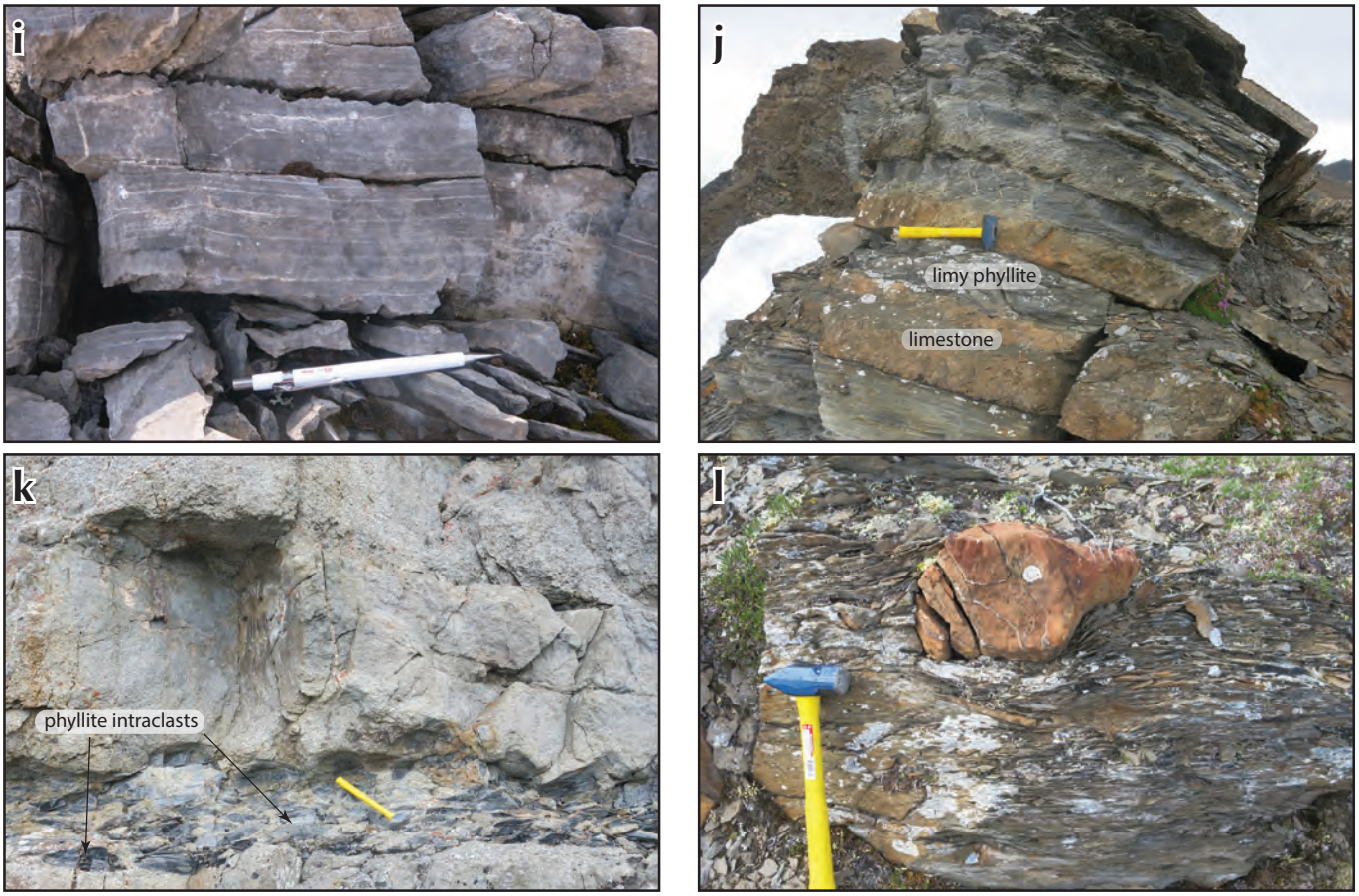


Figure 3 (continued). *(i) Grey, thinly bedded fetid grainstone of unit* PЄHYml*. This limestone forms a prominent marker horizon in the middle Yusezyu Formation on either side of the Hyland fault. Pencil for scale. (j) Medium to thin beds of limestone and limy phyllite in the upper part of the Yusezyu Fm. Much of the upper part of the formation comprises fine-grained, variably calcareous metasediments. Hammer for scale. (k) Thick beds of granule-pebble conglomerate ('grit') in the upper part of the Yusezyu Fm. The base of the lower bed contains abundant rip-up clasts, now converted to phyllite. (l) An olistostrome forms a distinctive marker in the upper part of the Yusezyu Formation. Orange dolostone clasts sit in a matrix of green wacke, which contains abundant subangular quartz grains. Hammer for scale.*

The limestone member (PЄCHYul) that marks the top of the Yusezyu Formation is approximately 10-15 m thick. It includes thin-medium bedded grey limestone and thin to thick beds of calcirudite, each interbedded with cleaved laminated green mudstone (Fig. 3m). There are also thin beds of orange-weathering silty limestone with planar and ripple lamination (BC Bouma sequences) interbedded with green mudstone in the upper part of the member. The limestone member is gradational into the overlying Narchilla Formation and its top is defined as the uppermost limestone layer (Gordey and Anderson, 1993).

NARCHILLA FORMATION

The base of the Narchilla Formation consists of thinly bedded green shale and yellow-brown weathering, parallel laminated calcareous sandstone. These sandstone beds die out up-section over an interval of ~10-20 m. The remainder of the formation is dominated by laminated, graded, maroon, green and grey-green, well-cleaved mudstone (±siltstone) and shale (Fig. 3n). It also includes some sandstone beds and rare silty limestone layers. Sandstone forms thin to medium beds that weather white; they commonly show an upward progression in their internal structure, with massive bases overlain by intervals that display planar lamination, followed by cross-lamination; these progressions are interpreted as ABC Bouma sequences. The thickness of the Narchilla Formation is poorly constrained, but it is at least several hundreds of metres thick, and probably broadly similar to the thickness at its type section in the Little Nahanni River area to the north (750 m; Gordey and Anderson, 1993).

Parts of the Narchilla Fm that are bright maroon or green are friable and give rise to non-resistant shaly slopes made up of small rock fragments. Much of the upper part of the Formation, however, comprises relatively competent, bioturbated, pale green, olive green and green-grey, cleaved mudstone, which is more resistant than underlying shaly intervals and the overlying Gull Lake Formation. Roots *et al.* (1966) interpreted this variation as a stratigraphic transition and included the resistant rocks in what is now referred to as Vampire Formation (unit 3 of Roots *et al.*, 1966). As the basal Gull Lake Formation sits above both bright green/maroon friable rocks and duller, more competent rock, this would require an unconformity with significant relief beneath Gull Lake Formation. While such an unconformity may exist (see below), boundaries between colourful variegated shales and duller more competent rock are geometrically complex, and range from gradational to sharp, suggesting a secondary, non-stratigraphic control. Here, all of the rock between the top of the Yusezyu Formation and Gull Lake Formation is included in a single unit (Narchilla Formation) and patchy variation in the colour/competence is interpreted to reflect heterogeneous diagenesis/alteration of the rocks.

VAMPIRE FORMATION

The Early Cambrian Vampire Formation (Fritz, 1982) crops out in the northeast corner of the mapped area, in the hanging wall of the Sprogge fault. It is dominated by dark to steel grey phyllite, with lesser medium to very thick-bedded pale grey sandstone and rare thin calcareous phyllite layers. The phyllite forms compact outcrops that are more resistant than shale of the overlying Gull Lake Formation. In the region to the east of the mapped area, the Vampire Formation has a distinctive rusty reddish-brown weathering colour in the contact aureoles of mid-Cretaceous granitic plutons.

The Vampire Formation is considered to be a broadly coeval, palaeogeographically inboard equivalent to the Narchilla Formation (Gordey and Anderson, 1993; Martel *et al.*, 2011) and the two units are overlain by identical stratigraphy. Distinction between the formations can be difficult and in the Coal River area (95E), the position of the boundary is arbitrary (Pigage *et al.*, 2015). In the upper Hyland River area, the units can be distinguished on the basis that phyllite of the Vampire Formation is uniformly grey and less friable, and sandstone beds are thicker than in the Narchilla Formation. Colour differences may not be stratigraphically significant, however, and it is likely that the transition between the two formations is gradational.

GULL LAKE FORMATION

The basal member of the Gull Lake Formation (lЄGb) sharply overlies Narchilla and Vampire formations and varies from approximately 10 m to several tens of metres thick. The dominant rock type is grey limestone conglomerate, but non-conglomeratic pale grey limestone is common and laminated argillaceous limestone is also locally present. The conglomerate (Fig. 3o) is poorly sorted, with sub-angular to sub-rounded clasts of grey limestone in the pebble to boulder size range; in places clasts up to 1 m in diameter are present. The matrix to the conglomerate is variably calcareous, sandy, and generally weathers grey or yellow-orange. Much of the conglomerate is massive, but thick-bedded layers with a

resistant, sand-rich matrix are common in the upper part. The top of the basal member is locally marked by a thick bed of grey, medium to coarse-grained sandstone.

Archaeocyathids were observed within grey limestone clasts at a single locality. These fossils are characteristic of the basal unit of Gull Lake Formation and indicate the unit is Cambrian Stage 2 or younger. The Gull Lake Formation was considered to be conformable with the underlying Narchilla Formation in the Little Nahanni River type area (Gordey and Anderson, 1993). However, the contact is unconformable in the Rackla area of east-central Yukon (Moynihan, 2016a) and an unconformity of this age is also widespread on the Yukon block (see discussion in Abbott, 1997).

The basal member of Gull Lake Formation is sharply overlain by the main/upper unit (lЄG). This contains a few 10-15cm thick beds of cream coloured laminated limestone near its base (lowermost 3 metres) but is otherwise composed of >200 m of dark argillite and phyllite. The lower portion of lЄG is dark grey to black, carbonaceous, laminated argillite with local spherical phosphate(?) nodules. The upper part of the unit is paler grey, laminated and commonly has a mottled appearance due to bioturbation. Rusty brown weathering of fracture surfaces is characteristic of the entire unit (Fig. 3n), and many rusty surfaces display an iridescent sheen. The argillite/phyllite is recessive and typically forms smooth, black to chocolate-brown coloured scree slopes; in places, however, the upper part of the formation weathers pale blue-grey.

The original thickness of the Gull Lake Formation is unknown as it is progressively cut out beneath an unconformity at the base of the Rabbitkettle.

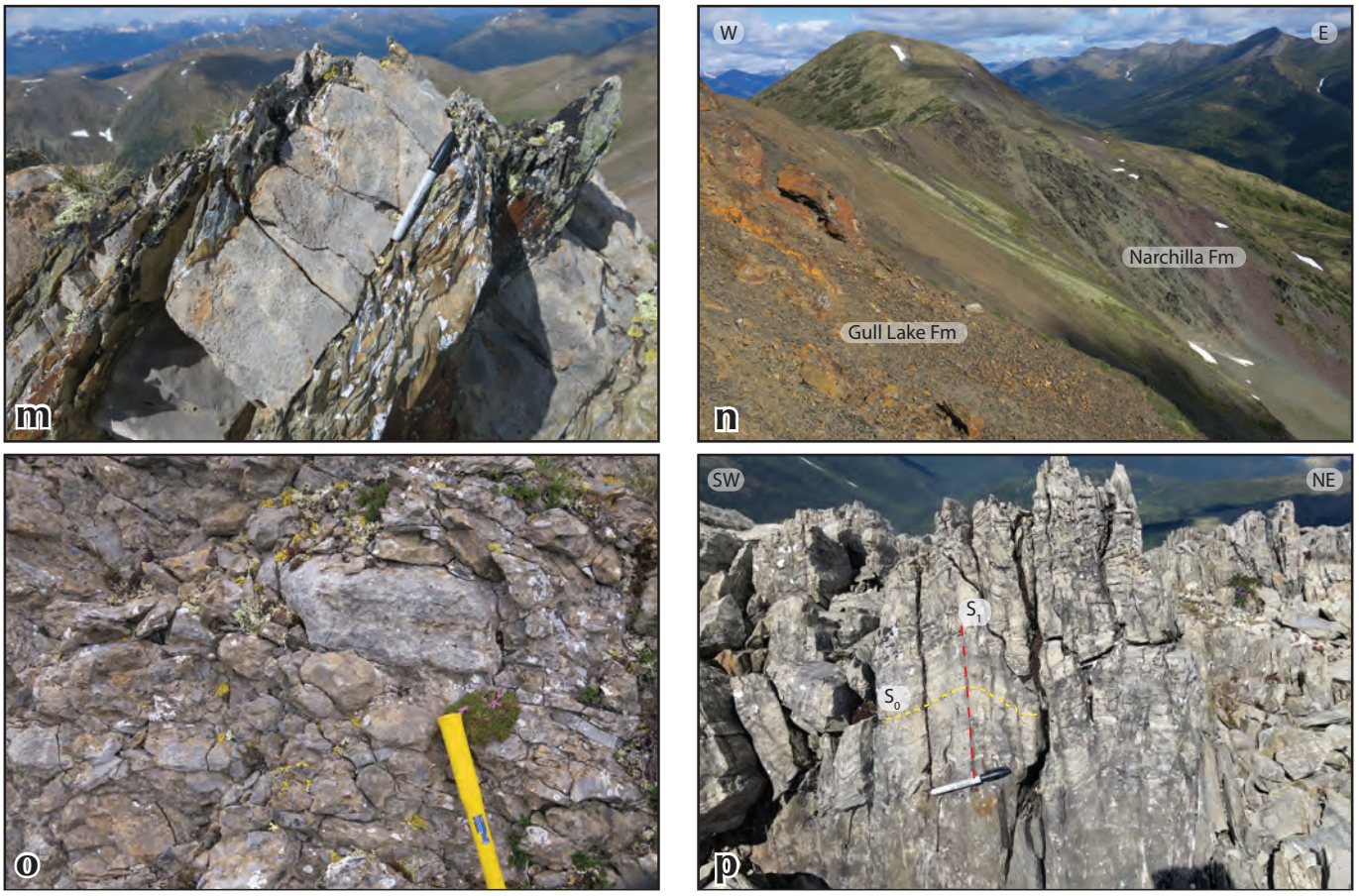


Figure 3 (continued). *(m) Interbedded grey limestone and green shale in the uppermost part of the Yusezyu Formation (limestone member, PЄHYul). This unit separates. (n) Rusty-weathering, brown shale of the Gull Lake Formation (foreground) overlies green and maroon mudstone of the Narchilla Formation. The distance from the photo site to the hilltop in the left side of the photo is approximately 1 km. (o) Limestone boulder conglomerate at the base of Gull Lake Formation. Rare archaeocyathids in limestone clasts indicate a maximum age of Cambrian series 2 for this unit. (p) Laminated argillaceous limestone of the Rabbitkettle Formation. Bedding (S_0) is disrupted across dark, graphite-rich, pressure-solution cleavage seams (S_1).*

RABBITKETTLE FORMATION

The Rabbitkettle Formation (ЄOR) comprises thin-bedded and laminated argillaceous limestone, with lamellae of limy argillite and lesser thin-bedded non-argillaceous fine-grained limestone (Fig 3p). Argillaceous limestone weathers cream, buff, grey and pale brown, whereas limestone layers weather pale grey. Limestone is locally replaced by sugary-textured, yellow to orange weathering dolostone. The Rabbitkettle Formation also contains numerous thin (tens of cm), altered mafic metavolcanic layers or dikes.

The Rabbitkettle Formation forms relatively vegetation-free, grey to yellow rubbly scree slopes. In some places the primary layering in the Rabbitkettle Formation is heavily disrupted across graphite-rich pressure solution cleavage planes. In these locations, discontinuous, lensoidal, secondary compositional layering is developed sub-parallel to cleavage.

The transition from underlying units to the Rabbitkettle is sharp and unconformable. The unconformable nature of its base is exemplified in east-central 105H/9, where the folded unconformity cuts down through the Gull Lake Formation (Fig. 7a).

Poorly preserved, non-age-diagnostic trilobite fragments were observed in one locality, but regionally the formation is Upper Cambrian-Lower Cambrian. Roots *et al.* (1966) indicate a number of fossil localities in this unit and assigned an age of Middle to Late Cambrian.

IGNEOUS ROCKS

The largest igneous body in the area is the Tyers Pass batholith, which forms part of the mid-Cretaceous Hyland Suite (mKgH). It is a northeast-dipping sheet-like body dominated by equigranular, medium grained biotite granodiorite and lesser hornblende-biotite granodiorite. Rocks are generally undeformed except near the base of the batholith, where it is locally weakly foliated. The batholith contains numerous screens of country rock and metasedimentary xenoliths are common. Xenocrysts of andalusite are also locally present. The boundary of the batholith is generally gradational, with abundant dikes in the adjacent country rock.

A dense network of dikes, similar in composition to the Tyers Creek batholith, affects large areas in the western part of the mapped area. These areas contain varying, sub-equal proportions of country rock and dike rock, and the dikes commonly coalesce to form numerous small plutons. The boundaries between these areas and those mapped as part of major batholiths are difficult to determine and, at least locally, arbitrary. Most dikes in this part of the area are equigranular and granodioritic, but quartz-feldspar porphyry dikes are also present, some of which weather pink.

Dikes and small intrusions are scattered throughout the area west of the upper Hyland fault. These include fine-grained green coloured dacitic (?) dikes. These are sub-equigranular, with some phenocrysts of hornblende and plagioclase in a fine-grained matrix. There are some small intrusions of medium-grained hornblende granodiorite, particularly in the Lower Yusezyu Formation east of the Hyland River (southern 105H/8). These are medium grained, commonly weather pink and are locally porphyritic.

Numerous felsic dikes intrude the Yusezyu Formation in the area around the Justin pluton, particularly to the south of the intrusion. These dikes contain mm-scale quartz phenocrysts in a white-weathering felsic matrix. One similar dike was observed in the Rabbitkettle Fm hanging wall of the Sprogge fault.

The northeastern part of 105H/9 also hosts numerous mafic dikes. These are dense, dark brown aphanitic, cpx-bearing vesicular rocks that commonly contain xenocrysts of spinel and a heterolithic suite of xenoliths. The dikes occupy brittle fracture sets and some show columnar jointing.

STRUCTURAL GEOLOGY

All (meta-) sedimentary rocks in the area are folded and penetratively deformed. The nature of the penetrative foliation ranges from phyllitic in eastern, low-grade parts of the area to schistose and gneissic in regions of higher metamorphic grade. Foliation dips to the northeast in most of the area, but there are large cross-strike differences in the orientation of folds and lineations, and the style of deformation. A cross-section (Fig. 4) illustrates some of this variation and the distribution of the six structural domains described below (Fig. 5). In broad terms, the area can be divided into three regions:

- A southwest-vergent fold and thrust belt in the northeast corner of the mapped area (domains 1-3). Folds in this area mostly trend NW (domains 1 and 2).

- A central region characterized by upright, NW-trending folds (domain 4)
- A highly deformed region in the southwest, characterized by tight-isoclinal folding, in which folds and stretching lineations trend at a high angle to strike (domains 5 and 6).

DOMAIN 1

Domain 1 includes rocks belonging to the Vampire, Gull Lake and Rabbitkettle formations in the northeast corner of 105H/9. The foliation (S_1) dips northeast at steep to moderate angles and is axial planar to open-close folds and has axes that mostly plunge at shallow angles to the northwest or southeast (Fig. 6a). Folds (F_1) are upright but mostly asymmetric, with relatively steep and short southwest-dipping limbs (Fig. 7a). There is large relief and good exposure in this area but the relative homogeneity of the Rabbitkettle Formation means that large-scale folds are not prominent.

SPROGGE FAULT

The boundary between domains 1 and 2 (and locally also the domain 1-3 boundary; Fig. 5) is marked by a northeast-dipping fault, or series of faults that separates Yusezyu Formation from Rabbitkettle Formation. This is interpreted as a northeast-side-down normal fault/fault zone.

For much of its length, the Yusezyu Fm-Rabbitkettle Fm boundary is marked by a simple fault/fault zone (here termed the Sprogge fault) that dips moderately steeply towards the northeast. The geometry is more complex, however, in the area southeast of the Justin pluton. On the ridge immediately south of the pluton (1.5 km to the southeast of its centre), the Yusezyu Fm-Rabbitkettle Fm boundary is marked by a steep normal fault (Kangas fault; Fig. 5) that is interpreted to offset the Sprogge fault (Fig. 7b). Rocks to the west of the Kangas fault are

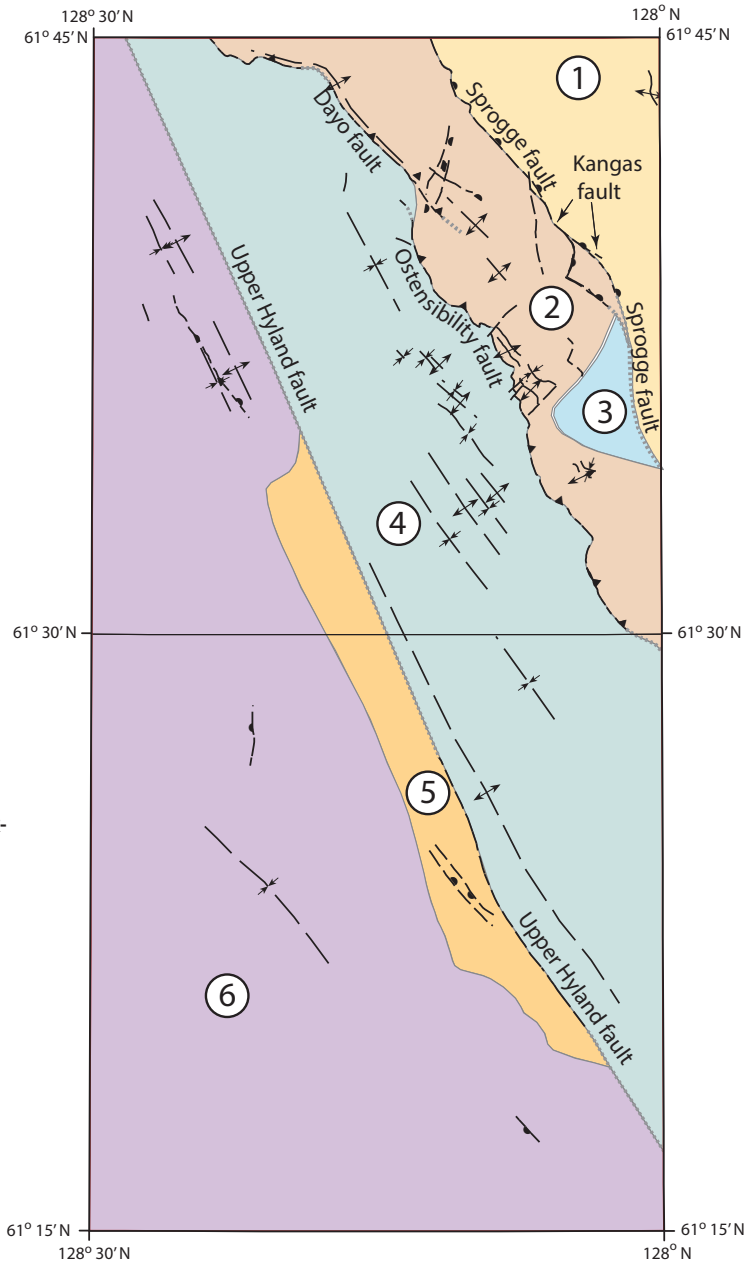


Figure 5. *Structural domains 1-6 and major faults referred to in the text. Symbols as in Figure 2.*

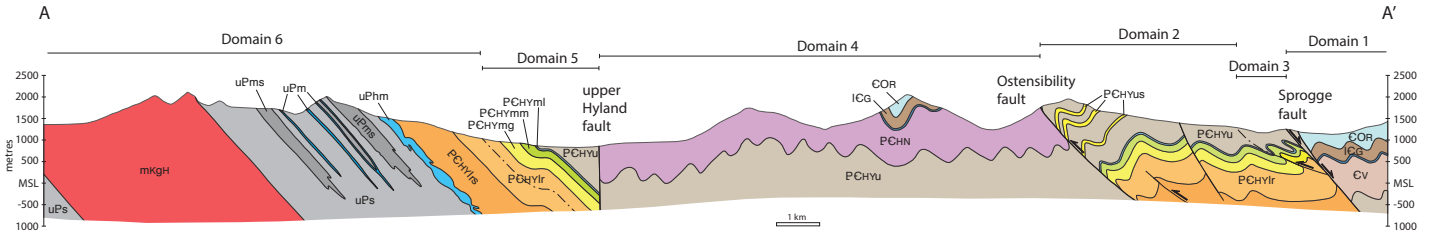


Figure 4. *Cross section across line A-A′; see Figure 2 for location of section line and legend.*

hornfelsed and host numerous small granitic intrusions, whereas dikes/sills are absent from rocks on its east side. This demonstrates post-mid-Cretaceous motion on the Kangas fault. Further south (~4 km to the south-southeast), a northeast-dipping sliver of basal Gull Lake Fm (limestone conglomerate and minor greenschist) is structurally intercalated between two panels of upper Yusezyu Fm

The Sprogge fault extends southeast into the Flat River area (95E, Gabrielse *et al.*, 1973), and continues northweast into the Little Hyland River valley, where it separates Yusezyu Formation (west side) from Vampire Formation (east side). Further up the valley to the northwest, hills to the west of the valley are underlain by Narchilla Fm, and it is not clear whether the fault continues the length of the valley or whether the Narchilla Fm-Vampire Fm contact is depositional.

Hart and Lewis (2006) interpreted the Sprogge Creek fault as a continuation of the March fault (Gordey and Anderson, 1993), a southwest-dipping thrust fault in the Little Nahanni River area that marks the northeastern limit of the Gull Lake Formation. However, this interpretation is subject to uncertainty, as there may not be physical continuity between the structures, they dip in opposite directions and there is Gull Lake Formation on either side of the Sprogge fault. Hart and Lewis (2006) further postulated that the March fault/Sprogge fault continues south into the Coal River area (95D) and continues along a magnetic anomaly that is coincident with the northern part of the Acland fault (Pigage *et al.*, 2015). As noted below, the Acland fault is more likely continuous with the Upper Hyland fault.

DOMAIN 2

Domain 2 is bounded by the Sprogge fault on the east and by two northeast-dipping faults in the west; the Ostensibility and Dayo faults.

The Ostensibility fault is a northeast-dipping reverse fault which marks the boundary between the Yusezyu Formation and the Narchilla Formation in the eastern part of 105H/9. Rocks adjacent to the fault are strongly foliated and compositionally banded. The location of the fault commonly coincides with discontinuous lenses of overturned limestone or brecciated orange-brown, sugary-textured dolostone. These rocks are interpreted as variably altered limestone from the uppermost part of the Yusezyu Fm (PЄHYul). The Dayo fault is north of and sub-parallel to the Ostensibility fault (parallel to Dayo Creek). It is a steeply-dipping fault that juxtaposes the grit member of the middle Yusezyu Formation (PЄHYmg) against the upper Yusezyu Formation. The fault is interpreted as a continuation of a thrust fault north of the 3 Aces (formerly 3Ace) prospect that also carries PЄHYmg in its hanging wall.

Foliation in Domain 2 dips at moderate to shallow angles to the northeast (Fig. 7c), and is axial planar to open-close folds that trend northwest (Fig. 6b). The axes of these folds generally plunge at shallow angles. Folds are asymmetric (Fig. 7d,e) and overturned to the southwest, adjacent to the Ostensibility Creek fault (Fig. 7f). Some fold trains are well defined by prominent sandstone/grit layers in the upper Yusezyu Formation (PЄHYu) and can be traced for several km along strike.

DOMAIN 3

This domain also lies within the corridor between the Sprogge Creek and Ostensibility Creek faults (Fig. 5). Foliation dips at shallow to moderate angles to the northeast, as in domain 2, but is instead axial planar to folds that plunge towards the north and northeast, approximately down the dip of the foliation (Fig. 6c). These folds are tight and commonly disharmonic, and layers that define folds are highly discontinuous; this lends a chaotic appearance to exposure viewed approximately down plunge.

The folds in this domain are interpreted to have been tightened and rotated towards their down-dip orientation during progressive deformation. Kinematic study is required to determine whether fold tightening was accompanied by thrust or normal sense shearing during foliation development; however, the fact that this zone appears to form a wedge within domain 2 suggests that it is a thrust-sense shear zone associated with the southwest-vergent deformation that characterizes domains 1 and 2.

Although the Selwyn fold and thrust belt generally verges towards the foreland (to the northeast/east), southwest-vergent deformation was also noted in the southern part of the Little Nahanni River area (Gordey and Anderson, 1993), and it is possible that it forms an extensive belt in SE Yukon.

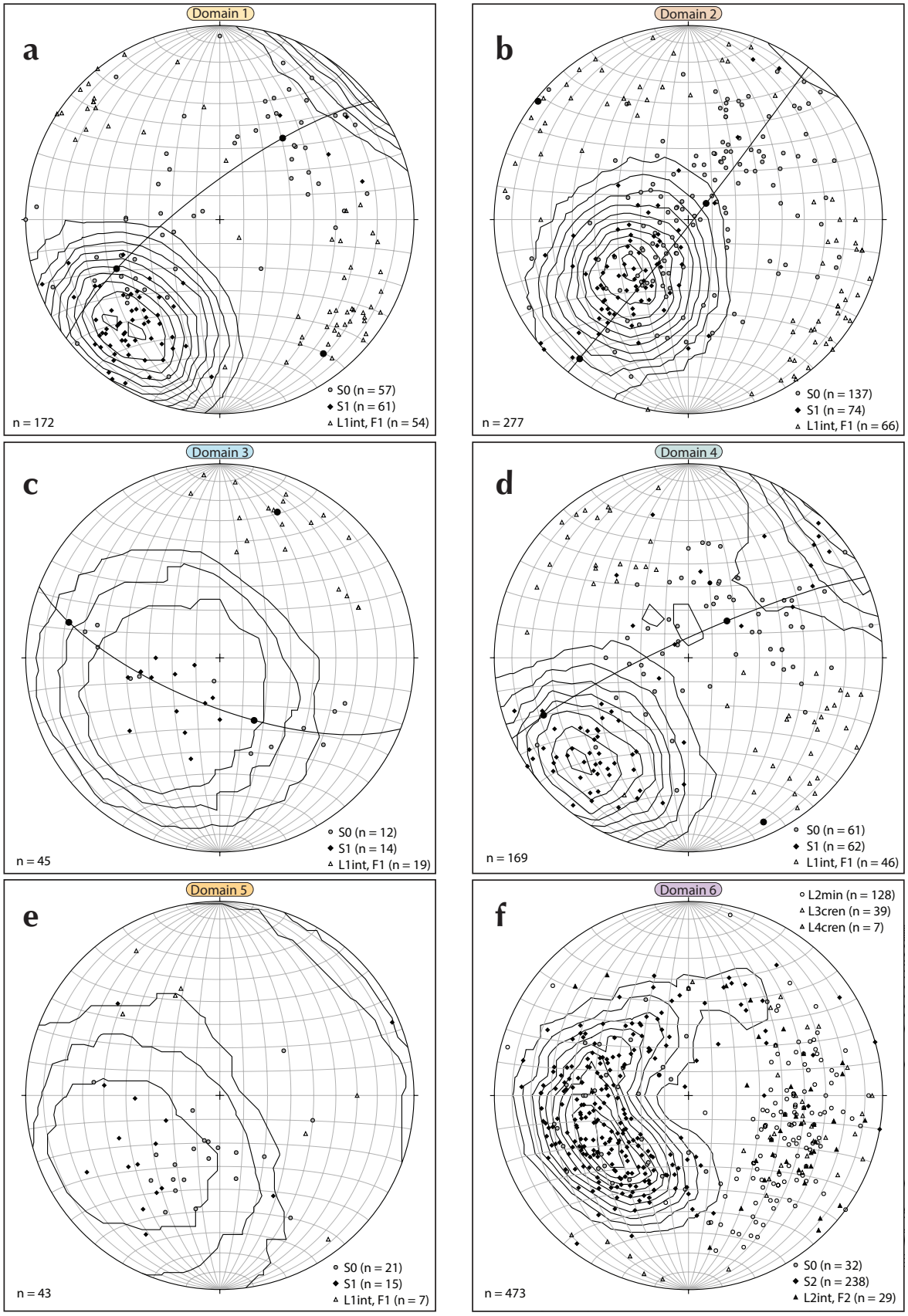


Figure 6. *Equal area, lower hemisphere projections showing the orientation of structures in each of the six structural domains. The dominant foliation in each domain (S_1, S_2) is contoured using the Kamb (1959) method, with contour intervals of 2σ.*

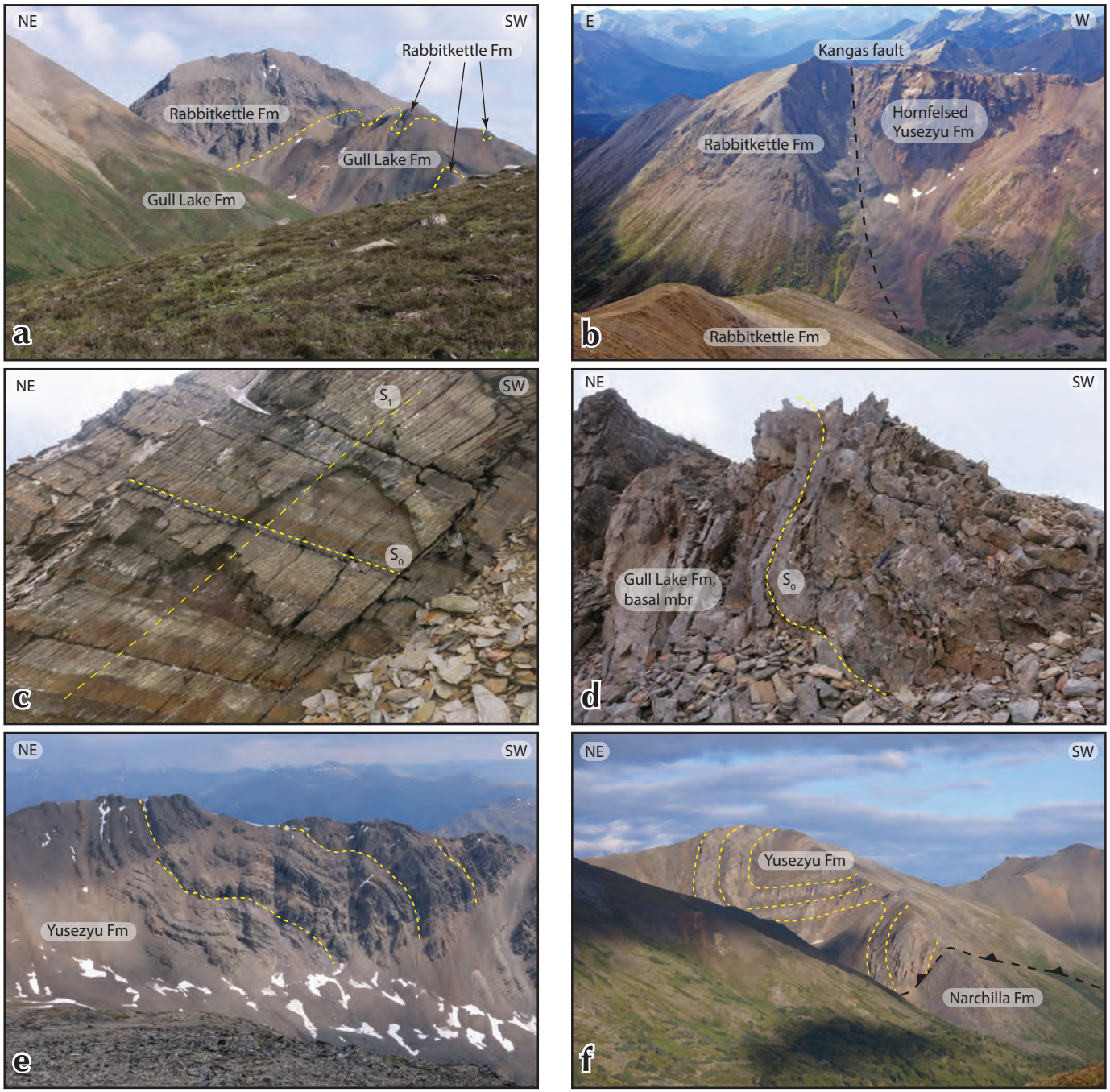


Figure 7. *(a) Folded contact between Gull Lake Fm and Rabbitkettle Fm on the eastern margin of 105H/9 (domain 1). Cleavage dips northeast and folds are asymmetric, with shorter, steeper southwest-dipping limbs. Elevation difference between the viewpoint and the highest mountaintop is approximately 650 m. (b) Fault contact between Rabbitkettle Fm and hornfelsed Yusezyu Fm approximately 2 km southeast of the Justin pluton in eastern 105H/9 (boundary between domains 1 and 2). The fault dips steeply and is interpreted to cut a lower-angle normal fault that marks the boundary between these formations in much of the northeastern part of the area. Relief between the valley bottom and ridge top is approximately 550 m. (c) Well-developed cleavage in brown-weathering, grey phyllite of the upper Yusezyu Formation (domain 2). Hammer for scale. (d) Southwest-verging folds in limestone conglomerate of the basal Gull Lake Formation. Gull Lake formation is tectonically intercalated with Yusezyu Formation at this location in the northeast part of 105H/9. Hammer for scale. (e) Large folds in the upper Yusezyu Formation, domain 2. Cleavage is axial planar to these folds and dips northeast moderately steeply. The cliff/steep slope facing the viewpoint is approximately 300 m high. (f) Overturned, southwest-verging folds in the immediate hanging wall of the Ostensibility thrust. The folds are outlined by two thick grit units in the upper Yusezyu Formation, which is thrust over the Narchilla Formation. The limestone member of the uppermost Yusezyu Fm is locally preserved along this contact. Visible relief is ~650 m.*

DOMAIN 4

Domain 4 includes a large region in the centre of the mapped area between the Ostensibility/Dayo faults and the Upper Hyland fault (Fig. 5). This area is mostly underlain by frost-heaved Narchilla Formation; topography is relatively subdued and except where Gull Lake and Rabbitkettle formations are exposed in the cores of synclines, large-scale fold geometries are difficult to discern. Foliation generally dips moderately to steeply northeast and locally steeply to the southwest (Fig. 6d). Folds are upright (Fig. 7g), open-close and have axes that plunge at shallow angles to the northwest or southeast. The structure is similar to that in domain 2, but in general folds are more symmetrical and the foliation dips more steeply.

UPPER HYLAND FAULT

A steeply-dipping, northwest-striking fault in the eastern part of 105H/8 juxtaposes oppositely dipping panels of Hyland Group. Southwest of the fault, rocks generally dip towards the northeast, and stratigraphy is truncated at a low angle by the fault. As the sequence strikes slightly counter-clockwise of the fault trace, progressively deeper levels are truncated towards the southeast. Northeast of the fault, rocks of the uppermost Hyland Group (upper Yusezyu and Narchilla formations) dip southwest towards the fault. Northeast of the fault, metamorphic grade in mudstones of the Narchilla Formation is very low, whereas rocks with similar protolith to the southwest are coarser-grained phyllites with rare biotite crystals in lower parts of the Yusezyu Formation.

To the southeast, the fault runs into a broad valley that separates Yusezyu Formation (west side) from Rabbitkettle Formation (east side). This boundary is probably a continuation of the fault, which is along strike from, and possibly continuous with, the Acland fault, a major structure in Coal River map sheet (105D) that Pigage *et al.* (2011) interpreted as a thrust.

To the northwest, the fault projects into the upper Hyland River valley, where it is interpreted to coincide with the eastern margin of a region of high magnetic susceptibility (Fig. 8). As the broad river valley is filled with Quaternary sediment and the Yusezyu Formation undivided on current maps, the northwestern extent of this fault is unknown. Although speculative, the convergence of magnetic lineaments and possible truncation of the east end of the Shannon pluton suggests the fault may extend northwest into the Little Nahanni River map area (105I; Fig. 8). The movement history of the fault is unknown, but its steep dip, linear trace and long strike-length are suggestive of strike-slip displacement.

DOMAIN 5

Domain 5 includes rocks of the middle and upper Yusezyu Fm that are located immediately west of the Upper Hyland fault. The stratigraphic sequence dips northeast, as does foliation (S_1), which is axial planar to folds that trend northwest or southeast (Fig. 6e). The structural style is similar to that in domain 4.

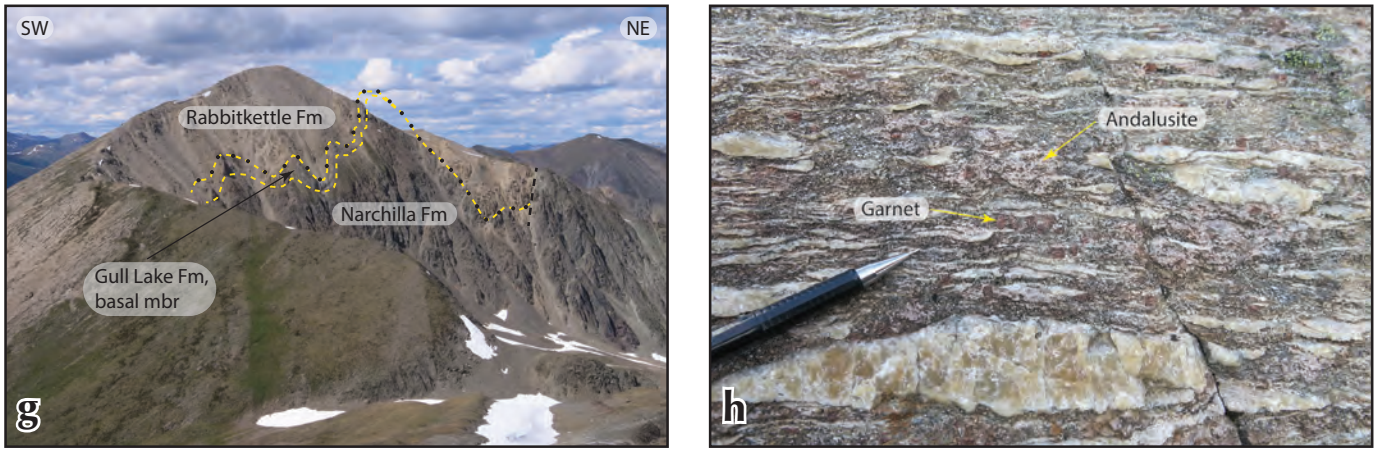


Figure 7 (continued). *(g) Upright folds in the east-central part of 105H/9 (domain 4). The basal member (limestone conglomerate) of the Gull Lake Fm is cut out beneath the folded, sub-Rabbitkettle unconformity (unconformity indicated with dots). The elevation difference between the saddle in the foreground and the peak is approximately 160 m. (h) Schistosity in Andalusite-zone schist in the western part of 105H/9. Partly preserved crenulations indicate this schistosity (S_2) overprints an earlier planar fabric (S_1). Pencil for scale.*

DOMAIN 6

Domain 6 includes most of the rocks on the west side of the upper Hyland River fault, including all of the amphibolite-facies rocks that fringe the Billings and Anderson batholiths. Whereas a single foliation is discernable in other domains, evidence that the main schistosity (S_2) overprints an earlier cleavage (S_1) is commonly preserved in thin section in domain 6. Further investigation of age relationships is required to reach a definitive conclusion, but this observation suggests that structures in domains 1-5, including the southwest-vergent folds and thrusts, pre-date the amphibolite-facies, penetrative deformation recorded in domain 6.

The foliation (S_2; Fig. 7h) generally dips northeast at shallow-moderate angles (Fig. 6f). Compositional layering is invariably parallel to the dominant schistosity, which is axial-planar to tight-isoclinal folds (Fig. 7i,j,k,l). Fold axes, intersection lineations, mineral lineations (Fig. 7m) and elongation lineations generally trend east-southeast, and pitch steeply on the foliation plane, perpendicular to boudin necks (Fig. 7n). Crenulations of S_2 with axes parallel to the mineral lineation are common throughout (F_3; Fig. 7o), and a later set of crenulations, at a high angle to the first, is locally developed east of the Hyland River (F_4). When viewed perpendicular to the lineation, structures are not obviously asymmetric and further kinematic study is required to establish whether penetrative deformation and east-southeast to west-northwest stretching in this area was accompanied by top to the east (normal sense) shearing, top to the west (thrust-sense) shearing, or neither.

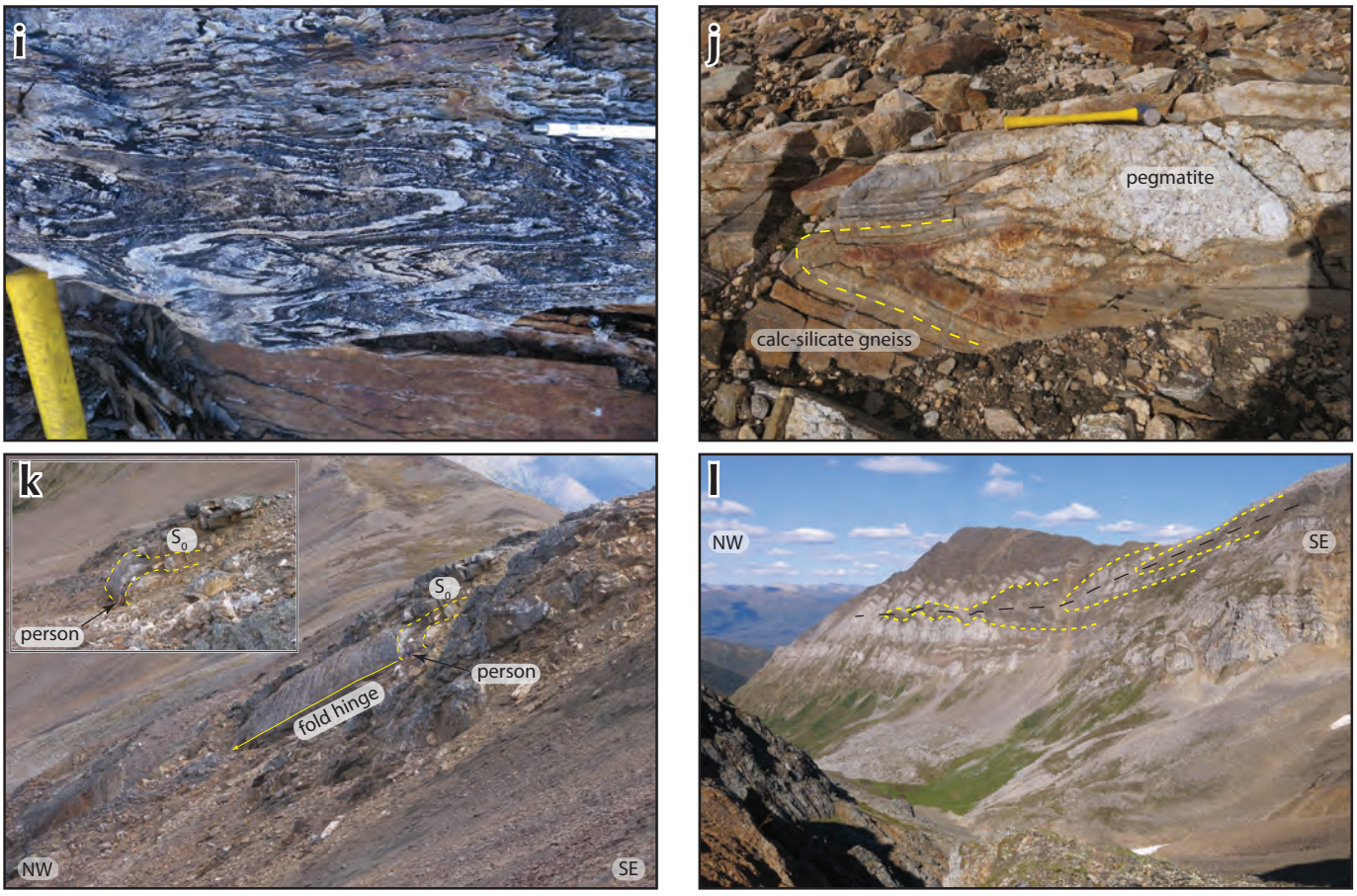


Figure 7 (continued). *(i) Tight similar folds in calc-silicate of unit* uPm. *Pencil for scale. (j)Tight folds in calc-silicate gneiss of unit* uPs. *The pegmatite cross-cuts layering but is itself deformed, suggesting it was intruded during deformation. (k) Tight to isoclinal fold of thick sandstone beds in low grade rocks of the Lower Yusezyu Formation, recessive unit. The large photo is an oblique view of the fold, whereas the inset photo shows the view looking down the plunge, towards the northeast. This is near the upper boundary of domain 6. Person for scale. (l) Isoclinal folds of marble and micaceous schist (units* uPm *and* uPs*, domain 6). The folds plunge towards the northeast, in the approximate dip-direction of the axial-planar foliation (S_2). The elevation difference between the valley bottom and the ridge top is approximately 400 metres.*

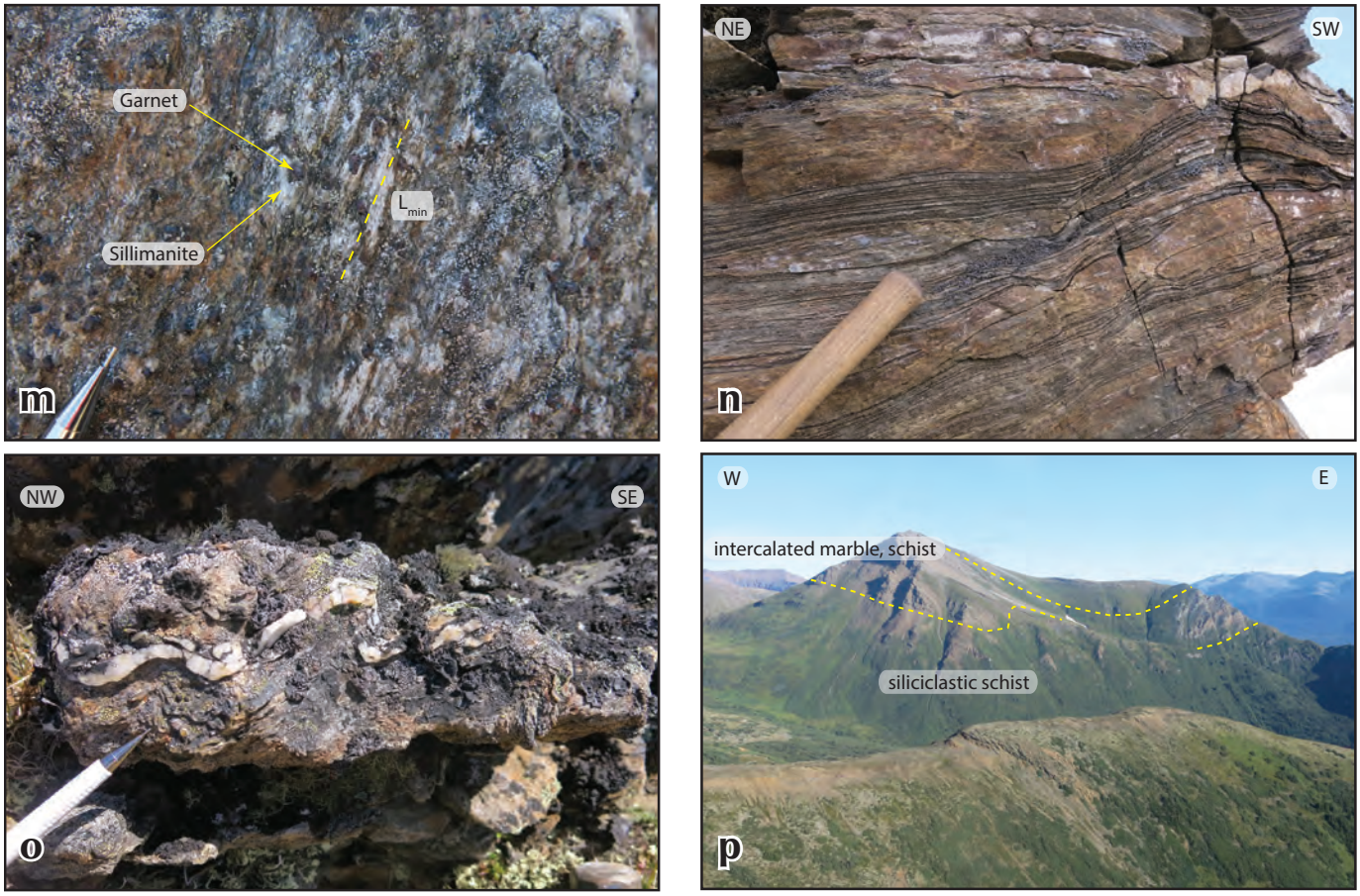


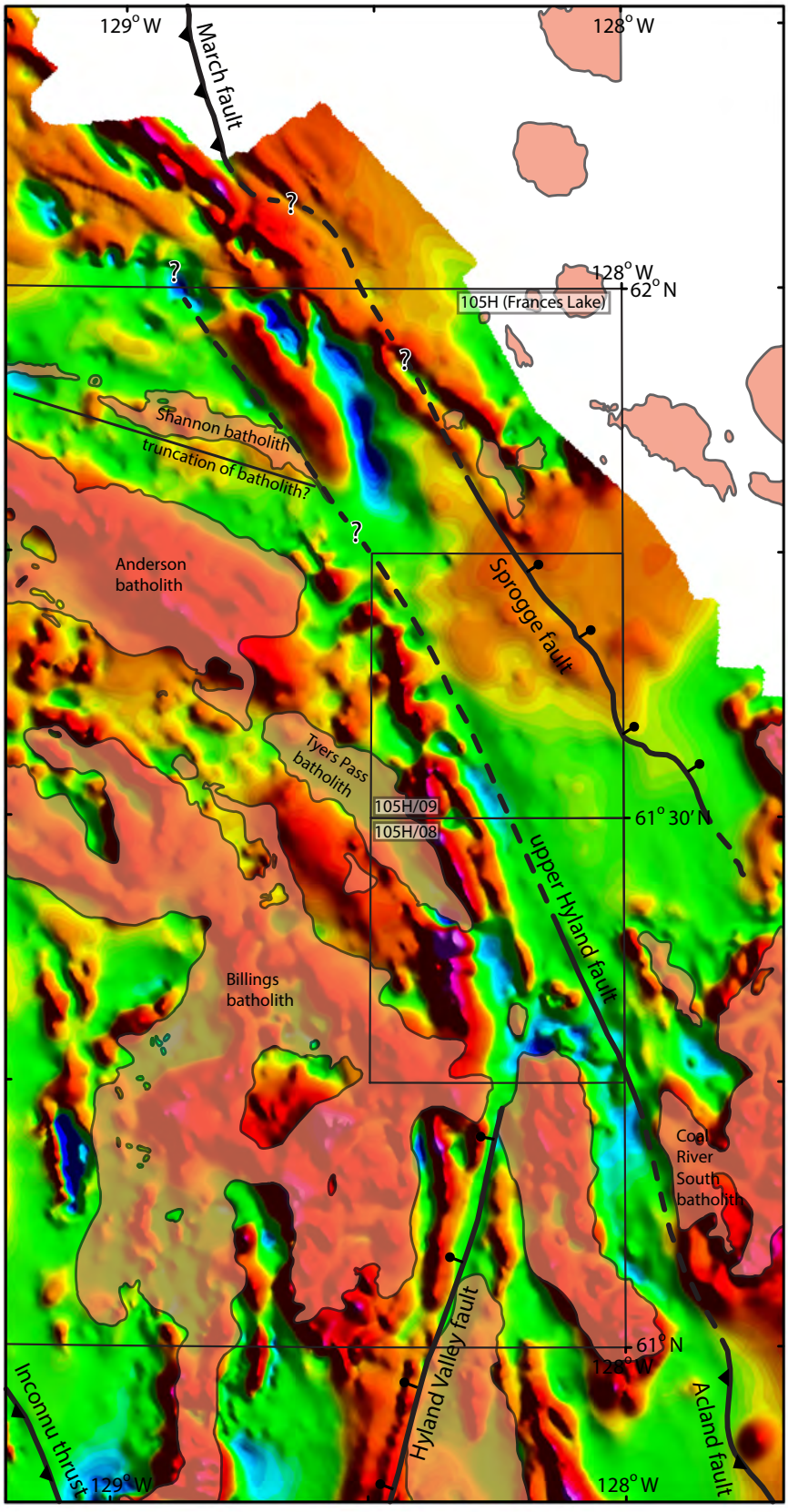
Figure 7 (continued). *(m) Mineral lineation defined by sillimanite crystals around garnet porphyroblasts. Pencil tip for scale. (n) Crenulations and small-scale folds of S_2 and quartz veins. Crenulations in domain 6 pitch steeply, and are generally coaxial with mineral lineations. Pencil for scale. (o) Boudinage structures in calc-silicate schist (*uPm*, domain 6). Boudin necks have gentle plunges, and are perpendicular to fold axes, mineral lineations and crenulations of the foliation (S_2). (p) The dominant foliation in domain 6 is overprinted by some open folds with axes that trend northwest. Elevation from valley bottom (left middle ground) to peak is approximately 550 m.*

The boundary between domains 5 and 6 lies within the unit PCHYlr, and is evidenced by a change in the orientation of folds/intersection lineations from approximately strike-parallel (domain 5) to steeply pitching (domain 6).

The S_2 foliation and associated structures are folded around late, upright open folds with axes that plunge shallowly to the northwest or southeast (Fig. 7p).

MINERALIZATION

The Upper Hyland River area hosts intrusion-related gold and W-Mo-Cu±Pb skarn prospects, as well as gold mineralization that has no obvious connection to igneous activity (Hart and Lewis, 2006). Recent exploration activity has been focused in the northeast part of the mapped area where there is intrusion-related Au-W mineralization around the Justin pluton (Higgs, 2009), and coarse, vein-hosted gold mineralization at 3 Aces (Schulze, 2010). 3 Aces is one of a number of gold occurrences hosted in the Yusezyu Formation east of the Hyland River to which Hart and Lewis (2006) ascribed a non-magmatic origin. They proposed that gold mineralization in this belt was related to metamorphic fluids that were generated in response to regional deformation and prograde metamorphism. However, as discussed above, there is uncertainty over the southeastern extent of the March fault, and its postulated extension – the Sprogge fault - appears to be a younger feature, which truncates structures that developed during low grade regional metamorphism.



ACKNOWLEDGEMENTS

Thanks to Colin Padget (2014) and Erin Bros (2015) for assistance in the field, and to JJ O'Donnell (Selwyn Chihong Resources) and Hendrik Falck (Northwest Territories Geoscience Office) for providing access to contract helicopters in 2014. Thanks also to Mike McCuaig of Aben Resources Ltd. for access to geophysical data of the Justin property and to Steve Israel for suggesting improvements to an earlier version of the manuscript.

Figure 8. *Total field aeromagnetic data from part of southeast Yukon, and postulated traces of major faults in the eastern part of the Frances Lake map area (105H). Plutonic rocks are indicated with a red semi-transparent overlay.*

REFERENCES

Abbott, J.G., 1997. Geology of the Upper Hart River area, eastern Ogilvie Mountains, Yukon Territory (116A/10, 116A/11). Exploration and Geological Services Division, Yukon, Indian and Northern Affairs Canada, Bulletin 9, 92p.

Colpron, M., Moynihan, D., Israel, S. and Abbott, G., 2013. Geological map of the Rackla belt, east-central Yukon (NTS 106C/1-4, 106D/1). Yukon Geological Survey, Open File 2013-13, 1:50 000 scale, 5 maps and legend.

Cecile, M.P., 2000. Geology of the Northeastern Niddery Lake map area, east-central Yukon and adjacent Northwest Territories. Geological Survey of Canada, Bulletin 533, 120 p.

Fritz, W.H., 1982. Vampire Formation, and new Upper Precambrian(?)/Lower Cambrian Formation, Mackenzie Mountains, Yukon and Northwest Territories. *In:* Current Research, Part B, Geological Survey of Canada, Paper 82-1B, p. 83-92.

Gabrielse, H., Blusson, S.L. and Roddick, J.A., 1973. Geology of Flat River, Glacier Lake and Wrigley Lake map areas, District of Mackenzie and Yukon Territory. Geological Survey of Canada, Memoir 366, 421 p.

Gordey, S.P. and Anderson, R.G., 1993. Evolution of the Cordilleran miogeocline, Nahanni map area (105I), Yukon and Northwest Territories. Geological Survey of Canada, Memoir 428, 214 p.

Hart, C.J.R. and Lewis, L.L., 2006. Gold mineralisation in the upper Hyland River area: A non-magmatic origin. *In:* Yukon Exploration and Geology 2005, D.S. Emond, G.D. Bradshaw, L.L. Lewis and L.H. Weston (eds.), Yukon Geological Survey, p. 109-125.

Higgs, A., 2009. Geological and geochemical report for the Sprogge (Justin) property, Watson Lake mining district, southeastern Yukon territory, 105H/09. Energy, Mines and Resources, Government of Yukon, Assessment Report 095153.

Kamb, W.B., 1959, Ice petrofabric observations from Blue Glacier, Washington, in relation to theory and experiment. Journal of Geophysical Research, vol. 64, p. 1891-1909.

MacLeod, W.A., 1982. Cal 81-144 mining claims, Watson Lake mining district, 105H/08W. Energy, Mines and Resources, Government of Yukon, Assessment Report 090867.

Martel, E., Turner, E.C. and Fisher, B.J. (eds.), 2011. Geology of the central Mackenzie Mountains of the northern Canadian Cordillera, Sekwi Mountain (105P), Mount Eduni (106A), and northwestern Wrigley Lake (95M) map area, Northwest Territories. NWT special Volume 1, NWT Geoscience Office, 423 p.

Moynihan, D.P., 2013. A preliminary assessment of low pressure, amphibolite-facies metamorphism in the upper Hyland River area (NTS 105H), southeast Yukon. *In:* Yukon Exploration and Geology 2012, K.E. MacFarlane, M.G. Nordling, and P.J. Sack (eds.), Yukon Geological Survey, p. 99-114.

Moynihan, D., 2016a. Bedrock geology compilation of the eastern Rackla belt, NTS 105N/15, 105N/16, 105O/13, 106B/4, 106C/1, 106C/2, east-central Yukon. Yukon Geological Survey, Open File 2016-2, 1:75 000 scale.

Moynihan, D., 2016b. Bedrock geology of parts of NTS 105H/8 and 105H/9, upper Hyland River area, southeast Yukon. Yukon Geological Survey, Open File, 1:50 000 scale, in prep.

Pigage, L.C., Roots, C.F. and Abbott, J.G., 2015. Regional bedrock geology for Coal River map area (NTS 95D), southeast Yukon. Yukon Geological Survey, Bulletin 17, 155 p.

Rasmussen, K., 2013. The timing, composition and petrogenesis of syn- to post-accretionary magmatism in the northern Cordilleran miogeocline, Eastern Yukon and southwestern Northwest Territories. Unpublished PhD thesis, University of British Columbia, Vancouver, Canada, 788 pages.

Roots, E.F., Green, L.H., Roddick, J.A. and Blusson, S.L., 1966. Geology, Frances Lake, Yukon territory and district of Mackenzie. Geological Survey of Canada, preliminary map 6-1966. 1:253 440 scale.

Ross, G.M., 1991. Tectonic setting of the Windermere Supergroup revisited. Geology, vol. 19, p.1125-1128.

Schulze, C.M., 2010. YMIP report on the phase 1 2010 geological and geochemical surveys on the 3Ace property, southeast Yukon, 73 pages. YEIP 2010-118.

Copper-gold±silver mineralization at the Stu occurrence, central Yukon (Yukon MINFILE 115I011)

P.J. Sack[1] and S. Casselman
Yukon Geological Survey

D. James
Consultant, Duncan, British Columbia

B. Harris
Midnight Mining Services Ltd.

Sack, P.J., Casselman, S., James, D. and Harris, B., 2016. Copper-gold±silver mineralization at the Stu occurrence, central Yukon (Yukon MINFILE 115I011). *In:* Yukon Exploration and Geology, K.E. MacFarlane and M.G. Nordling (eds.), Yukon Geological Survey, p. 207-222, plus digital appendices.

ABSTRACT

The Stu copper-gold±silver occurrence (Yukon MINFILE 115I 011) is located midway between the Minto and Carmacks Copper deposits in the eastern, Minto suite portion of the Granite Mountain batholith. The best known mineralization at Stu is in Zone A, where at least four foliated and mineralized bodies strike northwest and dip moderately to steeply to the northeast. These bodies grade 0.2 to 0.6% total Cu, though the best historic diamond drill intersection contains 3.5% Cu over 13.5 m. In plan and cross section view, the foliated and mineralized granodioritic orthogneiss bodies pinch and swell, appearing as lenses surrounded by unfoliated K-feldspar porphyritic granodiorite. Copper mineralization occurs as both fine-grained hypogene bornite and chalcopyrite, and supergene malachite, azurite, tenorite and chrysocolla. This study suggests that Stu mineralization is similar to that at the Carmacks Copper and Minto deposits as it is primarily hosted in multiple, discrete bodies of foliated granodioritic rock. In terms of ore body orientation, the moderate to steeply dipping nature at Stu is more reminiscent of Carmacks Copper than Minto, which likely explains the presence of significant supergene copper mineralization.

[1]*patrick.sack@gov.yk.ca*

INTRODUCTION

In 2014, the Yukon Geological Survey (YGS) initiated a multi-year project investigating Late Triassic to Jurassic plutonic rocks in Yukon with the aim of providing an updated metallogenic framework for associated deposits and occurrences; the most significant of these are the Minto (Yukon MINFILE 115I021) and Carmacks Copper (Yukon MINFILE 115I008) deposits. The Stu copper-gold±silver occurrence (Yukon MINFILE 115I011) is another significant, albeit poorly documented, occurrence located 10 km northwest of the Carmacks Copper deposit (oxide resource of 12 Mt grading 0.9% oxide Cu (1.07% total Cu), 0.5 g/t Au and 4.6 g/t Ag; Arseneau and Casselman, 2008) and 30 km southeast of the Minto mine (sulphide resource 70.8 Mt grading 1.2 % Cu, 0.5 g.t Au and 4.2 g/t Ag; recalculated from Mercer and Sagman, 2012).

Historic mapping, soil sampling, bull dozer trenching, diamond drilling and rotary air-blast (RAB) drilling were done on the Stu property between 1971 and 1989. With the notable exception of assay data, a reasonable amount of this information is in the public realm, mostly as assessment reports. However, a synthesis of existing data has not been done, and the occurrence has only received cursory research during studies focused on the Minto and Carmacks Copper deposits (*e.g.*, Tafti and Mortensen, 2004). Work at the Stu occurrence conducted in 2015 by YGS staff, in collaboration with Bill Harris the property owner, was done over a five day period. Core from three key, historic diamond drill holes was re-logged and resampled, two re-excavated trenches mapped and four re-excavated trenches sampled. Thirteen representative samples have been analyzed for whole-rock geochemistry, and twenty samples from diamond drill hole 80-6 have been re-assayed for sulphide and supergene Cu mineralization. Historic drill hole and trench geology has been digitized and combined with the new data to create an updated geologic model for the occurrence. In the present contribution, we document and characterize mineralization at the Stu occurrence so that it can be placed into the larger metallogenic framework being developed for Late Triassic to Jurassic plutonic rocks in Yukon.

REGIONAL GEOLOGY

Accretion of the Intermontane terranes (Yukon-Tanana, Stikinia, Quesnellia and Cache Creek) to the western margin of North America in the Late Triassic to Jurassic resulted in prolific arc magmatism throughout the northern Cordillera (Nelson *et al.*, 2013). This period of magmatism is particularly important metallogenically as it hosts many of the porphyry copper (±Au, Mo) deposits in British Columbia (Logan and Mihalynuk, 2014). Locally, rocks of this age host the enigmatic Minto and Carmacks Copper deposits, as well as the Stu occurrence (Tafti and Mortensen, 2004). New geochronological, geochemical and petrographic evidence collected during the YGS's Late Triassic to Jurassic plutons project will result in reinterpretation of the magmatic suites of this age range in Yukon. These suites will be described in detail in other publications (*e.g.* Joyce *et al.*, 2016), but updated terminology will used in this paper. In Yukon, Late Triassic to Jurassic plutonic rocks can be divided into four magmatic suites, from oldest to youngest these are: Late Triassic Stikine Suite, latest Triassic to Early Jurassic Minto suite, Early Jurassic Long Lake Suite, and Middle Jurassic Bennett-Bryde suite (Fig. 1; following subdivisions of Woodsworth *et al.*, 1991; Gordey and Makepeace, 2001 and Colpron *et al.*, 2016).

The Stu occurrence is hosted within the Granite Mountain batholith which intrudes Yukon-Tanana terrane rocks along its southwest margin, and is faulted against Stikinia rocks to the northeast along the Hoocheekoo fault (Fig. 1). To the northwest, the batholith is overlain by mafic to intermediate volcanic rocks of the Carmacks Group and to the southeast, the Miller fault juxtaposes Carmacks Group volcanic rocks against the batholith (Tempelman-Kluit, 1984). Broadly, the batholith is composed of a western Long Lake suite part and an eastern Minto suite part (Fig. 1); the contact between the two is poorly understood, and may be associated with a fault. The Granite Mountain batholith is intruded by dacite dikes related to the Early Cretaceous Mt. Nansen Group volcanic rocks, and by mafic feeder dikes of the overlying Late Cretaceous Carmacks Group volcanic rocks (Tempelman-Kluit, 1984).

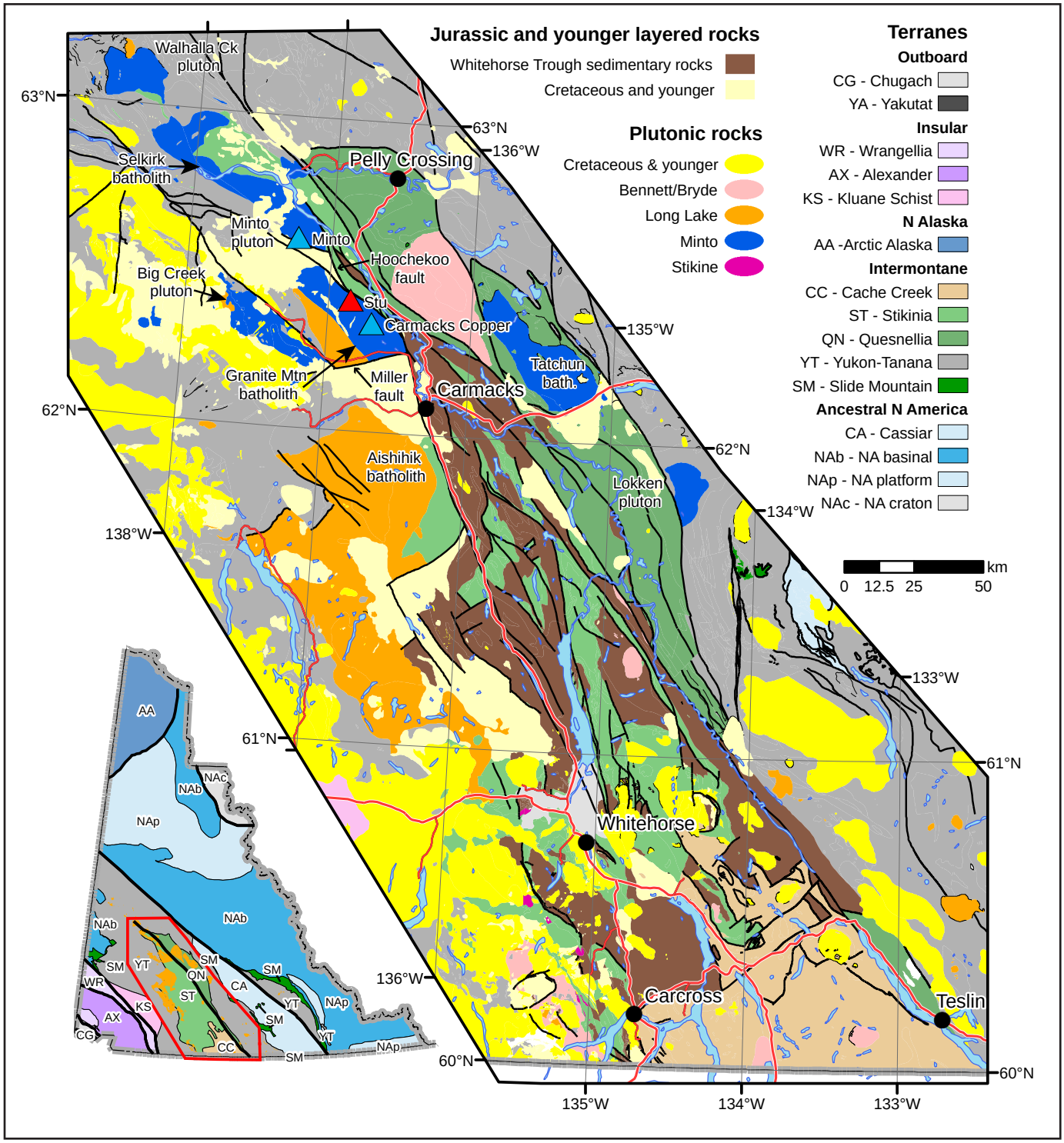


Figure 1. *Simplified geology of south central Yukon with emphasis on Late Triassic to Jurassic plutonic suites as described in text. Significant Early Jurassic Cu-gold±silver mineral occurrences shown by triangles, Stu in red. Inset, Yukon terrane map, area outlined in red shows the area of the main map. Geological data from Yukon Geological Survey (2015).*

PROPERTY GEOLOGY

Two main lithologies of plutonic rocks are recognized on the Stu property; for the purposes of the present paper we use the modal mineralogy QAP based classification of Le Bas and Streckeisen (1991). The southwestern margin of the property is underlain by a poorly understood equigranular quartz monzonitic rock while the majority of the property is underlain by variably foliated, fine to medium-grained, equigranular to K-feldspar porphyritic granodioritic rocks (Fig. 2). Geology and geophysical anomalies generally trend NW with the boundary between the quartz monzonitic rock and granodioritic rocks occurring in the transition between a relative magnetic low, to the southwest, and high to the northeast (Fig. 2 inset). Outcrop magnetic susceptibility

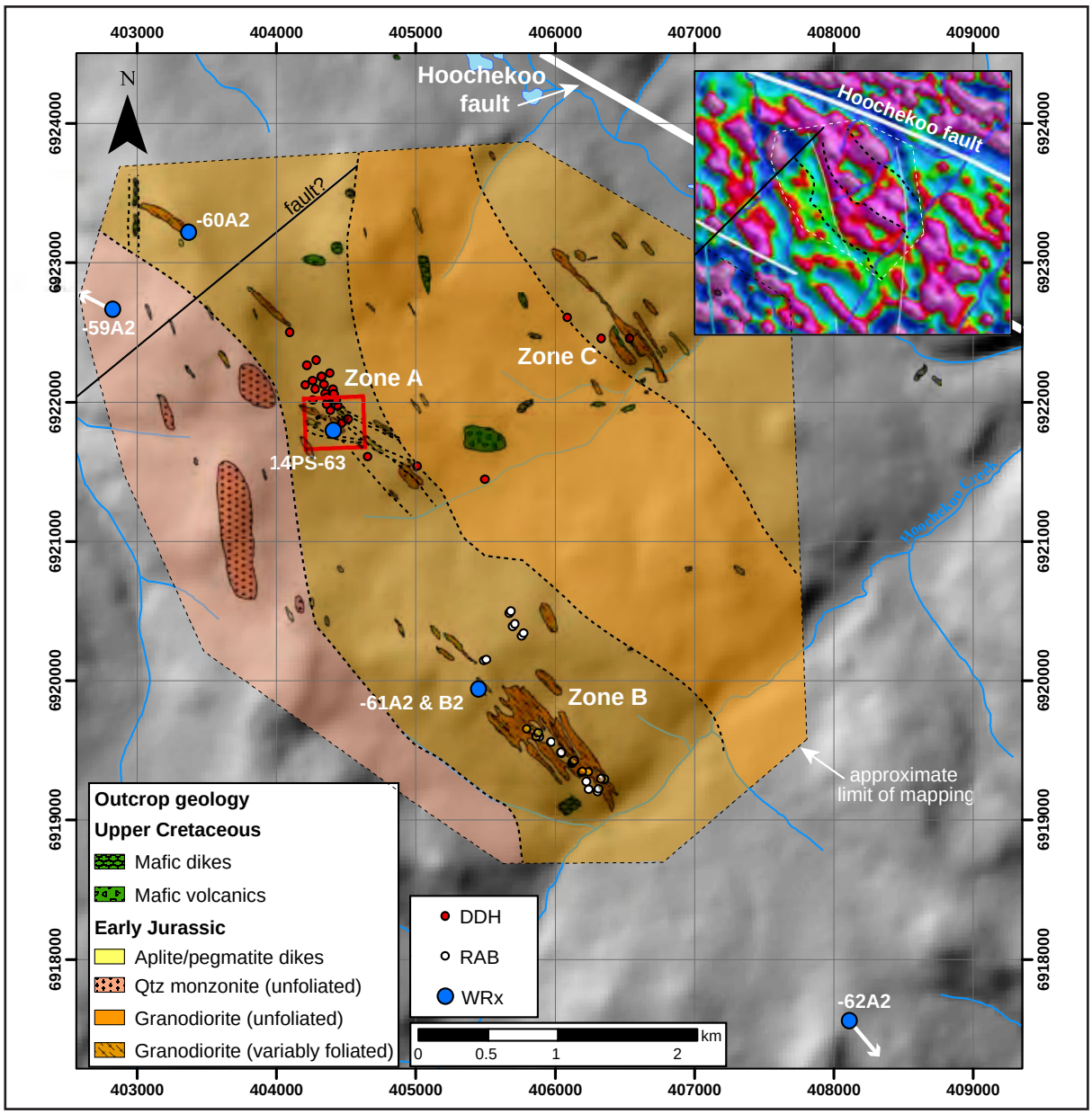


Figure 2. *Property outcrop map modified from Watson and Joy (1977); interpreted geology, in subdued colours, from the present study. Location of Figure 3 shown by red square. Samples -59A2 and -62A2 are approximately 4 and 1 km, respectively, off the map in the directions indicated by white arrow; coordinates for all samples are included in the digital appendices. Grid is UTM Zone 8, NAD83. Top right inset is the first vertical derivative of the enhanced magnetic field map from Hayward et al. (2012) and interpreted lineaments, in white, are from Sánchez et al. (2014). DDH=diamond drill hole collar, RAB=rotary air blast hole collar, WRx=whole-rock sample.*

measured at 63 stations throughout the Minto suite part of the Granite Mountain batholith average 4.13 x 10^3 SI units and range from 0.04 to 19.7. Supergene copper mineralization appears to be a relative magnetic low feature, likely due to oxidation effects on magnetite (Pautler, 2009).

The majority of bedrock exposed in trenches 600W and 800W (Fig. 3), and in diamond drill holes 80-6 (Fig. 4), 80-7 (Fig. 5), and 80-14, is weakly foliated to unfoliated K-feldspar porphyritic granodiorite. Within the porphyritic granodiorite are a series of strongly foliated bodies with a NW foliation dipping ~75° to the NE (Fig. 3). The bodies themselves appear to have a slightly shallower dip, between 40° and 70°, to the NE (Fig. 6; appendix 1). The degree of deformation and recrystallization of these rocks varies between unfoliated granodiorite, biotite schist and biotite orthogneiss (Figs. 4 and 5); with orthogneiss being more common than schist. Contacts between the three rock types are ambiguous. They generally transition over several cm, and locally K-feldspar phenocrysts in unfoliated

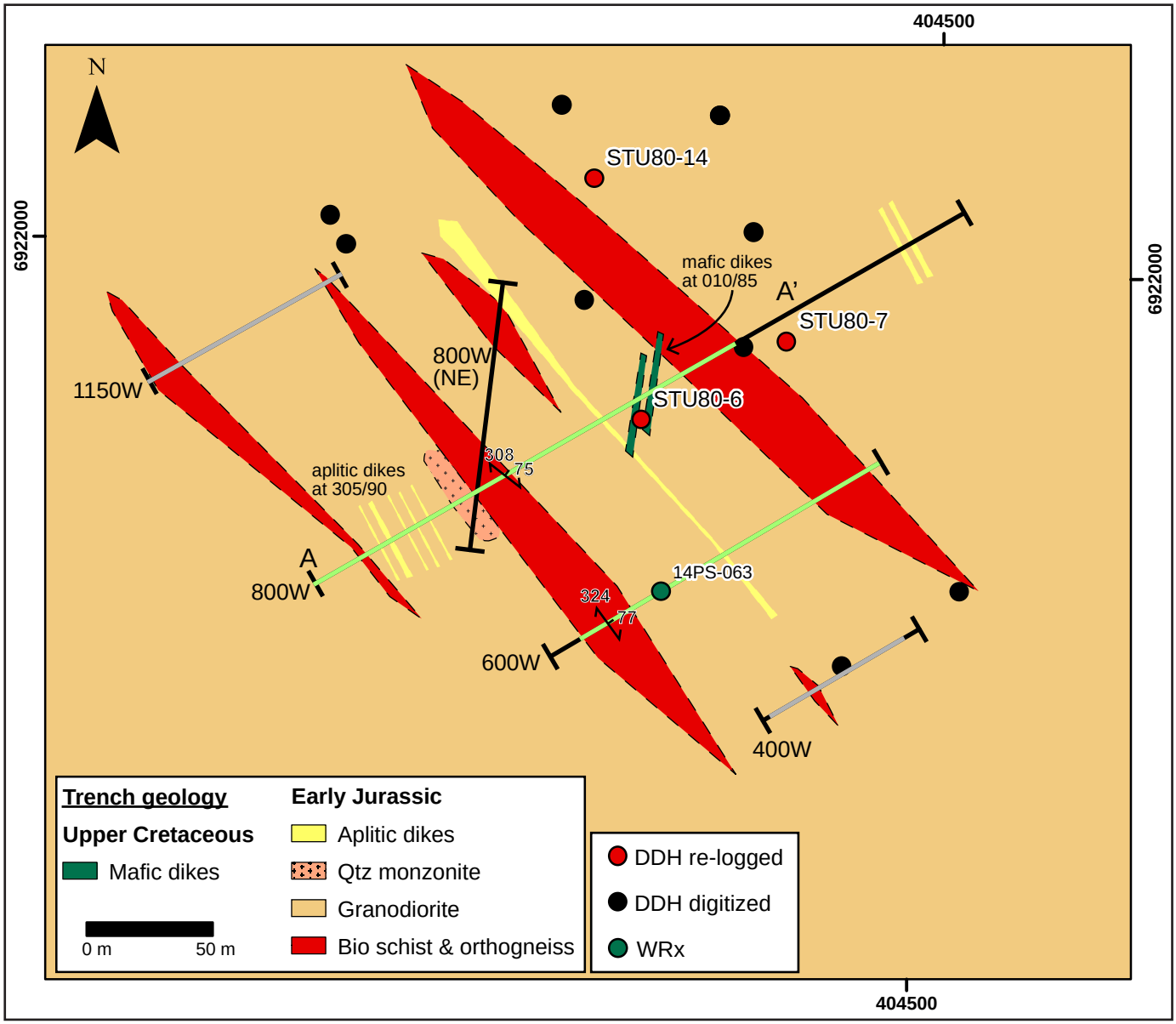


Figure 3. *Geologic sketch map of Zone A, based on 2015 trench mapping and reinterpretation of original trench mapping. Original 1978-79 trenches shown in black lines, parts of trenches shown in green were re-excavated, re-mapped and resampled in 2015, those in grey were not re-mapped but were resampled. Foliated and mineralized schist and gneiss shown in red is projected vertically to surface where not intersected by trenching. Cross section 800W in Figure 6 is A-A'. Bio = biotite, DDH = diamond drill hole, Qtz = quartz.*

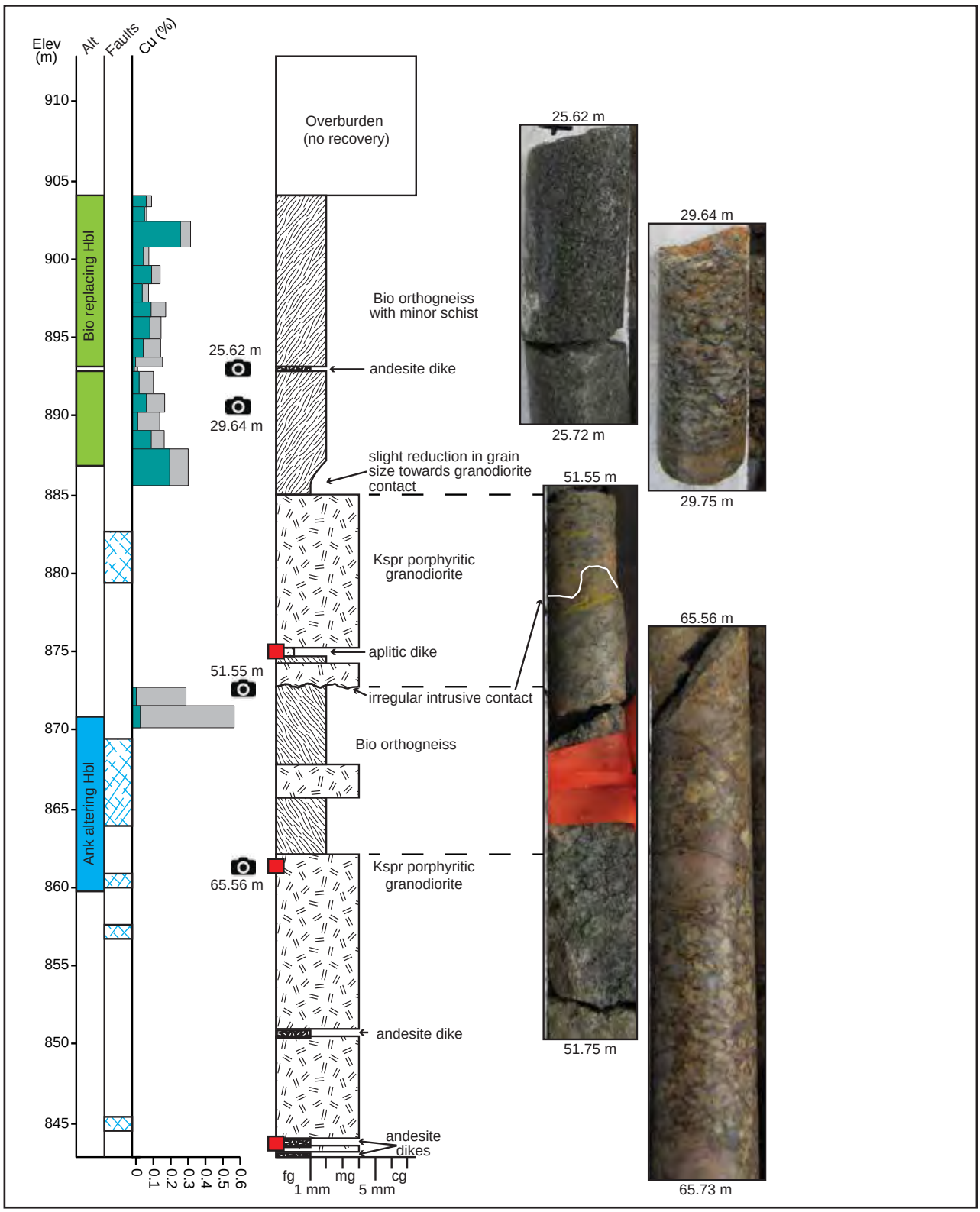


Figure 4. *Graphic log of diamond drill hole 80-6 re-logged and re-assayed in 2015 for the present study. Collar location shown on Figure 3. Pictures on right include from-to depths, above and below, respectively; all core is 3.65 cm diameter BQ size. Red squares show depths of 2015 samples. Alt = alteration; Cu = copper, reported as percentage of total Cu (grey) and supergene Cu (teal). Hbl = hornblende, Bio = biotite, Qtz = quartz, kspr = K-feldspar, Ank = ankerite, fg = fine-grained, mg = medium-grained, cg = coarse-grained.*

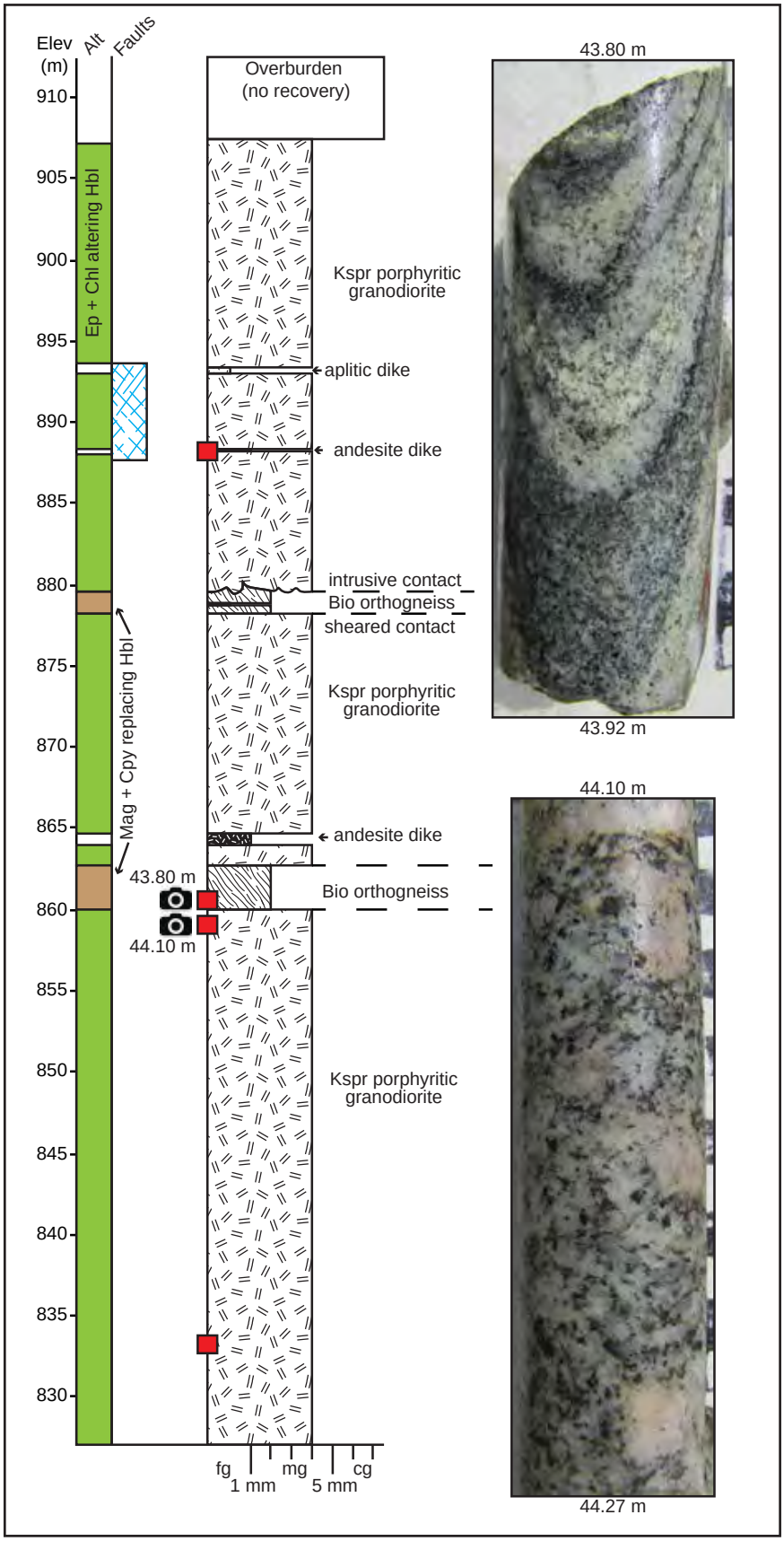


Figure 5. *Graphic log of drill hole 80-7 re-logged in 2015 for the present study, but not re-assayed. Collar location shown on Figure 3. Pictures on right shown include from-to depths above and below respectively; all core is 3.65 cm diameter BQ size. Ep=epidote, Mag=magnetite, Chl=chlorite, Cpy=chalcopyrite, other abbreviations and symbols same as Figure 4.*

granodiorite impinge foliated rocks suggesting that the contact is primarily intrusive. This coupled with overall rock distribution (Fig. 6) suggests that the unfoliated granodiorite engulfed earlier foliated varieties. Copper mineralization occurs as both supergene and sulphide minerals depending on level of oxidation (Fig. 6). Copper (Au ± Ag) mineralization is mostly associated with biotite schist and orthogneiss, though locally supergene copper minerals are found in unfoliated granodiorite.

Other intrusive rock types recognized locally, but not represented at the property map-scale include aplite and pegmatite dikes, microdiorite and andesite dikes. Small outcrops of Carmacks Group mafic volcanic rocks are found on the hilltops between Zone A and C (Fig. 2). Swarms of aplite and pegmatite dikes <1 m thick are generally steeply dipping with a NW strike. These dikes are found proximal to contacts between foliated and unfoliated varieties of granodiorite suggesting these contacts are zones of weakness. The aplite and pegmatite dikes are mineralogically and compositionally similar to the quartz monzonitic rocks, and are interpreted as late stage Early Jurassic intrusions related to the cooling of the Granite Mountain batholith. Based on crosscutting relationships, the interpreted intrusive sequence from oldest to youngest is: granodioritic orthogneiss – unfoliated granodiorite – quartz monzonite – aplite/pegmatite – microdiorite – andesite dikes (*e.g.*, Fig. 7).

PETROGRAPHY

Unmineralized massive porphyritic samples have a medium-grained groundmass of embayed and anhedral to subhedral felsic minerals (quartz, plagioclase and K-feldspar) with subhedral to euhedral randomly oriented mafic minerals (biotite and hornblende). Accessory titanite, magnetite and magmatic epidote are also present. Magmatic epidote is of particular interest as it has been used as petrographic evidence of a relatively deep emplacement depth for the plutons (>25 km crustal depth; Zen and Hammarstrom, 1984). Potassium feldspar phenocrysts are 1 to 3 cm long and are also randomly oriented. Groundmass plagioclase and K-feldspar (groundmass and phenocrysts) are moderately saussauritized. Quartz, plagioclase and hornblende all occur as inclusions within K-feldspar phenocrysts. The unfoliated granodiorite is generally unaltered to weakly

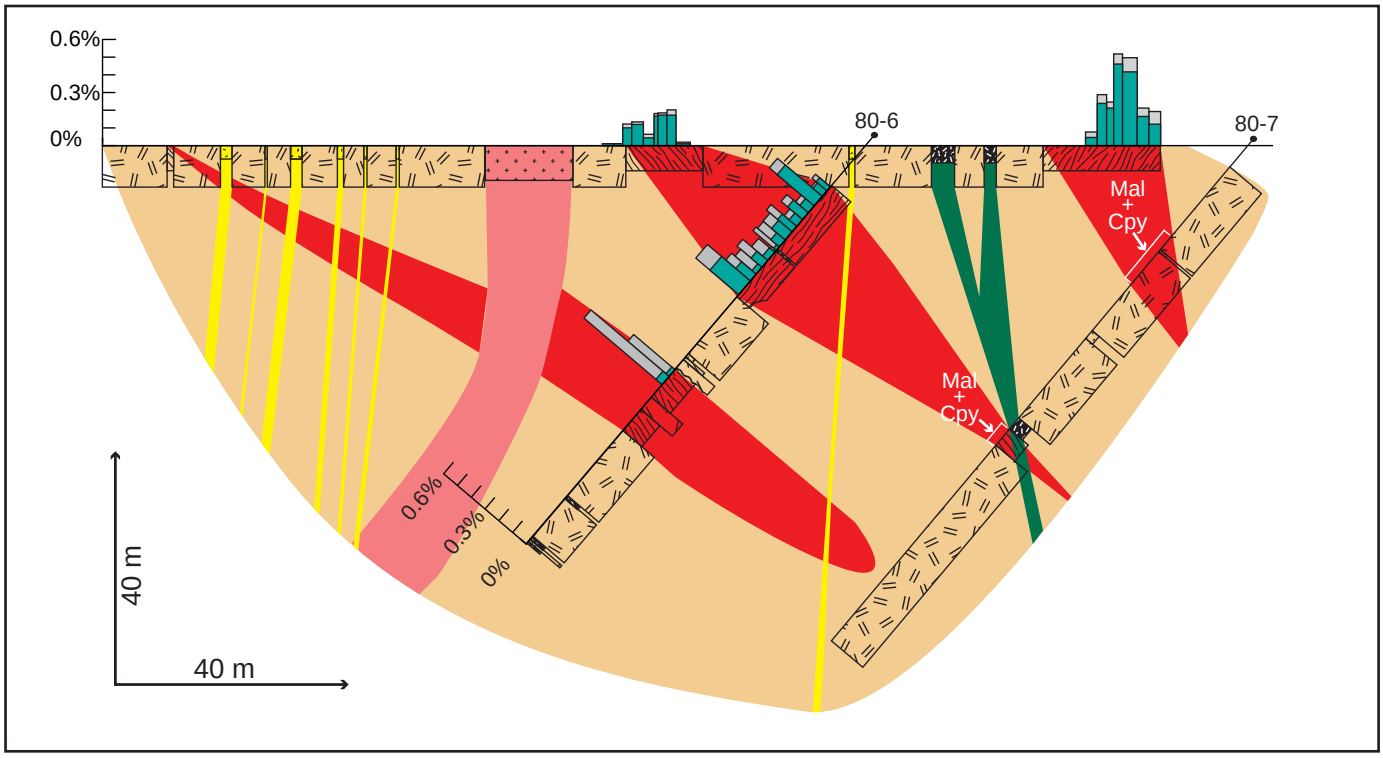


Figure 6. *Cross section of trench 800W from Zone A of the Stu occurrence, looking NW; location A-A′ shown on Figure 3. Graphic logs same as Figures 4 and 5, trench geology from 2015 re-mapping. Bar graphs show 2015 re-assayed total Cu (grey) and supergene Cu (teal) values. Diamond drill hole 80-7 was not re-assayed and mineralized zones are based on visible Cu mineralization as noted in original logs. Rock units same as Figure 3. Mal=malachite, Cpy=chalcopyrite.*

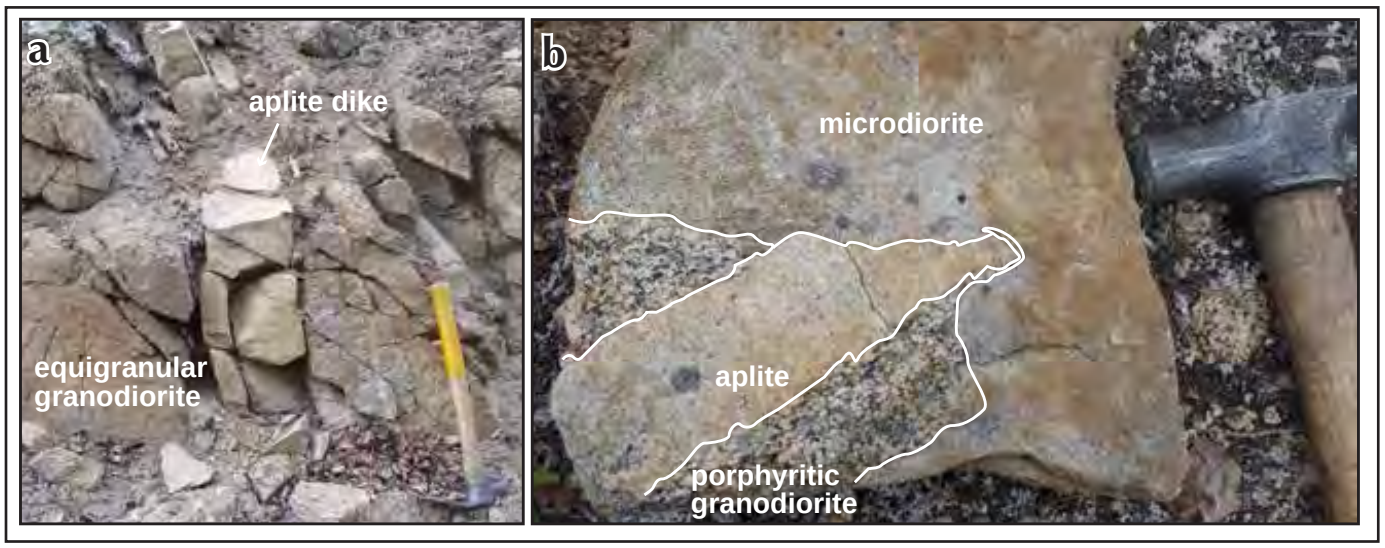


Figure 7. *Crosscutting relationship between granitoid intrusions at the Stu occurrence. (a) 20 cm thick aplite dike crosscutting equigranular granodiorite in trench 600W. (b) Three phases of granitoid intrusions in float from the B Zone. Porphyritic granodiorite cut by aplite dike, both cut by the microdiorite.*

chlorite altered with minor alteration of mafic minerals. Based on modal mineralogy, massive porphyritic rocks from the Stu property plot in, or on the lower boundary of, the granodiorite field of the Le Bas and Streckeisen (1991) classification (Fig. 8).

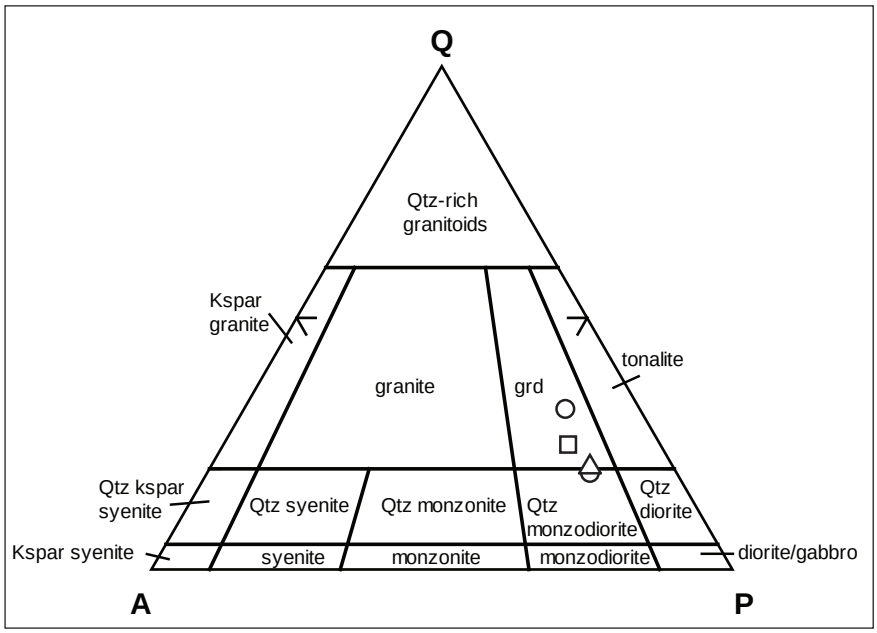


Figure 8. *Quartz-alkali feldspar-plagioclase (QAP) classification for plutonic rocks with <90% mafic mineral content (Le Bas and Streckeisen, 1991) using modal mineralogy determined by trained classification method on scans of cobaltinitrite stained slabs using ImageJ software. Qtz=quartz, Kspr=K-feldspar, grd=granodiorite. Circles=unfoliated granodiorite, square=biotite gneiss and triangle=mafic xenolith.*

Foliated and mineralized rocks also have a granodiorite composition (Fig. 8) but are equigranular and have higher biotite content than the porphyritic granodiorite. Modal mineralogy consists of quartz, plagioclase, K-feldspar, biotite, and hornblende with accessory titanite, epidote (both magmatic and deuteric), apatite and zircon (Fig. 9). The following petrographic description of foliated samples is mostly summarized from Fonseca (2008). Felsic minerals are generally anhedral to subhedral and elongate parallel to the dominant foliation. Mafic minerals typically form 5 to 15% of the rock, though locally they can reach 50%, and are subhedral to euhedral grains defining foliation. Hornblende is closely associated with biotite and locally partially biotite altered. Magnetite is the most abundant opaque mineral and forms 2 to 4% of melanocratic foliated domains as subhedral to euhedral octahedral grains that can be weakly replaced by hematite along microfissures. Hydrothermal alteration minerals are poorly developed and consist of clay and chlorite. Clay minerals alter growth zones in plagioclase and chlorite can locally partially replace biotite and hornblende along cleavage planes. Supergene copper mineralogy is

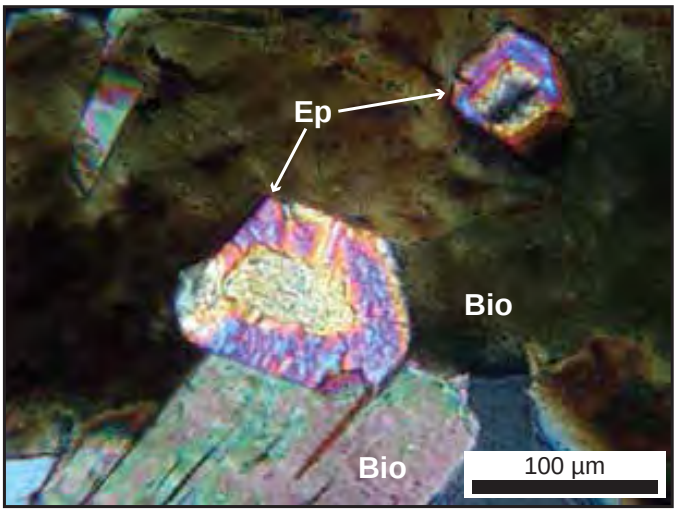


Figure 9. *Photomicrograph of euhedral magmatic epidote intergrown with euhedral magmatic biotite. Sample is a mineralized, moderately foliated granodiorite from Zone C in trench 1150E (from Fonseca, 2008). Field of view = 400 µm.*

dominantly malachite with lesser chrysocolla, azurite and tenorite. Hypogene copper mineralogy includes very fine grained chalcopyrite and bornite. In one sample, malachite and azurite replace very fine grained Cu-sulphides interpreted to have replaced primary mafic minerals; in two samples very small native gold grains (<0.5 µm) are reported. These observations suggest that primary hypogene copper mineralization occurred early in the intrusive history and, at least partly, as replacement of magmatic mafic minerals. Supergene copper is related to oxidation extent and decreases with depth (Fig. 6).

GEOCHEMISTRY

WHOLE-ROCK ANALYSES

As described above, most plutonic rocks from the Stu property (Fig. 2, 4 and 5) plot in the granodiorite field of the Le Bas and Streckeisen (1991) classification. A similarly restricted range in degree of fractionation is apparent in the whole-rock geochemical data, though there is a slight spread in the alkalinity (Fig. 10a,b). Two geochemical groups, corresponding to the quartz monzonitic and granodiorite compositions identified on the property, are separable in a variety of geochemical plots with granodiorite samples slightly less fractionated than the quartz monzonitic samples (Figs. 10 and 11). All samples are typical volcanic arc (I-type) granitoid rocks with a magnesian, calc-alkalic, metaluminous character. The one orthogneiss sample analyzed is chemically very similar to the unfoliated K-feldspar porphyritic granodiorite, and a mafic xenolith within the porphyritic granodiorite also has similar chemistry to its host, but is slightly more alkalic (Figs. 10 and 11). The aplite sample is chemically similar to the quartz monzonitic samples (Figs. 10 and 11). All whole-rock analytical results are included in appendix 2.

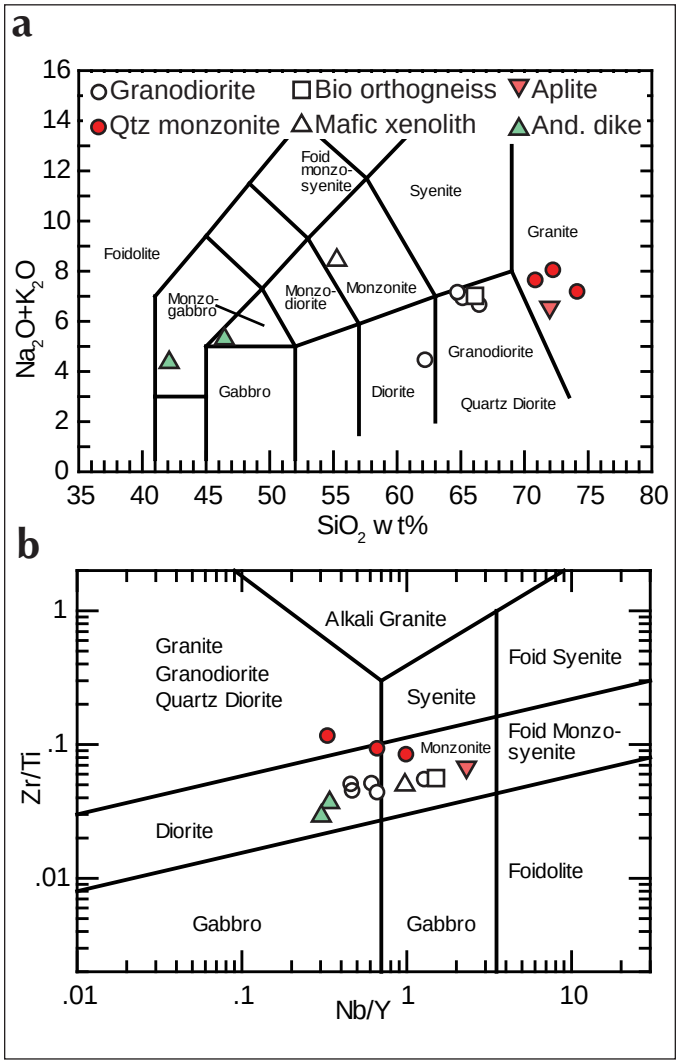


Figure 10. *Whole-rock composition plots. Symbols shown in Figure 10a. (a) Total alkali-silica plot using mobile elements (Le Bas et al., 1986), alkalinity increases on the Y-axis and degree of fractionation on the X-axis; (b) immobile element Zr/Ti vs. Nb/Y diagram of Winchester and Floyd (1977) modified by Pearce (1996), alkalinity increases on the X-axis and degree of fractionation on the Y-axis. Filled symbols are from quartz monzonitic samples on the western part of the property and have slightly more fractionated geochemistry but similar alkalinity to the granodioritic samples (hollow symbols).*

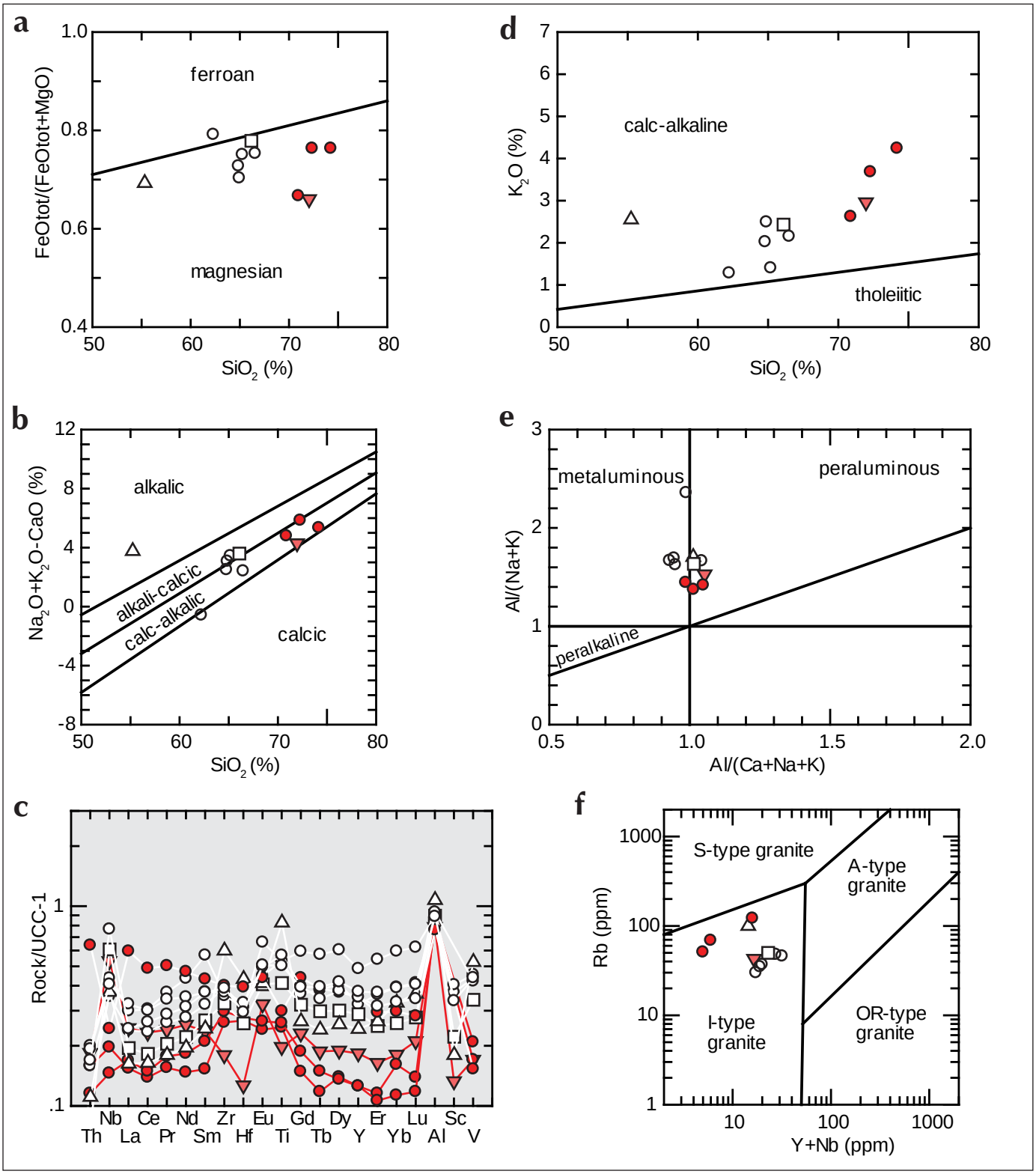


Figure 11. *Whole-rock geochemical plots. (a) Ferroan vs. magnesian granitoids (Frost and Frost, 2008); (b) modified alkali-lime index (Frost et al., 2001); (c) trace element patterns normalized to upper continental crust values of McLennan (2001); (d) Calc-alkaline vs. tholeiitic discrimination from Peccerillo and Taylor (1976); (e) alumina saturation plot of Shand (1927) from Maniar and Picolli (1989); and (f) tectonic discrimination diagram for collision zone intrusions (Harris et al., 1986). Symbols same as Figure 10a.* FeO_{tot} *=total Fe.*

ASSAY RESULTS

Samples were collected from diamond drill core and trenches. The drill core samples were collected from hole 80-6, a hole previously drilled and sampled in 1980. Most sample intervals had been split, sampled and presumably analyzed by previous operators, but the results are not available. Resampling of core left from previous work consisted of collecting composite samples, taking approximately 10 cm of remaining half-core piece every 30 cm over an average sample length of approximately 1.5 m. Trench samples were collected from trench walls as chip samples of 1 to 3 m intervals using standard exploration chip sampling methods. All assay results are included in appendix 3.

The samples collected from diamond drill hole 80-6 core were selected based on the presence of visible Cu mineralization. Sulphide and supergene Cu mineralization is generally observed in, or proximal to bodies of variably foliated granodioritic rock (Fig. 4). In the uppermost interval, from 11.58 to 35.66 m, total Cu content ranged from 0.03% to 0.34%, averaging 0.18% Cu over 24.08 m. The lowermost section is mineralized at the top of the interval, containing an average of 0.46% Cu over 3.35 m, but is unmineralized towards the bottom of the intersection (*i.e.*, <0.005% Cu). As would be expected, the ratio of supergene Cu oxide to total Cu is highest towards the top of the hole and decreases downwards. Based on this section, significant oxidation (*i.e.*, > 50% oxide to total Cu) occurs to a depth of approximately 40 m vertically from surface. Gold concentration in this hole is generally low (*i.e.*, <0.1 g/t Au), however two samples collected from the lower interval returned 0.128 and 0.272 g/t Au.

Results from trench sampling generally indicate multiple mineralized zones in each trench (Fig. 3). The ratio of Cu oxide to total Cu was >50%, indicating the majority of Cu is present as supergene Cu minerals. Gold values are generally low (*i.e.*, <0.1 g/t Au). The results of the resampling indicate three mineralized zones in trench 1150W: the eastern-most zone returned values of 0.153% total Cu and 0.083 g/t Au over 6.0 m; values from the centre include 0.124% total Cu and 0.026 g/t Au over 3.3 m; and 0.055% total Cu and 0.025 g/t Au over 14.0 m were return in the west. Trench 800W has two mineralized zones, 0.293% total Cu and 0.144 g/t Au over 12.8 m at the eastern end and 0.143% total Cu and 0.017 g/t Au over 9 m at the western end. Trench 600W does not have any significant mineralization at the eastern end, but in the west has 0.185% total Cu and 0.036 g/t Au over 27.0 m. Trench 400W has one zone containing 0.078% total Cu and 0.004 g/t Au over 6.0 m.

DISCUSSION

At least four foliated and mineralized bodies have been mapped in Zone A of the Stu property, they strike NW and dip moderately to steeply to the NE. The eastern body appears to be the largest (Fig. 3) with a minimum strike length of 200 m, a down dip extent of 80 m, and an approximate total Cu grade of 0.15%, along section 800W. Three significant intersections (>2.8 % Cu over 12.5 m or more), two within the eastern body, were drilled on the property in 1980 (Tempelman-Kluit, 1981). The best intersection to date, 3.51% Cu, 2.5 g/t Au and 18.4 g/t Ag over 13.5 m, is from hole 80-14 in Zone A (Tempelman-Kluit, 1981). In plan and cross section view, the foliated and mineralized bodies pinch and swell, appearing lensoidal in shape. Contacts between the foliated and unfoliated bodies are ambiguous but are interpreted as primarily intrusive in nature, though it is likely they were modified during deformation. Mineralized and foliated granodioritic rocks have been deformed and recrystallized to dominantly biotite orthogneiss with local biotite schist. This is similar to mineralized amphibolite, biotite schist and gneiss (Tafti and Mortensen, 2004) from Williams Creek, and foliated to gneissic banded granodiorite with mafic schlieren (Hood, 2012) from Minto.

Based on our re-assay of diamond drill core from hole 80-6, total Cu (%)/Au (ppm) ratios for Stu range from 2.2 to 10.2, supergene Cu/Au from 0.2 to 7.4, and sulphide Cu/Au from 1.3 to 9.2. Taking the two least oxidized sample intervals as representative of hypogene mineralization (Fig. 4), total Cu/Au averages 2.3 which is very similar to the ratios seen at the Minto and Carmacks Copper deposits (based on published resources of Mercer and Sagman, 2012, and Arseneau and Casselman, 2008, resepctively). The proportion of supergene Cu decreases with depth while the sulphide Cu increases (Fig. 4). Conversely Au and Ag are consistently low in shallow samples (~20 ppb and ≤1 ppm, respectively) compared to the deeper samples (200 ppb and 3 ppm, respectively). These trends suggest that Cu, Au and Ag have been mobilized during oxidation but only Cu has been re-deposited, and possibly enriched, during supergene processes.

The origin of the Minto and Carmacks Copper deposits is still debated. Early interpretations of the Minto ore bodies include metamorphosed and deformed syn-sedimentary

Cu mineralization (*e.g.*, red bed copper), or very early porphyry-style mineralization, followed by intrusion of the main unfoliated plutonic body (Pearson and Clark, 1979). Subsequent workers have utilized the presence of 'magmatic' epidote and Al-in-hornblende geobarometry to constrain the crystallization pressures of the unmineralized Granite Mountain batholith plutonic rocks to 6.1 to 6.6 kbar (equivalent to 22-24 km crustal depth; McCausland *et al.*, 2002; Tafti and Mortensen, 2004). The presence of 'magmatic' epidote in mineralized rock (*e.g.*, Fonseca, 2008) suggests models should accommodate a deeper crustal level than is typical in porphyry models (1-6 km; Seedorff *et al.*, 2005). This has been done by either, utilizing an early porphyry-style mineralization model, and invoking rapid vertical tectonic movement (Tafti and Mortensen, 2004), or using a shear-hosted magmatic-hydrothermal model whereby mineralization occurred in the mid-crustal roots of a porphyry system (Hood, 2012). Tafti and Mortensen (2004) also looked at the Carmacks Copper deposit and concluded the majority of mineralization was early porphyry-style in origin, but that supracrustal hosts (*i.e.*, metasedimentary and/or metavolcanic rocks) may have been locally important. At Carmacks Copper, others have concluded that the foliated and mineralized bodies may be rafts of mineralized volcanic rock (now amphibolite or schist; Archer, 1989; Kent *et al.*, 2014) similar to the early syn-sedimentary Cu interpretation at Minto of Pearson and Clark (1979).

The above models broadly incorporate the same key observations: 1) Cu-sulphide mineralization was emplaced early in the host rock history; 2) individual mineralized bodies have been deformed and recrystallized obscuring original characteristics; and 3) main unfoliated plutonic phases intrude, and possibly engulf the ore bodies. Observations at Stu are similar: Cu-sulphide minerals replace, at least partly, magmatic mafic minerals early in the host rock history; the host granodioritic rocks have been strongly deformed and recrystallized to the point they are now dominantly gneissic; and the primary contacts between unfoliated and foliated granodioritic rocks appear to have been intrusive in nature with the foliated and mineralized bodies surrounded by unfoliated K-feldspar porphyritic granodiorite. Limited rock exposure at the Stu, particularly of unoxidized hypogene mineralization, makes interpretation of a genetic model difficult. Based on our fieldwork, we suggest that Stu mineralization is similar to the Carmacks Cu and Minto deposits. It is primarily hosted in multiple discrete bodies of foliated granodioritic rocks striking NW and dipping to the NE. Mineralization occurs as both hypogene sulphide minerals, bornite and chalcopyrite, and supergene malachite, azurite, tenorite and chrysocolla. In terms of supergene processes, and ore body orientation, Stu is more similar to Carmacks Copper, though the overall similar character of hypogene mineralization at Carmacks Copper, Minto and Stu suggests a similar genetic model for all three. The primary difference between the three appears to be variation in the present orientation of the ore bodies which has likely influenced supergene processes.

ACKNOWLEDGMENTS

John Chapman of the Geological Survey of Canada provided whole-rock geochemical data from four samples near the Stu occurrence. Jean Pautler helped us early on with discussion and finding our way around the property. Josh Pillsbury and Don Lougheed provided superior assistance in the field. Jesse and Emily Halle and Nikolett Kovaks were gracious hosts at the Carmacks Copper camp and generously showed us their rocks.

REFERENCES

Archer, A.R., 1989. Bulk sampling and metallurgical investigations, Williams Creek Copper property, Carmacks area, Yukon Territory. Yukon Energy, Mines and Resources Assessment Report 092859.

Arseneau, G. and Cassleman, 2008. Resource Estimate of the No. 1, No. 4 and No. 7 zones Carmacks' Deposit, Yukon Territory. Internal report, Wardrop Engineering Inc., 73 p.

Colpron, M., Israel, S., Murphy, D.C., Pigage, L.C. and Moynihan, D., 2016. Yukon Bedrock Geology Map 2016. Yukon Geological Survey, Open File 2016-1, scale 1:1 000 000.

Fonseca, A., 2008. Petrographic survey of the Stu Cu-Au project, Carmacks Copper Belt, Dawson Range Yukon, Canada. Yukon Energy, Mines and Resources Assessment Report 095195.

Frost, B.R., Barnes, C.G., Collins, W.J., Arculus, R.J., Ellis, D.J. and Frost, C.D., 2001. A geochemical classification for granitic rocks. Journal of Petrology, vol. 42, p. 2033-2048.

Frost, B.R. and Frost, C.D., 2008. A geochemical classification for feldspathic igneous rocks. Journal of Petrology, vol. 49, p. 1955-1969.

Gordey, S.P. and Makepeace, A.J.(compilers), 2001. Bedrock geology, Yukon Territory. Indian & Northern Affairs Canada/Department of Indian & Northern Development: Exploration & Geological Services Division, Open File 2001-1, scale 1:1 000 000.

Harris, N.B.W., Pearce, J.A. and Tindle, A.G., 1986. Geochemical characteristics of collision-zone magmatism. *In:* Collision Tectonics, M.P. Coward and C.A. Ries (eds.), Special Publications 19, Geological Society London, p. 67-81.

Hayward, N., Miles, W. and Oneschuk, D., 2012. Detailed geophysical compilation project, Yukon Plateau, Yukon, NTS 115-I,J,K,N,O and 116A and B. Geological Survey of Canada, Open File 7279, scale 1:350 000.

Hood, S., 2012. Mid-crustal Cu-Au Mineralisation during Episodic Pluton Emplacement, Hydrothermal Fluid Flow, and Ductile Deformation at the Minto Deposit, YT, Canada. Unpublished MSc thesis, University of British Columbia, 231 p.

Joyce, N.L., Colpron, M., Allan, M.M., Sack, P.J., Crowley, J.L. and Chapman, J.B., 2016. New U-Pb zircon dates from the Aishihik batholith, southern Yukon. *In:* Yukon Exploration and Geology 2015, K.E. MacFarlane and M.G. Nordling (eds.), Yukon Geological Survey, p. 131-149.

Kent, A., Arseneau, G., Hester, M. G., Beattie, M. and Hull, J., 2014. Preliminary economic assessment of copper, gold and silver recovery at the Carmacks project, Yukon Territory, Canada. Internal report, Merit Consultants Internation Inc., 195 p.

Le Bas, M.J. and Streckeisen, A.L., 1991. The IUGS systematics of igneous rocks. Journal of the Geological Society, London, vol. 148, p. 825-833.

Logan, J.M. and Mihalynuk, M.G., 2014. Tectonic controls on Early Mesozoic paired alkaline porphyry deposit belts (Cu-Au ± Ag-Pt-Pd-Mo) within the Canadian Cordillera. Economic Geology, vol. 109, p. 827-858.

Maniar, P.D. and Picolli, P.M., 1989. Tectonic discrimination of granitoids. Geological Society of America Bulletin, vol. 101, no. 5, p. 635-643.

McCausland, P.J.A., Symons, D.T.A., Hart, C.J.R. and Blackburn, W.H., 2002. Paleomagnetism and geobarometry of the Granite Mountain batholith, Yukon: Minimal geotectonic motion of the Yukon-Tanana Terrane relative to North America. In: Yukon Exploration and Geology 2001, D.S. Emond, L.H. Weston and L.L. Lewis (eds.), Exploration and Geological Services Division, Yukon, Indian and Northern Affairs Canada, p. 163-177.

McLennan, S.M., 2001. Relationships between the trace element composition of sedimentary rocks and upper continental crust. Geochemistry, Geophysics, Geosystems, vol. 2, 24 p.

Mercer, B. and Sagman, J., 2012 Phase VI Preliminary Feasibility Report Minto Mine. Internal report, Minto Explorations Ltd., 368 p.

Nelson, J.L., Colpron, M. and Israel, S., 2013. The Cordillera of British Columbia, Yukon, and Alaska: Tectonics and metallogeny. *In:* Tectonics, Metallogeny and discovery: The North American Cordillera and similar accretionary setttings, M. Colpron, T. Bissig, B.G. Rusk and J.F. Thompson (eds.), Special Publication No. 17, Society of Economic Geologists, p. 53-109.

Pautler, J., 2009. Geological, geochemical, petrographic and compilation Assessment Report of the Stu property. Yukon Energy, Mines and Resources Assessment Report 095195.

Pearce, J.A., 1996. A user's guide to basalt discrimination diagrams. Trace element geochemistry of volcanic rocks. *In*: Wyman, D.A. (ed.), Geological Association of Canada - Mineral Deposits Division, p. 79-113.

Pearson, W.N. and Clark, A.H., 1979. The Minto copper deposit, Yukon Territory; a metamorphosed orebody in the Yukon crystalline terrane. Economic Geology, vol. 74, p. 1577-1599.

Peccerillo, A. and Taylor, S.R., 1976. Geochemistry of eocene calc-alkaline volcanic rocks from the Kastamonu area, Northern Turkey. Contributions to Mineralogy and Petrology, vol. 58, p. 63-81.

Sánchez, M.G., Allan, M.M., Hart, C.J.R. and Mortensen, J.K., 2014. Extracting ore-deposit-controlling structures from aeromagnetic, gravimetric, topographic, and regional geologic data in western Yukon and eastern Alaska. Interpretation, vol. 2, p. SJ75-SJ102.

Seedorff, E., Dilles, J.H., Proffett, J.M., Einaudi, M.T., Zurcher, L., Stavast, W.J.A., Johnson, D.A. and Barton, M.D., 2005. Porphyry deposits: Characteristics and origin of hypogene features. *In:* Economic Geology: One Hundredth Anniversary Volume, J.W. Hedenquist, J.F.H. Thompson, R.J. Goldfarb and J.P. Richards (eds.), Society of Economic Geologists, p. 251-298.

Shand, S.J., 1927. Eruptive rocks: Their genesis, composition, classification, and their relation to ore-deposits, with a chapter on meteorites. T. Murby & Co., London, 360 p.

Tafti, R. and Mortensen, J.K., 2004. Early Jurassic porphyry(?) copper (-gold) deposits at Minto and Williams Creek, Carmacks Copper Belt, western Yukon. *In:* Yukon Exploration and Geology 2003, D.S. Emond and L.L. Lewis (eds.), Yukon Geological Survey, p. 289-303.

Tempelman-Kluit, D.J., 1981. Description of the Stu property. *In:* Yukon Geology and Exploration 1979-80. Department of Indian and Northern Affairs, Geology Section, Whitehorse, Yukon, p. 262-263.

Tempelman-Kluit, D.J., 1984. Geology of Laberge (105E) and Carmacks (115I) map areas, Yukon. Geological Survey of Canada, Open File 1101.

Watson, K.W. and Joy, R.J., 1977. Geological, geochemical and geophysical report on the Stu claim group, Hoochekoo Creek area. United Keno Hill Mines Ltd., Yukon Energy, Mines and Resources Assessment Report 090248.

Winchester, J.A., Floyd, P.A., 1977. Geochemical discrimination of different magma series and their differentiation products using immobile elements. Chemical Geology 20, p. 325-343.

Woodsworth, G.J., Anderson, R.G. and Armstrong, R.L., 1991. Plutonic Regimes, Chapter 15. *In*: Geology of the Cordilleran Orogen in Canada, H. Gabrielse and C.J. Yorath (eds.), Geological Survey of Canada, Geology of Canada, no. 4, p. 491-531; *also Geological Society of America, The Geology of North America, vol. G-2*.

Yukon Geological Survey, 2015. Yukon Digital Bedrock Geology. <http://www.geology.gov.yk.ca/update_yukon_bedrock_geology_map.html> [accessed November 20, 2015].

Zen, E. and Hammarstrom, J.M., 1984. Magmatic epidote and its petrologic significance. Geology, vol. 12, p. 515-518.

APPENDICES

The three appendices for this paper are only available digitally. The 3D geologic model in Appendix 1 requires a free software viewer, see details below. Appendices 2 and 3 are separate tabs within one Microsoft Excel spreadsheet.

Appendix 1. A simplified 3D geological model for the Zone A occurrence on the Stu property is included in this digital appendix. The model was created from a series of sections (e.g., Fig. 6), using geological information from the three diamond drill holes and trenches logged in this study and from digitized historic drill sections for the remaining holes in Zone A. The model includes drill hole and trench geological data, assay data collected from this study, and historically reported drill intercepts. The model can be viewed and manipulated using Geosoft Montaj Viewer; free software available for download from the Geosoft website (http://www.geosoft.com/support/downloads/viewers/oasis-montaj-viewer). The Geosoft website provides directions for downloading and configuring the freeware. Once the file containing the model (STU 3D view.gpf) is open in Geosoft Montaj Viewer, the user can manipulated the model in 3D space by selecting the 3D tab in the top menu bar then selecting the rotation, zoom or pan options in the 3D window menu. Geologic units in the model same as Fig. 3.

Appendix 2. Whole-rock geochemical analyses. Whole-rock analysis of 13 samples was conducted at Activation Laboratories Ltd., Ancaster, Ontario, using the 4Lithoresearch analytical package, a lithium metaborate/tetraborate fusion followed by analysis using Inductively Coupled Plasma Mass Spectrometry (ICPMS). For major elements, the quality of these data meet or exceeds fusion x-ray fluorescence data. For trace elements, the fusion process provides total dissolution of refractory minerals such as zircon, sphene and monazite, and gives accurate rare earth and high field strength element data. Using this analytical package, detection limits for major elements are 0.001% to 0.01% and trace elements are typically better than 1 ppm.

Appendix 3. Assay data, including sulphide and supergene Cu analyses. Geochemical analyses were conducted by Bureau Veritas Mineral Laboratories Ltd. using standard preparation and analytical techniques. Each sample was

prepared by crushing then pulverizing to 200 mesh. The 200 mesh pulps were analyzed for 41 elements by 4-acid digestion and Inductively Coupled Plasma Emission and Mass Spectrometry (ICPES/ICPMS) depending on the best technique for each element. Gold was analyzed by fire-assay fusion with an atomic absorption analysis (FA-AAS) and supergene Cu was analyzed by weak sulphuric acid digestion (5% H_2SO_4) followed by an ICPMS analysis.

Late Holocene fluctuations of the north lobe of Llewellyn Glacier, Upper Yukon River Basin

M. Samolczyk[1]
School of Science, Yukon College

S. Laxton
Yukon Geological Survey

J.J. Clague
Department of Earth Sciences, Simon Fraser University

Samolczyk, M., Laxton, S. and Clague, J.J., 2016. Late Holocene fluctuations of the north lobe of Llewellyn Glacier, Upper Yukon River Basin. *In:* Yukon Exploration and Geology 2015, K.E. MacFarlane and M.G. Nordling (eds.), Yukon Geological Survey, p. 223-231.

ABSTRACT

Llewellyn Glacier contributes glacial meltwater to runoff entering the Yukon River, which flows through the hydroelectric power dam in Whitehorse, Yukon. An examination of lateral moraine stratigraphy, and radiocarbon and dendrochronological dating of *in situ* and detrital subfossil wood provide a record of fluctuations of Llewellyn Glacier over the past two millennia. Our data indicate the north lobe advanced sometime between AD 260 and AD 505, and reached within 70 m of its Little Ice Age maximum limit as early as the 17th century. The main lobe advanced as early as AD 1035, possibly between the First Millennium and Little Ice Age advances of the last two millennia, when glaciers have traditionally been considered more restricted. Results provide new information on the timing and frequency of fluctuations of Llewellyn Glacier, and can be used to assist with modelling the future impacts of climate change on glacial meltwater contributions to rivers and hydroelectric security in Yukon.

[1]*msamolczyk@yukoncollege.yk.ca*

INTRODUCTION

Glaciers at the headwaters of the Yukon River are important sources of the water that flows through the hydroelectric power dam in Whitehorse, Yukon. Concern over the impacts of climate change on hydroelectric security in Yukon has prompted examination of the contribution of glacial meltwater to runoff in the Upper Yukon River Basin, the fourth largest drainage basin in North America (Brabets *et al.*, 2000; Northern Climate Exchange, 2014). Llewellyn Glacier, an eastward flowing outlet glacier of the Juneau Icefield in British Columbia, contains at least half of the total ice in the Upper Yukon River Basin and was the single greatest contributor to runoff from glacier melt (7.3%) and glacier wastage (2.7%), as defined by Comeau *et al.* (2009), between 1981 and 2011 (Northern Climate Exchange, 2014).

Most glaciers around the world have thinned and retreated; cumulative losses of ice have increased from 226 Gt/year between 1971 and 2009 to 301 Gt/year between 2005 and 2009 (IPCC, 2013). In Yukon, the total area of glacier ice cover has decreased by 22% since the 1957-1958 International Geophysical Year (Barrand and Sharp, 2010). Like most other glaciers in Yukon, Llewellyn Glacier has thinned and retreated rapidly over the past several decades (Sprenke *et al.*, 1999; Clague *et al.*, 2010). Based on an analysis of remotely sensed and GIS data, the surface area of Llewellyn Glacier decreased 8.3% from 1948 to 2010 (Northern Climate ExChange, 2014).

Glaciers are sensitive to even minor changes in climate, and studies of geologic and dendrochronologic records in glacier forefields may provide evidence of past climatic conditions (Denton and Karlén, 1973). This paper presents evidence of recent fluctuations of the north lobe of Llewellyn Glacier. Our objective is to document the response of Llewellyn Glacier to past environmental change, which may provide insight into how the glacier will respond to future climate warming.

PREVIOUS WORK

Investigations based on Shuttle Radar Topographic Mission digital elevation model (SRTM DEM) data and Canadian digital elevation data (CDED DEM) indicate that the elevation of the surface of the lower part of Llewellyn Glacier decreased nearly 100 m between 1987 and 2000 (Northern Climate ExChange, 2014). Clague *et al.* (2010) studied the forefield of the main and south lobes of Llewellyn Glacier to construct a record of glacier expansion during the past two millennia. Based on the stratigraphy of lacustrine and deltaic sediments and on tree-ring and radiocarbon ages of detrital wood and glacially overridden stumps in growth position, they concluded that the glacier advanced between AD 300 and AD 500 and between AD 1035 and AD 1210, reaching within 400 m of its Little Ice Age (LIA) maximum limit in the later advance. The times of these advances are not fully consistent with previous interpretations that glaciers in northwest North America advanced during two broad intervals in the past two millennia: one near the start of the first millennium AD, referred to as the First Millennium Advance (FMA; Reyes *et al.*, 2006); and a second during the Little Ice Age (LIA), which began around AD 1200 and culminated in the eighteenth and nineteenth centuries (Clague *et al., 2010)*. Clague *et al.* (2010) argued that glacier behavior in northwest North America during the past two millennia is more complex than this simple view would suggest. Investigations at Bromley Glacier (Hoffman and Smith, 2013) and at Franklin Glacier (Mood and Smith, 2015) support this interpretation by showing that these glaciers advanced during the period between the FMA and LIA. Our study provides additional data pertinent to this issue from the north lobe of Llewellyn Glacier, which has not been previously examined.

STUDY AREA

Llewellyn Glacier, with an area of approximately 427 km^2, is one of the largest glaciers in British Columbia (Arendt *et al.*, 2014). It flows east from the Juneau Icefield toward the southern end of Atlin Lake (Fig. 1). The Juneau Icefield lies at the crest of the northern Boundary Ranges of the Coast Mountains and is the fifth largest icefield (4000 km^2) in North America (Sprenke *et al.*, 1999). Llewellyn Glacier flows from elevations of 1830 to 1980 m above sea level and terminates in three lobes between about 700 and 900 m above sea level. The largest lobe (herein referred to as the 'main' lobe) flows east and two smaller lobes, the 'north' and 'south' lobes, are located, respectively, north and south of the main lobe. Extensive lateral and end moraines, as well as trimlines, are preserved in the forefield area of the glacier and mark its maximum Holocene extent.

A weather station in Atlin BC, 54 km northeast of the toe of the north lobe of Llewellyn Glacier, records daily average January and July temperatures of -12.8°C and 13.4°C, respectively (Environment Canada, 2015). Average precipitation for January and July is 45.6 mm and 32.8 mm (water equivalent), respectively.

Our focus was on the lateral and end moraines of the north lobe of Llewellyn Glacier (study area 1; Fig. 1). An additional site on the north lateral moraine of the main lobe, approximately 4 km from its terminus, was also examined (study area 2; Fig. 1). Meltwater issuing from the north lobe enters a small proglacial lake and then flows into Hobo Creek, which discharges into Willison Bay of Atlin Lake. The north lobe occupies a narrow valley (~1.5 km wide) flanked by lateral moraines and is approximately 3.5 km long, terminating about 2.6 km up-valley from a sharp-crested LIA end moraine.

METHODS

The stratigraphy of lateral moraines was examined and recorded in June and August 2014 and samples of *in situ* and detrital subfossil wood associated with paleosurfaces of older buried moraines were collected for radiocarbon dating. Additional samples were collected for dendrochronologic analysis from living and dead trees on the distal slope of an end moraine of the north lobe (Fig. 1). Radiocarbon ages of the outer rings of glacially overridden, *in situ* stumps date the time when a glacier advanced over and killed the trees. *In situ* wood also provides a minimum age for the surface on which it grew. Ages of detrital wood are more difficult to interpret, but nevertheless, in the case of till, detrital wood ages are maxima for the time of deposition from ice with enclosing sediments at the location from which the wood was recovered.

Eleven samples of wood were radiocarbon dated using the accelerator mass spectrometry (AMS) method at Beta Analytic Inc. and the Keck Carbon Cycle AMS facilities (Table 1). Radiocarbon ages were calibrated using the calibration dataset of Reimer *et al.* (2013) in OxCal v. 4.2.4 (Bronk Ramsey, 2013). Calibrated ages in brackets are

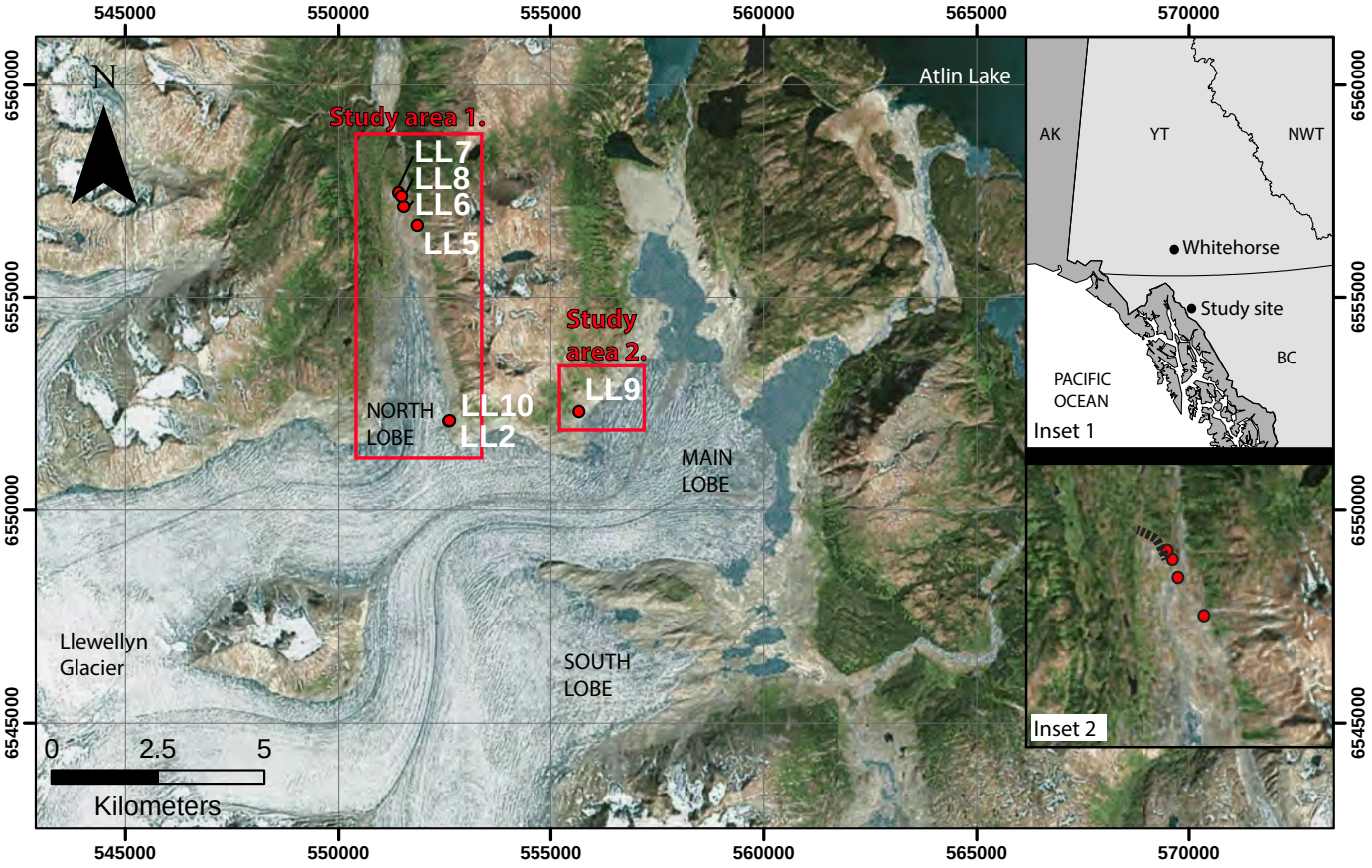


Figure 1. *Satellite imagery of Llewellyn Glacier, British Columbia, Canada, with study areas 1 and 2 outlined (numbered black boxes). Red dots indicate location of sample sites. Inset map 1 shows location of Llewellyn Glacier relative to Whitehorse, Yukon. Inset map 2 shows close-up of sites LL5 to LL8 in study area 1 with dashed black line showing crest of the end moraine.Background imagery: Esri, DigitalGlobe, GeoEye, Earthstar Geographics, CNES/Airbus DS, USDA, USGS, AEX, Getmapping, Aerogrid, IGN, IGP, swisstopo and the GIS.*

Table 1. *Sample site locations and reported radiocarbon ages.*

Radiocarbon age (^{14}C yr BP)[a]	Calendric age (AD)[b]	Laboratory number[c]	Site number (Fig. 1)	UTM coordinate (zone 8N)	Elevation (m)	Dated material
1705±30	252 - 401	UCIAMS-149293	LL2	552612, 6552090	1099	Branch or root[d]
1750±30	222 - 385	Beta-384639	LL2	552612, 6552090	1099	Branch or root[e]
1665±30	258 - 506	UCIAMS-149294	LL2	552612, 6552090	1099	Woody organic fragments
185±30	1650 - present	UCIAMS-149295	LL5	551867, 6556683	949	Branch or root[e]
80±30	1690 - 1926	UCIAMS-149296	LL6	551555, 6557143	797	Tree stump[e,f]
370±30	1446 - 1634	UCIAMS-149297	LL6	551555, 6557143	797	Tree stump[d,f]
145±30	1668 - 1948	UCIAMS-149298	LL7c	551427, 6557486	874	Tree trunk[d,g]
155±30	1666 - present	UCIAMS-149300	LL8	551503, 6557383	875	Branch or root[e]
910±30	1033 - 1204	UCIAMS-149301	LL9	555636, 6552368	834	Branch or root[e]
1775±30	138 - 339	UCIAMS-149302	LL10	552622, 6552092	unknown	Tree trunk[d]
1785±30	134 - 332	UCIAMS-149303	LL10	552622, 6552092	unknown	Tree trunk[e]

[a]Error terms reported by Laboratories are 1σ
[b]Age determined from the calibration curve of Reimer *et al.* (2013) in OxCal v.4.2.4 (2σ ranges reported).
[c]Laboratories: UCIAMS, Keck Carbon Cycle AMS Facility; Beta, Beta Analytic Inc.
[d]Inner wood
[e]Outer wood
[f]Sample contains 136 rings
[g]Sample contains 147 rings

reported as 2σ ranges and rounded to the nearest decade or mid-decade year. Three samples of wood were dated using dendrochronology. Disks from the trees were cut with a chainsaw, air-dried, and sanded with progressively finer sand paper until the ring boundaries were clearly discernable. Tree rings were counted at the University of Victoria Tree-Ring Laboratory using a WinDENDRO™ tree-ring imaging system (Guay *et al*., 1992).

RESULTS

STUDY AREA 1 – NORTH LOBE OF LLEWELLYN GLACIER

Paleosurfaces containing subfossil tree fragments were found at three sites along the east lateral moraine of the north lobe of Llewellyn Glacier (LL2, LL10 and LL5) and at two sites on the valley floor within 100 m of the LIA end moraine (LL6 and LL8; Fig. 1). Tilted dead and living trees growing just behind the LIA end moraine were also dated (LL7; Fig. 1).

A well-developed buried paleosol containing woody debris and two organic horizons is exposed at site LL2 on the flank of the east lateral moraine, approximately 77 m above the glacier surface and about 500 m down-valley from where the north lobe separates from the main lobe (Fig. 2a,b). A 1 m vertical section through the paleosol is exposed on the fresh steep face of the lateral moraine. The upper organic horizon, <35 cm thick, contains woody fragments, plant macrofossils and roots up to 15 cm in diameter in an olive-gray to brown mottled silt. This unit grades downward into a 52-cm-thick, yellow-brown sandy silt to silty sand containing discontinuous black peat lenses. A sharp contact separates the sand-silt unit from a lower, 1–2-cm-thick, organic horizon that contains black peat with woody roots and rootlets. An oxidized gravel unit, approximately 10-cm-thick, underlies the lower organic horizon and grades into till at the base of the section. A sample of the outer rings of a 15 cm-diameter branch or root from the upper organic horizon and another sample of its pith and adjacent inner rings, yielded radiocarbon ages, respectively, of 1750±30 ^{14}C yr BP (AD 220-385; Beta-384639) and 1705±30 ^{14}C yr BP (AD 250-400; UCIAMS 149293). A sample of the peat from the lower organic horizon returned a radiocarbon age of 1665±30 ^{14}C yr BP (AD 260-505; UCIAMS-149294).

An *in situ* subfossil tree stump is exposed at site LL10 (Fig. 3), approximately 15 m down-valley from site LL2 and at about the same height (76 m) above the glacier surface. At this site, the steeply sloping bedrock surface crops out on the face of the east lateral moraine and the stump is rooted at the till-bedrock contact on the stoss side of the

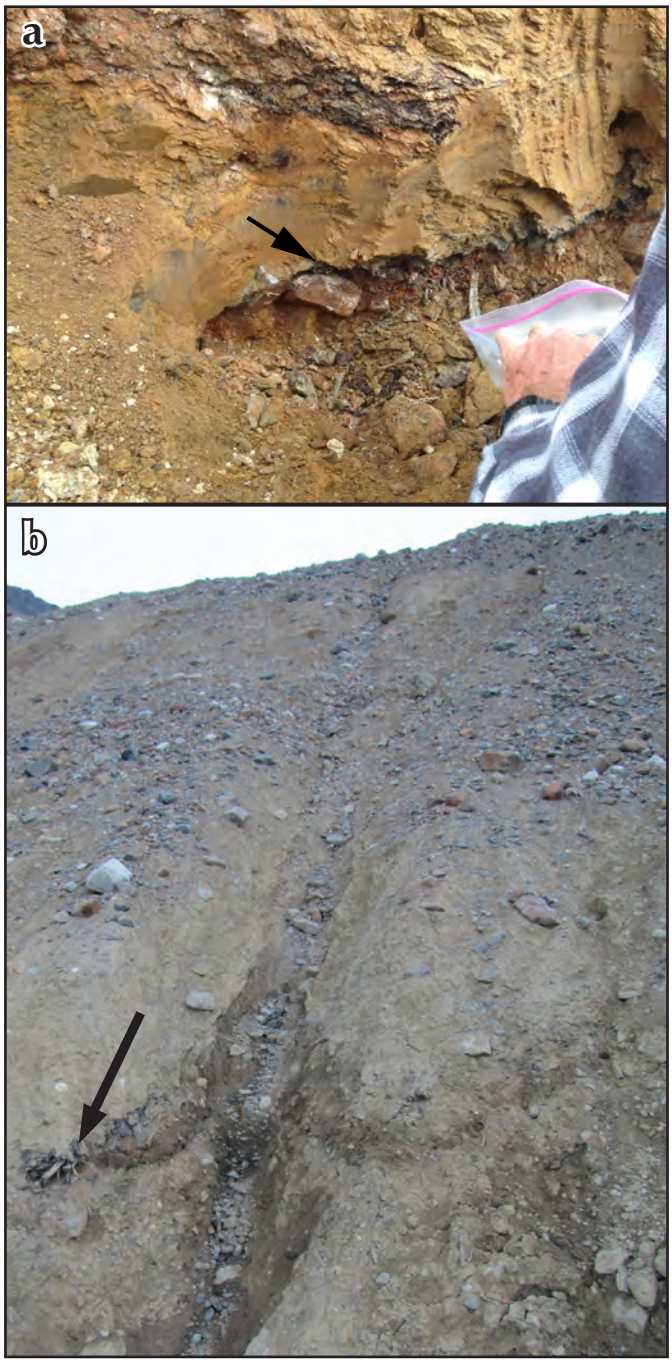


Figure 2. *(a) Excavation at site LL2 showing the dated lower organic horizon (1–2 cm thick; indicated by an arrow). Also shown are the overlying yellow-brown sand-silt unit (~50 cm thick) and the underlying oxidized yellow-brown gravel. The dated upper organic horizon that overlies the sand-silt unit is not shown in this image. Person for scale. (b) Location of site LL2 below the right lateral moraine crest of the north lobe of Llewellyn Glacier. Arrow indicates location of wood protruding from the dated upper organic horizon. The paleosol is located approximately 30 m below the moraine crest.*



Figure 3. *Sheared tree stump shown protruding from contact between till and bedrock outcrop at site LL10. Northward ice flow direction is indicated by arrow. Photographer is aiming camera down the face of the east lateral moraine toward the base of the moraine. Pencil for scale.*

bedrock exposure. Samples of the outermost rings and the pith and adjacent rings of the stump yielded radiocarbon ages of, respectively, 1785±30 ^{14}C yr BP (AD 135-330; UCIAMS-149303) and 1775±30 ^{14}C yr BP (AD 135-340; UCIAMS-149302).

At site LL5, 5.3 km down-valley from where the north lobe separates from the main lobe and 1.8 km beyond the terminus of the glacier, a paleosol containing a dark brown organic horizon with fibrous peat and *in situ* roots and fragments of detrital wood dips 30° from near the crest of the east lateral moraine toward the valley floor (Fig. 4). Fifteen to 30 cm of altered sediments with orange staining directly underlie the organic horizon, which can be traced discontinuously along the proximal slope of the moraine in gully exposures for about 20 to 30 m until it is about 15 m below the moraine crest. A gray matrix-



Figure 4. *Dipping paleosol at site LL5, showing exposed organic horizon. Moraine crest lies approximately 0.5 m above the paleosol. Pencil for scale.*



Figure 5. *Sample LL6, an in situ tree stump sheared by a glacial advance. Handheld radio for scale.*

supported diamicton composed of a silt-sand matrix and 25–30% subangular to rounded clasts (cobble- to boulder-size), some with striations, overlies the organic horizon. A grayish-brown clast- to matrix-supported diamicton with angular to sub-angular clasts, as large as boulder-sized, underlies the organic horizon. The entire package is weakly stratified and dips 30° towards the valley floor. The outer rings of a 10 cm diameter, *in situ* tree stem protruding from the organic horizon near the moraine crest yielded a radiocarbon age of 185 ± 30 ^{14}C yr BP (AD 1650-present; UCIAMS-149295). The same horizon approximately 25 m farther down-valley comprises a large wood mat with several protruding stems, but was inaccessible.

An *in situ* subfossil tree stump about 30 cm in diameter with 136 rings was found in the forefield area of the north lobe, just up-valley (<70 m) from the LIA end moraine at site LL6 (Fig. 5). In this area, ice flowed over and around both sides of a large bedrock knob on the valley floor. Hobo Creek has incised through till on the east side of the bedrock knob, leaving a thin discontinuous veneer of till or reworked diamicton on the flank of the knob. The roots of the glacially sheared stump penetrate a bedrock crevice about 6.8 m above Hobo Creek. A sample of the outermost rings and another comprising the pith and adjacent rings yielded radiocarbon ages of, respectively, 80 ± 30 ^{14}C yr BP (AD 1690-1925; UCIAMS-149296) and 370 ± 30 ^{14}C yr BP (AD 1445-1635; UCIAMS-149297).

The sharp-crested end moraine of the north lobe of Llewellyn Glacier abuts the aforementioned bedrock knob on its west side. The top of the bedrock knob is vegetated with a mature stand of subalpine fir (*Abies lasiocarpa* (Hooker) Nuttall), slide alder (*Alnus viridis* (Chaix) DC.) and shrubs. Titled dead and live subalpine fir trees are present on the distal side of the moraine crest. At site LL7, a tilted, living subalpine fir with 147 rings growing on the distal side of the moraine, 4 m below its crest, had cambial scars on the proximal side of the trunk (sample LL7c; Fig. 6a,b). The inner pith and adjacent rings of this tree returned a radiocarbon age of 145 ± 30 ^{14}C yr BP (AD 1670-1950; UCIAMS-149298). Another living subalpine fir (sample LL7b), which had been damaged and was leaning along the ground, had 95 growth rings, but was not radiocarbon dated.

A patchy veneer of till with weakly developed O and A soil horizons overlies bedrock at the top of the bedrock knob at site LL8, only metres down-valley from site LL6 (Fig. 7). Outer rings of a detrital branch 20 cm below the soil surface returned a radiocarbon age of 155 ± 30 ^{14}C yr BP (AD 1665-present; UCIAMS-149300).

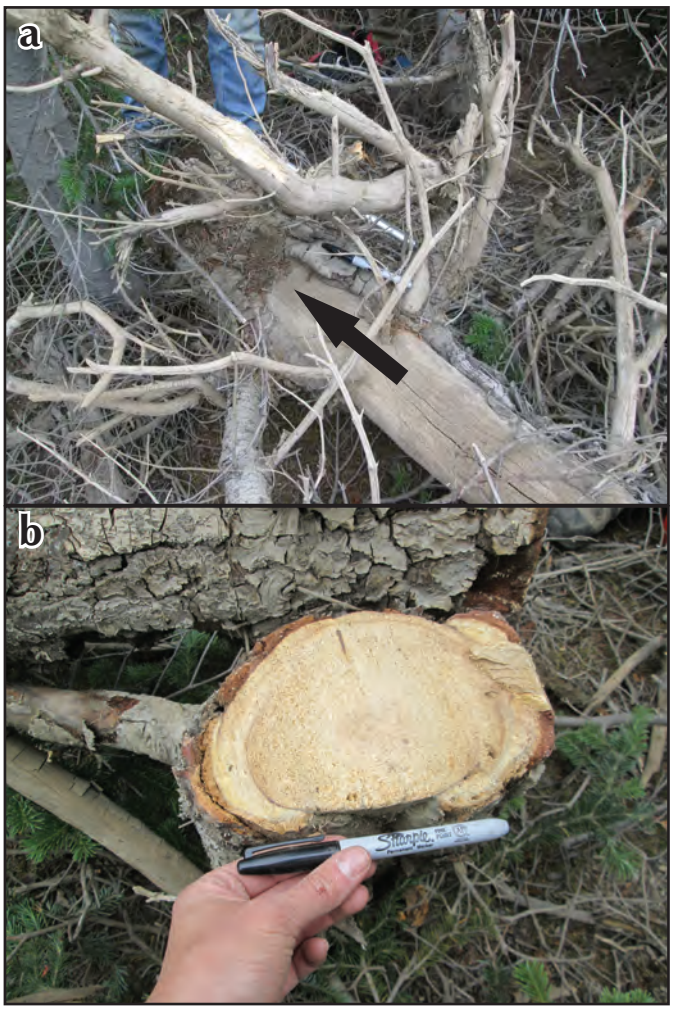


Figure 6. *(a) Black arrow indicates location of cambial scarring on sample LL7b. Marker for scale. (b) Cross section of damaged tree at site LL7. Marker for scale.*



Figure 7. *Sample LL8 protruding from till veneer. Pencil for scale.*

STUDY AREA 2 – MAIN LOBE OF LLEWELLYN GLACIER

A large gully is incised into the north lateral moraine of the main lobe of Llewellyn Glacier about 65 m above the present glacier surface (site LL9; Fig. 1). Several pieces of wood protrude from till at different elevations in this gully. Exposed along a stream flowing against the gully's southwest wall is approximately 2 m of matrix-supported, massive diamicton containing faceted striated stones up to boulder size overlying 0.5 m of weakly stratified, clast-supported diamicton (Fig. 8). Stratification in the lower unit and the sharp contact between the upper and lower units dip about 25° down the gully toward the glacier. A radiocarbon age of 910±30 ^{14}C yr BP (AD 1035-1205; UCIAMS-149301) was obtained from the outer rings of a detrital subfossil branch or stem, approximately 10 cm in diameter, that protruded from the contact between the upper and lower diamicton units.



Figure 8. *Red arrow points to sample LL9 protruding from a contact between coarse fluvial sediments (bottom) and till (top). Person for scale.*

DISCUSSION

The north lobe of Llewellyn Glacier deposited till on top of a paleosurface developed on its east lateral moraine, about 70 m above the present ice surface, sometime between AD 260 and AD 505, based on the evidence at sites LL2 and LL10. Because the dated surface supported well-developed soil horizons and rooted trees, it is likely that the surface was exposed for at least several hundred years prior to being overridden by Llewellyn Glacier during the first half of the first millennium AD. The record at sites LL2 and LL10 is consistent with evidence that the main and south lobes advanced into mature forest between AD 300 and AD 500 (Clague *et al.*, 2010).

Clague *et al*. (2010) presented evidence that the main lobe of Llewellyn Glacier was within 400 m of its maximum Holocene limit in the late 17th century prior to the maximum LIA advance. The radiocarbon-dated root in the paleosol at site LL5, about 4.8 km down-valley from sites LL2 and LL10, indicates that the north lobe of the glacier overtopped its lateral moraine and overrode a vegetated surface after AD 1650. The north lobe overrode a mature forest on the side of the bedrock knob about 5–10 m above the present valley floor near the LIA limit between AD 1690 and AD 1925, based on dates of the outermost rings of the sheared stump at site LL6 (Fig. 5). The stump contains 136 rings and the inner pith was dated to between AD 1445 and AD 1635, indicating that the tree was likely killed sometime in the late 16th to 18th centuries. When the glacier reached its LIA maximum position, it overrode trees and shrubs growing at the top of the bedrock knob. A date from detrital wood at site LL8 indicates that sediment was deposited on the bedrock knob sometime after AD 1665. Taking into account the findings of Clague *et al*. (2010) and evidence from sites LL5, LL6 and LL8, the north and main lobes probably reached their maximum LIA limits at the same time, after AD 1690.

The main lobe of Llewellyn Glacier was advancing as early as the 11th century. The dated stem or branch protruding from a contact between what is interpreted to be coarse fluvial sediments and overlying till in a gully on the north lateral moraine of the main lobe suggests that the glacier reached an elevation 65 m above the present ice surface after AD 1035. Crude stratification within the till dips parallel to the ground surface, indicating that at this site till was plastered onto the hillslope as the glacier thickened. Our data are consistent with an advance of the terminus of the main lobe of Llewellyn Glacier into mature forest between AD 1030 and AD 1210 (Clague *et al.*, 2010).

CONCLUSION

Data from sites along the margins of the north and main lobes of Llewellyn Glacier are in agreement with previous research findings that indicate a history of complex glacier fluctuations over the past two millennia. The north lobe thickened and advanced in the first half of the first millennium AD and probably repeatedly during the second half of the second millennium AD. Evidence found supports an advance of the main lobe of Llewellyn Glacier after AD 1035, possibly during a period between the FMA and LIA advances during which glaciers have traditionally been thought to have been more restricted. These data add to a growing body of evidence on past rates and magnitudes of glacier fluctuations in northwest North America and provide context for hydrologic models used to predict the effect of climate variability on hydroelectric security in Yukon River Basin.

ACKNOWLEDGEMENTS

We acknowledge Yukon Energy Corporation and the Natural Sciences and Engineering Research Council (NSERC) for their financial support. We are grateful for the field assistance provided by Chad Bustin, and lab and analytical support from Bryan Mood at the University of Victoria Tree-Ring Lab. The authors would also like to thank Jeff Bond for his thoughtful review of the manuscript.

REFERENCES

Arendt, A., Bliss, A., Bolch, T., Cogley, J.G., Gardner, A.S., Hagen, J.O., Hock, R., Huss, M., Kaser, G., Kienholz, C., Pfeffer, W.T., Moholdt, G., Paul, F., Radic, V., Andreassen, L., Bajracharya, S., Barrand, N., Beedle, M., Berthier, E., Bhambri, R., Brown, I., Burgess, E., Burgess, D., Cawkwell, F., Chinn, T., Copland, L., Davies, B., De Angelis, H., Dolgova, E., Filbert, K., Forester, R., Fountain, A., Frey, H., Giffen, B., Glasser, N., Gurney, S., Hagg, W., Hall, D., Haritashya, U.K., Hartmann, G., Helm, C., Herreid, S., Howat, I., Kapustin, G., Khromova, T., König, M., Kohler, J., Kriegel, D., Kutuzov, S., Lavrentiev, I., LeBris, R., Lund, J., Manley, W., Mayer, C., Miles, E.S., Li, X., Menounos, B., Mercer, A., Mölg, N., Mool, P., Nosenko, G., Negrete, A., Nuth, C., Pettersson, R., Racoviteanu, A., Ranzi, R., Rastner, P., Rau, F., Raup, B., Rich, J., Rott, H., Schneider, C., Seliverstov, Y., Sharp, M., Sigurðsson, O., Stokes, C., Wheate, R., Winsvold, S., Wolken, G., Wyatt, F. and Zheltyhina, N., 2014. Randolph Glacier Inventory – A dataset of global glacier outlines, version 4.0. Global Land Ice Measurements from Space, Boulder Colorado, USA, Digital Media, 56 p.

Barrand, N.E. and Sharp, M.J., 2010. Sustained rapid shrinkage of Yukon glaciers since the 1957-1958 International Geophysical Year. Geophysical Research Letters, vol. 37, L07501.

Brabets, T.P., Wang, B. and Meads, R.H., 2000. Environmental and hydrologic Overview of the Yukon River Basin, Alaska and Canada. United States Geological Survey, Water-Resources Investigations Report 99-4204, Anchorage, Alaska. 106 p.

Bronk Ramsey, C., 2013. OxCal v. 4.2.4, <http://c14.arch.ox.ac.uk/oxcal> [accessed October, 2015].

Clague, J.J., Koch, J. and Geertsema, M., 2010. Expansion of outlet glaciers of the Juneau Icefield in northwest British Columbia during the past two millennia. The Holocene, vol. 20, issue 3, p. 447-461.

Comeau, L.E., Pietroniro, A. and Demuth, M.N., 2009. Glacier contribution to the North and South Saskatchewan Rivers. Hydrological Processes, vol. 23, issue 18, p. 2640-2653.

Denton, G.H. and Karlén, W., 1973. Holocene climatic variations: their pattern and possible cause. Quaternary Research, vol. 3, issue 2, p. 155-205.

Environment Canada, 2015. National Climate Data and Information Archive, <http://climate.weather.gc.ca/climate_normals> [accessed September, 2015].

Guay, R., Gagnon, R. and Morin, H., 1992. A new automatic method and interactive tree-ring measurement system based on a line scan camera. Forestry Chronicle, vol. 68, p. 138-141.

Hoffman, K. and Smith, D.J., 2013. Late Holocene glacial activity at Bromley Glacier, Cambria Icefield, northern British Columbia Coast Mountains, Canada. Canadian Journal of Earth Sciences, vol. 50, issue 6, p. 599-606.

IPCC, 2013. Climate change 2013: The physical science basis. Contribution of Working Group I to the Fifth Assessment Report of the Intergovernmental Panel on Climate Change. Stocker, T.F., Qin, D., Plattner, G.-K., Tignor, M., Allen, S.K., Boschung, J., Nauels, A., Xia, Y., Bex, V. and Midgley, P.M. (eds.). Cambridge University Press, Cambridge, United Kingdom and New York, NY, USA, 1535 p.

Mood, B. and Smith, D.J., 2015. Latest Pleistocene and Holocene behaviour at Franklin Glacier, Mt. Waddington area, British Columbia Coast Mountains, Canada. The Holocene, vol. 25, issue 5, p. 784-794.

Northern Climate ExChange, 2014. Projected future changes in glaciers and their contribution to discharge of the Yukon River at Whitehorse. Northern Climate ExChange, Yukon Research Centre, Yukon College, Whitehorse, YT, 44 p.

Reimer, P.J., Bard, E., Bayliss, A., Beck, J.W., Blackwell, P.G., Bronk Ramsey, C., Buck, C.E., Cheng, H., Edwards, R.L., Friedrich, M., Grootes, P.M., Guilderson, T.P., Haflidason, H., Hajdas, I., Hatté, C., Heaton, T.J., Hoffmann, D.L., Hogg, A.G., Hughen, K.A., Kaiser, K.F., Kromer, B., Manning, S.W., Niu, M., Reimer, R.W., Richards, D.A., Scott, E.M., Southon, J.R., Staff, R.A., Turney, C.S.M. and van der Plicht, J., 2013. IntCal13 and Marine13 radiocarbon age calibration curves 0-50,000 years cal BP. Radiocarbon, vol. 55, issue 4, p. 1869-1887.

Reyes, A.V., Wiles, G.C., Smith, D.J., Barclay, D.J., Allen, S., Jackson, S., Larocque, S., Laxton, S., Lewis, D., Calkin, P.E. and Clague, J.J., 2006. Expansion of alpine glaciers in Pacific North America in the first millennium AD. Geology, vol. 34, issue 1, p. 57-60.

Sprenke, K.F., Miller, M.M., McGee, S.R. and Adema, G.W., 1999. Canadian Landform Examples – 36: The high ice plateau of the Juneau Icefield, British Columbia: Form and dynamics. The Canadian Geographer, vol. 43, issue 1, p. 99-104.

Crustal depth of emplacement of the Early Jurassic Aishihik and Tatchun batholiths, west-central Yukon

***M.J. Topham*[1]**
Department of Earth, Ocean, and Atmospheric Sciences, The University of British Columbia

M.M. Allan*[2]*, J.K. Mortensen, C.J.R. Hart
Mineral Deposit Research Unit, University of British Columbia

M. Colpron, P.J. Sack
Yukon Geological Survey

Topham, M.J., Allan, M.M., Mortensen, J.K., Hart, C.J.R., Colpron, M. and Sack, P.J., 2016. Crustal depth of emplacement of the Early Jurassic Aishihik and Tatchun batholiths, west-central Yukon. *In:* Yukon Exploration and Geology 2015, K.E. MacFarlane and M.G. Nordling (eds.), Yukon Geological Survey, p. 233-251, including appendices.

ABSTRACT

Early Jurassic plutons in west-central Yukon were emplaced during accretion of the Intermontane terranes onto the western North American margin, and their exhumation is recorded in the sedimentological and geochronological record. Here the aluminum-in-hornblende geothermobarometer is applied to the 200-197 Ma Tatchun batholith and the 188-180 Ma Aishihik batholith, to estimate crystallization depths and exhumation rates. The Tatchun batholith crystallized at 6.4-7.2 kbar (23-26 km), whereas the Aishihik batholith was emplaced at 3.4-4.2 kbar (12-15 km). The Tatchun batholith exhumed at a rate of ~1.2-2.0 mm/a after crystallization, and was likely exposed at surface by the Middle Jurassic. Although subvolcanic equivalents of the Tatchun batholith have been lost to erosion, it could be prospective for deformed copper deposits such as Minto and Carmacks Copper. Hypabyssal and water-saturated phases of the Aishihik batholith suggest that portions of the batholith could be at, or just below, an appropriate crustal level for magmatic-hydrothermal mineralization.

[1]*matthewjtopham@gmail.com*

[2]*mallan@eos.ubc.ca*

INTRODUCTION

Late Triassic to Early Jurassic arc-related plutons of the British Columbia, Yukon and eastern Alaska Cordillera record the growth of the metallogenically significant Stikinia and Quesnellia arc terranes, and their accretion to the western North American margin (*e.g.*, Mortensen *et al.*, 2000; Nelson *et al.*, 2013). Current field mapping and geochronological studies have led to the definition of four discrete arc-related plutonic suites in Yukon of this age range (Gordey and Makepeace, 2001; Joyce *et al.*, 2016): the Stikine suite (220-206 Ma), which represents the plutonic roots of the peri-Laurentian Stikinia and Quesnellia arc terranes; the Minto suite (204-195 Ma), which likely represents the onset of arc accretion and continental arc magmatism; and the Long Lake (188-180 Ma) and Bryde suites (178-160 Ma), which record continental arc magmatism associated with the evolving Cordilleran orogeny (Nelson *et al.*, 2013; Fig. 1).

As indicated by regional cooling ages (Breitsprecher and Mortensen, 2004; Joyce *et al.*, 2015) and the Early to Middle Jurassic sedimentological and detrital zircon record (Dickie and Hein, 1995; Hart *et al.*, 1995; Hart, 1997; Lowey, 2004; Colpron *et al.*, 2015), Late Triassic to Early Jurassic batholiths were emplaced into crust that exhumed in the Early to Middle Jurassic to form the fault-bound flanks of the subsiding Whitehorse trough terrestrial to marine basin. The depth and timing of pluton emplacement, the rate of crustal exhumation and the age of sedimentation from igneous source rocks are generally poorly constrained, but are important considerations for tectono-structural reconstructions of the evolving Cordilleran orogeny in the Jurassic. These factors also bear on the likelihood of forming and preserving Late Triassic to Early Jurassic porphyry copper deposits in Yukon.

In this contribution, we build on previous geothermobarometric investigations of Early Jurassic plutons (McCausland *et al.*, 2002; Tafti, 2005) by applying the same empirical aluminum-in-hornblende geothermobarometer to the Aishihik and Tatchun batholiths of west-central Yukon, which represent the Long Lake and Minto plutonic suites, respectively (Fig. 1; Joyce *et al.*, 2016). This pressure-depth information is combined with magmatic ages (Joyce *et al.*, 2016) and cooling ages of the plutons (Joyce *et al.*, 2015) to estimate rates of crustal exhumation and to gauge the likelihood of preserving shallow magmatic-hydrothermal systems.

GEOLOGIC SETTING

The latest Triassic to Jurassic evolution of the Cordilleran hinterland in Yukon is characterized by accretion of the Intermontane terranes (Quesnellia, Slide Mountain terrane, Stikinia, Yukon-Tanana terrane, Cache Creek terrane) to the western North American margin, accompanied by tectonic thickening and continental arc magmatism, and followed by concurrent exhumation and synorogenic basin formation (Whitehorse trough; *e.g.*, Mihalynuk *et al.*, 1994, 2004; Nelson *et al.*, 2013; Colpron *et al.*, 2015). The distribution of upper Triassic volcanic and sedimentary rocks of Stikinia and Quesnellia (Lewes River Group) in southern Yukon tapers northwestward, where northwest of the confluence of the Pelly River and Yukon River, only age-equivalent plutonic rocks of the Stikine suite are exposed (Fig. 1).

Lewes River Group rocks are unconformably overlain by Lower to Middle Jurassic (Hettangian to Bajocian) terrestrial to marine sedimentary rocks of the Laberge Group, which were fed igneous detritus derived from mountainous terrain via river systems into the Whitehorse trough (Fig. 1; Hart *et al.*, 1995; Hart, 1997; Lowey, 2008; Colpron *et al.*, 2015). The Laberge Group is divided into two distinct facies: the Richthofen Formation in the south, which consists of distal deep-marine facies turbidite rocks and mass flow conglomerate rocks, and the Tanglefoot Formation in the north, which is dominated by proximal-facies, shallow-marine to fluvial sandstone and conglomerate, as well as mudstone and minor limestone (Lowey, 2008; Colpron *et al.*, 2015). Interbedded horizons of Nordenskiold tuff, with U-Pb zircon ages between 188 and 186 Ma, occur in both the Tanglefoot and Richthofen formations, and are coeval with, and derived from, Long Lake suite magmatism (Hart, 1997; Fillmore, 2006; Colpron and Friedman, 2008; Joyce *et al.*, 2016). The stratigraphy of the Laberge Group is interpreted to record the exhumation of Late Triassic to Early Jurassic plutons of the Stikine, Minto, Long Lake and Bryde plutonic suites that were emplaced during the Cordilleran orogeny (Hart, 1997; Colpron *et al.*, 2015). Specifically, Late Pliensbachian (183 Ma) and younger conglomerate rocks of the Tanglefoot Formation contain approximately 60 to 80% plutonic clasts derived from the adjacent Late Triassic to Early Jurassic plutons (Dickie and Hein, 1995; Lowey, 2008).

Latest Triassic to Early Jurassic plutonic rocks are exposed as large batholiths outboard and inboard of exposures of the Lewes River Group (Fig. 1). Minto suite plutons include the Granite Mountain batholith and Minto pluton, which

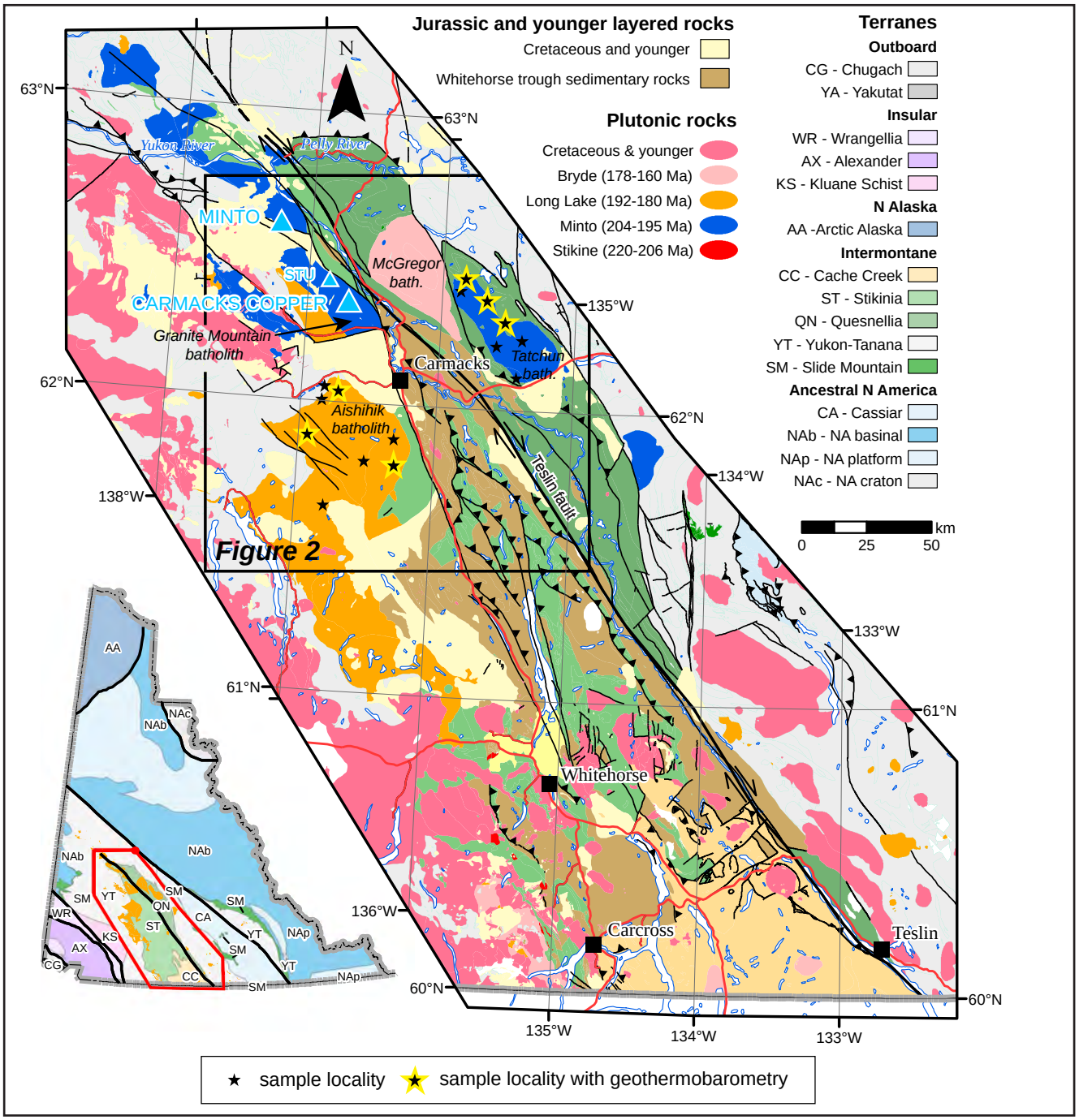


Figure 1. *Simplified regional geologic map of the Whitehorse trough region, highlighting Late Triassic to Early Jurassic plutonic suites. Geological data from Yukon Geological Survey (2015). Sample localities are indicated with the black stars, and samples used for geothermobarometry are highlighted in yellow.*

host the Carmacks Copper and Minto Cu-Au-Ag deposits, respectively. North of the mid-Cretaceous dextral strike-slip Teslin fault system, the Minto suite is represented by the *ca.* 200-197 Ma Tatchun batholith (Fig. 1; Colpron, 2011). The Aishihik batholith, located east of Aishihik Lake and southwest of Carmacks, is composed of 188-180 Ma granitoid rocks of the Long Lake suite (Johnston *et al.*, 1996; Hart, 1997; Joyce *et al.*, 2016). The Minto and Long Lake plutonic suites are compositionally heterogeneous, generally metaluminous, and demonstrate continental arc geochemical signatures (Mortensen *et al.*, 2000; Joyce *et al.*, 2016). Plutons of the Bryde suite include the McGregor

batholith north of Carmacks (Figs. 1 and 2) and several smaller plutons in southern Yukon (Fig. 1), but are not addressed in this study.

The regional tectonic fabric of the study area is a series of west-verging-thrust sheets, in which the Aishihik batholith is interpreted as an east-dipping, foliation-parallel, tabular intrusion (Hart, 1997; Johnston and Canil, 2007; Mira Geoscience, 2014). A weakly to moderately developed magmatic foliation is especially well developed near the margins of the pluton, which is consistent with a syntectonic interpretation (Johnston and Canil, 2007). Similarly, the Tatchun batholith is bound by southwest-verging thrust faults (Buffett *et al.*, 2006). The Tatchun batholith intrudes the Semenof block, which consists of Devonian to Permian volcanic and sedimentary arc rocks of the Boswell assemblage, which forms the basement to Mesozoic arc assemblages of Quesnellia (Semenof Formation; Templeman-Kluit, 1984, 2009; Simard and Devine, 2003; White *et al.*, 2012). Regional geophysical inversion modeling (Mira Geoscience, 2014) confirms previous interpretations by Colpron (2011) that the Tatchun batholith is a subhorizontal body. The tectonic setting of the Tatchun batholith is broadly similar to that suggested for the Aishihik batholith by Johnston and Canil (2007), in that it was emplaced into actively amalgamating lithotectonic domains.

Late Triassic to Early Jurassic plutonic rocks of west-central Yukon were exhumed shortly after their emplacement, as indicated by the preponderance of Early to Middle Jurassic cooling ages of batholiths and their country rocks (Breitsprecher and Mortensen, 2004; Colpron, 2011; Joyce *et al.*, 2015). Likewise, the eventual exposure and erosion of these plutons at surface is marked by the steady supply of igneous-derived detritus throughout the Early to Middle Jurassic sedimentation history of the Laberge Group (Hart *et al.*, 1995; Hart, 1997; Lowey, 2008; Colpron *et al.*, 2015). By the Late Jurassic, magmatic activity waned considerably, and by the end of the Jurassic, both crustal exhumation of plutonic rocks and sedimentation in the Whitehorse trough had ceased (Colpron *et al.*, 2015).

METALLOGENIC SETTING

In British Columbia, Late Triassic to Early Jurassic arc magmatism in Quesnellia and Stikinia has a well-documented connection to porphyry Cu-(Mo-Au) mineralization (*e.g.*, Logan and Mihalynuk, 2014). In Yukon, the plutonic roots of these arcs are exposed as the Stikine and Minto suites. However, possible examples of age-equivalent subvolcanic porphyry Cu-Au mineralization are restricted to a small number of occurrences in southern Yukon (*e.g.*, King Lake, Yukon MINFILE 115D 104 and Red Ridge, Yukon MINFILE 115D 100). In general, plutons of the Stikine and Minto suites were emplaced at mid-crustal pressures, as indicated by previous geothermobarometric studies (*e.g.*, McCausland *et al.*, 2002; Tafti, 2005) and by the presence of magmatic epidote (Tafti, 2005; Johnston *et al.*, 1996), which is indicative of high pressure (Zen and Hammarstrom, 1984). Accordingly, plutons of this age are generally poor targets for coeval, shallow-crustal porphyry, skarn, or epithermal mineralization.

Regardless, the Minto and Carmacks Copper deposits (Figs. 1 and 2) are two significant Yukon examples of intrusion-related Cu-Au-Ag mineralization associated with latest Triassic to Early Jurassic plutons. They are broadly characterized by sulphide mineralization hosted by schistose to gneissic to migmatitic rocks that have subsequently been intruded by massive granodiorite at mid-crustal levels in excess of 20 km (Tafti, 2005; Hood, 2012). These deposits have been variably interpreted as deformed porphyry systems (Mortensen *et al.*, 2000; Tafti and Mortensen, 2004), shear-hosted magmatic-hydrothermal deposits (Hood, 2012), iron-oxide copper gold (Mercer and Sagman, 2012), and sediment-hosted copper deposits (Pearson and Clark, 1979). Although the details of ore genesis at Minto and Carmacks Copper have been controversial, the association of mineralization with deeply emplaced plutonic rocks implies a unique exploration target.

PREVIOUS PRESSURE-DEPTH CONSTRAINTS

Estimations of the crustal depth of magma emplacement require an independent constraint on the pressure of crystallization, such as a pressure-sensitive mineral or mineral assemblage geobarometer. One such geobarometer is based on the empirical correlation between the total Al content of calcic amphibole and its pressure (P) of crystallization (Hammarstrom and Zen, 1986). The Al-in-hornblende geobarometer initially calibrated compositional analyses of hornblende from various Cordilleran plutons with independently constrained crystallization pressures derived from stratigraphic arguments or equilibrium mineral assemblages in contact metamorphic aureoles (Hammarstrom and Zen, 1986; Hollister *et al.*, 1987). The geobarometer was corrected for

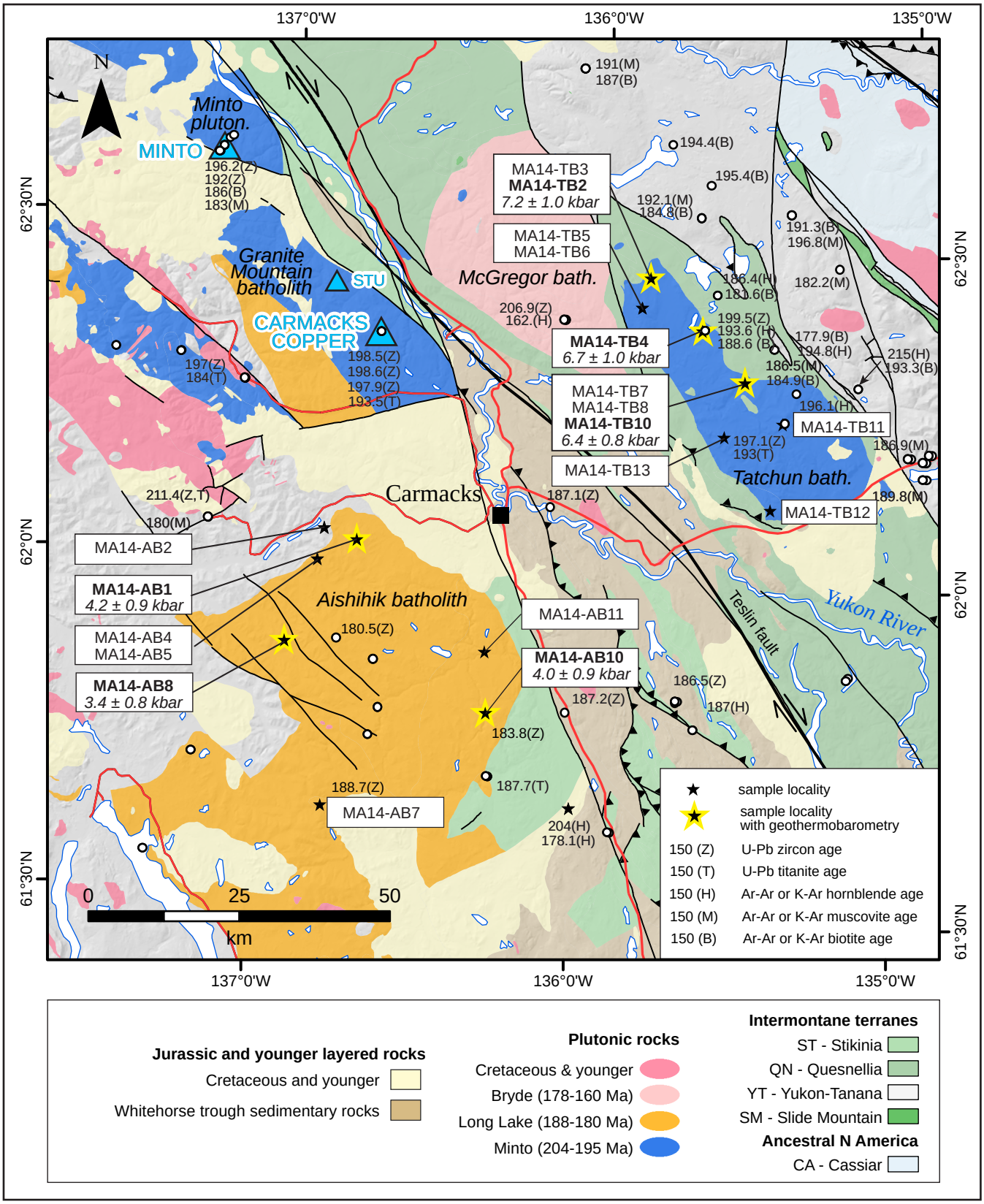


Figure 2. *Simplified geologic map of the study area, indicating published geochronological data from Late Triassic to Middle Jurassic. Sources of geochronological data: Breitsprecher and Mortensen (2004); Colpron (2011); Joyce et al. (2015, 2016). Geological data from Yukon Geological Survey (2015).*

the influence of temperature (*T*) by Anderson and Smith (1995), by taking into account the temperature-dependent equilibria between amphibole and plagioclase (Blundy and Holland, 1990; Holland and Blundy, 1994).

The temperature-corrected Al-in-hornblende geobarometer (referred to herein as "Al-in-hornblende geothermobarometer") was previously applied by McCausland *et al.* (2002) and Tafti (2005) to samples of the Minto pluton and Granite Mountain batholith. Crystallization pressures in the Minto pluton were in the range of 6.1-6.6 kbar (Tafti, 2005), equivalent to ~22-24 km depth under a lithostatic crustal column of 2800 kg/m^3 density. McCausland *et al.* (2002) indicate two spatially separate hornblende populations in the Granite Mountain batholith, with more aluminous, higher-pressure hornblende in the east (5.6-6.6 kbar) and less aluminous, lower-pressure hornblende in the west (4.9-5.8 kbar). Recent investigations (Colpron and Sack, unpublished mapping and data) indicate that the batholith has an eastern lobe composed of older and more deeply exhumed Minto suite granitoid rocks, and a western lobe composed of substantially younger Long Lake suite granitoid rocks (Figs. 1 and 2).

Geobarometric constraints from hornblende and magmatic epidote led Tafti (2005) to conclude that batholiths that post-dated mineralization and deformation at Minto and Carmacks Copper were emplaced at a depth of greater than 20 km. Therefore, Minto and Carmacks Copper deposits are interpreted by Tafti (2005) to represent porphyry systems that formed at shallower crustal depths of a few kilometres, but which were subsequently tectonically buried, deformed, incorporated into intrusions at depth, and subsequently exhumed, all within a few million years. Hood (2012) interprets that the Minto deposit instead formed from magmatic-hydrothermal fluids that focused into active brittle-ductile shear zones in the mid-crust, bypassing the requirement for tectonic burial of shallowly formed mineralization.

A previous study of the Aishihik batholith by Johnston *et al.* (1996) indicates a likely depth of magma emplacement of greater than 30 km. This constraint is based on the regular occurrence of magmatic epidote and a greater than 8 kbar metamorphic assemblage of sillimanite-kyanite-staurolite in pelitic country rocks. Johnston *et al.* (1996) suggests extremely rapid exhumation of the Aishihik batholith to explain melt crystallization at 186.0±2.8 Ma (U-Pb zircon), followed by cooling through ~600°C by 184-185 Ma, as indicated by U-Pb titanite ages.

SAMPLES

A suite of 19 granitoid samples of the Aishihik and Tatchun batholiths were collected during helicopter-supported fieldwork in 2014 (Table 1; Figs. 1 and 2). Cut and hydrofluoric acid-etched rock slabs were stained with sodium cobaltinitrite to identify K-feldspar and with amaranth red to identify plagioclase. Modal mineralogy and rock names were derived from stained slab observations and by petrographic investigations of polished thin sections (Table 1). The Aishihik batholith samples include medium to coarse-grained granodiorite, K-feldspar-phyric granodiorite, granite, aplitic granite and tonalite. The 11 Tatchun batholith samples include K-feldspar-phyric quartz diorite, pegmatitic diorite, K-feldspar-phyric quartz monzonite, quartz monzonite, granodiorite, quartz monzodiorite and aplitic granite.

Samples were first screened for their igneous mineral assemblages; six (three from each of the Aishihik and Tatchun batholiths) were determined to have the requisite equilibrium assemblage of quartz, plagioclase, orthoclase, hornblende, biotite, magnetite (or ilmenite), titanite, melt and vapour, to satisfy the thermodynamic requirements of the Al-in-hornblende geobarometer (Hammarstrom and Zen, 1986). These samples ranged in composition from granodiorite to tonalite to quartz diorite. Hornblende-plagioclase grain boundaries, on each of the six samples, were scrutinized for alteration by transmitted light petrography and scanning electron microscopy (SEM). Only hornblende and plagioclase grains that were texturally intergrown were considered for analysis (Fig. 3). Samples in which hornblende was euhedral or where co-precipitation of hornblende and plagioclase could not be petrographically satisfied were avoided.

Epidote is present in 16 of the 19 samples, including all six of the samples selected for geothermobarometry. In 15 of these, epidote occurs as anhedral replacements of biotite or hornblende, and therefore, is interpreted as a product of deuteric alteration. However, one Tatchun batholith sample (MA14-TB6) contains magmatic epidote as elongate, prismatic, euhedral grains in textural association with, but not replacing hornblende.

METHODOLOGY

Amphibole and plagioclase compositions were determined by electron microprobe analysis (EMPA) at the Electron Microbeam/X-ray Diffraction Facility in the Department of Earth, Ocean, and Atmospheric Sciences at the University

Table 1. *Sample descriptions and locations.*

Sample	Latitude (NAD83)	Longitude (NAD83)	Description	QAP norm (vol.%)			QAP
				K-feldspar	Plagioclase	Quartz	Rock Type
Aishihik batholith							
MA14-AB1*	62.03821	-136.72737	pale pink weathering; fresh grey-pink; weakly foliated, medium-grained sparesely Kfs-porphyritic biotite granodiorite, cut by minor aplite dikes	12	59	29	granodiorite
MA14-AB2	62.05304	-136.83230	tan-weathering 2m-wide aplite dike (cutting biotite orthogneiss)	41	18	41	granite
MA14-AB4	62.00563	-136.84785	fine-grained leucogranite (cutting foliated biotite granite)	38	21	41	granite
MA14-AB5	62.00563	-136.84785	medium-grained foliated biotite granite (cut by fine-grained leucrogranite)	29	41	29	granite
MA14-AB7	61.64092	-136.78826	buff-pink weathering; fine- to medium-grained equigranular, moderately chloritized biotite-hornblende(?) granite	41	18	41	granite
MA14-AB8*	61.88171	-136.93471	white weathering; white fresh; coarse-grained, weakly to moderately foliated, Kfs-porphyritic biorite-hornblende granodiorite	22	44	33	granodiorite
MA14-AB10*	61.79234	-136.28922	weakly foliated, medium-grained hornblende tonalite; accessory titanite and epidote	6	71	24	tonalite
MA14-AB11	61.88325	-136.30288	fine to medium-grained, massive, equigranular hornblende-biorite granite; euhedral 4-6mm biotite grains	21	37	42	granite
Tatchun batholith							
MA14-TB2*	62.45180	-135.82699	white weathering; weakly foliated medium-grained hornblende quartz diorite	6	88	6	quartz diorite
MA14-TB3	62.45180	-135.82699	white weathering; pegmatite leucodiorite	5	94	1	diorite
MA14-TB4*	62.37656	-135.66535	moderately epidotized hornblende phyric quartz diorite (cut by pegmatite leucodiorite)	6	88	6	quartz diorite
MA14-TB5	62.40720	-135.86282	foliated K-feldspar porphyritic medium-grained biotite-hornblende quartz monzonite (cut by fine-grained equigranular granodiorite and granite pegmatite)	44	39	18	quartz monzonite
MA14-TB6	62.40720	-135.86282	fine-grained equigranular granodiorite (cutting foliated bt-hbl granodiorite; cut by granite pegmatite)	13	56	31	granodiorite
MA14-TB7	62.30312	-135.52239	grey, foliated, medium-grained epidotized hornblende quartz diorite	6	88	6	quartz diorite
MA14-TB8	62.30312	-135.52239	hornblende quartz monzodiorite	25	67	8	quartz monzodiorite
MA14-TB10*	62.30312	-135.52239	unfoliated medium-grained hornblende quartz diorite	2	91	8	quartz diorite
MA14-TB11	62.24422	-135.39588	fine-grained equigranular leucogranite	35	24	40	granite (dike)
MA14-TB12	62.11541	-135.42423	K-feldspar porphyritic (5 - 40 mm) medium-grained biotite quartz monzonite; rare fine-grained mafic xenoliths	32	53	16	quartz monzonite
MA14-TB13	62.22087	-135.57949	white weathering; medium-grained equigranular hornblende biotite quartz monzonite	36	46	18	quartz monzonite

Notes:
* denotes sample selected for geothermobarometry

of British Columbia on a fully-automated CAMECA SX-50 instrument operating in wavelength-dispersion mode. For both minerals, the instrument operated with an excitation voltage of 15 kV, beam current of 20 nA, peak count time of 20 s (except 40 s for F in amphibole), background count time of 10 s (except 20 s for F in amphibole), and a spot diameter of 5 μm.

For the elements considered in feldspar, the following standards, X-ray lines and crystals were used: albite, NaKα, thallium acid phthalate (TAP); anorthite, AlKα, TAP; diopside, MgKα, TAP; anorthite, SiKα, TAP; orthoclase, KKα, pentaerythritol (PET); anorthite, CaKα, PET; synthetic rhodonite, MnKα, lithium fluoride (LIF); and synthetic fayalite, FeKα, LIF. For the elements considered in hornblende, the following standards, X-ray lines and crystals were used: synthetic phlogopite, FKα, TAP; albite, NaKα, TAP; kyanite, AlKα, TAP; diopside, MgKα, TAP; diopside, SiKα, TAP; scapolite, ClKα, PET; orthoclase, KKα, PET; diopside, CaKα, PET; rutile, TiKα, PET; synthetic magnesiochromite, CrKα, LIF; synthetic rhodonite, MnKα, LIF; synthetic fayalite, FeKα, LIF; and synthetic Ni_2SiO_4, NiKα, LIF. Data were reduced according to the 'PAP' $\phi(\rho Z)$ method of Pouchou and Pichoir (1985).

Four to six unaltered hornblende-plagioclase grain boundary locations were selected from each of the geothermobarometric samples; for each grain pair, two to four points per hornblende and plagioclase grain rim were analyzed. Rim spots were selected within a few tens of microns of grain boundaries, and additional spot analyses in grain cores were carried out to test for possible alteration or compositional zoning effects. In all cases, core compositions are within the variance of rim compositions, but only rim compositions were used for *P-T* calculations.

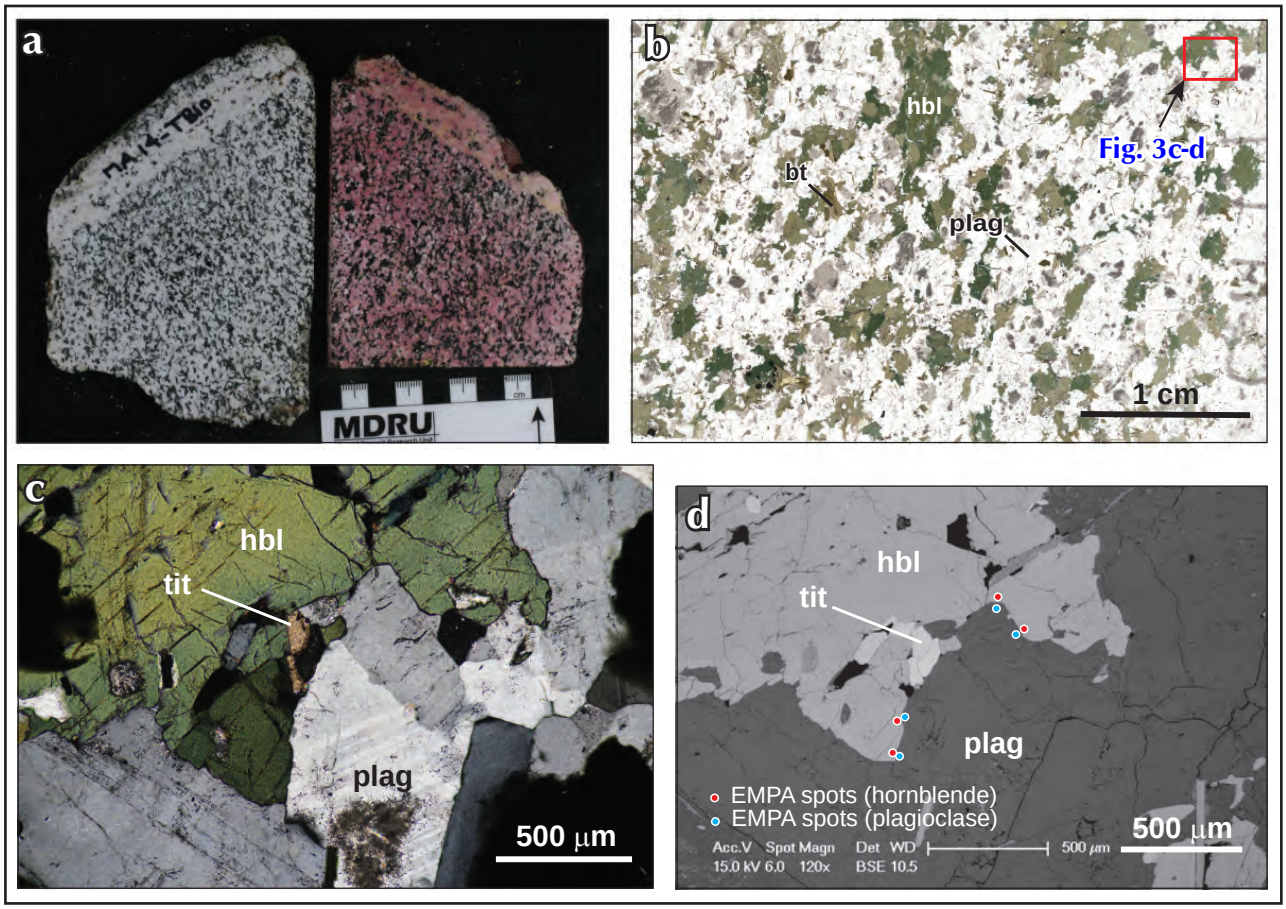


Figure 3. *Sequence of images for hornblende quartz diorite from the Tatchun batholith (MA14-TB10): (a) cut slabs, both unstained (left) and stained sequentially with amaranth red (for plagioclase) and sodium cobaltinitrite (for K-feldspar; right); (b) polished thin section of same sample, showing the location of a hornblende-plagioclase grain pair for EMPA analysis (red box); (c) cross-polarized microphotograph showing intergrown hornblende-plagioclase grain boundary; (d) backscattered electron image of (c), showing the location of EMPA points along grain rims of hornblende (red dots) and plagioclase (blue dots). Mineral abbreviations: bt=biotite; hbl=hornblende; plag=plagioclase; tit=titanite.*

Electron microprobe analyses of amphibole rims (Appendix A) were converted to amphibole formulae (Table 2) using the routine of Holland and Blundy (1994). All hornblende grains analyzed are calcic and range from hastingsitic to Mg-hastingsitic in Tatchun samples and Mg-hastingsitic to edenitic in Aishihik samples (Table 2). Within-grain variability is generally significantly greater than analytical uncertainty for the main mineral-forming elements, so the standard deviation of element concentrations among EMPA points is used to estimate the compositional uncertainty of a given mineral grain (Table 2).

A rigorous approach was used to determine the error in the aluminum content of hornblende, applying the same statistical technique commonly used for establishing error-weighted mean ages in geochronological analysis (Appendix B; Ludwig, 2008). For each hornblende grain, an inverse-variance weighted mean wt% Al_2O_3 was determined, and if the probability-of-fit was above 0.15, the error was derived from the internal (analytical) errors. If the probability-of-fit was below 0.15, the error was calculated as the product of the Student's t-value and the square root of the mean square weighted deviation. For a given rock sample, a mean wt% Al_2O_3 for all the hornblende grains analyzed was determined using the same routine, yielding a single hornblende composition and statistically robust error determination. The relative error in the total Al content (Al^{TOT}) of the hornblende composition is ~1% for most samples.

Mineral composition data were validated against the allowable plagioclase and hornblende compositional ranges for which the hornblende-plagioclase geothermobarometer has been calibrated. In all samples, the average ratio of ferric Fe to total Fe (Fe^{3+}#) is above the requisite value of 0.25, and the average Fe number (Fe# = Fe*/(Mg + Fe*)) is between the allowable range of 0.40 and 0.65 (Anderson and Smith, 1995). These requirements are critical given that low oxygen fugacity results in over-estimation of crystallization pressure (Anderson and Smith, 1995). The mole fraction of anorthite in plagioclase is between An_{15} and An_{38}, somewhat greater than the range of An_{25} and An_{35} typically applied for Al-in-hornblende geothermobarometry (*e.g.*, Anderson and Smith, 1995).

Temperatures of crystallization were calculated using the edenite + albite = richterite + anorthite mineral thermometer of Holland and Blundy (1994; Table 2), and pressures of crystallization were calculated according to the geothermobarometer of Anderson and Smith (1995):

$$P\ (\pm 0.6\ \text{kbar}) = 4.76\ Al^{TOT} - 3.01 - \{(T - 675)/85\} \times \{0.530\ Al^{TOT} + 0.005294(T - 675)\} \quad \text{(Equation 1)}$$

where T is the temperature of crystallization in °C and Al^{TOT} is the total aluminum content of hornblende. Calculations were performed using an MS Excel spreadsheet prepared by J.L. Anderson that was obtained from R. Tafti (pers. comm., 2014). For the mean hornblende and plagioclase compositions of a given sample, *P-T* conditions were calculated iteratively using an initial *P-T* condition calculated with equations in Schmidt (1992) and Holland and Blundy (1994). All pressure results are well above the lower 2 kbar calibration limit of Anderson and Smith's (1995) geothermobarometer.

The temperature-sensitivity of the Al-in-hornblende geobarometer is well-documented (*e.g.*, Anderson and Smith, 1995), so multiple mineral geothermometers were tested. The alternative edenite + 4 quartz = tremolite + albite geothermometer (Blundy and Hollard, 1990; Holland and Blundy, 1994) returned temperatures that were 20-170°C higher than those obtained with the edenite + albite = richterite + anorthite geothermometer (above). A possible explanation for the discrepancy is that quartz may have precipitated late in the crystallization sequence in the Aishihik and Tatchun batholith samples, and was not actually involved in the exchange of components between plagioclase and amphibole. The Ti-in-hornblende geothermometer of Otten (1984) was tested as an alternative, but yielded consistently low temperatures, potentially arising from exsolution of a Ti-bearing phase from amphibole during cooling (Ernst and Liu, 1998). Although petrographic observations support an equilibrium assemblage of quartz, plagioclase, orthoclase, hornblende, biotite, magnetite and titanite in all samples analyzed, it is cautioned that deviations from an equilibrium condition affect the quantitative validity of our *P* and *T* calculations.

Table 2. *Summary of average hornblende compositions.*

Sample		Aishihik batholith			Tatchun batholith		
		MA14-AB1	MA14-AB8	MA14-AB10	MA14-TB2	MA14-TB4	MA14-TB10
SiO_2	%	43.00	45.00	42.34	40.00	38.51	40.44
TiO_2	%	0.85	0.82	0.96	0.94	1.04	0.80
Al_2O_3	%	9.66	7.86	10.00	12.82	13.28	11.70
FeO*	%	18.47	17.13	18.32	18.89	21.17	20.41
MgO	%	10.12	11.35	10.01	8.89	7.18	8.24
MnO	%	0.82	0.74	0.74	0.33	0.48	0.50
CaO	%	11.58	11.40	11.49	10.62	10.50	11.16
Na_2O	%	1.16	1.26	1.11	2.61	2.58	1.82
K_2O	%	1.10	0.90	1.20	1.47	1.66	1.62
F	%	0.40	0.41	0.24	0.22	0.16	0.22
Cl	%	0.04	0.02	0.05	0.01	0.01	0.03
Sum	%	97.21	96.88	96.45	96.79	96.57	96.92
Element	**Site[a]**						
Si	T	6.485	6.756	6.425	6.124	5.982	6.224
Al^{IV}	T	1.515	1.244	1.575	1.876	2.018	1.776
Al^{VI}	M1,2,3	0.202	0.147	0.215	0.437	0.414	0.346
Ti	M1,2,3	0.097	0.092	0.109	0.108	0.121	0.093
Fe^{3+}	M1,2,3	0.813	0.656	0.831	0.610	0.738	0.661
Mg	M1,2,3	2.274	2.539	2.263	2.028	1.662	1.891
Mn	M1,2,3	0.104	0.095	0.095	0.042	0.063	0.065
Fe^{2+}	M1,2,3	1.510	1.471	1.487	1.774	2.002	1.944
Fe^{2+}	M4	0.007	0.024	0.008	0.035	0.011	0.022
Ca	M4	1.872	1.834	1.869	1.742	1.748	1.840
Na	M4	0.122	0.142	0.123	0.224	0.241	0.139
Na	A	0.218	0.226	0.203	0.550	0.535	0.404
K	A	0.211	0.172	0.231	0.287	0.330	0.319
OH	OH	1.794	1.799	1.873	1.890	1.918	1.886
F	OH	0.197	0.196	0.115	0.106	0.079	0.107
Cl	OH	0.010	0.005	0.012	0.004	0.003	0.007
Sum cations		15.429	15.398	15.434	15.837	15.865	15.722
Al^{TOT}	%	1.717	1.391	1.790	2.314	2.432	2.122
$Fe^{3+}\#$[b]		0.349	0.305	0.357	0.252	0.268	0.252
Fe#[c]		0.506	0.459	0.507	0.544	0.623	0.581
Amphibole type:		Mg-hastingsite	edenite	Mg-hastingsite	Mg-hastingsite	hastingsite	hastingsite

Notes:
[a] Amphibole sites: T = tetrahedral; M1,2,3 = octahedral; M4 = large octahedral; A = alkali vacancies; OH = anionic
[b] $Fe^{3+}\# = Fe^{3+}/Fe^*$
[c] $Fe\# = Fe^*/(Mg + Fe^*)$

RESULTS - GEOTHERMOBAROMETRY

The *P-T* conditions of crystallization and corresponding lithostatic emplacement depths have been calculated for the Aishihik and Tatchun batholith samples and are presented in Table 3. To assess the statistical significance of these calculated values, three sources of error are considered: (a) the approximate ±0.6 kbar regression error associated with uncertainties in the *P-T* correlation of the Anderson and Smith (1995) geothermobarometer; (b) the error associated with the input variable Al^{TOT}, which itself is a function of analytical precision and both within-grain and between-grain variability (Appendix B); and (c) uncertainty in the temperature of crystallization, which can be estimated from uncertainty in plagioclase compositions. The error in pressure arising from uncertainties in Al^{TOT} and *T* was propagated from known errors of the input variables in Equation 1, which yielded a combined error $\sigma_{Al,T}$ of ±0.23 to ±0.37 kbar. An estimate of the total error σ_{TOT} is given by the sum of the regression error (σ_{REG}) and propagated Al and *T* errors, and is between ±0.8 to ±1.0 kbar for all samples (13-24% error, equivalent to ±3.0 to ±3.5 km). All quoted errors are at the 1σ level of uncertainty, but a more conservative ±1.6 to ±2.0 kbar error at the 2σ level is perhaps more appropriate, especially if one considers other possible sources of error in the temperature estimate (*e.g.*, there is a ±0.8 kbar error associated with a ±50°C temperature uncertainty; Anderson and Smith, 2005).

Nevertheless, samples of the Aishihik and Tatchun batholiths define two statistically distinct pressure/depth regimes (Fig. 4). Aishihik samples range from 3.4-4.2 kbar (12-15 km), whereas Tatchun samples are consistently higher pressure at 6.4-7.2 kbar (23-26 km). Re-calculated *P-T* conditions of crystallization using the EMPA data of McCausland *et al.* (2002) and Tafti (2005) indicate that the broadly coeval Tatchun batholith, Minto pluton, and eastern Granite Mountain batholith (Minto suite) were emplaced at similar crustal depths of ~20-26 km, whereas magmas of the Long Lake suite in the Aishihik batholith were emplaced at distinctly shallower levels (~12-15 km). The broadly coeval western part of the Granite Mountain batholith was emplaced at somewhat greater depths of ~18-21 km (McCausland *et al.*, 2002).

Table 3. *Geothermobarometry results.*

Sample	Plagioclase X_{An} [a]	±1σ [b]	Amphibole Al^{TOT}	±1σ [c]	T (°C)	±1σ [d]	P (kbar)	±1σ_{REG} [e]	±1σ_{Al} [f]	±1σ_{T} [g]	±1$\sigma_{Al,T}$ [h]	±1σ_{TOT} [i]	Depth (km)	±1σ [j]
Aishihik Batholith														
MA14-AB1	0.320	0.028	1.717	0.034	**734**	10	**4.18**	0.6	0.16	0.19	0.31	0.91	**15.2**	3.3
MA14-AB8	0.213	0.015	1.391	0.014	**694**	7	**3.42**	0.6	0.07	0.07	0.23	0.83	**12.4**	3.0
MA14-AB10	0.377	0.036	1.790	0.006	**764**	12	**4.03**	0.6	0.03	0.27	0.31	0.91	**14.7**	3.3
Tatchun Batholith														
MA14-TB2	0.147	0.028	2.314	0.015	**724**	15	**7.15**	0.6	0.07	0.16	0.37	0.97	**26.0**	3.5
MA14-TB4	0.187	0.037	2.432	0.024	**765**	17	**6.69**	0.6	0.12	0.44	0.37	0.97	**24.4**	3.5
MA14-TB10	0.206	0.019	2.122	0.019	**721**	8	**6.36**	0.6	0.08	0.15	0.23	0.83	**23.1**	3.0

Notes:
[a] X_{An} refers to mole fraction of anorthite component in plagioclase
[b] error in plagioclase composition is estimated from the standard deviation of plagioclase compositions (both within-grain and between-grain)
[c] error in Al^{TOT} is calculated from the 1σ error in Al_2O_3 (Appendix)
[d] error in *T* is propagated from the error in the plagioclase composition (at fixed hornblende composition)
[e] σ_{REG} refers to the approximate 1σ regression error of the Anderson and Smith (1995) geothermobarometer
[f] σ_{Al} refers to the 1σ error in pressure due to uncertainty in the Al^{TOT}
[g] σ_{T} refers to the 1σ error in pressure due to uncertainty in crystallization temperature
[h] $\sigma_{Al,T}$ is the propagated 1σ error in pressure due to errors in Al^{TOT} and *T*
[i] σ_{TOT} is the estimated total error in pressure calculated by adding the regression error and propagated (Al^{TOT} and *T*) errors
[j] error in depth taking into account the combined uncertainty in pressure (σ_{TOT})

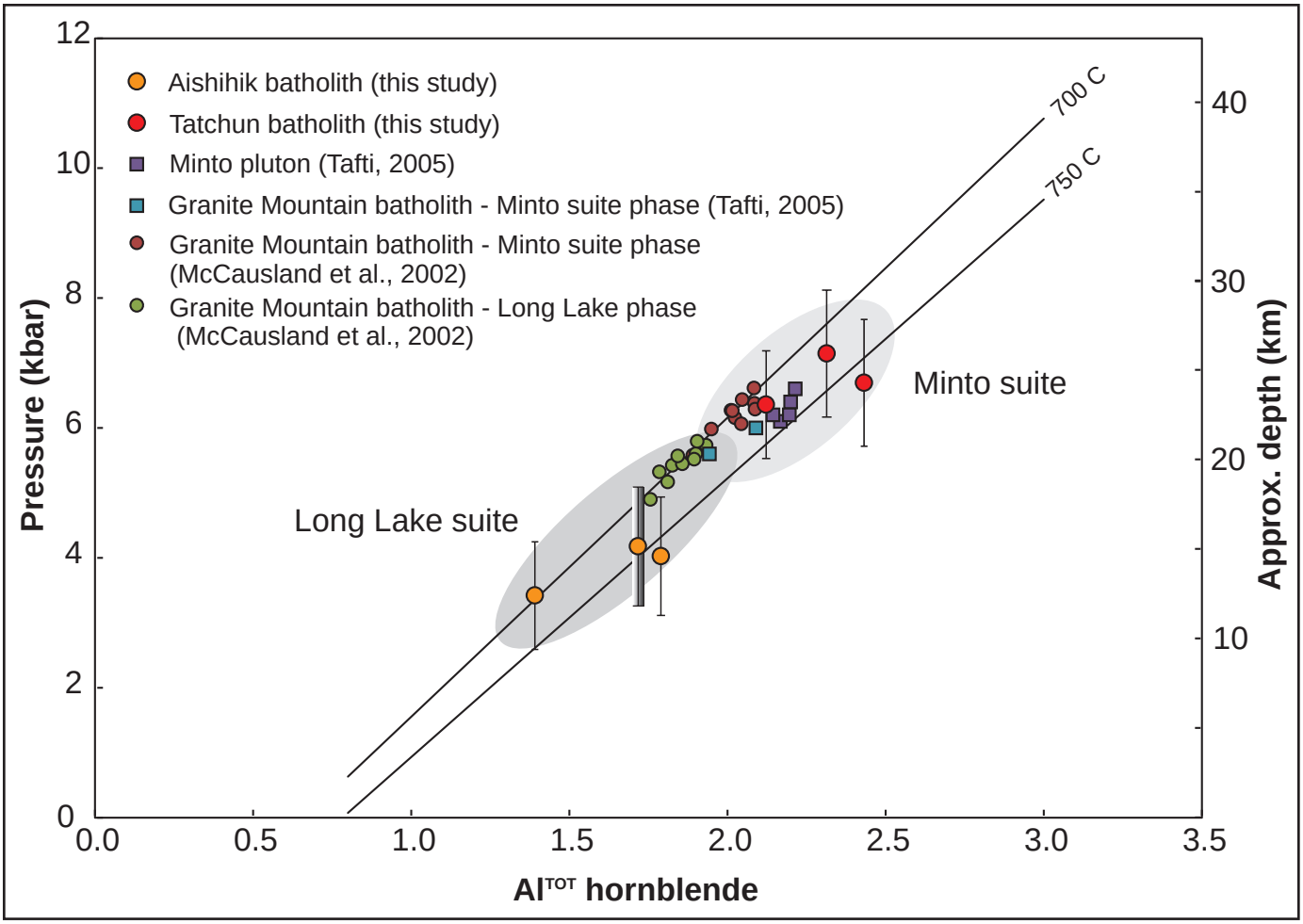


Figure 4. *Plot showing the relationship between Al^{TOT} in hornblende and calculated pressures and depths (at 2800 kg/m^3). Error bars represent 1σ_{TOT} uncertainty in pressure and errors in Al^{TOT} are less than the symbol width. Data from McCausland et al. (2002) and Tafti (2005) are included for comparison (errors omitted for clarity). Samples from the Minto suite (pale grey ellipse) were emplaced at systematically higher pressure than those of the Long Lake suite (medium grey ellipse).*

DISCUSSION

Geothermobarometric results indicate that the Tatchun batholith was emplaced at a depth of approximately 23 to 26 km, which is consistent with the pressure/depth estimates of Tafti (2005) and McCausland *et al.* (2002) for the age-equivalent Minto pluton and eastern part of the Granite Mountain batholith (Figs. 1 and 2). Following crystallization of the Tatchun batholith *ca.* 200-197 Ma, magmatic biotite records an Ar-Ar cooling age of 188.6 ± 1.1 Ma (Colpron, 2011; Joyce *et al.*, 2015). Assuming that the biotite age is the result of regional cooling through ~300°C, and with an average geothermal gradient of ~30°C/km, the Tatchun batholith was exhumed to ~10 km depth within 8 to 11 m.y. of emplacement. Therefore, Tatchun batholith's average exhumation rate over this time was ~1.2-2.0 mm/a. At a constant exhumation rate, the batholith would have been exposed at surface by ~184-180 Ma.

The ~1.2-2.0 mm/a rate of exhumation estimated for the Tatchun batholith is modest given higher rates of erosion in active collisional orogens. For example, the St. Elias Mountains in southwest Yukon, which are currently being uplifted due to collision of the Yakutat block with the western margin of North America in southeast Alaska since approximately 10-5 Ma, are undergoing rates of erosion of 5.1 mm/a (Sheaf *et al.*, 2003). In the

northwestern Himalayas, Indus river bedrock incision rates as equated to bedrock uplift rates during the Quaternary range from 2 to 12 mm/a (Burbank *et al.*, 1996). Furthermore, thermochronometric measurements along a segment of the Alpine fault in the Southern Alps of New Zealand indicate vertical exhumation rates ranging from 6-9 mm/a (Little *et al.*, 2005). Therefore, Early Jurassic exhumation rates in the Cordilleran orogen need not have been exceptional by global standards.

The Aishihik batholith crystallized between 188 and 180 Ma (Joyce *et al.*, 2016) and at depths of ~12 to 15 km – significantly shallower than plutons of the Minto suite. Results of this study differ markedly from the Johnston *et al.* (1996) interpretation that the Aishihik batholith was emplaced in excess of 30 km. The discrepancy could be due to emplacement of the batholith well after, and at shallower crustal level than the peak metamorphic conditions responsible for the sillimanite-kyanite-staurolite assemblage in pelite west of the batholith.

Perhaps the best control on exhumation of the Aishihik batholith is given by a 185.9±2.0 Ma U-Pb zircon age on a porphyritic phase of the batholith (sample MA14-AB9; Joyce *et al.*, 2016). The very fine grained matrix of the sample is typical of upper crustally emplaced (<10 km?), structurally controlled intrusions emanating from an underlying, fluid-saturated magma chamber. Elsewhere in the batholith, miarolitic cavities and dikes of granitic pegmatite and aplite are direct evidence of fluid exsolution, which is favoured at shallower levels in the crust due to the lower solubility of water in silicate melt at lower pressure. Although the pressure or depth of these features cannot be constrained, field relationships are reasonably explained by unroofing of the batholith during the 8 m.y. magmatic timespan of the Aishihik batholith.

K-Ar biotite cooling ages in the Aishihik batholith range from 170 to 164 Ma (Johnston *et al.*, 1996; Breitsprecher and Mortensen, 2004), indicating that parts of the batholith had cooled below ~300°C by this time. At an assumed geothermal gradient of 30°C/km, interpretation of K-Ar data would imply that the batholith was still at ~10 km depth 10 to 16 m.y. after final crystallization around 180 Ma. Therefore, if exhumation was rapid during the 188-180 Ma window of batholith emplacement, exhumation likely tapered off or stalled by the Middle Jurassic. This interpretation is consistent with the waning of regional cooling by Middle to Late Jurassic over much of Yukon's Cordilleran hinterland (Colpron, 2011; Allan *et al.*, 2013; Nelson *et al.*, 2013).

CONCLUSIONS

This study establishes that the earliest Jurassic Tatchun batholith of the Minto suite (200-197 Ma) was emplaced at a depth of ~23 to 26 km, similar to that previously proposed for the Minto pluton and Granite Mountain batholith. Geochronological and thermal constraints suggest that the Tatchun batholith likely exhumed at a reasonably modest rate of ~1.2-2.0 mm/a, although additional data from the Tatchun and other Minto suite plutons are required.

The Aishihik batholith of the Long Lake suite (188-180 Ma) was emplaced at a crustal depth of ~12 to 15 km, which contrasts strongly with the greater than 30 km estimate of Johnston *et al.* (1996). Crosscutting porphyritic and fluid-saturated phases of the Aishihik batholith are reasonably explained by exhumation of the batholith to shallower (<10 km?) depths during the ~8 my duration of magmatism. Exhumation rates slowed dramatically after magmatism ceased, as indicated by Middle Jurassic K-Ar biotite cooling ages.

Minto suite plutons are deeply unroofed and therefore unprospective for coeval subvolcanic porphyry copper deposits (*e.g.*, Chapman, 2014). However, the Minto and Carmacks Copper Cu-Au-Ag deposits are evidence that these plutons are prospective for somewhat older, deformed mineralization, which formed or was metamorphosed at deep magmatic levels. In contrast, fluid-saturated and hypabyssal phases of the Aishihik batholith suggest a magmatic environment permissible for magmatic-hydrothermal mineralization.

Additional geothermobarometric studies of various other Late Triassic to Early Jurassic plutons will be integrated with geochronological studies of the same intrusions to further resolve the evolution of magmatism and structure during this important stage of Cordilleran tectonics.

ACKNOWLEDGEMENTS

This contribution builds on a University of British Columbia BSc Honours project by MJT, which was supported by the Yukon-Alaska Metallogeny Project – a research partnership between the Mineral Deposit Research Unit, Yukon Geological Survey, Kaminak Gold Corp., and Sumac Mines Ltd. This study contributes to a comprehensive characterization study of Late Triassic to Early Jurassic plutonic suites in Yukon by the Yukon Geological Survey and Geological Survey of Canada.

REFERENCES

Allan, M.M., Mortensen, J.K., Hart, C.J.R., Bailey, L.A., Sanchez, M.G., Ciolkiewicz, W., McKenzie, G.G. and Creaser, R.A., 2013. Magmatic and metallogenic framework of west-central Yukon and eastern Alaska. *In*: Tectonics, Terranes, Metallogeny and Discovery in the northern circum-Pacific region, M. Colpron, T. Bissig, B. Rusk and J. Thompson (eds.), Society of Economic Geologists, Special Publication vol. 17, p. 111-168.

Anderson, J.L. and Smith, D.R., 1995. The effects of temperature and fO2 on the Al-in hornblende barometer. American Mineralogist, vol. 80, p. 549-559.

Blundy, J.D. and Holland, T.J.B., 1990. Calcic amphibole equilibria and a new amphibole-plagioclase geothermometer. Contributions to Mineralogy and Petrology, vol. 104, p. 208-224.

Breitsprecher, K. and Mortensen, J.K. (compilers), 2004. YukonAge 2004: A database of isotopic age determinations for rock units from Yukon Territory. Yukon Geological Survey (CD-ROM).

Buffett, G., White, D., Roberts, B. and Colpron, M., 2006. Preliminary results from the Whitehorse Trough seismic survey, Yukon Territory. Geological Survey of Canada, Current Research 2006-A2, 9 p.

Burbank, D.W., Leland, J., Fielding, E., Anderson, R.S., Brozovic, N., Reid, M.R. and Duncan, C., 1996. Bedrock incision, rock uplift and threshold hillslopes in the northwestern Himalayas. Nature, vol. 379, p. 505-510.

Chapman, J.B., 2014. Are there elephants hiding in the Early Jurassic of Yukon? A tectono-magmatic perspective on porphyry prospectivity. *In:* Annual Geological Society of America Meeting in Vancouver British Columbia, Programs with Abstracts, vol. 46, p. 590.

Colpron, M. (compiler), 2011. Geological compilation of Whitehorse trough - Whitehorse (105D), Lake Laberge (105E), and part of Carmacks (115I), Glenlyon (105L), Aishihik Lake (115H), Quiet Lake (105F) and Teslin (105C). Yukon Geological Survey, Geoscience Map 2011-1, 1:250000 scale.

Colpron, M. and Friedman, R.M., 2008. U-Pb zircon ages for the Nordenskiold Formation (Laberge Group) and Cretaceous intrusive rocks, Whitehorse trough, Yukon. *In:* Yukon Exploration and Geology 2007, D.S. Emond, L.R. Blackburn, R.P. Hill and L.H. Weston (eds.), Yukon Geological Survey, p. 139-151.

Colpron, M., Crowley, J.L., Gehrels, G., Long, D.G.F., Murphy, D.C., Beranek, L. and Bickerton, L., 2015. Birth of the northern Cordilleran orogen, as recorded by detrital zircons in Jurassic synorogenic strata and regional exhumation in Yukon. Lithosphere, vol. 7, p. 541-562.

Dickie, J.R. and Hein, F.J., 1995. Conglomeratic fan deltas and submarine fans of the Jurassic Laberge Group, Whitehorse trough, Yukon Territory, Canada - Fore-arc sedimentation and unroofing of a volcanic island-arc complex. Sedimentary Geology, vol. 98, p. 263-292.

Ernst, W.G. and Liu, J.L., 1998. Experimental phase-equilibrium study of Al- and Ti-contents of calcic amphibole in MORB – A semiquantitative thermobarometer. American Mineralogist, vol. 83, p. 952-969.

Fillmore, J.A., 2006. Character and origin of the Lower Jurassic (Pliensbachian) Nordenskiold dacite, Whitehorse trough, Yukon Territory, Canada. Unpublished BSc Honours thesis, Laurentian University, Ontario, 28 p.

Gordey, S.P. and Makepeace, A.J., 2001. Bedrock geology, Yukon Territory. Geological Survey of Canada, Open File 3754, scale 1:1000000; *also Yukon Geological Survey, Open File 2001-1*.

Hammarstrom, J.M. and Zen, E., 1986. Aluminum in hornblende: An empirical igneous geobarometer. American Mineralogist, vol. 71, p. 1297-1313.

Hart, C.J.R., 1997. A Transect across Northern Stikinia: Geology of the Northern Whitehorse Map Area, Southern Yukon Territory (105D/13-16). Exploration and Geological Services Division, Yukon Region, Indian and Northern Affairs Canada, Bulletin 8, 112 p.

Hart, C.J.R., Dickie, J.R., Ghosh, D.K. and Armstrong, R.L., 1995. Provenance Constraints for Whitehorse Trough Conglomerate: U-Pb Zircon Dates and Initial Sr Ratios of Granitic Clasts in Jurassic Laberge Group, Yukon Territory. *In:* Jurassic Magmatism and Tectonics of the North American Cordillera, Geological Society of America Special Paper 299, p. 47-63. doi 10.1130/SPE299-p47.

Holland, T.J.B. and Blundy, J.D., 1994. Non-ideal interactions in calcic amphiboles and their bearing on amphibole-plagioclase thermometry. Contributions to Mineralogy and Petrology, vol. 116, p. 433-447.

Hollister, L.S., Grissom, G.C., Peters, E.K., Stowell, H.H. and Sisson, V.B., 1987. Confirmation of the empirical correlation of Al in hornblende with pressure of solidification of calc-alkaline plutons. American Mineralogist, vol. 72, p. 231-239.

Hood, S.B., 2012. Mid-crustal Cu-Au mineralization during episodic pluton emplacement, hydrothermal fluid flow, and ductile deformation at the Minto deposit, YT, Canada. Unpublished MSc thesis, The University of British Columbia, British Columbia, 220 p.

Johnston, S.T., Mortensen, J.K., and Erdmer, P., 1996. Igneous and metaigneous age constraints for the Aishihik metamorphic suite, southwest Yukon. Canadian Journal of Earth Sciences, vol. 33, p. 1543-1555.

Johnston, S.T. and Canil, D., 2007. Crustal architecture of SW Yukon, northern Cordillera: Implications for crustal growth in a convergent margin orogen. Tectonics, vol. 26, p. 1-18.

Joyce, N.L., Ryan, J.J., Colpron, M., Hart, C.J.R., and Murphy, D.C., 2015. A compilation of $^{40}Ar/^{39}Ar$ age determinations for igneous and metamorphic rocks, and mineral occurrences from central and southeast Yukon; Geological Survey of Canada, Open File 7924, 1 .zip file. doi:10.4095/297446

Joyce, N., Colpron, M., Allan, M.M., Sack, P.J., Crowley, J.L. and Chapman, J.B., 2016. New U-Pb zircon ages from the Aishihik batholith, southern Yukon. *In*: Yukon Exploration and Geology 2015, K.E. MacFarlane and M.G. Nordling (eds.), Yukon Geological Survey, p. 129-147.

Little, T.A., Cox, S., Vry, J.K. and Batt, G., 2005. Variations in exhumation level and uplift rate along the oblique-slip Alpine fault, central Southern Alps, New Zealand. GSA Bulletin, vol. 117, p. 707-723.

Logan, J.M. and Mihalynuk, M.G., 2014. Tectonic controls on Early Mesozoic paired alkaline porphyry deposit belts (Cu-Au ± Ag-Pt-Pd-Mo) within the Canadian Cordillera. Society of Economic Geologists, Economic Geology, vol. 109, p. 827-858.

Lowey, G.W., 2004. Preliminary lithostratigraphy of the Laberge Group (Jurassic), south-central Yukon: Implications concerning the petroleum potential of the Whitehorse trough. *In*: Yukon Exploration and Geology 2003, D.S. Emond, L.L. Lewis (eds.), Yukon Geological Survey, p. 129-142.

Lowey, G.W., 2008. Summary of the stratigraphy, sedimentology and hydrocarbon potential of the Laberge Group (Lower–Middle Jurassic), Whitehorse trough, Yukon. *In*: Yukon Exploration and Geology 2007, D.S. Emond, L.R. Blackburn, R.P. Hill and L.H. Weston (eds.), Yukon Geological Survey, p. 179-197.

Ludwig, K.R., 2008. Isoplot 3.70: A Geochronological Tookit for Microsoft Excel, Berkeley Geochronology Center.

McCausland, P.J.A, Symons, D.T.A., Hart, C.J.R. and Blackburn, W.H., 2002. Paleomagnetism and geobarometry of the Granite Mountain batholith, Yukon: Minimal geotectonic motion of the Yukon-Tanana Terrane relative to North America. *In*: Yukon Exploration and Geology 2001, D.S. Emond, L.H. Weston and L.L. Lewis (eds.), Exploration and Geological Services Division, Yukon, Indian and Northern Affairs Canada, p. 163-177.

McMillan, W.J., Thompson, J.F.H., Hart, C.J.R. and Johnston, S.T., 1995. Regional geological and tectonic setting of porphyry deposits in British Columbia and Yukon Territory. *In*: Porphyry Deposits of the Northwestern Cordillera of North America, T.G. Schroeter (ed.), Canadian Institute of Mining and Metallurgy, Special Volume 46, p. 40-57.

Mercer, B. and Sagman, J., 2012. Phase VI preliminary feasibility study technical report, Minto mine. Minto Explorations Ltd., 368 p. <http://capstonemining.com/i/pdf/PFS.pdf> [accessed December 9, 2012].

Mihalynuk, M.G., Nelson, J.A. and Diakow, L.J., 1994. Cache Creek terrane entrapment: Oroclinal paradox within the Canadian Cordillera. Tectonics, vol. 13, p. 575-595.

Mihalynuk, M.G., Erdmer, P., Ghent, E.D., Cordey, F., Archibald, D.A., Friedman, R.M. and Johannson, G.G., 2004. Coherent French Range blueschist: Subduction to exhumation in <2.5 m.y.? Geological Society of America Bulletin, vol. 116, p. 910-922.

Mira Geoscience, 2014. Geologically-constrained inversion of magnetic and gravity data over parts of the Yukon-Tanana terrane and Whitehorse trough. Yukon Geological Survey, Miscellaneous Report MR-10, Mira Geoscience Project No. 3984, 81 p.

Mortensen, J.K., Emon, K., Johnston, S.T. and Hart, C.J.R., 2000. Age, geochemistry, paleotectonic setting and metallogeny of Late Triassic-Early Jurassic intrusions in the Yukon and eastern Alaska: a preliminary report. *In*: Yukon Exploration and Geology 1999, D.S. Edmond and L.H. Weston (eds.), Exploration and Geological Services Division, Yukon Region, Indian and Northern Affairs Canada, p. 139-144.

Nelson, J.L., Colpron, M. and Israel, S., 2013. The Cordillera of British Columbia, Yukon, and Alaska: Tectonics and Metallogeny. *In*: Tectonics, Terranes, Metallogeny and Discovery in the northern circum-Pacific region, M. Colpron, T. Bissig, B. Rusk and J. Thompson (eds.), Society of Economic Geologists, Special Publication vol. 17, p. 53-109.

Otten, M.T., 1984. The origin of brown hornblende in the Artfjallet gabbro and dolerites. Contributions to Mineralogy and Petrology, vol. 86, p. 189-199.

Pearson, W.N. and Clark, A.H., 1979. The Minto copper deposit, Yukon Territory: A metamorphosed orebody in the Yukon crystalline terrane. Economic Geology, vol. 74, p. 1577-1599.

Pouchou, J.L. and Pichoir, F., 1985. PAP $\phi(\rho Z)$ procedure for improved quantitative microanalysis. Microbeam Analysis, vol. 1985, p. 104-106.

Schmidt, M.W., 1992. Amphibole composition in tonalite as a function of pressure: An experimental calibration of the Al-in hornblende barometer. Contributions to Mineralogy and Petrology, vol. 110, p. 304-310.

Sheaf, M.A., Serpa, L. and Pavlis, T.L., 2003. Exhumation rates in the St. Elias Mountains, Alaska. Tectonophysics, vol. 367, p. 1-11.

Simard, R.L. and Devine, F., 2003. Preliminary geology of the southern Semenof Hills, Yukon (105E/1,7,8). *In*: Yukon Exploration and Geology 2002, D.S. Emond and L.L Lewis (eds.), Exploration and Geological Services Division, Yukon Region, Indian and Northern Affairs Canada, p. 213-222.

Tafti, R., 2005. Nature and origin of the Early Jurassic copper (-gold) deposits at Minto and Williams Creek, Carmacks Copper Belt, western Yukon: Examples of deformed porphyry deposits. Unpublished MSc thesis, The University of British Columbia, British Columbia, 213 p.

Tafti, R. and Mortensen, J.K., 2004. Early Jurassic porphyry-copper (-gold) deposits at Minto and Williams Creek, Carmacks copper belt, western Yukon. *In*: Yukon Exploration and Geology 2003, D.S. Emond and L.L. Lewis (eds.), Yukon Geological Survey, p. 289–303.

Tempelman-Kluit, D.J., 1984. Geology, Laberge (105E) and Carmacks (105I), Yukon Territory. Geological Survey of Canada, Open File 1101, 1:250 000 scale.

Tempelman-Kluit, D.J., 2009. Geology of Carmacks and Laberge map areas, central Yukon: Incomplete draft manuscript on stratigraphy, structure and its early interpretation (ca. 1986). Geological Survey of Canada, Open File 5982, 399 p.

White, D., Colpron, M. and Buffett, G., 2012. Seismic and geological constraints on the structure of the northern Whitehorse trough, Yukon, Canada. Bulletin of Canadian Petroleum Geology, vol. 60, p. 239-255.

Yukon Geological Survey, 2015. Yukon Digital Bedrock Geology, <ftp://ftp.geomaticsyukon.ca/GeoYukon/Geological/>, [accessed November 15, 2015].

Yukon MINFILE, 2015. Yukon MINFILE - A database of mineral occurrences. Yukon Geological Survey, <http://data.geology.gov.yk.ca> [accessed November 30, 2015]

Zen, E. and Hammarstrom, J.M., 1984. Magmatic epidote and its petrologic significance. Geology, vol. 12. p. 515-518.

APPENDIX A. *Hornblende EMPA results (summary results per grain).*

	SiO_2	TiO_2	Al_2O_3	FeO*[a]	MgO	MnO	CaO	Na_2O	K_2O	F	Cl	Sum
average RSD (%):	**0.39**	**3.6**	**0.66**	**0.93**	**0.81**	**7.2**	**0.76**	**3.0**	**2.4**	**47**	**48**	
Grain (no. analyses)	**MA14-AB1 (Aishihik batholith)**											
B (n = 2)	43.27	0.79	9.39	18.38	10.18	0.82	11.58	1.16	1.10	0.43	0.04	97.15
± 1s	1.20	0.30	0.98	0.77	0.58	0.08	0.09	0.09	0.10	0.05	0.02	1.86
C (n = 2)	42.49	0.48	10.22	19.38	9.57	0.83	11.64	1.17	1.05	0.39	0.03	97.24
± 1s	0.36	0.01	0.45	0.24	0.37	0.02	0.16	0.06	0.04	0.00	0.01	0.75
D (n = 3)	43.35	0.90	9.38	18.12	10.50	0.83	11.62	1.14	1.06	0.45	0.03	97.37
± 1s	0.26	0.18	0.20	0.58	0.31	0.05	0.18	0.03	0.03	0.09	0.00	0.78
E (n = 2)	42.91	1.25	9.66	18.02	10.23	0.79	11.50	1.18	1.18	0.35	0.05	97.09
± 1s	0.09	0.06	0.11	0.01	0.13	0.02	0.15	0.09	0.02	0.14	0.00	0.30
Average	**43.00**	**0.85**	**9.66**	**18.47**	**10.12**	**0.82**	**11.58**	**1.16**	**1.10**	**0.40**	**0.04**	**97.21**
	MA14-AB8 (Aishihik batholith)											
A (n = 3)	45.13	0.75	7.73	17.43	11.36	0.71	11.48	1.34	0.90	0.39	0.01	97.24
± 1s	0.50	0.08	0.23	0.48	0.24	0.04	0.07	0.10	0.05	0.04	0.00	0.79
B (n= 2)	44.68	0.83	8.14	16.30	10.98	0.67	10.81	1.12	0.94	0.34	0.03	94.86
± 1s	1.03	0.09	1.36	0.51	0.93	0.05	0.95	0.06	0.17	0.12	0.02	2.23
C (n= 2)	45.02	0.57	7.87	17.48	11.40	0.76	11.53	1.31	0.86	0.39	0.01	97.19
± 1s	0.93	0.47	0.43	0.10	0.24	0.01	0.34	0.19	0.20	0.13	0.01	1.24
D (n = 2)	45.48	0.83	7.63	17.18	11.45	0.85	11.57	1.22	0.91	0.38	0.01	97.50
± 1s	1.09	0.06	0.92	0.72	0.79	0.01	0.00	0.12	0.21	0.03	0.01	1.80
E (n = 3)	44.59	1.00	7.97	17.35	11.36	0.73	11.33	1.48	0.91	0.38	0.03	97.13
± 1s	0.09	0.10	0.18	0.50	0.21	0.04	0.05	0.04	0.02	0.03	0.01	0.59
F (n = 1)	45.08	0.92	7.83	17.02	11.54	0.74	11.68	1.11	0.87	0.56	0.02	97.38
± 1s	N/A	N/A	N/A	N/A	N/A	N/A	N/A	N/A	N/A	N/A	N/A	N/A
Average	**45.00**	**0.82**	**7.86**	**17.13**	**11.35**	**0.74**	**11.40**	**1.26**	**0.90**	**0.41**	**0.02**	**96.88**
	MA14-AB10 (Aishihik batholith)											
A (n = 4)	42.00	0.92	10.20	18.29	9.90	0.73	11.47	1.00	1.27	0.18	0.04	96.00
± 1s	0.73	0.11	0.49	0.70	0.26	0.04	0.17	0.08	0.04	0.07	0.01	1.18
B (n = 3)	42.11	0.92	10.35	18.72	9.72	0.74	11.62	1.05	1.22	0.15	0.03	96.63
± 1s	0.17	0.07	0.02	0.17	0.10	0.03	0.05	0.03	0.05	0.02	0.01	0.29
C (n = 3)	43.12	1.10	9.31	17.75	10.52	0.75	11.40	1.09	1.10	0.33	0.05	96.52
± 1s	1.17	0.08	0.86	0.74	0.55	0.05	0.13	0.03	0.12	0.05	0.01	1.73
D (n = 3)	42.27	0.75	10.17	18.61	10.03	0.76	11.54	1.18	1.17	0.26	0.03	96.78
± 1s	0.40	0.15	0.13	0.19	0.05	0.03	0.30	0.05	0.08	0.04	0.01	0.58
E (n = 3)	42.15	0.84	10.20	18.28	9.82	0.74	11.54	1.17	1.18	0.27	0.04	96.22
± 1s	0.22	0.10	0.51	0.44	0.35	0.01	0.19	0.01	0.16	0.16	0.02	0.85
F (n = 4)	42.40	1.21	9.78	18.27	10.06	0.72	11.39	1.16	1.23	0.23	0.08	96.53
± 1s	0.57	0.11	0.53	0.20	0.40	0.02	0.10	0.09	0.10	0.06	0.02	0.92
Average	**42.34**	**0.96**	**10.00**	**18.32**	**10.01**	**0.74**	**11.49**	**1.11**	**1.20**	**0.24**	**0.05**	**96.45**

APPENDIX A *continued.*

	MA14-TB2 (Tatchun batholith)											
A (n = 4)	39.82	0.76	13.07	18.95	8.89	0.31	10.72	2.63	1.54	0.21	0.01	96.92
± 1s	0.04	0.18	0.14	0.22	0.10	0.04	0.08	0.17	0.16	0.03	0.01	0.42
B (n = 4)	39.86	0.86	12.85	18.99	8.82	0.34	10.60	2.56	1.53	0.24	0.02	96.65
± 1s	0.42	0.24	0.54	0.12	0.27	0.03	0.13	0.15	0.17	0.08	0.01	0.83
C (n = 4)	40.11	1.05	12.61	19.03	8.84	0.31	10.46	2.56	1.41	0.17	0.02	96.56
± 1s	0.34	0.09	0.08	0.26	0.19	0.02	0.13	0.11	0.02	0.09	0.01	0.52
D (n = 4)	40.08	0.93	12.87	18.74	8.91	0.33	10.64	2.60	1.48	0.24	0.01	96.83
± 1s	0.49	0.13	0.29	0.12	0.15	0.01	0.13	0.13	0.15	0.09	0.01	0.66
E (n = 4)	40.15	1.10	12.71	18.75	8.99	0.34	10.68	2.67	1.39	0.22	0.01	97.01
± 1s	0.18	0.06	0.13	0.22	0.16	0.02	0.09	0.05	0.03	0.02	0.01	0.37
Average	**40.00**	**0.94**	**12.82**	**18.89**	**8.89**	**0.33**	**10.62**	**2.61**	**1.47**	**0.22**	**0.01**	**96.79**
	MA14-TB4 (Tatchun batholith)											
A (n = 3)	38.49	1.01	13.12	20.29	7.69	0.48	10.44	2.66	1.59	0.16	0.01	95.95
± 1σ	0.88	0.06	0.63	0.80	0.57	0.03	0.12	0.14	0.23	0.03	0.00	1.50
B (n = 3)	37.96	0.92	13.63	21.68	6.80	0.46	10.50	2.44	1.88	0.19	0.01	96.46
± 1σ	0.05	0.08	0.20	0.20	0.13	0.03	0.11	0.05	0.17	0.05	0.01	0.39
C (n = 4)	38.49	1.13	13.35	21.00	7.21	0.50	10.46	2.65	1.54	0.15	0.01	96.50
± 1σ	0.17	0.10	0.18	0.17	0.16	0.02	0.15	0.08	0.14	0.08	0.01	0.43
D (n = 3)	38.58	1.05	13.40	21.35	7.09	0.46	10.53	2.68	1.64	0.10	0.02	96.88
± 1σ	0.48	0.00	0.39	0.33	0.15	0.04	0.16	0.10	0.15	0.07	0.00	0.76
E (n = 3)	39.05	1.07	12.90	21.54	7.11	0.50	10.58	2.45	1.68	0.19	0.01	97.08
± 1σ	0.16	0.21	0.22	0.45	0.23	0.02	0.08	0.04	0.06	0.03	0.01	0.62
Average	**38.51**	**1.04**	**13.28**	**21.17**	**7.18**	**0.48**	**10.50**	**2.58**	**1.66**	**0.16**	**0.01**	**96.57**
	MA14-TB10 (Tatchun batholith)											
A (n = 4)	40.72	0.82	11.29	20.22	8.43	0.50	11.15	1.84	1.59	0.25	0.03	96.83
± 1σ	0.21	0.13	0.22	0.22	0.15	0.03	0.05	0.05	0.15	0.08	0.01	0.46
B (n = 4)	40.21	0.77	12.02	20.41	8.23	0.50	11.17	1.84	1.66	0.24	0.03	97.07
± 1σ	0.16	0.03	0.07	0.29	0.15	0.06	0.08	0.16	0.09	0.07	0.01	0.43
C (n = 4)	40.63	0.89	11.38	20.47	8.23	0.52	11.08	1.79	1.56	0.17	0.03	96.75
± 1σ	0.35	0.06	0.24	0.30	0.16	0.04	0.05	0.09	0.05	0.06	0.01	0.57
D (n = 4)	40.52	0.74	11.84	20.22	8.35	0.50	11.17	1.78	1.61	0.28	0.02	97.04
± 1σ	0.28	0.15	0.12	0.31	0.22	0.01	0.05	0.05	0.03	0.05	0.01	0.52
E (n = 4)	40.12	0.79	11.96	20.71	8.00	0.47	11.21	1.83	1.69	0.14	0.03	96.93
± 1σ	0.42	0.19	0.35	0.24	0.39	0.03	0.09	0.07	0.14	0.08	0.02	0.76
Average	**40.44**	**0.80**	**11.70**	**20.41**	**8.24**	**0.50**	**11.16**	**1.82**	**1.62**	**0.22**	**0.03**	**96.92**

Notes:
[a] FeO* denotes total Fe as FeO
[b] ±1σ errors are within-grain standard deviations in EMPA results (analytical error not included)

APPENDIX B. *Error treatment for Al-in-hornblende analyses.*

Grain	n	wt% Al	error (95%)	Al_2O_3	error (95%)	error (1σ)
MA14-AB1 (Aishihik)						
B	2	4.9	4.7	9.26	8.88	4.53
C	2	5.4	2.1	10.20	3.97	2.02
D	3	4.96	0.26	9.37	0.49	0.25
E	2	5.11	0.52	9.66	0.98	0.50
weighted average:				**9.44**	**0.43**	**0.22**
MA14-AB8 (Aishihik)						
A	3	4.09	0.31	7.73	0.59	0.30
B	2	4.3	6.4	8.12	12.09	6.17
C	2	4.2	2	7.94	3.78	1.93
D	2	4	4.4	7.56	8.31	4.24
E	3	4.22	0.24	7.97	0.45	0.23
F	1	4.1436	N/A	7.83	N/A	N/A
weighted average:				**7.88**	**0.17**	**0.09**
MA14-AB10 (Aishihik)						
A	4	5.39	0.42	10.18	0.79	0.40
B	3	5.48	0.04	10.35	0.08	0.04
C	3	4.9	1.1	9.26	2.08	1.06
D	3	5.38	0.17	10.17	0.32	0.16
E	3	5.39	0.67	10.18	1.27	0.65
F	4	5.16	0.46	9.75	0.87	0.44
weighted average:				**10.34**	**0.07**	**0.04**
MA14-TB2 (Tatchun)						
A	4	6.92	0.12	13.08	0.23	0.12
B	4	6.79	0.46	12.83	0.87	0.44
C	4	6.672	0.039	12.61	0.07	0.04
D	4	6.81	0.24	12.87	0.45	0.23
E	4	6.72	0.11	12.70	0.21	0.11
weighted average:				**12.66**	**0.19**	**0.10**
MA14-TB4 (Tatchun)						
A	3	6.94	0.82	13.11	1.55	0.79
B	3	7.21	0.26	13.62	0.49	0.25
C	4	7.06	0.16	13.34	0.30	0.15
D	3	7.09	0.51	13.40	0.96	0.49
E	3	6.83	0.29	12.91	0.55	0.28
weighted average:				**13.32**	**0.31**	**0.16**
MA14-TB10 (Tatchun)						
A	4	5.97	0.18	11.28	0.34	0.17
B	4	6.36	0.038	12.02	0.07	0.04
C	4	6.02	0.2	11.37	0.38	0.19
D	4	6.26	0.1	11.83	0.19	0.10
E	4	6.32	0.3	11.94	0.57	0.29
weighted average:				**11.95**	**0.24**	**0.12**

Digitizing and spatially analyzing historic placer exploration data from Dominion Creek: A pilot project

Sydney van Loon[1]
Yukon Geological Survey

van Loon, S., 2016. Digitizing and spatially analyzing historic YCGC drill data from Dominion Creek: a pilot project. *In:* Yukon Exploration and Geology 2015, K.E. MacFarlane and M.G. Nordling (eds.), Yukon Geological Survey, p. 253-280, including appendices.

Abstract

Compilation of historic geologic data can help identify deposits of unmined gold-bearing gravel and promote further exploration on under-explored ground. Archival documents of the Yukon Consolidated Gold Corporation (YCGC) contain detailed, accurate prospecting data, and can be used to identify dredge localities and production values. With dredge inefficiency and crude mining techniques, areas heavily worked in the past may contain both technogenic and remnant *in situ* gold-bearing gravel. These types of placer deposits have been the target for many miners on previously worked ground, but with the aid of historic data, these deposits can be identified and evaluated for their potential prior to any ground work. Although there are some limitations and challenges associated with the historic documents, the data contained within them can significantly support placer exploration in both mined and unmined areas of Yukon.

[1]*sydney.vanloon@gov.yk.ca*

INTRODUCTION

Higher gold prices, more economical and efficient mining methods, and growth in the placer industry have resulted in new targets being explored and historic creeks analyzed for their missed potential. Uncovering remnants of untouched gravels on previously mined creeks has been a target for many miners, but these remnants are primarily found by coincidence and anecdotal evidence. Using historic geological data, targets can be identified in previously explored creeks that can lead to discoveries of virgin gravel. An extensive and detailed resource of historic placer geology data exist in the Yukon Consolidated Gold Corporation (YCGC) archival files; YCGC was a prominent company in the Klondike while in operation from 1923 to 1966 (Green, 1977). Geological data obtained from the collection consist of surficial material depth, depth to bedrock, gold grade, ground condition (permafrost), bedrock and surface elevation, as well as historic activity localities such as dredge limits, drilling and shafting locations. Documents from the collection can be used to piece together new and missed potential that exists in the Klondike. The archival files of the YCGC include data primarily from the Klondike mining district, as well as a small amount of reconnaissance exploration data from other placer districts.

While a small number of YCGC documents handed down from the previous generation still circulate in the Klondike, the bulk of the YCGC archival collection is housed at the Canadian National Archives in Ottawa. Identified by the Yukon placer mining industry as a valuable resource, Yukon Geological Survey (YGS) has undertaken a project to identify, scan and make available documents of geological interest pertaining to Yukon. This repatriation project has involved scanning more than 1000 documents and maps. In order to evaluate the potential of the historic geologic data to modern placer exploration, YGS completed a digital compilation for Dominion Creek.

The objective of this project is to demonstrate how to incorporate YCGC data into a geographic information system (GIS) in order to assess its potential for placer exploration. This process highlights the challenges, limitations and accuracy of bringing historic data into a modern analytical environment.

A pilot project was completed on a section of the Dominion Creek drainage where sufficient YCGC data have been recovered. Data includes drilling information on gold grades, material thickness, presence of permafrost and depth to bedrock. In addition, data on areas dredged (dredge limits) and gold produced are also captured. Through analyses of this information two important economic questions are addressed: (1) what are the pay channel characteristics; and (2) where are the exploration targets?

STUDY AREA: DOMINION CREEK

Dominion Creek, a tributary of the Indian River, is a significant placer gold-bearing stream which has been actively mined since the early 1900s. A total of 2.73 million ounces of placer gold has been produced from Dominion Creek; hand mining produced 1,000,000 ounces, dredging produced 775,000 ounces, and mechanized mining produced 621,000 ounces (YGS, 2010). Twenty five historic documents on drilling, shafting and dredging are present for the middle reaches of Dominion Creek; for this reason the pilot project was chosen in this area (Fig. 1). The section investigated is approximately 9 km long, extending from the mouth of Nevada Creek downstream to the mouth of Arkansas Creek, and includes claims 76 to 177. Three historic drilling maps from 1936 were used in this project, YCGC Map numbers 1103 to 1105 (Fig. 2).

METHODS

Bringing historic geological maps into modern Geographical Information Systems (GIS) provides opportunities for advanced analysis and the creation of new maps that can be significantly more intuitive and easier to use than the original maps. For the Dominion Creek pilot project, the following steps were taken to incorporate the historic data into a modern mapping system.

GEOREFERENCING

In order to digitize data contained on the historic maps, scanned maps were imported into ESRI ArcGIS, and stable control points (stream junctions and valley orientation) were used to initially place the dataset to known positions. The dataset was then georeferenced by matching the vertices of historic placer claims with the Yukon Government's placer claim dataset. Quality of georeferencing was assessed by comparing actual known historic claim locations, which were located and recorded in the field.

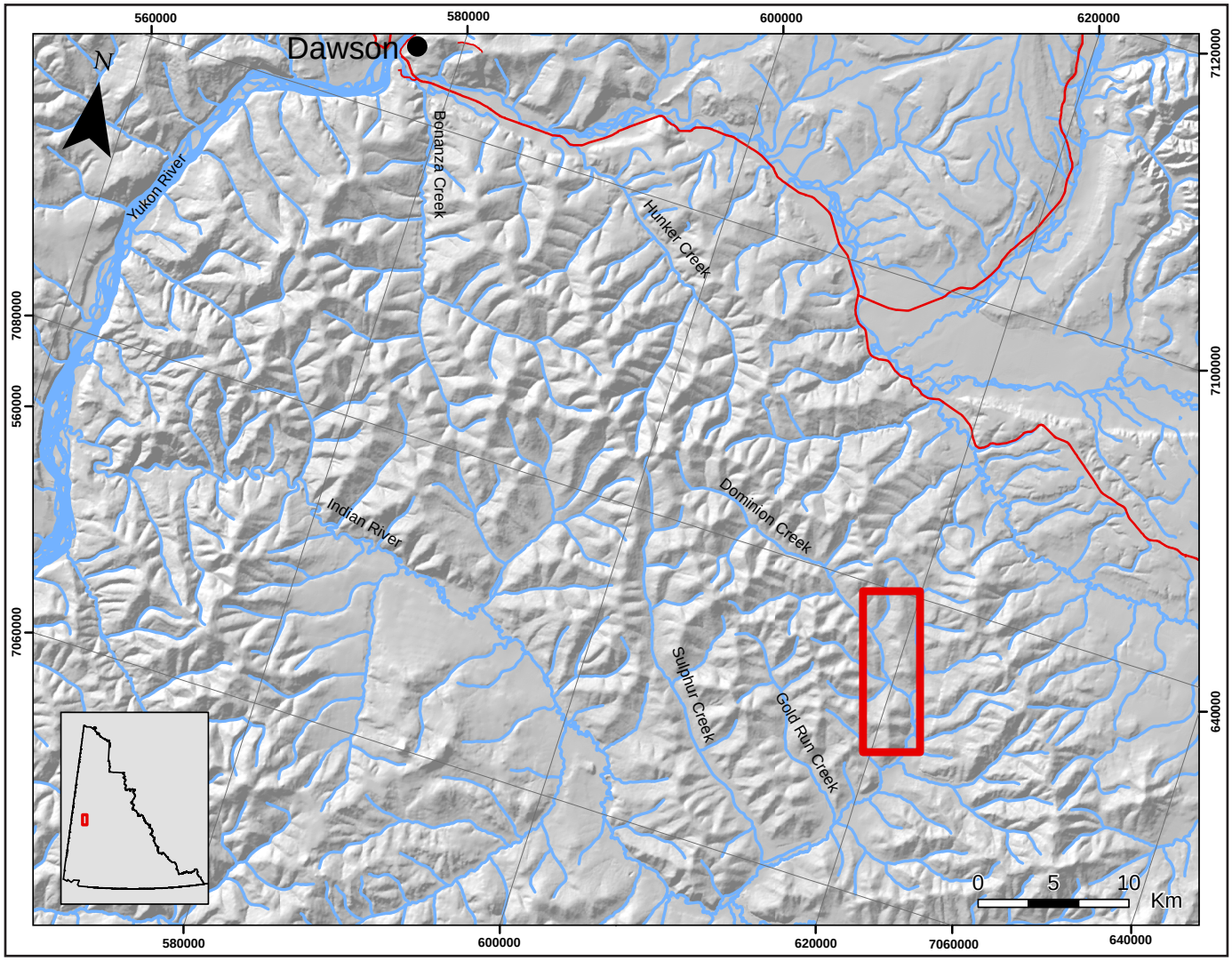


Figure 1. *Study area (outlined in red) south of Dawson City on mid-Dominion Creek.*

DIGITIZING

The 450 drill hole collars within the study area were manually digitized inside a point feature class, and attributed with their associated geological data (Appendix 1). The geological data include drill hole number, ground condition (frozen, partial or thawed), surface elevation, bedrock elevation, depth of overburden, depth of dredge section (pay gravel plus bedrock), and grade measured in dollars per cubic yard (gold at CDN $20.67). Dredge limits, both original and revised, were also digitized from the maps. Satellite imagery from July 2009 was used to compare georeferenced dredge limit locations with actual dredge limits by identifying dredge piles and undisturbed ground. The resulting digitized drill hole dataset and dredge limits formed the basis of the analysis (Appendix 2).

CONVERSIONS

Calculations were performed to convert measurements from imperial to metric. Depth in feet for overburden and dredge section were converted to metres. Within the attribute table of the drill hole data layer, a new column labeled 'total section depth' was generated from the sum of overburden plus dredge section. This was completed using the Field Calculator function in ArcGIS. The value of gravel in cents per cubic yard, was converted from the historic price of CDN $20.67 to today's price of CDN $1400.00. This was completed by converting cents to dollars, dollars to number of fine ounces, and multiplying the ounces by CAD $1400 to determine modern grade.

CORRECTIONS

Drill holes labeled with TR (trace) grades were digitized as 0.1 cents per cubic yard to show that gold was present, despite the low quantity. Several bedrock elevation values were too faintly transcribed to be reliable and were removed from the dataset. Drill hole 134-8 produced an historic grade of 2132.7 cents per cubic yards (gold at CDN $20.67), which was 527% higher than the next highest value in the dataset (404.8 cents per cubic yard). We considered this value to be the result of the nugget affect, and therefore, assigned a value that averaged its neighbouring drill holes to reduce the emphasis of the location.

SPATIAL ANALYSIS

Once the raw data were reviewed and corrected, spatial analyses were performed to create a series of raster datasets; each dataset highlights the various measurements associated with the drill hole data. In order to create the raster surfaces, the ArcGIS Spatial Analyst tool 'Inverse Distance Weighting' (IDW) algorithm was used to interpolate each attribute associated with the drill hole points. Contours at various intervals were then derived, using ArcGIS Spatial Analyst 'Surface' tool, from each of the resulting raster datasets to determine which interval gives the best representation of the data. For example, larger contour intervals of bedrock topography highlighted

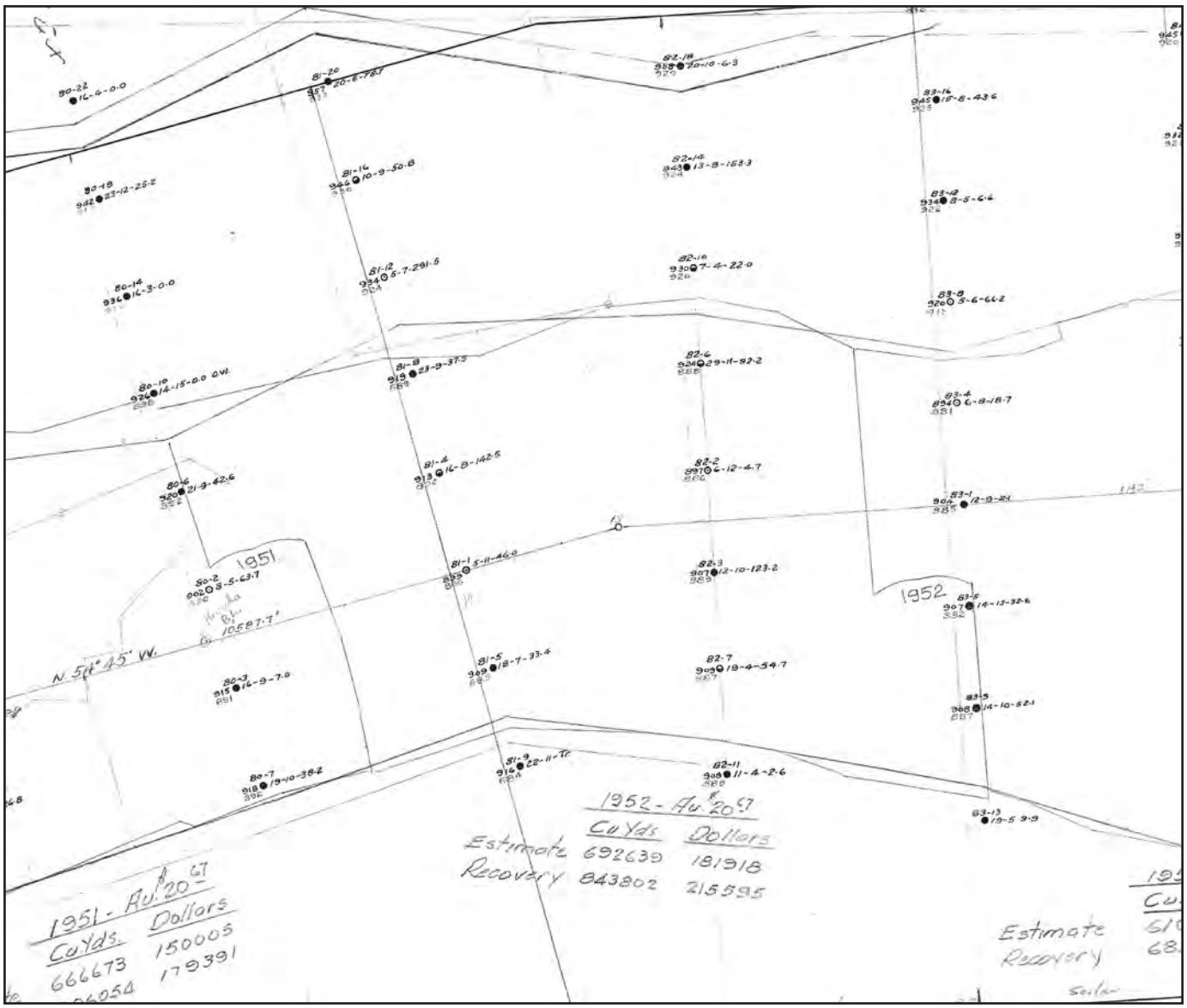


Figure 2. *Clip of drill map no. 1103, September 1936 (YCGC, 1936).*

bench features and small intervals highlighted undulations. The pay channel location was accentuated when grade contours were presented at coarser intervals (10 m), whereas detailed channel morphological features were highlighted under finer (2 m) contours.

Of particular value was the development of a bedrock topography map. In order to illustrate the bedrock topography, a digital elevation model (DEM) was visually represented with a hillshade image produced from the Spatial Analyst tool 'Hillshade' algorithm.

INTERPRETATIONS

The resulting points, rasters, and contours were then used to produce a series of maps (Appendices 3 to 7). A bedrock-low channel was digitized by following the contours (Appendix 8). Similarly, the pay channel was reconstructed and digitized by connecting the zones of the highest grade. Pay channel patterns and characteristics were derived from viewing single and multiple layer raster data. Likewise, exploration targets were generated by overlaying multiple sets of raster data and using the dredge limit polygon to further subdivide target types.

DATA LIMITATIONS

Several limitations exist within the dataset and must be taken into consideration when working with and interpreting the data. The main challenge associated with the historic map documents is their lack of geographical reference. Most maps have no grid reference, and at best, have base lines and claim blocks. To orient a map, several maps may be required to correlate references such as claim block numbers, old cabins, or contour lines. Incomplete legends add a significant limitation and legends from other YCGC maps were relied upon to interpret symbology. Data must be critically analyzed; highs and lows are removed from the dataset as a precaution and to not skew extrapolated raster data. Once raster data are generated, interpretation must consider the extent of the data, as in our case the data do not cover the entire width of the valley. The margins of the raster dataset are represented by an extrapolation from the nearest data point and therefore are zones of reduced data confidence. The radius of extrapolation on the margin measured 200 m.

Drilling accuracy can be affected by variables such as inconsistent recovery from varied ground conditions, nugget effect and sampling procedures. The reliability of the drill data was determined by comparing it to the dredge production data. Dredge estimate and actual production data are labeled on the maps for ten annual blocks. Six dredge blocks underestimated their production by an average 23%, while four overestimated their production by an average 14%. This speaks directly to drilling accuracy, as the drill data on average underestimated recovery by 8%.

RESULTS: MAPPING THE PAY CHANNEL

The paleo-channel and its associated patterns were reconstructed using raster data of gold grade (Appendix 9). The reconstructed high-grade channel width is ~45 m as defined by a grade greater than $150 per cubic yard. The channel width is approximately the same on the bench as it is in the valley bottom, indicating that as the stream incised, the reworking process did not greatly affect the lateral distribution of gold grains. The position of the pay channel in the valley bottom is offset towards the left limit and does not follow the bedrock low on the right limit (Appendix 8). This disconnection between bedrock topography and gold distribution could be attributed to the resilience of gold to move laterally during the reworking process. Therefore, the enriched channel is a reflection of an earlier channel thalweg and primarily moved vertically during reworking.

The gold grade data also provide us with an opportunity to assess grade continuity within the channel and interpret patterns. A common pattern is the accumulation of gold immediately upstream from the mouths of left limit tributaries. This could be the result of stream hydraulics or resulting dilution from the tributaries. If the tributaries were major gold contributors, you might expect to see more consistent grade throughout the channel rather than sporadic spikes. Bedrock undulations also appear to affect the grades. The pay channel appears to become more dispersed when the bedrock topography is more undulatory. Grade also increases where locally steep gradients in bedrock exist, which could reflect a more channelized flow and limited lateral gold movement.

Across the valley from the mouth of Hunter Creek (Fig. 3), a canyon and irregular bedrock surface is visible from modern elevation contours and bedrock contours. Also at this location, the reconstructed pay channel follows the bedrock low through a section measuring approximately 230 m wide. Grade is affected as a result of a change in channel hydraulics from the canyon, with a hotspot present both upstream and downstream from it.

At the downstream end of the study area the channel appears to dissipate after Arkansas Creek, which could be a function of the valley widening causing both stream flow and gold transport to decrease (Appendix 9). In addition, a dissipating channel could reflect changes in bedrock and a decrease in gold sources.

RESULTS: IDENTIFYING EXPLORATION PROSPECTS

The second objective of the pilot project was to identify exploration prospects. This was completed by analyzing single and multiple layer raster data for both dredged and unmined areas.

Targets inside the dredge limits can be identified by:

- A total section depth that exceeds the dredge maximum digging depth of 9.1 m (30 ft). These areas can be field verified by looking for rounded clasts on tailings piles indicating that the dredge did not reach bedrock and left behind *in situ* gold-bearing gravel and gold-enriched bedrock; and
- Bedrock undulations observed in the bedrock topography raster. Uneven bedrock surfaces would have been difficult to clean using dredge buckets, providing potential for *in situ* gravel to remain.

Four targets with a total section depth exceeding 9.1 m were identified, with the largest target measuring 650 m long by 105 m wide (Appendix 10). Undulations are evident throughout the length of the study area and accentuated at the mouth of Sullivan Creek, approximately 1 km downstream from Nevada Creek and Hunter Creek. The presence of bedrock undulations warrants large parts of the dredged area to be re-examined, with approximately ⅓ of the study area having prospective undulatory bedrock topography. These areas may yield increased grade due to channelized flow resulting in lag concentrations, particularly for coarser gold. In addition, channel irregularities, similar to the canyon near Hunter Creek, could cause an increased concentration of gold due to changes in gradients or stream velocity. Other prospects inside the dredge limits include technogenic deposits such as tailing piles, cat push, and historic settling ponds that offer a potential mineable resource due to poor gold recovery techniques in the past.

Targets outside the limits of both dredging and modern excavations include:

- High grade areas derived from extrapolated grade data from the nearest drilling location;
- Areas identified with shallow overburden and a thick gravel package; and
- Favourable ground conditions, such as selecting thawed areas that would be less expensive to mine.

Significant areas of extrapolated high grade include a 2-km-long left limit zone at the mouth of Nevada Creek, a 0.5-km-long left limit section between Jensen and Kentucky creeks, and a 1 km-long section, on both limits of Dominion Creek, near the mouth of Arkansas Creek Appendix 3). Additional extrapolated high grade zones also extend approximately 1 km up and down-stream from Hunter Creek on both limits of Dominion Creek. A significant prospect of a thawed, thick gravel package exists on the left limit of Dominion Creek, across from Hunter Creek. Appendix 4 and Appendix 7 display the gravel depth and thawed conditions of this target, which is approximately 1 km in length and 0.5 km in width, with thawed gravels ranging from 6 to 10 m thick.

Additional prospects could be identified by adding supplementary data that may exist, such as shafting results, modern geology maps, and additional dredge and modern production data. In dredge blocks where production was less than anticipated, potential for economic gravel deposits could remain due to dredge inefficiencies. In these areas, exploration targets may include reworking tailing piles that were inadequately processed or assessing the bedrock interface for missed pay gravel.

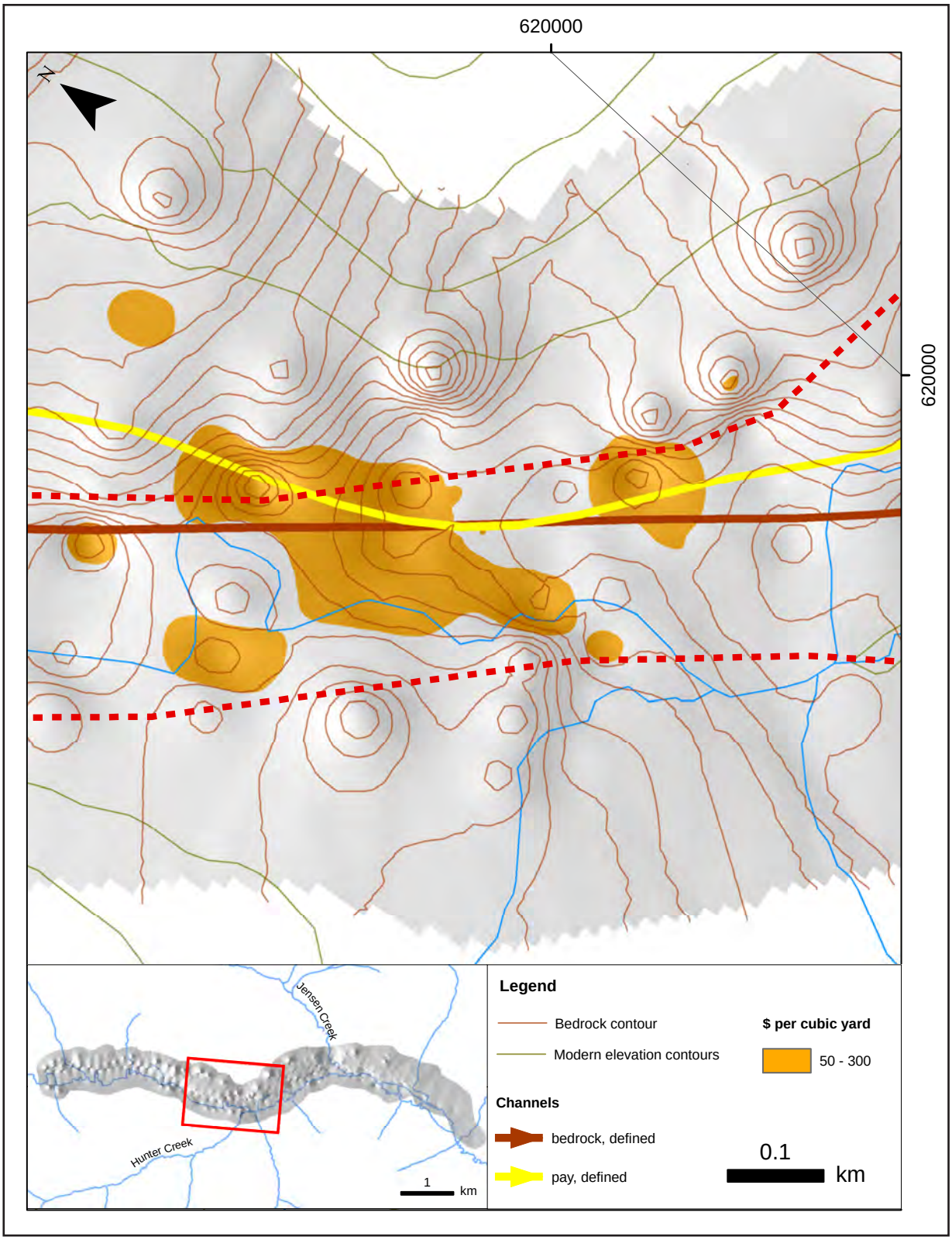


Figure 3. *Canyon at the mouth of Hunter Creek, causing a channel irregularity to affect gold grade. A bedrock contour map with gold grade near the mouth of Hunter Creek. The yellow line defines the approximate center of the pay channel and the brown line defines the bedrock topographic low. The distribution of gold (orange shade) appears irregular and may be attributed to the uneven bedrock surface.*

CONCLUSION

The Dominion Creek YCGC pilot project has shown that bringing historic map data into modern GIS mapping systems can provide new and encouraging ways to view and interpret archival data. With the ability to characterize the pay channel in terms of width, distribution and grade, we can hypothesis about drainage evolution and the mechanics of gold transport and deposition. An understanding of the gold deposition system, when used with thaw, overburden depth and bedrock depths allows prospectors to make informed decisions when identifying potential targets. Compilations larger than the one presented here would likely result in a greater ability to interpret channel dynamics and have an increased understanding of gold transport within the creek system. This could also lead to exploration of tributaries and nearby creeks with similar valley morphologies.

YCGC data are available for most major tributaries in the Klondike goldfields. Archival data include drilling results, shafting locations and dredge reserves, all of which could assist miners and prospectors in the placer mining industry to locate pockets of unmined areas in historic placer regions. While there are some challenges to using the data, the substantial wealth of exploration knowledge contained in the YCGC archives makes it a worthwhile tool for investigating placer potential.

ACKNOWLEDGMENTS

Many thanks are owed to the placer miners along Dominion Creek - Adrian Hollis, Dean Russell, Lucky Strike Ventures Ltd. and the Sailer family - that permitted access to their properties and engaged in many conversations about the creek and its local history. Thank you to Jeff Bond and Kristen Kennedy for the abundant field and office support. A special thanks to Brett Elliot for his guidance in digitizing and analysing the data within ArcMap. Thanks are also owed to Bailey Staffen for technical assistance, Karen MacFarlane and Monica Nordling for editorial review, and Bill LeBarge for the discussions and feedback on the YCGC data.

We thank the miners for all their contributions and the industry for supporting the acquisition of the YCGC data collection.

REFERENCES

Green, L., 1977. The Gold Hustlers. Alaska Northwest Publishing Company, Anchorage.

Yukon Consolidated Gold Corp., 1936. Middle Dominion drill holes - Claims 77 to 99 below lower discovery. Energy, Mines and Resources Property File Collection, YCGC 1103.

Yukon Consolidated Gold Corp., 1936. Middle Dominion drill holes - Claims 99 to 137 below lower discovery. Energy, Mines and Resources Property File Collection, YCGC 1104.

Yukon Consolidated Gold Corp., 1936. Middle Dominion drill holes - Claims 137 to 159 below lower discovery. Energy, Mines and Resources Property File Collection, YCGC 1105.

Yukon Geological Survey, 2010. Yukon Placer Database – Geology and mining activity of placer occurrences. Yukon Geological Survey, CD-ROM.

APPENDICES

Appendix 1. Attribute table; from historic drill maps.

Note: Appendices 2 through 10 are oversized maps.

Appendix 2. Satellite imagery of Dominion Creek study area with YCGC drilling data, dredge limits, and 2015 placer operation locations.

Appendix 3. Dredge limits and gold grade, gold at $1,400.

Appendix 4. Dredge section thickness, pay gravel plus bedrock.

Appendix 5. Overburden depth.

Appendix 6. Total section depth, overburden plus dredge section.

Appendix 7. Bedrock topography and ground condition.

Appendix 8. Bedrock topography with bedrock low and pay channel highlighted.

Appendix 9. Pay channel reconstruction using modern grade raster information.

Appendix 10. Total section depth with dredge limit and high grade zones.

APPENDIX 1. *Attribute table of geological information obtained from historic drill maps.*

DRILL HOLE ID	GROUND CONDITION	SURFACE ELEVATION	BEDROCK ELEVATION	OVERBURDEN (M)	DREDGE SECTION (M)	CENTS PER CUBIC YARD
99-9	Frozen	859	839	5.49	1.52	170
99-5	Frozen	860	837	5.18	2.13	4.9
99-4	Frozen	868	846	1.83	5.18	0
99-21	Partial	879	862	1.52	3.96	5.2
99-17	Frozen	872	863	1.22	2.13	10.4
99-13	Partial	864	861	0.3	0.91	20.1
99-1	Frozen	861	836	5.79	3.66	51.9
98-7	Frozen	863	842	5.49	1.83	78.1
98-6	Partial	882	875	0.91	1.22	0
98-3	Frozen	863	837	5.79	3.35	99.6
98-2	Frozen	869	844	6.71	1.22	29.9
98-19	Frozen	881	870	2.74	0.91	0.1
98-15	Frozen	868	857	1.83	1.83	2.7
98-11	Frozen	863	849	3.66	1.22	178.4
97-9	Frozen	866	854	3.05	1.52	1.6
97-5	Frozen	866	840	6.1	3.05	314.6
97-4	Frozen	890	874	1.83	3.35	4
97-21	Frozen	883	859	5.18	2.44	0
97-17	Frozen	869	850	5.49	1.52	181.6
97-13	Frozen	865	860	0.91	1.22	18.4
97-1	Frozen	873	866	1.22	1.22	10.3
96-7	Frozen	875	864	2.74	0.91	0
96-6	Frozen	912	877	8.53	3.05	102.5
96-3	Frozen	886	875	1.52	2.44	33.6
96-23	Frozen	884	858	7.62	0.61	9.6
96-2	Frozen	899	876	4.57	3.35	65.8
96-19	Frozen	870	845	4.88	3.66	13.1
96-15	Frozen	869	847	5.79	1.83	54.8
96-14	Frozen	947	895	14.94	1.22	0
96-14	Frozen	947	895	14.94	1.22	0
96-11	Frozen	870	840	7.01	2.74	94.4
96-10	Frozen	928	880	13.11	2.13	45.3
95-9	Frozen	877	851	5.49	3.05	120.2
95-8	Frozen	922	880	10.67	2.44	18.7
95-5	Frozen	886	870	3.35	1.83	9.1
95-4	Frozen	909	879	7.32	2.44	82.6
95-23	Frozen	880	861	5.18	0.91	0
95-21	Frozen	870	850	4.88	1.52	13.2
95-17	Frozen	872	848	6.1	2.13	19.8
95-13	Frozen	872	841	5.49	4.27	5.7
95-12	Frozen	934	882	14.33	2.13	10.1

Appendix 1. *continued*

DRILL HOLE ID	GROUND CONDITION	SURFACE ELEVATION	BEDROCK ELEVATION	OVERBURDEN (M)	DREDGE SECTION (M)	CENTS PER CUBIC YARD
95-1	Frozen	896	879	4.27	1.83	57.8
94-7	Frozen	881	870	2.13	1.52	30.5
94-6	Frozen	907	885	5.49	2.13	122
94-3	Frozen	888	873	3.66	1.83	171.3
94-21	Frozen	<Null>	<Null>	<Null>	<Null>	0
94-2	Frozen	897	880	4.57	1.52	74
94-19	Frozen	875	843	7.32	3.05	28.6
94-18	Frozen	955	915	10.97	1.52	0
94-15	Frozen	873	852	5.49	1.52	18.9
94-14	Frozen	937	893	11.89	1.83	73.8
94-11	Frozen	875	852	5.49	1.83	40.4
94-10	Frozen	922	889	7.92	3.05	36.6
93-9	Frozen	877	854	6.1	2.13	12.5
93-8	Frozen	917	889	6.4	3.35	145.7
93-5	Frozen	883	876	1.83	1.83	178.3
93-4	Frozen	904	884	5.18	1.52	157.8
93-20	Frozen	963	929	9.14	1.52	0
93-19	Frozen	<Null>	<Null>	<Null>	<Null>	0
93-17	Frozen	876	863	5.49	1.83	72.4
93-16	Frozen	946	889	15.24	2.44	10.9
93-13	Frozen	878	855	5.49	2.44	30.4
93-12	Thawed	931	889	10.67	3.05	39.7
93-1	Frozen	893	880	2.74	2.44	404.8
92-7	Frozen	881	856	5.79	2.44	27.4
92-6	Frozen	902	889	1.83	2.74	68.2
92-3	Partial	876	871	0.91	0.91	0.1
92-2	Frozen	888	880	1.22	1.83	16.3
92-14	Frozen	930	887	8.23	2.13	4.2
92-11	Frozen	880	856	6.4	1.22	5.9
92-10	Frozen	916	893	3.35	4.88	75
91-9	Frozen	887	861	6.71	1.52	8.8
91-8	Partial	895	892	0.61	0.61	0
91-5	Frozen	883	857	5.79	3.35	15.4
91-4	Frozen	893	875	4.57	1.22	3.5
91-16	Frozen	958	917	8.84	3.66	0
91-12	Frozen	928	894	7.62	3.05	13.7
91-1	Frozen	884	860	6.1	1.52	52.6
90-9	Frozen	890	873	1.22	4.27	0
90-7	Frozen	886	860	6.4	2.74	25.1
90-6	Partial	905	900	1.52	0.61	0.1

Appendix 1. *continued*

DRILL HOLE ID	GROUND CONDITION	SURFACE ELEVATION	BEDROCK ELEVATION	OVERBURDEN (M)	DREDGE SECTION (M)	CENTS PER CUBIC YARD
90-3	Frozen	884	861	4.88	2.74	28.2
90-2	Frozen	890	870	2.44	4.88	75.1
90-14	Frozen	953	946	0.91	1.22	0
90-11	Frozen	902	894	0.61	2.13	0
90-10	Partial	932	920	0.91	3.05	6.2
89-9	Frozen	889	861	6.4	2.74	60.6
89-5	Frozen	889	865	5.79	2.44	69
89-4	Partial	891	883	0.91	1.22	3.5
89-16	Frozen	962	929	3.96	6.4	0
89-12	Frozen	938	915	5.49	2.13	51.3
89-11	Frozen	899	887	2.74	1.22	7.3
89-1	Frozen	880	865	5.79	1.52	18.4
88-7	Frozen	891	867	5.49	2.44	12
88-6	Frozen	908	885	7.32	0.91	20.3
88-3	Frozen	886	863	1.52	4.27	1.3
88-2	Frozen	894	872	7.01	1.22	8.6
88-18	Frozen	963	940	6.4	0.91	0
88-14	Frozen	941	910	7.62	2.13	3.7
88-11	Frozen	898	870	7.92	0.91	16.9
88-10	Frozen	923	904	5.18	1.22	74.8
87B-8	Frozen	899	875	6.71	2.44	274
87B-7	Frozen	<Null>	<Null>	<Null>	<Null>	0
87B-5	Frozen	895	867	6.1	3.05	35.2
87B-20	Frozen	951	913	9.45	2.44	2
87B-16	Frozen	936	911	6.1	1.83	18.4
87B-12	Thawed	908	908	0	0.61	8.3
87B-1	Frozen	891	872	4.27	2.13	3.9
87A-6	Frozen	894	873	4.88	2.13	29.9
87A-3	Frozen	898	872	4.57	3.66	1.5
87A-2	Frozen	895	874	5.79	1.52	43.7
87A-18	Frozen	940	914	5.79	2.74	5.1
87A-16	Frozen	929	914	2.44	2.74	21.8
87A-14	Frozen	918	911	0.91	1.52	25.3
87A-10	Frozen	901	874	7.01	1.83	36.7
878-4	Frozen	891	870	5.18	1.83	133.4
87-8	Frozen	888	876	2.44	1.52	5.7
87-5	Frozen	894	874	3.35	3.05	0.1
87-4	Frozen	896	874	5.18	2.44	17.4
87-24	Frozen	954	929	5.18	2.74	0
87-20	Frozen	933	915	5.49	2.44	43.4

Appendix 1. *continued*

DRILL HOLE ID	GROUND CONDITION	SURFACE ELEVATION	BEDROCK ELEVATION	OVERBURDEN (M)	DREDGE SECTION (M)	CENTS PER CUBIC YARD
87-16	Frozen	925	915	1.83	2.74	30.9
87-12	Frozen	912	889	6.71	1.22	152.6
87-1	Frozen	896	874	3.66	3.66	14.3
86-7	Frozen	900	878	5.49	1.52	19.5
86-6	Frozen	897	881	2.74	3.05	7.8
86-3	Frozen	899	878	4.88	2.74	39
86-22	Frozen	947	923	6.71	1.22	19.5
86-2	Frozen	896	880	4.88	0.91	8.2
86-18	Frozen	930	916	2.44	3.05	117.5
86-14	Frozen	918	900	3.66	2.74	76.8
86-10	Frozen	906	882	6.71	1.22	43.8
85-9	Frozen	899	880	3.66	2.74	26.7
85-8	Frozen	907	885	5.18	2.74	136.6
85-5	Frozen	900	878	5.18	2.13	8.7
85-4	Frozen	893	883	1.52	1.83	2.7
85-16	Thawed	931	922	1.22	1.83	3.9
85-13	Frozen	903	881	5.18	1.83	4.2
85-12	Frozen	917	903	3.05	1.22	170.4
85-1	Frozen	900	881	5.18	0.91	5.5
84-7	Frozen	905	879	5.49	3.05	47.1
84-6	Partial	894	884	2.44	0.91	6.2
84-3	Frozen	903	880	4.57	3.05	72.1
84-26	Thawed	960	926	12.8	1.22	0
84-22	Frozen	960	926	7.92	3.35	91
84-2	Frozen	902	882	4.57	1.83	7.6
84-18	Partial	945	920	5.49	2.44	46.6
84-15	Thawed	916	882	9.14	2.13	83.9
84-14	Partial	932	921	1.83	3.05	189.4
84-11	Frozen	905	881	5.18	2.44	0.1
84-10	Frozen	919	910	2.13	1.22	61.6
83-9	Frozen	908	887	4.27	3.05	52.1
83-8	Thawed	920	911	1.52	1.83	66.2
83-5	Frozen	907	882	4.27	3.96	32.6
83-4	Thawed	894	881	1.83	2.44	18.7
83-20	Frozen	957	930	6.71	1.83	6.6
83-16	Frozen	945	925	4.57	2.44	43.6
83-13	Frozen	910	886	5.79	1.52	9.9
83-12	Frozen	934	922	2.44	1.52	6.6
83-1	Frozen	904	885	3.66	2.74	2.1
82-7	Partial	909	887	5.79	1.22	54.7
82-6	Partial	924	888	8.84	3.35	92.2

Appendix 1. *continued*

DRILL HOLE ID	GROUND CONDITION	SURFACE ELEVATION	BEDROCK ELEVATION	OVERBURDEN (M)	DREDGE SECTION (M)	CENTS PER CUBIC YARD
82-3	Frozen	907	889	3.66	3.05	123.2
82-2	Thawed	897	886	1.83	3.66	4.7
82-18	Frozen	958	929	6.1	3.05	6.3
82-14	Frozen	943	924	3.96	2.44	153.3
82-11	Frozen	909	889	3.35	1.22	2.6
82-10	Partial	930	920	2.13	1.22	22
81-9	Frozen	916	884	6.71	3.35	0.1
81-8	Frozen	919	889	7.01	2.74	37.3
81-5	Frozen	909	885	5.49	2.13	33.4
81-4	Partial	913	892	4.88	2.44	142.5
81-24	Frozen	967	937	7.92	1.52	0
81-20	Frozen	957	933	6.1	1.83	78.7
81-16	Partial	946	930	3.05	2.74	50.8
81-12	Thawed	934	924	1.52	2.13	291.5
81-1	Thawed	899	886	1.52	3.35	46
80-7	Frozen	918	892	5.79	3.05	38.2
80-6	Frozen	920	892	6.4	2.74	42.6
80-3	Frozen	915	891	4.88	2.74	7
80-22	Frozen	<Null>	<Null>	<Null>	<Null>	0
80-2	Thawed	902	890	2.44	1.52	63.7
80-18	Frozen	942	910	7.01	3.66	25.2
80-14	Frozen	936	919	4.88	0.91	0
80-10	Frozen	926	898	4.27	4.57	0
78-8	Partial	918	895	4.57	3.05	57
78-5	Frozen	919	893	6.1	3.05	26.8
78-4	Partial	915	895	1.22	5.18	6.1
78-24	Frozen	957	934	0.91	6.4	3.2
78-20	Partial	948	928	2.74	2.13	22
78-16	Partial	936	930	0.91	1.83	42.5
78-12	Partial	924	920	0.61	0.91	99.9
78-1	Frozen	916	893	3.96	4.57	88.7
77-7	Frozen	930	895	8.84	3.05	46.3
77-6	Partial	918	894	5.49	2.44	64.4
77-3	Frozen	918	893	5.49	2.74	26.3
77-22	Partial	956	938	3.35	2.44	59.8
77-2	Frozen	920	895	4.57	3.96	71.1
77-18	Partial	940	933	1.22	1.22	3.4
77-15	Frozen	970	921	13.72	1.83	6.1
77-14	Frozen	930	910	5.49	0.91	4.8
77-11	Frozen	948	910	9.45	3.35	19
77-10	Thawed	923	891	7.32	2.74	11.9

Appendix 1. *continued*

DRILL HOLE ID	GROUND CONDITION	SURFACE ELEVATION	BEDROCK ELEVATION	OVERBURDEN (M)	DREDGE SECTION (M)	CENTS PER CUBIC YARD
151-18	Frozen	795	769	4.57	4.88	22.3
151-14	Frozen	792	766	4.57	4.88	5.4
149-6	Partial	793	774	4.27	2.13	30.9
149-14	Frozen	798	772	4.88	3.66	58.7
149-10	Frozen	795	774	4.27	2.74	50.7
147-30	Frozen	823	789	8.84	2.44	6.9
147-26	Frozen	814	787	5.49	3.35	15.2
147-22	Frozen	807	786	5.49	1.52	40.4
147-18	Frozen	801	785	3.05	2.13	3.7
147-14	Frozen	798	779	5.18	1.52	101.8
145-6	Frozen	805	783	4.27	2.74	26.6
145-30	Frozen	837	793	10.36	3.96	10.9
145-26	Frozen	828	794	5.49	5.18	5.1
145-22	Frozen	819	792	4.27	4.57	23.9
145-18	Frozen	812	791	3.66	3.05	0.6
145-14	Frozen	808	791	3.05	3.05	24.8
145-10	Frozen	807	788	3.66	3.96	48.8
143-6	Frozen	814	798	2.44	3.35	11.2
143-26	Frozen	<Null>	<Null>	4.27	5.79	1.7
143-22	Frozen	828	800	6.1	3.05	23.5
143-2	Frozen	808	788	3.35	3.66	22.6
143-18	Frozen	823	800	4.27	3.05	1.7
143-14	Frozen	819	799	3.35	3.35	10.3
143-10	Frozen	817	798	3.05	3.66	53
142-7	Frozen	<Null>	<Null>	4.27	3.96	10.3
142-6	Frozen	<Null>	<Null>	3.96	3.05	9.5
142-5	Frozen	<Null>	<Null>	3.96	4.57	3.3
142-4	Frozen	<Null>	<Null>	4.88	3.35	3.6
142-3	Frozen	<Null>	<Null>	5.18	4.88	6.9
142-2	Frozen	<Null>	<Null>	4.57	6.4	1.2
142-1	Thawed	<Null>	<Null>	3.66	8.23	1.7
141-b	Frozen	<Null>	<Null>	6.1	3.05	6.9
141-a	Frozen	<Null>	<Null>	4.57	3.35	4.7
141-6	Frozen	821	804	3.05	2.74	2
141-18	Frozen	836	815	4.57	2.74	1.9
141-14	Frozen	831	809	5.18	2.13	61.3
141-10	Partial	825	809	3.05	2.74	161.8
140-8	Frozen	828	812	3.35	1.83	119
140-5	Frozen	814	794	4.57	1.83	2.9
140-4	Frozen	825	794	7.92	2.13	28.1
140-28	Frozen	848	<Null>	7.32	1.52	10.6

Appendix 1. *continued*

DRILL HOLE ID	GROUND CONDITION	SURFACE ELEVATION	BEDROCK ELEVATION	OVERBURDEN (M)	DREDGE SECTION (M)	CENTS PER CUBIC YARD
140-24	Frozen	844	820	6.1	1.83	17.5
140-20	Frozen	838	818	4.57	3.66	43.3
140-16	Frozen	835	815	4.27	2.13	41
140-12	Frozen	831	814	3.66	1.83	28.7
140-1	Frozen	821	796	6.1	1.83	5.5
139-b	Frozen	<Null>	<Null>	6.4	1.22	35.7
139-a	Frozen	<Null>	<Null>	3.05	2.74	10.5
139-7	Frozen	818	795	5.18	2.13	24.9
139-6	Frozen	823	812	1.22	2.74	21
139-3	Frozen	819	796	3.66	3.66	1.5
139-2	Frozen	820	799	3.96	2.74	4.3
139-18	Frozen	835	818	1.83	3.66	2.9
139-15	Frozen	817	793	3.96	3.66	3.4
139-14	Frozen	832	818	1.52	3.66	41.6
139-11	Frozen	818	795	5.79	1.52	16.1
139-10	Frozen	827	813	2.13	2.74	43.7
138-b	Frozen	<Null>	<Null>	5.18	2.74	1.8
138-a	Frozen	<Null>	<Null>	3.05	3.96	72.8
138-9	Frozen	820	798	5.18	1.83	4.3
138-8	Frozen	827	813	2.74	2.13	40.7
138-5	Frozen	821	803	3.66	2.44	4.3
138-4	Frozen	822	808	2.44	1.83	4.2
138-20	Frozen	844	824	4.57	1.83	7.2
138-16	Frozen	838	823	2.13	3.35	66.4
138-12	Frozen	832	822	1.52	2.74	70.1
138-1	Frozen	821	804	4.27	1.52	8.4
137-7	Frozen	823	796	4.57	3.96	0
137-6	Frozen	829	820	1.52	1.83	28.7
137-30	Frozen	877	844	3.05	7.32	5
137-3	Frozen	822	805	4.27	2.13	2.5
137-28	Frozen	872	835	2.44	9.14	3
137-26	Frozen	868	836	6.1	4.27	15.1
137-22	Frozen	858	850	3.66	5.18	5
137-2	Frozen	824	817	1.22	1.22	7.3
137-15	Frozen	849	835	3.35	1.83	8
137-14	Partial	842	827	4.57	0.91	6.5
137-10	Frozen	836	826	1.22	2.13	2.7
137-1	Frozen	815	782	6.4	3.66	1.5
136-9	Frozen	826	799	5.18	3.66	14.5
136-8	Frozen	837	828	2.44	1.22	37.8
136-5	Frozen	826	800	5.79	2.44	3.1

Appendix 1. *continued*

DRILL HOLE ID	GROUND CONDITION	SURFACE ELEVATION	BEDROCK ELEVATION	OVERBURDEN (M)	DREDGE SECTION (M)	CENTS PER CUBIC YARD
136-4	Frozen	829	821	1.22	1.52	11
136-26	Frozen	877	838	8.84	3.35	8.5
136-24	Frozen	871	838	7.92	2.74	34.3
136-22	Frozen	866	835	7.32	2.44	5
136-20	Frozen	861	835	6.71	2.13	6.5
136-16	Frozen	852	833	3.66	1.83	2.1
136-12	Frozen	845	832	1.83	2.44	8.2
136-1	Frozen	824	802	4.88	2.13	11.2
135-9	Frozen	829	804	3.96	4.27	3.2
135-7	Frozen	828	799	5.49	3.66	7.5
135-6	Partial	837	825	2.13	1.83	75.3
135-3	Frozen	827	805	6.1	1.22	30.4
135-22	Partial	869	835	6.1	5.18	4.4
135-2	Frozen	827	808	4.57	1.83	45.9
135-18	Frozen	860	837	5.18	3.35	41.3
135-14	Frozen	851	834	1.22	4.88	173.7
135-11	Frozen	822	795	7.92	1.22	31.4
135-10	Thawed	844	832	1.22	2.74	5.2
134-9	Frozen	828	807	4.57	2.44	17.1
134-8	Frozen	849	837	3.35	1.22	237
134-5	Partial	829	820	0.91	2.13	0.1
134-4	Frozen	841	829	2.44	2.44	368.7
134-16	Frozen	867	840	5.18	3.35	2.9
134-15	Frozen	<Null>	<Null>	<Null>	<Null>	0
134-13	Frozen	831	805	6.1	2.13	4.8
134-12	Partial	857	838	4.57	1.83	105.3
134-1	Thawed	835	829	0.61	1.52	90.9
133-7	Thawed	830	811	4.57	1.52	7.5
133-6	Thawed	841	835	0.91	2.13	11.8
133-3	Thawed	838	828	1.22	2.13	11.8
133-2	Thawed	840	830	0	3.66	75.6
133-18	Partial	882	865	1.52	4.57	9.1
133-17	Frozen	<Null>	<Null>	<Null>	<Null>	2.4
133-15	Frozen	833	806	6.4	2.13	18.4
133-14	Partial	870	848	4.88	4.27	21.7
133-11	Frozen	831	808	5.49	1.83	2.7
133-10	Partial	861	836	4.88	2.74	28.7
132-9	Frozen	832	810	6.1	1.52	43.3
132-8	Thawed	849	838	0.61	3.05	3.3
132-5	Partial	834	820	3.66	0.91	4.5
132-4	Thawed	841	839	0.61	0.91	6.2

Appendix 1. *continued*

DRILL HOLE ID	GROUND CONDITION	SURFACE ELEVATION	BEDROCK ELEVATION	OVERBURDEN (M)	DREDGE SECTION (M)	CENTS PER CUBIC YARD
132-13	Frozen	834	811	3.35	4.27	27
132-12	Partial	866	849	3.35	2.13	0
132-1	Thawed	843	839	1.22	0.3	0
131-7	Frozen	834	817	3.35	2.13	0
131-6	Frozen	842	810	6.1	1.52	0
131-3	Frozen	836	811	5.18	3.35	51.6
131-2	Frozen	839	819	4.88	1.52	0
131-19	Frozen	832	807	3.66	4.27	6.9
131-15	Frozen	834	811	6.71	0.91	113.5
131-11	Frozen	833	811	5.49	1.52	9.3
131-10	Frozen	845	820	7.32	1.22	0.1
130-9	Frozen	833	805	5.79	3.35	18.2
130-8	Frozen	841	823	2.74	1.52	0.1
130-5	Frozen	832	806	4.57	3.66	17.5
130-4	Frozen	838	824	3.35	1.22	1.3
130-11	Thawed	836	807	7.32	2.13	6.7
130-1	Frozen	837	816	4.27	1.83	100.9
129-7	Frozen	837	819	4.57	1.52	36.5
129-6	Frozen	842	825	2.44	2.44	73.7
129-3	Frozen	835	816	3.66	2.74	32.7
129-2	Partial	839	831	0.61	2.13	26
129-18	Partial	867	856	0.91	4.57	4.9
129-14	Partial	858	848	1.22	2.13	42.7
129-11	Frozen	838	808	7.01	2.44	16.9
129-10	Frozen	849	842	1.52	0.91	5.7
128-9	Frozen	840	812	5.18	3.66	5.3
128-8	Thawed	845	834	2.13	1.52	8.2
128-5	Frozen	839	817	5.79	1.22	5.9
128-4	Thawed	842	835	1.83	1.83	275.3
128-24	Frozen	898	854	2.74	1.22	0
128-20	Frozen	885	855	5.49	2.74	0
128-16	Frozen	873	849	3.35	4.27	7.9
128-13	Thawed	862	805	13.41	3.66	27.2
128-12	Frozen	860	845	2.13	2.74	105.2
128-1	Frozen	839	814	4.88	0.91	16.7
127-7	Frozen	841	817	4.88	3.05	5
127-6	Partial	846	838	1.52	1.22	3.5
127-3	Frozen	841	820	5.49	1.83	105.2
127-2	Partial	848	834	3.05	1.52	13.1
127-18	Partial	896	855	11.58	1.22	7.6
127-14	Frozen	878	850	6.71	2.74	24.4

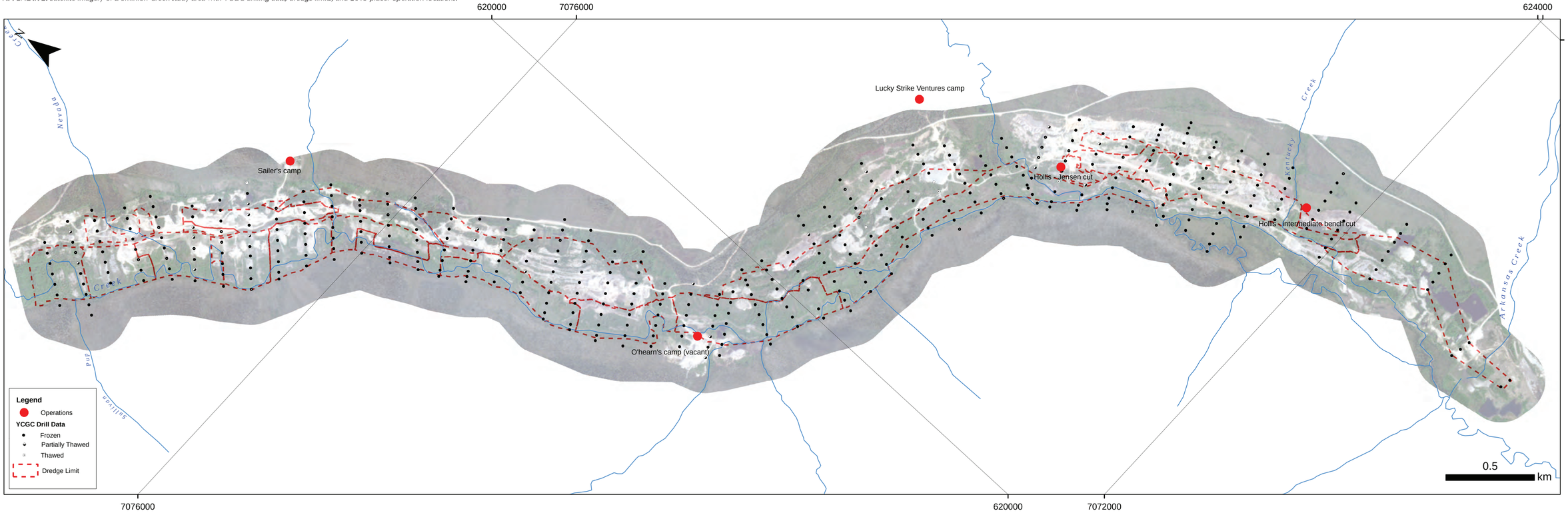
Appendix 1. *continued*

DRILL HOLE ID	GROUND CONDITION	SURFACE ELEVATION	BEDROCK ELEVATION	OVERBURDEN (M)	DREDGE SECTION (M)	CENTS PER CUBIC YARD
127-11	Frozen	857	830	6.4	2.13	1.7
127-10	Frozen	865	842	6.1	1.83	49.3
126-9	Frozen	845	821	5.18	2.44	5.4
126-8	Partial	850	844	0.91	1.22	29.7
126-5	Frozen	843	823	5.49	0.91	22.2
126-4	Partial	855	848	1.52	0.91	7.8
126-28	Frozen	938	890	9.14	5.79	0
126-24	Partial	924	856	18.59	2.74	41.1
126-20	Frozen	910	858	14.63	1.83	9.3
126-16	Frozen	894	858	9.14	2.13	42.3
126-12	Partial	875	845	7.92	1.83	88.6
126-1	Partial	843	825	2.13	3.96	58.9
125-7	Frozen	846	824	5.18	2.44	14.2
125-6	Thawed	852	844	1.22	1.83	105.2
125-3	Frozen	845	822	5.79	1.52	19.3
125-26	Partial	948	867	21.34	4.27	3.5
125-22	Thawed	929	861	18.29	2.74	19.5
125-2	Frozen	850	826	6.4	1.22	0
125-18	Partial	911	852	14.63	3.66	1.3
125-15	Frozen	854	822	8.84	1.22	18.4
125-14	Frozen	894	850	11.28	3.05	46.4
125-11	Frozen	847	824	5.79	1.83	51.4
125-10	Thawed	870	839	7.32	2.44	12.6
124-9	Frozen	847	828	4.88	1.52	20.9
124-8	Frozen	880	849	7.92	2.13	59.7
124-5	Partial	847	831	4.57	0.91	5
124-4	Frozen	867	847	4.27	3.35	99.8
124-20	Frozen	926	866	13.11	5.49	0
124-17	Frozen	851	820	7.32	3.05	13.9
124-16	Frozen	910	863	9.14	5.49	0.8
124-13	Frozen	848	828	4.88	1.52	20.9
124-12	Frozen	893	851	11.89	1.83	65.5
124-1	Partial	847	842	1.22	0.61	0.1
123-7	Frozen	850	826	5.49	2.44	29.3
123-6	Frozen	876	851	6.4	2.13	117.3
123-3	Frozen	852	831	4.88	1.83	10.1
123-22	Frozen	940	908	8.53	1.52	0
123-2	Frozen	862	840	6.4	0.91	206.7
123-19	Frozen	872	821	13.72	2.13	0
123-18	Frozen	921	865	14.63	1.83	62.2
123-15	Frozen	850	820	5.18	5.18	41.9

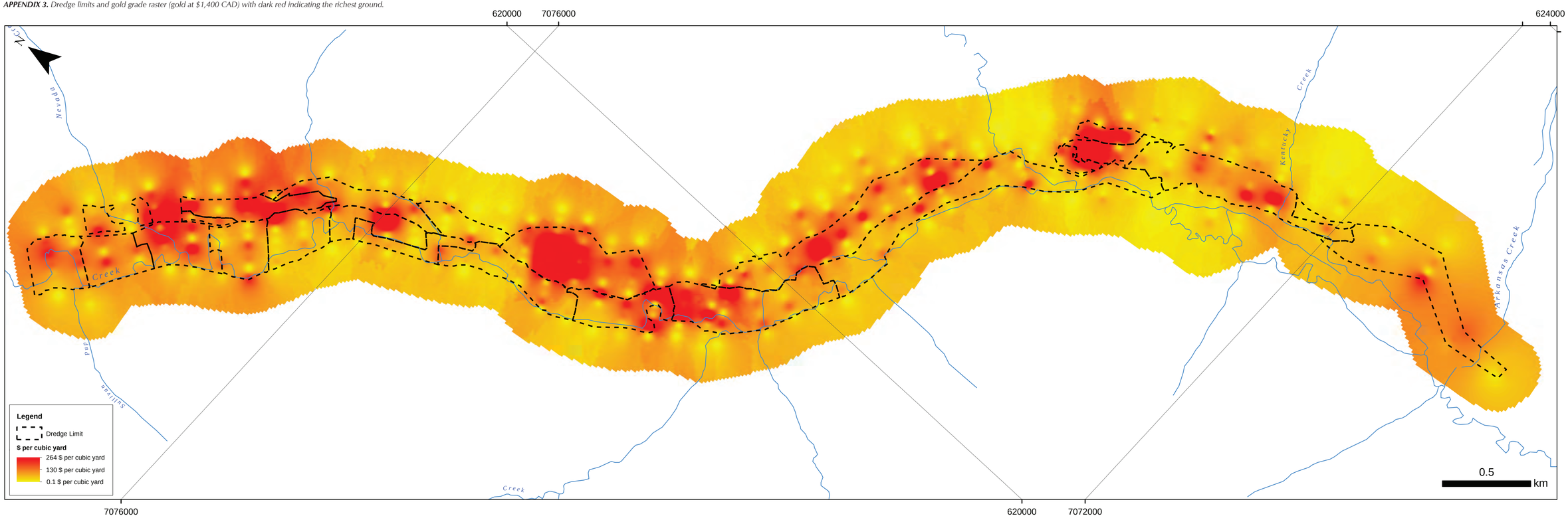
Appendix 1. *continued*

DRILL HOLE ID	GROUND CONDITION	SURFACE ELEVATION	BEDROCK ELEVATION	OVERBURDEN (M)	DREDGE SECTION (M)	CENTS PER CUBIC YARD
123-14	Partial	904	857	11.28	3.66	24.3
123-11	Frozen	850	830	5.18	1.52	22.6
123-10	Frozen	890	852	7.62	4.27	8
122-8	Partial	880	857	7.01	1.22	56.2
122-5	Frozen	852	833	5.18	0.91	29.9
122-4	Frozen	867	842	7.01	1.22	46.7
122-2	Frozen	898	859	4.88	7.32	0
122-17	Frozen	858	825	7.62	1.83	6.6
122-13	Frozen	852	825	5.79	3.66	36.3
122-1	Frozen	855	834	5.79	1.22	78.2
121-7	Frozen	847	823	5.79	2.13	10.6
121-6	Partial	878	856	4.88	3.05	47.6
121-3	Frozen	855	841	3.66	0.91	16.4
121-2	Partial	865	855	1.22	2.13	14
121-15	Frozen	859	832	6.1	2.44	4.3
121-14	Frozen	909	878	4.27	5.49	0
121-11	Frozen	854	827	5.79	3.05	57.4
121-10	Frozen	892	860	4.57	5.18	9.2
120-9	Frozen	855	833	5.18	1.83	23.9
120-8	Frozen	881	866	3.35	2.13	80.8
120-5	Frozen	855	829	5.49	3.05	50.7
120-4	Frozen	865	837	7.32	1.83	35
120-17	Frozen	860	838	6.1	1.22	8.6
120-14	Partial	<Null>	<Null>	<Null>	<Null>	0
120-13	Frozen	859	837	5.18	2.13	66.1
120-10	Frozen	<Null>	<Null>	<Null>	<Null>	15.6
120-1	Frozen	856	834	4.57	2.44	10.9
100-7	Frozen	858	844	3.35	1.52	0.1
100-6	Partial	866	860	0.61	1.52	0
100-3	Frozen	860	837	5.18	3.35	58.7
100-2	Frozen	858	832	6.1	3.05	308
100-19	Frozen	871	851	4.88	1.52	0
100-15	Partial	867	847	4.88	1.52	9.6
100-11	Frozen	862	840	4.88	2.44	88

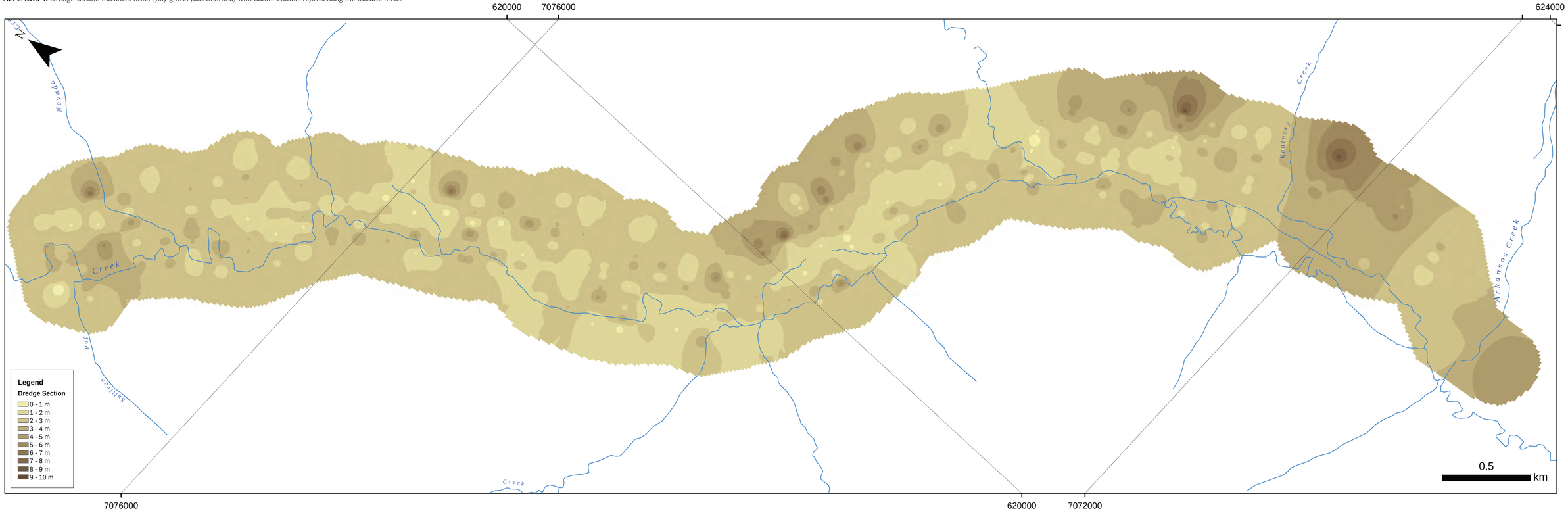
APPENDIX 2. *Satellite imagery of Dominion Creek study area with YCGC drilling data, dredge limits, and 2015 placer operation locations.*



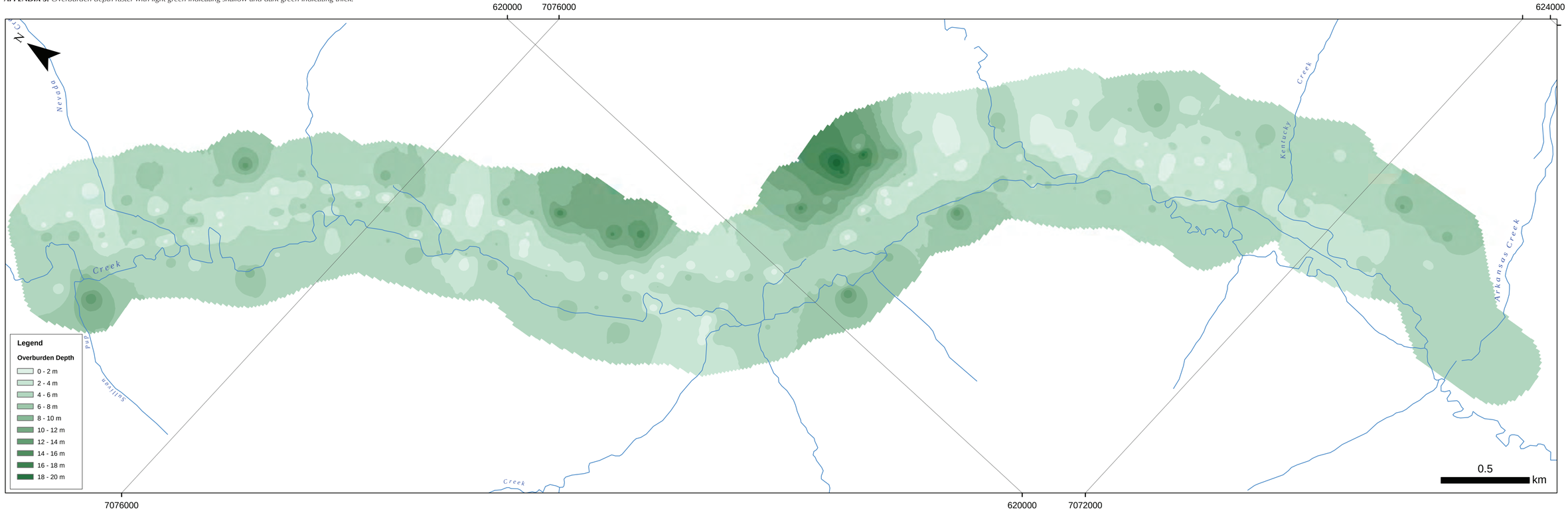
APPENDIX 3. *Dredge limits and gold grade raster (gold at $1,400 CAD) with dark red indicating the richest ground.*



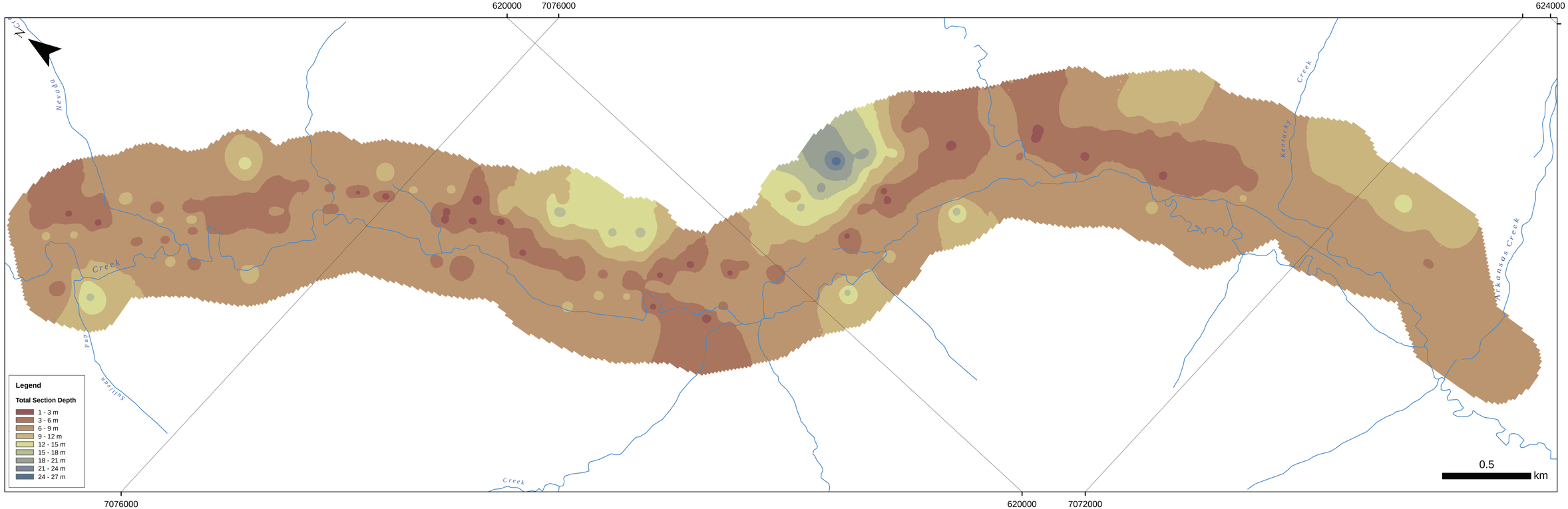
APPENDIX 4. *Dredge section thickness raster (pay gravel plus bedrock) with darker colours representing the thickest areas.*



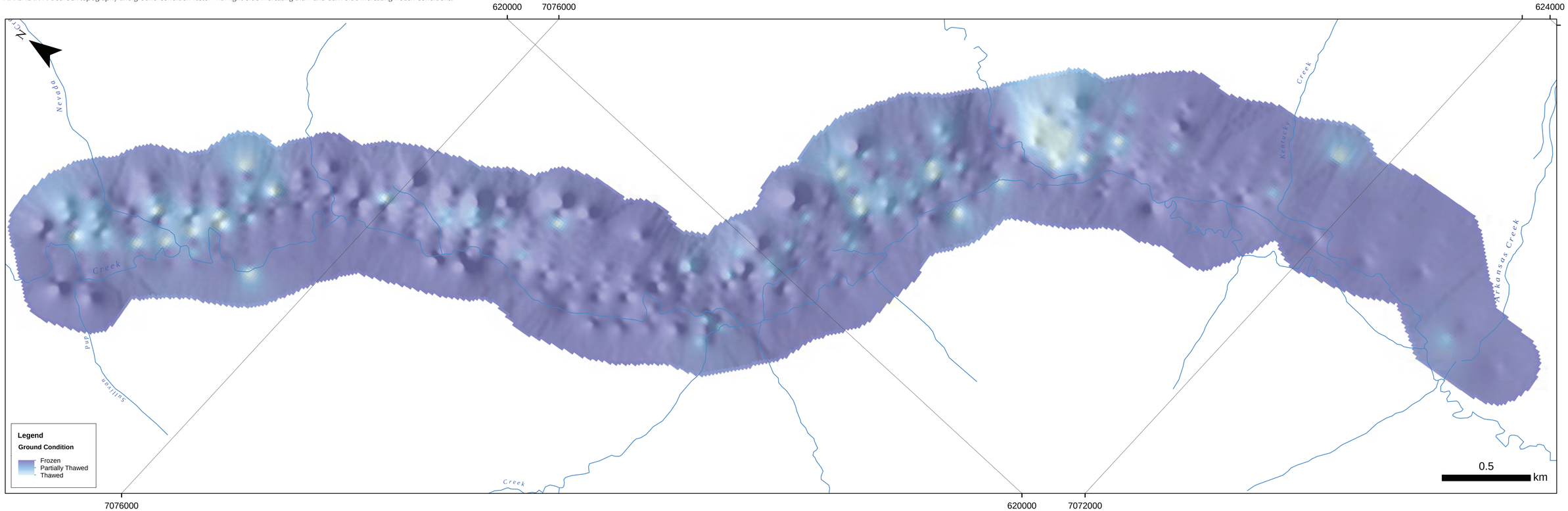
APPENDIX 5. *Overburden depth raster with light green indicating shallow and dark green indicating thick.*



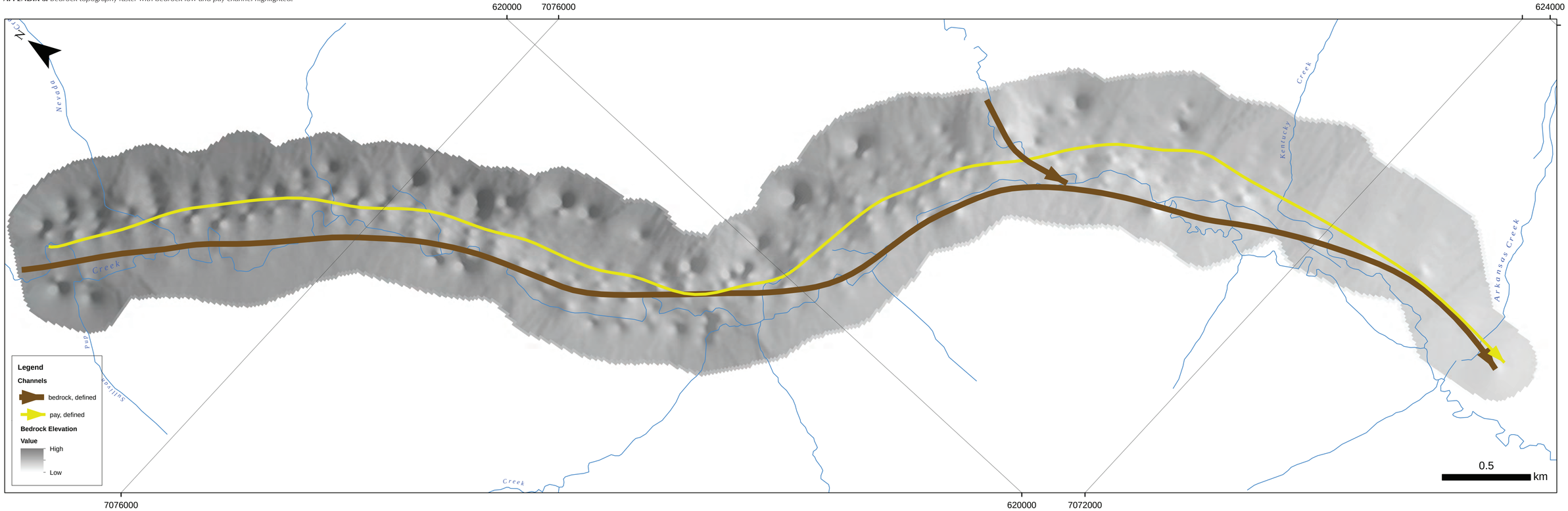
APPENDIX 6. *Total section depth raster (overburden plus dredge section) with depth increasing as brown lightens to blue.*



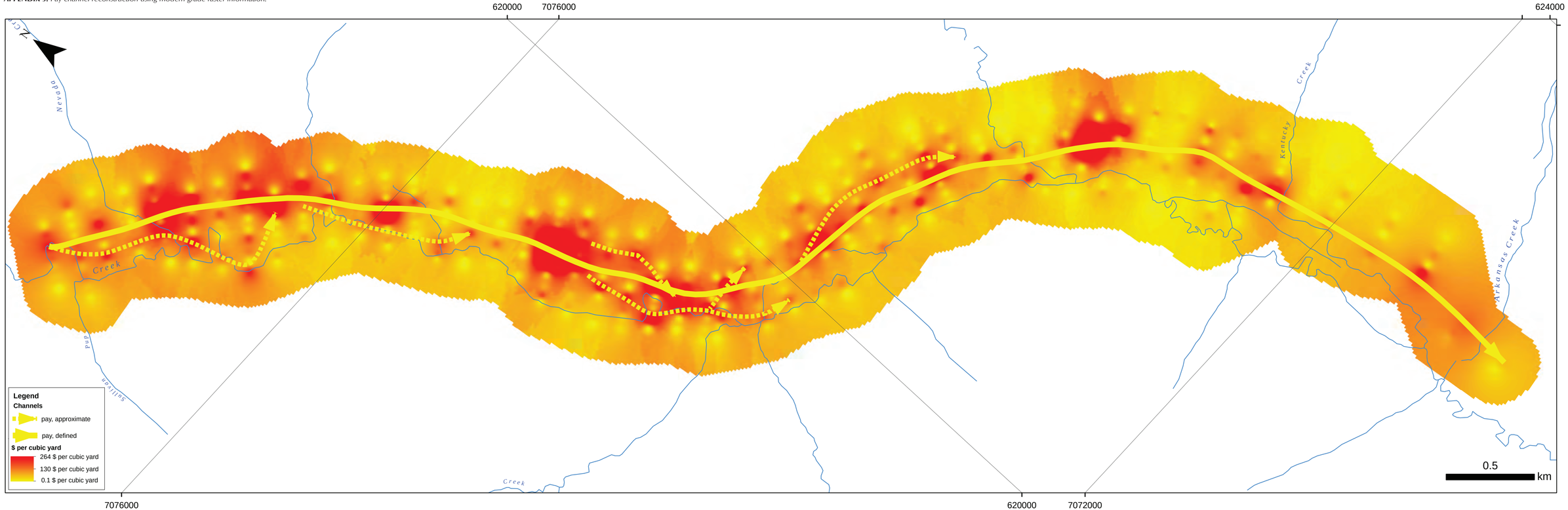
APPENDIX 7. *Bedrock topography and ground condition raster with light blue indicating thaw and dark blue indicating frozen conditions.*



APPENDIX 8. *Bedrock topography raster with bedrock low and pay channel highlighted.*



APPENDIX 9. *Pay channel reconstruction using modern grade raster information.*



APPENDIX 10. *Total section depth with dredge limit and high grade zones.*

